5-1985

Applications of a Direct Fast Field/Reflectivity Method to Wave Propagation Modeling in Underwater Acoustic and Solid Earth Seismic Environments

Gerard Joseph Tango
University of New Orleans

APPLICATIONS OF A DIRECT FAST FIELD/REFLECTIVITY METHOD TO WAVE PROPAGATION MODELING IN UNDERWATER ACOUSTIC AND SOLID EARTH SEISMIC ENVIRONMENTS

A Thesis

Submitted to the Graduate School Faculty
of the University of New Orleans LA
in partial fulfillment of
the requirements for the degree of
Master of Applied Physics
in
the Department of Physics, UNO

by

Gerard Joseph Tango
B.S., Cornell University, 1977
May, 1985

TABLE OF CONTENTS

		Pages
ACKNOWLEDGEMENTS.		i
TABLE OF CONTENTS		iii
LIST OF FIGURES		v
ABSTRACT.		xix
1.0	PRELUDE	1
2.0	THEORETICAL DERIVATIONS	
2.A	Historical Introduction	7
2.B	General Model & Derivation of Field Equations	26
2.C	Finite Element/Finite Wave Element Analogy.	68
2.D	Direct Global Matrix Strategy	81
2.E	Rapid Assembly & Implementation using Index Pointers	91
2.F	Global Matrix Solution via Gaussian Elimination.	100
2.G	Numeric Integration: Contour Order & Representation	110
2.H	Numeric Integration: Path	115
2.I	Numeric Integration: FFP algorithm.	128
2.J	Theoretical Stability & Accuracy Tests of Global Matrix output.	134
2.K	Computer Accuracy tests of Green's function: Results.	153

3.0 APPLICATIONS

3.A. Overview of Applications. 195

3.B Very Low Frequency Seis-Acoustic Ocean Bottom Propagation 199

3.C Forward Seismic Modeling of LVL Transition Zones in E. Basin & Range province 225

3.D Synthetic Vertical Seismic Profiles 369

4.0 ONGOING & FUTURE EXTENSIONS

4.A Overview of Ongoing & Future Extensions 567

4.B Spherically-stratified Media. 569

4.C 3-D "Gaussian beam" source 570

4.D Range-dependent propagation 578

5.0 SUMMARY, CONCLUSIONS AND RECOMMENDATIONS FOR

5.A FURTHER STUDY. 590

5.B THESIS CONTRIBUTIONS 598

LIST OF REFERENCES 602

VITA 622

List of Figures

Figures for Chapter 1 pages

Figure 1 SAFARI Numerical Model 29

Figure 2 Cross-Interface Continuity of Normal & Tangential Displacement & Stress 62

Figures for Chapter 2 pages

Figure 3	Schematic of Sparse banded block bidiagonal global matrix	.67
Figure 4	Schematic of Connectivity relations for Finite element & Finite Wave element models	.75-6
Figure 5	Mapping between Local and Global systems of equations	.89-90
Figure 6	Indicial Pointer system for Local to Global mapping.	.94
Figure 7	Computational features of SAFARI Direct Global Matrix solution.	.98
Figure 8	Heuristic flowchart of SAFARI DGM algorithm.	.99
Figure 9	Schematic of the Stability of complex Exponentials along DGM main diagonal.	.105
Figure 10	Programming features of SAFARI	.109
Figure 11	Contour integration path in complex wavenumber plane used by SAFARI.	.118
Figure 12a -g	Full plane wave (line source) solution & Outgoing-only + asymptotic point source approximation	.122-5
Figure 13	Typical Green's function integrand	.137
Figure 14a b c	Typical time domain "ringing" distortion full wave synthetic seismograms due to Gibb's oscillations (too abrupt a truncation of frequency spectrum)	.146-8
Figure 15a b	Typical time domain "wraparound" aliasing (time window too small).	.151-3

Figure 16a Comparative Accuracy tests of SAFARI:
b Green's function integrands and
c Transmission loss curves
d as derived from SAFARI
e and IFDPE (Parabolic Equation)
f SNAP (adiabatic Normal Mode)
g and Kutschale (FFP)
h overlay plots of Normal mode,
i Kutschale FFP and IFDPE results;
j SAFARI FFP results for NK=16384;
k PE & SAFARI contured TL plots. 158-68

Figure 17a Comparative Accuracy tests of SAFARI:
b Results from SAFARI FFP and Kutschale FFP for Green's functions 171-2

Figure 18 Theoretical dispersion curve for solid Basalt basement. 176

Figure 19a Theoretical Green's function and
b synthetic water wave arrival at 2 ranges (after PEKERIS, 1948; FRAZIER and RUDMAN, 1978). 180-1

Figure 20a -c S* inhomogeneous arrival (after GUTOWSKI et al, 1984) 185-7

Figure 21a Hypothetical horizontal seismic profile
b for MOHO1 Model (after BRAILE
c & SMITH, 1975) 189

Figure 22a Velocity/depth profile and
b corresponding fullwave synthetic seismogram for crustal seismic wave tunnelling (after FUCHS & SCHULTZ,1975). 191-2

Figures for Chapter 3, Section One pages

Figure 23 Pekeris model shallow water environment. 204

Figure 24
a Transmission loss curves:
b Basalt (no shear), f=50Hz
c Basalt (no shear), f=5Hz
d Basalt (shear), f=50Hz
Basalt (shear), f=5Hz 207-10

Figure 25a
b Simulation of net shear loss via addition of additional P wave attenuation (in a no shear model). 211-13

Figure 26a
b
c Theoretical Green's function for Basalt
f=5Hz
f=3Hz
. 215-6

Figure 27 Fullwave synthetic seismic (Scholte wave) pulse for Basalt (f_{center}= 5Hz; f_{mx}=12.5; f_{mn}=0) 219

Figure 28 Fullwave synthetic vertical seismic profile for Basalt 221

Figure 29 Depth-range contoured Transmission loss for Basalt. 222

Figures for Chapter 3, Section Two pages

Figure 30 Schematic plot of generalized Reduced-time deep crustal seismic arrival types 235

Figure 31 Fullwave synthetic seismogram for LVL6 Model, showing interfering complex of Pg arrival(s) (after BRAILE & SMITH, 1975) 239

Figure 32 Fullwave Hypothetical VSP for LVL6 Model. 244

Figure 33 Reflectivity and Fullwave synthetic seismograms for LVL6 Model 249

Figure 34 Detailed fullwave hypothetical VSP for LVL6 Model 251-4

Figure 35a b Velocity/depth profile & corresponding synthetic reflectivity seismogram for simple 2-layer crustal model (after TATEL & TUVE; from PAKISER, 1985) 256-8

Figure 36 Field record section of refraction seismic data from DELTA West-Shoal from PRODEHL (1979) 265

Figure 37a b c d Corresponding synthetic reflectivity seismograms for PRODEHL Model 1 using 3 different maximum angles of wavenumber integration 270-3

Figure 38a General Prodehl-derived velocity-depth model, w/o LVL (all-discontinuity)
b c Corresponding reflectivity synthetic seismograms for 2 maximum angles
d e Fullwave synthetic seismograms for 2 maximum horizontal wavenumbers 277-81

Figure 39a General Prodehl-derived velocity-depth model w/o LVL (all gradients)
b Corresponding reflectivity synthetic. 284-91

Figure 40a — General Prodehl-derived velocity-depth model w/LVL and gradients
b — Corresponding reflectivity synthetic 286-7

Figure 41a — General Prodehl-derived velocity-depth model w/o LVL, having near-surface & deeper crustal structure
b — Corresponding reflectivity synthetic 288-9

Figure 42a — General Prodehl-derived velocity-depth model w/o LVL, having more complex near surface & deeper crustal structure (nonlinear gradients)
b — Corresponding reflectivity synthetic 290-1

Figure 43a
b — Velocity/depth profile and corresponding reflectivity synthetic for LVL6 Model 293

Figure 44a
b — Velocity/depth profile and corresponding reflectivity synthetic for generalised Basin and Range model (after KELLER,SMITH & BRAILE,1975) 294-5

Figure 45a
b — Velocity/depth profile and corresponding reflectivity synthetic for generalised Basin and Range model (after BRAILE & SMITH, 1975) 296-7

Figure 46a
b — Velocity/depth profile and corresponding reflectivity synthetic for proposed DELTA West-Shoal model N7 (after MULLER & MUELLER, 1979). 302-3

Figure 47 — Fullwave synthetic seismogram for Muller-Mueller Model N7. 304

Figure 48a
b — Velocity/depth model and corresponding reflectivity synthetic for generalized Basin & Range LVL (after BANDA & DEICHMANN, 1983). 310-11

Figure 49 — Reflectivity synthetic for Banda & Deichmann LVL model,using maximum angle of wavenumber integration. 312

Figure 50 Velocity/depth model and corresponding reflectivity & fullwave synthetic seismogram for structured LVL (after MCMECHAN, 1984) 314-6

Figure 51a b Velocity/depth model and corresponding reflectivity synthetic for Muller-Mueller nearsurface and LVL model, incorporating Prodehl subLVL. 322-3

Figure 52a b Velocity/depth profile and corresponding reflectivity synthetic for Muller-Mueller +Prodehl model, with thicker LVL. 324-5

Figure 53a b Velocity/depth profile and corresponding reflectivity synthetic for Muller-Mueller +Prodehl model, with LVL of greater velocity contrast 327-8

Figure 54a b Velocity/depth profile and corresponding reflectivity synthetic for Muller-Mueller+Prodehl model, with additional velocity gradient 330-1

Figure 55a b Velocity/depth profile and corresponding reflectivity synthetic for Muller-Mueller +Prodehl model, with maximum LVL velocity contrast. 332-3

Figure 56a b Velocity/depth profile and corresponding reflectivity synthetic for Muller-Mueller +Prodehl model, with second LVL in nearsurface 337-8

Figure 57a b Velocity/depth profile and corresponding reflectivity synthetic for Muller-Mueller +Prodehl model, with second LVL in nearsurface, of greater velocity contrast 339-40

Figure 58a b Velocity/depth profile and corresponding reflectivity synthetic for Muller-Mueller +Prodehl model, with 2nd LVL (as in Figure 56), and third LVL below central LVL. 344-5

Figure 59a b — Velocity/depth model and corresponding reflectivity synthetic for Muller-Mueller +Prodehl model, with single thin high velocity layer centered in main LVL 347-8

Figure 60a b — Velocity/depth model and corresponding reflectivity synthetic for Muller-Mueller +Prodehl model, with single thin high velocity layer centered in main LVL, of higher velocity contrast 349-50

Figure 61a b — Velocity/depth model and corresponding reflectivity synthetic for Muller-Mueller +Prodehl model, with many thin high velocity layers alternating with low velocity layers centered in main LVL (laminated complex) 353-4

Figure 62 — Composite velocity/depth model, derived from previous SAFARI results and published proposals (KOSMINSKYA et al, 1972) for a generalized crust with LVL 357

Figure 63a b — Partial digitized version of Kosminskya LVL velocity/depth model, and corresponding fullwave synthetic 359-60

Figures for Chapter 3, Section Three

		pages
Figure 64	Data acquisition and wave arrival types for shallow-depth Vertical & Horizontal seismic profiles.	.371
Figure 65	Schematic of travel paths for horizontal and vertical seismic profiles	.378
Figure 66	Summary of extant synthetic VSP modelling algorithms	.390
Figure 67	Representation of SAFARI single and multiple offset VSP modelling capabilities	.394
Figure 68	Velocity/depth profile for a (full shear) elastic multilayered model of 50 layers, representing Ruhr valley coal seams (after TEMME & MULLER, 1982)	.400-1
Figure 69	Synthetic reflectivity horizontal seismic profile for Temme & Muller v/z profile	.403
Figure 70a b c	Fullwave synthetic VSP (point source) for full shear elastic v/z profile, at three extreme nearfield source-receiver offsets	.406-8
Figure 71a b	Fullwave synthetic VSP (line source) for full shear elastic v/z profile, at two extreme nearfield source-receiver offsets	.410-1
Figure 72	Fullwave synthetic VSP, line source (plane wave), for acoustic-only Temme-Muller v/z profile; x_{offset}= .3 km	.418
Figure 73	Fullwave synthetic VSP, plane wave for acoustic-only Temme-Muller v/z profile, x_{offset}=.3km; with #receivers=46	.420
Figure 74	Fullwave synthetic VSP, plane wave for acoustic-only Temme-Muller v/z profile, x_{offset}=.3km; with f_{center}=100Hz, f_{max}=225Hz	.422

Figure 75 Fullwave synthetic VSP, plane wave, for acoustic-only Temme-Muller v/z model, with f_{center}=25Hz, f_{max}=50Hz. 423

Figure 76a b c Velocity/depth models and fullwave synthetic VSP, plane wave, for acoustic-only Temme-Muller v/z model,
(a) No nearsurface [deep seams only]
(b) No deep seams [nearsurface only]
(c) total response 425-9

Figure 77a b Fullwave synthetic VSP, plane wave, for acoustic-only Temme-Muller v/z model, x_{offset}=.3km, for values of Low and High intrinsic attenuation 433-4

Figure 78a b Velocity-depth model (variation of Temme-Muller) and fullwave synthetic VSP, plane wave, acoustic-only model, x_{offset}=.3km, with 1st major coal seam replaced by "seismically-equivalent" cyclic sequence of thin alternating high and low velocity layers 437-40

Figure 79a b c d e f g h i Synthetic fullwave VSP, plane wave, for acoustic-only Temme-Muller v/z model, over a range of increasing source/receiver offsets
x=.1km
x=.3km
x=.5km
x=.7km
x=.9km
x=1.1km
x=1.3km
x=1.5km
x=1.7km
demonstrating maximum amplitude enhancement of successively deeper horizons with progressively greater offsets. 442-50

Figure 80 Fullwave synthetic VSP, plane wave, for acoustic-only Temme-Muller v/z model, with increased thickness and velocity of 1st major seam (z_{seam}=720m) 455-6

Figure 81a–f Fullwave synthetic VSP, plane wave, for full-shear elastic Temme-Muller v/z model, over a range of offsets
a x=.1km
b x=.3km
c x=.5km
d x=.7km
e x=.9km
f x=1.1km
demonstrating increased P-S conversion from localised layers with increased offset 459-64

Figure 82 Plane wave reflexion coefficients (PP & PS) for the same model as Figure 81 466-70

Figure 83 VSPs for same model and offsets as Figure 81, with f_{center}=25 and f_{max}=50Hz horizontal particle velocity records 474-9

Figure 84a–f VSPs for same model and offsets as Figure 81, over extreme farfield offsets
a x=1.3km
b x=1.5km
c x=1.7km
d x=1.9km
e x=2.1km
f & split panel: acoustic & seismic VSPs. . . .482-7

Figure 85a–b Raitt Ocean crustal velocity/depth model and corresponding reflectivity horizontal seismic profile with a suite of Green's function integrands 492-50

Figure 86a–e Fullwave synthetic VSPs, plane wave full shear elastic Raitt v/z model, over selected range of OSE offsets
a–d x_{min}= 1km; x_{max}= 5km;
e Geophone records of Vertical particle velocity. 503-7

Figure 87a Fullwave synthetic VSPs, plane wave
b full shear elastic Raitt v/z model,
c over selected range of OSE offsets
d x_{min}= 1km; x_{max}= 5km;
e Hydrophone records of pressure
f = - normal stress 508-12

Figure 88a Fullwave synthetic VSPs, plane wave
b full shear elastic Raitt ocean v/z
c model, over selected range of OSE
offsets (x_{min}= 1km; x_{max}= 5km)
e Geophone records of horizontal
f particle velocity 513-7

Figure 89a Fullwave synthetic VSPs, plane wave
b full shear elastic Raitt ocean v/z
model, x_{off}= 3km, With and Without
Free surface reflection effects 521-2

Figure 90a Raitt v/z profile, modified to
include a nominally thin sediment
layer atop crust Layer 1
(after WHITE & STEPHEN, 1980);
corresponding plane wave bottom loss
curves over all grazing angles, and
frequencies from f=0 to f=25
for 3 sediment thicknesses 526-41

Figure 91a Full wave VSPs, plane wave, full shear
b thin sediment + Raitt ocean v/z model
c layer w/positive velocity gradient, at
d 5 offset ranges (x=1,2,3,4,5 km)
e (Geophone-Vertical particle velocity). . . .544-7

Figure 92a Full wave VSPs, plane wave, full shear
b thin sediment + Raitt ocean v/z model
c layer w/positive velocity gradient,at
d 5 offset ranges (=1,2,3,4,5 km)
e (Geophone-Horizontal particle velocity). . .548-52

Figure 93a Fullwave HSP, point source, full
b shear elastic v/z model of sediment
c +Raitt crust for a suite of OBS
d receivers in horizontal and vertical
particle velocity, and pressure. 555-6

Figure 94a Fullwave HSP, point source, full
b shear elastic v/z model from Costa
Rica DSDP experiment (after STEPHEN et
al, 1984), for receivers at 2 depths
(Direct Water wave root) 559-64

Figures for Chapter 4

pages

Figure 95a f — Outline of governing field equations for 3d source version of SAFARI (after SCHMIDT & GLATTETRE, 1985) 572-6

Figure 96 — Schematic of basic finite wave element concept 580

Figure 97 — Overview table of total SAFARI capability. .597

ABSTRACT

A new method is discussed for exact rapid computation of the depth-dependent Green's function occuring in full integral solutions to the acoustic and elastic Helmholtz wave equation, allowing calculations of underwater acoustic propagation loss and full wavefield synthetic seismograms, in range-independent plane stratified media.

This algorithm, " SAFARI " , (SAclant FAst field program for Range-Independent environments), developed by SCHMIDT (1982,1983), is based upon an explicit approach to the Pekeris layered media model of Ewing, Jardetzky and Press. " SAFARI " permits arbitrary location of any number of sources and receivers in a flat n-layered ocean/earth, via a more direct, economical and unconditionally stable solution, resulting in a novel numerical model of wide generality and application, without limitations inherent to propagator-matrix based solutions.

This direct-global-matrix/finite-wave-element approach to Green's function computations of SCHMIDT is here developed in detailed analogy to the direct finite element method, generalized to the case of n arbitrary elastic layers in terms of scalar potentials. The direct global matrix approach of " SAFARI " is then compared with the recursive local propagator matrix method of Thomson-Haskell, common to FFP, reflectivity and discrete wavenumber techniques, and the integration scheme employed reviewed.

Selected representative examples of the broad range of validity and application of the " SAFARI " approach are presented for the cases of

shallow water ocean acoustic propagation at very low frequencies

deep crustal synthetic seismic modeling of crust/mantle low velocity transition zones, and

synthetic vertical seismic profile simulation

computed using a VAX 11/780 + attached array processor version of " SAFARI ". These application cases are discussed in detail via comparison to available results of other numerical modeling programs, as well as available experimental data. Application specific extensions and further theoretical developments of the " SAFARI " method are outlined.

Section 1.0

Prelude.

A direct procedure to evaluate the Green's function response, for an arbitrarily layered visco-elastic halfspace, to any number of arbitrary buried point sources is presented, after the work of SCHMIDT (1982). The complex (discrete) wavenumber domain formulation is here based upon the direct approach of Ewing, Jardetzky and Press (EJP), to represent globally the solution to the Pekeris layered problem in terms of a direct simultaneous superposition of up and downgoing waves in all layers, resulting from a separable product solution under the Langer approximation (with P-SV coupling only at layer interfaces). The sparse banded block bidiagonal form of the resulting matrix (for the case of N layers having a free surface) gives 4n-2 linear equations in 4n-2 unknown wavefield coefficients and allows efficient and unconditionally stable solutions by simple standard methods, such as Gaussian elimination with partial pivoting, without additional recourse to any iterative or approximate schemes.

Time domain results of pressure quantities versus range in (eg) underwater acoustics are directly obtained, and for seismogram synthesis may be arrived at by integration over wavenumber or slowness with Fourier synthesis over frequency (or vice versa),

in any one of several asymptotic or exact numerical techniques. The procedure for both Green's function and field quantity solution, as encoded in a new algorithm of SCHMIDT, " SAFARI ", are complete and valid for all frequencies, wavenumbers and layer properties, are applicable to fluid, solid and/or mixed layers of any number or configuration; incorporates any chosen law of material attentuation or source type, and calculates automatically the received wavefields from N arbitrary receiver arrays, at very small additional computational costs, making it ideal when the number of source-receiver combinations is very large.

The accuracy, completeness and stability of the SAFARI direct global matrix procedure and associated computer programs have been established thru this research, by comparisons with solutions obtained via other analytic and numerical methods, for simple representative test case models. In particular, the results obtained by the present direct global matrix approach for (N) buried point source(s) have been successfully compared for the underwater acoustic case with the results obtained by Pekeris, Normal Mode and earlier FFP methods.

For layered solid earth media, the displacements and stresses generated by a buried point source, as calculated by the present algorithm, were compared with those obtained by use of the reflectivity method of Fuchs-Mueller and Kennett. The excellent agreement obtained for a wide range of frequencies,

source/receiver geometries and ranges, number and thickness of layers and elastic parameter values indicates the reliablility and complete flexibility of the direct global matrix method for elastodynamic Green's function solution embodied in " SAFARI ". Since the wavefield is necessarily computed for the entire layer stack, by employing the inbuilt facility of utilising vertical receivers within the media, the results of both standard surface receiver based seismology and insitu borehole seismometry (VSP) may be automatically modeled and analysed more completely, with little additional computational cost when additional adjacent boreholes in range are considered.

The computer time required to perform the Green's function matrix solution calculations depends only upon the frequency bandwidth, horizontal complex wavenumber spectrum and number of layers considered. For the simplest ocean modeling case, involving only 1 layer, at least an order of magnitude CPU time savings has been observed in routine comparisons to extant propagator matrix based solution algorithms. In a deep crustal seismic simulation involving a buried source located in the nearsurface of a layered halfspace comprising 50 layers, the computation of the displacement/stress fields for a surface receiver array of 90 equispaced receivers over 90 km required only 6 minutes on a VAX 11/780, and 40 seconds on a VAX 11/780 with FPS 164 attached array processor. For vertical seismic profiling configurations of 25 subsurface receivers to 1 source of bandwidth 0-125 Hz, the computer times were 2000 seconds and 6000 seconds on an FPS 164

for acoustic & elastic models respectively, in a 50 layer model.

As will be demonstrated, the direct global matrix approach of SCHMIDT in "SAFARI" directly embodies & results from only the basic physics of wave propagation in a layered (waveguide) medium. When developed in formal analogy to well-established matrix techniques basic to the direct finite element method, it clearly provides a direct intuitive grasp of how depth-dependent layering affects seismic-acoustic wavefield propagation. The technique is developed entirely independent of any considerations or use of propagator matrices.

Since the "SAFARI" formulation is perfectly general in respect of fluid, solid or mixed media, number & type of sources and/or receivers, and frequency/wavenumber range, it naturally also encompasses a broad spectrum of ultrasonic & physical acoustic applications, besides those of underwater & seismic acoustic wave propagation modeling (SCHMIDT & JENSEN, 1984). Further, because the direct global matrix/finite wave element method as implemented by SCHMIDT is unconditionally stable for all boundary conditions & layer configurations, as well as computationally comparable to or faster than other extant seismic acoustic modeling algorithms of the same "complete solution" type, it can readily accomodate more realistic earth stratification conditions qua treating much larger numbers of transition isovelocity steps, to better approximate real earth elastic parameter gradients.

In the solid earth seismic as in the underwater acoustic case, where " SAFARI " can easily serve as an established reference solution for model-data comparisons, " SAFARI " can also function as a benchmark to other partial approximate or numeric solution methods.

The theoretical development and analysis of the direct global matrix/finite wave element approach in " SAFARI " presented here is an extended form of that due to SCHMIDT (1982;1983), SCHMIDT and JENSEN (1984) and SCHMIDT and TANGO (1984), with special emphasis on presenting both the detailed derivations and the diverse applications of this new complete solution algorithm. In particular, the resulting form of the direct global matrix, and the techniques used to solve for the depth dependent Green's function wavefield coefficients, will both be shown to be very closely related to the global stiffness matrix and the specific indicial mapping techniques employed in the direct finite element method. These guarantee stable and accurate numeric behaviour from within the framework of established and well understood methods for solving large linear systems by sparse banded matrix techniques. The exact and complete nature of the full wavefield solution, as well as the natural ability of this traveling-wave formulation to encompass automatically the numerical modeling requirements of vertical seismic and other vertical receiver array simulations will also be stressed.

In contrast to similar independent recent work by CHIN et al (1984) and HA (1984) on matrix methods in seismology, the approach adopted by SCHMIDT and also this thesis is decidedly geophysical, and therefore comparatively 'nonformal' in the sense that computational details and theoretical machinery or equivalences of a purely mathematical nature, as common in propagator matrix discussions, are described only insofar as necessary to develop the direct global matrix/finite wave element approach for general seismic-acoustic applications.

This thesis thus attempts an essentially self-contained overview of selected recent work in numerical modeling of acoustic and elastodynamic wave propagation in plane homogeneous media. Based primarily on the results of joint ongoing investigations of the author with Dr. Henrik SCHMIDT, the present effort also reports the outcome of a concerted literature survey in several areas of numerical methods and theoretical seismology, given here as background to the current undertaking.

While only underwater acoustic and seismic modeling are considered here, it must be emphasised that the technique for Green's function matrix solution, and the underlying 'finite wave element' philosophy, is equally well applicable, not only elsewhere in physical acoustics and theoretical and applied mechanics, but also to electromagnetic propagation studies in plane media.

Section 2: Theoretical Derivation of "SAFARI" formalism

2(a) Historical Introduction

As recently reviewed by DEAVENPORT & DINAPOLI (1980) and JENSEN (1983) for underwater acoustics, and by MOONEY (1982), KENNETT (1983) and CHAPMAN & ORCUTT (1984) for seismology, over the past 25 years, a number of diverse integral transform methods to estimate the exact dynamic Green's function impulse response of a multilayered homogeneous halfspace have been developed. In general the type of transform-domain solution, method and/or order of integration & inverse transformation have served to distinguish these approaches. Along with purely numeric (BOOTH, 1971) and 'hybrid' techniques (DEAVENPORT & DINAPOLI, 1978; KORN, 1982), extant solution methods fall in general into catagories of ray, mode and wave types, into the last of which groupings falls the topic of this thesis.

As distinct from the approximate ray or mode summation approaches (PEKERIS, 1948; CERVENY, 1978; BEN MENAHEM & SINGH, 1980; KENNETT, 1983), the other wave class of exact integral transform techniques (involving discrete wavenumber & frequency synthesis integrations) has existed in principle since the first analytic investigations of transient elastic wave propagation in plane layered media (see references; EWING JARDETZKY and PRESS,

1957; BREKHOVSKIKH, 1960; CERVENY and RAVINDRA, 1970; MIKLOWITZ, 1978; AKI and RICHARDS, 1980).

Various 'exact' formulations of solutions to the layered waveguide problem have been developed, and the numerous and varied attempts to reduce the many difficulties arising from complexity of the solution integrals has been closely determined by (1) the presence of a guiding conceptual model for specific applications, and (2) the existing state-of-the-art in numerical computation (as concerns both mathematical methods and computer hardware).

To cite the many outstanding individual contributions to this fundamental problem of determining the complete theoretical response of a spherical point source from a plane seis-acoustic boundary entails consideration of an extensive historic reference bibliography (for an introduction to these, see CAGNIARD, 1939,1960; EWING JARDETZKY and PRESS, 1957; REDWOOD, 1959; BREKHOVSKIKH, 1960; BUDDEN, 1962; MUELLER, 1968; CERVENY and RAVINDRA, 1971; MIKLOWITZ, 1978; AKI and RICHARDS, 1980).

However, despite the previous computational convenience of both the nonwave (approximate) and restricted wave (partial) solutions, the advantages, implications and common insights of a vast amount of previous effort on elastic transients in a layered halfspace have often been missed. This is due precisely to the nature and formulation of the restricted solutions obtained for

realistic exact cases, or the inutility of complete exact solutions available for highly idealised models. Both approaches have typically involved serious limits on source, receiver and layer number and location, resulting wave types and orders.

As a consequence, theoretical investigation of a more general approach to acoustic/elastic wave propagation for point sources in a homogeneous medium has historically attracted repeated attention since the original work of LAMB (1904). A central concern here has been identification of an exact and complete framework and problem formulation, sufficiently general to comprehend the major classes of experimental (source/receiver configurations) and environmental (media properties) conditions, while at the same time clearly preserving the basic physics common to all waveguide problems.

It has long been known (LAME,1852;CAGNIARD,1939,1962) that the total displacement-stress field resulting from one or more point sources within a homogeneous multilayered planar waveguide can always be described in terms of general field variables continuous across layer **interfaces**. For example, all LAMB's (1904) basic problems concerning transient elastic wave propagation for both surface and buried point or line sources in a simple halfspace -as well as most all of the other derived canonic problems of theoretical seismology- fall into the above catagory.

In this connection, the work of PEKERIS (1940,1948,1952,1957) is central. Here the basic models are fluid, solid or mixed layered halfspace waveguides, with one layer typically containing an explosive point source for P or SH waves. Using this wave model, PEKERIS (1948) theoretically calculated, for one and two layer fluid/solid ocean models, the wave motion resulting from a buried monochromatic point source, expressing sound wave propagation as the sum of up and downgoing travelling waves (subsequently demonstrating in this fashion the equivalence of normal mode and exact ray theories for propagation description when computing synthetic seismograms for a transient source).

Since its inception, this integral representation of a total displacement/stress field has been the core of many advances made through solution of boundary value problems in linear elastodynamics. It is here clear that the general problem of seismic-acoustic wave propagation in a general multilayered medium is correctly and completely solved if it is somehow possible to find a **general** solution model and method, sufficiently stable and swift so as to be suitable for routine numeric computation of all contributions to the exact full wavefield solution, and also valid for all experimental and environmental conditions.

Dealing with a very simple axisymmetric plane layered waveguide model, of the kind now canonic in underwater acoustics (PEKERIS, 1948), theoretical and applied mechanics (MIKLOWITZ, 1978) and

also both seismic and electromagnetic wave propagation (BREKHOVSKIKH, 1958; BUDDEN, 1960; TOLSTOY, 1974; WAIT, 1982), Ewing Jardetzky and Press (1957) in the seismic elastic case proposed the most general integral transform representation of the total wavefield solution for this waveguide model. The physical displacement and stress quantities are replaced by the total real contour horizontal wavenumber integral over an unknown field solution, satisfying the homogeneous Helmholtz wave equation, superposed with a forcing term due to one or more arbitrary sources within any layer. These are both expressed in terms of up and downgoing scalar wavefield potentials.

This general approach was first explicitly developed by JARDETZKY (1953) and KEILIS-BOROV (1953), in the context of determining theoretic surface wave dispersion curves, for general multilayered media with a single source/receiver configuration. For the few-layered cases originally considered in exact format, such a Green's function solution kernel is found analytically in a straightforward fashion. However, despite the potential generality of their 'global' methodology, for any media models more complex than simple few layer/halfspace combinations, the approach soon becomes impractical for routine application, by virtue of sheer arithmetic and algebraic complexities. It was further objected (HASKELL, 1953; EWING JARDETZKY and PRESS, 1957; HARKRIDER, 1964) that not only would finite computer accuracy and long runtimes preclude computationally correct calculations with 'global' matrices of such large order, but that in fact such

theoretically complete results would be undesirable, on account of the belief that such a global formulation could not inherently provide insight into the individual separable effects of receiver depth, source depth and layering on the total Green's function response.

For precisely these reasons, traditionally the Green's function representation has to date been solved for through 'local' matrizant or propagator matrix based computational techniques (AKI and RICHARDS, 1980, Chapter 5), as introduced into seismology by THOMSON (1951) and later varyingly modified (HASKELL, 1953; HARKRIDER, 1962; WOODHOUSE, 1980; APSEL, 1983; FRANSSENS, 1984). The essence of all these layer-propagation methods (reviewed in URSIN, 1982; see also KENNETT, 1983) is that the solution to a **global** multipoint **boundary value** problem is approximated by the set of **local initial value** solutions computed for each layer and matched at each interface. In this way, the **global** response for all layers is simply the product of the individual **local** layer propagator matrices.

Despite their numerous conceptual and practical advantages in many applications, however, this local matrix formalism has oftentimes entailed serious complications and limitations on scope and accuracy of application, as well as clarity of implementation. In contrast to its relatively straightforward operation in simpler optical transmission (VAN CITTERT, 1938), electrical (SCHULNEKOFF, 1934) and acoustical impedence

calculations (WATSON, 1946) as well as field computations for fluids (GILBERT, 1982), in seismology for solid elastic media the propagator matrix has not always proven readily suitable for the full range of practical numeric calculations. This is basically due to (1) chronic instability of its exponential transfer terms in the evanescent wavenumber regime, for arbitrarily thick layers with respect to the dominant seismic wavelength. In addition (2), the fact that repetitive field calculations are required with a local layer-to-layer formalism, even for only 1 source/receiver depth combination, in order to propagate the field thru a given layer and across the interface in question. The former problem in particular arises due to the well-known difficulties from incomplete cancellation of growing by dying exponentials (CHIN et al, 1984), inevitably arising in arithmetic roundoff on finite word-length computers.

Extensive theoretical development over the last 15+ years has thus focused precisely on overcoming these problems with propagator matrices by various correction/extension techniques (e.g., 'delta matrix' methods) or else application-specific reformulations (the 'invariant embedding' reflectivity approach of KENNETT; also WOODHOUSE, 1980). Although varyingly successful for particular applications, the general result of such efforts as remain within the propagator matrix solution philosophy have been time-consuming algorithms arising from an increasingly pure-mathematical approach to the computational physics problem at hand. Here the basic full wavefield solution properties in the

integral transform approach to Green's function solution of layered waveguide problems can be lost, or at least obscured to the wider audience of seismologists & acousticians, because of the extensive ancilliary mathematics required by utilizing an inherently ill-conditions initial value approximation (propagator matrix) to what is in actuality a multipoint boundary value problem (CHIN et al, 1984). In addition, as the theoretical seismology literature of recent years has shown (JOHNSON, 1974), practical Green's function calculations for application to seismogram synthesis over all source & receiver ranges & depths requires additional numerical stabilisation as well as many separate recursions. Total calculation time is here proportional to the total number of sources & receivers, often being prohibitive for many environmental & experimental configurations of interest. In addition, many formally-convenient local matrix schemes have proven difficult if not impossible to implement in practice (KENNETT, 1984). For these reasons, local separability of source, receiver & layer effects, although in principle achievable in this manner, has to date been practically unattainable via propagator matrix approaches originally proposed for this purpose.

To consider the computational (as opposed to conceptual) limits of local matrix methods in seismic-acoustics, as cited above, for the few-layered cases originally considered in exact format, such a Green's function solution kernel is in most cases easily found

analytically in a straightforward fashion, but soon becomes impractical for routine application to all but the simplest multilayered models. Before the advent of large digital computers and associated large-scale matrix solver software in numerical analysis, the required Green's function computation has historically been tackled by recursive Thomson-Haskell propagator matrix methods, as the previously best-available operation technique. However, in light of the development of extensive direct matrix solver software and extended computer memory since the original formulations of EJP (1957), the propagator matrix solution approach is no longer necessarily the only technique of choice for all applications.

In point of fact, the underlying ("global") idea in propagation of local layer solutions as well as the original EJP-PEKERIS layered waveguide model used in this procedure is both more general and directly accessible from the viewpoint of basic 'waveguide physics' than might at first be seen. In the method of SCHMIDT, a more direct and global **Physical** approach is taken to efficient stable solution of the global Green's function layer system matrix. This seeks to more readily preserve the theoretically desirable features of EJP's original multipoint boundary value problem solution, now however more widely generalised as implemented within the framework of modern sparse matrix solution techniques for large linear systems [as arise in diverse underwater acoustic, elastodynamic, seismic modeling and finite element applications (GEORGE and LIU, 1980)].

The purpose and method of all **local** propagator matrix solution techniques has been to seek to provide a computational mechanism for incorporating the boundary conditions and linking together the local wave equation solutions for all individual layers to eventually give the total (global) wavefield at one given receiver. Here, in what might be termed a direct global matrix approach, the seismic pressure/stress-displacement wavefield for a general n layer complex is considered as a global superposition of inhomogeneous wavefields produced by m arbitrary sources per layer, in the absence of boundaries, and an unknown homogeneous field, expressed in travelling wave potentials satisfying the homogeneous reduced Helmholtz equation. The unknown field is then simply determined directly from applying the classical boundary conditions of continuity of normal and tangential displacement and stress, to be simultaneously satisfied globally at each and every layer **interface**.

Thus, rather than resorting to ' local ' propagator matrix schemes for propagating displacements and stresses thru n halfspace layers, the resulting linear system of equations in the Hankel/Fourier transforms (in cylindrical/cartesian coordinates) of the scalar potentials, indexed per each interface, is directly assembled and written down in a global matrix form. Due to the simple cross connectivity arising from the here 4 specific boundary conditions of continuity, the resulting global matrix, directly assembled from all local interface submatrices, is positive definite, sparse and in this case banded block

bidiagonal, closely analogous to the global stiffness matrix arising in the direct finite element method (ZIENKIEWICZ, 1973; SCHMIDT, 1977). The solution of this global system of equations, in the seismic-acoustic case, can as in finite elements therefore be determined by simple Gaussian elimination with partial pivoting, directly yielding the exact total (global) wavefield in all layers simultaneously.

This direct global matrix/Finite Wave Element (DGM/FWE) approach, independently developed subsequently by CHIN et al (1984) from the perspective of propagator matrix extension, is seen to be exactly equivalent to the original technique formulated much earlier by JARDETZKY (1953) and EJP to derive analytic solutions (though not in closed form) for special solid/fluid waveguide models having only a 1 or 2 layer structure. The DGM/FWE model and algorithm of SCHMIDT (1982) described here is in fact precisely a general applications numerical implementation of the Pekeris-EJP approach to solution for the multilayer Green's response function. The "SAFARI" solution algorithm was developed in extenso by SCHMIDT, in recognition of the basic power and clarity of exact integral transform methods, after previous work in numeric finite element applications to both acoustic emission and ultrasonic nondestructive testing (SCHMIDT, 1975; SCHMIDT and KRENK, 1982).

The close formal analogy between the present finite wave element technique and the well-known finite element method of structural

mechanics is not accidental (SCHMIDT, 1982; KENNETT, 1984, personal communication). This can in fact be profitably used to motivate and develop more intuitively not only the underlying direct local-to-global matrix mapping concepts employed, but also to outline its successful algorithmic solution properties, within the framework of established straightforward matrix solver methods, completely independent of any considerations or use of propagator matrices and their subsequent developments. It is this approach which is taken in the present account.

Finally, despite the analytical equivalence of local recursive propagator and direct global matrix solutions (on a hypothetically infinite word length computer) for the multilayer Green's function, when compared to the original and the modified Thomson-Haskell propagator matrix based solution technique, as exist today in underwater acoustics and seismology, there are a number of important theoretical and pragmatic advantages of the DGM method for applications in these areas, as well as in theoretical and applied mechanics:

1. there are no longer any restrictions whatsoever on the number and type of sources, both within each layer and in total.

2. any number of receiver depths can easily be treated, with only 1 solution pass, since the total unknown wavefield potentials are found in all layers simultaneously.

3. for even only 1 source/receiver combination, the present direct global matrix - finite wave element algorithm yields a code which is almost an order of magnitude faster than existing programs using a modified Thomson-Haskell technique.

4. the resulting nonrecursive structure lends itself immediately to even further runtime savings via vectorised programming.

5. in contrast to propagator matrix based techniques, mixed fluid/solid layer cases are readily treated in an efficient manner.

6. no time-consuming stability assurance problems arise, these being removed automatically from this direct global matrix solution technique by simple judicious choice of appropriate natural local coordinate system, within each layer.

7. this kind of direct global matrix/finite wave element representation can also be obtained for a very wide class of seismic acoustic and elastodynamic propagation problems, within plane homogeneous media, allowing a vast array of media conditions to be modeled within the framework of a single common program.

8. ready extensions to more complex media and source conditions (spherical stratification, 3D source and range-dependent media) are equally possible from within the same direct global matrix/finite wave element framework.

This thesis presents an initial comparative study of the direct global matrix technique, as embodied in the full wave/fast field/ reflectivity program "SAFARI" of SCHMIDT. The theoretical model & basis for seismic acoustic wave propagation in a plane homogeneous stratified visco-elastic waveguide is described in Section 2(b), closely following PEKERIS (1948), EJP (1957), MIKLOWITZ (1978) and SCHMIDT (1982;1983;1984), where the numeric Green's function solution technique, particular to this direct global matrix model, is described in mathematical detail in Section 2(d) and developed in formal analogy to the finite element method in Section 2(c). Following an outline of the central DGM assembly thru use of index pointers in the "SAFARI" algorithm in Section 2(e), Section 2(f) describes efficient stability features in both the DGM formulation & solution via Gaussian elimination. Theoretic numerical integration options and optimum parameterization are treated in Sections 2(g) and 2(h) repsectively. Selected benchmark test problems which detail the basic accuracy speed and scope of the resulting DGM/FWE Green's function solution are given in Sections 2(i), 2(j) and 2(k).

Emphasis on comparative applications of this new fast field technology to the current representative problems of

A). Underwater Acoustic Propagation loss prediction at very low frequencies (VLF)

B). Deep Crustal Seismogram synthesis for modelling complex LVL and MOHO zones

C). Vertical Seismic Profiling (VSP) simulation for both deep crustal & exploration boreholes

is presented in overview in Section 3, and in detail in Sections 3(a), 3(b) and 3(c). Section 4(a) summarizes theoretic and applications results, 4(b) describes particular alternate embodiments, as well as several extensions of the DGM/FWE method in 4(c), and in 4(d) aspects of extant global and local methods in need of further consideration. Section 5 summarizes the content and results of this thesis.

In the progress of both the present research project, and comparative discussions with others active in this area (GILBERT, 1983; THIGPEN, 1984; MULLER, 1984; KENNETT, 1984: personal communications), it is the author's opinion that the generalized DGM/FWE approach of SCHMIDT, as embodied in the "SAFARI" algorithm can, for many seismic acoustic problems in both fluid and solid media, be the more physically direct and intuitive, if not the most economical, allowing possible extension to even further areas not yet fully explored by propagator matrix formalisms. Furthermore, many advantages offered by an exact and complete full wavefield solution (Green's function nearfield information) have as yet to be fully recognized and exploited. It is thus felt that these factors, together with its inate computational stability and economies as well as structural clarity in implementation, more than answer any possible criticisms of its necessarily complete (nonpartial) wavefield solution for all layers. To this it can be further answered that traditional reflectivity seismograms follow naturally from the DGM approach; in addition, CHIN et al have employed a global matrix formalism for the case of a Biot medium precisely to decompose the total field into individual generalized ray summations (CISTERNAS et al, 1973). These "limitations" of the direct global matrix approach for Green's function solution are in fact an apparent necessity imposed by transmuting an essentially "local" mathematical notation into a "global" one. The general DGM/FWE method of SCHMIDT presented here is thus in no way claimed as displacing local propagator matrix solutions,

but is offered rather as an elegant (and at times optimal) complementary alternative approach to monofrequency and pulse seismic propagation studies.

This thesis presents an initial comparative study of the direct global matrix technique, as embodied in the full wave/fast field/ reflectivity program "SAFARI" of SCHMIDT. The theoretical model & basis for seismic acoustic wave propagation in a plane homogeneous stratified visco-elastic waveguide is described in Section 2(b), closely following PEKERIS (1948), EJP (1957), MIKLOWITZ (1978) and SCHMIDT (1982;1983;1984), where the numeric Green's function solution technique, particular to this direct global matrix model, is described in mathematical detail in Section 2(d) and developed in formal analogy to the finite element method in Section 2(c). Following an outline of the central DGM assembly thru use of index pointers in the "SAFARI" algorithm in Section 2(e), Section 2(f) describes efficient stability features in both the DGM formulation & solution via Gaussian elimination. Theoretic numerical integration options and optimum parameterization are treated in Sections 2(g) and 2(h) repsectively. Selected benchmark test problems which detail the basic accuracy speed and scope of the resulting DGM/FWE Green's function solution are given in Sections 2(i), 2(j) and 2(k).

Section 2(b)

General Model and Derivation of Field Equations

The representation of the total seismic wavefield in terms of integral solutions for a multilayered Green's function here closely follows the presentations originally given by PEKERIS (1948), EWING, JARDETZKY and PRESS (1957), and subsequently by MIKLOWITZ (1978) and SCHMIDT and KRENK (1982).

The model environment is assumed to be an arbitrarily plane stratified set of n layer elements in welded interfacial contact, all elements, including the upper and lower halfspaces, considered homogeneous and isotropic viscoelastic continua with Lame constants λ and μ and density ρ. The subscript j here refers to the layer number, **bold underline j** indicating **interface** index.

The elastic medium, e.g. representing a multilayered ocean or solid earth crust, has elastic parameters assumed to be homogeneous within each j-th layer, on the whole taken to vary arbitrarily with depth while remaining constant in horizontal range. As JEFFREYS (1970) and more recently CHAPMAN and ORCUTT (1984) have discussed, the number of composite layers has to be taken large enough for the differences between consecutive layers to be a " sufficiently small " fraction (of order 1/n) of the

whole variation, when real earth gradients at depth are stepwise approximated. We adopt the usual '1st order' Langer approximation; of assuming that P and SV waves propagate independently (with no coupling), so that interconversion occurs only at the **interfaces** of discontinuities with respect to elastic parameters, between isovelocity layers). (As is well known (OFFICER, 1958), in a fluid media, if a linear c^2 velocity distribution is assumed, exact field solutions are obtainable in terms of Airy functions.)

Although spherical symmetry does not persist during propagation in a plane layered media, in many cases axial symmetry qua cylindrical coordinates thru the source can be assumed. The field equations are thus derived here in cylindrical coordinates; derivation of the corresponding field representations in plane Cartesian geometry has been given by SCHMIDT and JENSEN (1984).

A cylindrical coordinate system in $\{r,z,\theta\}$ is thus introduced, with the z coordinate axis perpendicular to the interfaces and referenced positive direction downwards [**Figure** 1]. The z axis is chosen to pass thru one or more colinear point sources, making the resulting field independent of azimuthal angle. In cylindrical coordinates, the governing displacement relations (u,v,w) for the general 3D case in terms of scalar potentials (ϕ,ψ,Λ) (SCHMIDT and KRENK, 1982) are

Figure 1

"SAFARI" numerical model and representative environment, showing generalized source/receiver configurations.

SAFARI NUMERICAL MODEL

KNOWN:
SOURCE
CONTRIBUTION(S)

UNKNOWN:
REFLECTED AND
TRANSMITTED FIELD

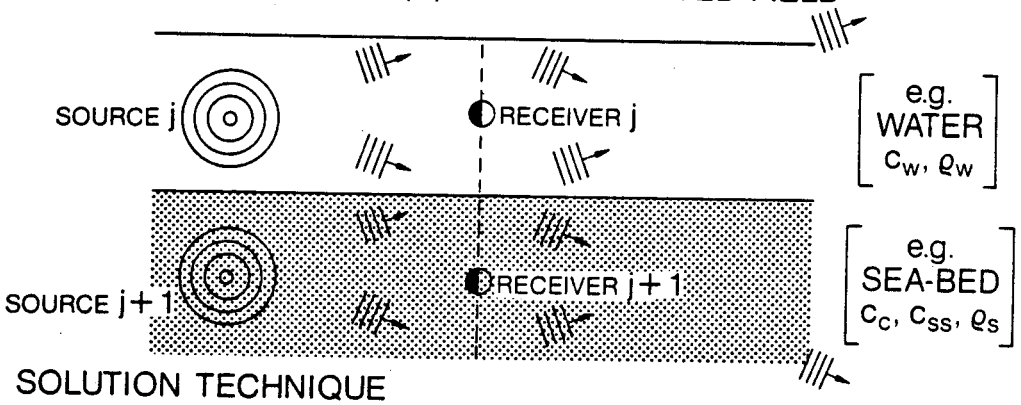

SOLUTION TECHNIQUE

1) SOURCE CONTRIBUTION DECOMPOSED INTO UP AND DOWNGOING PLANE WAVES IN EACH LOCAL LAYER

2) CORRESPONDING PLANE-WAVE COMPONENTS OF UNKNOWN FIELD FOUND BY MATCHING BOUNDARY CONDITIONS IN ALL LAYERS ACROSS ALL INTERFACES

3) TOTAL GLOBAL FIELD AT ALL DEPTHS IS CALCULATED VIA SUPERPOSITION OF ALL LOCAL LAYER WAVEFIELDS
(*DEFINING DEPTH-DEPENDENT GREEN'S FUNCTION*)

4) TOTAL FIELD AT ALL RANGES IS CALCULATED BY NUMERICAL INTEGRATION OF DEPTH-DEPENDENT GREEN'S FUNCTION OVER HORIZONTAL WAVENUMBER K_r
(*DEFIING FREQUENCY-DOMAIN TRANSFER FUNCTION*)

5) SYNTHETIC TIME SERIES FOUND BY NUMERICAL INTEGRATION OVER EACH FREQUENCY ω VIA INVERSE FOURIER TRANSFORM
(*DEFINING SYNTHETIC SEISMIC TIME SERIES*)

$$u = \frac{\partial \phi}{\partial r} + \frac{1}{r}\frac{\partial \Lambda}{\partial \theta} + \frac{\partial^2 \psi}{\partial r \partial z}$$

$$v = \frac{1}{r}\frac{\partial \phi}{\partial \theta} - \frac{\partial \Lambda}{\partial r} + \frac{1}{r}\frac{\partial^2 \psi}{\partial \theta \partial z}$$

$$w = \frac{\partial \phi}{\partial z} - \left(\frac{1}{r}\frac{\partial}{\partial r} r \frac{\partial}{\partial r} + \frac{1}{r^2}\frac{\partial^2}{\partial \theta^2}\right) \psi \quad .$$

In the absence of body forces (MIKLOWITZ, 1978, pp.119ff) plane strain imposes

$$v = 0$$

Hence, where σ is the resulting strain,

$$\sigma_{z\theta} = \sigma_{r\theta} = 0$$

reducing to expressions in u and w only (given zero angular/θ dependence. Thus the resulting equations of motion will be satisfied if the nonvanishing displacement field components {u,v,w} in each layer j are then re-expressed in terms of the scalar displacement potentials $\{\phi,\psi\}$ as

$$u(r,z) = \frac{\partial \phi}{\partial r} + \frac{\partial^2 \psi}{\partial r \partial z} \qquad (1)$$

and

$$w(r,z) = \frac{\partial \phi}{\partial z} - \frac{1}{r} \frac{\partial}{\partial r} r \frac{\partial}{\partial r} \psi \qquad (2)$$

(with the corresponding stress potential relations following directly from Hooke's law (EWING JARDETZKY & PRESS, 1957)

$$\sigma_{zz}(r,z) = (\lambda + 2\mu) \frac{\partial w}{\partial z} + \lambda \frac{\partial u}{\partial r} \qquad (3)$$

and

$$\sigma_{rz}(r,z) = \mu \left(\frac{\partial u}{\partial z} + \frac{\partial w}{\partial r}\right) \qquad (4)$$

and where each of the (uncoupled) P and S wavefield potentials separately satisfies the corresponding wave equations

$$\left(\nabla^2 - \frac{1}{c_p^2} \frac{\partial^2}{\partial t^2}\right) \phi = 0 \qquad (5)$$

and

$$(\nabla^2 - \frac{1}{c_s^2}\frac{\partial^2}{\partial t^2})\,\psi = 0 \qquad (6)$$

Here $c_p(z)$ and $c_s(z)$ are the velocities of compressional and shear waves respectively, constant within each layer:

$$c_p(z) = \sqrt{\frac{\lambda + 2\mu}{\rho}} \qquad (7)$$

and

$$c_s(z) = \sqrt{\frac{\mu}{\rho}} \qquad (8)$$

The initial model is thus seen to be closely related to Lamb's first problem for a buried point load source (AKI and RICHARDS, 1980; BATH, 1984), and hence the prototype for a wide class of past and present seismic modeling problems. If the medium is fluid, ψ vanishes, and only the compressional potential ϕ remains. This (equivalent to SH/Acoustic only) propagation can

however be considered as a special example of the general solid layer case and is treated separately in SCHMIDT and JENSEN (1984).

The point sources S1, S2, S3 ... are taken to be harmonic and vibrate with a common angular frequency ω. In complex notation a common time dependence of the form $\exp(i\omega t)$ is assumed; here however this common factor will be dropped in all following expressions. Viscoelastic attenuation can be accounted for by letting the Lame constants be complex (AKI and RICHARDS, 1980; CHIN, 1982). It is important to note that, with the present formalism, more than one source, of both point and distributed types, can be readily introduced as arbitrary layer forcing functions, with considerably more utility and flexibility than standard stress-displacement discountinuities and required 'source interfaces', as are common in propagator matrix solutions; see below, Section 2 and Section 4; HARKRIDER, 1964 for a discussion of the utility and generality of the point source representation.

The resulting wave equations, Eqs. 5 and 6, now take the reduced Helmholtz form

$$(\nabla^2 + k_p^2)\,\phi = 0 \qquad (9)$$

and

$$(\nabla^2 + k_s^2)\,\psi = 0 \qquad (10)$$

k_p and k_s being the total horizontal wavenumbers for compressional and shear waves respectively are:

$$k_p^2 = \left(\frac{\omega}{cp}\right)^2 = \frac{\omega^2\rho}{\lambda + 2\mu} \qquad (11)$$

and

$$k_s^2 = \left(\frac{\omega}{cs}\right)^2 = \frac{\omega^2\rho}{\mu} \qquad (12)$$

A direct procedure (EWING, JARDETZKY and PRESS, 1957,pg.10ff) for Green's function solution begins with the most general solution form possible and adjusts this solution to the physical-geometric boundary conditions of the specific problem. The most general solution here must subsequently hold for all cases of seismic-acoustic wave propagation in a welded homogeneous isotropic

layered media, for an arbitrary number of buried sources and/or receivers with arbitrary axial positions as well as for any boundary conditions which can be imposed at the delimiting boundaries of the medium.

Due to the horizontal stratification inherent in this discretely layered model, integral transforms are more readily treated than the expressions in the function domain themselves; by applying Hankel transforms for this cylindrically symmetric case to Eqs. 9 and 10, the following integral transform representations are obtained for the **homogeneous** wavefield solutions within the general j-th layer:

$$\phi(r,z) = \int_0^\infty \left[A_j^-(k_r) e^{-z\alpha_j(k_r)} + A_j^+(k_r) e^{+z\alpha_j(k_r)} \right] J_0(k_r r)\, k_r\, dk_r \qquad (13)$$

$$\psi(r,z) = \int_0^\infty \left[B_j^-(k_r) e^{-z\beta_j(k_r)} + B_j^+(k_r) e^{+z\beta_j(k_r)} \right] J_0(k_r r)\, dk_r \qquad (14)$$

Here A-, A+, B- and B+ are arbitrary wavefield functions in the horizontal wavenumber k_r --from which plane wave reflection coefficients may be readily derived; see below-- where

$$\alpha(k_r) = \sqrt{(k_r^2 - k_p^2)} \qquad (15)$$

$$\beta(k_r) = \sqrt{(k_r^2 - k_s^2)} \qquad (16)$$

Note that the Eqs. (13) and (14) above are just simple decompositions of the total (spherical) wavefield into up- and down-going conical waves (subsequently integrated over all horizontal wavenumbers/angles of incidence). When the field becomes evanescent, the solution is automatically a linear combination of growing and decaying exponentials, whose expressions must satisfy the relevant continuity, source and boundary conditions. This point is important to remember later when considering algorithmic implementation of this 'mapping' via topology matrices analogous to those employed in the Finite Element Method; see Section 2(d) below.

In the most general treatment of seismic-acoustic wave propagation in terms of complex exponentials, we retain both the positive and negative values of the layer coefficients of z for each local layer whose thickness is some arbitrary value z_j (not

writing the imaginary factor i explicitly but absorbing it into the layer coefficients α and β). These terms distinctly correspond to upward and downward travelling waves in each homogeneous layer sufficient ot account for all seismic-acoustic wave types (HUDSON, 1978). It should be noted here, however, that for an actual solid continuous medium, mathematically speaking, the net wavefield no longer has such a simple unambiguous decomposition (SCHELKUNOFF, 1951; SLUITJER, 1970; CLAERBOUT, 1976); ie, the terms --representing the approximate response of a truly continuous medium-- include both up and downgoing wave characteristics. It is precisely this unique linear decomposability in the discretised-multilayer case which is the basis of the complete exact VSP solution obtainable in the direct global matrix algorithm of SCHMIDT; Section 3(c); GANLEY, 1980).

For each value in the (laterally homogeneous) horizontal range, in the most general solid case, to solve the boundary value problem for the welded-interface model, the local equations at each interface are totally independent of those comprising all other layers. Unlike the propagator matrix approach (of eliminating unknown A/B amplitudes when "propagating" across each layer), to solve for A+/- and B+/- in the present method, only the 4 basic governing physical boundary conditions must be satisfied; normal and tangential displacement and stress must be everywhere continuous across each layer interface in sequence. In addition, in the upper and lower halfspaces, the arbitrary

wavefield functions A-, B-, A+ , B+ must vanish due to the Sommerfeld radiation condition (EWING JARDETZKY & PRESS, 1957).

In seeking the total wavefield solution over all frequencies for any number of given ranges, the first objective is to determine tht specific form of A and B. Written as given, the potential solutions do not yet contain an inhomogeneous/source component arising from one or more point or other sources in one or more layers. Although from a strictly analytical viewpoint, homogeneous and source-term solutions could be treated in one pass, here (with the hindsight of numeric computational implementation of the actual "SAFARI" algorithm), the homogeneous and source terms are in fact treated separately (because the continuity of the respective kernel's cannot be formally stated at this point). In addition, it will be subsequently seen that this separate treatment of source and resultant wavefields allows complete generality as to the number and location of any type of source or sources in one or more layers -a significant advantage over existing propagator matrix algorithms.

HOMOGENEOUS Solutions

To develop the working expressions for the 4 continous physical field parameters involved in the boundary conditions, we start with normal and tangential displacements, where normal and tangential stresses will subsequently be expressed in terms of these. For **u**, from Eq.1 above

$$u = \int_0^\infty -k_r(A^- e^{-z\alpha} + A^+ e^{+z\alpha}) J_1(k_r r) k_r \, dk_r$$

$$+ \int_0^\infty -k_r(-\beta B^- e^{-z\beta} + \beta B^+ e^{+z\beta}) J_1(k_r r) \, dk_r \qquad (17)$$

$$u = \int_0^\infty (-k_r A^- e^{-z\alpha} + k_r A^+ e^{+z\alpha} + \beta B^- e^{-z\beta} - \beta B^+ e^{+z\beta}) k_r J_1(kr) \, dk_r \qquad (18)$$

For **w**,

$$w = \frac{\partial \phi}{\partial z} - (\frac{1}{r} \frac{\partial}{\partial r} r \frac{\partial}{\partial r}) \psi = \frac{\partial \phi}{\partial z} + (\frac{\partial^2}{\partial z^2} + k_s^2) \psi \; . \qquad (19)$$

Upon substitution of the general up and downgoing wavefield

solutions into Eq. 19 above, we obtain

for a general j-th layer

$$W = \int_0^\infty [\, -A^- \alpha\, e^{-z\alpha} + A^+ \alpha\, e^{+z\alpha}\,] \, J_o(k_r r) k_r dk_r$$

$$+ \int_0^\infty [\, B^- \beta^2 e^{-z\beta} + B^+ \beta^2 e^{+z\beta}\,] \, J_o(k_r r)\, dk_r$$

$$+ k_s^2 \int_0^\infty [\, B^- e^{-z\beta} + B^+ e^{+z\beta}\,] \, J_o(k_r r)\, dk_r \qquad (20)$$

$$= \int_0^\infty [\, -A^- \alpha\, e^{-z\alpha} + A^+ \alpha\, e^{+z\alpha}] \, J_0(k_r r)\, k_r\, dk_r$$

$$+ \int_0^\infty \beta^2 [\, B^- e^{-z\beta} + B^+ e^{+z\beta}] \, J_0(k_r r)\, dk_r$$

$$+ \int_0^\infty k_s^2 \, [\, B^- e^{-z\beta} + B^+ e^{+z\beta}] \, J_0(k_r r)\, dk_r$$

$$= \int_0^\infty [\, -A^- \alpha\, e^{-z\alpha} + A^+ \alpha\, e^{+z\alpha}] \, J_0(k_r r)\, k_r dk_r$$

$$+ \int_0^\infty (\beta^2 + k_s^2) \, [B^- e^{-z\beta} + B^+ e^{+z\beta}] \, J_0(k_r r)\, dk_r \qquad (21)$$

Since $\beta = \sqrt{k_r^2 - k_s^2}$ and thus $\beta^2 + k_s^2 = k_r^2$, the above becomes

$$= \int_0^\infty [-A^- \alpha\, e^{-z\alpha} + A^+ \alpha\, e^{+z\alpha}] \, J_0(k_r r)\, dk_r$$

$$+ \int_0^\infty [k_r^2 \, B^- e^{-z\beta} + k_r^2 \, B^+ e^{+z\beta}] \, J_0(k_r r)\, dk_r \qquad (22)$$

so that finally

$$w = \int_0^{\infty} [-\alpha A^- e^{-z\alpha_+} \; \alpha A^+ e^{+z\alpha_+} \; k_r B^- e^{-z\beta_+} \; k_r B^+ e^{+z\beta_+}] \; J_0(kr) \; k_r dk_r \quad (23)$$

Using Hooke's law in cylindrical coordinates, directly relating stresses with (previously-derived) displacements

$$\sigma_{zz} = \lambda \nabla.u + 2\mu \frac{\partial w}{\partial z} \tag{24}$$

$$= \lambda \left[\frac{1}{r} \frac{\partial}{\partial r} (ru) + \frac{\partial}{\partial z} w \right] + 2\mu \frac{\partial w}{\partial z} \tag{25}$$

$$= \lambda \left[\frac{\partial}{\partial r} + \frac{1}{r} \right] u + (\lambda + 2\mu) \frac{\partial w}{\partial z} \tag{26}$$

By use of the recurence relation (9.1.27, ABRAMOWITZ and STEGUN, 1964,pg.361)

$$\left(-\frac{\partial}{\partial r} \pm \frac{m}{r}\right) J_m(k_r r) = +k_r \pm J_{m+1}(k_r r) \tag{27}$$

upon substitution into the above expression for σ_{zz}

$$\sigma_{zz} = \int_0^\infty \lambda\left(\frac{\partial}{\partial r} + \frac{1}{r}\right)\left(-k_r A^- e^{-z\alpha} - k_r A^+ e^{+z\alpha} + \beta B^- e^{-z\beta} - \beta B^+ e^{+z\beta}\right) k_r J_1(kr)\,dk_r$$

$$+ \ (\lambda + 2\mu)\left(\frac{\partial w}{\partial z}\right), \qquad (28)$$

and substituting from the previous for $\partial w/\partial z$

$$= \lambda \int_0^\infty \left(-k_r A^- e^{-z\alpha} - k_r A^+ e^{+z\alpha} + \beta B^- e^{-z\beta} - \beta B^+ e^{+z\beta}\right) k_r^2 J_0(kr)\,dk_r$$

$$+ \ (\lambda+2\mu)\int_0^\infty \left(\alpha^2 A^- e^{-z\alpha} + \alpha^2 A^+ e^{+z\alpha} - k\beta B^- e^{-z\beta} + k\beta B^+ e^{+z}\right) k_r J_0(kr)\,dk_r$$

(29)

Bringing in one power of k_r into the first integral kernel term, and using $\alpha^2 = k_r^2 - k_p^2$ and $(\lambda + 2\mu)k_p^2 = \mu\, k_s^2$ one obtains, upon substitution in Eq. (29)

$$= \lambda \int_0^\infty \left[\left(-k_r^2 A^- e^{-z\alpha} - k_r^2 A^+ e^{+z\alpha} + k\beta B^- e^{-z\beta} - k\beta B^+ e^{+z\beta}\right) + \right.$$

$$\left.(\lambda+2\mu)\int_0^\infty \left((k_r^2-k_p^2)A^- e^{-\alpha z} + (k_r^2-k_p^2)A^+ e^{+z\alpha} - k\beta B^- e^{-z\beta} + k\beta B^+ e^{+z\beta}\right)\right] k J_0(kr)\,dk_r$$

(30)

which, upon expansion around $(\lambda+2\mu)$, cancellation of k_r^2 terms around λ, and regrouping of remaining k_p^2 terms in A+/- in λ and 2μ,

$$= (\lambda+2\mu)\int_0^\infty \left(-k_p^2 A^- e^{-z\alpha} - k_p^2 A^+ e^{+z\alpha}\right) k_r J_0(kr) \, dk_r$$

$$+ \quad (2\mu)\int_0^\infty \left(-k_\beta B^- e^{-z\beta} + k_\beta B^+ e^{+z\beta}\right) k_r J_0(kr) \, dk_r$$

$$+ \quad (2\mu)\int_0^\infty \left(k_r^2 A^- e^{-z\alpha} + k_p^2 A^+ e^{+z\alpha}\right) k_r J_0(kr) \, dk_r \quad . \qquad (31)$$

Substituting the expression $(\lambda + 2\mu) k_p^2 = (\mu) k_s^2$ into the above, and grouping all remaining A+/- and B+/- terms around $(2k_r^2 - k_s^2)$ and $2 k_r \beta$ respectively, one obtains

$$\sigma_{zz} = \mu\int_0^\infty \left[(2k_r^2 - k_s^2)[A^- e^{-z\alpha} + A^+ e^{+z\alpha}] + (2k_\beta)[-B^- e^{-z\beta} + B^+ e^{+z\beta}]\right] k_r J_0(kr)$$

(32)

Finally, for σ_{zr}, using the definition

$$\sigma_{zr} = \mu \left(\frac{\partial u}{\partial z} + \frac{\partial w}{\partial r} \right) \qquad (33)$$

substituting $\beta^2 = k_r^2 - k_s^2$, grouping around B+/-, one obtains

$$\sigma_{zr} = \mu \int_0^\infty [(2\alpha k_r)[A^- e^{-z\alpha} - A^+ e^{+z\alpha}] - (2k_r^2 - k_s^2)[B^- e^{-z\beta} + B^+ e^{+z\beta}]] J_1(kr) k_r dk_r$$

(34)

These representations for the **homogeneous** solution are identical to those given by SCHMIDT (1982) & SCHMIDT and JENSEN (1984).

As the preceding intermediate steps have shown, although alternate (and mathematically equivalent) formulae for the above are clearly possible, from computational hindsight, the present formulation has been shown to be critical (SCHMIDT, 1984, personal communication) for unconditional stability of the DGM formulation and solution.

SOURCE Contributions

To now consider the specific Source (inhomogeneous) term contribution(s), for one or more buried compressional wave point sources, from the Weyl-Sommerfeld integral (EWING JARDETZKY and PRESS, 1957, pg.13, Eq.1-41) for the pressure in a fluid (= bulk stress in a solid)

$$P(r,z) = + \frac{ik_p \rho c}{4\pi} S_\omega \int_0^\infty J_0(k_r r)\, e^{-\alpha(k_r)|z-z_s|} \frac{k_r\, dk_r}{\alpha(k_r)} \qquad (35)$$

where S_ω is a source normalisation term.

To obtain the normal and tangential displacements and stresses for the **source** contributions, as per the homogenous solutions above, since $\psi = 0$,

$$u^*_{\text{source } j} = \frac{\partial \phi}{\partial r}\text{source} + \frac{\partial^2 \psi}{\partial r \partial z}\text{source} = \frac{\partial \phi}{\partial r}$$

$$= \frac{\partial}{\partial r}\left[\frac{iS_\omega}{4\pi} \int_0^\infty \frac{e^{-|z - z_s|\,\alpha_j}}{\alpha_j}\, k_r J_0(k_r r)\, dk_r\right]$$

$$= \frac{-iS_\omega}{4\pi} \int_0^\infty \frac{e^{-|z - z_s| \alpha_j}}{\alpha_j} k_r^2 J_1(k_r r)\, dk_r = \underline{u^*_{\text{source } j}} \qquad (36)$$

$$\underline{w^*_{\text{source } j}} = \frac{\partial \phi}{\partial z} + \left(\frac{\partial}{\partial^2 z} + k_s^2\right) \psi_j =$$

$$\frac{\partial \phi}{\partial z} = \frac{\partial}{\partial z} \left[\frac{iS_\omega}{4\pi} \int_0^\infty \frac{e^{-|z - z_s| \alpha_j}}{\alpha_j} k_r J_0(k_r r)\, dk_r \right.$$

$$= \frac{\pm iS_\omega}{4\pi} \int_0^\infty e^{-|z - z_s| \alpha_j} k_r J_0(k_r r)\, dk_r = \underline{w^*_{\text{source } j}} \qquad (37)$$

and likewise for σ_{zr} and σ_{zz}

$$\underline{\sigma^*_{\text{source } j}} = \left(\frac{\partial}{\partial z} u_j + \frac{\partial}{\partial r} w_j\right)$$

$$= \frac{\partial}{\partial z}\left(\frac{-iS}{4\pi\omega} \int_0^\infty \frac{e^{-|z-z_s|\alpha_j}}{\alpha j} k_r^2 J_1(k_r r)\, dk_r\right)$$

$$+ \frac{\partial}{\partial r}\left(\frac{\pm iS_\omega}{4\pi} \int_0^\infty e^{-|z-z_s|\alpha_j} k_r J_0(k_r r)\, dk_r\right)$$

$$= \pm \frac{2iS_\omega}{4\pi} \int_0^\infty e^{-|z-z_s|\alpha_j} k_r^2 J_1(k_r r)\, dk_r = \sigma^*_{zr\,\underline{\text{source j}}} \qquad (38)$$

for σ_{zz}

$$\sigma^*_{zz\,\underline{\text{source j}}} = \lambda\left(\frac{\partial}{\partial r} + \frac{1}{r}\right)u + (\lambda + 2\mu)\frac{\partial w}{\partial z}$$

since $\left(\frac{\partial}{\partial r} + \frac{1}{r}\right)J_1(k_r r) = -k_r J_0(k_r r)$

$$= \lambda\left(\frac{\partial}{\partial r} + \frac{1}{r}\right)\left[\frac{-iS\omega}{4\pi} \int_0^\infty \frac{e^{-|z-z_s|\alpha_j}}{\alpha j} J_1(k_r r)\, k_r^2 dk_r\right)$$

$$+ (\lambda+2\mu)\frac{\partial}{\partial z}\left[\frac{\pm iS\omega}{4\pi} \int_0^\infty e^{-|z-z_s|\alpha_j} J_0(k_r r)\, dk_r\right)$$

Simultaneous division and multiplication by α results in

$$= \frac{iS\omega}{4\pi}\left[-\lambda \int_0^\infty \frac{e^{-|z-z_s|\alpha_j}}{\alpha j} k_r^2 \, k_r \, J_0(k_r r)\, dk_r\right.$$

$$\left. + (\lambda+2\mu) \int_0^\infty (k_r^2 - k_p^2)\frac{e^{-|z-z_s|\alpha_j}}{\alpha j} k_r J_0(k_r r)\right] dk_r$$

The $2\lambda k_r$ terms cancel, and substituting $k_s^2\mu = k_p^2(\lambda+2\mu)$ obtains

$$= \{2\mu \int_0^\infty k_r^2 \frac{e^{-|z-z_s|\alpha_j}}{\alpha j} k_r J_o(k_r r)\, dk_r$$

$$- \mu \int_0^\infty k_s^2 \frac{e^{-|z-z_s|\alpha_j}}{\alpha j} k_r J_o(k_r r)\}dk_r$$

$$= \frac{iS}{4\pi\omega}\mu \int_0^\infty (2k_r^2 - k_s^2) \frac{e^{-|z-z_s|\alpha_j}}{\alpha j} k_r J_o(k_r r)\, dk_r = \sigma^*_{zz\ \underline{\text{source j}}} \qquad (39)$$

We have now determined the total normal and tangential displacements and stresses as a sum of **homogeneous** and **source** contributions. Since these parameters must be continuous at all ranges, it is required that the respective integrand kernels be equal. For a general j-th layer, bounded above and below by the j-1th and jth **interfaces** respectively (here appearing as **bold underlined** superscripts)

Total u^{j}_{j-1} = Total u^{j}_{j}

$$-kA^{-}_{j-1}e^{-z_j\alpha_{j-1}} - kA^{+}_{j-1}e^{+z_j\alpha_{j-1}} + \beta_{j-1}B^{-}_{j-1}e^{-z_j\beta_{j-1}} - \beta_{j-1}B^{+}_{j-1}e^{+z_j\beta_{j-1}}$$

$$- \frac{e^{-|z_j - z_{sj}|\alpha_{j-1}}}{\alpha_{j-1}} k_r \left[\frac{i\, S_{\omega j}}{4\pi}\right]$$

=

$$-kA^{-}e^{-z_j\alpha_j} - kA^{+}e^{+z_j\alpha_j} + \beta_j B^{-}_j e^{-z_j\beta_j} - \beta_j B^{+}_j e^{+z_j\beta_j}$$

$$- \frac{e^{-|z_j - z_{sj}|\alpha_j}}{\alpha_j} k_r \left[\frac{i\, S}{4\pi}\omega_j\right]$$

(40)

total w^{j}_{j-1} = total w^{j}_{j}

$$-\alpha_{j-1}A^{-}_{j-1}e^{-z_j\alpha_{j-1}} + \alpha_{j-1}A^{+}_{j-1}e^{+z_j\alpha_{j-1}} + k_r B^{-}_{j-1}e^{-z_j\beta_{j-1}} + k_r B^{+}e^{+z_j\beta_{j-1}}$$

$$- e^{-|z_j - z_s|\alpha_{j-1}} k_r \left[\frac{i\, S}{4\pi}\omega_j\right]$$

=

$$- \alpha_j A^{-}_j e^{-z_j\alpha_j} + \alpha_j A^{+}_j e^{+z_j\alpha_j} + k_r B^{-}_j e^{-z_j\beta_j} + k_r B^{+}_j e^{+z_j\beta_j}$$

+

$$e^{-|z_j - z_{sj}|\alpha_j} \left[\frac{i\, S}{4\pi}\omega_{j-1}\right] \qquad (41)$$

$$\underline{\text{total}\ {}_{zz}\sigma^{\underline{j}}_{j-1}} = \underline{\text{total}\ {}_{zz}\sigma^{\underline{j}}_{j}}$$

$$(2k_r^2-k_s^2)[A^-_{j-1}e^{-z\alpha_{j-1}}_{\underline{j}} + A^+_{j-1}e^{+z\alpha_{j-1}}_{\underline{j}}] + (2k\beta_{j-1})[-B^-_{j-1}e^{-z}_{\underline{j-1}}{}^{\beta_j} + B^+_{j-1}e^{+z}_{\underline{j-1}}{}^{\beta_j}]$$

$$+\mu_{j-1}\frac{(2k_r^2-k_s^2)\ e^{-|z-z_s|\alpha_{j-1}}_{\underline{j}}\ [\frac{i\,S}{4\pi}\omega_{\underline{j}}]}{\alpha_{\underline{j}}}$$

$$=$$

$$(2k_r^2-k_{sj}^2)[A^-_j e^{-z\alpha_j}_{\underline{j}} + A^+_j e^{+z\alpha_j}_{\underline{j}}] + (2k_r\beta_j)[-B^-_j e^{-z\beta_j}_{\underline{j}} + B^+_j e^{+z\beta_j}_{\underline{j}}]$$

$$+\frac{u_j(2k_r^2-k_{sj}^2)\ e^{-|z-z_s|\alpha_j}_{\underline{j}}[\frac{i\,S}{4\pi}\omega_{j-1}]}{\alpha_j} \qquad (42)$$

$$\underline{\text{total}\ {}_{zr}\sigma^{\underline{j}}_{j-1} = \text{total}\ {}_{zr}\sigma^{\underline{j}}_{j}}$$

$$\mu_{j-1}(2\alpha_{j-1}k_r)[A^-_{j-1}e^{-z\alpha_{j-1}}_{\underline{j}} - A^+_{j-1}e^{+z\alpha_{j-1}}_{\underline{j}}] + (2k_r^2-k_s^2)[B^-_{j-1}e^{-z\beta_{j-1}}_{\underline{j}} + B^+_{j-1}e^{+z\beta_{j-1}}_{\underline{j}}]$$

$$+2e^{-|z-z_s|\alpha_{j-1}}_{\underline{j}}\ k_r\ [\frac{i\,S}{4\pi}\omega_{j-1}]$$

$$=$$

$$\mu_j(2\alpha_j k_r)[A^-_j e^{-z\alpha_j}_{\underline{j}} - A^+_j e^{+z\alpha_j}_{\underline{j}}] + (2k_r^2-k_{sj}^2)[B^-_j e^{-z\beta_j}_{\underline{j}} + B^+_j e^{+z\beta_j}_{\underline{j}}]$$

$$+2e^{-|z-z_s|\alpha_j}_{\underline{j}}\ k_r\ [\frac{i\,S}{4\pi}\omega_j] \qquad (43)$$

Separating source terms on the right hand side, for each of the 4 quantities above,

$$-k_r\left(A^-_{j-1}e^{-\underline{j}z\alpha_{j-1}} + A^+_{j-1}e^{+\underline{j}z\alpha_{j-1}}\right)$$

$$+\beta_{j-1}\left(B^-_{j-1}e^{-\underline{j}z\beta_{j-1}} - B^+_{j-1}e^{+\underline{j}z\beta_{j-1}}\right) \qquad \underline{\text{tangential}_u \text{ displacement}}$$

$$+ \quad k_r\left(A^-_j e^{-\underline{j}z\alpha_j} + A^+_j e^{+\underline{j}z\alpha_j}\right)$$

$$+\beta_j\left(B^-_j e^{-\underline{j}z\beta_j} - B^+_j e^{+\underline{j}z\beta_j}\right) = -\left(\frac{e^{-\underline{j}|z-z_s|\alpha_j}}{\alpha_j} + \frac{e^{-\underline{j}|z-z_s|\alpha_{j-1}}}{\alpha_{j-1}}\right)\left[\frac{iS}{4}\omega_{\pi j}\right]$$

(44)

$$-\alpha_{j-1}\left(A^-_{j-1}e^{-\underline{j}z\alpha_{j-1}} + A^+_{j-1}e^{+\underline{j}z\alpha_{j-1}}\right)$$

$$+k_r\left(B^-_{j-1}e^{-\underline{j}z\beta_{j-1}} + B^+_{j-1}e^{+\underline{j}z\beta_{j-1}}\right) \qquad \underline{\text{normal}_w \text{ displacement}}$$

$$+\alpha_j\left(A^-_j e^{-\underline{j}z\alpha_j} - A^+_j e^{+\underline{j}z\alpha_j}\right)$$

$$-k_r\left(B^-_j e^{-\underline{j}z\beta_j} + B^+_j e^{+\underline{j}z\beta_j}\right) = \left(e^{-\underline{j}|z-z_s|\alpha_j} + e^{-\underline{j}|z-z_s|\alpha_{j-1}}\right)\left[\frac{iS}{4}\omega_{\pi j-1}\right]$$

(45)

$$(2k_r^2-k_s^2)[A_{j-1}^- e^{-z\alpha_{j-1}} + A_{j-1}^+ e^{+z\alpha_{j-1}}]$$

$$+(2k_r\beta_{j-1})[-B_{j-1}^- e^{-z\beta_{j-1}} + B_{j-1}^+ e^{+z\beta_{j-1}}] \qquad \text{normal stress } \sigma_{zz}$$

$$+$$

$$-(2k_r^2- k_{sj}^2)[A_j^- e^{-z\alpha_j} + A_j^+ e^{+z\alpha_j}]$$

$$-(2k_r\beta_j)[-B_j^- e^{-z\beta_j} + B_j^+ e^{+z\beta_j}] = \mu_j(2k_r^2-k_{sj}^2)e^{-|z-z_{sj}|} \pm \mu_j(2k_r^2-k_s^2)e^{-|z-z_{sj}|}$$

(46)

$$\left[\frac{i}{4\pi} S_{\omega j-1}\right]$$

$$\mu_{j-1}(2\alpha_{j-1}k_r)[A_{j-1}^- e^{-z\alpha_{j-1}} - A_{j-1}^+ e^{+z\alpha_{j-1}}]$$

$$+(2k_r^2- k_s^2)[B_{j-1}^- e^{-z\alpha_{j-1}} + B_{j-1}^+ e^{+z\alpha_{j-1}}] \qquad \text{tangential stress } \sigma_{zr}$$

$$-$$

$$\mu_j(2\alpha_j k_r)[A_j^- e^{-z\alpha_{j-1}} - A_j^+ e^{+z\alpha_{j-1}}]$$

$$-(2k_r^2-k_{sj}^2)[B_j^- e^{-z\beta_j} + B_j^+ e^{+z\beta_j}] = 2e^{-|z-z_{sj}|}\alpha_j k_r - 2e^{-|z-z_{sj}|}\alpha_{j-1}k_r$$

(47)

$$\left[\frac{i\ S}{4\pi}\omega_j\right]$$

Restating the Homogeneous Equations for the generalised j-th layer:

normal Displacement

$$\underline{u_j} = \int_0^\infty \{-kA_r^- e^{-z\alpha} + kA_r^+ e^{+z\alpha} + \beta B^- e^{-z\beta} - \beta B^+ e^{+z\beta}\}_j \, J_1(k_r r) \, k_r dk_r$$

normal Stress

$$\underline{w_j} = \int_0^\infty \{-\alpha A^- e^{-z\alpha} + \alpha A^+ e^{+z\alpha} + kB_r^- e^{-z\beta} + kB_r^+ e^{+z\beta}\}_j \, J_0(k_r r) \, k_r dk_r$$

tangential Displacement

$$\underline{\sigma_{zz\,j}} = \mu_j \int_0^\infty \{(2k_r^2 - k_s^2)[A^- e^{-z\alpha} + A^+ e^{+z\alpha}] + (2k_r\beta)[-B^- e^{-z\beta} + B^+ e^{+z\beta}]\}_j$$

$$k_r J_0(k_r r) \, dk_r$$

tangential Stress

$$\underline{\sigma_{zr\,j}} = \mu_j \int_0^\infty \{(2\alpha k_r)[A^- e^{-z\alpha} - A^+ e^{+z\alpha}] - (2k_r^2 - k_s^2)[B^- e^{-z\beta} + B^+ e^{+z\beta}]\}_j$$

$$k_r J_1(k_r r) \, dk_r$$

Reviewing the (4) previous Source contributions

tangential displacement

$$\underline{u_j^*} = -\frac{iS\omega}{4\pi}\int_0^\infty \frac{e^{-|z-z_s|\alpha_j}}{\alpha_j} k_r^2 J_1(k_r r)\, dk_r$$

normal displacement

$$\underline{w_j^*} = \pm\frac{iS\omega}{4\pi}\int_0^\infty e^{-|z-z_s|\alpha_j} k_r J_o(k_r r)\, dk_r$$

normal stress

$$\underline{\sigma_{zr\,j}^*} = \pm\frac{iS\omega}{4\pi}\int_0^\infty e^{-|z-z_s|\alpha_j} k_r^2 J_1(k_r r)\, dk_r$$

tangential stress

$$\underline{\sigma_{zz\,j}^*} = +\frac{iS\omega}{4\pi}\int_0^\infty \frac{e^{-|z-z_s|\alpha_j}}{\alpha_j}(2k_r^2 - k_s^2) k_r J_o(k_r r)\, dk_r$$

TOTAL Field Superposition

If the above equation for a generalised buried p-wave point source is inserted into the previous governing relations for continuity of normal and tangential displacements and stresses, in each layer the homogeneous and source field contributions are superposed, so that the resulting field parameters are

$$u_{total} = u_{homogeneous} + u^*_{source}$$

$$w_{total} = w_{homogeneous} + w^*_{source}$$

$$\sigma_{zz\,total} = \sigma_{zz\,homogeneous} + \sigma^*_{zz\,source}$$

$$\sigma_{zr\,total} = \sigma_{zr\,homogeneous} + \sigma^*_{zr\,source} \qquad (48)$$

The resulting total field parameters are now expressed in 2 different integral representations, such that, for continuity at any interface $F^{j=\underline{\text{interface}}\ \text{index}}_{j-1=\text{layerindex}} = F^j_j$ and likewise

[Figure 2]

$$
\begin{aligned}
u^j_{j-1} &= u^j_j \\
w^j_{j-1} &= w^j_j \\
\sigma_{zz}\ ^j_{j-1} &= \sigma_{zz}\ ^j_j \\
\sigma_{zr}\ ^j_{j-1} &= \sigma_{zr}\ ^j_j
\end{aligned}
\qquad (49)
$$

Figure 2

Cross-interface continuity of Normal and Tangential displacements and stresses (classical boundary conditions used in "SAFARI")

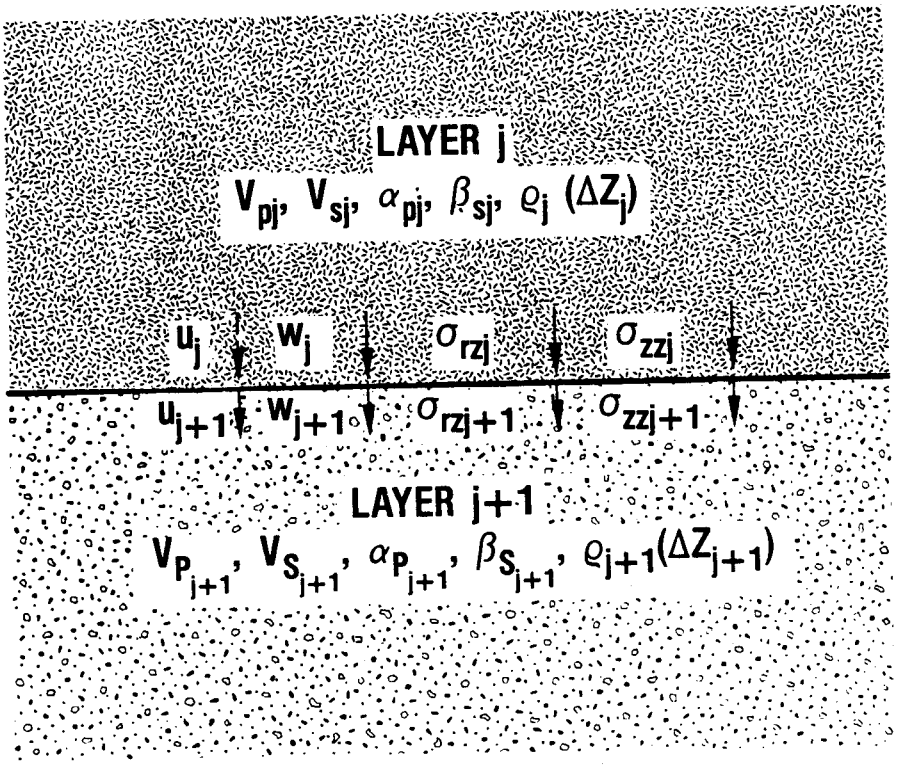
LAYER j
V_{pj}, V_{sj}, α_{pj}, β_{sj}, ϱ_j (ΔZ_j)
u_j
w_j
σ_{rzj}
σ_{zzj}
INTERFACE j
u_{j+1}
w_{j+1}
σ_{rzj+1}
σ_{zzj+1}
LAYER j+1
$V_{P_{j+1}}$, $V_{S_{j+1}}$, $\alpha_{P_{j+1}}$, $\beta_{S_{j+1}}$, $\varrho_{j+1}(\Delta Z_{j+1})$

Similarly, corresponding sets of equations with right and left hand separated into source and homogeneous wavefield contributions respectively, can likewise be written for all other interfaces. In addition, in both the upper and lowermost bounding halfspaces, the arbitrary wavefield functions A-,B- and A+,B+ must vanish due to the Sommerfeld radiation condition.

This is all that is required to assemble the **global** coefficient matrix for the entire layer system, as derived **directly** from application of the governing classical boundary conditions of continuity to the generalised solution forms at each **local** layer **interface**. In total this gives a system of 4n-2 linear equations in the 4n-2 unknown arbitrary wavefield amplitude functions A+, A-, B+, B- (EWING JARDETZKY and PRESS, 1957, Chapter 4). When this system has been solved, the depth-dependent Green's function solution to the total inhomogeneous Helmholtz equation follows directly by superposition of the resulting homogeneous solution with the source kernels. The total field in range is then obtained by (numeric) evaluation of the integral transforms.

As mentioned above, for simple systems comprising only a very limited number of layers, these equations can of course be solved analytically, as done for the special 1, 2 and 3 layer cases in PEKERIS and EJP, but for a more general environment such an analytic solution is pragmatically prohibitive. This solution technique (as first applied to numerical analysis of surface wave dispersion) was thus originally perceived as requiring the then-infeasible inversion of large order matrices (e.g. for computation of the Rayleigh determinant in dispersion curve calculation; EWING JARDETZKY and PRESS, 1957; KNOPOFF, 1970; CISTERNAS et al, 1973). The global system of equations, however, can be shown to form the basis for a more general numerical solution to this multilayered Green's function problem, well

suited for fast matrix solution, due to its sparse block bidiagonal bandstructure and its analytically well-behaved nature for all values of frequency and horizontal wavenumber (excepting of course those corresponding to surface poles and trapped modes, treated with appropriate contour integration; see Section 2(e) below). An efficient and entirely general numerical solution scheme for the complete wavefield is presented in the following section, and subsequently discussed in the context of formal Finite Element Method (FEM) and Finite Wave Element (FWE) direct global matrix structure and solution strategies.

Figure 3

Schematic representation of sparse positive-definite banded block bi-diagonal global coefficient matrix in "SAFARI", resulting from writing normal and tangential displacements and stresses in each layer as LHS, and source or sources as RHS elements of total system of equations to be solved, for all layers.

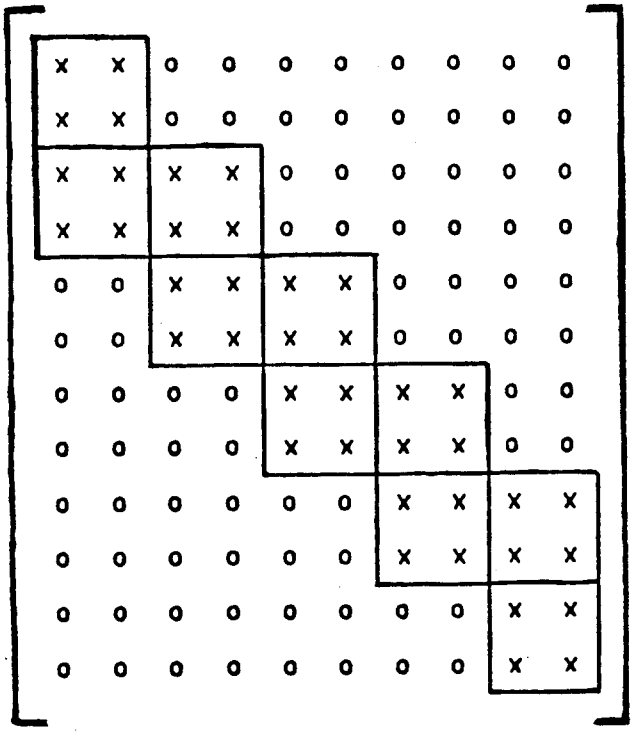
x x o o o o o o o o
x x o o o o o o o o
x x x x o o o o o o
x x x x o o o o o o
o o x x x x o o o o
o o x x x x o o o o
o o o o x x x x o o
o o o o x x x x o o
o o o o o o x x x x
o o o o o o x x x x
o o o o o o o o x x
o o o o o o o o x x

Section 2(c)

Finite Element/Finite Wave Element Analogy

The purpose of this section is to outline the Green's function solution method, by a Direct Global Matrix/Finite Wave Element approach as developed by SCHMIDT (1982), to illustrate the chief features and advantages of the technique (in comparison to propagator matrix based solutions), to discuss the nature and computationally-relevant properties of the global coefficient matrices that arrive, and finally to describe the main method of solution of the governing equation system. The discussion here will be limited to that of the plane-stratified homogeneous isotropic case (whose governing field equations were derived above), for seismic acoustic wave propagation from arbitrary buried (point, or other) sources, as treated in the numerical algorithmds "SAFARI" (1982;1983).

As in all ocean acoustic and synthetic seismic modeling methods based upon integral transform techniques (e.g., FUCHS-MULLER and KENNETT reflectivity, KUTSCHALE FFP and BOUCHON-AKI discrete wave number method), the numerical solution for the total wavefield problem is divided into two general parts. First the unknown arbitrary wavefield functions are founds at a discrete number of

horizontal wavenumber k_r from the basic system of equations (in A+/- and B+/-) which express the governing boundary conditions of condituity (in normal and tangential displacement are stress) to

be satisfied. This is equivalent to obtaining a Green's function solution to the basic 2-point boundary value problem of Chin et al, 1984. Second, the transfer functions are then found at all selected depths and ranges by evaluation of the integral Hankel/Fourier transforms, followed (for seismogram synthesis) by Fourier synthesis over frequency to yield the time-domain synthetic seismic response. As repeated computational experience of over 15 years has shown (CHAPMAN and ORCUTT, 1984), for almost all cases of Green's function calculation involving propagator matrices, the first part -the exact Green's function solution- is by far the most critical in relation to total computation time. It is precisely here, in the **direct global matrix** method, that the present model differs in computational approach from recursive local propagator matrix techniques (of THOMSON-HASKELL) of the same integral transform class. Emphasis is therefore focused on this first part in the following (for a review of pertinent literature, for ocean acoustics, see JENSEN, 1983; for seismology, CHAPMAN and ORCUTT, 1984; KENNETT, 1983; URSIN, 1982; MULLER and SCHOTT, 1979).

As is well known in numerical modeling, the use of digital computers in solving field problems in continuous media in general requires some kind of discretisation. One possibility is to set up the Exact field Equations (in an EXACT problem formulation) for the continuum and then to find an approximate solution by **discretisation of the equations.** This is the approach taken in finite difference techniques for solving the partial

differential equations; for example, the parabolic approximation to the acoustic Helmholtz wave equation (TAPPERT, 1977; GILBERT, 1981).

The other possibility is to **discretise the continuous medium** itself, and then in effect let the computer numerically determine an exact solution to this APPROXIMATED problem, now defined in terms of Approximate Equations.

Perhaps the most well known example of the latter approach is the Finite Element Method (FEM) (ZIENKIEWICZ,1973). This numerical technique is based precisely upon division of a given medium continuum into an assemblage of finite layers, blocks or elements, interconnected at a finite number of discrete interface points or nodes. Exact local solutions for the single elements, together with the governing boundary conditions of continuity between the elements concentrated at the nodes, leads directly to an exact solution for the global response problem (comprising all layers). This direct global approach requires the solution of large linear system of equations in the unknown degrees of freedom (in engineering mechanics FEM, typically node displacements, in response to applied forcing functions). Despite the fact that lack of sufficient appropriate computer power has, until the last two decades, somewhat obstructed practical use of this powerful technique, it is today the most widely employed methodology in many different fields, such as structural

mechanics, fluid mechanics and numerical elastodynamic modeling.

Considering again the question of solving the 4n-2 system of linear equations representing seismic wave propagation in the n-layered case, in contrast to recursive propagator matrix techniques, one can directly observe (SCHMIDT, 1982;1983;1984) that solution of the exact wave equation for horizontally stratified environments by integral transform methods (as derived above) is of the latter ('finite element type') catagory. Here the **local** expressions for the depth-dependent Green's function are exact within each layer (element). Thus an exact **global** solution for all layers can be obtained **directly**, via application of the classical boundary conditions of continuity to be satisfied at all interfaces (nodes), to obtain a characteristically sparse banded block (bi) diagonal matrix for the multilayer Green's function directly reflecting these connectivity conditions, precisely as is the case in FEM. It is therefore not suprising that the practically-implemented solution of this present exact seismic acoustic finite wave element matrix problem can be performed in close analogy to finite element 'stiffness' matrix solutions. In this case it possible to use many of the wellknown and efficient numerical tools created for matrix operations during the recent decades of FEM methodological development. This is the basis of the analogous " finite wave element " solution of SCHMIDT used in the general applications algorithm " SAFARI ".

A rigorous study of the mathematical bases of FEM is beyond the scope and purpose of this thesis (see ZIENKIEWICZ, 1978; HINTON and OWENS, 1980). In order to formally develop this FEM/FWE analogy, the basic principles of the finite element method (in its 'direct' or 'displacement' form) pertinent to this DGM/FWE method will be briefly outlined at this point.

The simplest possible static element shown in [Figure 4a] is chosen as a representataive example for this discussion. It has 4 degrees of freedom, the 4 plane-layered node displacements (u1,u2,u3,u4). An exact expression can be set up for the corresponding node forces (p1,p2,p3,p4):

$$\begin{Bmatrix} P \\ 1 \\ P \\ 2 \\ P \\ 3 \\ P \\ 4 \end{Bmatrix} = \begin{bmatrix} & & \\ & & \\ & K & \\ & & \\ & & \\ & & \\ & & \\ & & \end{bmatrix}_j \begin{Bmatrix} u \\ 1 \\ u \\ 2 \\ u \\ 3 \\ u \\ 4 \end{Bmatrix} \tag{50}$$

Using the potential energy formulation of FEM (ZIENKIEWICZ, 1978), the elastic energy stored in the element is

$$E_j = = 1/2 \begin{Bmatrix} u1 \\ u2 \\ u3 \\ u4 \end{Bmatrix}_j \begin{bmatrix} \\ \\ k_j \\ \\ \end{bmatrix} \begin{Bmatrix} u1 \\ u2 \\ u3 \\ u4 \end{Bmatrix}_j \tag{51}$$

Figure 4

Schematic diagram of connectivity (continuity/topology) relations for Finite Element and Finite Wave Element models

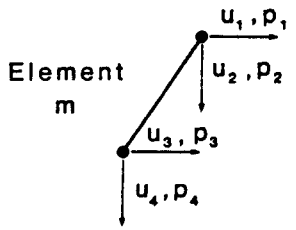

$$\begin{Bmatrix} p_1 \\ p_2 \\ p_3 \\ p_4 \end{Bmatrix}_m = \begin{bmatrix} k \end{bmatrix}_m \begin{Bmatrix} u_1 \\ u_2 \\ u_3 \\ u_4 \end{Bmatrix}_m$$

a. Finite element

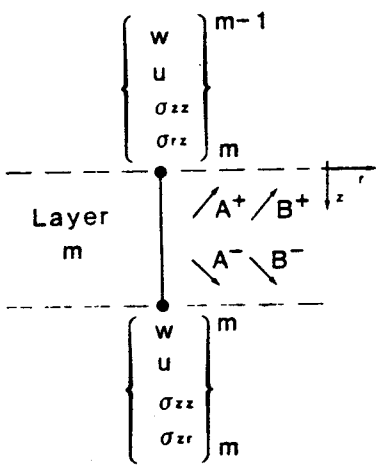

$$\begin{Bmatrix} w \\ u \\ b_{zz} \\ b_{rz} \end{Bmatrix}^{m-1}_{m} = \begin{bmatrix} d \end{bmatrix}_m \begin{Bmatrix} A^- \\ B^- \\ A^+ \\ B^+ \end{Bmatrix}$$

$$\begin{Bmatrix} w \\ u \\ b_{zz} \\ b_{rz} \end{Bmatrix}^{m}_{m} = \begin{bmatrix} d \end{bmatrix}_m \begin{bmatrix} e \end{bmatrix}^{m}_{m} \begin{Bmatrix} A^- \\ B^- \\ A^+ \\ B^+ \end{Bmatrix}$$

b. Finite wave element

Analogy to Finite Element Method.
a. Finite element with 4 degrees of freedom.
b. Finite wave element with 4 degrees of freedom.

a. Finite element

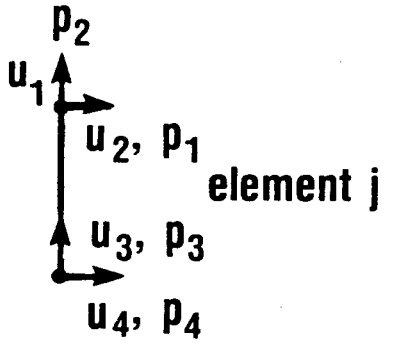

$$\begin{Bmatrix} p_1 \\ p_2 \\ p_3 \\ p_4 \end{Bmatrix}_j = [k]_j \begin{Bmatrix} u_1 \\ u_2 \\ u_3 \\ u_4 \end{Bmatrix}$$

b. Finite wave element

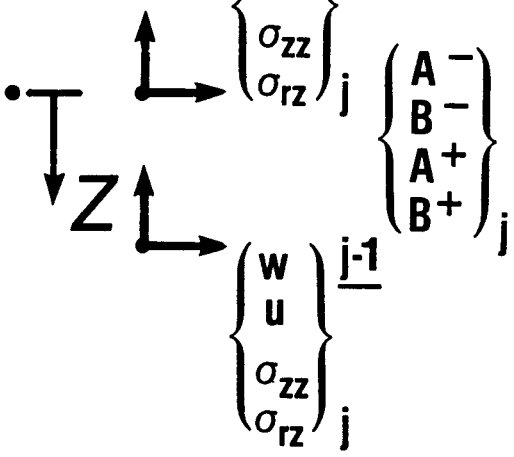

$$\begin{Bmatrix} w \\ u \\ \sigma_{zz} \\ \sigma_{rz} \end{Bmatrix}_j^{j-1} \quad \begin{Bmatrix} A^- \\ B^- \\ A^+ \\ B^+ \end{Bmatrix}_j$$

$$\begin{Bmatrix} w \\ u \\ \sigma_{zz} \\ \sigma_{rz} \end{Bmatrix}_j^{j-1} = [d]_j \begin{Bmatrix} A^- \\ B^- \\ A^+ \\ B^+ \end{Bmatrix}_j$$

$$\begin{Bmatrix} w \\ u \\ \sigma_{zz} \\ \sigma_{rz} \end{Bmatrix}_j^{j} = [d]_j [e]_j \begin{Bmatrix} A^- \\ B^- \\ A^+ \\ B^+ \end{Bmatrix}_j$$

c. Propagator matrix

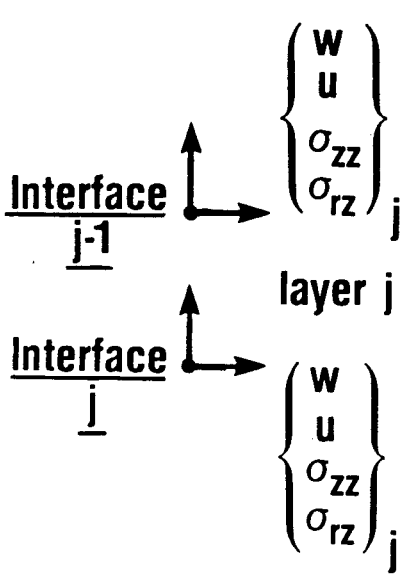

$$\begin{Bmatrix} w \\ u \\ \sigma_{zz} \\ \sigma_{rz} \end{Bmatrix}_j^{j} = [p] \begin{Bmatrix} w \\ u \\ \sigma_{zz} \\ \sigma_{rz} \end{Bmatrix}_{j-1}^{j-1}$$

$$[p]_j = [d]_j [e]_j [d]_j^{-1}$$

where the k's are nodal displacement coefficients for the general j-th layer.

If external forces or loads are acting on the jth layer element, these are again concentrated in the node forces (r1,r2,r3,r4), so that the net potential energy or work performed by these can be expressed as

$$w = 1/2 \begin{Bmatrix} u1 \\ u2 \\ u3 \\ u4 \end{Bmatrix}_j^T \begin{Bmatrix} u1 \\ u2 \\ u3 \\ u4 \end{Bmatrix}_j \qquad (52)$$

As the nodes/interfaces are in general common for more than one element, it is here convenient to introduce a global degree of freedom vector {U} defined by

$$\begin{Bmatrix} u1 \\ u2 \\ u3 \\ u4 \end{Bmatrix}_j = \begin{bmatrix} & L & \end{bmatrix}_j \{ u \} \qquad j=1,2,3...N \qquad (53)$$

local global

where [L] is the topology, transformation or connectivity matrix for layer element j (ZIENKIEWICZ, 1973). In finite element applications, the topology matrix is an extremely sparse identifier matrix or mapping, here with only 4 nonvanishing elements, which are unity, directly reflecting the number and kinds of continuity/connectivity conditions governing the layer system in question at each interface. Using this notation, we may

symbolically construct the local to global transformation for the nodal displacements as:

$$\{u_{local}\} = [\ L\ ]\ \{u_{global}\}\ , \tag{54}$$

where the topology matrix [L] is of the form

$$[\ L\ ] = \begin{bmatrix} [t] & [0] & [0] & [0] \\ [0] & [t] & [0] & [0] \\ [0] & [0] & [0] & [t] \end{bmatrix} \tag{55}$$

where the number of nonzero matrix elements [t] in [L] equals the number of layer element nodes/interfaces, and the number of columns is the total number of degrees of freedom (in this example = 4), Insertion of (49) into (51) and (52) above yields

$$E_j = 1/2\ \{u\}^T\ [\ L\ ]^T_j\ [k]_j\ [\ L\ ]_j\ \{u\} \tag{56}$$

and

$$w_j = 1/2\ \{\ u\ \}^T\ [\ L\ ]^T \begin{Bmatrix} \{r1\} \\ \{r2\} \\ \{r3\} \\ \{r4\} \end{Bmatrix}_j \tag{57}$$

respectively. Hamilton's principle of stationary energy requires that

$$\delta\left(\sum (E_j - W_j) \right) = 0 \tag{58}$$

leading to the following linear system of equations to be satisfied

$$[\,K\,]\{\,U\,\} = \{\,R\,\} \tag{59}$$

where [K] is the global stiffness matrix

$$[\,K\,] = \sum_j [\,L\,]_j^T [k]_j [L]_j \tag{60}$$

and [R] is the global forcing/source function vector

$$[\,R\,] = \sum_j [\,L\,]_j^T \begin{Bmatrix} r1 \\ r2 \\ r3 \\ r4 \end{Bmatrix} \tag{61}$$

After modification of [K] to account for prescribed displacements (the details of which are outside the scope of this discussion; ZIENKIEWICZ, 1973), the assembled global coefficient matrix for finite element method in the simplest linear element form is seen to be positive definite, diagonally dominant and symmetric. In the displacement version of FEM, the overall governing equation is

$$[K]\{u\} = \{P\} \tag{62}$$

where [K] is the assembled global stiffness matrix, properly contracted to account for the governing physical boundary conditions of cross-interface continuity, {u} the vector of unknown displacements of the interfaces/nodal points and {P} the vector for source/loading functions. The matrix [K] can be shown to be real, symmetric and positive definite, as well as (in most structural FEM applications), sparse and generally dense-banded (diagonally dominant) along the main diagonal, whose width and arrangement depends upon the node topology and the manner in which the nodes and degrees of freedom of the element structure are ordered and indexed (RICE, 1980). The vector of unknown displacements {u} can then be directly evaluated by simply inverting [K] according to standard solution methods, such as one of the variants of Gaussian elimination (HINTON and OWEN, 1980; BATHE and WILSON, 1976).

Section 2(d)

Direct Global Matrix Solution

Returning to the determination of the elastodynamic depth-dependent Green's function for modeling seismic wave propagation in plane layered solid media, the fact that horizontal range dependence on r has been removed (in the solution of the depth-separable Helmholtz wave equation) yieldsthe possibility of effectively representing each discrete layer as a one-dimensional " finite wave element ", shown in **Figure** 4, in a direct formal analogy to the basic matrix solution of standard finite elements discussed above. The degrees of freedom for this finite-wave-element are here simply the corresponding generalized scalar potential wave amplitudes $A^{+/-}_j$ and $B^{+/-}_j$, and these are likewise conveniently collected in an analogous local layer degree-of-freedom vector {a},

$$\{a\}_j = \begin{Bmatrix} A^- \\ B^- \\ A^+ \\ B^+ \end{Bmatrix} , \qquad (63)$$

where the subscript j refers as above to the **layer** number. If the kernels for the field parameters of displacement and stress involved in the boundary conditions (Eqs 40-43) are expressed similarly in vector form as

$$\{ v(z) \} = \begin{Bmatrix} w(z) \\ u(z) \\ \sigma_{zz}(z) \\ \sigma_{zr}(z) \end{Bmatrix} , \qquad (64)$$

the following matrix relation is obtained for the homogeneous part of the wavefield solution

$$\{ v(z) \}_j = [c(z)]_j \{a\}_j \qquad (65)$$

The matrix $[c(z)]_j$ is a function of the horizontal wavenumber k_r and of depth z. As the depth-dependence is present only in the exponentials, this matrix can itself be factorised further as

$$[c(z)]_j = [d]_j [e(z)]_j \qquad (66)$$

where $[d]_j$ is a depth-independent matrix containing only simple functions of k_r, and $[e(z)]$ is a diagonal matrix containing the exponentials. Explicit expressions for these matrices are given in CHIN et al, 1984.

In terms of the above, the following expressions are now obtained for the field parameters from considering the homogeneous solution at the associated interfaces j-1 and j:

$$\{ v \}_j^{j-1} = [d]_j \{a\}_j \qquad (67)$$

and

$$\{ v \}_j^j = [d]_j \, [e]_j^j \{a\}_j \tag{68}$$

with the **superscripts** identifying the **interface**. For convenience the upper interface j-1 has been chosen as the origin of a local coordinate system making the corresponding exponential matrix $[e]_j^{j-1}$ the identity matrix. (We will return later to this specific choice in relation to the numerical stability of the present direct global matrix solution algorithm "SAFARI" of SCHMIDT; see Section 2(e)).

As in the Finite Element Method, the (homogeneous) field parameters in Eqs. 18,23,32,34 are now superposed with the corresponding forcing terms due directly to the sources within layer j, to yield the total wave field expression. The classic boundary conditions, of simultaneous continuity in normal and tangential displacements and stresses at all interfaces, now yields a corresponding global linear system of equations in the unknown wave amplitudes. The rules governing the assembly and solution processes can be shown (below) to directly correspond in a natural analogy to those procedures used in the matrix solution of framed structures and discrete networks in FEM (ZIENKIEWICZ, 1973; RUBINSTEIN, 1979; DESAI & ABEL, 1979).

Using the notation from above, continuity of the superposed field parameters at interface # $\underline{j}$ can be expressed:

$$\{ v \}^{\underline{j}}_{j} + \{ \overset{*}{v} \}^{\underline{j}}_{j} = \{ v \}^{\underline{j}}_{j+1} + \{ \overset{*}{v} \}^{\underline{j}}_{j+1} \qquad (69)$$

where $\{\overset{*}{v}\}^{\underline{j}}_{j}$ and $\{\overset{*}{v}\}^{\underline{j}}_{j+1}$ are the source contributions arising from the sources in layer number j and j+1 respectively. If Eq. 69 is rewritten as

$$\{ v \}^{\underline{j}}_{j} - \{ v \}^{\underline{j}}_{j+1} = \{ \overset{*}{v} \}^{\underline{j}}_{j+1} - \{ \overset{*}{v} \}^{\underline{j}}_{j+1} \qquad (70)$$

it then directly expresses cancellation of the discontinuity in the source fields by the discontinuity in the homogeneous solution, in direct correspondence to cancellation conditions in propagator matrix formalism (KENNETT,1983;AKI & RICHARDS,1980). The interface discontinuity vector {v}j is therefore introduced as

$$\{ v \}^{\underline{j}} = \{ v \}^{\underline{j}}_{j} - \{ v \}^{\underline{j+1}}_{j} \qquad j=1,2,3...N-1 \qquad (71)$$

and similarly for the source field discontinuity $\{\overset{*}{v}\}$.

In order to assemble the 4N-2 **local** equations (u) into 1 **global** system, the global degree of freedom vector in [A] (the up and

downgoing wavefield scalar potential amplitudes) is first introduced, defined by the unique local-to-global mapping (SCHMIDT, 1983)

$$\{ a \}_j = [S]_j \{A\} \tag{72}$$

one	all
Local	Global
layer	layers

After insertion of Eqs. 72 into 68 and 71, the local discontinuity in the homogeneous solution at interface $\underline{j}$, the result takes on the form

$$\{ v \}^{\underline{j}} = ([d]_j [e]_j^{\underline{j}} [S]_j - [d]_{j+1} [S]_{j+1}) \{A\} \tag{73}$$

We now introduce a second unique mapping, collecting the Local field discontinuity vectors {v} into one Global vector {V}

$$\{ V \} = \sum_{j=1}^{N-1} [T]^{\underline{j}} \{v\}^{\underline{j}}$$

$$= \sum_{j=1}^{N-1} [T]^{\underline{j}} \left\{ [d]_j [e]_j^{\underline{j}} [S]_j - [d]_{j+1} [S]_{j+1} \right\} \{A\} \tag{74}$$

Similarly the global source field discontinuity vector $\{\overset{*}{V}\}$ is

$$\{ \overset{*}{V} \} = \sum_{j=1}^{N-1} [T]^{\underline{j}} \left\{ \{\overset{*}{v}\}^{\underline{j}}_{j} - \{\overset{*}{v}\}_{j+1} \right\} \tag{74}$$

The global cancellation condition therefore requires the following linear system of equations to be satisfied

$$\{ V \} = - \{ \overset{*}{V} \} \tag{76}$$

or

$$[C] \{A\} = - \{ \overset{*}{V} \} \tag{77}$$

where [C] is the global coefficient matrix

$$[C] = \sum_{j=1}^{N-1} [T]^{\underline{j}} \left\{ [d]_j [e]^{\underline{j}}_{j} [S] - [d]_{j+1} [S]_{j+1} \right\} \tag{78}$$

As can be observed, the above global system, Eq. 77, is in both form and function clearly analogous to the finite element stiffness system. The mapping matrices $[T]^{\underline{j}}$ and $[S]_j$ employed are exactly equivalent to the topology/connectivity matrices [L] defined for FEM in Eq. 55 previously. However, because the governing boundary conditions for the wave equation are not set up in the unknown potentials directly, but in derived physical

quantities, two sets of topology matrices are needed here, one for local-to-global mapping of the degrees-of-freedom (the wavefield amplitudes A+/- and B+/-, described above) and one for A/B conversion of the physical field parameters (normal and tangential displacements and stresses) involved in the boundary conditions of continuity.

In sum, the wave amplitudes (expressed as potentials for the entire global layer assemblage) may be written as an Nx1 vector. If we considerthe element/interface and element/layer indices separately, we can directly write the expanded global coefficient matrix and sources as NxN square matrices and Nx1 vectors respectively (in direct analogy to the FEM stiffnesses and loads). These are then readily constructed in full global form by inserting the known wavefield coefficients and sources (stiffness coefficients and loads) in their proper locations in 2 sets of 4x4 blocks along the diagonal (via topology matrices), and filling the remaining global matrix locations with zeroes. This is shown in **Figure 5.**

Figure 5

Schematic of unique algebraic mapping between Local and Global systems of equations used in DGM method of "SAFARI" (after SCHMIDT, 1982)

MAPPING BETWEEN LOCAL AND GLOBAL SYSTEMS OF EQUATION

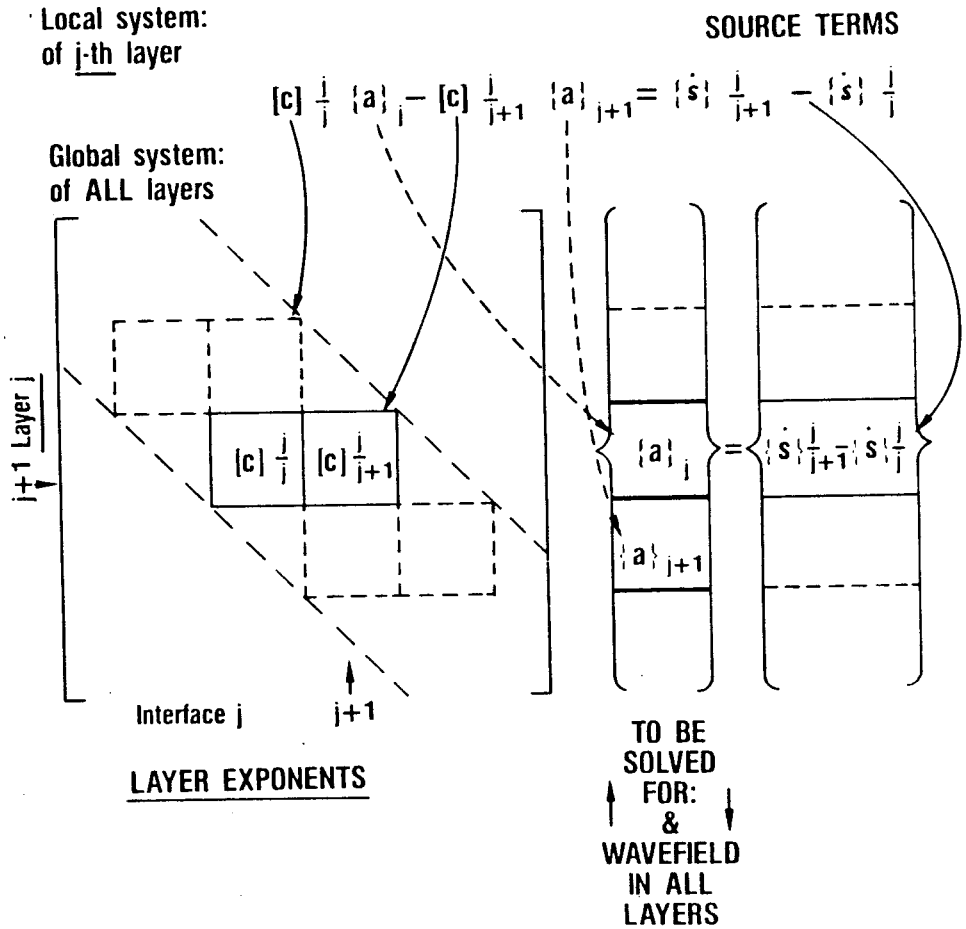

$$[c]_{j}^{j-1} = \begin{bmatrix} -\alpha_{j-1} e^{-z_j \alpha_{j-1}} & +k_r e^{-z_j \beta_{j-1}} & +\alpha_{j-1} e^{+z_j \alpha_{j-1}} & +k_r e^{+z_j \beta_{j-1}} \\ -k_r e^{-z_j \alpha_{j-1}} & +\beta_{j-1} e^{-z_j \beta_{j-1}} & -k_r e^{+z_j \alpha_{j-1}} & -\beta_{j-1} e^{+z_j \beta_{j-1}} \\ (2k_r^2 - k_s^2) & (2k_r \beta_{j-1}) & (2k_r^2 - k_s^2) & (2k_r \beta_{j-1}) \\ \bullet & \bullet & \bullet & \bullet \\ e^{-z_j \alpha_{j-1}} & -e^{-z_j \beta_{j-1}} & -e^{+z_j \alpha_{j-1}} & +e^{+z_j \beta_{j-1}} \\ (2\alpha_{j-1} k_r) & -(2k_r^2 - k_s^2) & (2\alpha_{j-1} k_r) & (2k_r^2 - k_s^2) \\ \bullet & \bullet & \bullet & \bullet \\ e^{-z_j \alpha_{j-1}} & e^{-z_j \beta_{j-1}} & -e^{+z_j \alpha_{j-1}} & e^{+z_j \beta_{j-1}} \end{bmatrix}$$

Section 2(e)

Discussion: Index Pointer System in Rapid Numeric Implementation of Direct Global Matrix method for Green's function Solution

From the above, it is clear that the main task in formulating the Green's function solution by the Direct Global Matrix method is that of synthesizing the appropriate sparse banded block diagonal (stiffness type) matrix from its component layer elements. This is accomplished by judicious use of Eqs. 72 and 74, the coding or indicial pointer system which efficiently related local & global nodal/interface indexes for a given layer/element (SCHMIDT,1982).

When solving large matrix systems on a computer, it is well known that in almost all cases, the largest part of total solution cost arises from the mechanics of data structuring, storage and transfer (TEZCON, 1963). To achieve satisfactory program performance (to optimise I/O operations without imposing excessive overhead or limiting problem size), special coding or mapping procedures must be developed.

To given an example from FEM, the global stiffness matrix file can be stored as a sequential array, identified by a single index subscript (j). A directory file is made containing special index pointers to the individual component submatrices. In this way,

using double indices, if the contents of a stiffness matrix are to be read, the i-th directory record is first accessed. This accessory information is scanned and the pointer to the submatrix in question is then returned & itself used to extract the proper record from the total stiffness matrix file.

In the DGM algorithm of SCHMIDT, this same representation scheme is employed. The topology matrices, transformation vectors or mapping arrays [S] and [T] given above are extremely sparse, containing only zeroes and ones, which (seen as a 2D network specifying all member element locations) effectively maps each **local** matrix element into its appropriate **global** matrix location. In operational terms, the formal matrix mappings of Eqs. 72 and 74 however need never be actually performed as such. Formal pointer matrices can instead be readily replaces by these two unique set of pointers, connecting respectively the interface elements of the local system with those of the global system, and subsequently converting scalar potential coefficients into physical displacements and stresses; see **Figure 6**. More precisely, the topology matrix $[\ T\ ]^{\underline{j}}$ defines a set of row pointers and $[\ S\ ]_j$ the corresponding column pointers.

As is the case in most FEM programs, in SAFARI the topology matrices as such are never set up to be explicitly solved-for in the actual computer code. Instead an array is used which relates the local and global nodal/interface indices for the given element/layer, allowing simple assembly of the individual local

Figure 6

Representation of indicial pointer system used for economic referencing and operations with Local to Global matrix mapping as employed in "SAFARI"

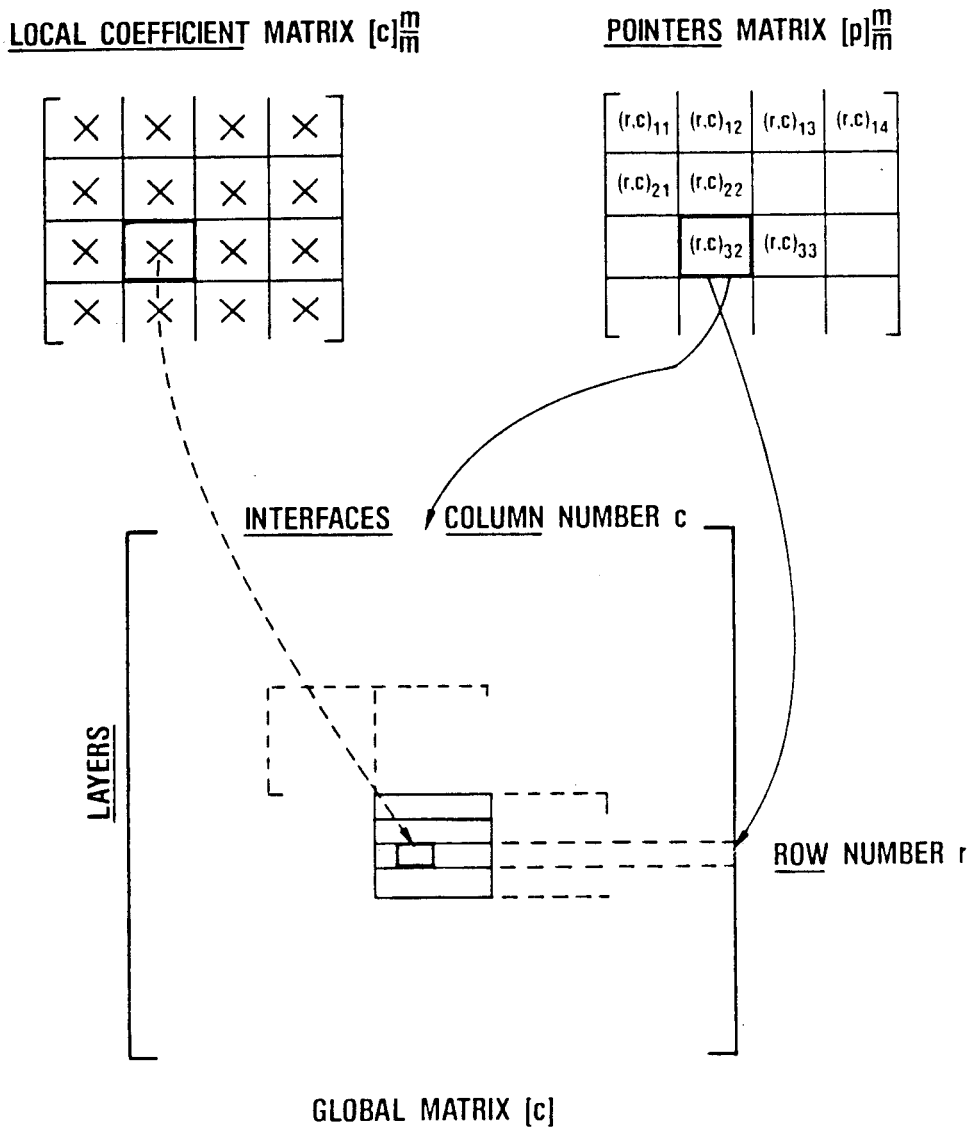
LOCAL COEFFICIENT MATRIX $[c]^m_m$
POINTERS MATRIX $[p]^m_m$
$(r,c)_{11}$ $(r,c)_{12}$ $(r,c)_{13}$ $(r,c)_{14}$
$(r,c)_{21}$ $(r,c)_{22}$
$(r,c)_{32}$ $(r,c)_{33}$
INTERFACES
COLUMN NUMBER c
LAYERS
ROW NUMBER r
GLOBAL MATRIX [c]

layer submatrices [a] into the appropriate locations in the overall global system matrix [A]. Similarly it is possible to appropriately map the subvectors of the elemental layer sources {v} into the proper positions of the overall global source vector {V}. As noted above, this general algorithmic strategy, of replacing serial operations with an equivalent (more economic) vector representation is common in many other areas of matrix-based computations; HINTON and OWENS, 1980. It is, for example, also found as an explicit option in the 'Pascal' programming language, as a structure of ordered array, whose values are precisely the address in computer memory of 1 or more variables. Because of their compact (and vectorisable) form, pointer-type constructs can be readily used to create flexible and powerful data structures where needed.

In addition to the significant computational economies gained by this technique (described below; see also ZIENKIEWICZ, 1973), the formal use of topology matrix mapping strategy is however also very convenient when seeing to comprehend the most general fluid/solid/vacuum case involving mixed layers of any arbitrary combination, as the topology matrix [S] can be set up to include only the non-vanishing wavefield amplitudes, and [T] only to involve the actual local boundary conditions. This reduces the total number of equations and unknowns compared to propagator matrix schemes for the pure solid case, totally eliminating, for example, the time-consuming problems of zero-fill via matrix dimension equalization (KUTSCHALE, 1972).

In this notation, to build the global coefficient matrix for subsequent Green's function solution via the pointer indices defined in Eqs. 72 and 74 above, it is only necessary to calculate the elements of the matrix [d], which are seen to be very simple functions of the horizontal wavenumber (CHIN et al, 1984, and the transfer exponentials in [e], for each layer in turn. This operation sequence is well suited for efficient vectorization on modern parallel computers (see below). The subsequent solution then yields the total wavefield in all layers simultaneously.

Considering their physical significance, the pointer indices defining the mappings of Eqs. 72 and 74 are dependent solely upon the topology/connectivity of the environmental model in question (directly reflecting the number and type of boundary conditions maintaining across each interface), and hence can be determined a priori in advance of actual solution (Figures 7 & 8).

Figures 7 - 8

7)
List of selected computational features of 'SAFARI'/Direct Global Matrix solution

8)
Heuristic flowchart of central "Calint" DGM algorithm used in 'SAFARI' (CW Fip version)

COMPUTATIONAL FEATURES OF SAFARI: DIRECT GLOBAL MATRIX SOLUTION

1. Sparse diagonally-dominant global matrix form (small bandwidth)
2. Simple local component matrices of exponential and algebraic factors
3. Numerically well-conditioned and unconditionally stable
4. Readily vectorizable (via index move pointers)
5. Executed and adapted within the framework of known and established software (from finite element method)

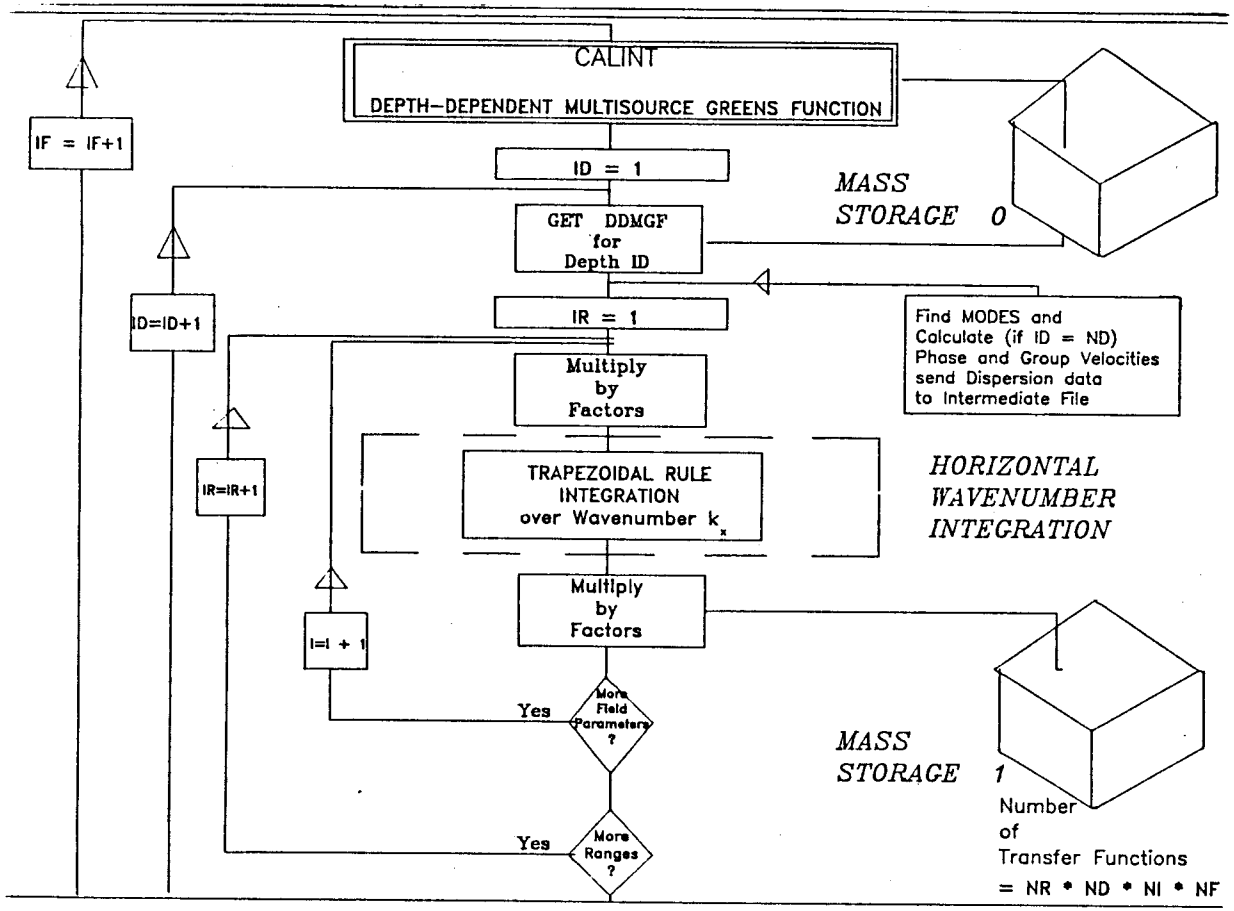
CALINT
DEPTH–DEPENDENT MULTISOURCE GREENS FUNCTION
IF = IF+1
ID = 1
MASS STORAGE 0
GET DDMGF for Depth ID
ID=ID+1
IR = 1
Find MODES and Calculate (if ID = ND) Phase and Group Velocities send Dispersion data to Intermediate File
Multiply by Factors
IR=IR+1
TRAPEZOIDAL RULE INTEGRATION over Wavenumber k
HORIZONTAL WAVENUMBER INTEGRATION
Multiply by Factors
I=I + 1
Yes
More Field Parameters ?
MASS STORAGE 1
Number of Transfer Functions = NR * ND * NI * NF
Yes
More Ranges ?

Section 2(f)

Consideration of Global Matrix Solution by Gaussian Elimination with Partial Pivoting

Detailed discussion of the theoretic stability, algorithmic design and implementation of Direct Global solution methods for Green's function computation is beyond the scope of this presentation (see SCHMIDT and JENSEN, 1984 and CHIN et al, 1984). A full account would require detailed stability computations unique to the particular linear system in question, as well as comprative evaluations using two or more matrix solution techniques. However, several computatationally-significant advantages can be immediately pointed out for the simple Gaussian elimination with partial pivoting employed by SCHMIDT.

Many numbers which would be zero in exact ('infinite word length') arithmetic are almost certainly nonzero inactual floating point (finite word length) implementation, because of the inevitable roundoff-truncation errors (WILKINSON, 1962). This simple fact is the basic cause of numerical problems with propagator matrices, and the motivation for both stability and accuracy analysis in linear system solutions in general.

As is commonly the case in direct solutions for large order structured matrices of the DGM type (see below; RICE, 1980; MOLER and VAN LOAN, 1977), for the sake of numerical stability in operations with growing/dying exponential terms, it is here advisable to carefully examine and if necessary rearrange the direct global matrix by subsequently pre-pivoting appropriate columns. When this is undertaken on the global matrix system as directly obtained from continuity boundary conditions applied to the scalar potential solutions. In addition to an improved exponential stability, one obtains simulateneously a natural termination of the global matrix at the upper and lower halfspace boundaries.

The above equations show that the difference in absolute dimension between displacements and stresses computed for the individual layer matrices can yield several orders of magnitude difference between the coefficients in the corresponding rows for both local and global matrix system. It is well known in such cases (RICE, 1980; SAMEH et al, 1978) that simple Gaussian elimination, whether with or without partial pivoting, will not by itself guarentee unconditional numeric stability. This occurs owing to the cumulative roundoff errors arising from enforced finite word length arithmetic on digital computers. In the present scheme (whose algorithmic realization by SCHMIDT in "SAFARI" is described by SCHMIDT & JENSEN, 1984 and SCHMIDT and TANGO, 1985), the above equations for displacement and stress are therefore additionally prescaled before solution, in order to

make all coefficients physically dimensionless, thereby insuring frequency and geometry-independent numerical stability.

To consider numeric solution of the particular layer equations, although from a theoretical viewpoint the origin of the above-mentioned layer coordinate system can (like the source position(s)) be chosen quite arbitrarily, its specific choice is in point of fact very critical for stability when large real arguments of the exponential functions appear. As noted, this commonly occurs for thick layers and large values of horizontal wavenumber (see discussion in FRANSSENS, 1984 and CHIN et al, 1984). As is further discussed in SCHMIDT and JENSEN (1984), for purely imaginary arguments, the exponential functions correspond to wavefields in the presence of visco-elastic attenuation (CHIN, 1981). For real arguments, however (for the evanescent regime encompassing both modal and interface type waves), large differences in the order of magnitude of exponential functions can again occur. In this case the resulting differences appear within the rows, and thus row-scaling itself as before is inapplicable. Although scaling during solution could in principle be applied in the colums (via defactorization of the growing exponentials, as suggested by CHIN et al, 1984), this step generally requires additional computations at each horizontal wavenumber.

It can be shown (SCHMIDT and JENSEN, 1984) that such additional scaling is in fact unnecessary when Gaussian elimination with

partial pivoting is used to solve the global matrix system. This follows from the fact that a simple combination of appropriate pre-pivoting and pre-scaling prior to solution, together with a judiciously chosen local coordinate system (as above), effectively removes the troublesome exponentials from the interface submatrix [c]. In the resulting matrix, all large-argument exponential functions now automatically all lie closest to the global matrix diagonal [**Figure 9**]. At the same time, this forces the condition that the A+/- and B+/- wave amplitudes corresponding to the growing exponentials will vanish after triangularization and back-substitution during Gaussian elimination.

Apart from conditions intrinsic to the precise equations used by SCHMIDT in "SAFARI", there are several other important general aspects of direct global matrix solution by Gauss elimination to be considered. For example, the fact that the direct global matrix, here solved in straightforward manner, is itself a banded block bidiagonal allows application of special data storage/CPU time efficient 'band' and 'envelope' solver techniques in a modular configuration (as per those in FEM). Because the bandwidth is both small and constant in this case (5 super- and 5-sub-diagonals, plus 5 extra diagonals from pivoting for a total of 16), these allow the total matrix to be effectively collapsed into a compact array of nonzero elements, with specific advantage in solution organization taken of both the limited bandwidth and diagonal dominance. In this particular case, the form of the

Figure 9

Schematic of the basis for numerical stability of complex exponential factors along the main diagonal of the Direct Global matrix (after SCHMIDT & JENSEN, 1984)

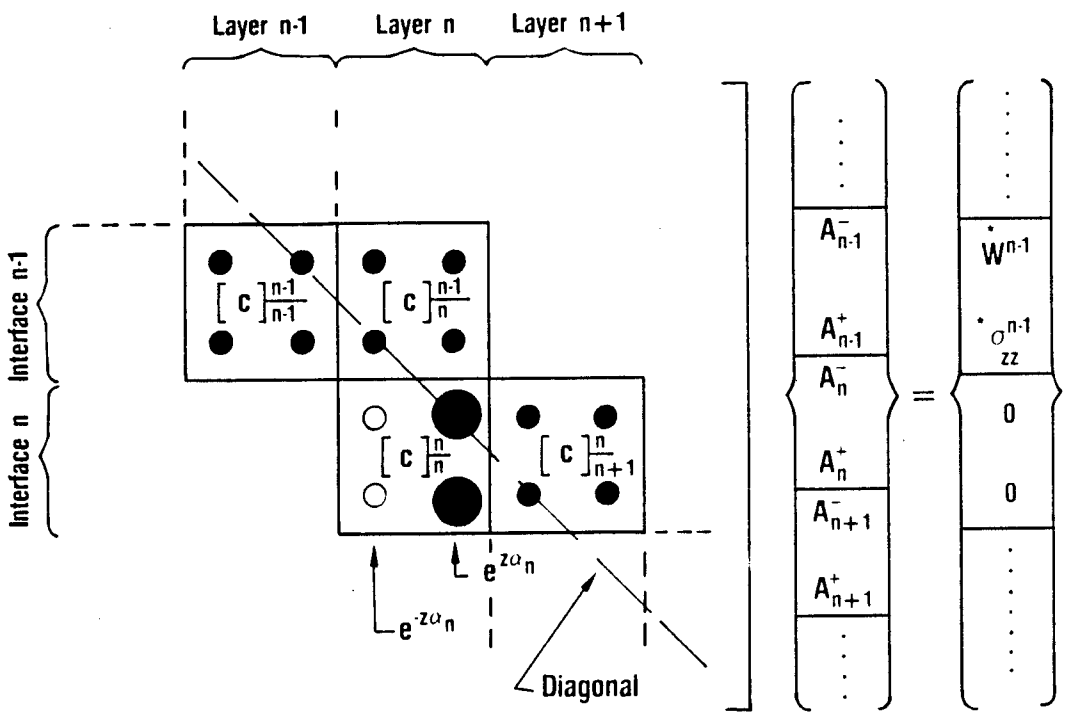

● Number $\gg$ 1 in evanescent case

● Number $\sim$ 1 in evanescent case

○ Number $\ll$ 1 in evanescent case

global matrix is such as to allow of efficient solution, using an envelope matrix solver in the forward elimination stage, and a banded solver in back substitution. Furthermore, in the required pivoting due to the "almost diagonally-dominant" form of the direct global matrix, due to the fact that for fluid/solid cases there are an unequal number of columns (DEBOOR and WEISS, 1983), all additional nonzero elements due to fill in during reduction (occuring exclusively above and outside the central bandwidth can be determined a priori and allowed for by calculating the new bandwidth dynamically during pivoting.

The total problem of accuracy, conditioning-stability and economy in Gaussian elimination, as well as particular requirements of sparse and block matrix types, represent a large and complex topic of applied mathematics (the outlines of which only can be treated here). The problem is further compounded by the necessity of considering in detail stability and accuracy behaviours of problems specific to the applications equations in question.

From the above, it will be seen that although there exist several theoretically-equivalent (mathematical) realisations of the direct global matrix method for Green's function solution, these are in fact not necessarily equal, according to both the practical specifics of their respective (algorithmic) implementation, as well as current (machine-imposed) limits in terms of numeric accuracy and economics. Because of the desirable propertiss of FEM-type global matrices, no special numerical

efforts, except for simple pre-pivoting, pre-scaling and local coordinate system normalization, are needed to insure unconditional numeric stability, when solving the direct global matrix by Gaussian elimiation with partial pivoting in the present "SAFARI" program of SCHMIDT. This (together with the indicial pointer system above; Section 2(e)) is believed to be one of the major reasons for both the unconditional stability and order of magnitude improvement in computational speed over those local recursive propagator matrix algorithms involving modified Thomson-Haskell techniques. Due to the sparse and diagonally-dominant form of the global matrix, solution by nothing more complex than prescaled Gauss elimination with partial pivoting alone can be performed very efficiently (**Figure** 10).

Figure 10

List of selected programming-algorithm features of "SAFARI"

PROGRAMMING FEATURES OF SAFARI:

1. Optimizes use of (small) high speed FPS memory
2. Employs extensive software pipelining (loop unwinding)
3. Critical I/O statements replaced with reads/writes to array buffers
4. Customed optimized microcoded sparse band/envelope solver

Section 2(g)

Numeric Integration: Theoretical Considerations of Integration Order and Representation

The Green's function contains complete information fully characterizing the exact elastodynamic layered media response. When the global system of equations has been solved, by matrix techniques as given above, the Green's response function kernels can then be readily evaluated at any depths of interest, the only additional quantities needed are $\exp(+/- z_j)$. All other k_r functions and expressions have at this point been already evaluated while setting up the global equation system. In accord with the recommendations of CHIN et al (1984), precisely because (1) effective unconditionally-stable Green's function solution is here coordinated algorithmically with (2) efficient subsequent (Hankel) integral transform evaluation for field quantities, the present SAFARI algorithm of SCHMIDT is extremely cost-effective and naturally suited to cases where the total wavefield is to be determined (for arbitrarily many receivers) at arbitrarily many depths (see Section 3(c), Vertical Seismic Profiling). In addition, because of its automatically complete wavefield representation, the method is ideal where an exact total solution is critical (in analysis of "leaky" modes; Section 3(b)).

In the standard "Spectral" integration sequence with a real contour (CHAPMAN, 1978;KENNETT, 1983) currently employed in SAFARI, the **first** numeric integration over k_r is standard interpolative **quadrature** using e.g. the simple trapezoidal rule (as has routinely been employed in reflectivity programs; FUCHS, 1968). A second alternative k_r integration is the **FFP** (discussed below) making use of the Fast Fourier transform (FFT) to directly integrate the Green's function solution. The **FFT** is also used here to carry out the **second** numeric intregation over ω (via an inverse FFT). The present Spectral integration order is widely used in both crustal and exploration modeling applications (KENNETT, 1983). It should be stressed, however, that the discretised Green's function solution technique described above, is completely valid for any order, path or method of integration, over both real and complex values of horizontal wavenumber and frequency, as well as for all possible source/receiver configurations;(THIGPEN, 1980). Consequently any complex integration contour, fast transform, interpolative or adaptive quadrature, or generalised Filon type numeric method of integration could equally well be chosen (FRAZIER, 1979; FRAZIER et al, 1984).

Since the original work of PEKERIS (1948;1956) in underwater acoustics and seismology, it is clear that for guided propagation even in lossless media, the above kernels to be evaluated over range in the integral transforms of k_r and ω will inevitably

require k_r to be extended to complex values, necessitating application of residue theory in the complex wavenumber plane for k_r integration (TOLSTOY, 1974). This arises because the solutions to the depth-separated wave equation become imaginary at certain k_r, wherein α and β become real and the waves decay exponentially. Since integration contours cannot cross any discontinuity, the complex plane must be cut into an appropriate number of branch lines so as to insure the integrand is always analytic (BÅTH, 1984).

For given kp/ks and k, as is well known, the Green's function integrand has singularities or poles at points defined by situations where the determinant of the global matrix becomes zero (EWING JARDETZKY and PRESS, 1957).Here, in general, over certain ranges of kp and k values, these poles on the real k_r axis interfere with possible integration paths, corresponding to trapped/normal eigenmodes and surface/interface waves, for the equivalent layered waveguide structure (REDWOOD, 1962). In these cases, a direct numerical integration along the real axis is at this stage both inconvenient and uneconomical, where an exact and complete representation of the most general seismic-acoustic wavefield is desired.

When further considering complex wavenumber k_r integration of the resulting Green's function, there are in general two ways in which this problem can be overcome. One is to deliberately deform

the complex integration contour into the complex k_r plane (as per the method of CAGNIARD-deHOOP; AKI and RICHARDS, 1980), in what will eventually be a mixed numeric/locally analytic solution. The other approach is to additionally introduce physically realistic attenuation in all layers. This will effectively result in moving the otherwise troublesome poles out onto the 1st and 3d quadrants of the complex wavenumber plane, and consequently make rapid real axis numeric integration feasible, at the same time complying more closely with known real-earth material (attenuative) behavior (KENNETT, 1974; MULLER and SCHOTT, 1979; O'NEILL and HILL, 1979). Notwithstanding the above, the influence of particular surface wave excited mode poles can in many cases still be strongly felt out on the integration contour, even for large attenuation-constant values, making exact choice of numeric integration parameters for k_r integration in general a matter of considerable attention (see Section 2(i) below).

At this point, having obtained (by DGM) the Green's function integrand for the layered system, and having then determined the order and path of integration for k_r and ω, the chief difficulties that now remain are precisely those of (1) correctly and completly interpreting and accounting for the often difficult implications of complex singularities on the k_r plane (see e.g. DOLPH and SCOTT, 1982), and of (2) correctly evaluating numerically the integrands in k_r and ω by some sufficient and specifiably accurate discrete quadrature or other method.

This choice must be undertaken with considerable care, given that some techniques may have only a restrictingly-small range of validity, whereas others may require computational times prohibitively long even on large digital computers (TSANG et al,1974). In addition, unless careful planning and numeric testing are instituted for the unique integrand conditions of every layered model whose response is sought, serious corruptive computational errors, inaccuracies and blatant numeric artifacts can result, both from improper choice of numeric integration method and/or integration limits and sampling. The following discussion in Section 2(h) considers integration method choice from the viewpoint of theoretic completeness of solution; Section 2(i) subsequently presents guidelines for correct parameterisation and implementation.

Section 2h

Numeric Integration Path

Here we consider the question of reducing cpu time on wavenumber integration within a more convenient framework (a method also applicable for the subsequent ω integration) than that of standard quadrature methods. Since the work of DINAPOLI (1972), KUTSCHALE (1971;1973), HARRISON (1982) etc, an often standard procedure in developing 'fast' field approximations to exact integration over the Bessel's range function involves effectively (1) replacing the original $J_0(k_r r)$ with a decomposition into an equivalent pair of Hankel transforms in terms of $H_0^{(1)}(k_r r)$ and $H_0^{(2)}(k_r r)$; (2) neglecting $H_0^{(1)}(k_r r)$; and (3) replacing $H(\frac{2}{0})$ with its large argument asymptotic expansion (this later having the advantage of easy computation via an FFT); COOLEY et al, 1967). This is the computational basis of numeric integration in both the socalled Fast Field Program (FFP) in ocean acoustics and the Discrete Wavenumber Method in theoretical seismology (MARSH et al, 1967, who first employed the method in electromagnetic field computations).

Briefly, the first step consists in replacing the original zeroth-order Bessel transform $J_0(k_r r)$ by a decomposition into the

equivalent Hankel function representation (ABRAMOWITZ and STEGUN, 1964; #9.1.3-4) [Figure II]

$$J_{m=0}(k_r r) = 1/2 \left(H_0^{(1)}(k_r r) + H_0^{(2)}(k_r r)\right)$$

The above integrals are in this case effectively split into two, one involving $H_0^{(1)}$ which, with the present choice of time factor corresponds to outgoing waves which diverge from the source, the other order Hankel function then corresponding to ingoing waves (references: GILBERT, 1968; PHINNEY, 1961; ROSENBAUM, 1960).

Although in general only erratically discussed in the literature, the relative significance of these two in and outgoing wavefield contributions can be considered, in a nonrigorous semiqualitative sense, using complex contour integration (ROSENBAUM, 1960; PHINNEY, 1961; see review of DOLPH and SCOTT, 1978 for detailed discussion and bibliography).

The contour for the first integral involving $H_0^{(1)}$ can be closed in the lower half plane, with vanishing contribution from the first quadrant in the complex plane (easily demonstrated by replacement of the remaining Hankel function H with its large argument/farfield asymptotic approximation; see below). All poles, corresponding to surface waves, trapped and 'leaky' modes, are due to the attenuation encircled by this contour.

Figure 11

Contour integration path in the complex horizontal wavenumber plane employed by "SAFARI" (after SCHMIDT & KRENK, 1980)

$$h^{(1)}_{m+2j+1}(-Z)j_{m+2l+1}(-Z) = h^{(2)}_{m+2j+1}(Z)j_{m+2l+1}(Z).$$

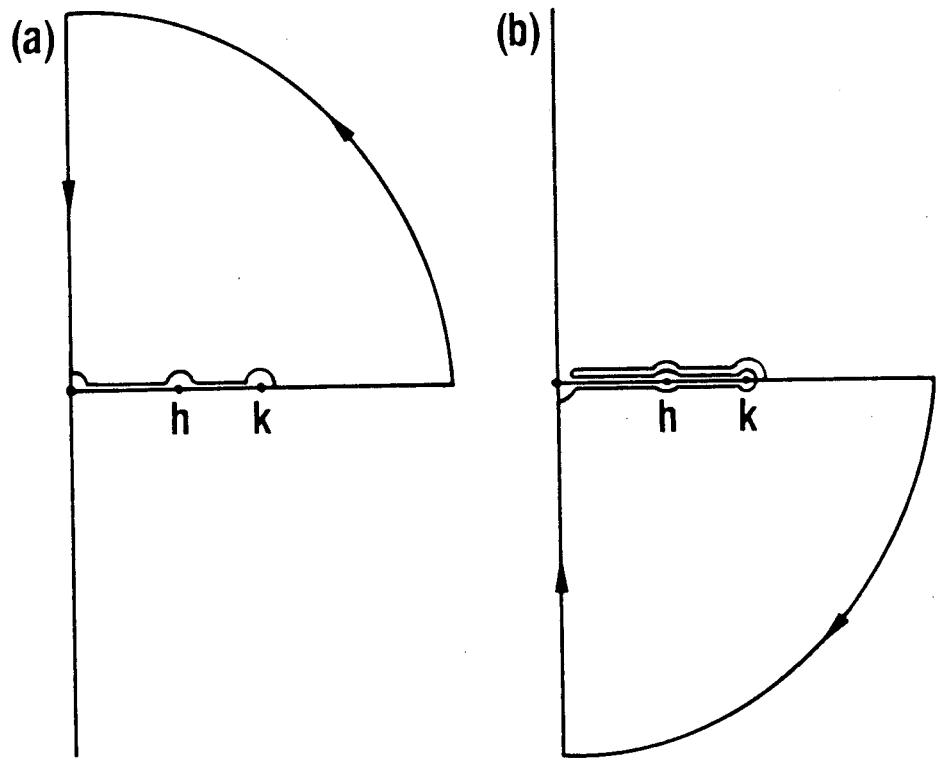

The full integral above can therefore be replaced by the corresponding residues plus branch line integrals corresponding to the continuous wavenumber spectrum, and a contribution from the contour along the negative imaginary axis. The contour for the second integral involving $H_0^{(1)}$ can be similarly closed in the upper halfplane, but as neither poles nor branch cuts are present here, only the integral along the imaginary axis contributes. The Hankel function of pure imaginary argument, however, now becomes a modified Bessel function of the 2nd kind, which is an exponentially decaying function of the argument $k_r r$.

It can be shown (KRENK and SCHMIDT, 1982) that this integral therefore gives significant contribution only at very small values of $k_r r$, at extremely short receiver source-receiver offset ranges with respect to the dominant seismic wavelength, and for very steep angles of incident, NB at very low frequencies, over most material configurations of practical interest (GILBERT, 1968;). In point of fact, this integral together with the corresponding contribution to the H ($k_r r$) integral can be seen to represent vertically standing waves in the nearfield along the source axis above and below the source, as an interference complex having no clear distinction with respect to coupling between P and SV wave types. This has also been described as an oscillatory nonpropagating continuum, "constituting nonrealisable pulse terms and modal oscillations that are insignificant compared with those from the outward

traveling waves" (PHINNEY, 1961). It can be further shown by contour integration that the ingoing Hankel function becomes a modified Bessel function of the 2nd kind, having no phase change with range. Because of this, the integral involving H is therefore often neglected, with complete correctness for many practical ocean acoustic and solid earth seismic modeling applications (those involving realistic source/receiver offsets and relatively "short" period signals). This is the procedure followed here with the SAFARI program and hence for the numerical applications of SAFARI that follow in Section 3. A more quantitative justification of the farfield approximation has been given by DINAPOLI and DEAVENPORT (1980) through numeric experiments with underwater acoustic transmission loss modeling, via response comparisons of Green's function results when computed by the truncated asymptotic Hankel function approximation and by the full Bessel's function/nonasymptotic solution of TSANG et al (1974). KENNETT (1984, personal communication; DOLPH and SCOTT, 1978; GILBERT, 1968; ROSENBAUM, 1960) have noted possible instances when the nearfield and ingoing contributions can potentialy have a significant effect for sufficiently complex multi-layered media. Further detailed study for the seismic nearfield case in Vertical Seismic Profiling (VSP) will be found elsewhere (TANGO and SCHMIDT, 1985).

Some idea of the magnitude and type of effects arising from neglecting ingoing wave contributions can be had from comparison

Figure 12 (a-d)

a/ Full plane wave (line source) exact solution for fluid medium

b/ Outgoing-only + asymptotic spherical wave (point source) solution for fluid medium

c/ Full plane wave (line source) exact solution for fluid 1/2 space

d/ Outgoing-only + asymptotic spherical wave (point source) solution for fluid 1/2 space

showing amplitude error (singularity) at extreme nearfield ranges (closer than $k_r r < 3$)

LINE SOURCE IN LIQUID MEDIUM (WHOLE SPECTRUM)

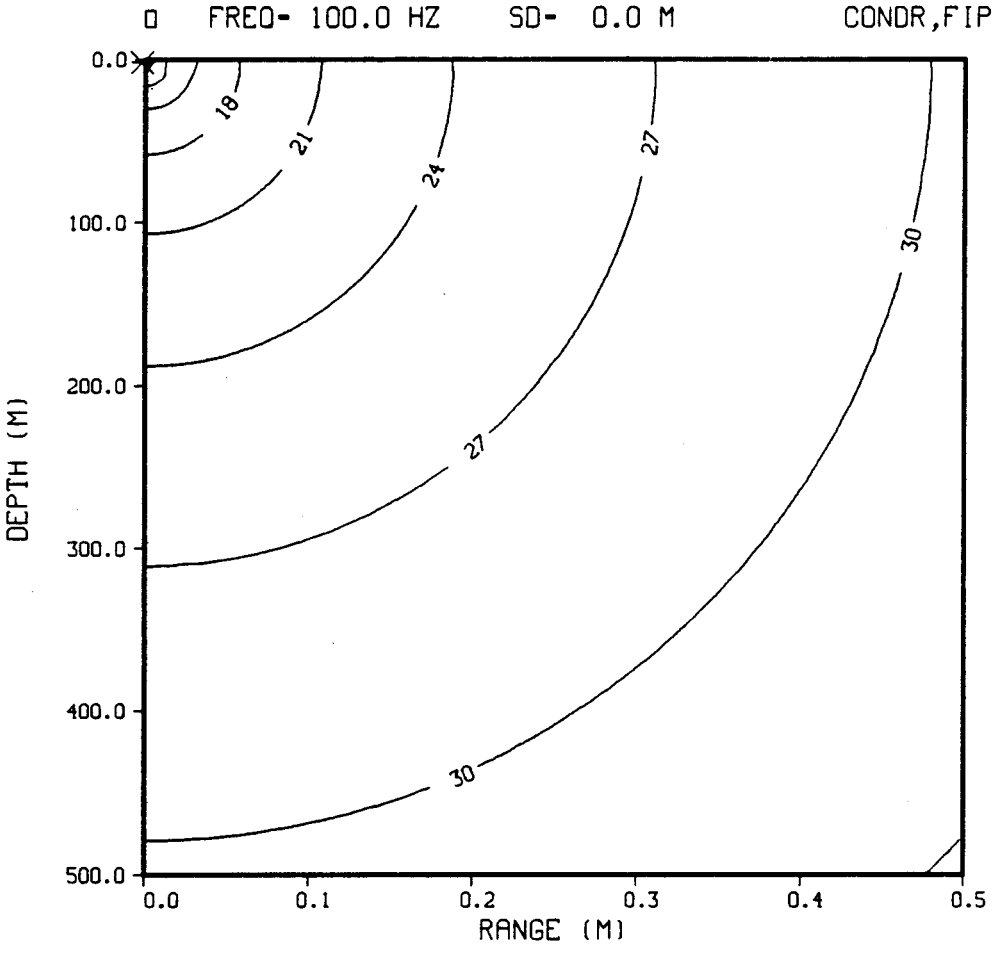

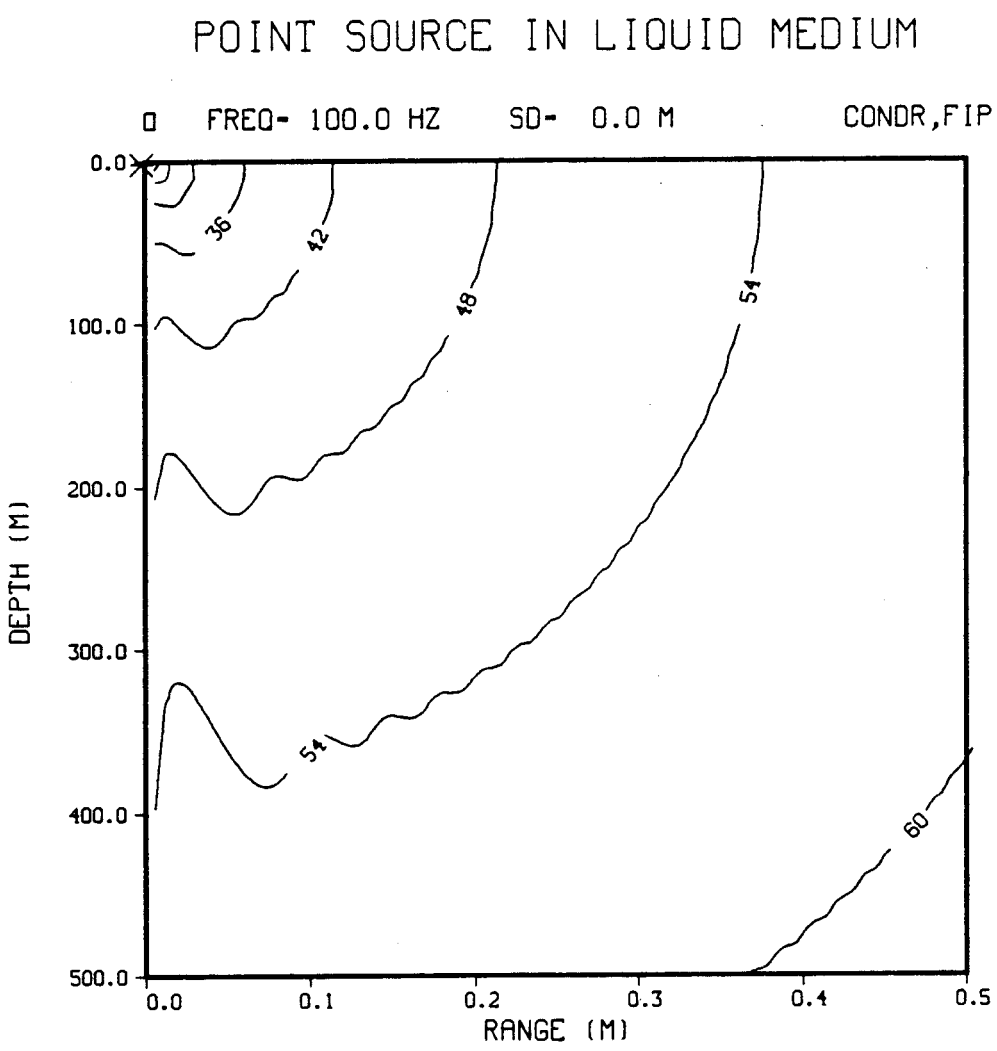
POINT SOURCE IN LIQUID MEDIUM
0 FREQ- 100.0 HZ SD- 0.0 M CONDR,FIP
0.0
100.0
200.0
300.0
400.0
500.0
DEPTH (M)
36
42
48
54
54
60
0.0
0.1
0.2
0.3
0.4
0.5
RANGE (M)

LINE SOURCE IN LIQUID 1/2 SPACE (WHOLE SPECTRUM)

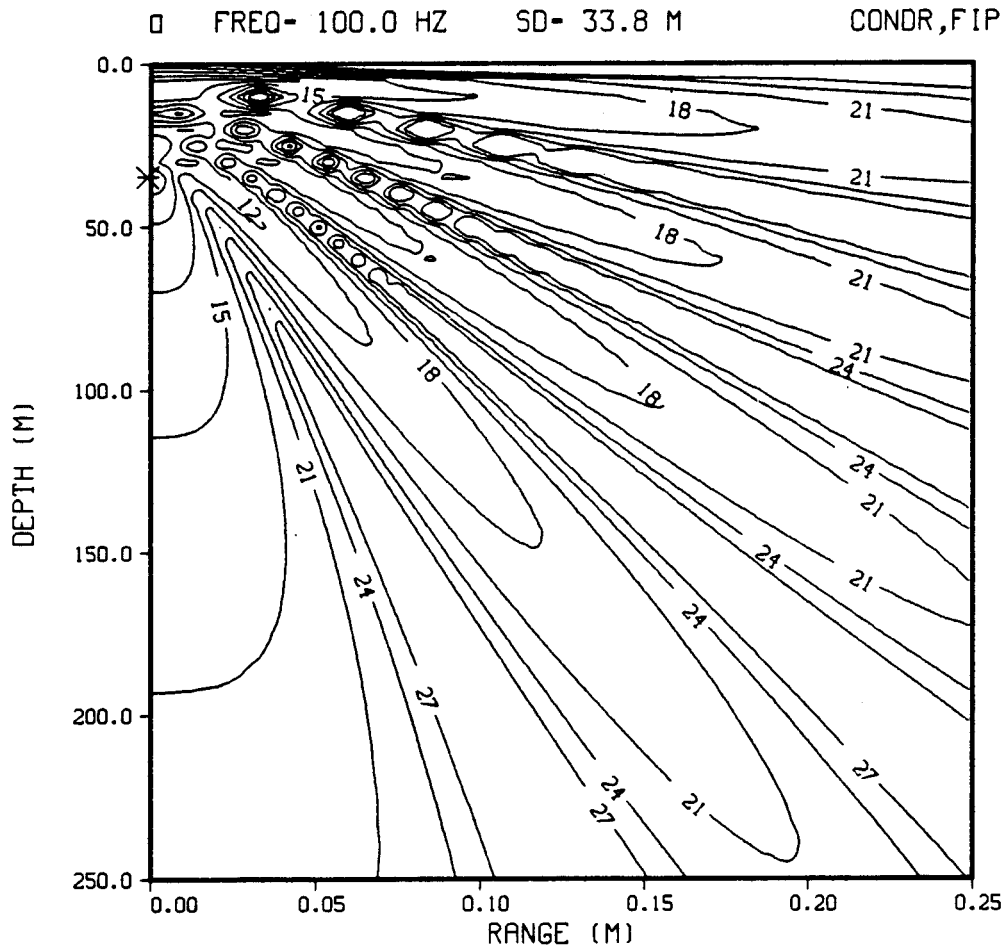

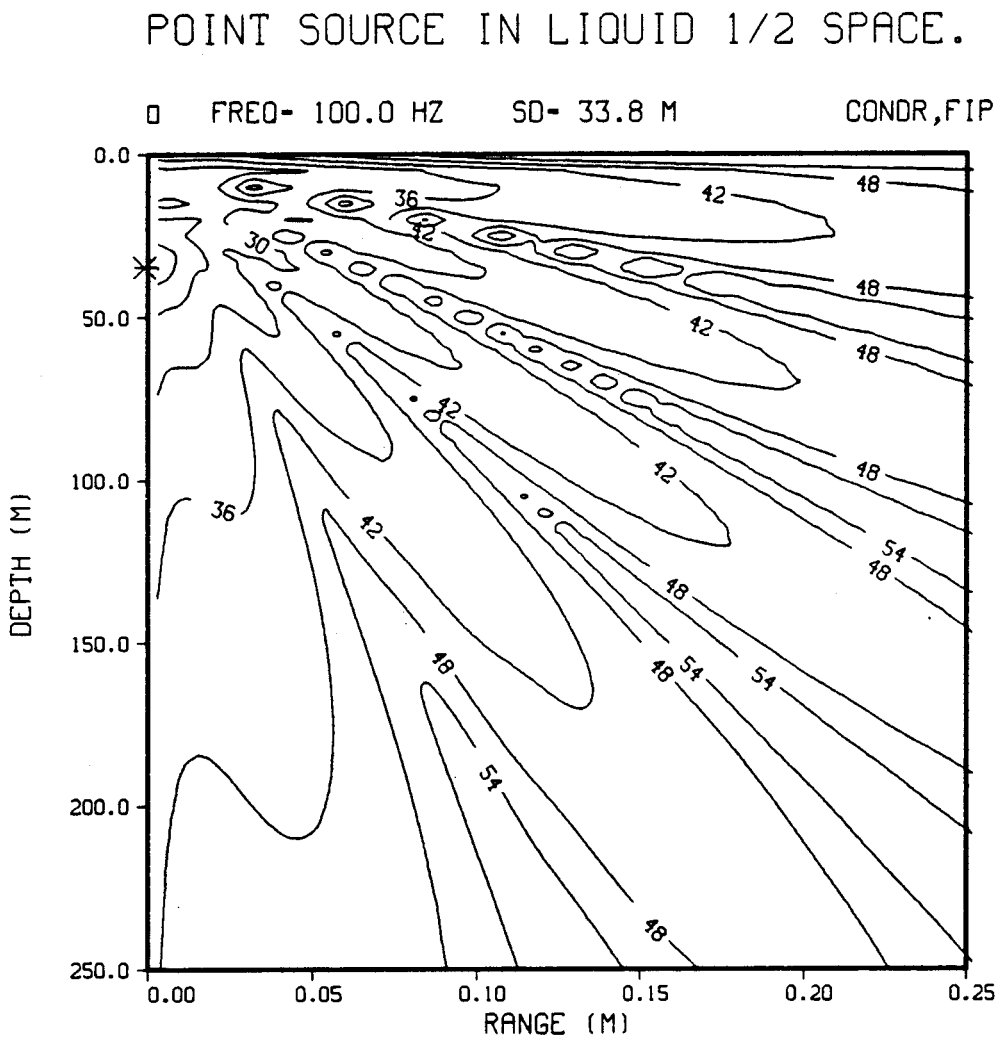
POINT SOURCE IN LIQUID 1/2 SPACE.
FREQ- 100.0 HZ
SD- 33.8 M
CONDR,FIP
DEPTH (M)
RANGE (M)
0.0
50.0
100.0
150.0
200.0
250.0
0.00
0.05
0.10
0.15
0.20
0.25
30
36
42
48
54

of **Figures 12a** and **12b**, showing full planewave and outgoing-only responses in a fluid halfspace to a single imbedded point source. Here it is seen that while the plane wave response is valid at all ranges and incident angles, the spherical wave response taking outgoing waves only in a farfield approximation causes amplitude discontinuities at steep angles and close ranges approaching the source position. It should be noted here, however, that the neglect of the ingoing wave term here is completely arbitrary, and that the complete Bessel function (of both in- and out-going waves) could readily be used if desired, with however an associated additional cost in CPU time (TSANG et al, 1974).

Having neglected the incoming $H_0^{(1)}$, we can now replace the remaining Hankel function $H_0^{(2)}$ as noted above with its large-argument asymptotic expansion (ABRAMOWITZ and STEGUN, 1964, 2.33.4)

$$H_0^{(2)}(k_r r) = \left[\frac{2}{\pi k_r r} \right]^{1/2} e^{-i(k_r r - \pi/4)}$$

This asymptotic farfield approximation is generally valid for horizontal source-receiver offset ranges sufficiently large that $k_r r > 3$, although as source frequency decreases the minimum offset for a given accuracy should be decreased (FUCHS, 1969; KENNETT, 1984, personal communication). Thus the equations above may be written as

$$w(r,z) \simeq \frac{e^{i(m+1/2)\pi}}{(2\pi r)^{1/2}} \int_0^\infty W(k_r,z)\,(k_r)^{1/2}\; e^{-i\,k_r r}\, dk_r$$

Section 2i

FFP Algorithm

In order to evaluate this numerically via a fast transform approach, at a series of N equally spaced range points, with sample spacing Δr, both the horizontal wavenumber k_r and horizontal range r are discretised so as to be evaluated only at:

$$k_{r_n} = k_{r_o} + n\,\Delta k_r \qquad n=0,1,2,\ldots(N-1)$$

$$r_m = r_o + m\,\Delta r \qquad m=0,1,2,\ldots(N-1)$$

where the Fourier condition (BRIGHAM, 1975) must hold that

$$\Delta r\,\Delta k_r = 2\pi/N, \text{ where } N = 2^L, \quad L=0,1,2\ldots$$

using a standard radix-2 FFT program.

The field integrals can now be evaluated over k_r as

$$F(r,z) = (2\pi)^{-1/2}\, e^{i(m+1/2)\pi/2} \int_o^\infty f(k_r,z)\,(k_r)^{1/2}\, e^{-irk_r}\, dk_r$$

which can be rewritten in discrete form as

$$F(r,z) \equiv \Delta k_r e^{-i[k_{ro} rm - (m+1/2)\pi/2]} \sum_{n=o}^{m-1} \left(f(k_{r_n}, z) e^{-ir_o n\Delta} e^{-i2\pi mn/N} \right)$$

When N is 2 raised to an integral power, the discrete wavenumber summation can be rapidly performed via an FFT for the quantity in (brackets), which is input to the Fast Fourier Transform.

This yields the range-frequency domain representation of the wavefield at all m discrete (unaliased) ranges, essentially simultaneously. As has long been realised, this approach is ideally suited for rapid computation of the total seismic/acoustic wavefield over multiple ranges, for a single frequency ω, once the central Green's function kernel has been obtained (in ocean acoustic transmission loss modeling; see Section 3(b)).

The FFP integration method was originally instituted for both k_r and ω integrations in SAFARI, for both CW acoustic and pulse seismic computations. However, for more complex multilayered models (where pulse applications requiring Fourier synthesis over a wide bandwidth is desired), due to the relation between the horizontal wavenumber k_r and range discretisation Δr, the Fast Field integration technique did not always prove very convenient or fast. This is especially the case when transfer functions have to be determined over a wide frequency bandwith, for multiple fixed receiver ranges, as is the case when most standard synthetic seismograms are to be generated.

A direct trapezoidal rule, as originally described, was found to be more effective in the k_r integration in SAFARI for the synthetic seismic applications pursued below (see Section 3(b) and 3(c)), with no significant negative effects on total calculation time for most realistic cases considered (SCHMIDT, 1984, personal communication).

As a third alternative numeric integration strategy, since the Green's function integrand is in general very oscillatory only in restricted regions of the k_r spectrum (requiring denser sampling only in these regions), FUCHS and MULLER (1971), in their original "reflectivity" formulation of a complete wavefield solution, introduced the transformation $k = \omega/\alpha$ from horizontal wavenumber to angle of incidence, where α_{max} is the maximum phase velocity and α the incident angle,

$\theta = \sin^{-1}(\alpha / c_{max})$.

While a convenient expedient for fast estimates of overall Green's function behaviour, integration over real angles only has the potentially serious shortcoming of excluding surface and leaky/trapped mode effects, which can be very significant in marine vertical seismic and teleseismic crustal modeling. For surface wave studies and/or very near source-receiver configurations, the reflection angle integration must thus be extended to complex angles of incidence (STEPHEN, 1977).

When k_r integration is complete, the spectral transfer function so obtained is the complete frequency response for the multilayered medium for one or more given source configurations, the standard output of ocean acoustic transmission loss calculations (see Section 3(b) below) for a given receiver location. For synthetic seismogram generation, this frequency domain response is then itself multiplied by an appropriately chosen input source spectrum (typically the weighted double sine pulse of KUEPPER, 1958; FUCHS and MULLER, 1971), followed by the frequency-to-time inverse FFT, over a discrete set of frequencies, to yield the final full wavefield synthetic time series seismogram response.

It should be noted that, once the Green's function impulse response has been calculated, it is possible to choose any

source wavelet for convolution with the frequency-integrated response series to generate synthetic seismogram records. However, it has often proven desirable to select an input source wavelet which is both symmetric and zero everywhere except for a limited time interval (for optimal resolution). The wavelet cited above, having functional form

$$f = \sin\omega t - n/n+2 \sin(n+2/n\omega t),\ n=1,2,3\ldots$$

first given by MARTIN (1935) and KUEPPER (1958) fits this purpose ideally, where n is the number of wavelet extrema and t the pulse duration.

Other possible numeric integration schemes (for example, generalised Filon and adaptive quadrature) are discussed in FRAZIER et al, 1984).

Section 2(j)

Consideration of (Computational) Conditions Necessary for Accurate Green's Function Results

Since the Green's function (unit impulse response) embodies all the essential elastodynamic and seis-mechanical properties of the layered medium in question, and can subsequently be used to derive wavefield solutions in terms of physical quantities, the output of the DGM stage of "SAFARI" should be at least provisionally examined in terms of its absolute and machine-dependent accuracy. The references here are analytic problems with known exact solutions where possible, and otherwise against standard reference/benchmark test problems as computed by other known algorithms.

As is well known, the theoretically infinite sampling density in k_r, infinite representation accuracy and infinite integration range required for exact evaluation of the Green's function integrand cannot be practically realised in a computer. It is therefore first necessary to determine whether, for a given error tolerence ε (larger than the representation error inherent in the computer), the numeric algorithm and machine implementation thereof will calculate approximate values G* so that G-G* is always less than ε, for a specific subset over k_r of interest.

In fast field programs, considering numeric integration, the main errors are those related to "finite windowing" and "discrete sampling" of the continuous Green's function integrand. Whereas the error associated with discrete sampling of the continuous Green's function integrand can be shown to decrease to some limit with the number of samples in general, the typical error induced by the truncation plus smoothing operations are filter and problem dependent.

Such problems are particularly acute when considering the Green's function integrands resulting from large multilayered media models. This is because, as MULLER and SCHOTT (1979), KENNETT (1983) and FRAZER et al (1984) have recently discussed, the vast majority of Green's function integrands arising in both underwater acoustics and solid earth seismology, of the general form [Figure 3]

$$\text{Field} = \int_a^b G(k_r,z)\, J_m(k_r r)\, dk_r$$

inevitably have a rapidly oscillating and in general highly complicated structure, particularly when the integration path passes near the 'shoulders' of the poles displaced by attenuation from the real axis. The integrand $G(k_r z)$ can be seen to be composed of oscillatory terms, whose precise character depends in nontrivial fashion upon source number type and depth in each layer, distance between source and major layer boundaries as well

Figure 13

Typical oscillatory Green's impulse response function integrand (showing large few-featured zones and localised multi-featured region)

INTEGRAND

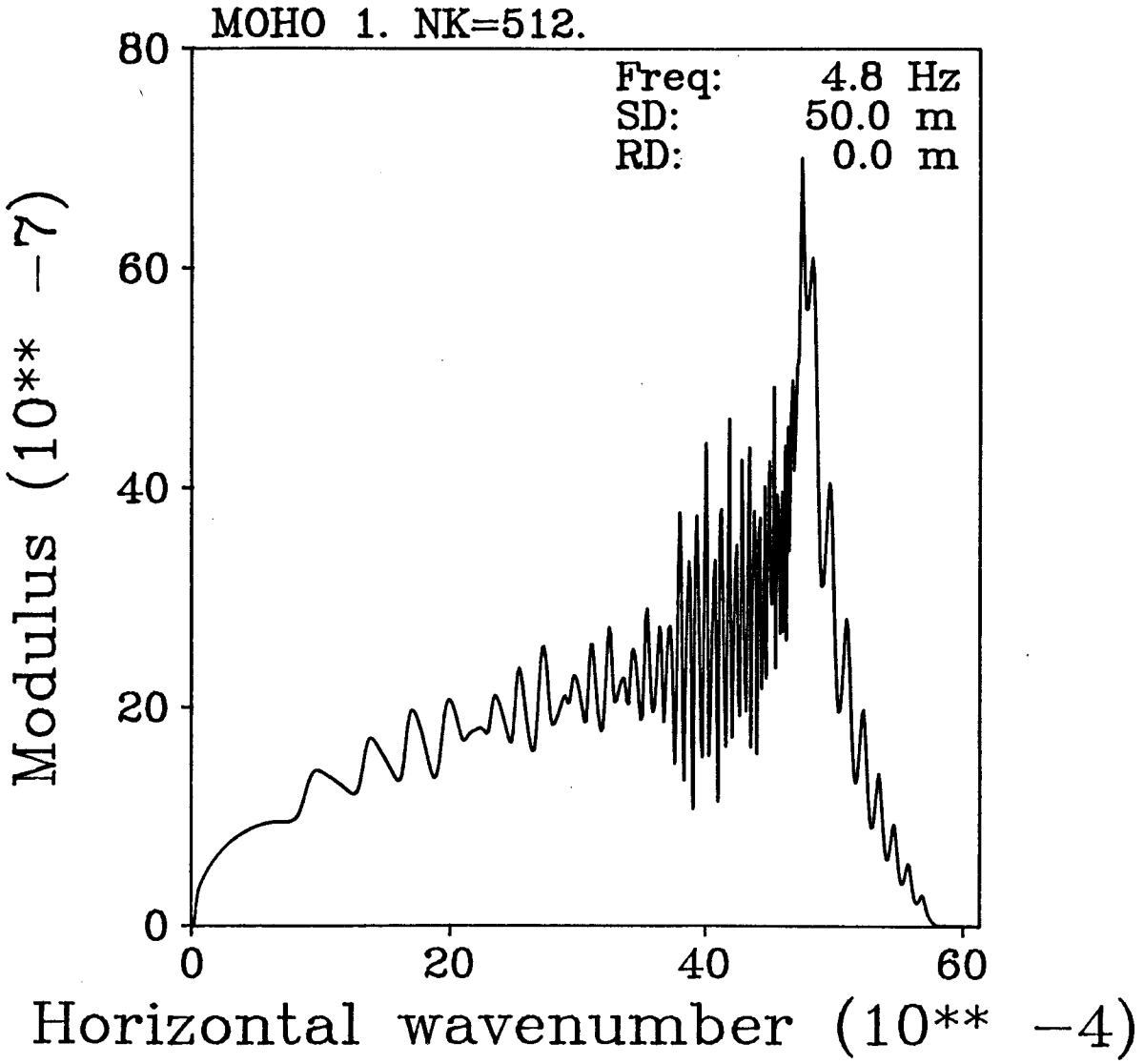
MOHO 1. NK=512.
Freq: 4.8 Hz
SD: 50.0 m
RD: 0.0 m
80
60
40
20
0
0
20
40
60
Modulus (10** −7)
Horizontal wavenumber (10** −4)

as the elastic properties of these, and the argument of the range-dependent Bessel's function itself (so that in general both J_o and the terms multiplying it can be highly oscillatory; HAMMING and EPSTEIN, 1972; LUKE, 1954). These factors make detailed considerations of comparative numeric integration options for specific applications of interest a serious requirement (in terms of both accuracy and runtime).

Considering the k_r integration limits first, k_r is typically a large parameter, which can be either real or complex. The Green's function integrand in general is here bounded by well-behaved values that approach zero at small and large wavenumbers. Thus the interval between these limiting wavenumbers kmin and kmax represent in general a partial segment of a longer contour in the complex wavenumber plane. As a consequence, a further complication common to all complete wavefield solutions requiring direct numeric integration of the Green's function integrand is the problem of appropriately choosing kmin and kmax, related to phase velocities cmax and cmin respectively by the relation $k=2\pi f/c$. If the integration interval is too small or too abrupt, not only can significant physically-real wave types be ignored, but for the later case unphysical truncation artifacts can lead to noncausal arrivals in subsequently computed synthetic seismograms. On the other hand, if the interval is too large, the desired body wave response can be entirely swamped by the dominant high-amplitude surface wave modes. In addition,

computational time is increased as the total integration interval is made larger.

Thus for layered earth models where only partial (body wave information is desired, correctly chosen and implemented k_r integration requires optimal selection and application of a smoothing filter over the k_r limits to avoid Gibb's oscillation phenomena. This has been shown to be of particular concern for specific surface source/receiver configurations, where decay of the Green's function kernal as a function of k_r is slower than otherwise.

To consider the integration complexities presented by the Green's function in more detail, in many underwater acoustic and solid earth seismic modeling scenarios, the Green's response function curve is characterised, even at high wavenumbers, by a succession of many closely separated narrow peaks, related directly to the eigenmodes of the effective waveguide in question (which will resonate strongly as attenuation is decreased). It has been found in synthetic seismic modeling that use of the discrete Green's function integrand can additionally lead to distorted waveform results, on account of computer inability to treat the often very large numbers represented by (unattenuated) Green's function peaks.

As a general conclusion from the above, it is clear that care must be taken to avoid confusing localised sampling or smoothing dependent artifacts for real response features. For the general integrand, it remains unclear exactly how to determine the precise connections between (1) satisfaction of straightforward mathematical error reduction criteria for convergence on the one hand, and (2) the actual geophysical approach of discrete Green's function values to the real solution.

Originally, as in the Fuchs-Mueller reflectivity technique, a simple low-order procedure (trapezoidal) or equivalent interpolatory quadrature rule for numeric integration was employed. In applying the trapezium rule for numeric integration, for large k_r, the integration intervals are divided into a "sufficiently large" number of small horizontal sampling intervals Δk_r, the usual criteria for choice of increment size/number of increments depending in simple fashion upon the rate and kind of oscillations observed for the integrand in question. If quadrature type methods are used to evaluate this type Green's function integrand, for most cases very many small (in general equispaced) integration steps will be required in order to track "sufficiently well" the "major" oscillations of the integrand. This leads to many integral sampling points and thus in general a large storage requirement for each frequency ω. Overall Green's function convergence for quadrature rules thus generally requires less sampling for a given accuracy as frequency decreases.

However, as can be seen by inspection, in many circumstances the Green's function is typified by many high peaks in particular narrow wavenumber intervals, separated however by relatively sparsely-populated "no-peak" zones of low or no oscillations. In other words, the convergence of the numeric Green's function solution to the exact value is in general not necessarily uniform when considered as a function of horizontal wavenumber k_r. These questions are further complicated in the SAFARI case, where both multiple receivers and source depths are possible, resulting in a generally nontrivial depth dependence of the Green's function response.

A brute force approach to numeric integration accuracy can be taken, by attempting for any given case to use excessive numbers of sampling points (and working backwards to lesser sample sizes, observing the sampling rate at which "significant" changes appear in the integrand). Here, however, not only is it not always feasible (in terms of computation time) to use gross oversampling, but more fundamentally, precisely when critical wavenumber intervals change/appear/disappear as the sampling is changed, it is not apriori clear whether what is being observed is a real wavefield feature, or whether a certain degree of numeric resolution enforced by the computer has been reached. In such events, the actual width has simply become so small as to be practically unobservable.

The major source of difficulties in specifying a generally optimal numeric integration scheme for highly oscillatory integrands arises precisely from the problem of stating a priori the relations between response position and height and the distribution, depths, thicknesses and elastic parameters of the medium in question. As noted above, a practical criterion is to choose the number of sample points so that Δk_r comprehends the smallest expected Green's function feature width.

As has been suggested elsewhere, a truly rigorous study of numerical convergence and accuracy of this fundamentally-important (Green's function) integrand should be carried out, insofar as possible, directly on the discretised equations themselves qua discrete representations. A corresponding further attempt should be made thereby to identify, in comparison with computer imposed resolution limits, the actually expected widths of critical wavenumber intervals, for at least a series of canonic or extremal problems whose responses are well known (either analytically or by alternate integration paths). Alternate numeric integration should be investigated, with emphasis upon those which can adapt sample requirements to observed integrand behaviour while still remaining computationally economical.

As MULLER and SCHOTT (1980) and others have discussed, both finite source frequency bandwidth and Nyquist frequency requirements impose practical limits on the upper frequency of **k** integration. The synthetic seismic time series obtained after DFT is necessarily of fixed length and cyclic nature (BRACEWELL, 1978; BRIGHAM, 1977), so that the possibility of 'time aliasing' of later in earlier arrivals must be specifically allowed for. This proves especially important in exact synthetic VSP calculations for far source-receiver offset configurations. To date antialiasing has been achieved either by utilising a reversible amplitude scale-down scheme (ROSENBAUM, 1974) or more generally by employing a sufficiently large time window so as to contain all important high amplitude seismic arrivals of interest. The later has proven the most expedient method in the present studies.

As in **k** integration, because Fourier synthesis is necessarily computed over a finite frequency bandwidth, the transform must be carefully smoothed in truncation, to prevent parasitic Gibb's oscillations on either side of principle arrivals.

In FFT based **k** integration, the net waveform is available from t° to $t^{\circ} + 1/\Delta f$, where Δf is the frequency bandwidth $f_{max} - f_{min}$. Since the time duration of the received waveform will generally increase with increasing source-receiver offset, Δf must be small enough so that the time duration of the waveform is adequate at the largest offsets of interest. **Figures 14a-c** show typical

ringing on synthetic offset VSPs for the case of too small a frequency interval of integration, which increases with offset.

Figure 14

Typical time domain "ringing" in synthetic fullwave VSP seismogram due to Gibb's oscillations (arising from too abrupt a truncation of the frequency spectrum; oscillations increasing with offset)

VERTICAL PARTICLE VELOCITY

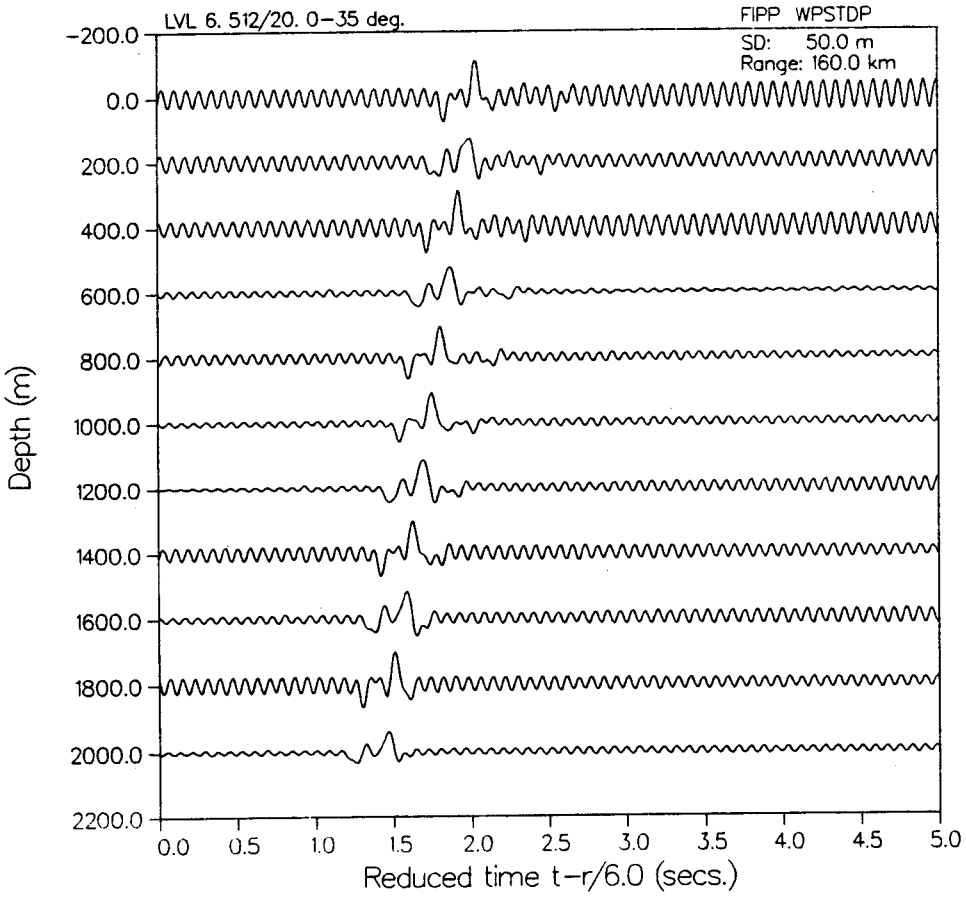

15.00.52 THUR 28 MAR, 1985 JOB-TRN0D , NORDA OISSPLA 9.2

VERTICAL PARTICLE VELOCITY

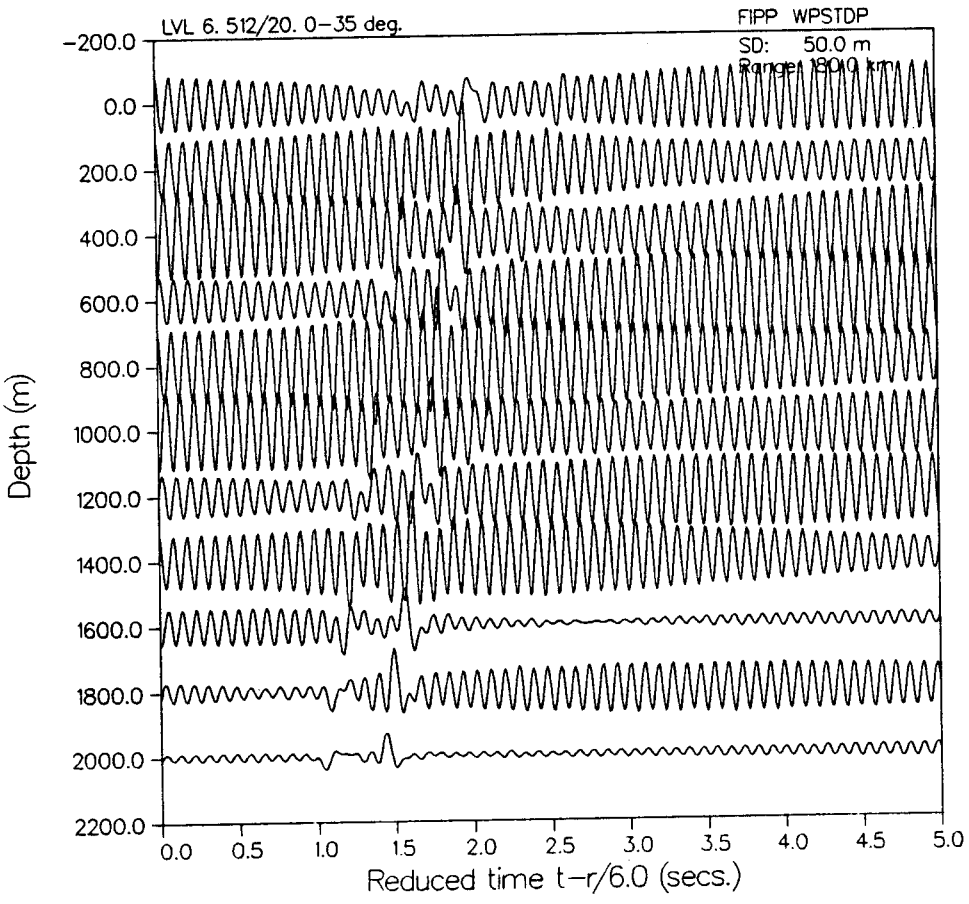

15.18.38 THUR 28 MAR, 1985 JOB-TRANS , NORDA DISSPLA 9.2

VERTICAL PARTICLE VELOCITY

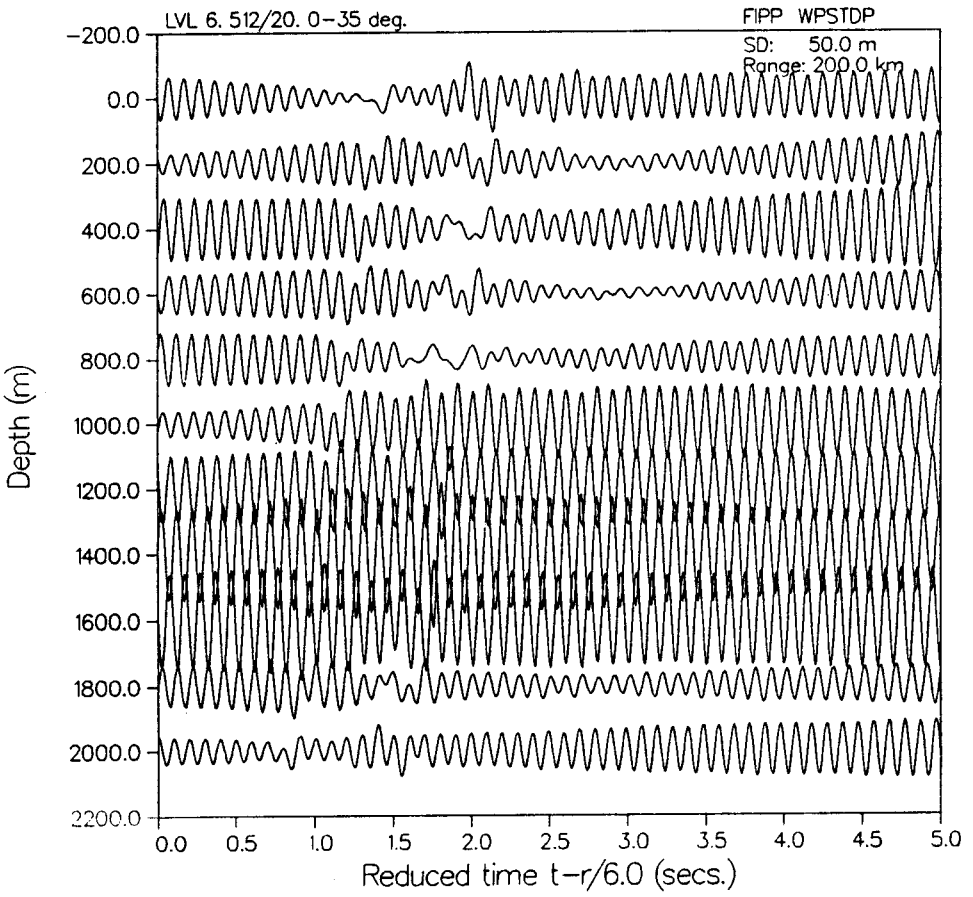

As is now long routine in deep crustal seismology (FOERTSCH, 1951; in GIESE et al,1976), in order to allow for following in detail only specific arrivals as localised within a smaller (and computationally faster) time window, the present "SAFARI" program also includes the option to generate a 'reduced' time seismogram, computed by multiplying the $G(r,\lambda)$ spectrum for each r by $\exp(-i\lambda r/c_{red})$, where c_{red} is chosen to correspond to the group velocity of the arrivals of interest (AKI and RICHARDS, 1980), or else selected to facilitate phase correlation of the maximum number of events within a specific time/range window. **Figure 15a** shows typical time domain wraparound aliasing which results from selecting too short a time integration window. **Figure 15b** shows the correct response.

Figure 15

a/ typical time domain "wraparound" aliasing in a reflectivity synthetic seismogram (arising from too small a total time integration window)

b/ correct response

VERTICAL PARTICLE VELOCITY

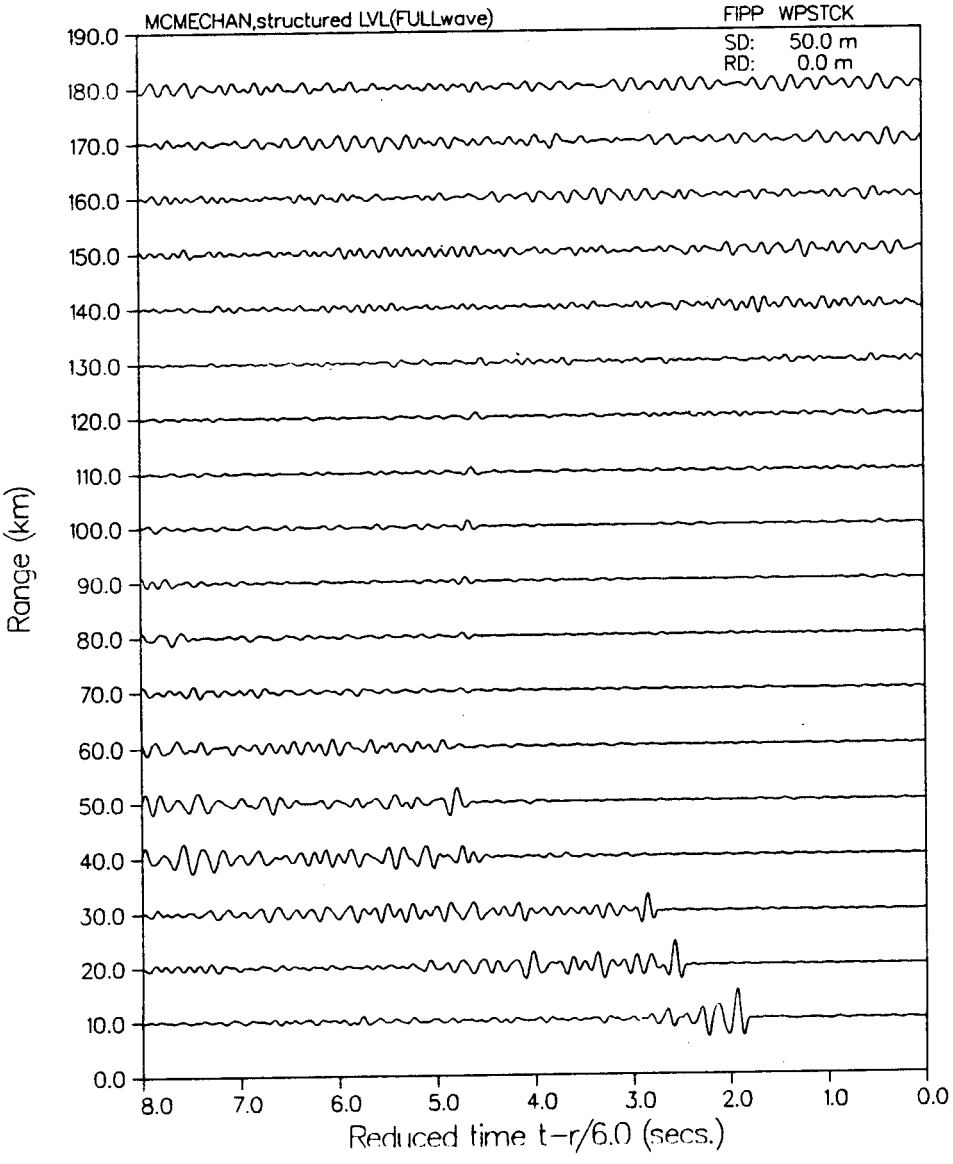

VERTICAL PARTICLE VELOCITY

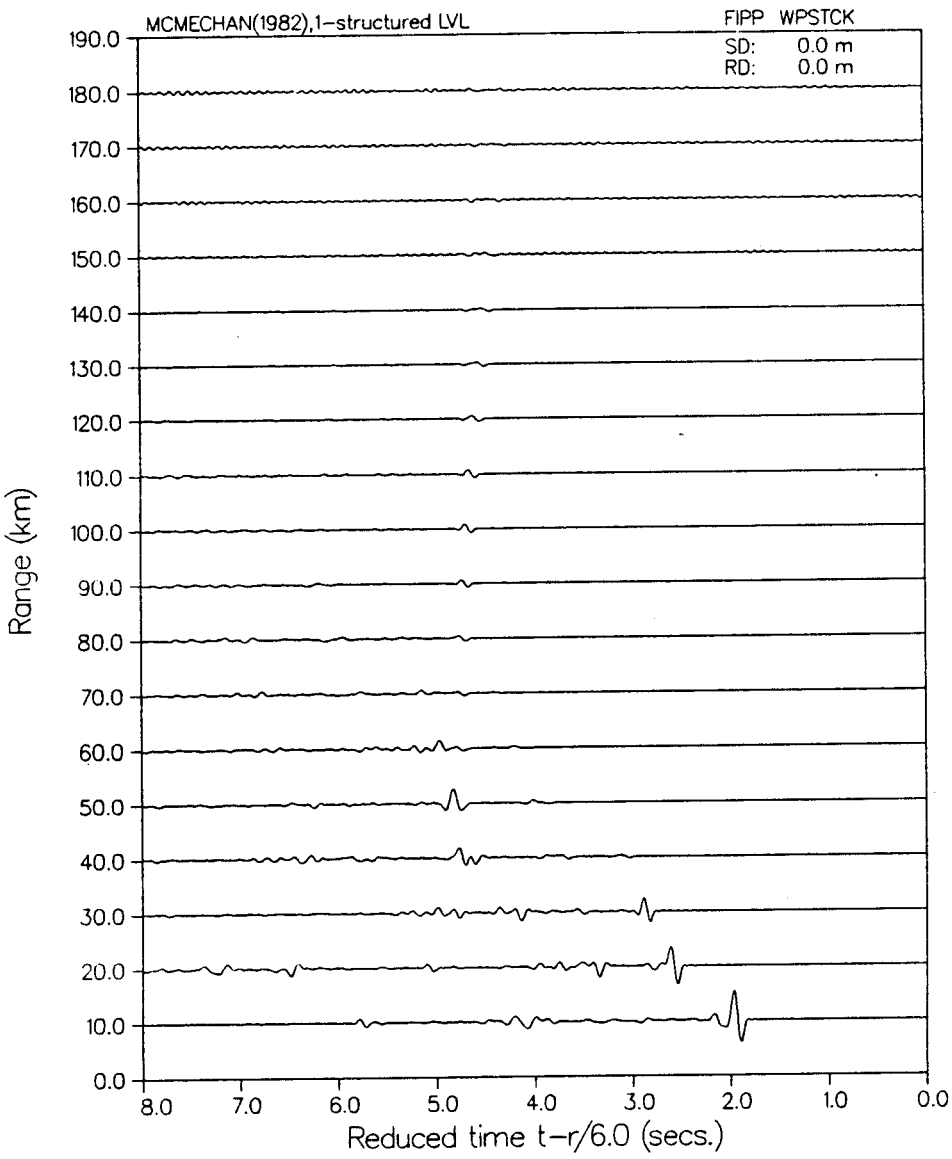

Section 2(k)

Accuracy Tests of Green's Function: Results

A representative set of numerical validation calculations, prior to employing the Green's function integrand (computed by the DGM/FWE method in SAFARI) for actual applications, is considered in this section, using a diverse selection of widely-known analytical and numeric reference solutions. The select numeric examples have been chosen to illustrate classic features of Green's function and synthetic wavefield behaviour for specific geomodels in both underwater acoustic and solid earth seismic modeling applications, emphasising requirements for practically attaining correct and complete solution representations from numeric integration.

It was infeasible to computationally validate SAFARI code behaviour in all respects against all possible test cases. Due to the further unavailability of particular algorithms for comparison testing, 5 basic external verification tests are given here, as comparisons of SAFARI output to both theoretically known (3 and 4) and other numerically-computed solutions (1,2,5), for both fluid (1,2,3) and solid (4,5) media, in both monofrequency (1,2) and multifrequency pulse applications (3,4,5). These tests were selected to fall within the same general classes of environmental properties and experimental configurations as

those routinely modeled in underwater acoustic, seismic and ultrasonic applications. Specific parameters were chosen to comprehend at least partially the extreme range of possible conditions encountered.

The first test compares SAFARI's reliability and accuracy when considering the canonic problem of a single fluid layer overlying a solid halfspace, for a monofrequency CW source in the water column. This is the classic Pekeris layered waveguide problem, routinely encountered in underwater acoustics as a test case (Test 3b in the NORDA Parabolic Equation Workshop; DAVIS et al, 1982), and here employed in both Test 1 (reference computed by Normal Mode solution; JENSEN and FERLA, 1980) and TEST 2 (computed by the FFP model of KUTSCHALE (1972)). This same 1 layer waveguide environment is employed again in Test 3, which computes the theoretical dispersion curves, as per EJP(1957) the Pekeris layer model is employed to compute the theoretically-expected received waveform for a single receiver at depth, for the same geomodel and experimental parameters as given by PEKERIS (1948) and FRAZIER and RUDMAN (1980). Finally, in Test 5 the completeness of the full wavefield seismic solution is examined for the MOHO1 and LVL6 test cases of synthetic crustal seismograms after BRAILE and SMITH (1975), the 'tunneling wave' model of FUCHS and SCHULTZ (1976), and the S* arrival model of CERVENY et al (1971).

Other additional comparison tests, against other numerical models and empirical data, from (i) VLF underwater acoustics, (ii) deep crustal and (iii) vertical seismic profiling, are given in Sections 3(b), 3(c) and 3(d) respectively below, and are further considered elsewhere (see references). More detailed accuracy and applications testing is underway.

No attempt is made here to delimit the absolute theoretic accuracy and/or program features of the comparison algorithms employed.

TEST 1: CW Point Source Response in a Single Layered Fluid Pekeris Waveguide

The first figures [Figures 16 a-g] constitute initial results of comparative numeric accuracy testing for the overall solution and specific arithmetic values of the Green's integrand response function. The reference case is Test Case 3b (DAVIS et al, 1982) for CW underwater acoustic propagation modeling, as computed by the SAFARI 'Fast Field' program of SCHMIDT (1982), and for reference by the SNAP Normal mode program of JENSEN and FERLA (1980).

This model is chosen here because it embodies all the essential features of shallow water propagation problems, routinely encountered in transmission loss prediction, geobottom environmental reconnaissance and detection simulation in underwater acoustic modeling.

For the case of a fluid layer overlying a solid halfspace, the wavenumber spectrum is comprised of discrete, continuous and evanescent modes, corresponding to trapped acoustic rays (reflecting between water column and bottom at precritical incident angles), 'leaky' acoustic rays/modes (partially reflected and refracted at postcritical angles) and seismic surface/interface waves at submodal cutoff frequencies. The Green's function resonance peaks for all 3 contributions are

Figure 16

Computational accuracy tests of "SAFARI" [CW FIP version]

a,c,e: Green's function integrands (NK=1024,2048,4096)

b,d,f: Corresponding TL vs range plots

g: Comparison of SNAP (SACLANT Normal Adiabatic Mode) and NORDA IFDPE (Parabolic Equation) TL results with Kutschale FFP

h,i: Comparison of PE and SAFARI range-depth TL contours

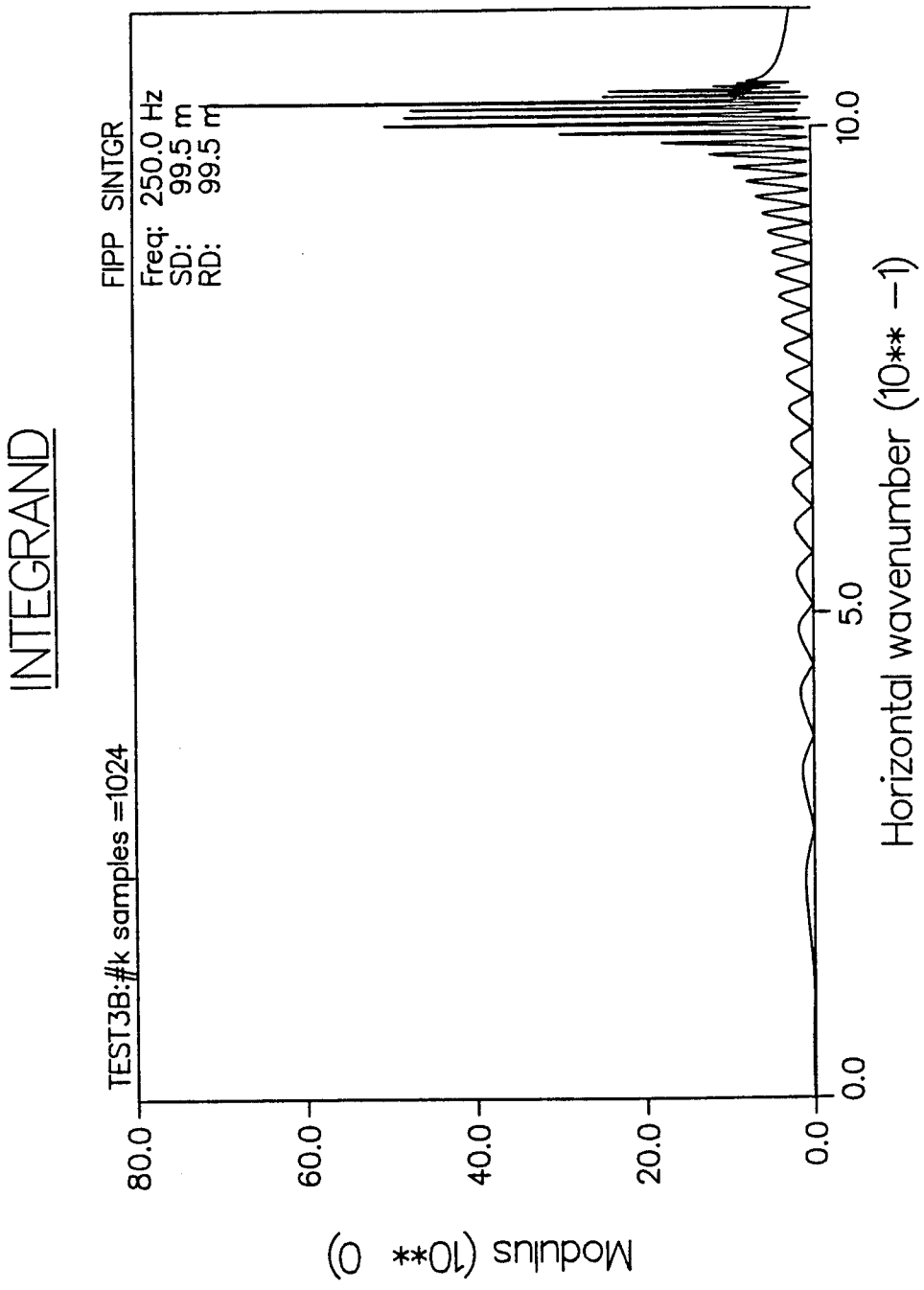
INTEGRAND
TEST3B:#k samples =1024
FIPP SINTGR
Freq: 250.0 Hz
SD: 99.5 m
RD: 99.5 m
80.0
60.0
40.0
20.0
0.0
Modulus (10** 0)
0.0
5.0
10.0
Horizontal wavenumber (10** −1)

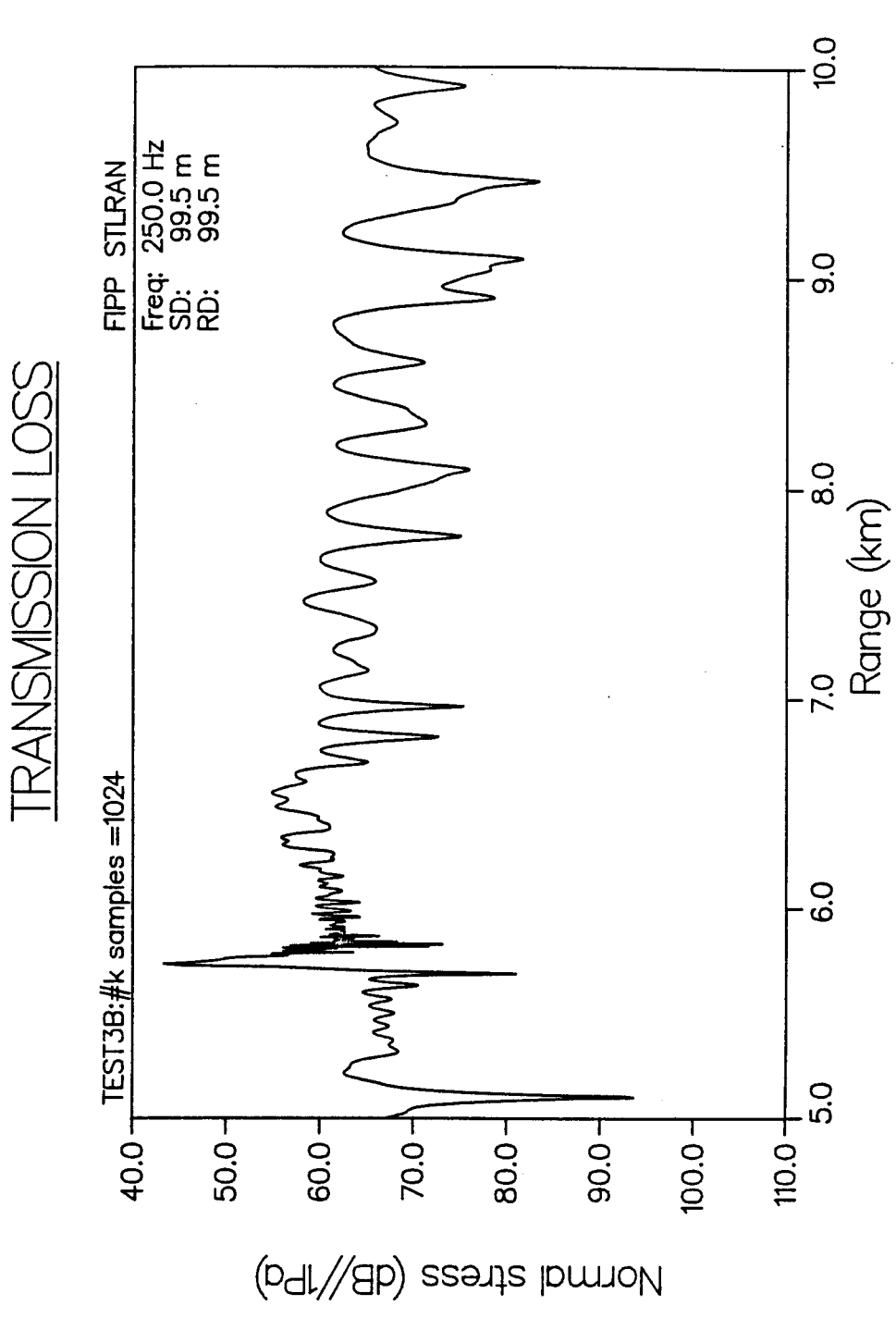
TRANSMISSION LOSS
TEST3B:#k samples =1024
FIPP STLRAN
Freq: 250.0 Hz
SD: 99.5 m
RD: 99.5 m
Normal stress (dB//1Pa)
40.0
50.0
60.0
70.0
80.0
90.0
100.0
110.0
5.0
6.0
7.0
8.0
9.0
10.0
Range (km)

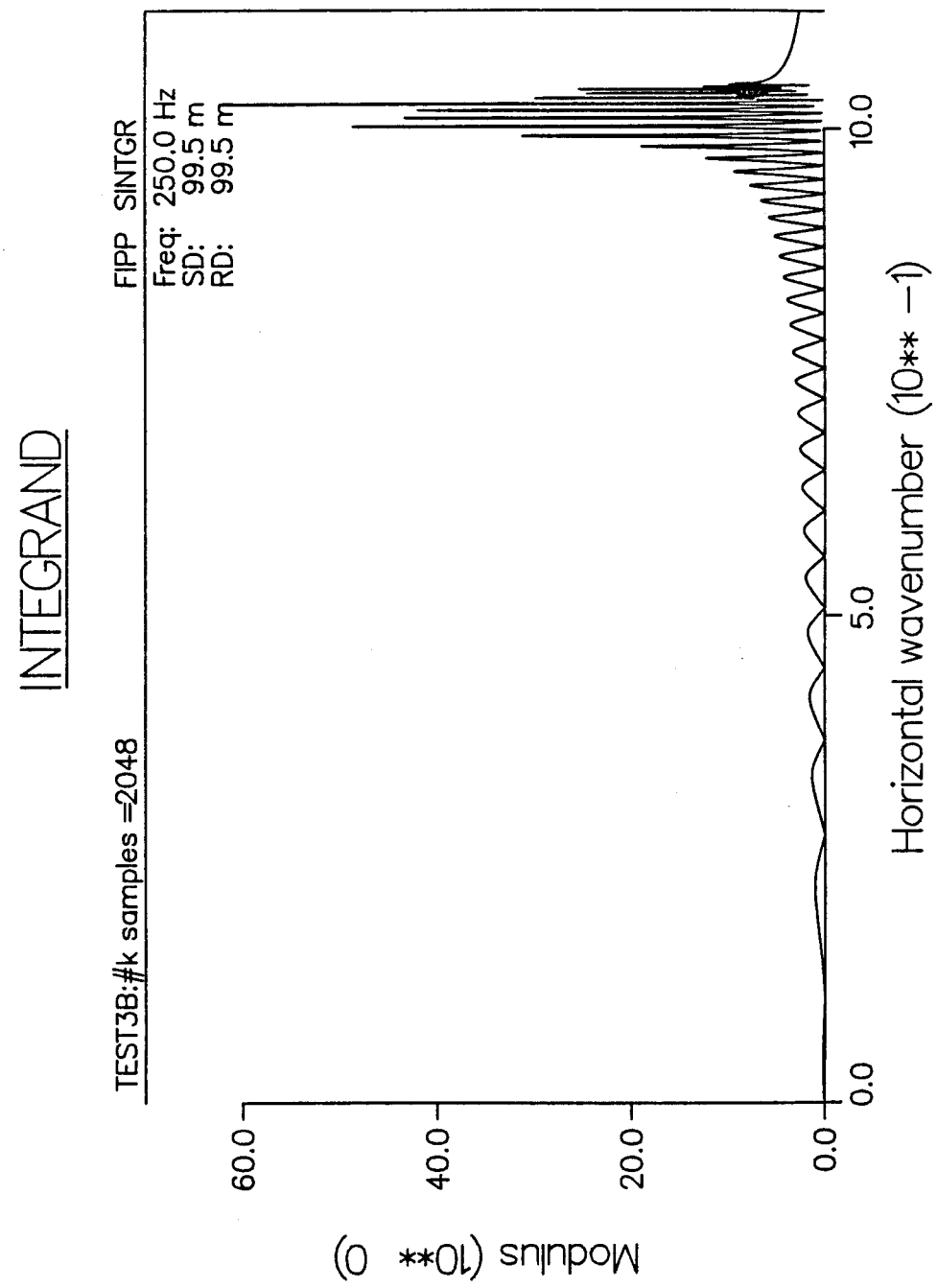
INTEGRAND
TEST3B:#k samples =2048
FIPP SINTGR
Freq: 250.0 Hz
SD: 99.5 m
RD: 99.5 m
60.0
40.0
20.0
0.0
Modulus (10** 0)
0.0
5.0
10.0
Horizontal wavenumber (10** −1)

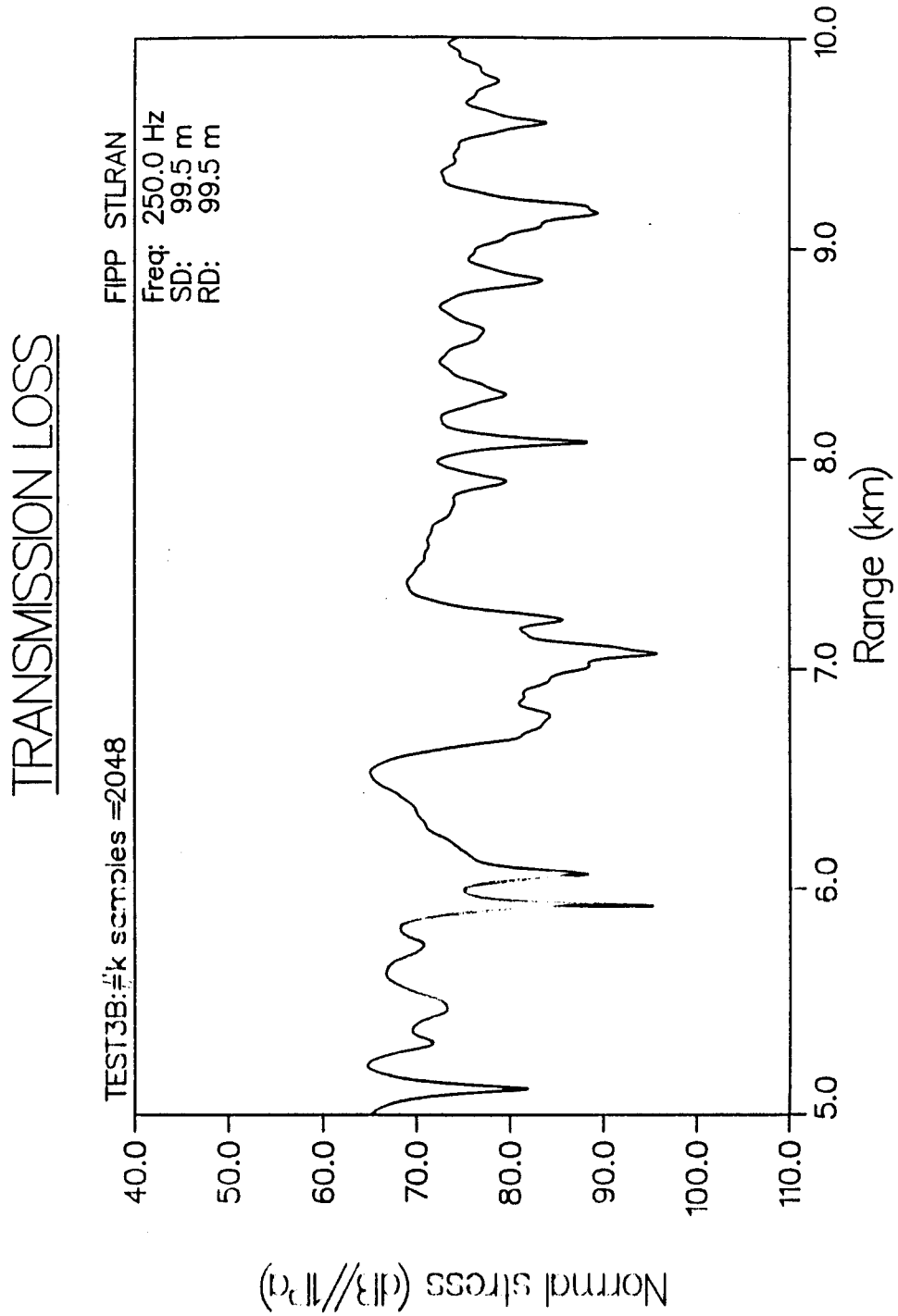
TRANSMISSION LOSS
TEST3B: #k samples =2048
FIPP STLRAN
Freq: 250.0 Hz
SD: 99.5 m
RD: 99.5 m
40.0
50.0
60.0
70.0
80.0
90.0
100.0
110.0
5.0
6.0
7.0
8.0
9.0
10.0
Range (km)
Normal stress (dB re 1 μPa)

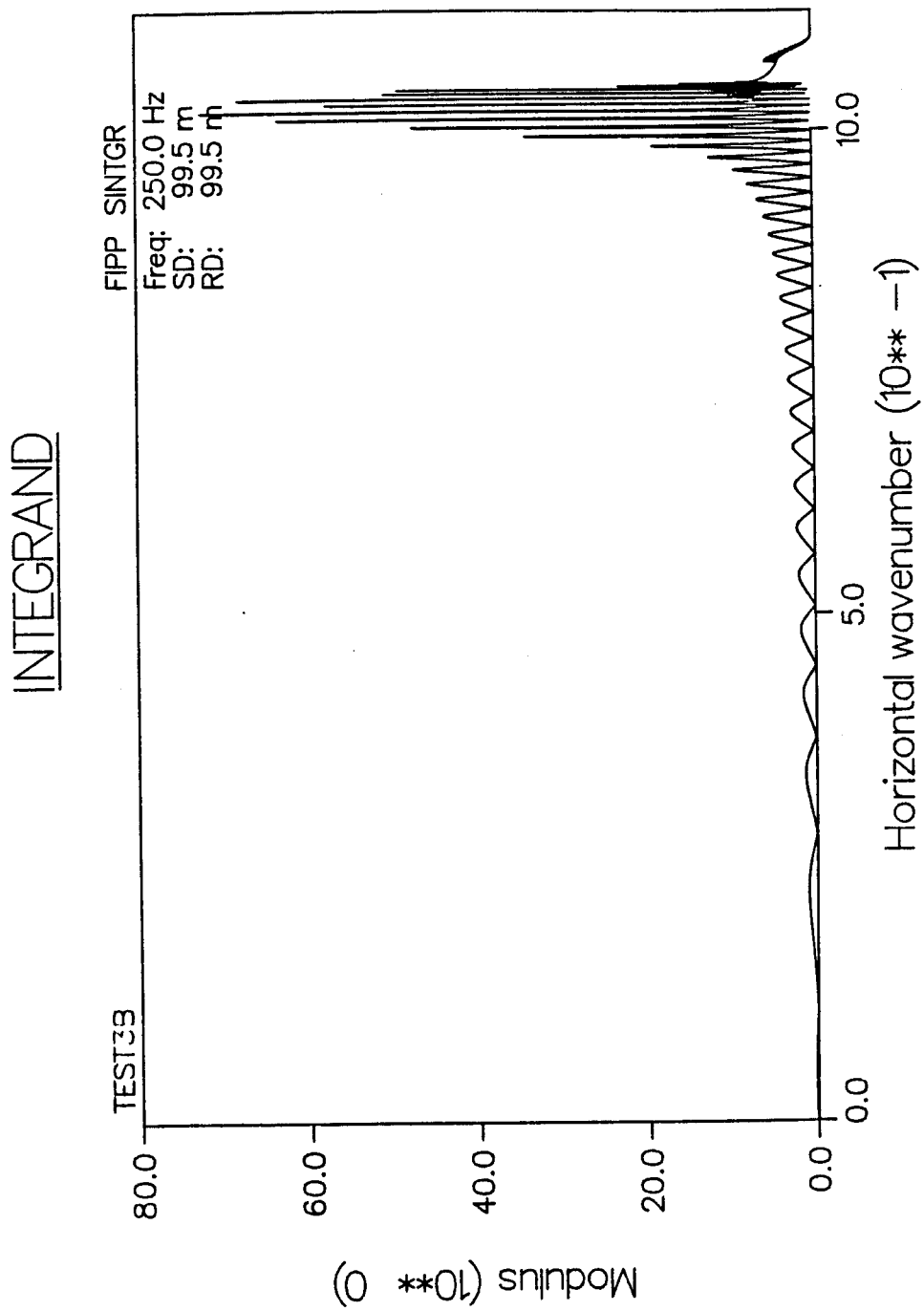
INTEGRAND
TEST33
FIPP SINTGR
Freq: 250.0 Hz
SD: 99.5 m
RD: 99.5 m
80.0
60.0
40.0
20.0
0.0
Modulus (10** 0)
0.0
5.0
10.0
Horizontal wavenumber (10** −1)

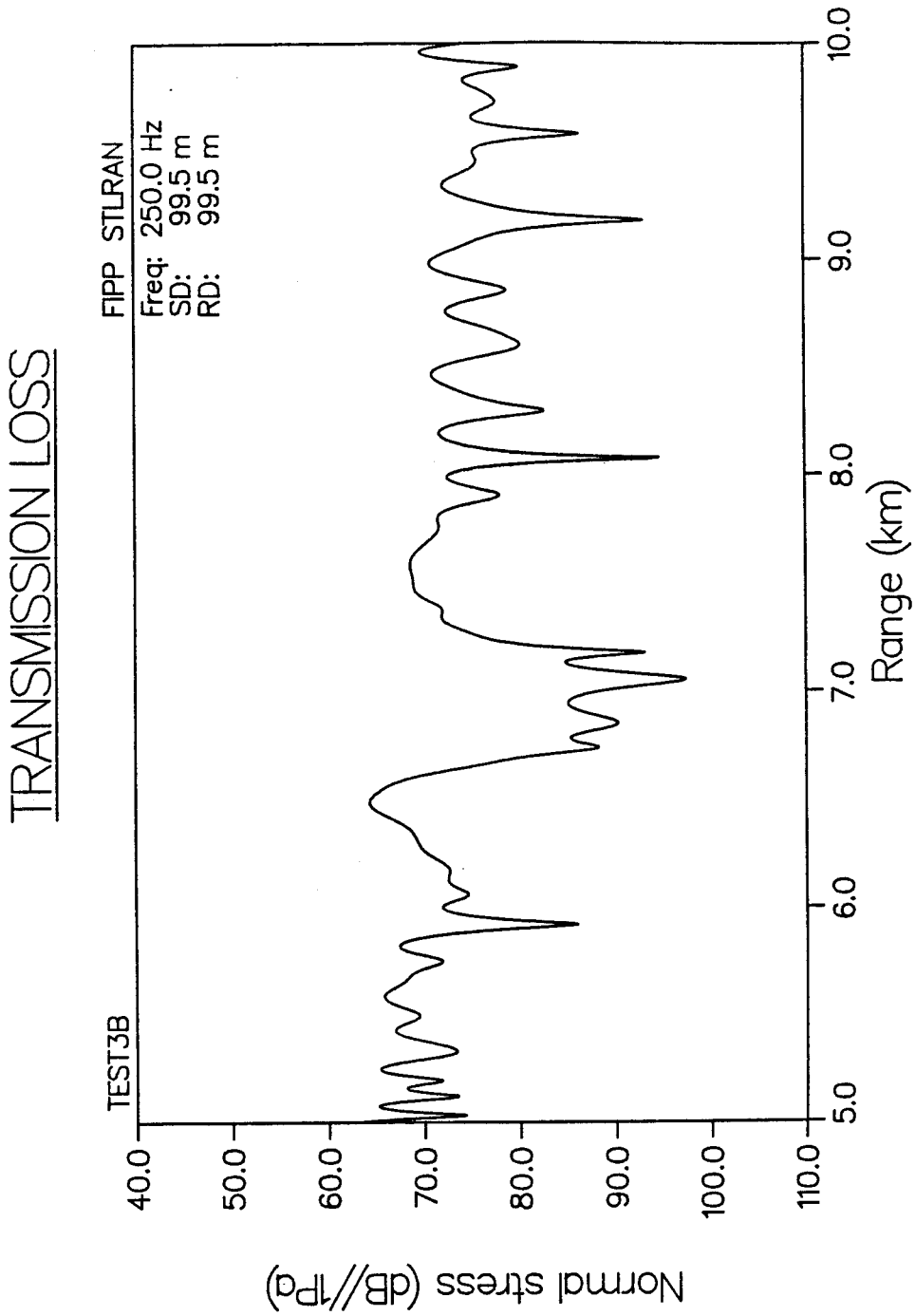
TRANSMISSION LOSS
TEST3B
FIPP STLRAN
Freq: 250.0 Hz
SD: 99.5 m
RD: 99.5 m
40.0
50.0
60.0
70.0
80.0
90.0
100.0
110.0
Normal stress (dB//1Pa)
5.0
6.0
7.0
8.0
9.0
10.0
Range (km)

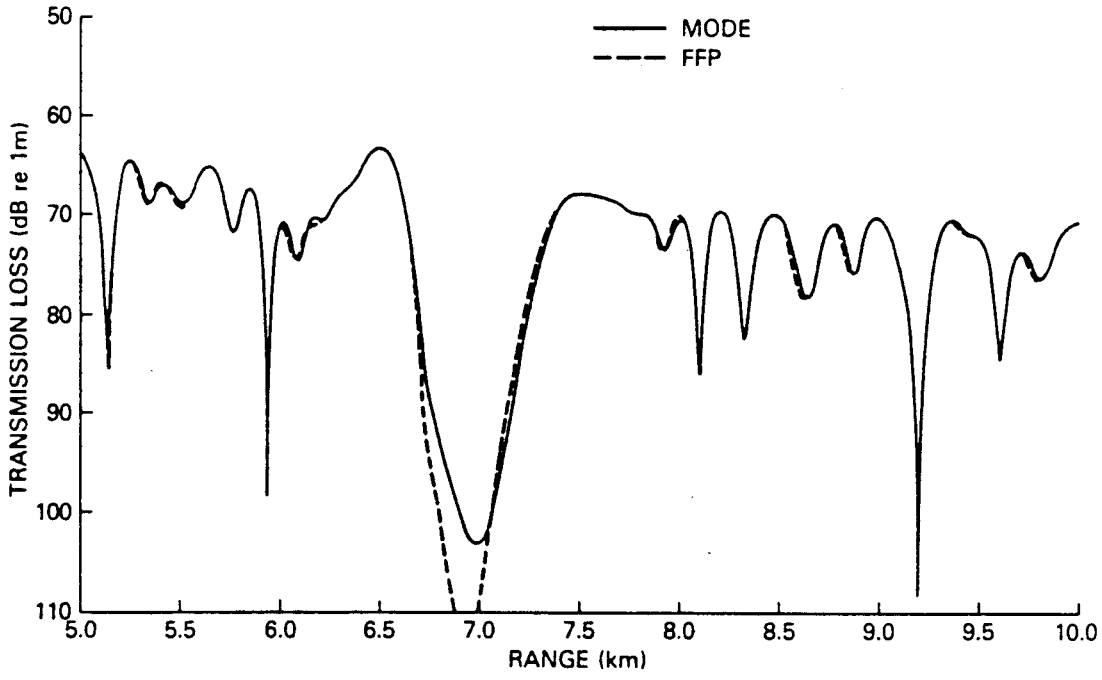

Comparison of MODE (SNAP) and FFP results for Test Case 3B

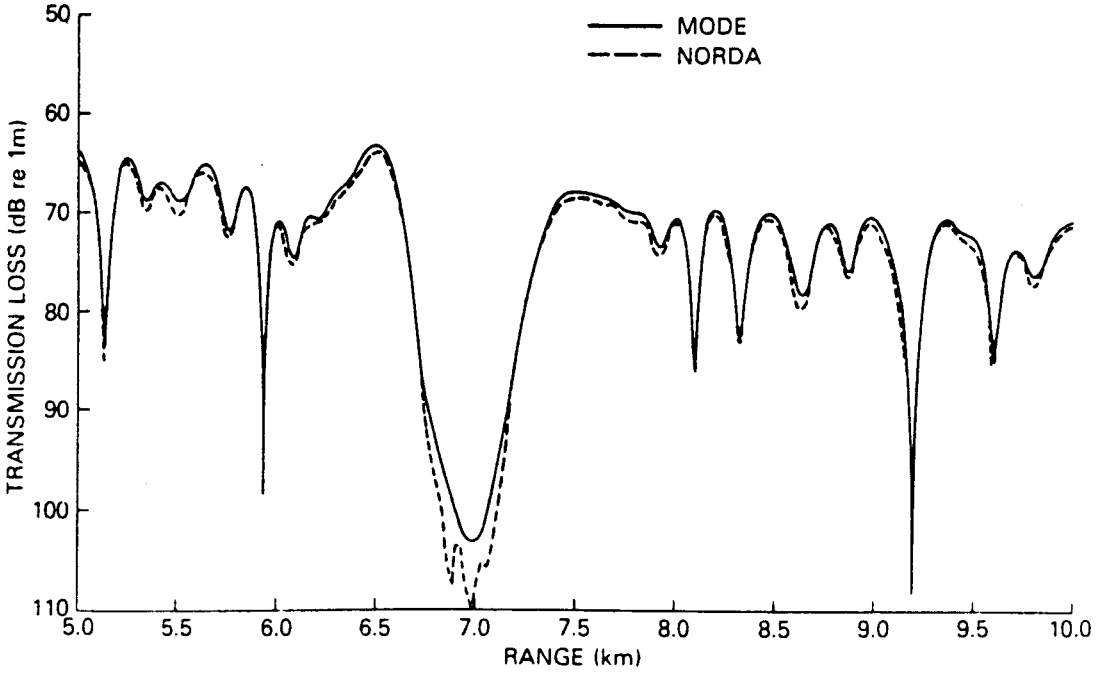

NORDA PE result compared with reference result (MODE) for Test Case 3B

attenuation broadened, both by material absorption in the water bottom and refraction loss thru propagation into the bottom.

Because the FFP technique employed here integrates the complete wavenumber spectrum, the solution obtained necessarily includes the entire discrete, continuous and evanescent mode spectrum, over all near or far field ranges, for all realistic elastic parameters of the media.

Comparing the Green's function integrand computed by SAFARI FFP and that by the SNAP Normal Mode programs, the curves are seen [**Figure 16g**] to agree exactly for all discrete and continuous modes. Direct comparison of exact arithmetic values of the integrand eigenvalues (not given here) shows full agreement at the decimal point limit of the computer employed (7 places; single precision on the VAX 11/780). Only the extreme nearfield shows any discernable difference, due to the absence of evanescent elastic interface waves, as a zeroth-order mode, in the acoustic eigenvalue solution of the adiabatic normal mode program employed. The significance of this difference can be shown to increase for very low (sub acoustic cutoff) frequencies in a geobottom where shear velocity is increased beyond a certain fraction of water column compressional sound speed (see Section 3(b) below).

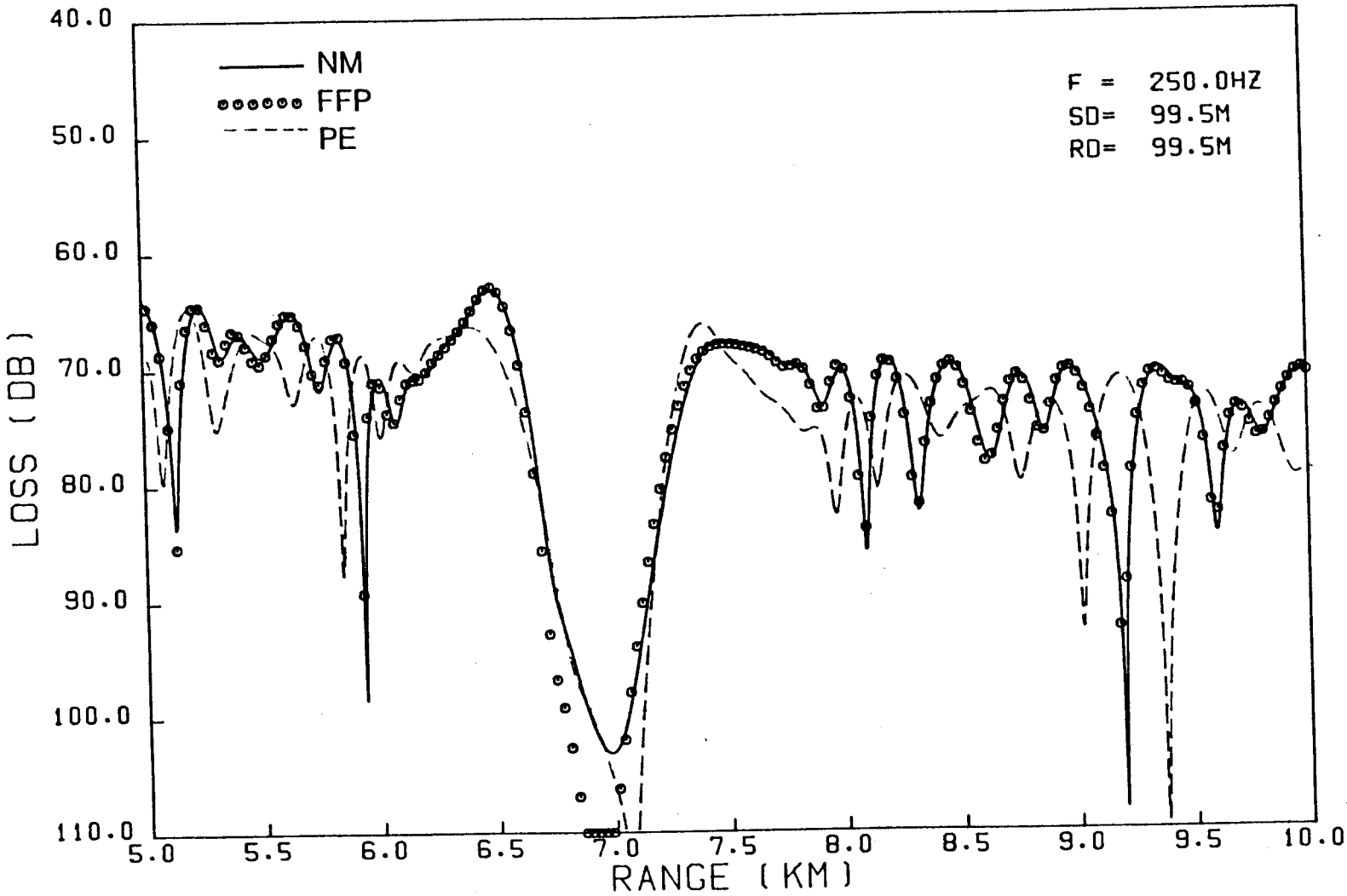

INTER-MODEL COMPARISON FOR CASE 3B

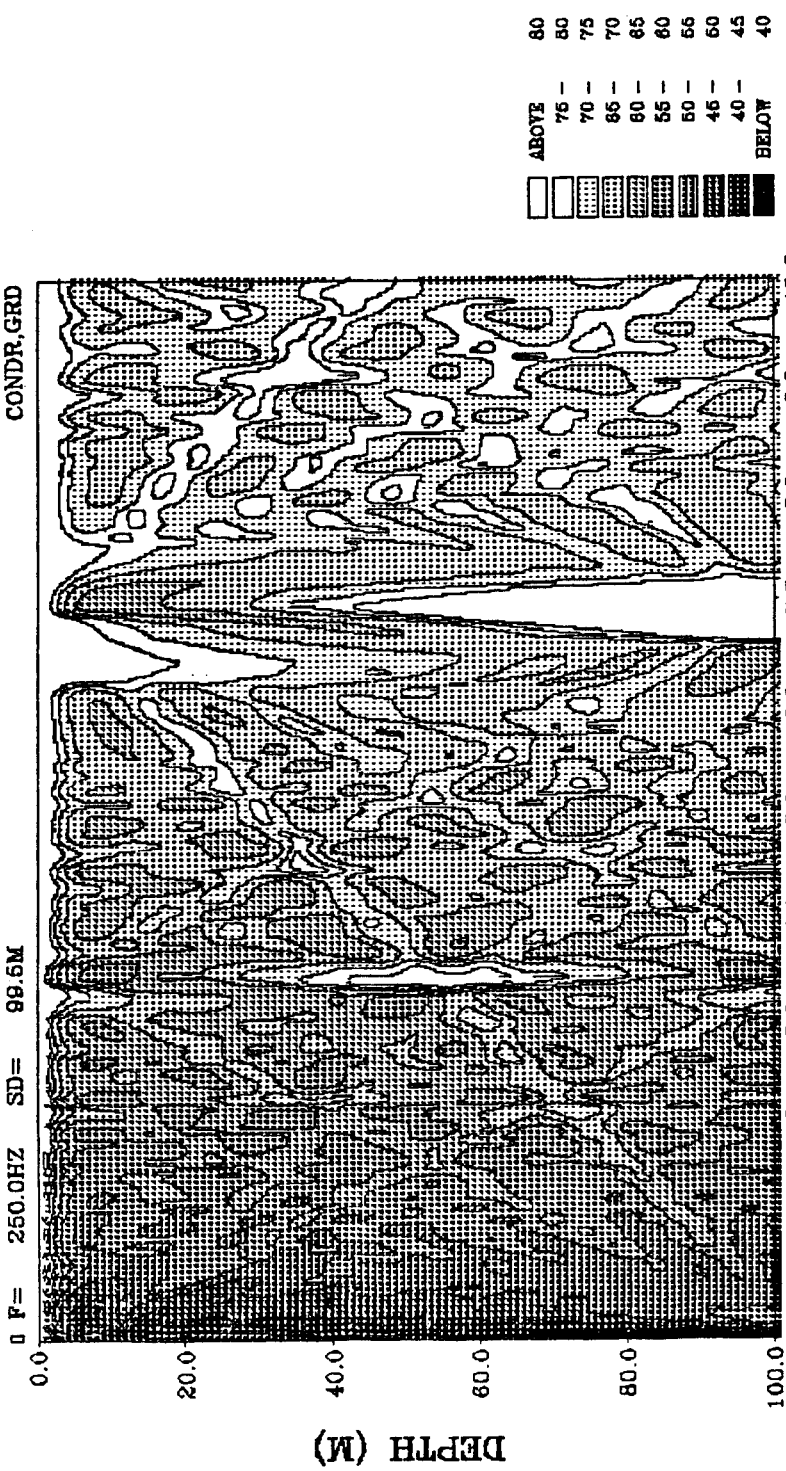

RangeIndependent ShallowWater TestCase 3b

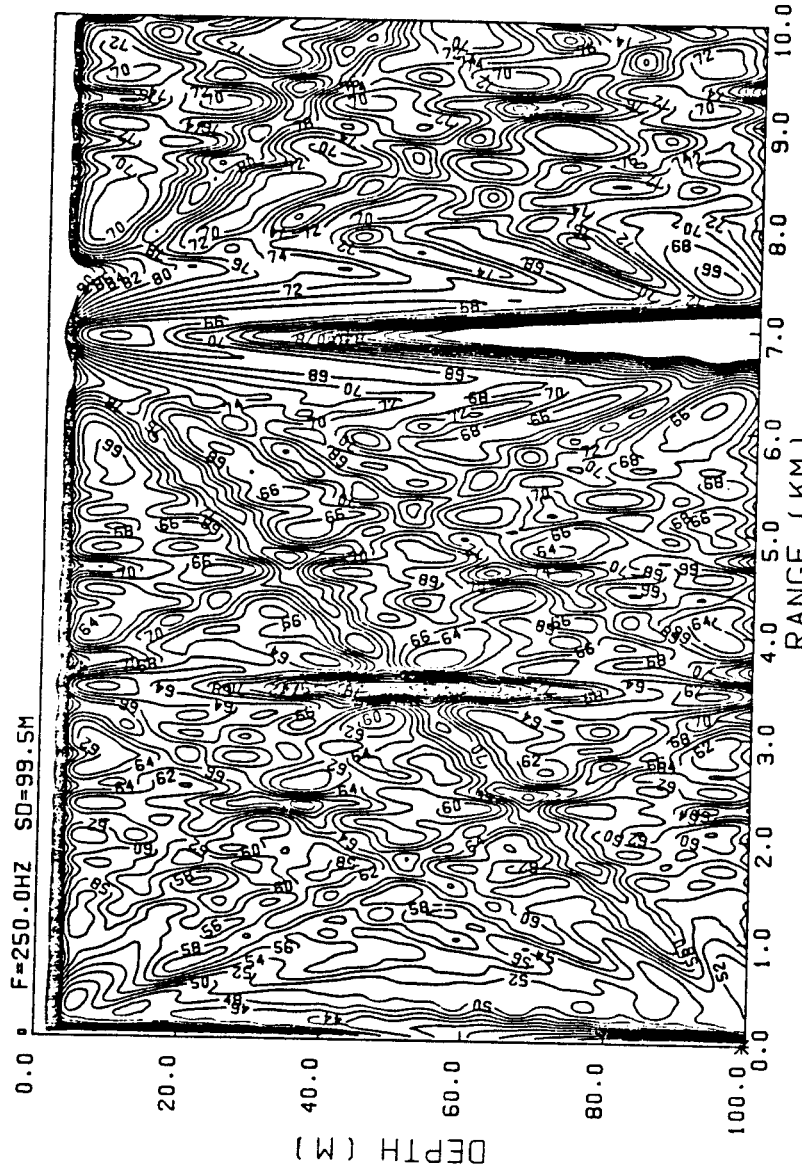

CONTOURED PROPAGATION LOSS FROM PE MODEL FOR CASE 3B

TEST 2: Comparison of Propagator/Global matrix FFP Solutions

In TEST 2, these calculations for the PEKERIS model are repeated, for Green's function integrands, using SAFARI FFP and the original general-purpose FFP of KUTSCHALE (1971). The method of numerical integration employed in both FFPs is identical, the only difference being that of the local and global matrix methods by which the depth-dependent Green's function is computed. This example corresponds to the well known TEST 2a case of the NORDA PE Workshop (DAVIS et al, 1981).

In this case, the integrands are shown to agree exactly, both in overall response behaviour, and in ultiamte numeric precision of computed eigenvalues (**Figures** 17a and 17b).

Because the local (uncorrected) propagator matrix method cannot be used to calculate very high or very low frequency solutions for elastic media, due to its global sensitivity to local roundoff error, the net error and accuracy loss incurred here effectively setting a limit to the

Figure 17

Comparative accuracy tests of "SAFARI" [CW Fip Version]:

NORDA SACLANT Test Case 2a:

a). Kutschale FFP Green's function (NK=4096)

b). "SAFARI" FFP Green's function (NK=4096)

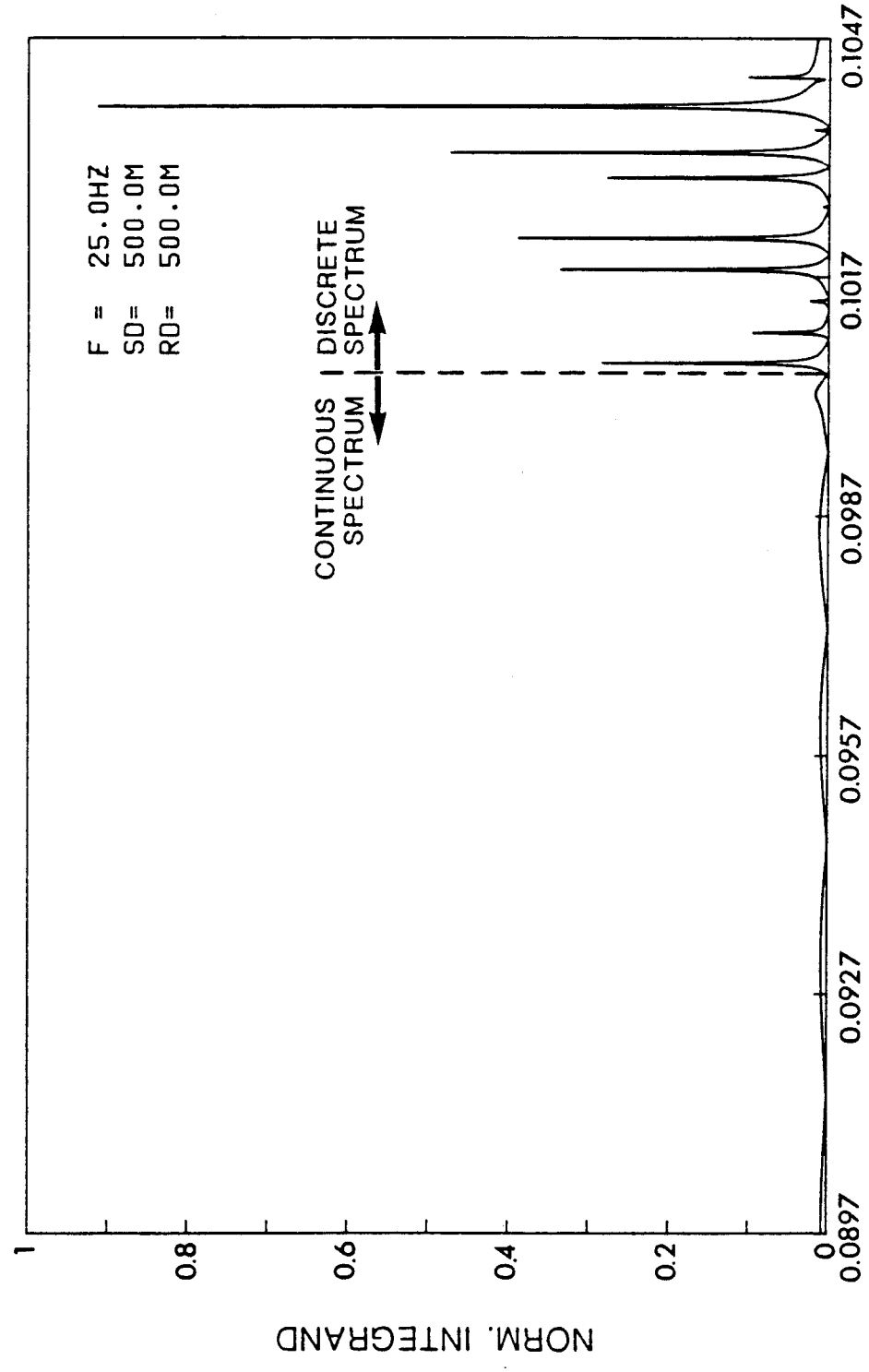

FFP INTEGRAND PLOT FOR CASE 2A (full spectrum)

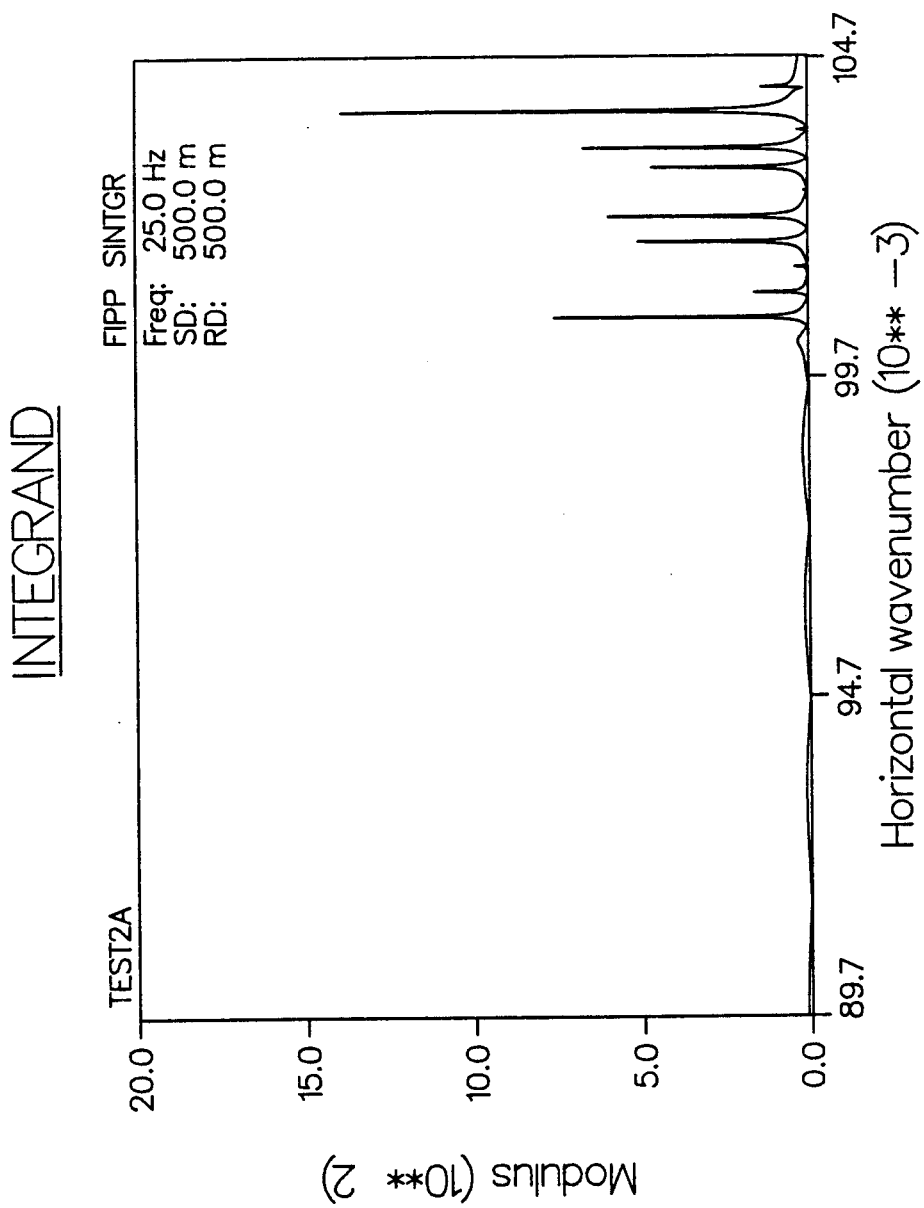
INTEGRAND
TEST2A
FIPP SINTGR
Freq: 25.0 Hz
SD: 500.0 m
RD: 500.0 m
20.0
15.0
10.0
5.0
0.0
Modulus (10** 2)
89.7
94.7
99.7
104.7
Horizontal wavenumber (10** -3)

number of layers that can be considered. Conversely, for a given layer thickness, numeric error growth imposes a corresponding maximum frequency limit.

It can be shown that the uncorrected propagator is unstable, and that even the corrected propagator formulation becomes impractical beyond number of layers N greater than about 25 , for a test frequency of 5000. A plot of the region of acceptable accuracy in f vs N is possible for both SAFARI and KUTSCHALE FFP; at present the maximum test case for SAFARI accuracy has involved 250 layers, a frequency bandwidth of 500 Hz, and a maximum monofrequency of several million Hz. Full accuracy was retained, the case in question limited only by present restrictions on available computer disk space for very large layer models.

Other Pekeris type waveguide comparison tests have been carried out, to examine the relative numeric stability of local/global based FFPs, specifically in respect to local exponential behaviour. This is reported on elsewhere (SCHMIDT and JENSEN, 1984).

TEST 3: Theoretical Dispersion Curve Calculation

In order to examine the comparative accuracy of the SAFARI programs for multifrequency pulsed seismic applications, the same Pekeris layered waveguide model was used for calculating the historically-original quantity of interest - theoretical dispersion curves - over a wide range of source frequencies, as first given analytically by PEKERIS (1948) and EWING JARDETZKY and PRESS (1957). Some of these latter are used for reference comparisons.

Figure 18 below shows a representative dispersion curve of group velocity versus frequency for a simple few layered waveguide model after PEKERIS (1948). Here, for a mixed fluid/solid medium, the eigenvibrations obtained by solving the wave equation subject to boundar conditions leads to Lambs secular equation (TOLSTOY, 1973). The eigenvalues are given as the values of the phase velocities for the various propagating wave modes within the waveguide, obtained as functions of frequency in a characteristic dispersion curve.

As can be seen, for the lowest abscissa values, only modes are present. As the frequency (or layer thickness) is increased, successively higher modes emerge, their cutoffs given by the layer thickness corresponding to a half-integer number of wavelengths for symmetric modes.

Figure 18

Theoretical dispersion curve (velocity vs frequency) for VLF seismic-modal wave propagation over a sediment-covered solid basalt basement

DISPERSION CURVES

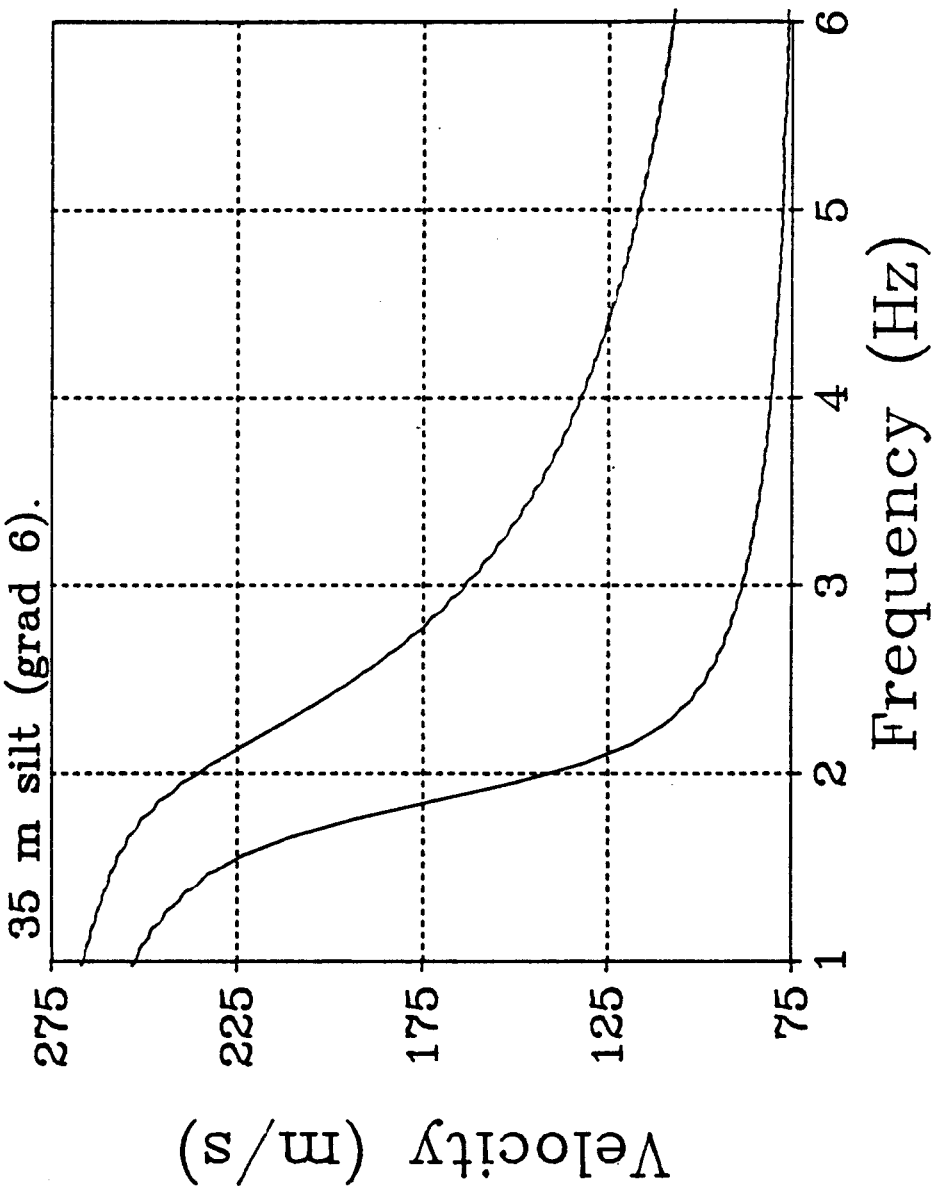

The calculations done with SAFARI are seen to agree exactly with those originally obtained by PEKERIS, and constitute a strong additional confirmation of the absolute numeric precision of the SAFARI algorithm.

TEST 4: Single Pulse Waveform Solution for Pekeris Waveguide

TEST 4 examines both the Green's function accuracy, and computed seismic waveform response, for the fluid/ocean layered media case represented previously. The Pekeris single layered waveguide with solid bottom have constant separate sound speeds in both media. The response is that due to single concentrated buried point transient source, as detected by a theoretic bottom receiver located on the bottom (source also at bottom, overlain by a water column 20m deep), for a 150 Hz simple sine pulse having power from 0 to 450 Hz.

This case was previously calculated by PEKERIS (1948) and more recently by FRAZIER and RUDMAN (1980) using an efficient numeric implementation of PEKERIS' original formulation. The latter is used for comparison here.

The synthetic Green's functions and waveforms at ranges x=6.4km and 8.3km are shown in **Figures 19a-b**. The amplitude and phase of the respective waveforms agrees well with those computed using the analytic solution of FRAZIER and RUDMAN, ie., the low frequency ground wave, Airy phase, first and (in this case) second modes. (The latter is excited here due to a probably higher input frequency employed).

Figure 19

(a) Theoretical Green's function

(b) Synthetic pulse water wave and modal arrivals for 2 source-receiver offset ranges

after PEKERIS, 1948 and FRAZIER & RUDMAN, 1978

(f_c = 100, f_{min}=0, f_{max}=425 Hz)

INTEGRAND

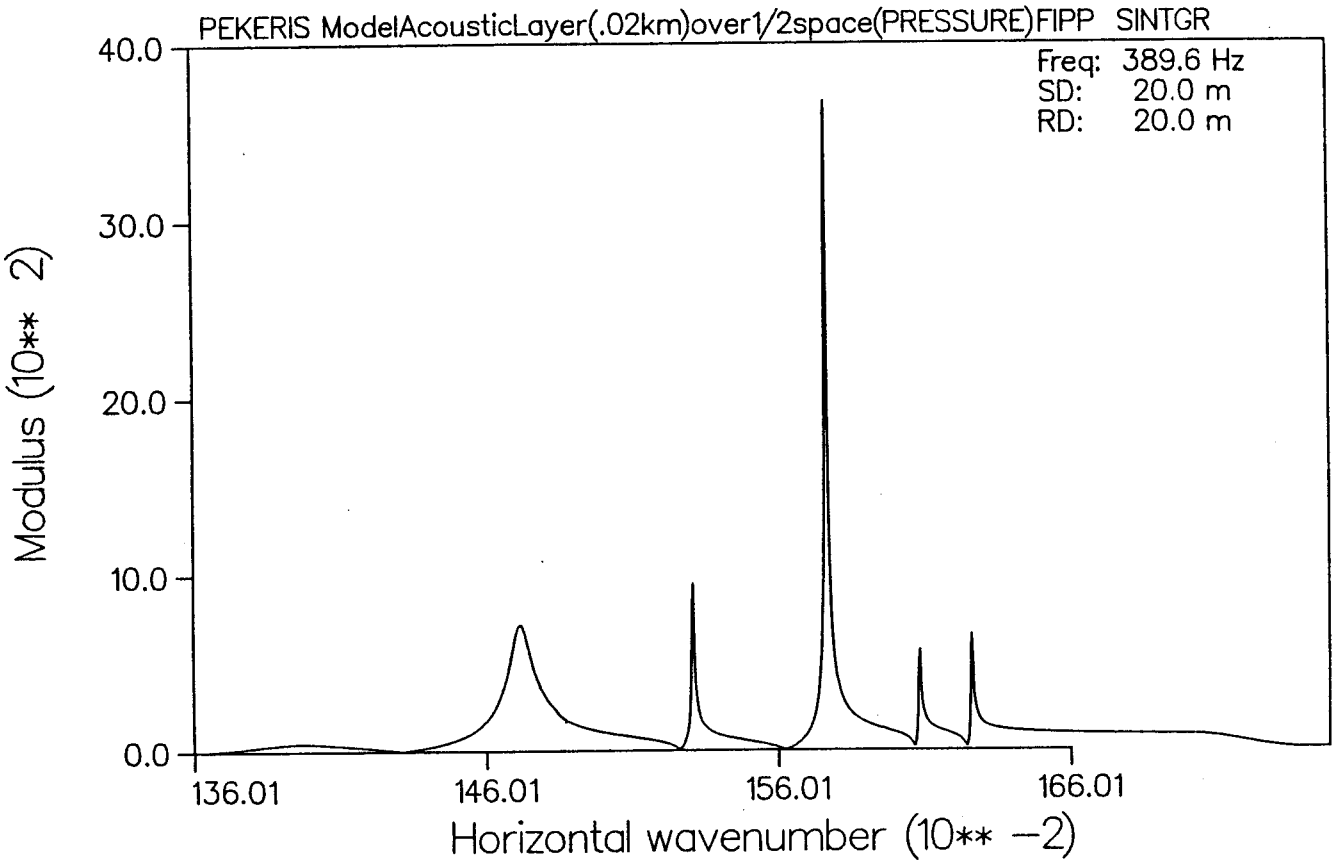
PEKERIS ModelAcousticLayer(.02km)over1/2space(PRESSURE)FIPP SINTGR
Freq: 389.6 Hz
SD: 20.0 m
RD: 20.0 m
40.0
30.0
20.0
10.0
0.0
Modulus (10** 2)
136.01
146.01
156.01
166.01
Horizontal wavenumber (10** −2)

NORMAL STRESS

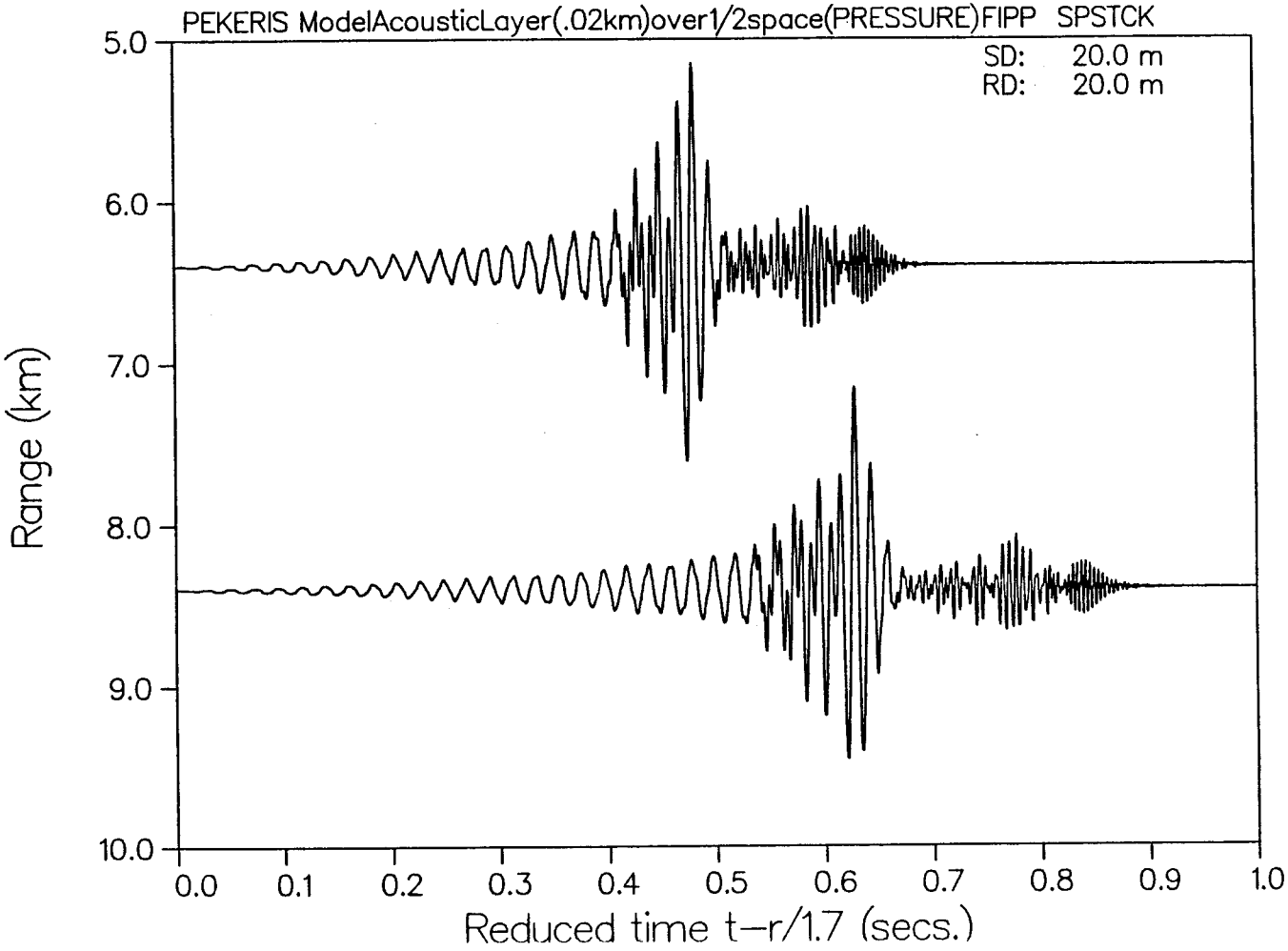

Other tests of seismic pulse waveform accuracy are reported elsewhere (SCHMIDT, 1982).

TEST 5: Theoretical Completeness of Full Wavefield and Reflectivity seismic solutions

The final tests presented here involve a comparison of multi-receiver range-stacked synthetic seismograms, in both the exact and complete full wavefield and approximate reflectivity solutions, for 3 representative solid earth crustal models. Test 5(a) comprises the 'inhomogeneous S* arrival example of CERVENY et al (1971), which is essentially that of Lamb's first problem in the limit as buried receiver depth from surface approaches zero. Test 5(b) considers the canonic MOHO1 model of BRAILE and SMITH (1975), representing all basic arrival types expected for an idealised 1 layer crust overlying a semi-infinite mantle halfspace. Test 5(c) is that of FUCHS and SCHULTZ (1976), for "tunnelling waves" between alternatingly thick and thin layers, which clearly reveals the exact wave nature of the SAFARI solution.

Recently 'rediscovered in theoretical seismology (also long known in e.g. atmospheric wave propagation; BUDDEN, 1962), these 'new' modes are effectively an extra inhomogeneous arrival type, not predicted nor describable via geometric ray theory, nor readily treated via other reflectivity type complete solution algorithms. **Figure 20a-c** reproduces the angular S* representation of GUTOWSKI et al (1984), vs angle, vs receiver depth, and vs receiver range respectively, where total agreement is obtained, with the

Figure 20

(a) S* inhomogeneous arrival vs. angle

(b) S* inhomogeneous arrival vs. receiver depth

(c) S* inhomogeneous arrival vs. receiver range

after GUTOWSKI et al, 1984

VERTICAL PARTICLE VELOCITY

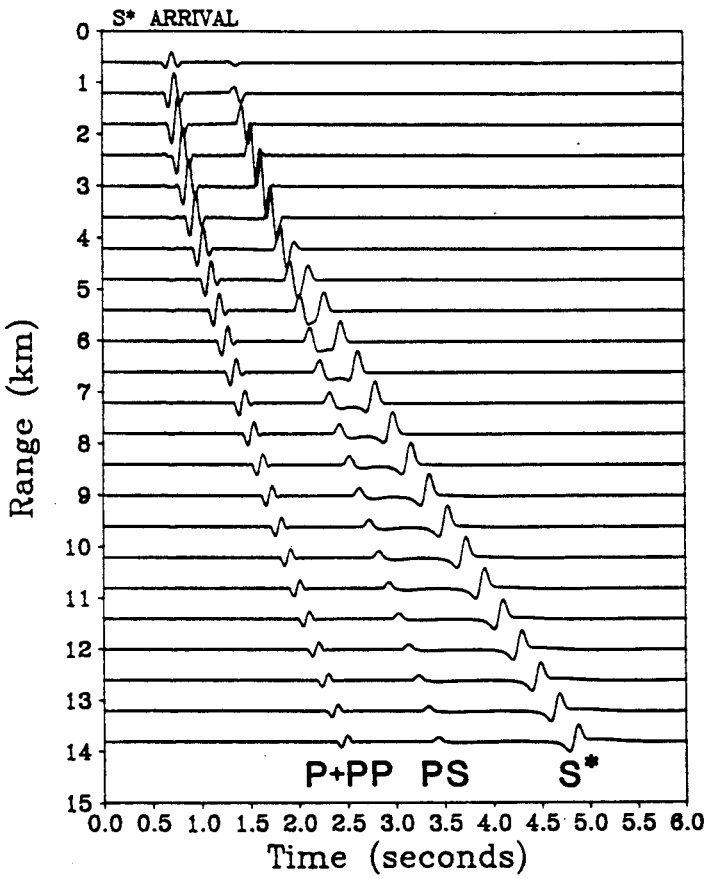

S* arrivals for source $\lambda/8$ below free surface.
Receiver depth 3 and ranges 0.5-11.5 λ (λ = 1200 m).
Amplitudes are multiplied by range.

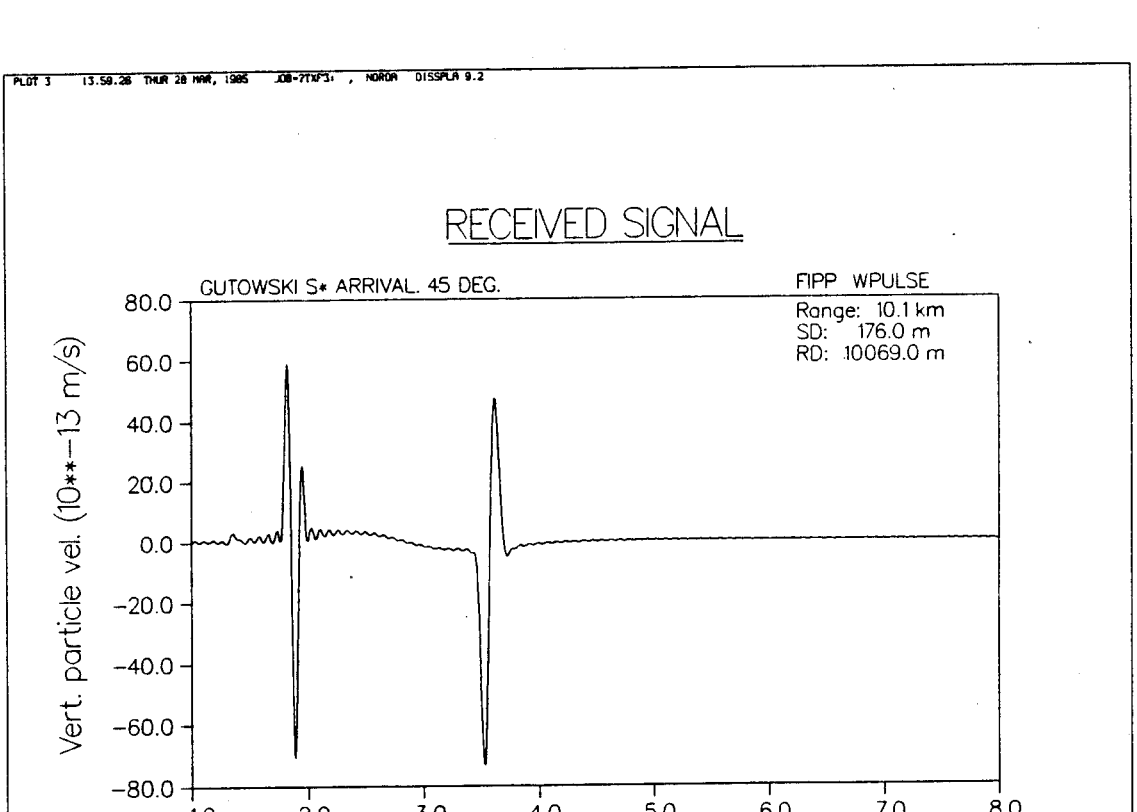
PLOT 3 13.59.26 THUR 28 MAR, 1985 JOB=7TXP3: , NORDA DISSPLA 9.2
RECEIVED SIGNAL
GUTOWSKI S* ARRIVAL. 45 DEG.
FIPP WPULSE
Range: 10.1 km
SD: 176.0 m
RD: 10069.0 m
Vert. particle vel. (10**-13 m/s)
80.0
60.0
40.0
20.0
0.0
-20.0
-40.0
-60.0
-80.0
1.0
2.0
3.0
4.0
5.0
6.0
7.0
8.0
Time (seconds)

VERTICAL PARTICLE VELOCITY

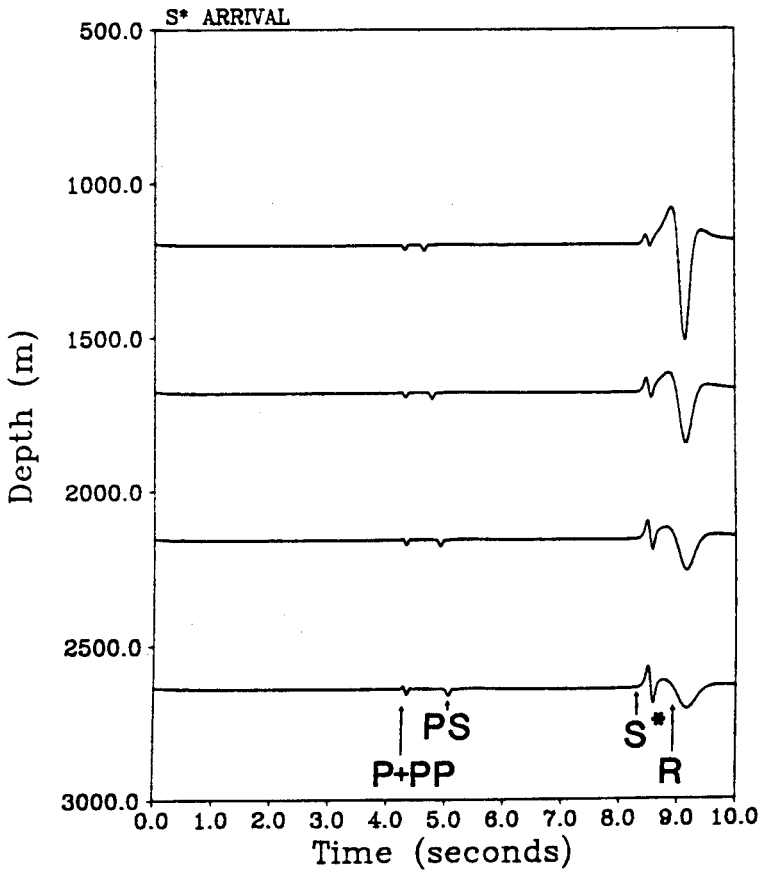

S* arrivals for source $\lambda/8$ below free surface.
Receiver range 21 and depths 1.0-2.2 λ (λ = 1200 m).

exception that in SAFARI, no numerical dispersion errors occur (as in Gutowski's hybrid reflectivity/finite difference formulation), since the SAFARI solution and integration technique is exact. Small oscillations around 20b are due to f truncation.

Figure 21a-c shows the results of computing hypothetical seismic profile response for surface geophones in the range of 10-150km offset from the source, using both full wavefield and reflectivity solutions. The idealised MOHO1 earth model is a single 30km layer overlying a semi-infinite halfspace. Perfect agreement in amplitude and phase is obtained, there being only very minor waveform shape and amplitude differences for the very first nearfield receivers, arising from the retention and neglect respectively of surface generated multiple reflections in the SAFARI anda reflectivity synthetics.

Finally, considering crustal seismic tunnelling waves, we adopt a simple representation of low seismic frequency penetration of waves from a low velocity zone thru "thin" high velocity zones, using a modification of the same canonic MOHO1 model as above. Here a crust of 30km depth overlying a solid halfspace mantle is interrupted at 25km by a single high velocity lens of elastic properties equal to those of the underlying subMOHO zone. As will be seen in **Figure 22b**, low pass frequency transmission and characteristic 'shadow' zones are clearly evident, agreeing with expected results as given previously (FUCHS and

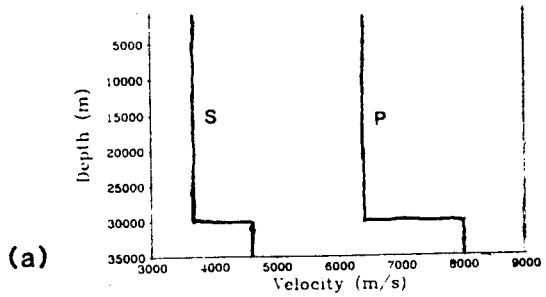

VERTICAL PARTICLE VELOCITY

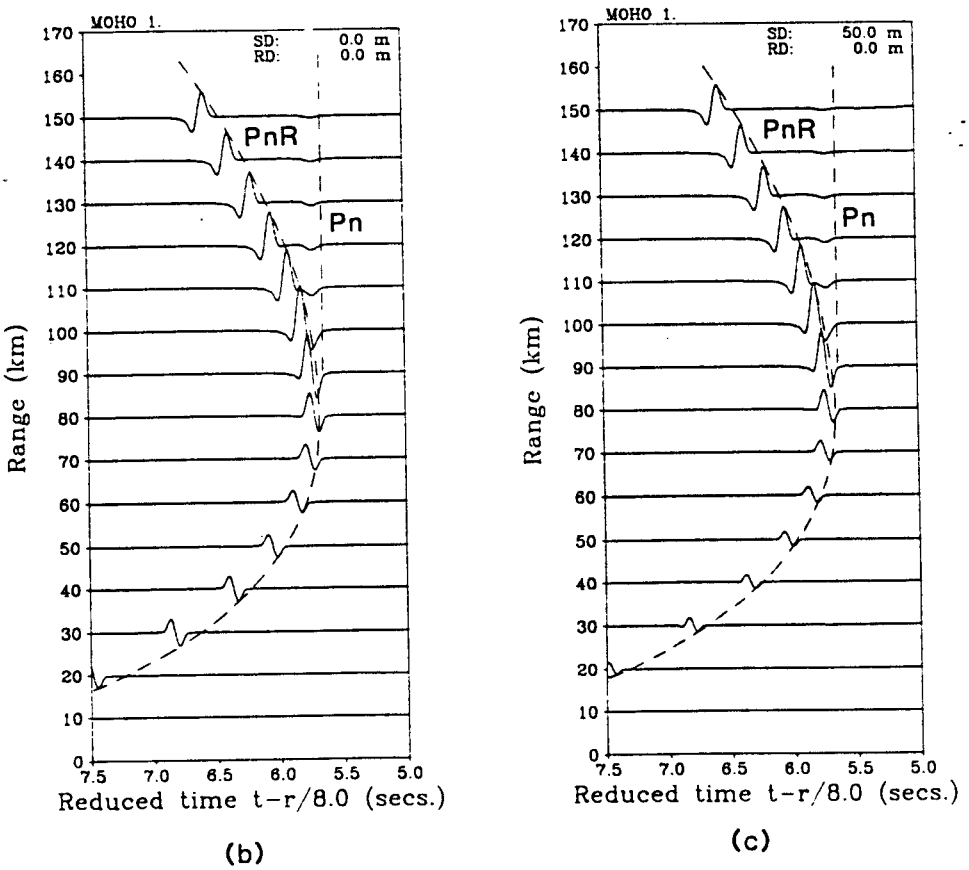

Figure 21 Synthetic seismograms for MOHO-1 crustal model. a. Velocity profile. b. Reflectivity approximation. c. Full wavefield solution. Amplitudes are multiplied by range.

Figure 22

Velocity/depth profile and corresponding fullwave synthetic seismogram for crustal seismic wave tunnelling through a single thin high-velocity layer (after FUCHS and SCHULTZ, 1975)

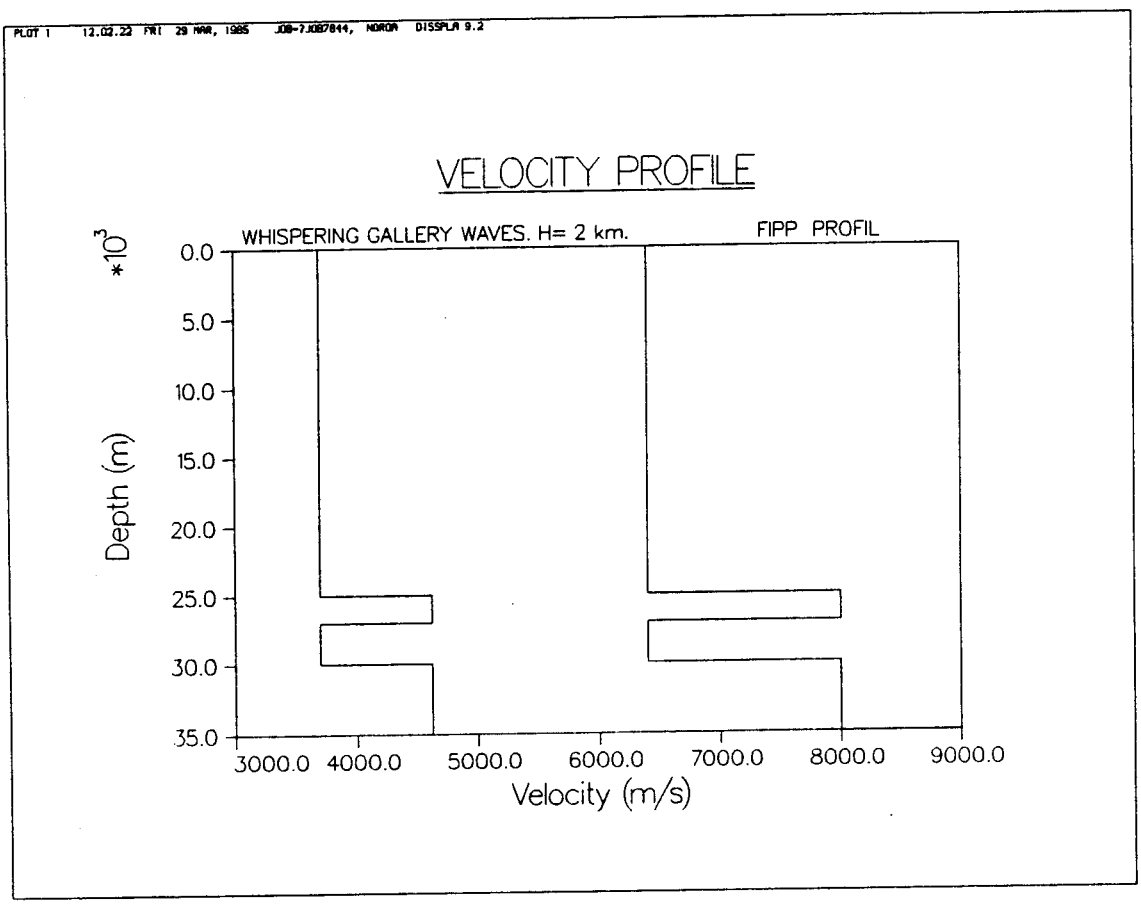
PLOT 1 12.02.22 FRI 29 MAR, 1985 JOB-7J087844, NORDA DISSPLA 9.2
VELOCITY PROFILE
WHISPERING GALLERY WAVES. H= 2 km.
FIPP PROFIL
*10^3
Depth (m)
0.0
5.0
10.0
15.0
20.0
25.0
30.0
35.0
3000.0
4000.0
5000.0
6000.0
7000.0
8000.0
9000.0
Velocity (m/s)

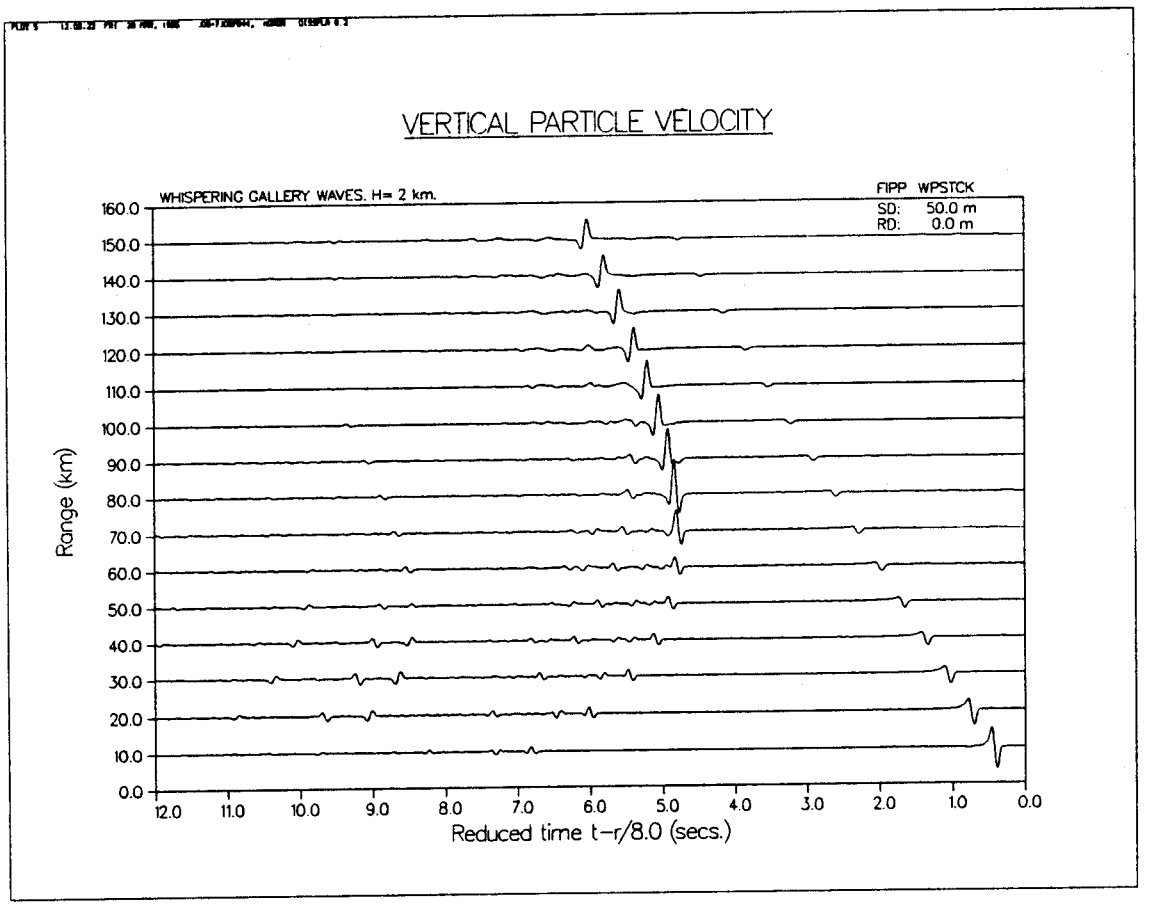
VERTICAL PARTICLE VELOCITY
WHISPERING GALLERY WAVES. H= 2 km.
FIPP WPSTCK
SD: 50.0 m
RD: 0.0 m
Range (km)
160.0
150.0
140.0
130.0
120.0
110.0
100.0
90.0
80.0
70.0
60.0
50.0
40.0
30.0
20.0
10.0
0.0
12.0
11.0
10.0
9.0
8.0
7.0
6.0
5.0
4.0
3.0
2.0
1.0
0.0
Reduced time t−r/8.0 (secs.)

SCHULTZ, 1976). Tunneling wave phenomena for other crustal seismic cases are considered again below (Section 3(c)).

The excellent agreement obtained by SAFARI for all test cases considered, over a wide range of media models, source/receiver configurations, wavenumber and frequency bandwidths confirms the reliability, accuracy and generality of the DGM/FWE method in CW and pulsed seismic applications, as implemented by SCHMIDT in SAFARI. Many other consistency tests of SAFARI could be carried out, with present and other reference programs, to further verify the complex total wavefield result for extreme model cases.

Additional computation and solution advantages and testing results of SAFARI are described by SCHMIDT and JENSEN, 1984 and SCHMIDT and TANGO (1984), and below in Section 3.

Section 3

(a): Overview of Applications & Numerical Examples

To illustrate that the direct global matrix/finite wave element model, as employed in the general applications code SAFARI of SCHMIDT (1982,1983,1984) provides exact & complete fullwavefiled solutions to seismic propagation in plane stratified (range-independent) environments, 3 representative cases are given, for which Green's function integrands, transmission loss and/or time domain synthetic seismograms are presented. These cases were selected to encompass both simple classic seis-acoustic wave propagation problems, such as Pekeris waveguides at very lo frequencies, as well as more complex multilayered deep crustal & exploration earth models. Both model-model & (when available)data -model comparisons are considered for the test cases below, to demonstrate the theoretic stability, precision & completeness as well as practical versatility afforded by the new SAFARI program. (For other applications see SCHMIDT & JENSEN,1984;TANGO,1985).

To show SAFARI's computational precision & accuracy for Green's function & transmission loss in CW/pulse study in ocean acoustic prediction, very low frequency (VLF) ocean propagation in a

fluid/solid waveguide channel is investigated, for the environmental and experimental regimes where shear-induced seismic interface waves can have important effects on overall tranmission loss. Significant additional implications for both detection and geo-bottom reconnaissance are presented, and optimal source/receiver configurations for marine interface wave detection and analysis are considered, following the work of ESSEN (1981), RAUCH (1982) and SCHMIDT (1982).

Theoretical completeness of the SAFARI full wavefield solution for crustal seismic investigations is detailed by examination of the agreement between SAFARI and reflectivity for canonic LVL transition models in the e. Basin and Range, following the work of PRODEHL (1971;1976), MUELLER and LANDISMANN (1972), BRAILE and SMITH (1975), MULLER and MUELLER (1979) and McMECHAN (1983). Complex interference head wave and mode conversions for post-critical offsets are analysed, as well as near normal incidence reflexions at small offsets, to initially investigate their information content for refraction seismic detection of pre-MOHO intermediate depth reflectors and deeper LVL transition zones.

Versatility and speed of SAFARI is shown by deriving both partial wavefield/reflectivity results, as well as exact full wavefield synthetic Vertical Seismic Profiles (VSPs), for hypothetical and real marine crustal and exploration stratigraphic borehole models of STEPHEN (1977;1984) and TEMME & MULLER (1982) respectively.

In all cases, except as noted, the source(s) are simple buried infinitesimal point sources with zero azimuthal dependence. Receivers record separately both vertical and horizontal particle velocity, and in agreement with current practice both the full wavefield and reflectivity synthetics are computed for both zero and reported average values of P and SV attenuation. In order to more rigourously and completely examine and compare the detailed arrival type and structure of the resulting synthetic seismograms, computations are carried out over a range of extreme nearfield, critical and post-critical/farfield source-receiver offsets. Unless otherwise stated, for computational convenience the corresponding synthetics are therefore plotted in standard reduced time format.

As a final note of nomenclature, the "full wavefield" response from the DGM/FEW algorithm "SAFARI", should be clearly distinguished from all numerically-derived, approximated or partial-wavefield (reflectivity) responses (CHAPMAN and ORCUTT, 1984). The DGM/FWE output is a theoretically complete and exact solution, in the sense of FFP solutions in underwater acoustics (and should in **no** way be confused with other 'full wave' synthetic seismograms as based on the asymptotic ray method of CHOY et al (1979)). The DGM/FWE solution, as derived from the **exact** Green's function layer matrix, and as **completely** integrated numerically along real contours, automatically includes all body and surface/interface waves and all orders of surface, interbed and internal multiples, as calculated simultaneously throughout

the entire layered halfspace model by direct global wave field solution of SAFARI.

Section 3(b)

Applications of SAFARI to Very Low Frequency (VLF) Seismic-Acoustic Propagation in Shallow Ocean Environments

Background

Very low frequency seis-acoustic propagation in a waveguiding channel, such as the shallow oceans comprising continental shelves, has traditionally been analysed in terms of simple or modified ray or normal mode numerical models (HECHT, 1978; KUPERMAN and JENSEN, 1980). With certain exceptions (coupled mode solutions), to date most such "exact" propagation models have been range-independent, or at most allow for only a limited range dependence as well as vertical variation in a restricted number of elasto-acoustic medium parameters. Where these approaches have been most successful, they have effectively treated the total water + bottom environment as a "fluid", or at best comprehend only a very limited number of solid layers, for CW sources only (CHAPMAN, 1984).

In these models, at frequencies sufficiently above modal cutoff, for a simple Pekeris environmental model, all rays/modes in the discrete wavenumber spectrum (ie, in the propagating field) inevitably have part of their pathlengths in the bottom, where

they undergo absorption dependent on bottom layer number and type(s). Although at sufficiently long ranges most of the energy contributing to the sound field is carried by rays/modes which do not penetrate deeply into the sediments, at lower frequencies approaching mode cutoff, over 'nearfield' ranges (for bottom environments with non-negligible shear) it is no longer clear that bottom interactions can be ignored in their effects on net transmission loss behaviour. In some cases, not only can a significant fraction of total energy be diverted thru/into the bottom by virtue of P-SV mode and head wave conversion (FRYER, 1978;CHRISTIANSEN et al, 1977), but seismic interface waves can also be generated. These two **seismic** propagation loss mechanisms have recently been shown to become increasingly important as frequency approaches or drops below mode cutoff (SCHMIDT, 1982). Such seismic effects are completely unaccounted for in fluid-only propagation models. In addition, even in modified ray or hybrid/coupled mode formulations, complete evaluation of all wavefield effects is hindered because the number of contributing modes/rays may be exceedingly large.

These shortcomings have led to other various attempts at either (1) incorporating approximate "shear phenomenology" into acoustically successful and efficient adiabatic normal mode or parabolic equation models, or (2) developing simple exact "problem specific" models, analytically treatable by an exact Hankel transform approach. Despite considerable theoretic effort

and development, the former shear-PE approach has as yet not proven feasible for even simple numerical modeling applications.

To satisfy geophysical evidence and runtime limitations, there has thus been increasing motivation to seek the later alternative. This approach includes simple exact waveguide solutions which intrinsically treat the total seismic-acoustic wavefield for simple Pekeris ocean-bottom models. In spite of their obvious theoretic correctness and utility for many applications (LYNCH et al, 1984, and references), these analytic Hankel transform solutions are limited in both the range of multilayered environments and experimental configurations treated.

Consequently, during the last decade, a great deal of interest has arisen in obtaining computationally simple and rapid algorithms of wide generality for the complete wavefield above and below the ocean bottom interface, correct for all source and receiver frequencies, numbers and configurations. As an exact (integral transform) solution, the Fast Field/reflectivity method has emerged, employing a generalised Pekeris model to obtain the complete seismic-acoustic wavefield in an arbitrary multilayered fluid/solid medium (DINAPOLI & DEAVENPORT, 1980).

In the FFP, by simply defining the model aspects of interest within this discrete Hankel transform representation, and performing (asymptotic or exact) numeric integration to evaluate

the multilayer Green's function (previously found by propagator matrix methods) over complex wavenumber and frequency, one automatically derives the complete and exact contributions of all normal and virtual modes, reflected-refracted, converted and interface excitations in one result.

However, despite their theoretic correctness and generality over specific-case solutions, the full potential of the integral transform/FFP approach to seismic-acoustic modeling has not previously been completely exploited, due to inherent instabilities and runtime diseconomies (of the propagator matrix based algorithms employed) at very low frequencies and multi-layered bottom environments.

Figure 23

Schematic of Pekeris waveguide shallow underwater environment and experimental configurations typifying VLF scenarios

STRATIFIED SHALLOW WATER ENVIRONMENT FOR (RANGE-INDEPENDENT)
CW PROPAGATION MODELLING

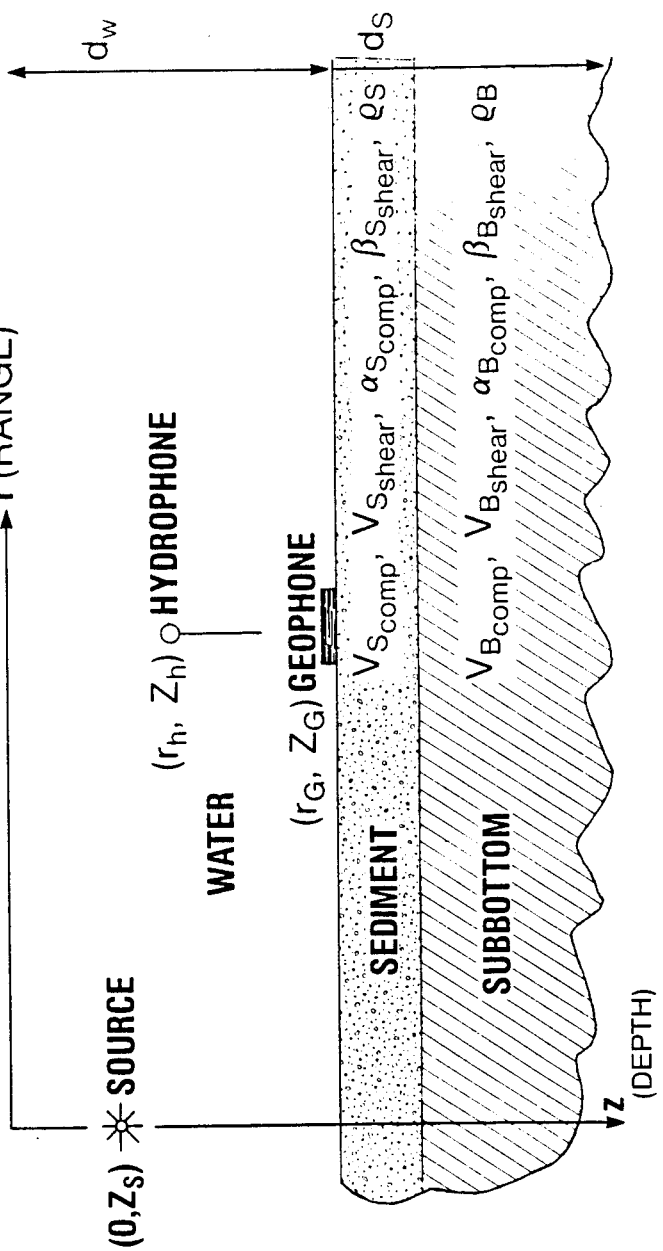

In this section, we present only the basic ingredients of a selected ocean VLF numerical modeling study, emphasising the fundamental underlying physics and geophysical conditions controlling seismic-acoustic propagation phenomena in the VLF regime.

Specifically, we examine here shear rigidity effects on VLF propagation loss prediction in shallow water channels, exploring the particular contributions to net transmission loss of seismic interface wave excited in a representative seabed environment (here **basalt**) over realistic source/receiver configurations of interest (**Figure** 23).

The input geomodel is a simple 2 layer bottom, comprising a single isovelocity fluid layer with 100m depth, overlying a solid halfspace (with properties approximating those of marine basalts; HAMILTON, 1975). A single point source and receiver are positioned a near-bottom depths, initially 95m and 100m respectively. Transmission loss is considered here over the nearfield ranges of 0 to 10km, for which interface wave amplitudes are generall important.

Figures 24a-d show the theoretical transmission loss at f=50 and f=5Hz respectively, for the cases of shear and no-shear velocity bottoms, with only nominal α and β attenuations.

Figure 24

VLF transmission loss vs. receiver range:

(a) Basalt (acoustic-only bottom), f=50Hz
(b) Basalt (acoustic-only bottom), f=5Hz
(c) Basalt (full elastic bottom), f=50Hz
(d) Basalt (full elastic bottom), f=5Hz

showing relative efficacy of shear-related (nb, Scholte seismic wave) effects as mechanism of TL loss in acoustic normal mode cutoff regime, at "nearfield" ranges

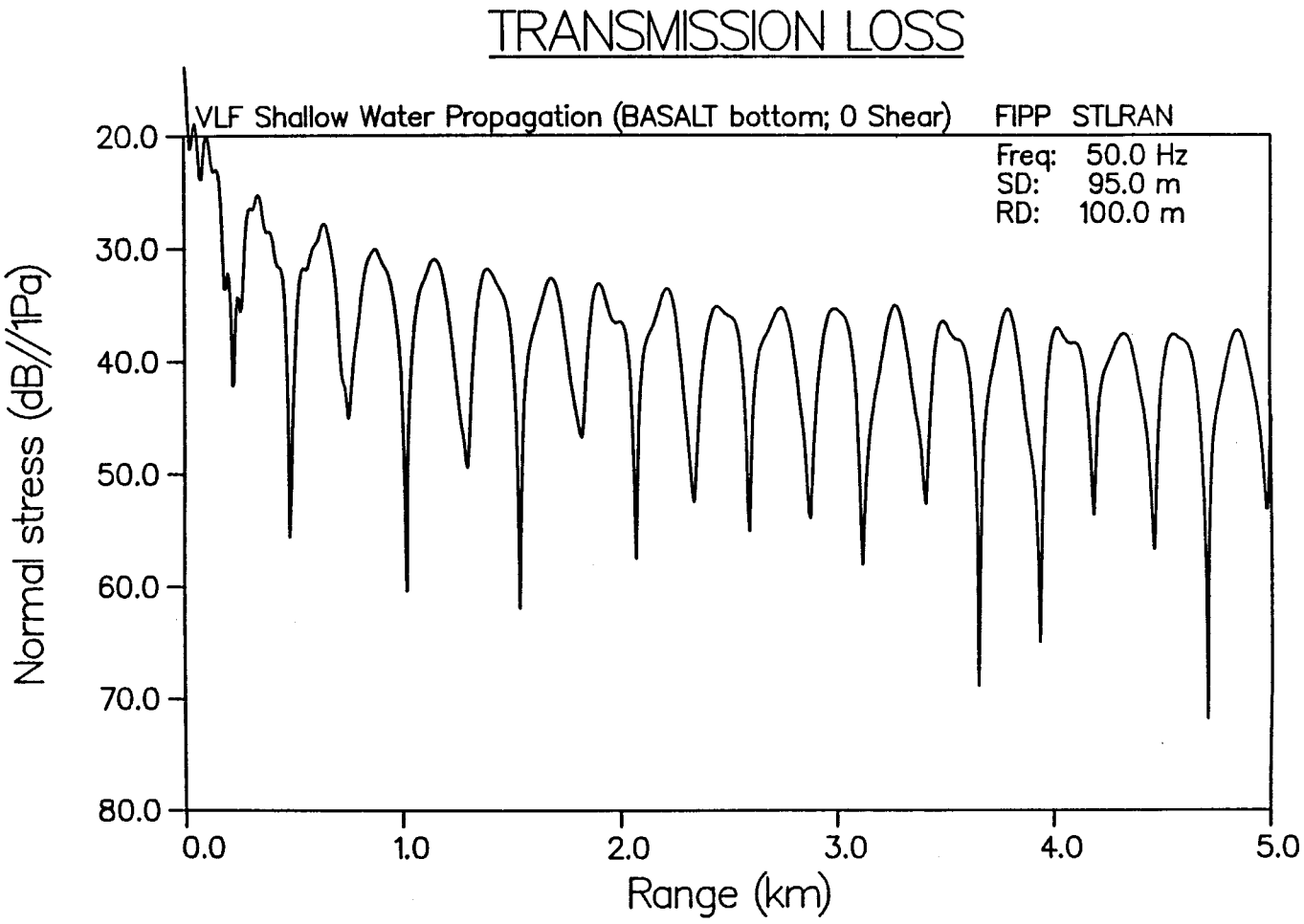
TRANSMISSION LOSS
VLF Shallow Water Propagation (BASALT bottom; 0 Shear)
FIPP STLRAN
Freq: 50.0 Hz
SD: 95.0 m
RD: 100.0 m
Normal stress (dB//1Pa)
20.0
30.0
40.0
50.0
60.0
70.0
80.0
0.0
1.0
2.0
3.0
4.0
5.0
Range (km)

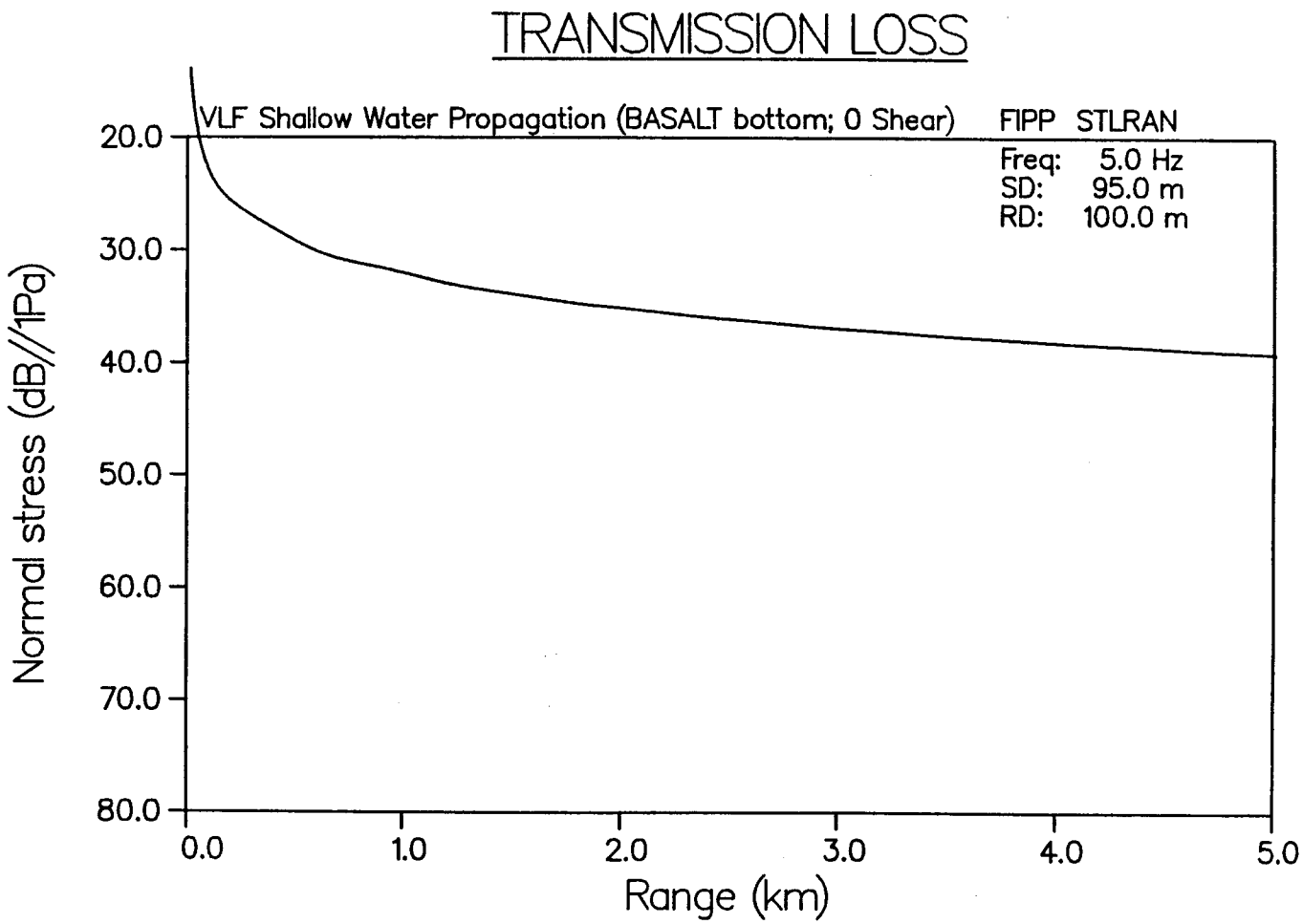
TRANSMISSION LOSS
VLF Shallow Water Propagation (BASALT bottom; 0 Shear)
FIPP STLRAN
Freq: 5.0 Hz
SD: 95.0 m
RD: 100.0 m
Normal stress (dB//1Pa)
20.0
30.0
40.0
50.0
60.0
70.0
80.0
0.0
1.0
2.0
3.0
4.0
5.0
Range (km)

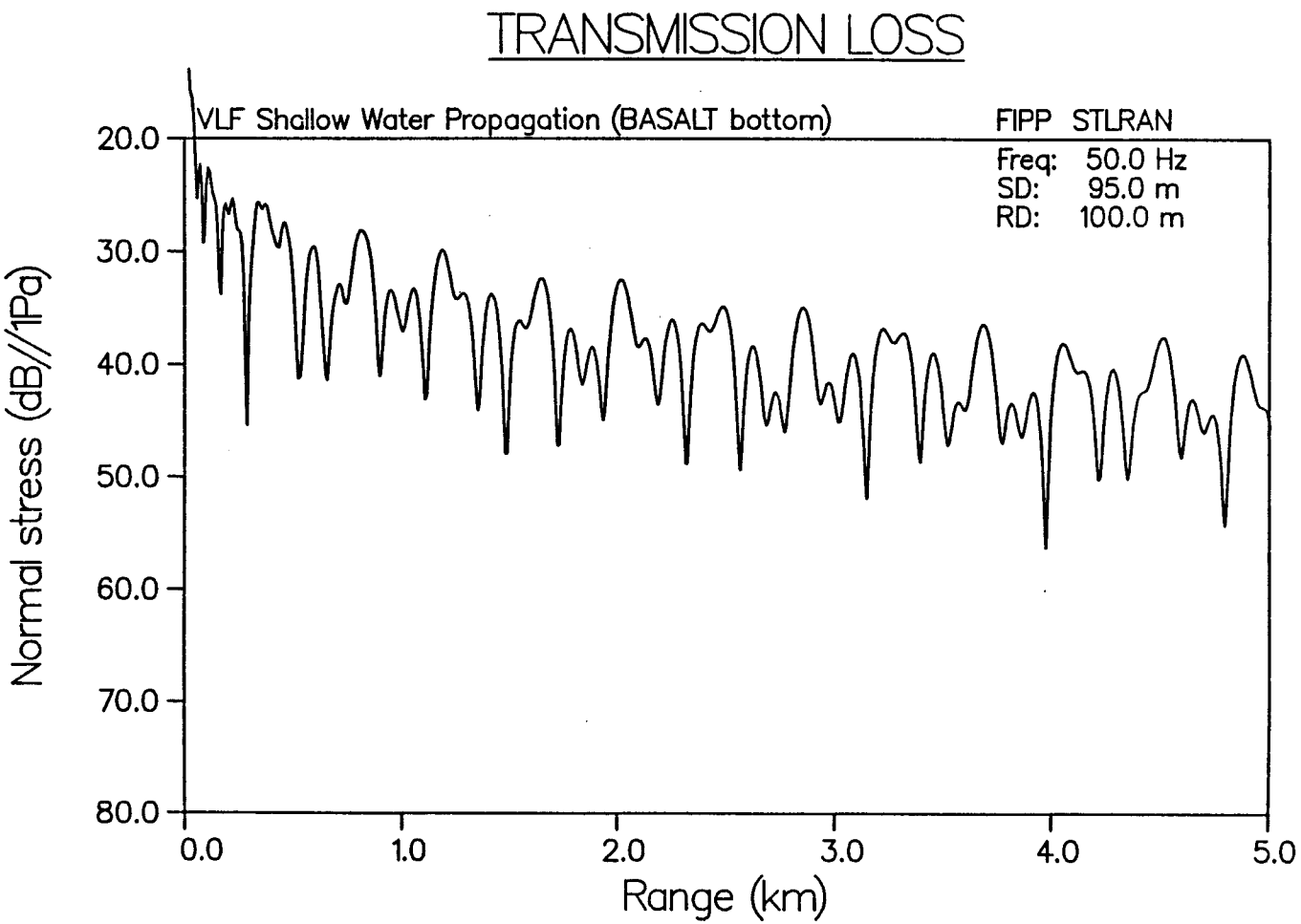
TRANSMISSION LOSS
VLF Shallow Water Propagation (BASALT bottom)
FIPP STLRAN
Freq: 50.0 Hz
SD: 95.0 m
RD: 100.0 m
Normal stress (dB//1Pa)
20.0
30.0
40.0
50.0
60.0
70.0
80.0
0.0
1.0
2.0
3.0
4.0
5.0
Range (km)

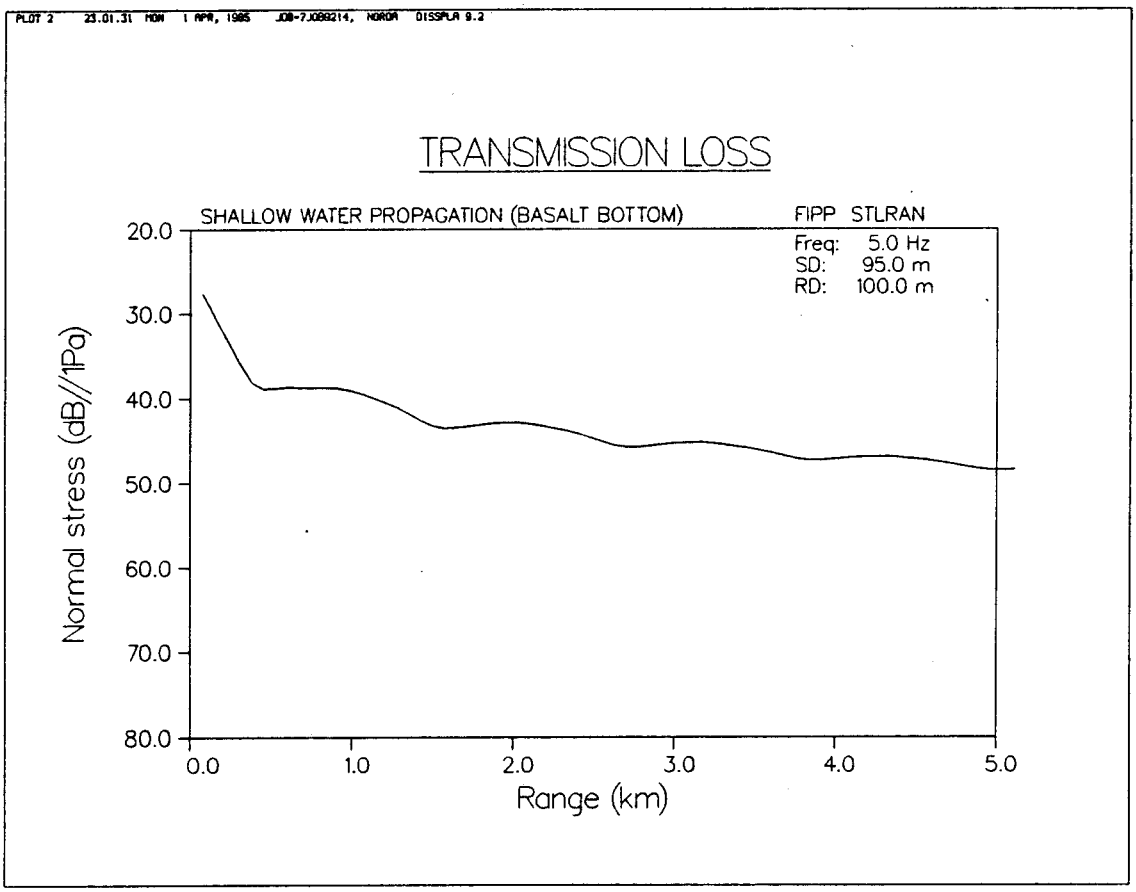
PLOT 2 23.01.31 MON 1 APR, 1985 JOB=7.J089214, NORDA DISSPLA 9.2
TRANSMISSION LOSS
SHALLOW WATER PROPAGATION (BASALT BOTTOM)
FIPP STLRAN
Freq: 5.0 Hz
SD: 95.0 m
RD: 100.0 m
Normal stress (dB//1Pa)
20.0
30.0
40.0
50.0
60.0
70.0
80.0
0.0
1.0
2.0
3.0
4.0
5.0
Range (km)

Figure 25

(a) effective simulation of net shear loss effect on TL in an acoustic-only bottom model via additional P wave attenuation (f = 5Hz, above acoustic modal cutoff)

(b) failure of effective attenuation strategy for frequencies below acoustic modal cutoff

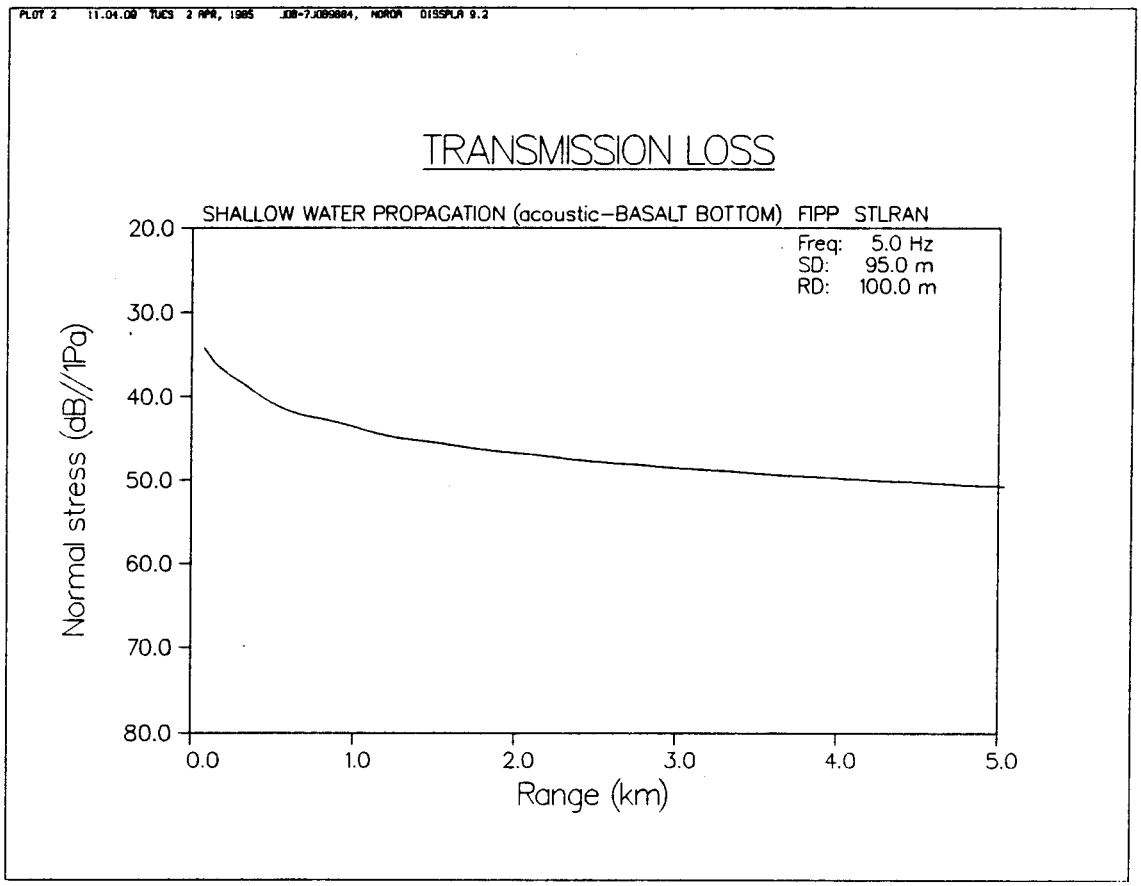
PLOT 2 11.04.09 TUES 2 APR, 1985 JOB-7.JOB9884, NORDA DISSPLA 9.2
TRANSMISSION LOSS
SHALLOW WATER PROPAGATION (acoustic–BASALT BOTTOM) FIPP STLRAN
Freq: 5.0 Hz
SD: 95.0 m
RD: 100.0 m
Normal stress (dB//1Pa)
20.0
30.0
40.0
50.0
60.0
70.0
80.0
0.0
1.0
2.0
3.0
4.0
5.0
Range (km)

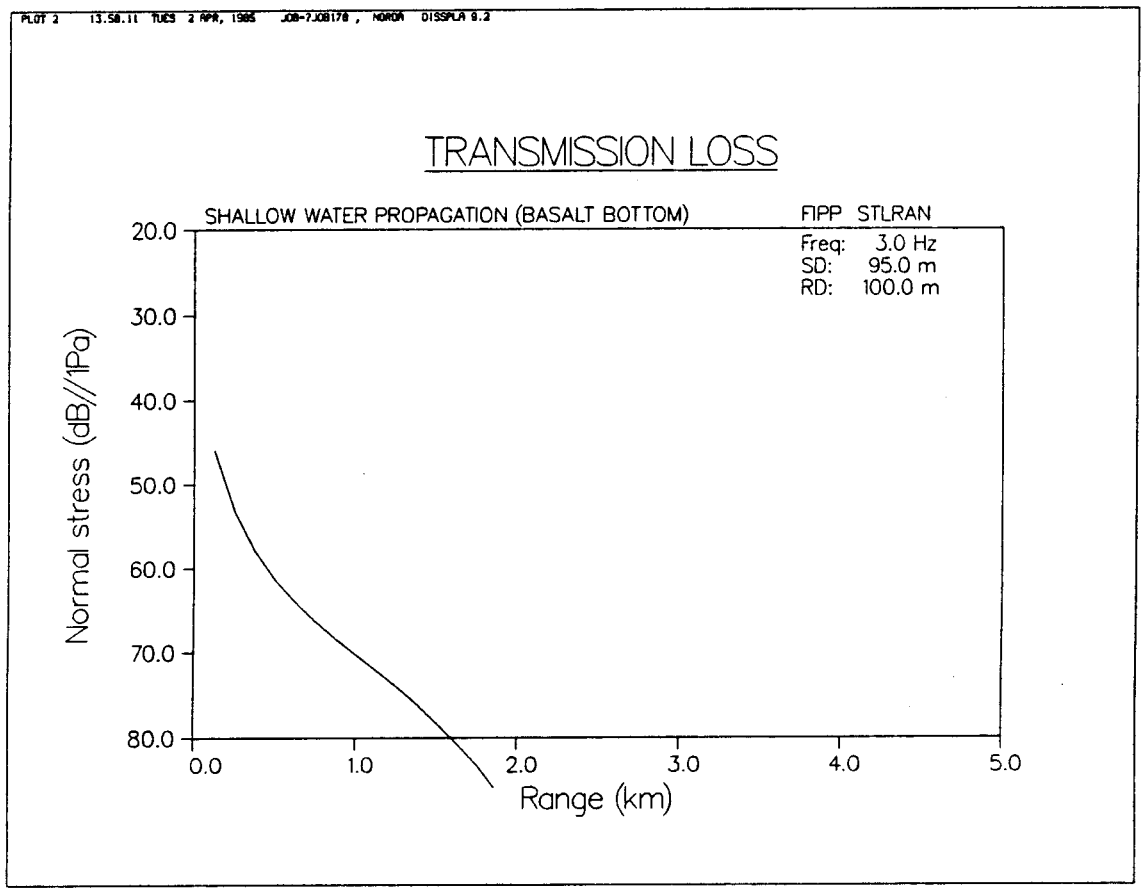
PLOT 2 13.58.11 TUES 2 APR, 1985 JOB-7J08178 , NORDA DISSPLA 8.2
TRANSMISSION LOSS
SHALLOW WATER PROPAGATION (BASALT BOTTOM)
FIPP STLRAN
Freq: 3.0 Hz
SD: 95.0 m
RD: 100.0 m
Normal stress (dB//1Pa)
20.0
30.0
40.0
50.0
60.0
70.0
80.0
0.0
1.0
2.0
3.0
4.0
5.0
Range (km)

Figure 26

Theoretical Green's function for

(a) acoustic-only basalt (f=5Hz)

(b) fullshear basalt (f=3Hz)

corresponding to the TL curves (a) and (b) in Figure 25 (above)

INTEGRAND

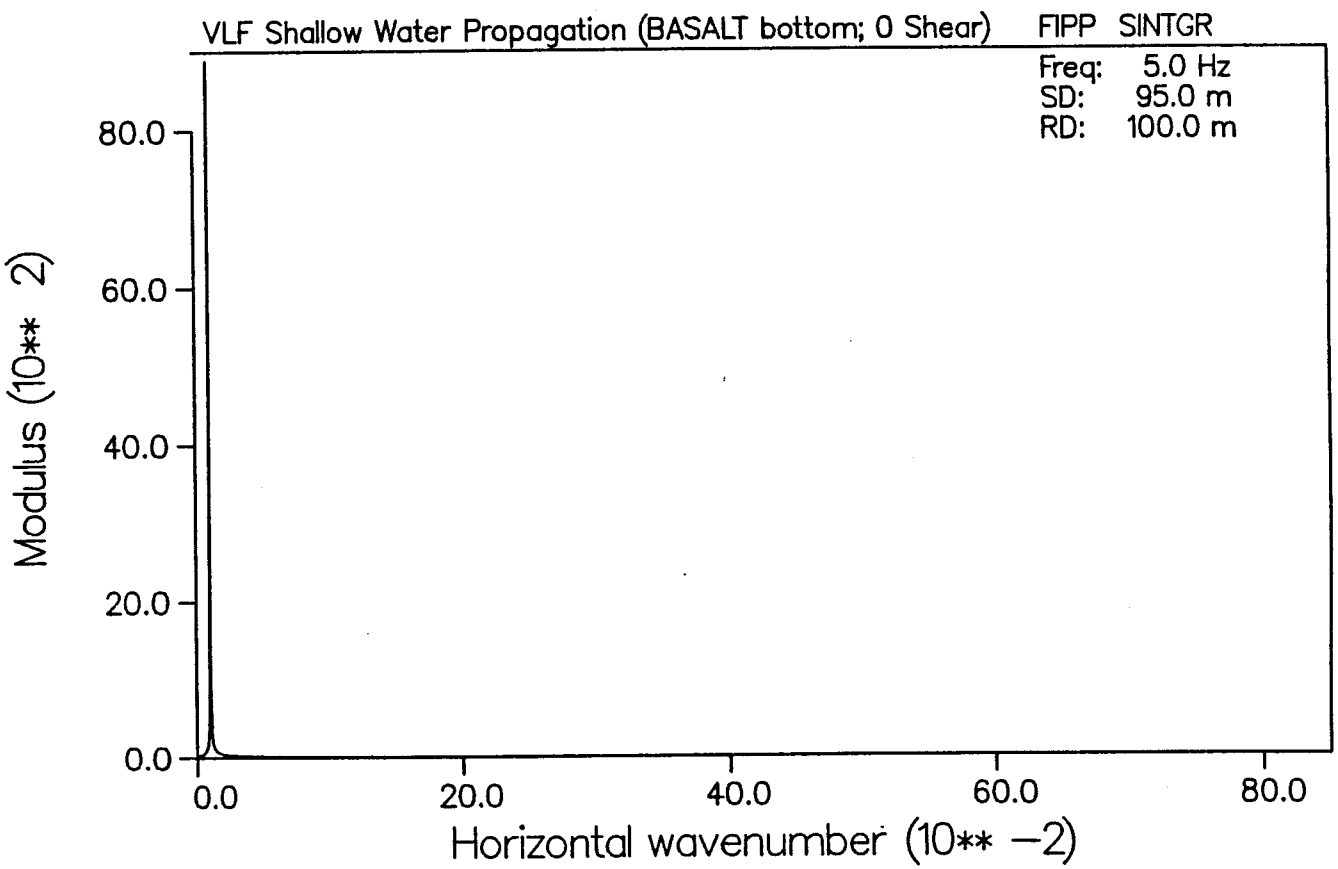
VLF Shallow Water Propagation (BASALT bottom; 0 Shear)
FIPP SINTGR
Freq: 5.0 Hz
SD: 95.0 m
RD: 100.0 m
Modulus (10** 2)
80.0
60.0
40.0
20.0
0.0
0.0
20.0
40.0
60.0
80.0
Horizontal wavenumber (10** −2)

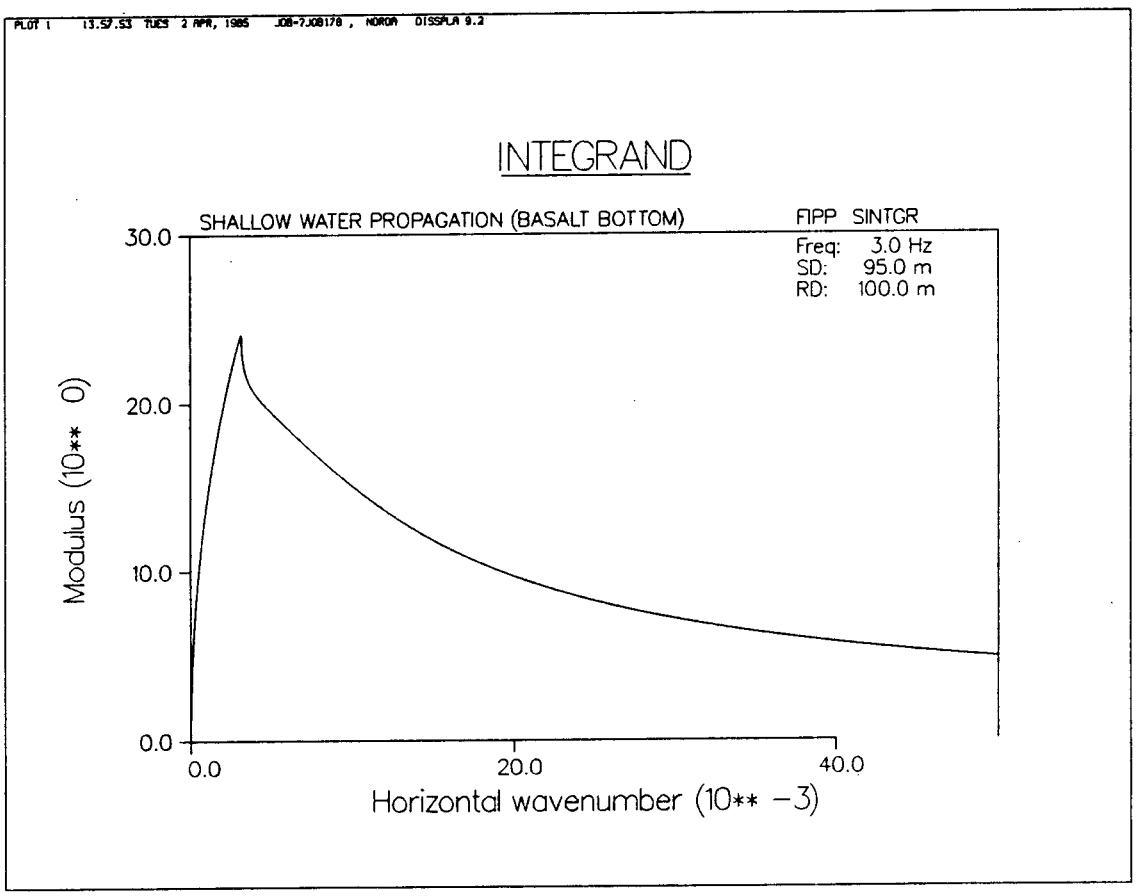
PLOT 1 13.57.53 TUES 2 APR, 1985 JOB-7J08178 , NORDA DISSPLA 9.2
INTEGRAND
SHALLOW WATER PROPAGATION (BASALT BOTTOM)
FIPP SINTGR
Freq: 3.0 Hz
SD: 95.0 m
RD: 100.0 m
30.0
20.0
10.0
0.0
Modulus (10** 0)
0.0
20.0
40.0
Horizontal wavenumber (10** -3)

pulse centered around f = 5 Hz. The dispersion behaviour and seismic waveform clearly indicate a surface seismic wave. In addition, it is known that (Scholte) interface wave amplitudes decrease exponentially with depth away from the interface; this is plainly observed in **Figure 28**, which shows the Scholte wave field as would be seen by a string of receivers buried at progressively greater depths below the ocean bottom interface. the net transmission loss level is likewise seen to vary rapidly with increased depth below the interface, as shown in a contoured plot of scaled pressure vs range and depth (**Figure 29**).

Figure 27

Fullwave synthetic seismic Scholte (marine interface) wave for fullshear elastic basalt bottom at nearfield source-receiver ranges

(clearly showing frequency dependent dispersion in waveforms)

NORMAL STRESS

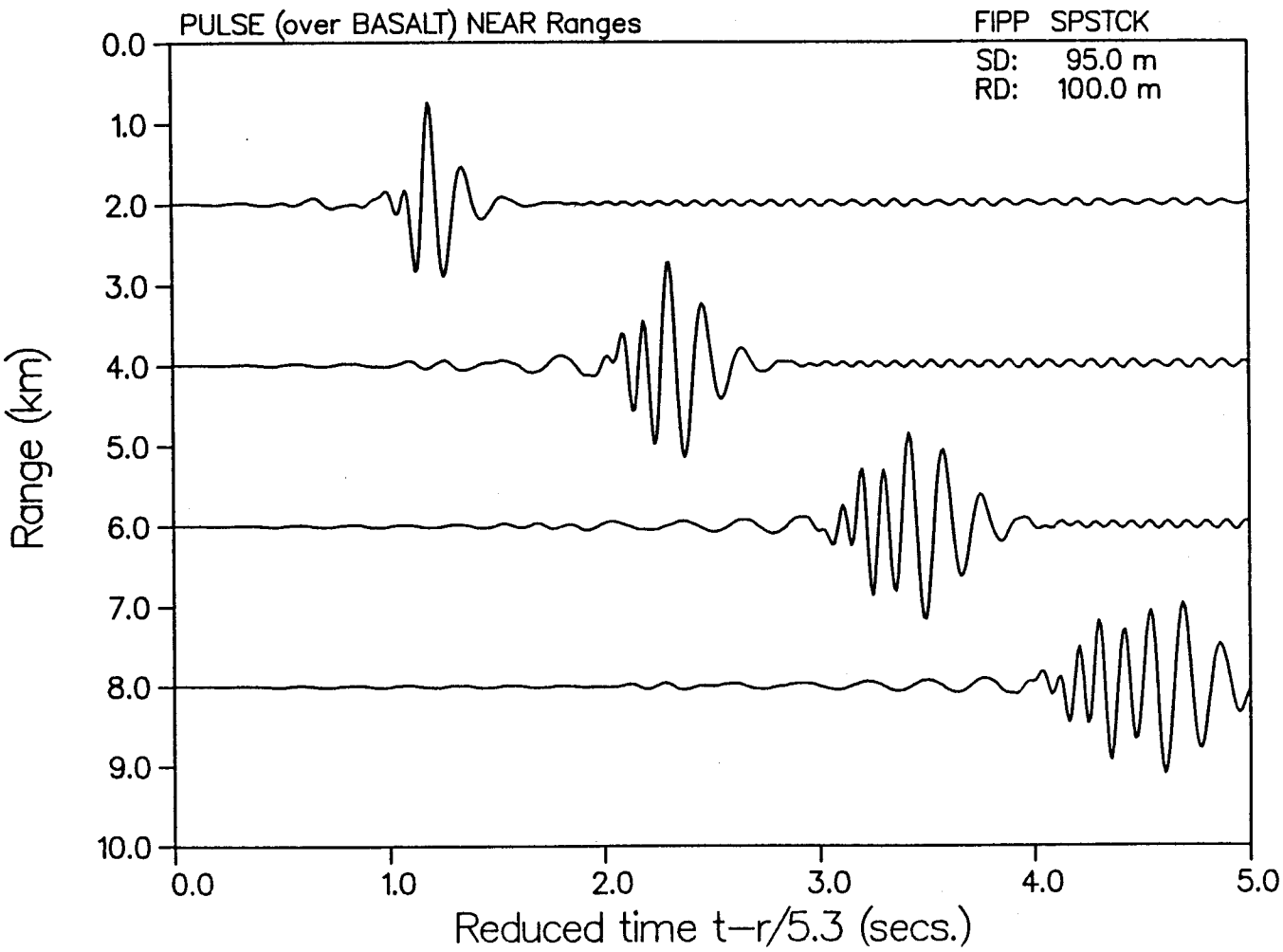

Figure 28

Fullwave synthetic VSP (vertical seismic profile) for full-shear elastic basalt bottom (#receivers=10), showing exponential amplitude decay of Scholte interface wave with increasing distance from interface

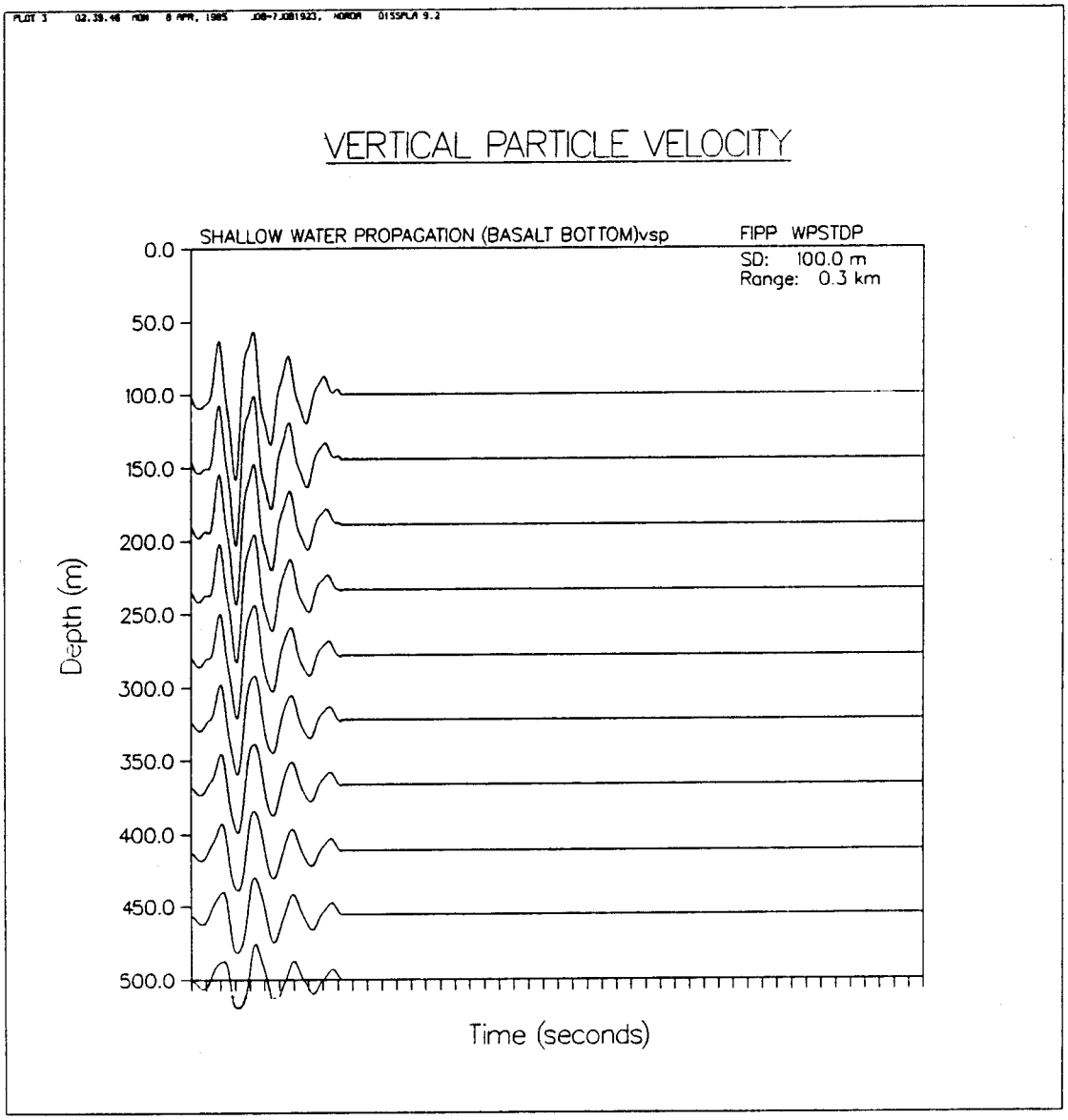
VERTICAL PARTICLE VELOCITY
SHALLOW WATER PROPAGATION (BASALT BOTTOM)vsp
FIPP WPSTDP
SD: 100.0 m
Range: 0.3 km
0.0
50.0
100.0
150.0
200.0
250.0
300.0
350.0
400.0
450.0
500.0
Depth (m)
Time (seconds)

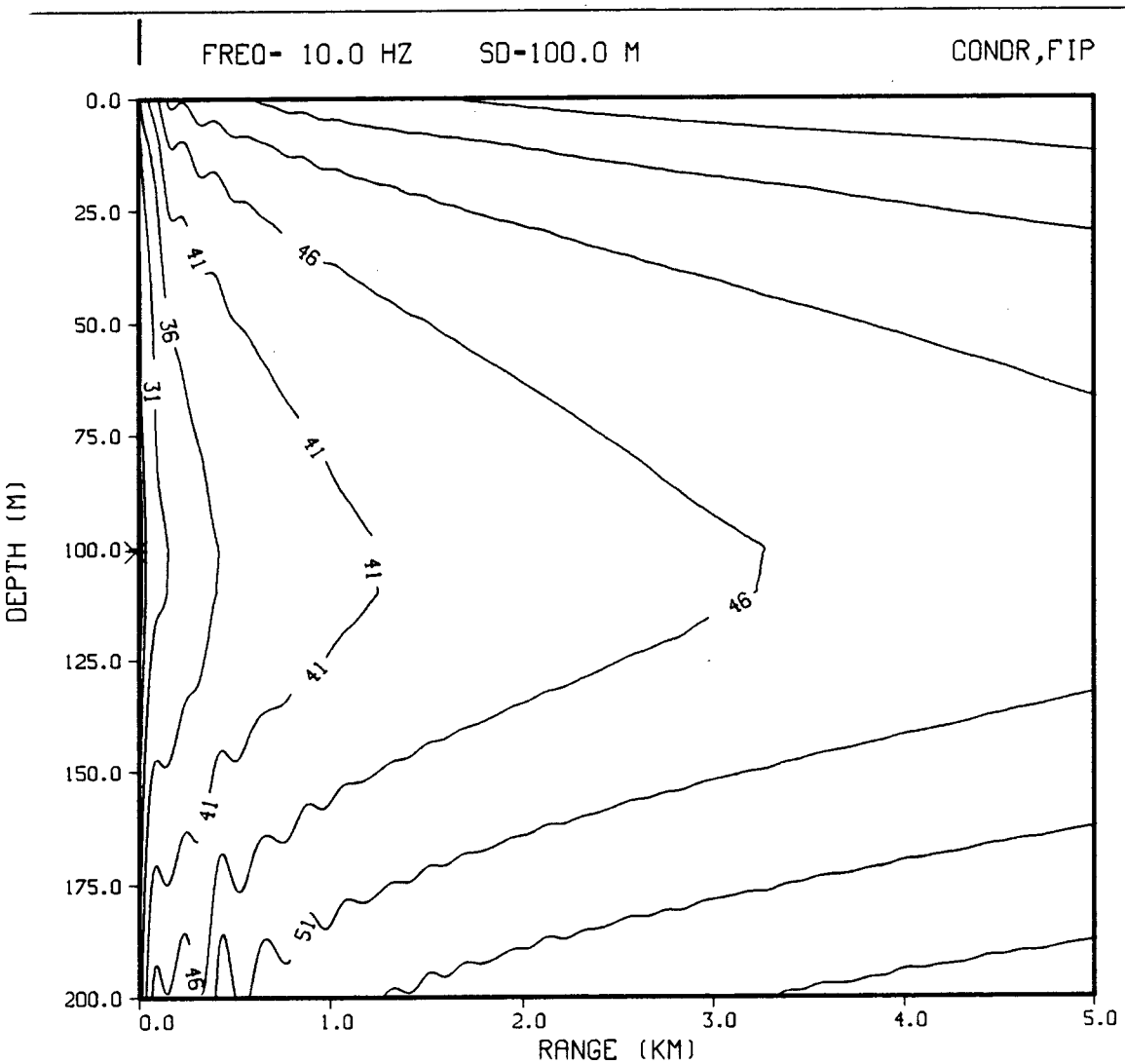

Figure 29 Depth-range contoured Transmission loss for Basalt (VLF)

The preliminary results obtained here with FFP SAFARI for simple idealised shallow water Pekeris models confirms the previous numeric and model-data comparisons reported by AKAL, ESSEN, RAUCH and SCHMIDT, and suggests major trends and sensitivity of transmission loss to gross experimental and environmental parameters for further investigation:

1. Repeat the above calculations for other pure and mixed geology bottom layers (those incorporating extreme ranges of low and high shear rigidity) to better delineate specific regimes and mechanisms of shear-related TL in common shallow water bottom stratigraphy.

2. Examine the effect of varying the total number, thickness and location of component bottom layers, to further specify the minimum "hidden depth" and fine-scale structure influencing TL at very low frequencies.

3. Systematically vary source and receiver depth and range configurations, and also type of source (nonpoint) and receiver(s) (hydrophone,geophone;water-surface,water-column,ocean bottom, subbottom) so as to assess the optimal conditions for a/. geobottom reconaissance and b/. detection.

4. Specifically study the effects of simple discontinuities, simple as well as higher order sub-bottom gradients, in both P/SV

wave velocities and attenuations, on fluid/bottom energy partitioning as well as specific contributions of P-Sv headwave and interface wave generation to net TL.

5. Couple Greens function and TL range plots with depth-contoured TL vs range and reflectivity plots to further constrain interpretation (complute and analyse contoured plots of horizontal and vertical particle velocities).

6. Test previous results from generalized ray modelling (SPUDICH, 1977) that:

a. primary features of ocean bottom response for shallow water VLF are dominated by the "solid" basement (for sufficiently thin overlying sediment cover: zSED < zGeometric turning depth)

b. this dominance becomes progressively stronger for increasing source/receiver separation

c. except for specific ranges at which gradients in P/Sv layer velocities generate diving rays thru sediments, where

d. strong P and Sv wave velocity gradient structure of this sediment to basement transition zone can crucially effect net ocean bottom response (WHITE & STEPHEN, 1980).

Section III(c)

Application of the Direct Fullwavefield/Reflectivity Method to Investigation of possible LVL transition zones in the eastern Basin and Range

The sensitivity of waveform shapes, arrival times and types to different crustal velocity-depth distributions has been the current basis for employing theoretical seismogram synthesis to forward modeling of gross real earth structure. One region for which many differing and often contradictory models have been proposed is the upper crust-mantle transition zone in the eastern Basin and Range province, an area of extreme geophysical and tectonic complexity (SMITH et al, 1980). PAKISER (1985) has extensively reviewed the history of explosion seismology and deep crustal models for the Basin and Range province.

This section is a provisional report of ongoing work seeking to systematically study predicted types of converted, refracted, multiple and inhomogeneous seismic arrivals produced by a wide range of features common to proposed first order discontinuity, gradient and mixed (discontinuity/gradient) velocity depth distributions. Complete full wavefield and reflectivity synthetics are computed using the SAFARI program of SCHMIDT (1983).

In the following, we first examine the differences in arrival types, time and waveforms seen in synthetic records for a basic generalized **low velocity layer (LVL)** model. After a brief synopsis of current reflectivity models, and a discussion of major crustal arrival phases as well as a brief review of the conceptual evolution of crustal models in general, we re-examine the DELTA WEST-SHOAL data (EATON et al, 1964), used by PRODEHL (1971;1979) to derive crustal velocity/depth models via GIESE's modified Herglotz-Wiechert inverse method. The full wavefield and reflectivity synthetic seismograms are computed for Prodehl's initial models, and compared with both Delta Shoal field data and with the general LVL model of BRAILE and SMITH (1975), and the Delta West reinterpretation of MUELLER and MULLER (1979). These later results are considered in terms of the thus-far unsuccessful attempts to identify additional (intermediate range/time) crustal arrival phases to further constrain velocity/depth models (PAKISER, 1985). We here specifically examine the suggestions of MCMECHAN (1982) and BANDA and DEICHMANN (1983). These respectively seek to associate additional intermediate reflection arrivals with either further shallow crustal structure, in the structured triangle-LVL model of McMECHAN, or else simply with additional arrivals automatically comprehended in the complete wavefield response for the simple unstructured LVL of BANDA and DEICHMANN.

Seeking to preserve the simplest velocity/depth model consistent with observed arrivals, as well as to examine the resulting

wavefield from recently-proposed LVL models, we then compute the full wavefield and reflectivity synthetic seismograms corresponding to the next order of crustal structure complexity, ie, that resulting from including (a) further linear fine structure within the single LVL of MUELLER-MUELLER, after DAVIDOYA (1975); (b) additional intermediary LVL zone, as per KIND (1974); and (c) the purely-theoretic 'random comb' crustal model of ZSCHAU and KOSCHYK (1976), and MEISSNER (1970). Each of the above models requires an increasing computational size, from (a) thru (c) spanning 30 to 90 + layers, computed over all wavenumbers, for a source frequency centered at 5 Hz, with spectral power from 0 to 12.5 Hz. In all the above, we have modelled velocity gradients via a series of thin isovelocity layers, under the criteria that the maximum thickness of each component layer be less than or equal to one quarter the prevailing shear wave velocity. The validity of using thin homogeneous layers to model a vertical velocity inhomogeneity was confirmed in every case by checking that the resulting seismogram converged to the same arrival curves and waveforms when the number of component layers was changed.

These results allow basic conclusions about the improved crustal modeling made possible by the direct global approach of SAFARI, and indicate further directions for future study to reduce ambiguity in crustal model selection for the eastern Basin and Range.

Background

The reflectivity method has been repeatedly re-discovered and modified by several investigators for numerous applications to both ocean acoustic and seismic applications. In this approach, a synthetic seismogram of surface and/or body waves at explosion seismic distances (where no earth flattening correction is needed) characterises the response from a specified subset of a multilayered plane homogeneous stratified medium to excitation by a harmonic point displacement or pressure source, via reflexion and transmission properties of major (lower) portions of the stratification. This was originally introduced by FUCHS (1968), MULLER (1969) and FUCHS and MULLER (1971) to describe an exact "generalised ray" technique in which all multiple reflexions and mode conversions are retained in a specifiably-lower part of the subsurface. PP reflexion coefficients for the major subsurface region $z > z_r$ are constructed for a stack of uniform plane layers, by modification of the classic propagator matrix method of THOMSON (1951) and HASKELL (1953). This was later extended by FUCHS (1976) to allow additional P-S conversions, and by KIND (1976) and STEPHEN (1977) to include the cases of a single buried source and receiver respectively. MULLER and KIND (1976) effectively move the reflexion zone to the surface by taking as an approximate nearsurface model a very

dense stratified acoustic fluid (having wavespeed of air overlying a stratified halfspace).

The Fuchs-Muller reflectivity representation of the two dimensional elastodynamic Green's function is developed in the complex horizontal wavenumber - frequency domain. Once the major effort of computing the total reflectivity matrix has been completed, one need only numerically integrate the above impulse response over wavenumber and inverse Fourier transform over frequency to generate standard synthetic seismic records for desired frequency bandwidths and angles of incidence.

As noted above, there already exist numerous reflectivity approximation and extension schemes for including/excluding specific seismic phases, frequency bands and/or velocity depth distributions. These utilise either hydrid combinations of reflectivity with generalised ray theory (FABER and MULLER, 1980) or reflectivity with finite differences (KORN and MULLER, 1982; ALEXEEV and MIKHAILENKO, 1980). In response to chronic problems of instability for high frequencies/large layer thicknesses in finite accuracy calculations with propagator matrices, WOODHOUSE (1980) and FRANSSENS (1983) have further developed improved 'delta matrix' techniques. As CHIN et al (1984) have recently discussed, KENNETT (1974) has alternatively reformulated the unstable propagator calculation into a stable ray-expansion recursion. This algorithm in principle allows selective decomposition of net received wavefield into contributions by

primaries and a specifiable order of multiples. However, despite major successes of these approaches to particular applications, it has often proven difficult to readily incorporate all arrivals, environmental and experimental conditions of interest for seismic modeling into one generally-applicable efficient and physically-transparent transfer matrix based algorithm.

As an alternative to "local" Green's function solution techniques, the algorithm SAFARI, originally developed by SCHMIDT (1982) for improved underwater acoustic modeling (as an extension of extant FFP techniques) comprises a Direct Global matrix approach that requires no correction or approximation of additional arrivals and/or effects. SCHMIDT (1982; 1983), SCHMIDT and JENSEN (1984) and SCHMIDT and TANGO (1985) have varyingly demonstrated that the complete exact Green's function spectral responses for an arbitrary stack of plane layers can be efficiently constructed in direct fashion from a global form of the Pekeris layered media solution, avoiding time consuming approximations or cumbersome analytic solutions. SCHMIDT and GLATETRE (1985) have shown an easy further extension of SAFARI to both distributed and 3-dimensional sources, and TANGO and SCHMIDT (1985) have discussed the natural applications of SAFARI to complete synthetic vertical seismic profiling (VSP).

The SAFARI complete exact wavefield solution, comprehending any arbitrary number and distribution of solid/fluid layers, sources and/or receivers, and having vastly decreased CPU time, opens up

many new avenues for examining total wavefield responses from large order crustal seismic models.

Main Wave Groups on Deep Crustal Refraction Profiles

Until the last decade, attention in model-data comparison for deep crustal seismic study has been focused primarily on results of very low frequency pulse seismic refraction data, using established generalised ray, modal summation or basic reflectivity type modeling programs. The advent of improved hi-density refraction, and of practical deep crustal reflexion seismic profiling (together with improvement of synthetic seismic modeling capabilities) have led increasingly to re-examining not only previously-interpreted data profiles, but the full range and type of seismic wave arrivals expected. This in turn has led to a reassessment of the basic types of possible crustal models derivable/detectable in terms of these.

As mentioned above, numerical modeling methods in theoretical and deep crustal seismology may differ with regard to both the number and kind of arrival types and branches as well as individual waveform features in each. Thus any generalisation of major crustal wave groups expected must be based on features of wavefields characteristic for each specific numerical model. Here the "extended-reflectivity" full wavefield solution of SAFARI is considered. This will allow accurate modeling of <u>all</u> expected wavefield features from a given class of crustal velocity/depth

as represented in the generalised reduced-traveltime diagram of **Figure** 30. These are discussed below, as per their range-traveltime occurance in the subcritical (nearfield), critical and postcritical (farfield) regimes.

Figure 30

Schematic plot of generalized reduced-time deep crustal seismic arrival types
(Major refraction phases indicated)

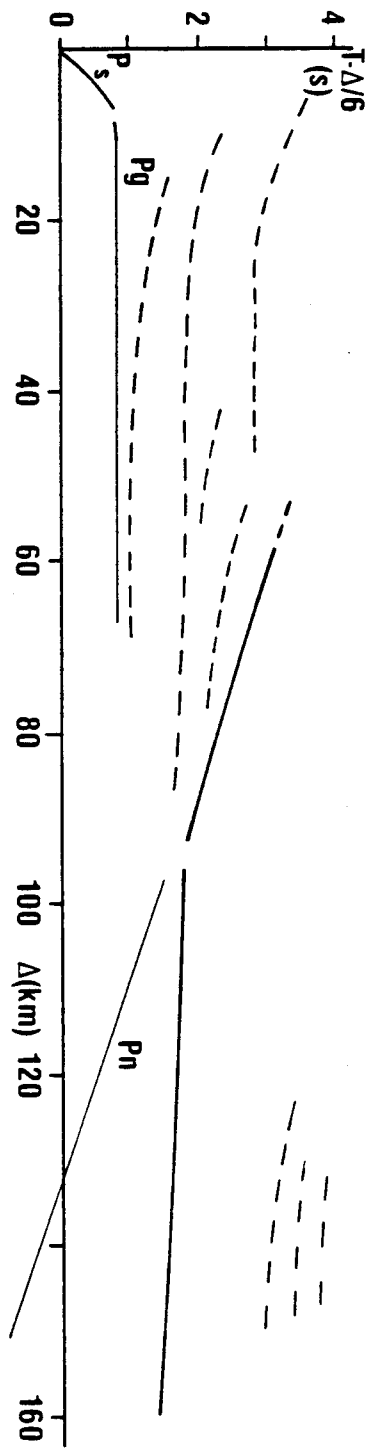
0
2
4
T-Δ/6
(s)
Ps
Pg
20
40
60
80
100
Δ(km)
120
Pn
160

Subcritical (including near-vertical incidence) Arrivals

Subcritical reflexions are waves reflected one or more times from one (or more) interfaces at small angles of incidence, important typically in source-receiver ranges from 0 - 40km. Having characteristically weak-concave traveltime curves, their (P1R) amplitudes are strongly enhanced by discontinuous velocity contrasts above and below the given reflecting interface, whereas a velocity transition zone (gradient) significantly decreases subcritical reflexion amplitude. An additional frequency-dependence in amplitude has been noted from theory (CERVENY, 1966), notably for near vertical reflexions from thin laminated transition zone layers. These 'stratigraphic' structures have long been noted elsewhere (OSTRANDER, 1984) for having frequency dependent reflexion coefficients at certain characteristic "tuning" frequencies, due to constructive wave interference, and have gained recent attention in discussion of COCORP results (HALES and THOMPSON, 1982; JONES and NUR, 1984).

Also notable in the nearfield, Pg headwaves often appear as a first arrival, showing characteristically zero or slightly convex traveltime curvature. Typically evident at distances up to 70 km offset, Pg arrivals have been generally conceived as a refracted head wave travelling in/along a major upper crustal interface, or else as two or more closely associated refracted arrivals showing

complex structures of first and secondary arrivals (if sedimentary cover is complexly varying).

GIESE et al (1976) notes the Pg arrival's inherently complex waveform, in the case of a subMoho velocity gradient. HILL (1971) and BRAILE and SMITH (1975) have shown that positive velocity gradients result in large Pg amplitudes, whereas negative gradients attenuate Pg. CERVENY and RAVINDRA (1971) have also shown (contrary to geometric ray theory results) that Pg amplitudes do not decrease monotonically with distance past the critical point, further suggestive of a complicated interference mechanism for their generation. Although rather quickly appearing as a single head wave type, in very near source-receiver ranges (typically 0~20 km) the complex interference nature of Pg arrivals can be clearly seen, when considering the synthetic reflectivity seismogram result for Model LVL6 in BRAILE and SMITH (1975) (**Figure** 31).

Despite the above conceptualisation of Pg phases, the seismic literature has repeatedly used the notations "P" and "Pg" interchangably, in reference to the often-noted resemblence between 'classical' Pg and the broad large amplitude P wave phase typically following Pn. An almost consistent group velocity of ~ 6 km/sec and propagation behaviour largely insensitive to details of deep crustal and mantle structure has led to the suggestion that P/Pg be best viewed as a mode phenomenon. This entails a model of multiply reflected P waves trapped within an overall

Figure 31

Fullwave synthetic seismogram generated by 'SAFARI' for LVL6 Model (after BRAILE and SMITH, 1975), showing interference headwave complex of Pg arrivals in nearfield, and dispersed arrival character for farfield

VERTICAL PARTICLE VELOCITY

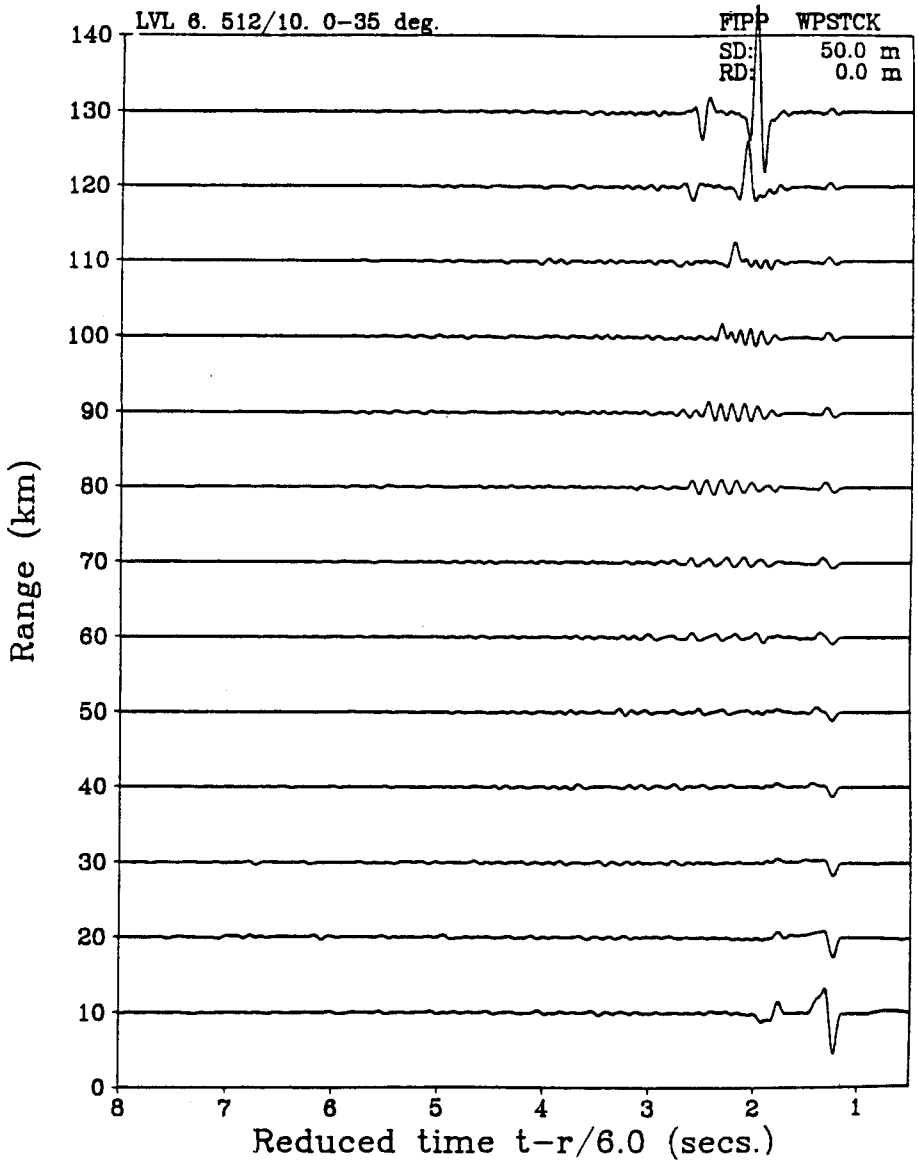

gross-scale crustal waveguide. Further studies from this approach over long ranges have been recently given by HADDON (1984).

Figure 32 shows a hypothetical seismic record computed by SAFARI in both reflectivity and fullwave mode from the simple LVL6 model after BRAILE and SMITH (1975), over a series of equispaced geophones at LVL depths (effectively constituting a theoretical Vertical Seismic Profile for the continental crust; PUJHOL et al, 1984). Here the interference nature of the Pg arrival is graphically demonstrated at depths corresponding to wavefield evolution through an LVL gradient zone.

Further insight into the Pg arrival can be gained when comparing a reflectivity synthetic (**Figure** 33b) with that resulting from the full wavefield SAFARI solution (as in **Figure** 33c). A distinct additional arrival is noted in the extreme near field immediately following the first Pg arrival. The exact nature of this additional surface-multiply reflected (ghost) P-SV converted- arrival can likewise be clearly shown here by computing the hypothetical VSP over depths, as above.

Although in general not as widely observed (BARANZANGI et al, 1982), SMITH et al (1976) have noted the recording of Sg and other corresponding shear converted modes on nearfield refraction survey traces, for which horizontal particle velocity records offer better detection response.

Figure 32

Full wavefield hypothetical VSP for LVL6 Model (after BRAILE and SMITH, 1975), showing mode conversion and interference nature of head wave arrivals

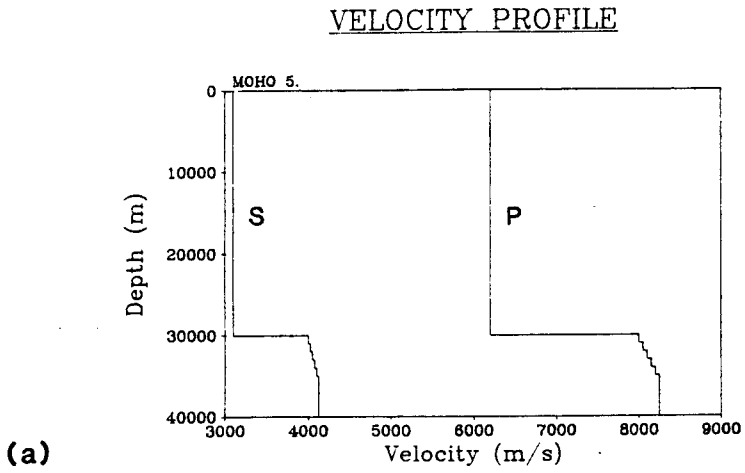

(a)

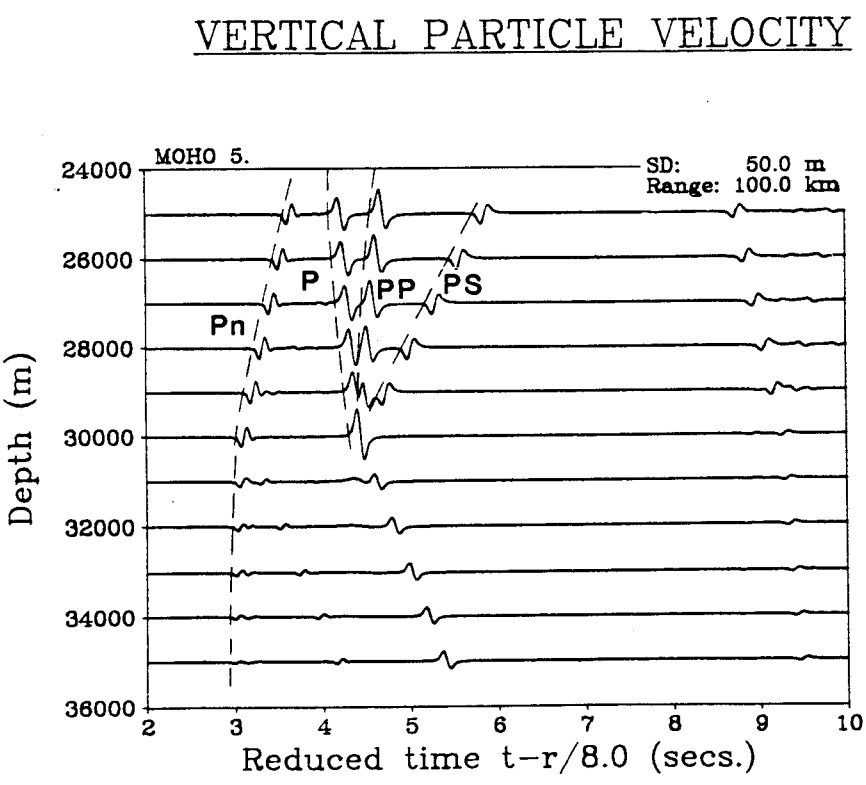

(b)

Synthetic seismograms for MOHO-5 crustal model. a. Velocity profile. b. Synthetic VSP at 100 km range and 25-35 km depth.

Figure 33

Comparative reflectivity and full wavefield synthetic seismograms for LVL6 Model (after BRAILE and SMITH, 1975), showing full agreement except in farfield for surface multiple and conversion effects

VELOCITY PROFILE

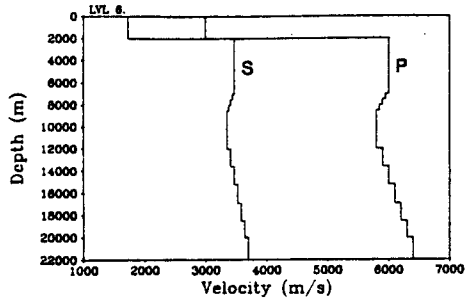

(a)

VERTICAL PARTICLE VELOCITY

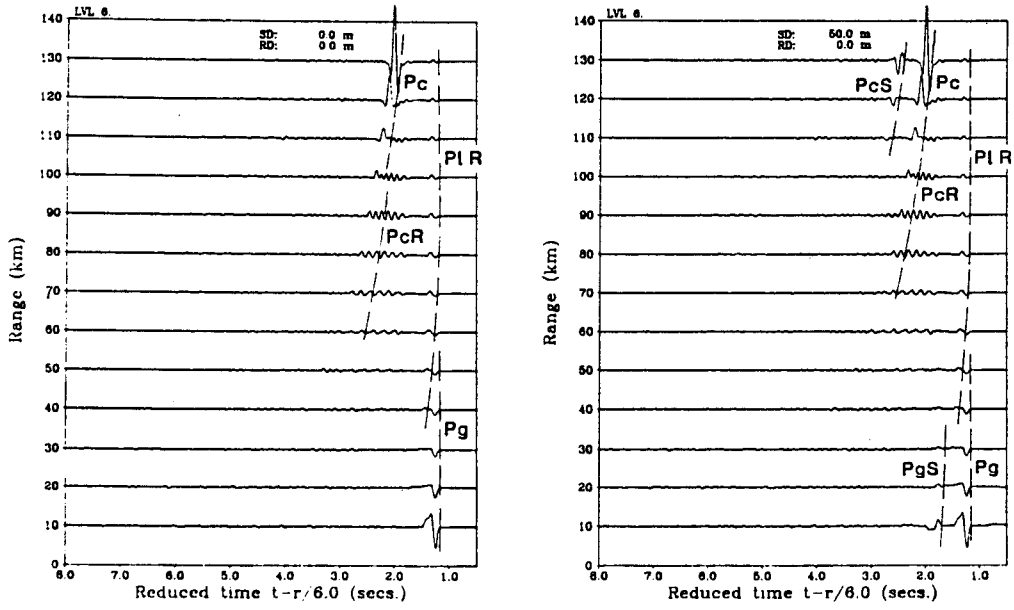

(b) (c)

Synthetic seismograms for LVL-6 crustal model.
a. Velocity profile. b. Reflectivity approximation.
c. Full wavefield solution. Amplitudes are multiplied by range.

Near-Critical Incidence

For an offset region near-to-just-beyond the geometric-ray theory critical distance for the major interface(s) of interest, the first subcritical reflected waves and head wave(s) interfere, resulting in large amplitude net arrivals having generally similar amplitude distance characteristics for most v/z models considered (BRAILE and SMITH, 1975). From exact wave theory it can be shown that these near-critical reflexions (PNR) have maximum amplitude at a distance beyond critical, the maximum amplitude distance discrepancy (between ray and wave theory predictions) decreasing as f approaches 0. It can also be shown that the reflected wavelet phase also changes gradually with distance near the geometric critical region. (One or more PnR phases are also often seen in weak or dispersed form in the extreme nearfield).

In contrast to pure "head" or refracted waves, as mentioned above interference head waves (Pn) exist whenever velocities below the plane reflecting interface vary rapidly with depth (CERVENY and RAVINDRA, 1971). Here an interference head wave is specifically defined as the effective sum of all waves propagated as head refracted waves along a lowermost layered halfspace, which however undergoes repeated reflections and refractions at one or more upper interfaces. Before the critical point, only reflected wave(s) exist; at critical incidence both reflected and head

waves are present. The characteristics of both waves change continuously across and beyond critical, throughout which path Pn exhibits negative traveltime slope.

The length of the interference zone of (subcritical) reflected and head waves is approximately δt, the duration of the input signal pulse. Beyond the critical point, whereas the amplitude of pure head waves decreases very rapidly (proportional to $r^{-1/2}$ $L^{-3/2}$ ($L = x - x_{crit}$), Pn interference head wave amplitudes actually increase with increasing source-receiver separation (**Figure** 21, BRAILE and SMITH MOHO1). The greater the velocity contrast across the interface depth, the farther the range of maximum amplitude lies from the source, and the greater the distance between $x_{max\ amp}$ and x_{crit}.

Supercritical/Wide Angle Arrivals

Prominent wide-angle reflexions from deeper horizons are found on nearly all refraction record sections (PcR) in far offset ranges, with amplitudes that decrease as ~ x^{-1} and phase shifts approaching 90° as range increases.

For many proposed LVL models, supercritical arrivals can be strong reflexions, showing sharp waveform characteristics for distinct discontinuities and a more dispersed character when deeper gradients are considered. As BRAILE and SMITH (1975) have shown, an additional (P1R) reflected arrival, with possible multiply-reflected phases of the primary PcR (PcR1, PcR2,...) as secondary arrivals can also occur, along strongly concave reduced travel time curves, in cases where an LVL is expected.

As discussed by MUELLER and LANDISMANN (1966), the (Pc) refraction arrival, typically found in lower super critical reflexion ranges (having nearly constant delay with respect to Pg) can be seen to occur between PcR and Pg, often intersecting the later at large offset ranges. For the case of a sufficiently large low velocity zone of sufficiently large velocity contrast, the Pc phase is a major arrival, but more typically is difficult to identify against the background of noise and other arrivals. As SHAW and ORCUTT (1984) and HADDON (1984) have discussed, Pc signals can be attributed to strong constructive interference

between large amplitude post critical reflexions and refracted head waves. (An abrupt lower boundary and sufficiently large (>.2 km/sec) velocity contrast between the layers below and above the LVL can result in strong Pc arrivals at comparatively small offset distances; see below). As studies (of FUCHS (1968)) have shown, wide angle reflexions often tend to be relatively weak in amplitude except in the near critical ranges. Appearance of additional "ringing" in PlR type reflexions (with higher order associated multiples) has been used as evidence to suggest additional fine-structured lamination layering in and/or around an LVL zone (LVL6; **Figures** 32 and 33). This is more clearly shown in the detailed hypothetical VSP for LVL 6 in **Figure** 34.

In the catagory of extremely long range arrivals, regional phases can also be used to further constrain LVL crustal models. For the current data set, regional information was not available.

VELOCITY PROFILE

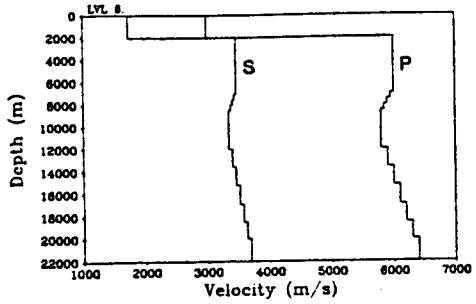

(a)

VERTICAL PARTICLE VELOCITY

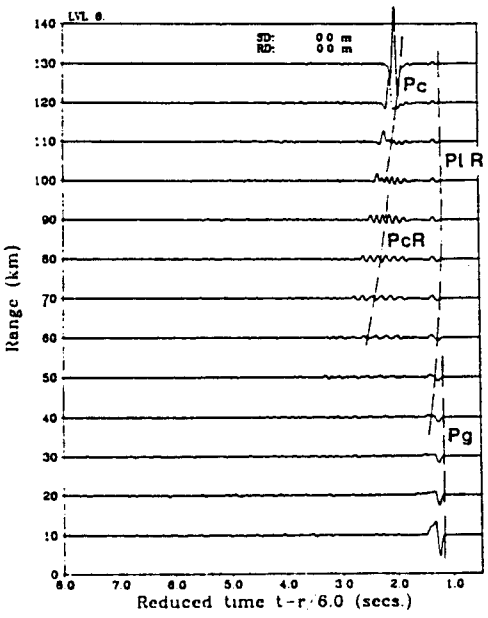

(b)

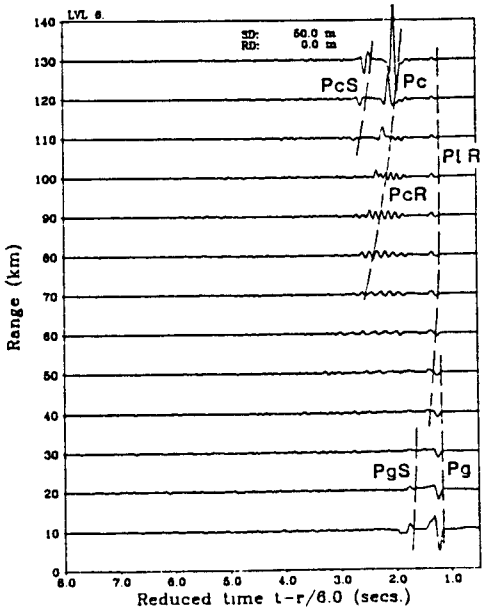

(c)

Synthetic seismograms for LVL-6 crustal model.
a. Velocity profile. b. Reflectivity approximation.
c. Full wavefield solution. Amplitudes are multiplied by range.

Figure 34

Fullwave (hypothetical) VSPs for LVL6 model (as per Figure 31) for 3 source-receiver offsets, showing dispersed anture of arrivals at about x=100km, and shear-converted arrival at about x=120,140km

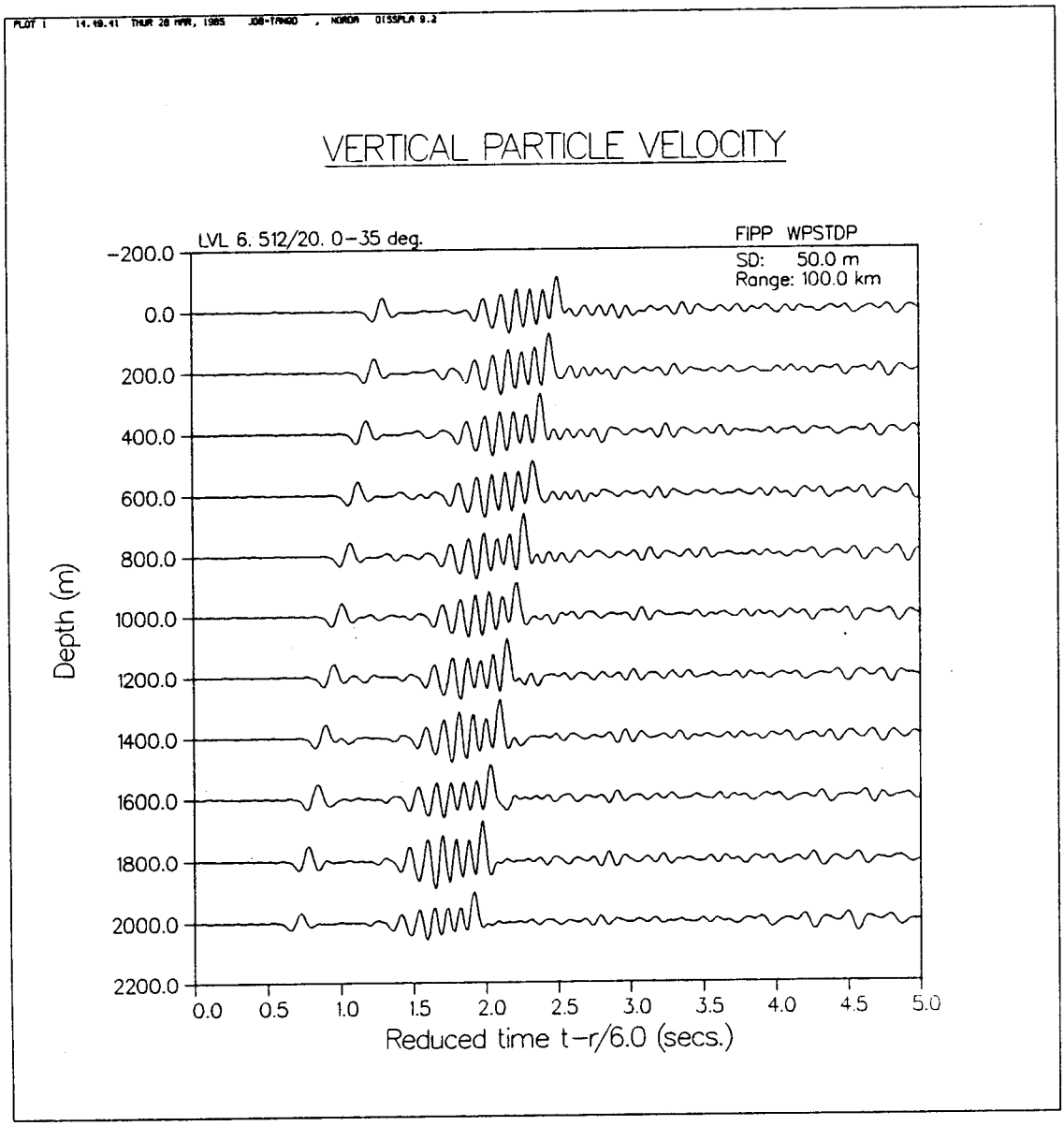
PLOT 1 14.49.41 THUR 28 MAR, 1985 JOB-TANGO , NORDA DISSPLA 9.2
VERTICAL PARTICLE VELOCITY
LVL 6. 512/20. 0-35 deg.
FIPP WPSTDP
SD: 50.0 m
Range: 100.0 km
Depth (m)
-200.0
0.0
200.0
400.0
600.0
800.0
1000.0
1200.0
1400.0
1600.0
1800.0
2000.0
2200.0
0.0 0.5 1.0 1.5 2.0 2.5 3.0 3.5 4.0 4.5 5.0
Reduced time t-r/6.0 (secs.)

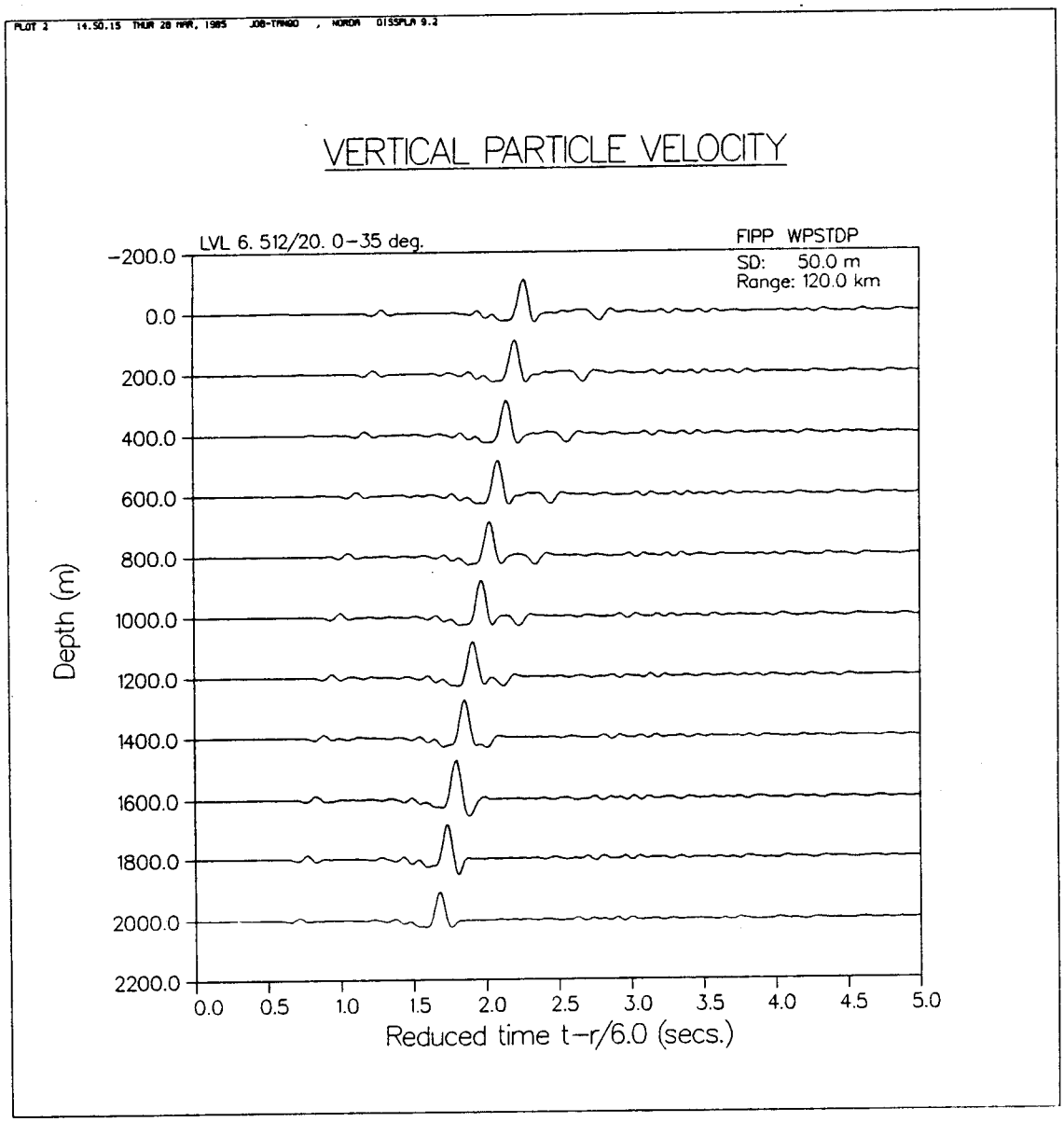
PLOT 2 14.50.15 THUR 28 MAR, 1985 JOB-TRNOD , NORDA DISSPLA 9.2
VERTICAL PARTICLE VELOCITY
LVL 6. 512/20. 0-35 deg.
FIPP WPSTDP
SD: 50.0 m
Range: 120.0 km
Depth (m)
-200.0
0.0
200.0
400.0
600.0
800.0
1000.0
1200.0
1400.0
1600.0
1800.0
2000.0
2200.0
0.0 0.5 1.0 1.5 2.0 2.5 3.0 3.5 4.0 4.5 5.0
Reduced time t-r/6.0 (secs.)

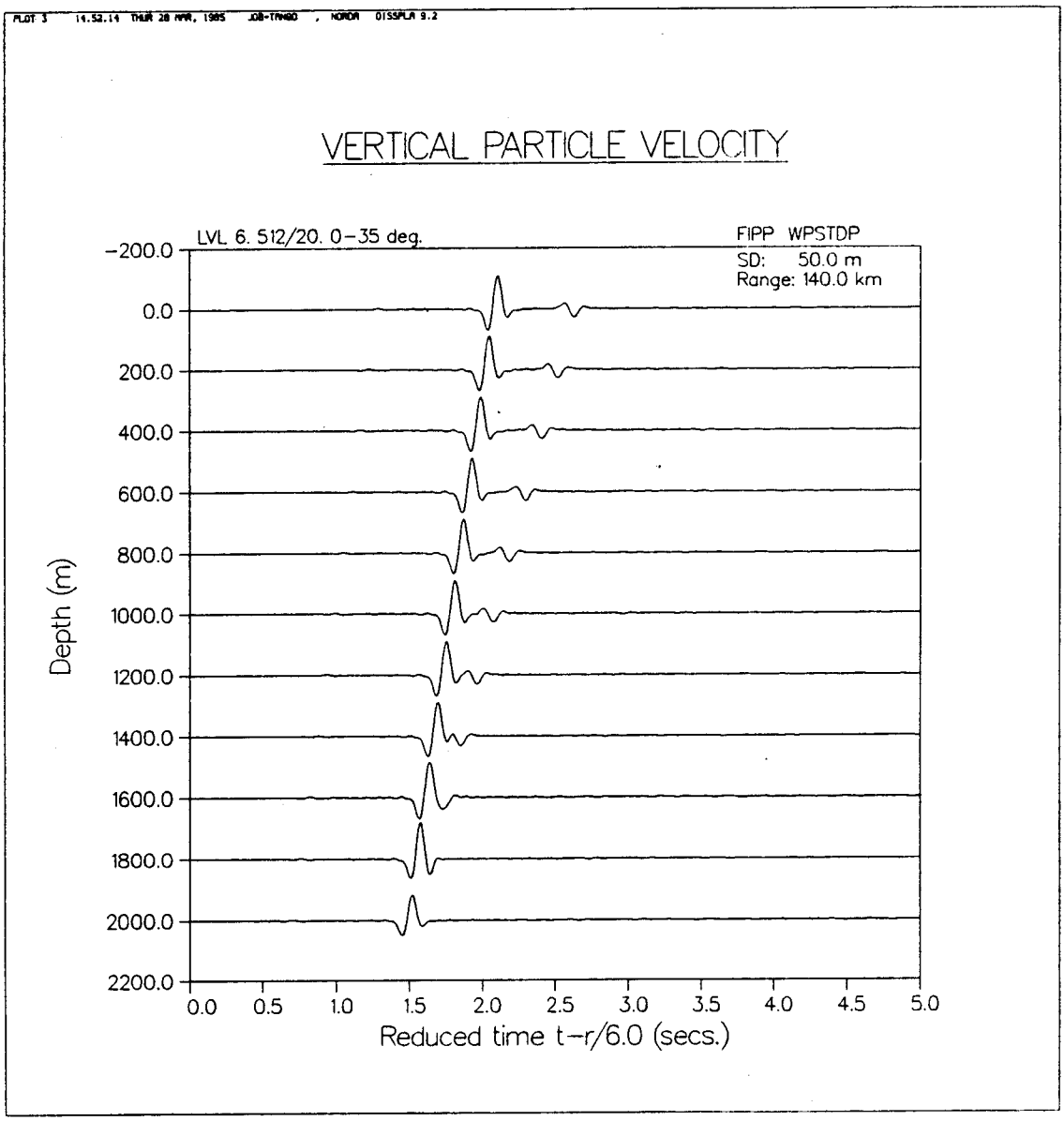
PLOT 3 14.52.14 THUR 28 APR, 1985 JOB-TANGO , NORDA DISSPLA 9.2
VERTICAL PARTICLE VELOCITY
LVL 6. 512/20. 0-35 deg.
FIPP WPSTDP
SD: 50.0 m
Range: 140.0 km
Depth (m)
-200.0
0.0
200.0
400.0
600.0
800.0
1000.0
1200.0
1400.0
1600.0
1800.0
2000.0
2200.0
0.0 0.5 1.0 1.5 2.0 2.5 3.0 3.5 4.0 4.5 5.0
Reduced time t-r/6.0 (secs.)

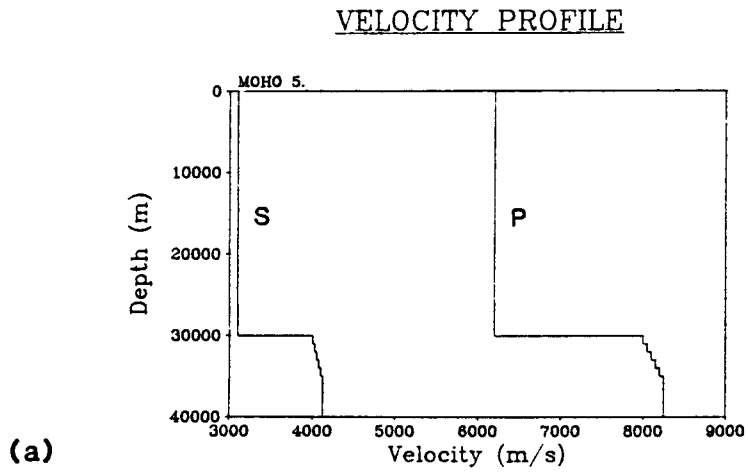

(a)

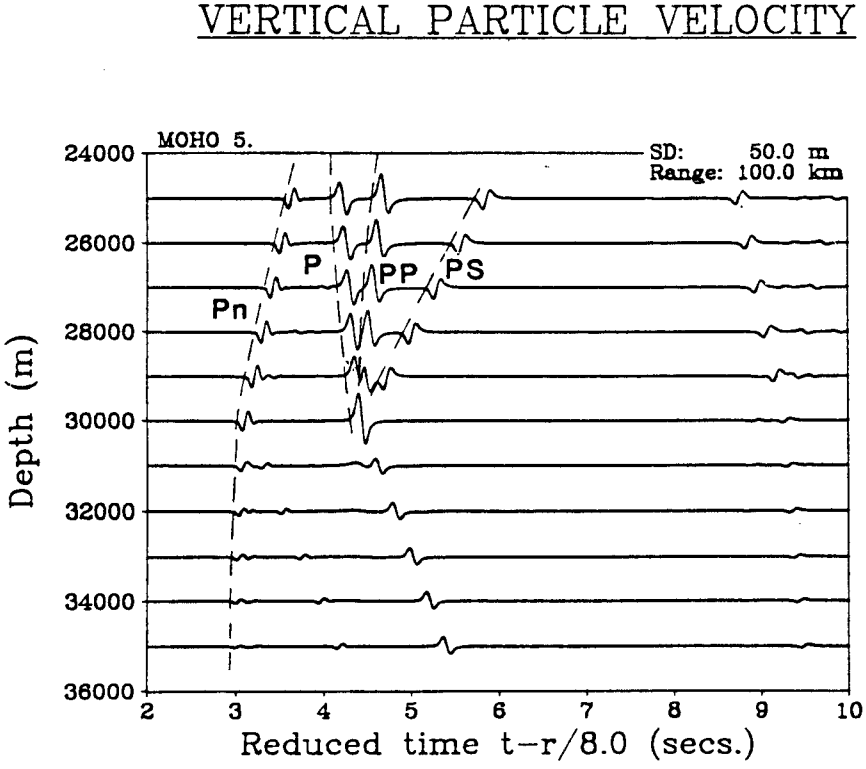

(b)

Synthetic seismograms for MOHO-5 crustal model. a. Velocity profile. b. Synthetic VSP at 100 km range and 25-35 km depth.

Figure 35

Velocity-depth profile and corresponding synthetic reflectivity seismogram for simple 2-layer crustal model (after TATEL & TUVE, 1955; as reviewed in PAKISER, 1985). Compare with MOHO1 model (BRAILE & SMITH, 1975) above.

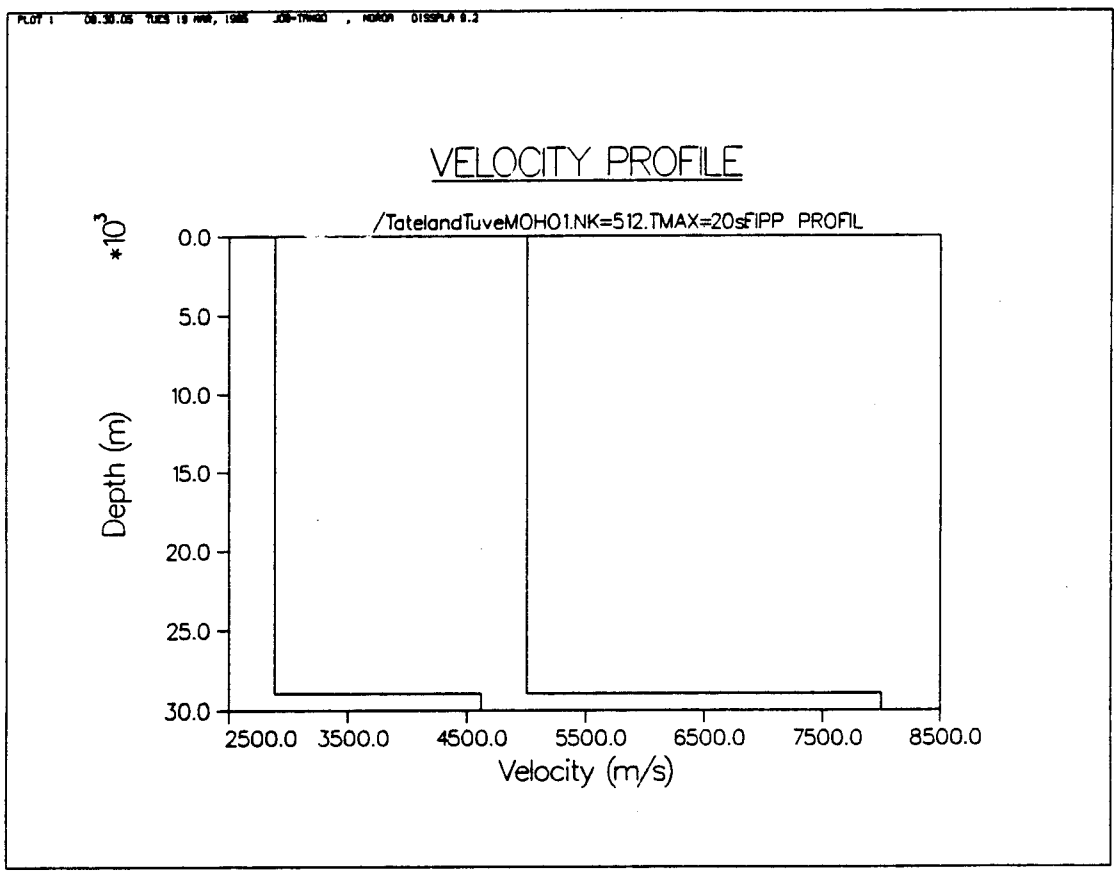
VELOCITY PROFILE
/TatelandTuveMOH01.NK=512.TMAX=20sFIPP PROFIL
*10^3
Depth (m)
0.0
5.0
10.0
15.0
20.0
25.0
30.0
2500.0
3500.0
4500.0
5500.0
6500.0
7500.0
8500.0
Velocity (m/s)

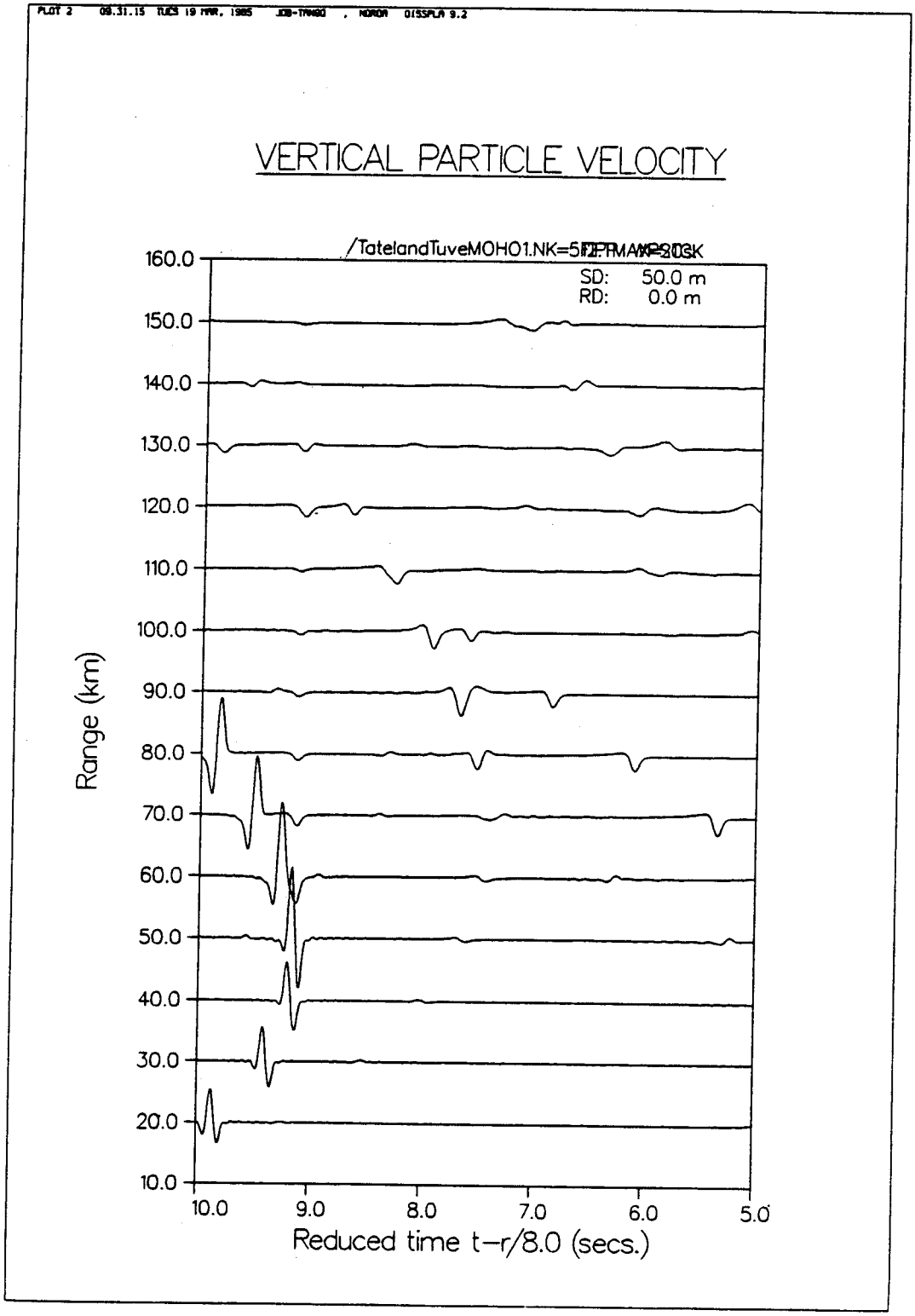
VERTICAL PARTICLE VELOCITY
/TatelandTuveMOH01.NK=5
SD: 50.0 m
RD: 0.0 m
160.0
150.0
140.0
130.0
120.0
110.0
100.0
90.0
80.0
70.0
60.0
50.0
40.0
30.0
20.0
10.0
Range (km)
10.0
9.0
8.0
7.0
6.0
5.0
Reduced time t−r/8.0 (secs.)

VERTICAL PARTICLE VELOCITY

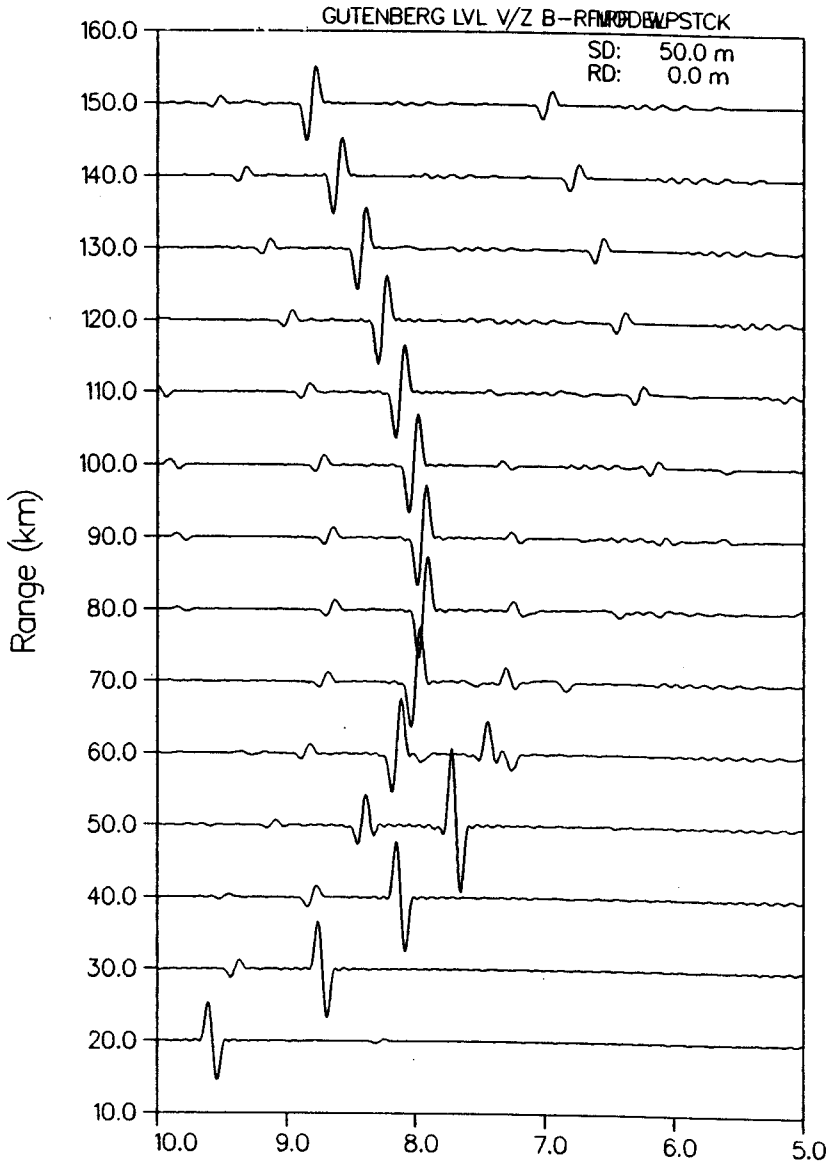

General Models of Crustal Velocity/Depth Structure

There is now a vast literature on the question of seismically-observable structure of continental aeep crustal features, particularly controversial when seeking to reconcile results of previous refraction with recent reflection crustal data. Present findings suggest an increasingly complex evolution of the basic conceptual models for deep crustal interpretation.

Initial crustal observations based on analysis of earthquake records (TATEL and TUVE, 1952) found no evidence of crustal structure, modeling the crust and mantle as a simple slab overlying a semi-infinite halfspace (**Figure 35**; see also MOHO1 in Figure 21). Into this basic 1 layer Moho, GUTENBERG (1955) first suggested introducing a single low velocity layer at the base of the crust to explain heretofore uninterpreted near-earthquake phases. Until the last decade, ie. since the beginning of large-scale seismic refraction and reflexion measurements, this basic "large scale" concept of only two or three isovelocity layers-one of which a low velocity layer (LVL) -has been widely used as a guiding basis for data-model deep crustal analysis.

Based on longer offset refraction and near-vertical reflexion seismics, subsequent detailed crustal investigations have

increasingly implied that this simple few layer block-discontinuity models can no longer satisfactorily fit observed the vast majority of recorded traveltime and arrival type and waveform data. Not only have certain originally-proposed boundaries or layer discontinuities like the "Conrad" been largely discounted as general features worldwide, but the very notion of worldwide uniform isovelocity layers and simple first-order discontinuities have by now become increasingly regarded as but themselves first order approximations of the "true" crustal velocity/depth distribution -which is itself now largely seen in a **local** statistical sense only (CAPON, 1973).

Strongly influenced both by the improved resolution and results of exploration and deep crustal reflexion seismology, one recent approach to explaining the often rapidly-varying reflexions occuring between the main known arrival phases has been to attempt to use a model of many stratified lamellae having many more layers of smaller and variable thickness (MEISSNER, 1967; FUCHS, 1969; CLOWES and KANASEWICH, 1970; MEISSNER, 1973; DAVYDOVA, 1975; GIESE et al, 1976; OLIVER et al, 1980; HALE and THOMPSON, 1982; JONES and NUR, 1984).

Pursuing this idea, several authors have investigated the nature and source of additional pre-MOHO events (between 'established' refraction arrival types) in terms of possible further finely-layered internal structure to both pre and post-MOHO regions, and within the LVL(s) itself; (MCMECHAN, 1982). These authors have

proposed one or more transition zones of highly variable and depth-extended natures, including varying combinations of both discontinuities and gradients. In addition, near vertically incident reflexion seismic results have likewise implied models involving many thin layers of both high and low velocities, each having thickness of anywhere from .1 to 1 km (HALE and THOMPSON, 1983).

To better meet the demands of a 'statistical' deep crustal interpretation on the one hand, and an increasing amount and complexity of detailed individual waveform and secondary arrival information from both seismic refraction and reflection data, gross step wise velocity layers have been increasingly replaced by a much larger number of layers to more closely approximate a 'random' semi-continuous distribution. However, at the same time as the number of possible layers and layer-distributions have increased, the question of the precise origin and nature of 'canonic' arrival types (as well as that of 'optimally' the true velocity-depth distributions responsible for these) becomes all the more problematic.

The above problem of complex arrival identification through wavefield decomposition, together with that of reconciling far-field (postcritical reflexion) with nearfield (precritical/'shadow zone') refraction data, has been particularly acute for the question of modeling possible

refraction and reflection returns from one or more LVL zones (from a geographic region for which good data exists).

DELTA Profile: proposed LVL in the eastern Basin and Range

The Delta West/Delta Shoal profiles (EATON et al, 1964) provide an excellent example of high-resolution seismic refraction records having implications for both refraction and reflexion seismic crustal interpretation. Extending westward in the Basin and Range province from Nevada (PRODEHL, 1971) thru Utah, the Delta West profile in particular has been repeatedly cited as giving strong evidence for the existence of a crustal LVL with fine structure.

Considering the basic data record, (Figure 36, from PRODEHL, 1979)) large amplitude near field arrivals, corresponding to one or more additional head wave arrivals, have been taken to indicate a possibly strong velocity contrast at the base of an extended zone of velocity variation. However, as has been known almost since the inception of the seismic refraction method, direct determination of detailed LVL interior layer structure is theoretically not possible from surface source refraction data alone. Refracted rays do not bottom within an LVL, so that seismic refractions are "blind" to velocity inversions. In addition, generally as many as 9+ phases have been identified and discussed in the literature (PRODEHL, 1971; GIESE et al, 1976; MCMECHAN, 1983), often in terms of multiply-reflected subcritical arrivals from one or more velocity inversions at localized depths. However, although in some cases relatively compact, these

Figure 36

Field record section of refraction seismic deep crustal data from DELTA West-Shoal profile (after PRODEHL, 1979)

note salient features of shadow zone (2-4 seconds, 60-70km offset) and high-amplitude interference complexes above and below the geometric shadow zone

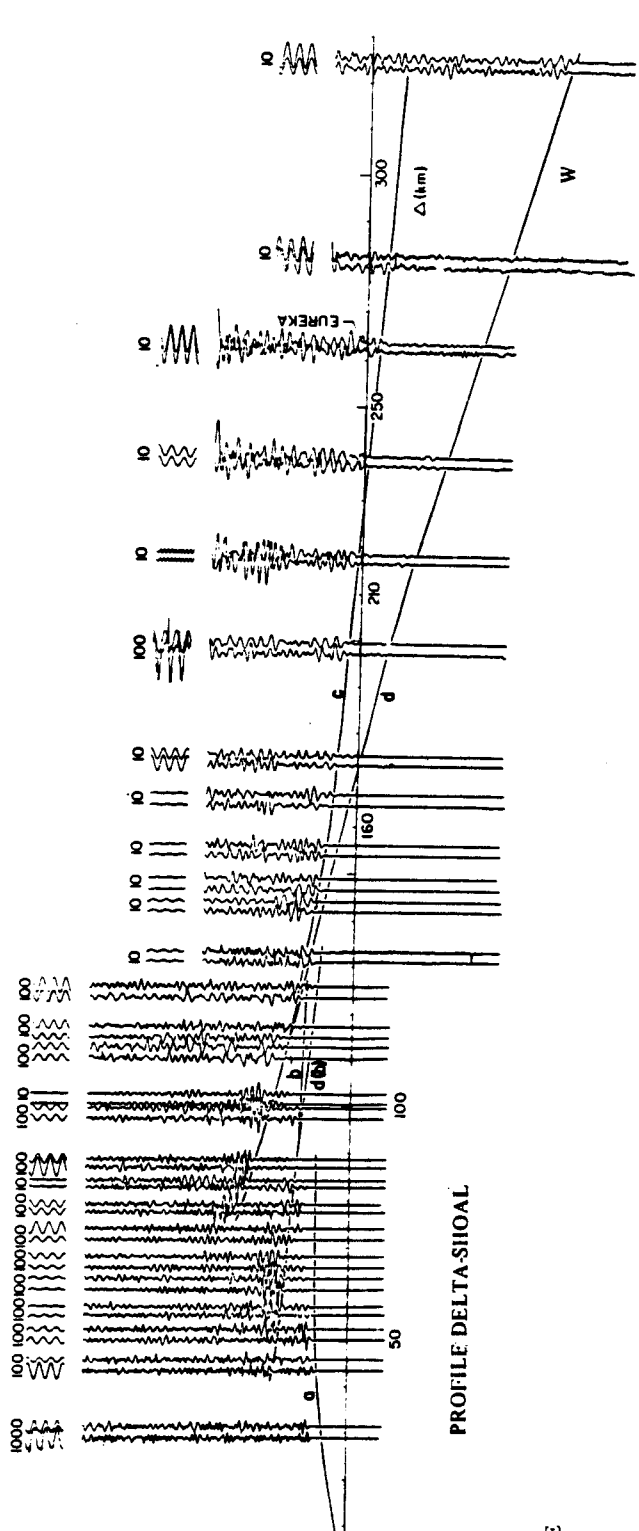

—Record section of the profile from Delta (16) to SHOAL (10). The numbers behind the shotpoints refer to figure 1, plate 1*A*, and table 1. Two traces of each seismogram are plotted. The corresponding calibration at the top of each trace is marked in microvolts. Section produced by S.W. Stewart and P.R. Stevenson, U.S. Geological Survey.

phases are usually traceable only over rather short (3-5km) segments of the total profile. Furthermore, they are often only poorly-distinguishable against a background of localized interference complexes of comparable or greater amplitude. As will be seen, ever since the initial analysis by PRODEHL (1971), at least 3 sources of difficulty have presented themselves in attempted forward modeling of proposed LVL crustal structures:

1). inherent theoretical weaknesses in the various (ray-theory) methods for approximate inverse modeling, by introducing artificial bottoming points (EARTH-model errors)

2). difficulties in discriminating algorithm-or-user-dependent variations in the forward numerical model for synthetically computed wavefield responses (PROPAGATION-model errors) from

3). observable differences due to ambiguities or errors in deep crustal structures themselves (GROUP/PHASE CORRELATION errors).

An example of problem type #2 is specification of the minimum and maximum limits of angular integration when computing a reflectivity or fullwave synthetic seismogram (**Figures** 37a-d).

In light of the above, in the following we consider 3 previous interpretations of the DELTA WEST Profile, due to PRODEHL (1971;1979), MUELLER and MULLER (1979), MCMECHAN (1982) and BANDA

and DEICHMANN (1983) and examine the agreement of synthetic with field seismogram for several theoretically-proposed general crustal models. In this way it is possible to further determine the sensitivity of main wavefield features to the degree and kind of actual subsurface geomodel variations proposed in the literature, but as yet only partially investigated.

Reduced traveltime curves are here used exclusively to enhance detection of LVL. This is not only for computational savings, but because the line connecting the termination points of first arrivals determines slope of the inversion top, whereas the envelope of reduced time arrival curves below a proposed LVL gives the slope at its bottom. The absolute difference in time between these two limits is proportional to variation in velocity from the overall trend.

DELTA WEST Profile Analysis

The observed Delta West seismogram from the eastern Basin and Range province is here compared to reflectivity and fullwave synthetic seismograms generated by the SAFARI algorithm, for a suite of variations on the velocity/depth model derived from Delta West data by PRODEHL (1971) using GIESE's modified Herglotz-Wiechert (ray theory) inverse method.

As noted above, owing to the existence of LVL's even in shallow near surface structures, the task of approximately inverting refraction traveltime data into a velocity depth function necessarily leads to a nonunique solution (AKI and RICHARDS, 1980). This is because the only direct information on detailed structure of an LVL layer is that provided by the:

1). range distance between beginning of first nearfield reflection and the termination of refracted Pg headwave

2). traveltime difference between the two corresponding reduced time curves

3). apparent group velocity at these points (equal for both)

These 3 parameters can be shown to be satisfied by an infinite number of different models of an LVL, so that in principle any velocity distribution of arbitrary shape and depth distribution is possible in the "refraction-hidden" LVL. Thus additional

Figure 37

Corresponding synthetic reflectivity seismogram for discretized realization of PRODEHL Delta Model 1, using 3 different maximum angles of wavenumber integration

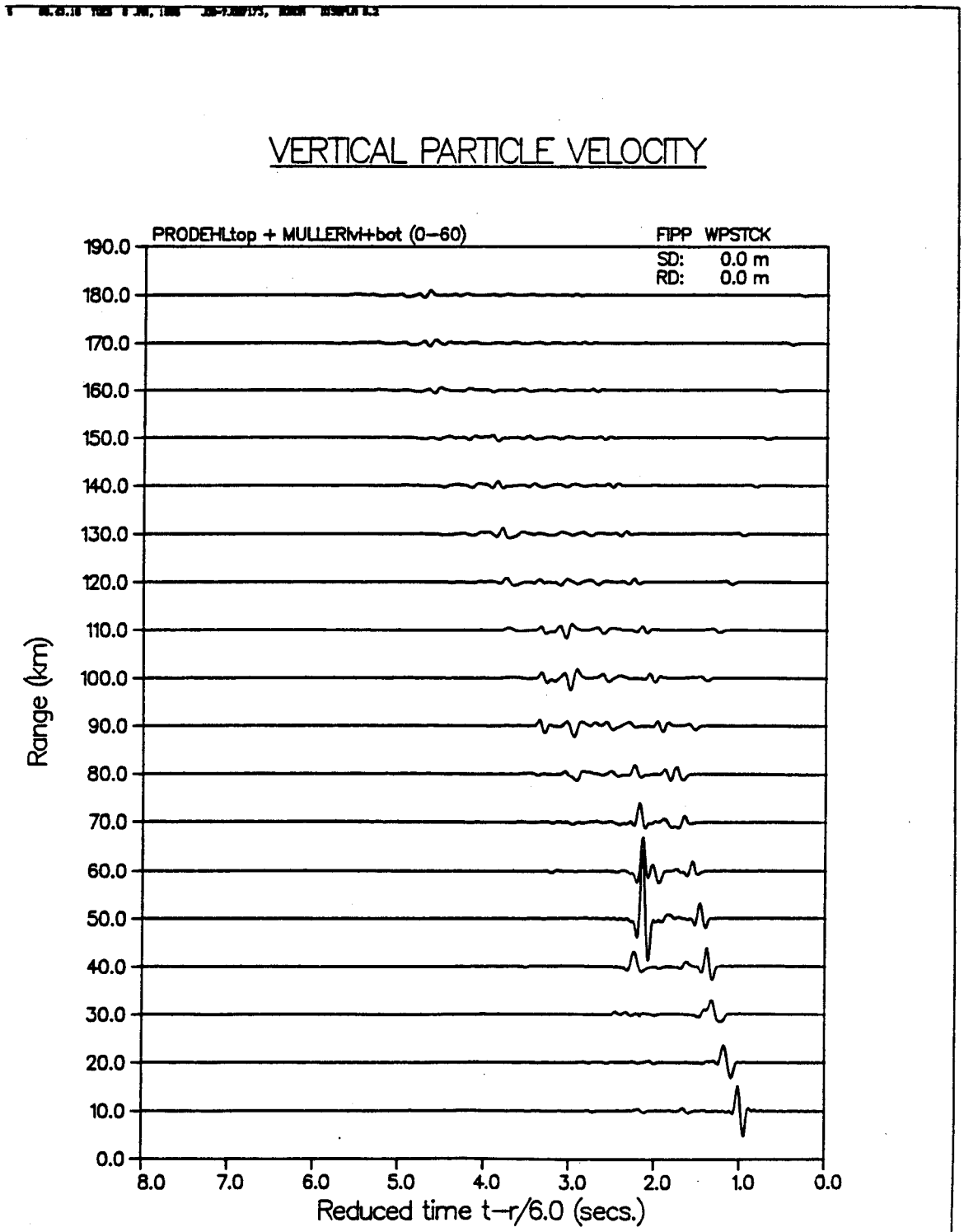
VERTICAL PARTICLE VELOCITY
PRODEHLtop + MULLERlvl+bot (0–60)
FIPP WPSTCK
SD: 0.0 m
RD: 0.0 m
Range (km)
190.0
180.0
170.0
160.0
150.0
140.0
130.0
120.0
110.0
100.0
90.0
80.0
70.0
60.0
50.0
40.0
30.0
20.0
10.0
0.0
8.0
7.0
6.0
5.0
4.0
3.0
2.0
1.0
0.0
Reduced time t–r/6.0 (secs.)

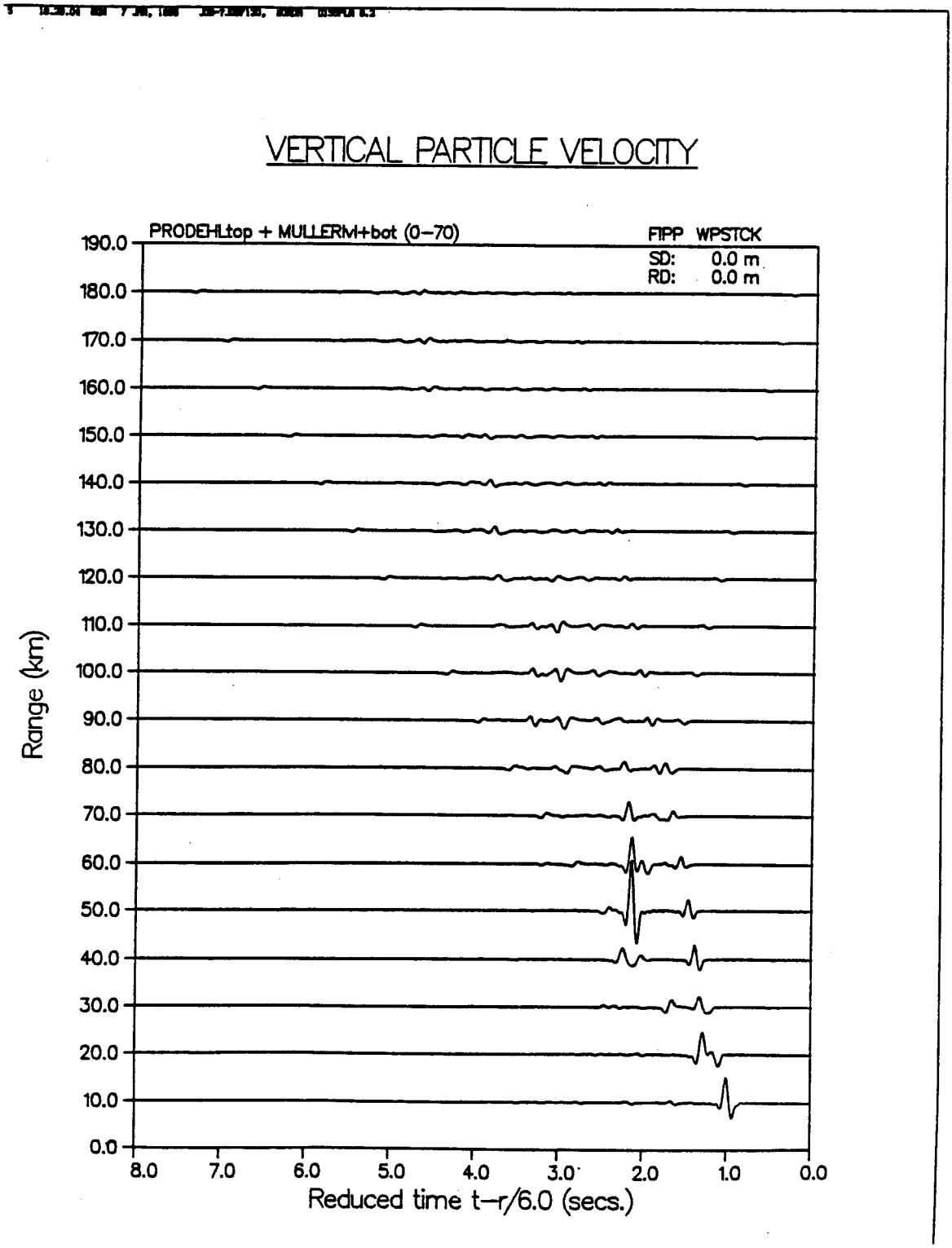
VERTICAL PARTICLE VELOCITY
PRODEHLtop + MULLERM+bot (0–70)
FIPP WPSTCK
SD: 0.0 m
RD: 0.0 m
Range (km)
190.0
180.0
170.0
160.0
150.0
140.0
130.0
120.0
110.0
100.0
90.0
80.0
70.0
60.0
50.0
40.0
30.0
20.0
10.0
0.0
8.0
7.0
6.0
5.0
4.0
3.0
2.0
1.0
0.0
Reduced time t–r/6.0 (secs.)

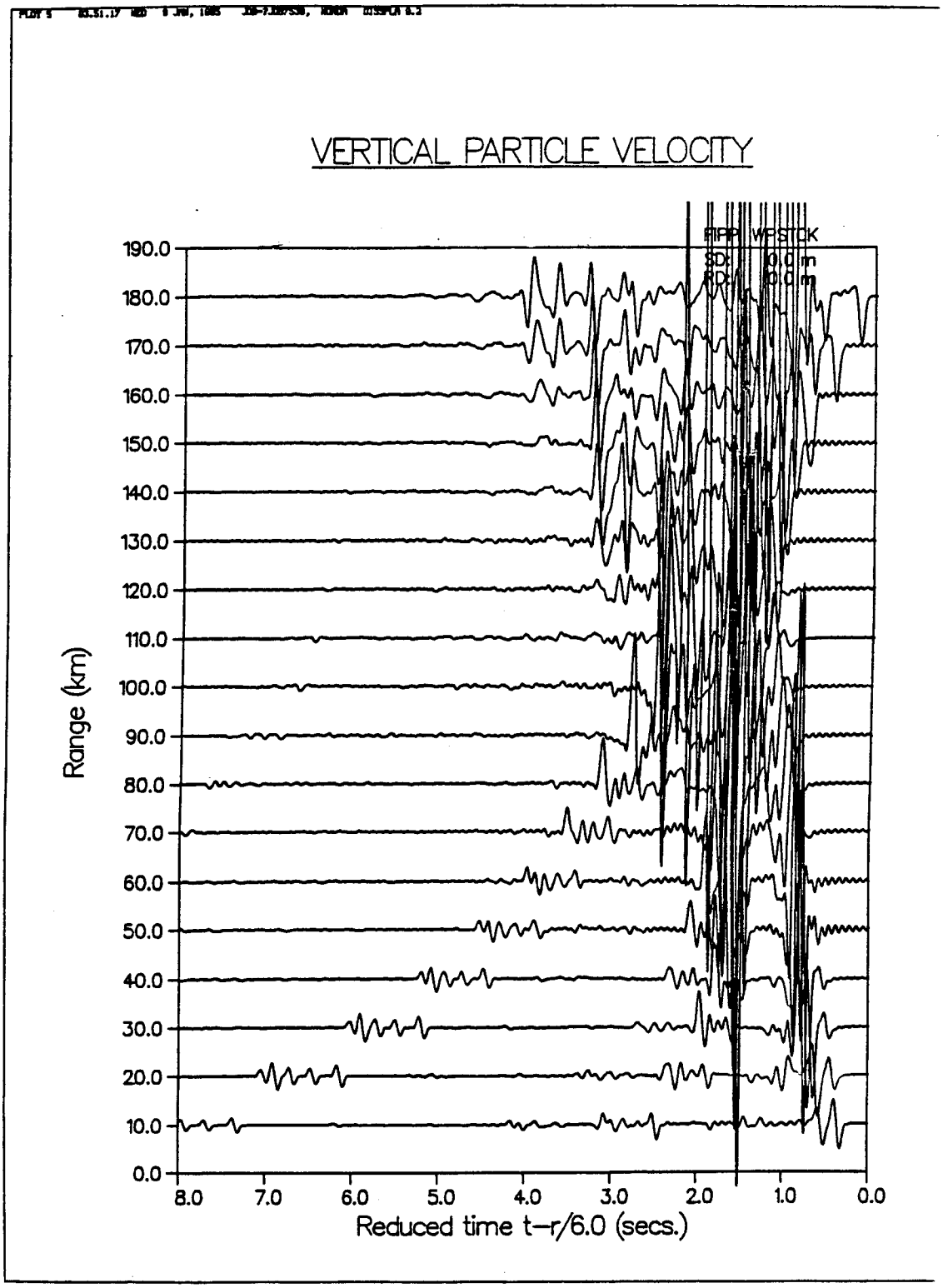
VERTICAL PARTICLE VELOCITY
RIPP WESTOK
SD: 0.0 m
RD: 0.0 m
Range (km)
190.0
180.0
170.0
160.0
150.0
140.0
130.0
120.0
110.0
100.0
90.0
80.0
70.0
60.0
50.0
40.0
30.0
20.0
10.0
0.0
8.0
7.0
6.0
5.0
4.0
3.0
2.0
1.0
0.0
Reduced time t−r/6.0 (secs.)

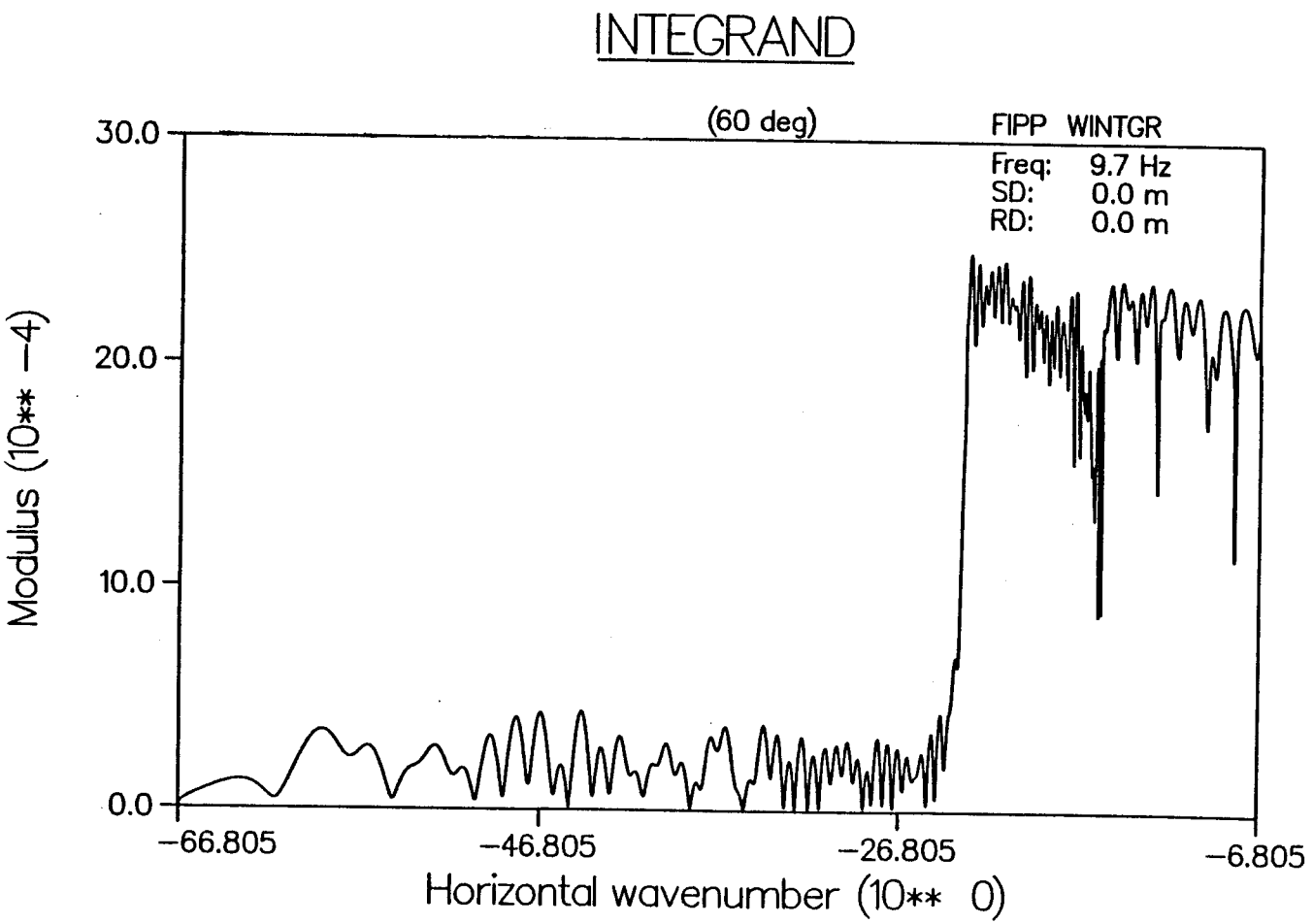
INTEGRAND
(60 deg)
FIPP WINTGR
Freq: 9.7 Hz
SD: 0.0 m
RD: 0.0 m
30.0
20.0
10.0
0.0
Modulus (10** -4)
-66.805
-46.805
-26.805
-6.805
Horizontal wavenumber (10** 0)

assumptions must be invoked for the interpretational ambiguity to be constrained.

In the absence of exact mode or wave inversion schemes based on propagation physics (excluding general linearised inversion schemes; BRAILE, 1972), one or another modification of the classic ray-trace scheme of Herglotz-Wiechert has been varyingly employed for inverse crustal modeling (AKI and RICHARDS, 1980). Strictly speaking, in the case where a true LVL exists, discontinuities appearing in the equations makes direct application of the Herglotz-Wiechert relations impossible. However, if a particular (simple) form for the velocity distribution within the inversion can be initially assumed, it is then possible to obtain a unique solution for the travel time curves following the LVL interuption zone. This has been developed by GIESE (1968) and GIESE and STEIN (1971), and discussed at length in GIESE et al (1976).

PRODEHL (1971) applied the modified Herglotz-Wiechert ray inversion scheme of GIESE (1968) to data records from the Delta profiles, and derived the 3 basic velocity depth models given in **Figures** 38-42. These comprise all-discontinuity (no gradient) in several reflectivity and fullwave versions, gradient without LVL, gradient with 'structured' LVL, gradient without LVL having simple near-surface and complex sub-LVL gradients, and gradient without LVL with complex near-surface and deep gradients.

The respective differences between the reflectivity and full wavefield synthetic seismograms computed by SAFARI for PRODEHL's v/z models are shown in **Figure** 38b-c and Figure 38d-e respectively. The computed reflectivity record sections the initial models is seen to agree in general traveltime features with the field profile, with better overall critical-offset detail in the two gradient models. Nearfield concave Pg traveltime curves on both record and the coarse-layered (no-gradient) synthetic are very similar, disagreeing only slightly in the critical point range of disappearence. The Pc head wave is also evident in correct time and critical point location. Additionally, both the PmP Moho reflection and PcR intermediate crustal return appear from near critical well into the far field, with convex traveltime and waveforms in general agreement with data.

However, it can be noted that field record amplitudes of refracted arrivals are larger at nearfield ranges, and the net arrival pattern shows distinctly more "ringing" than the synthetic (especially in the subcritical nearfield). These results are reminiscent of those seen in the LVL6 model of BRAILE and SMITH (1975).

An even more striking nearfield difference can also be found, when comparing the almost total absence of subcritical intermediate time arrivals in the synthetic to the complexly interfering and (at times) locally high amplitude arrivals on the

Figure 38

(a) General Prodehl-derived velocity-depth model, without LVL (all discontinuity; no gradients)

(b-c)corresponding reflectivity synthetic seismograms for 2 maximum angles of integration

(d-e)corresponding fullwave synthetic seismograms for 2 maximum horizontal wave numbers

on (d) and (e), near vertical surface multiples, especially of the direct source arrival, are progressively cut out as the maximum horizontal wavenumber is reduced. Minimum and maximum phase velocities were empirically determined for each general model type.

VELOCITY PROFILE

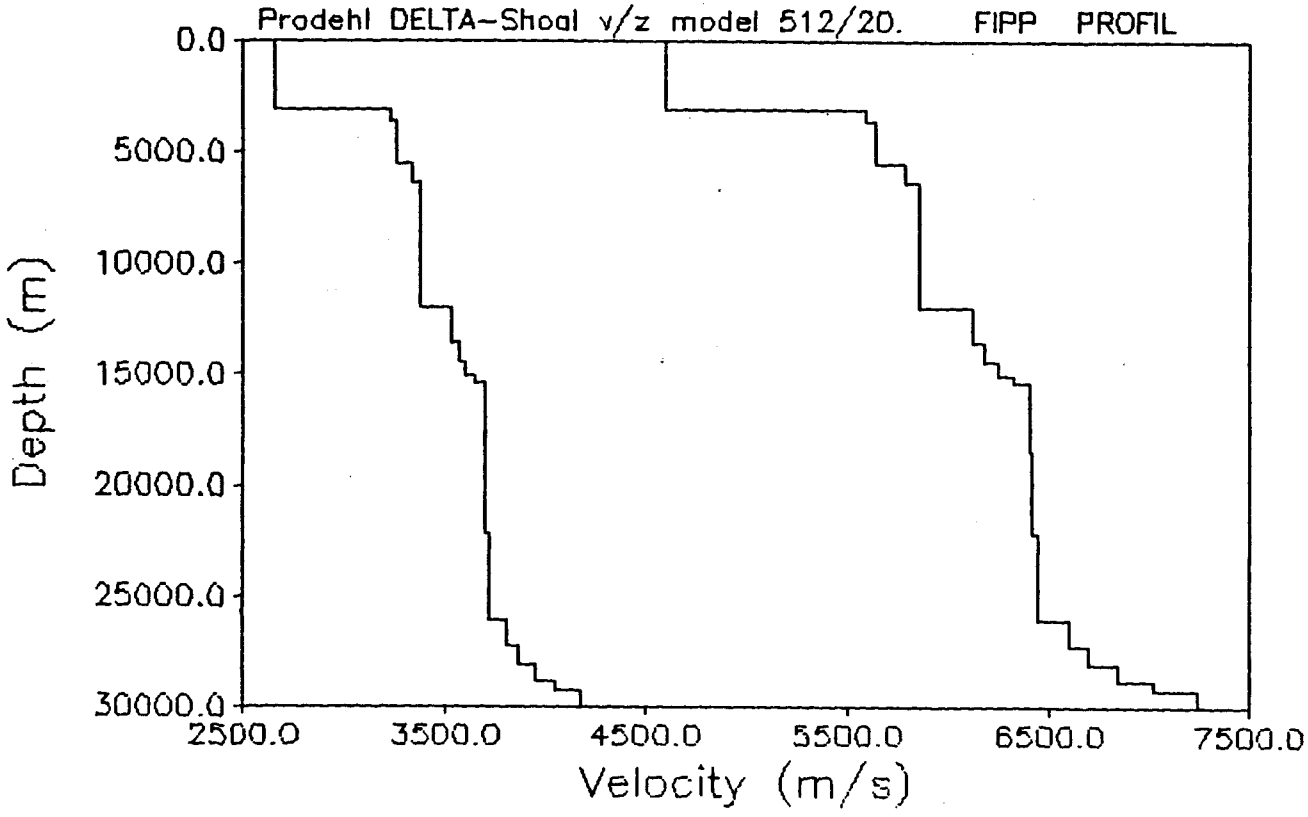

VERTICAL PARTICLE VELOCITY

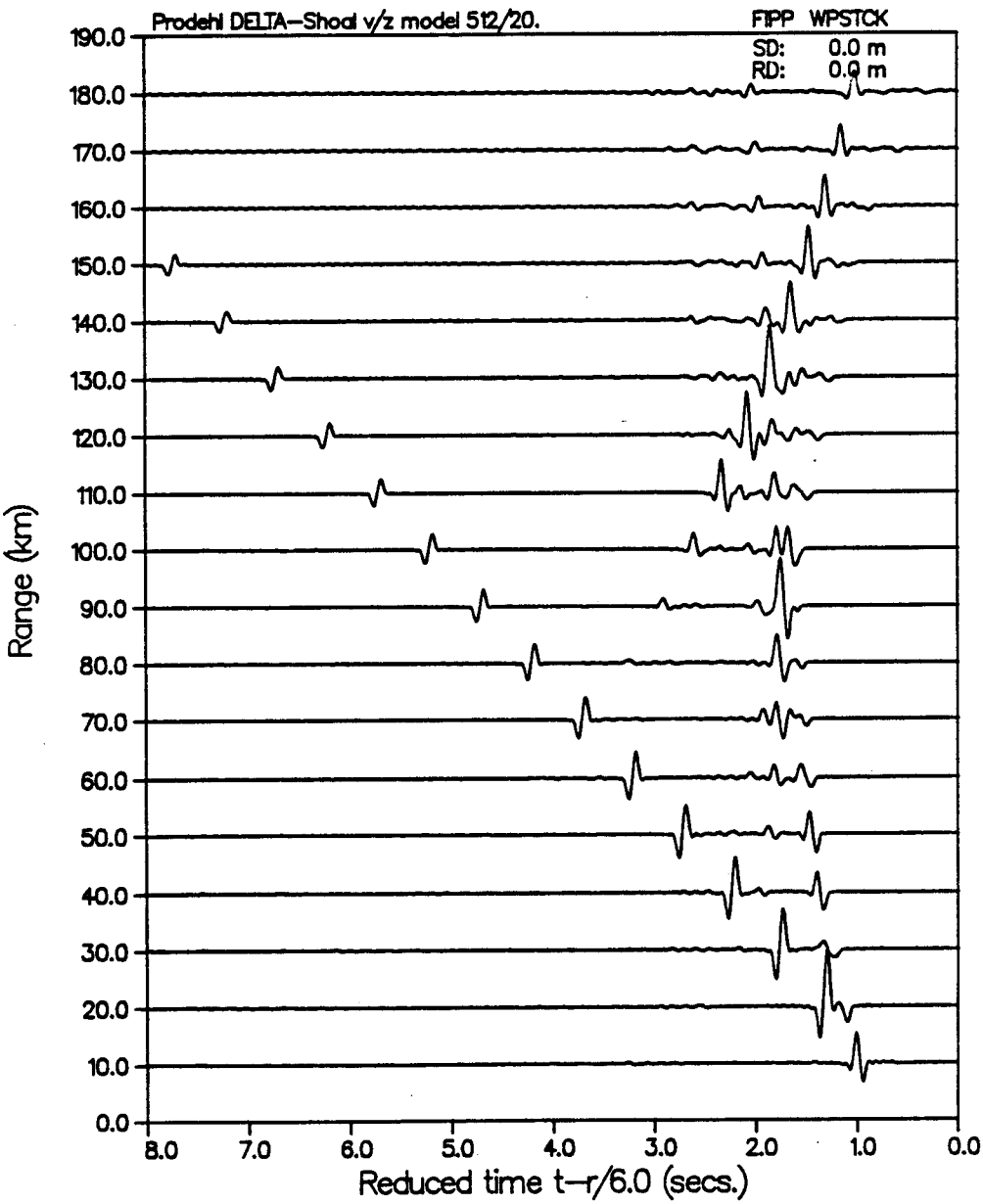

VERTICAL PARTICLE VELOCITY

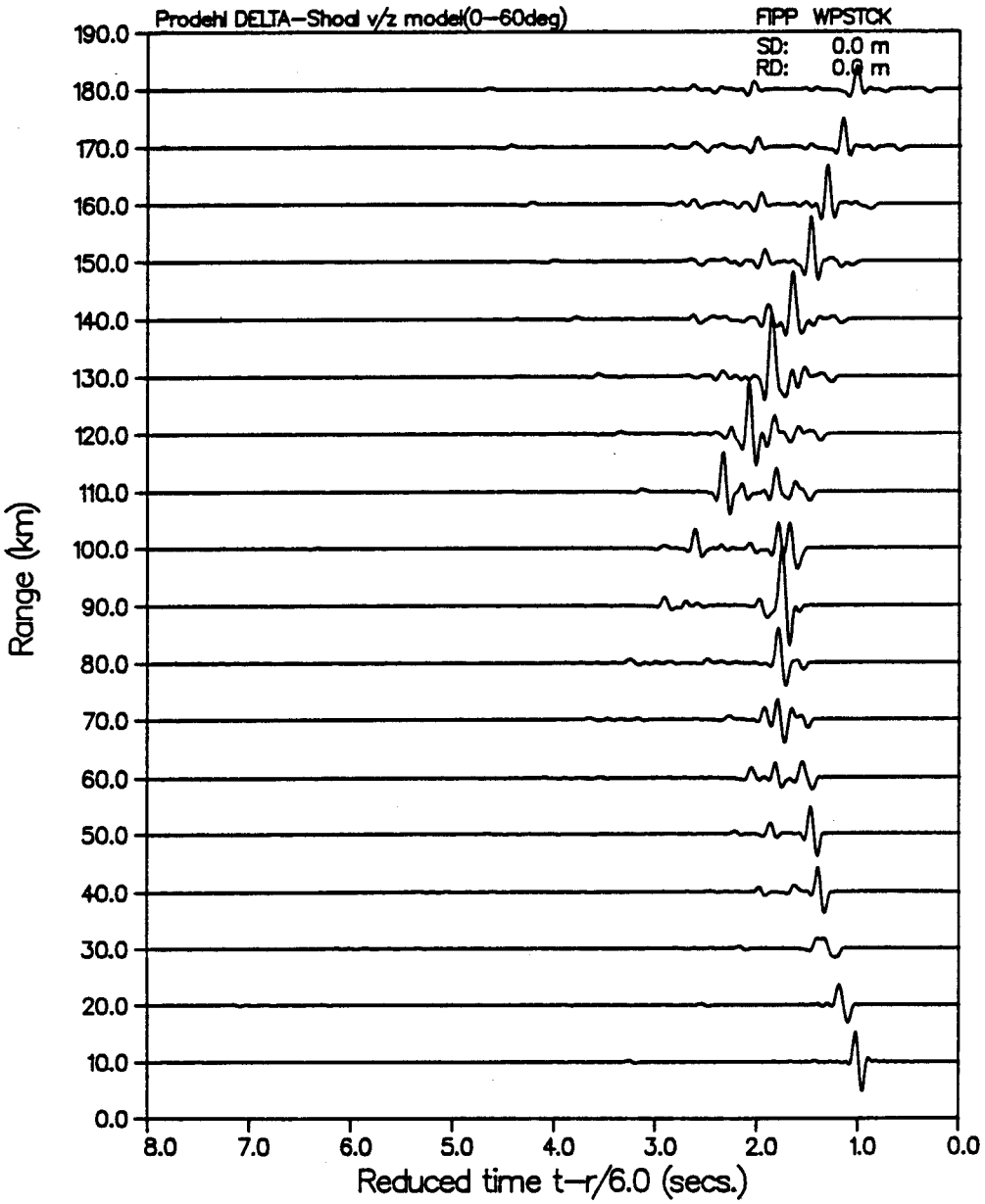

VERTICAL PARTICLE VELOCITY

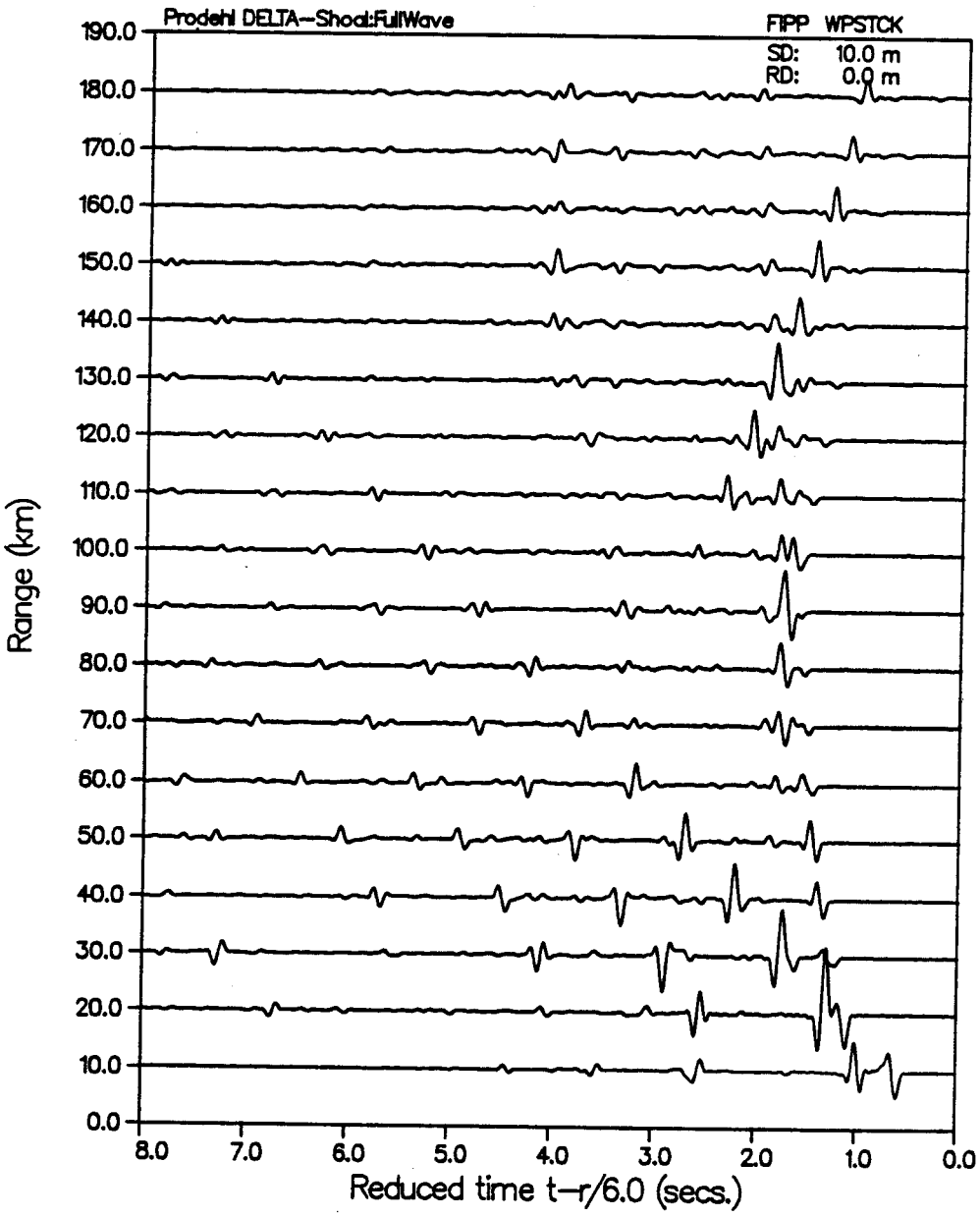

VERTICAL PARTICLE VELOCITY

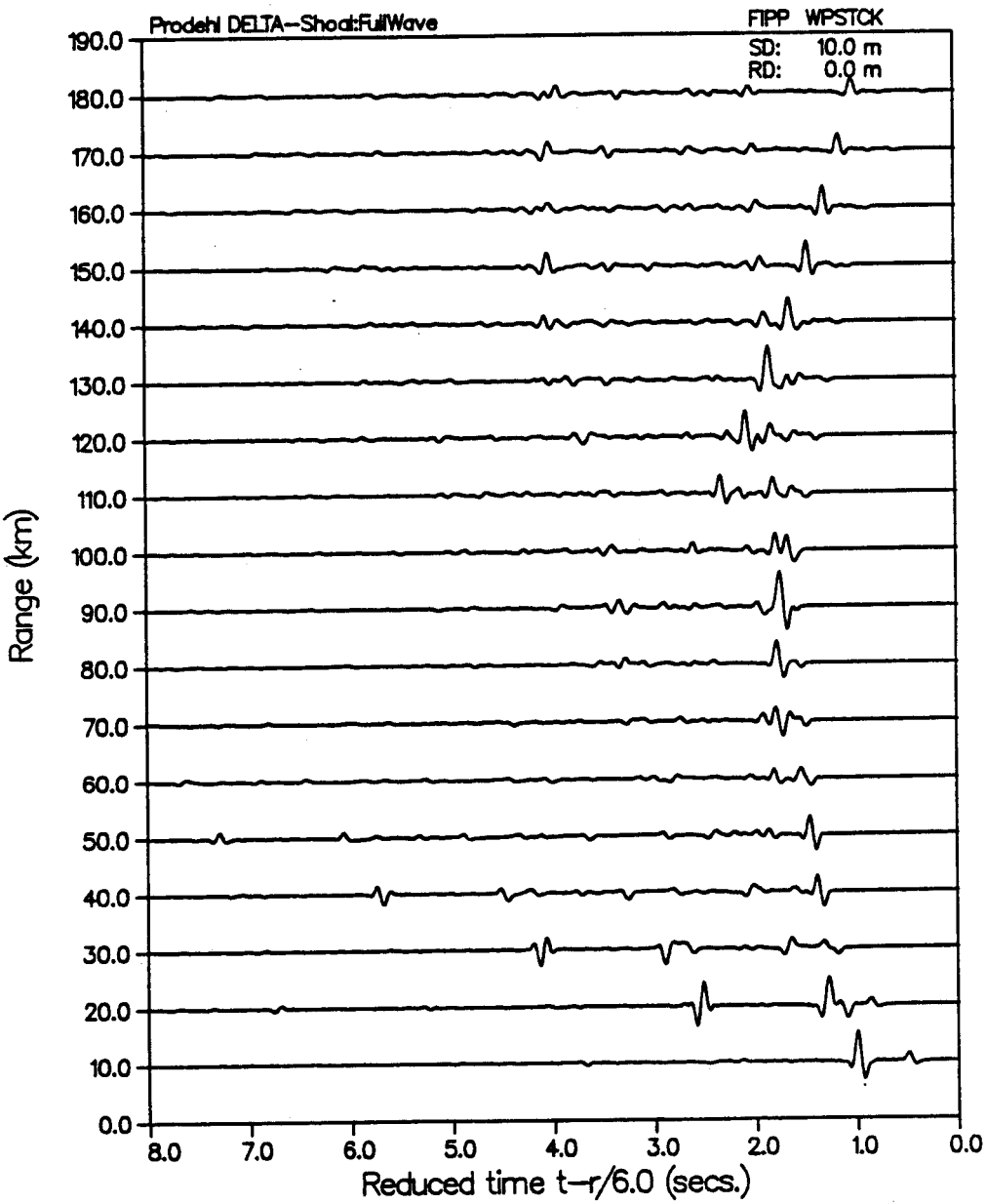

Delta profile data, thru which at least several additional arrival phases can be correlated over a considerable portion of the total profile.

Several additional synthetic seismic computations for the PRODEHL model were undertaken, introducing small uncertainty variations as well as both more finely spatial-sampled and alternative gradients in the same depth zones where LVL's have been proposed, without significant improvement in overall model-data agreement. To reduce complexity, we adopted next the above-mentioned 15 layer LVL6 model of BRAILE and SMITH (1975). As expected, although agreeing well in the farfield (in dispersed waveform character), it did not agree in the nearfield.

We thus recomputed reflectivity synthetic seismograms for BRAILE and SMITH's generalised Basin and Range model BR2 (nearly identical to that given in KELLER SMITH and BRAILE, 1975; PAKISER, 1985). The v/z model and corresponding synthetics are shown in **Figure** 45.

For these much simpler models -comprising only 4-6 layers overlying a halfspace- the corresponding synthetic wavefield is considerably more complex and less clearly discernable in terms of distinct arrival phases and critical points. Overall agreement in the existence of near-critical distance high amplitude interference zone as well as the presence and number of subcritical phases is markedly better than that of previous

Figure 39 - 42 part (a)

General velocity-depth profiles, derived after PRODEHL (1979):

(39) all-discontinuities with small LVL

(40) all-discontinuities without LVL

(41) linear gradients without LVL

(42) nonlinear gradients without LVL

The distinct absence of near field arrivals in all non-LVL models is evident. Near mantle depth linear and nonlinear gradients are shown to effect farfield arrivals only (nB, increasing Pn arrival amplitudes beyond x=120km).

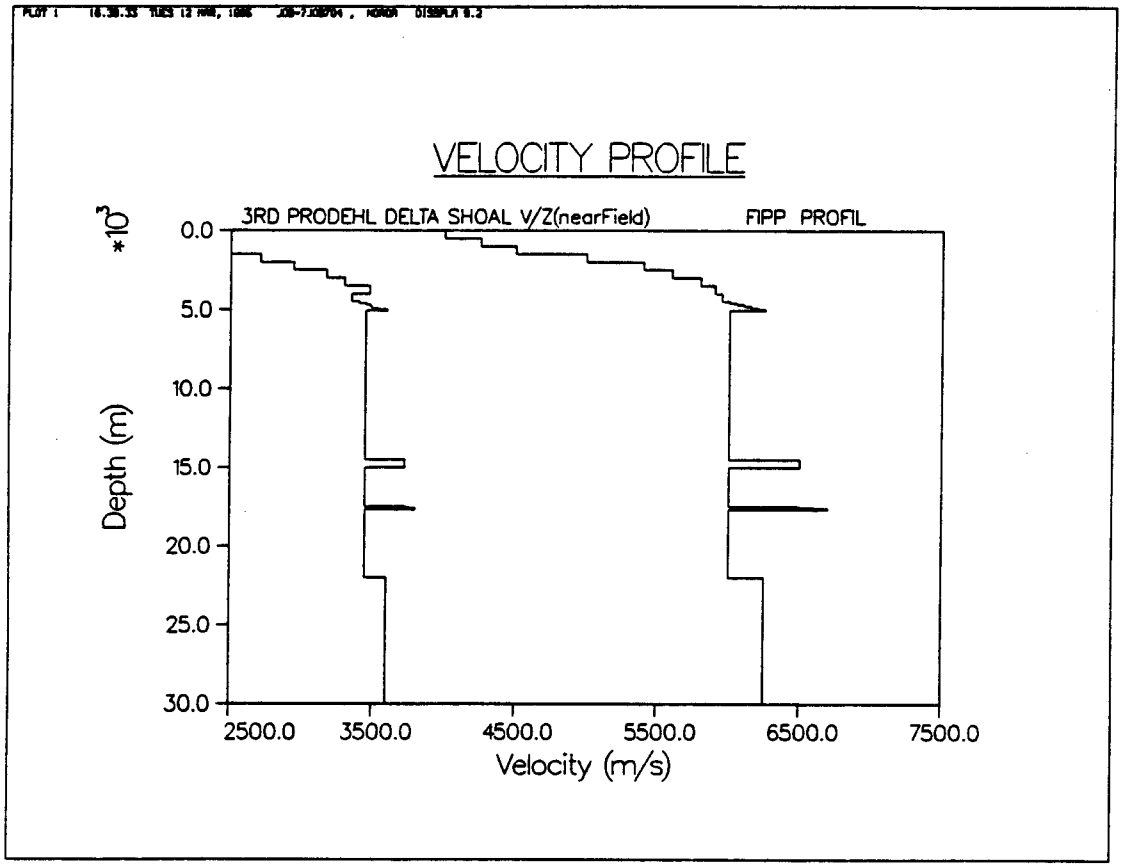
VELOCITY PROFILE
3RD PRODEHL DELTA SHOAL V/Z(nearField)
FIPP PROFIL
*10^3
Depth (m)
0.0
5.0
10.0
15.0
20.0
25.0
30.0
2500.0
3500.0
4500.0
5500.0
6500.0
7500.0
Velocity (m/s)

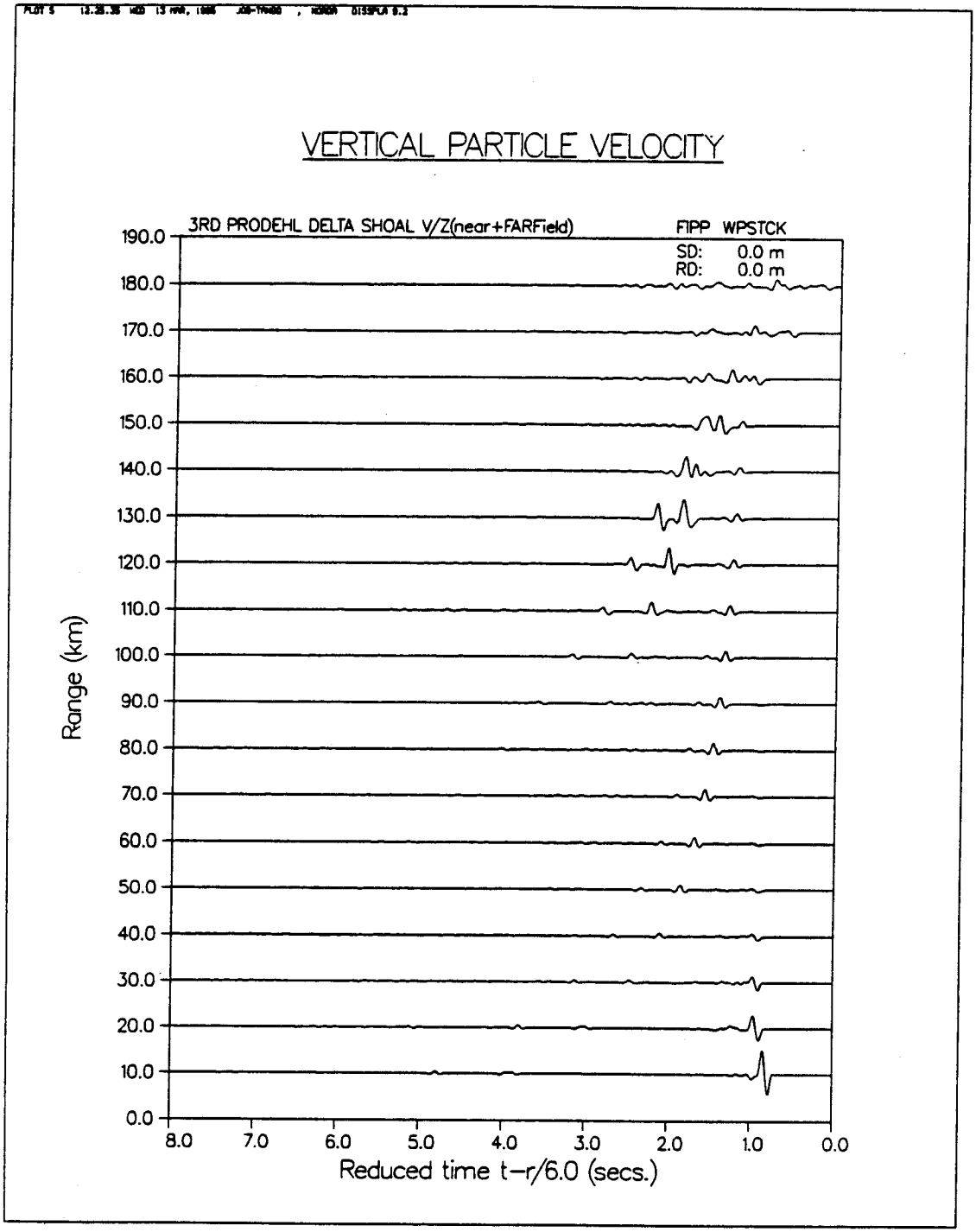
VERTICAL PARTICLE VELOCITY
3RD PRODEHL DELTA SHOAL V/Z(near+FARField)
FIPP WPSTCK
SD: 0.0 m
RD: 0.0 m
Range (km)
190.0
180.0
170.0
160.0
150.0
140.0
130.0
120.0
110.0
100.0
90.0
80.0
70.0
60.0
50.0
40.0
30.0
20.0
10.0
0.0
8.0
7.0
6.0
5.0
4.0
3.0
2.0
1.0
0.0
Reduced time t−r/6.0 (secs.)

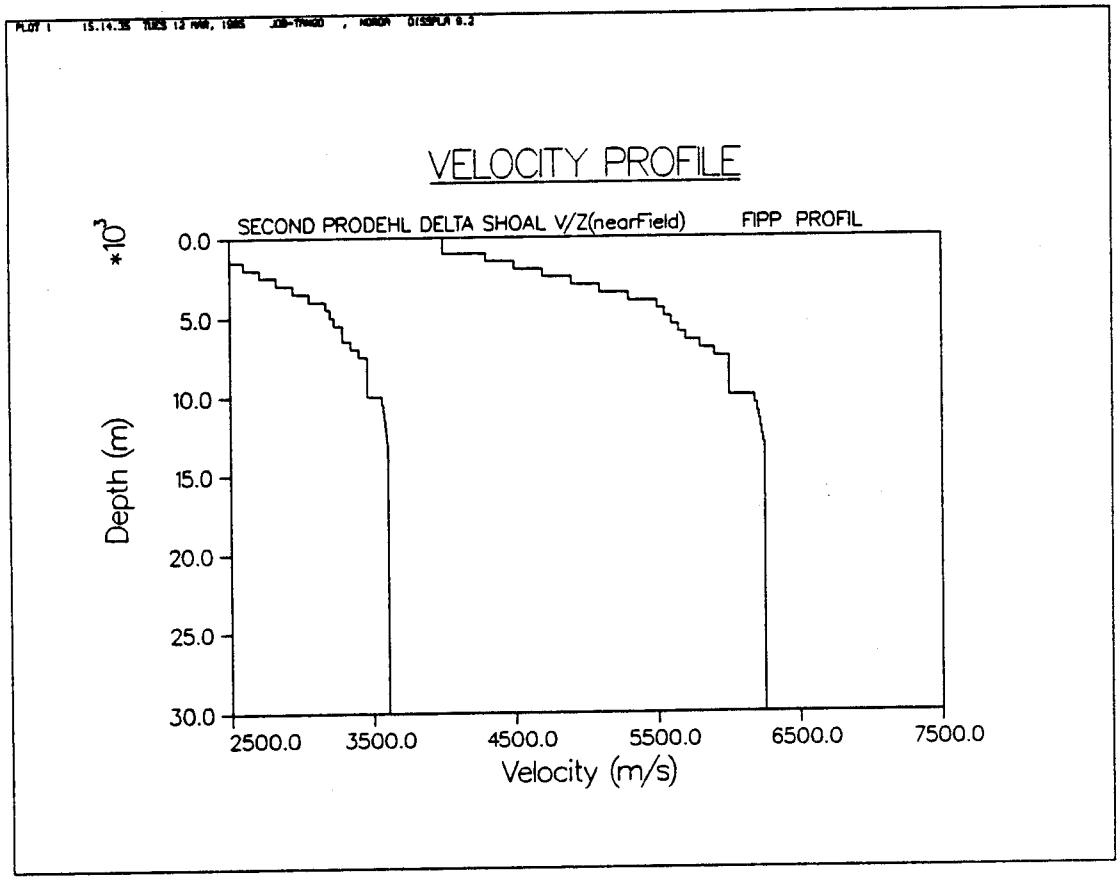
VELOCITY PROFILE
SECOND PRODEHL DELTA SHOAL V/Z(nearField) FIPP PROFIL
*10^3
Depth (m)
0.0
5.0
10.0
15.0
20.0
25.0
30.0
2500.0
3500.0
4500.0
5500.0
6500.0
7500.0
Velocity (m/s)

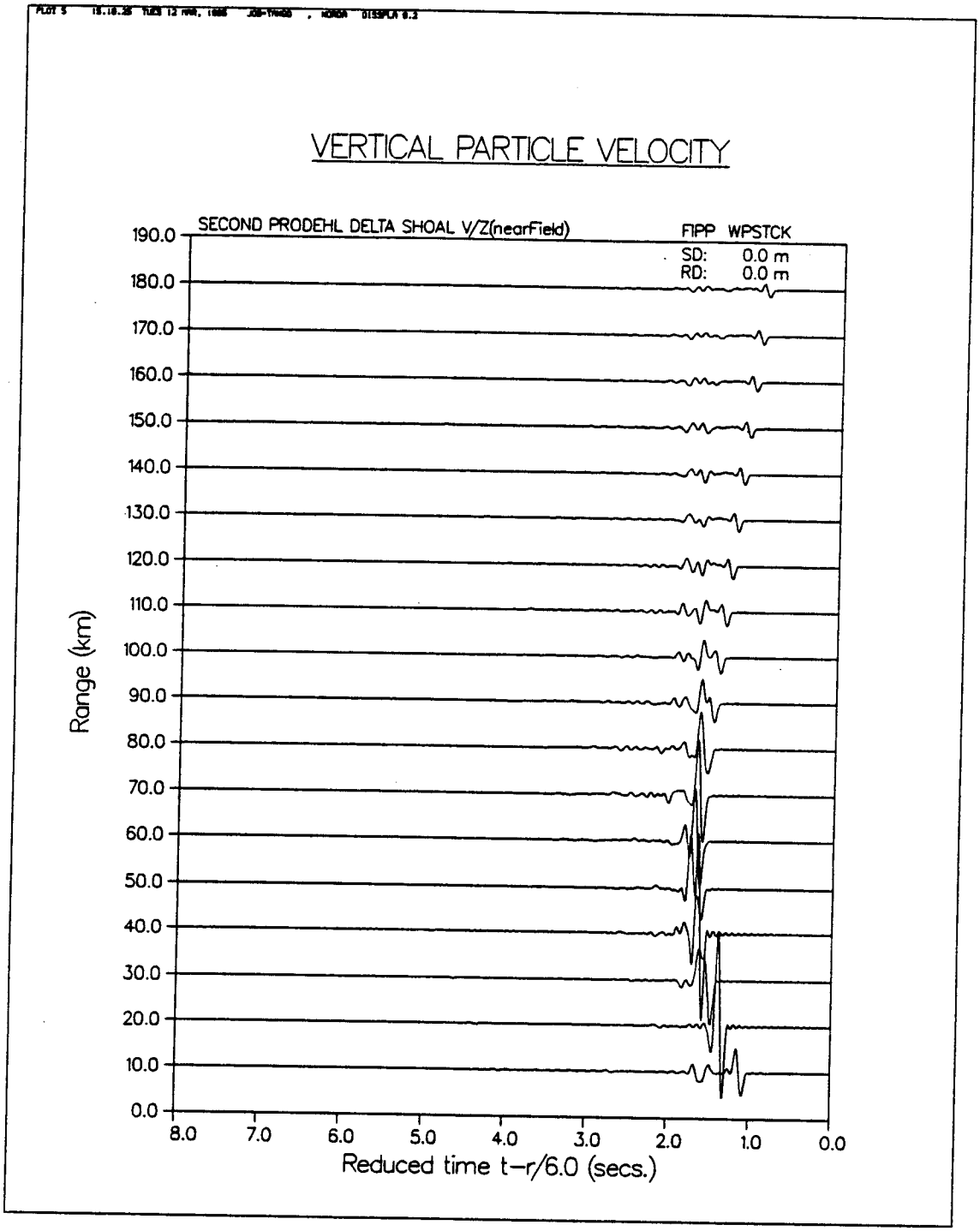
VERTICAL PARTICLE VELOCITY
SECOND PRODEHL DELTA SHOAL V/Z(nearField)
FIPP WPSTCK
SD: 0.0 m
RD: 0.0 m
Range (km)
190.0
180.0
170.0
160.0
150.0
140.0
130.0
120.0
110.0
100.0
90.0
80.0
70.0
60.0
50.0
40.0
30.0
20.0
10.0
0.0
8.0
7.0
6.0
5.0
4.0
3.0
2.0
1.0
0.0
Reduced time t−r/6.0 (secs.)

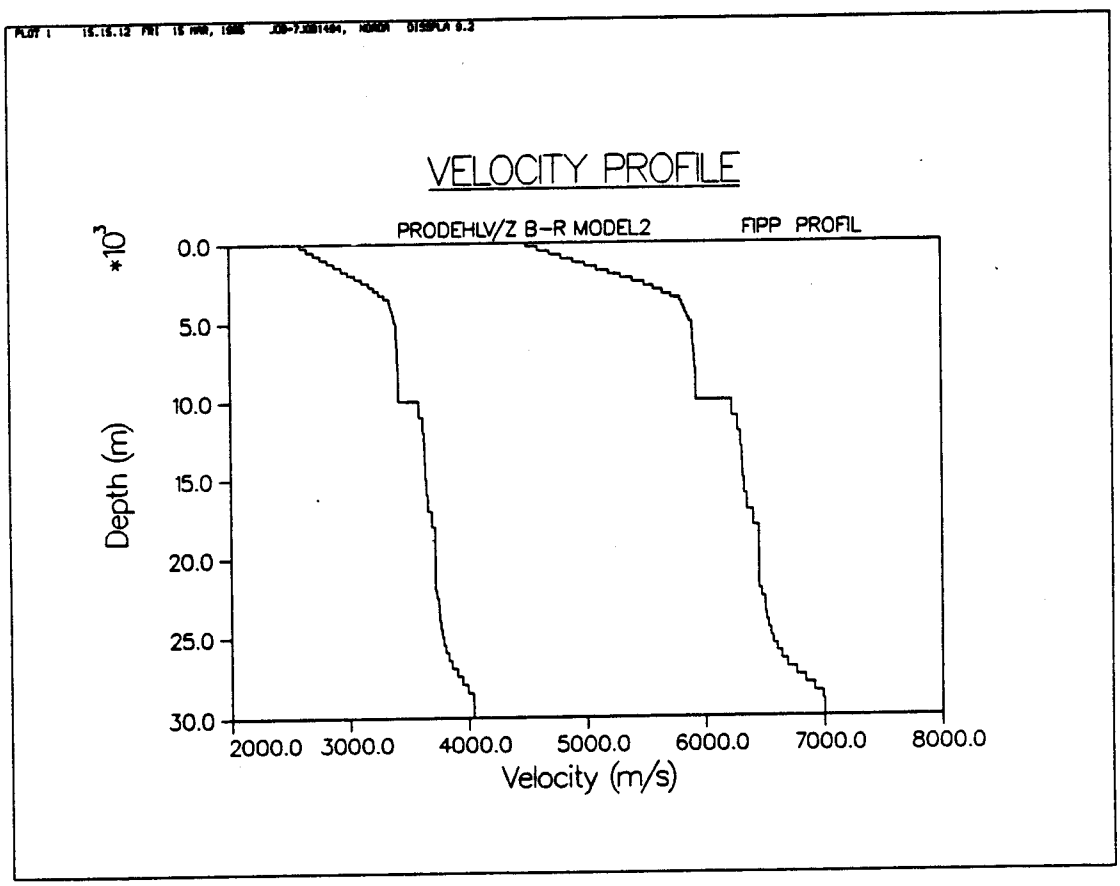
VELOCITY PROFILE
PRODEHLV/Z B-R MODEL2
FIPP PROFIL
Depth (m)
*10³
0.0
5.0
10.0
15.0
20.0
25.0
30.0
2000.0
3000.0
4000.0
5000.0
6000.0
7000.0
8000.0
Velocity (m/s)

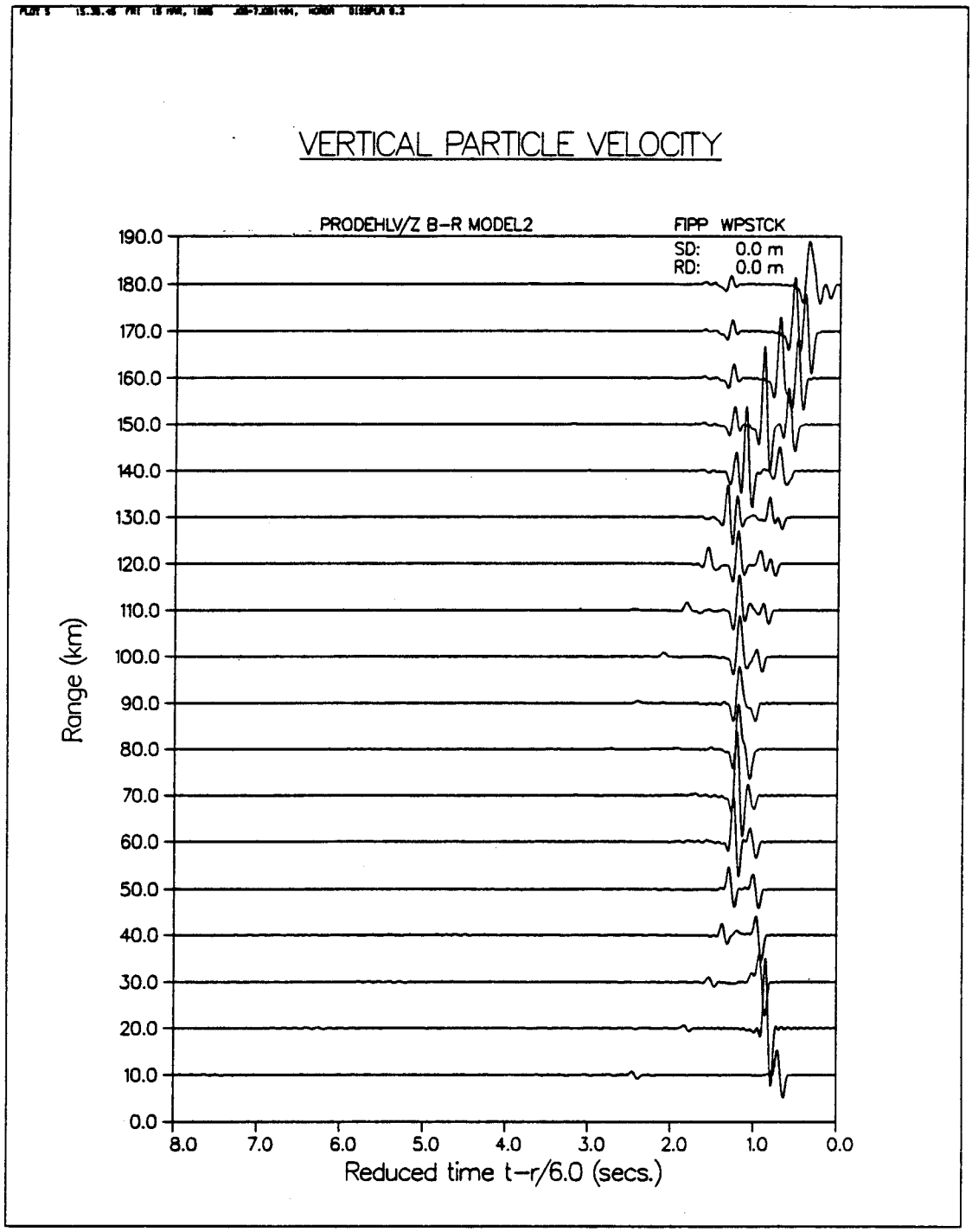
VERTICAL PARTICLE VELOCITY
PRODEHLV/Z B-R MODEL2
FIPP WPSTCK
SD: 0.0 m
RD: 0.0 m
Range (km)
190.0
180.0
170.0
160.0
150.0
140.0
130.0
120.0
110.0
100.0
90.0
80.0
70.0
60.0
50.0
40.0
30.0
20.0
10.0
0.0
8.0
7.0
6.0
5.0
4.0
3.0
2.0
1.0
0.0
Reduced time t-r/6.0 (secs.)

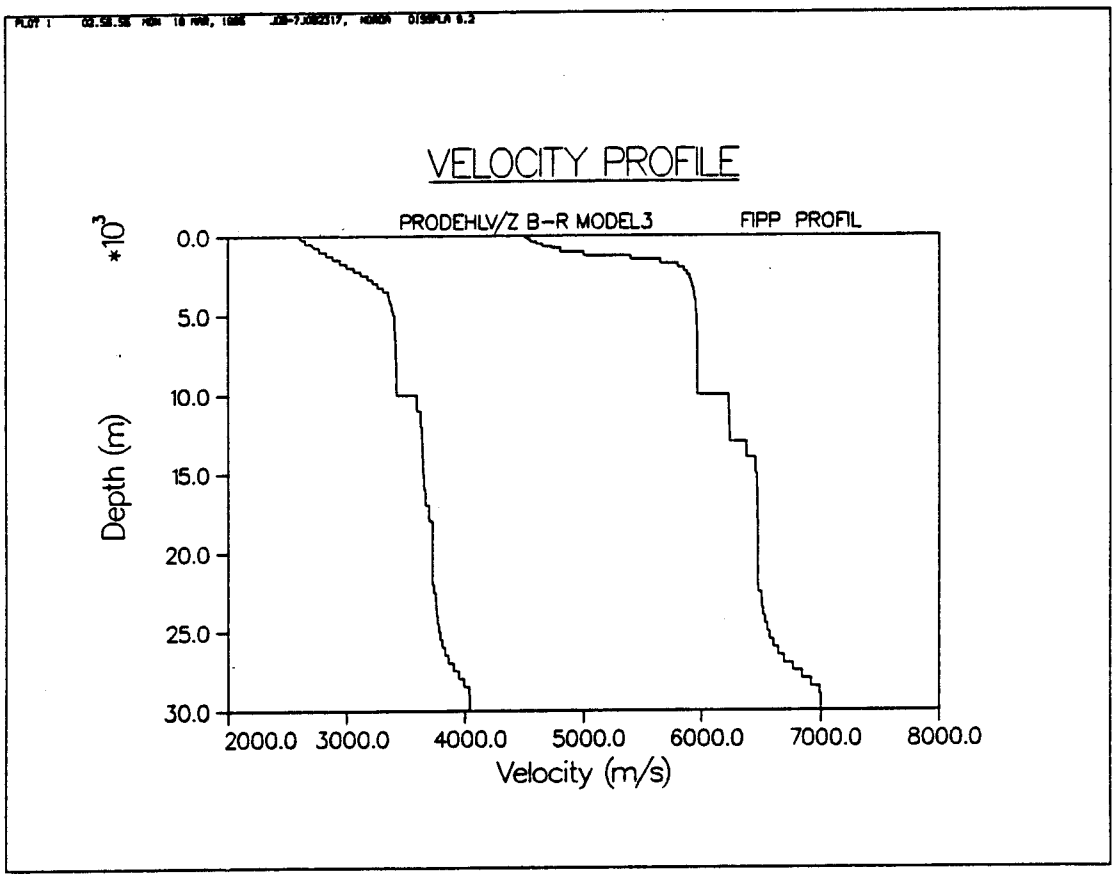
VELOCITY PROFILE
PRODEHLV/Z B-R MODEL3
FIPP PROFIL
Depth (m)
*10^3
0.0
5.0
10.0
15.0
20.0
25.0
30.0
2000.0
3000.0
4000.0
5000.0
6000.0
7000.0
8000.0
Velocity (m/s)

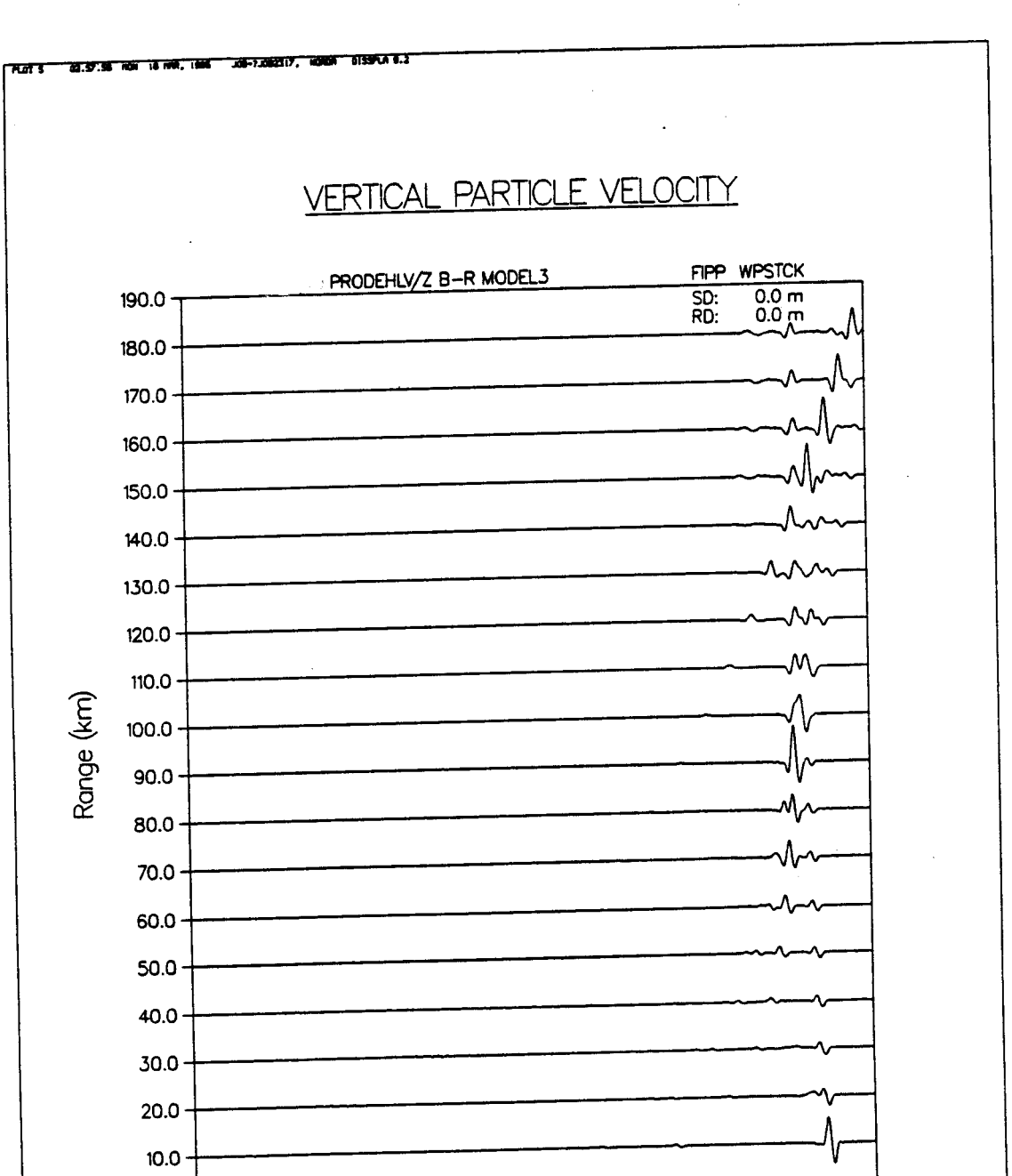
VERTICAL PARTICLE VELOCITY
PRODEHLV/Z B-R MODEL3
FIPP WPSTCK
SD: 0.0 m
RD: 0.0 m
Range (km)
190.0
180.0
170.0
160.0
150.0
140.0
130.0
120.0
110.0
100.0
90.0
80.0
70.0
60.0
50.0
40.0
30.0
20.0
10.0
0.0
8.0
7.0
6.0
5.0
4.0
3.0
2.0
1.0
0.0
Reduced time t-r/6.0 (secs.)

Figures 44 - 45

Velocity-depth profiles (including LVL) and corresponding synthetic reflectivity seismograms for generalized Basin and Range model, after KELLER,SMITH & BRAILE (1975) and BRAILE & SMITH (1975).

The inadequacy of few-layered (Nlayers=4,5) velocity depth models to correctly account for the number and character of nearfield multiple arrivals (nB figure 45) suggests importance of LVL and subLVL 'fine' structure

VELOCITY PROFILE

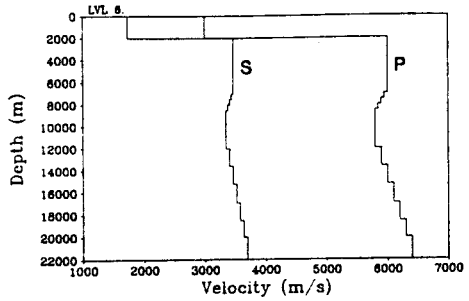

(a)

VERTICAL PARTICLE VELOCITY

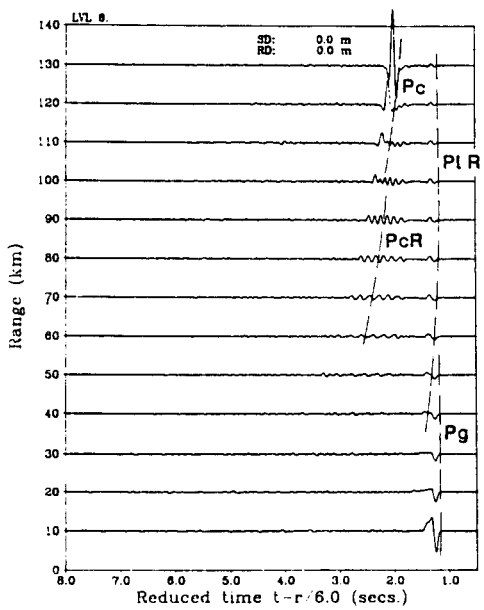

(b)

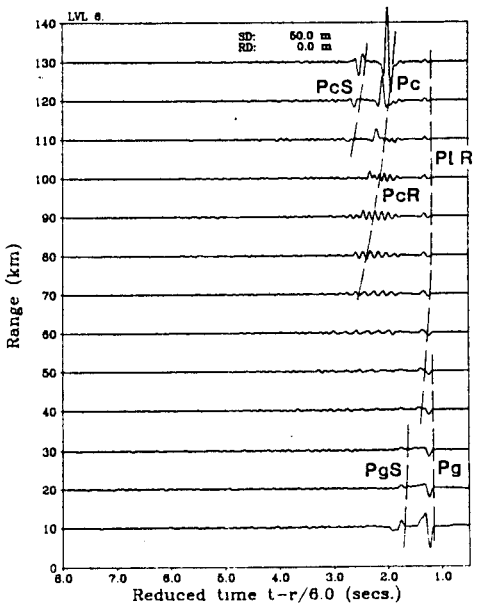

(c)

Synthetic seismograms for LVL-6 crustal model.
a. Velocity profile. b. Reflectivity approximation.
c. Full wavefield solution. Amplitudes are multiplied by range.

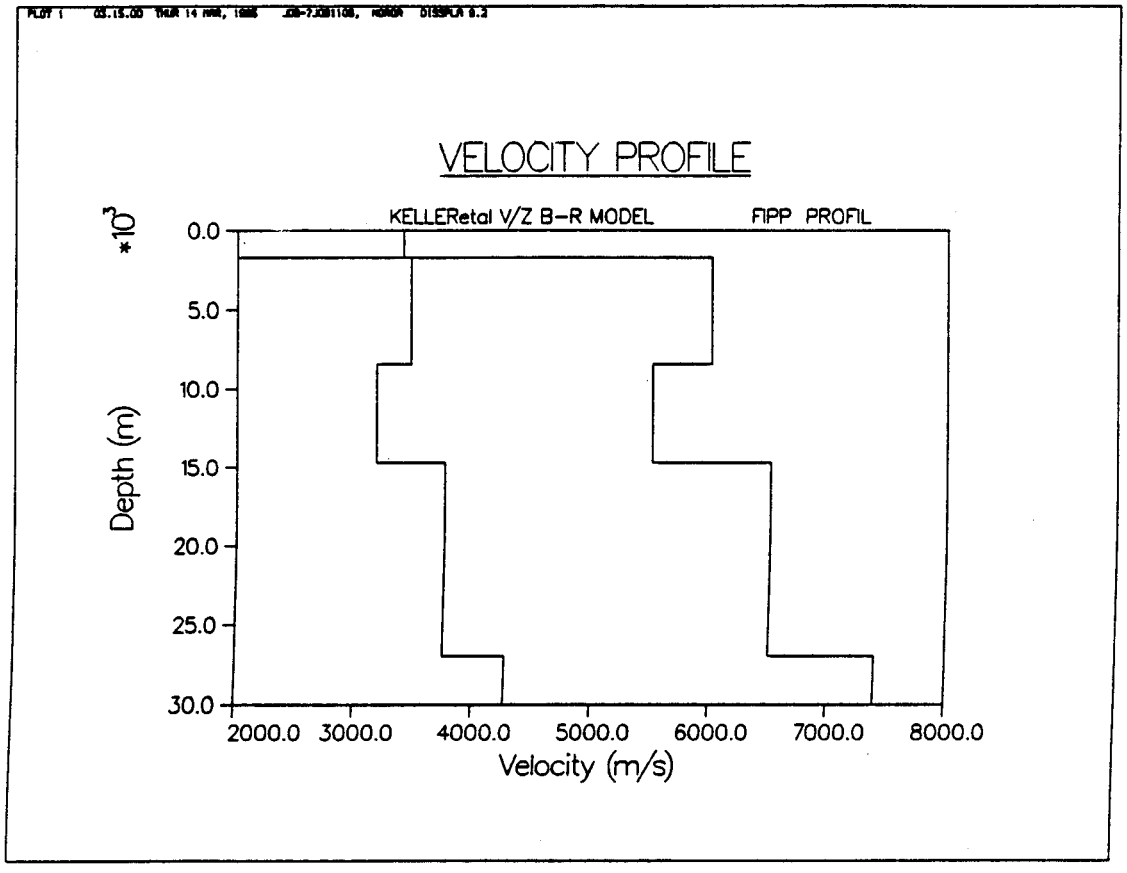
VELOCITY PROFILE
KELLERetal V/Z B-R MODEL
FIPP PROFIL
*10^3
Depth (m)
0.0
5.0
10.0
15.0
20.0
25.0
30.0
2000.0
3000.0
4000.0
5000.0
6000.0
7000.0
8000.0
Velocity (m/s)

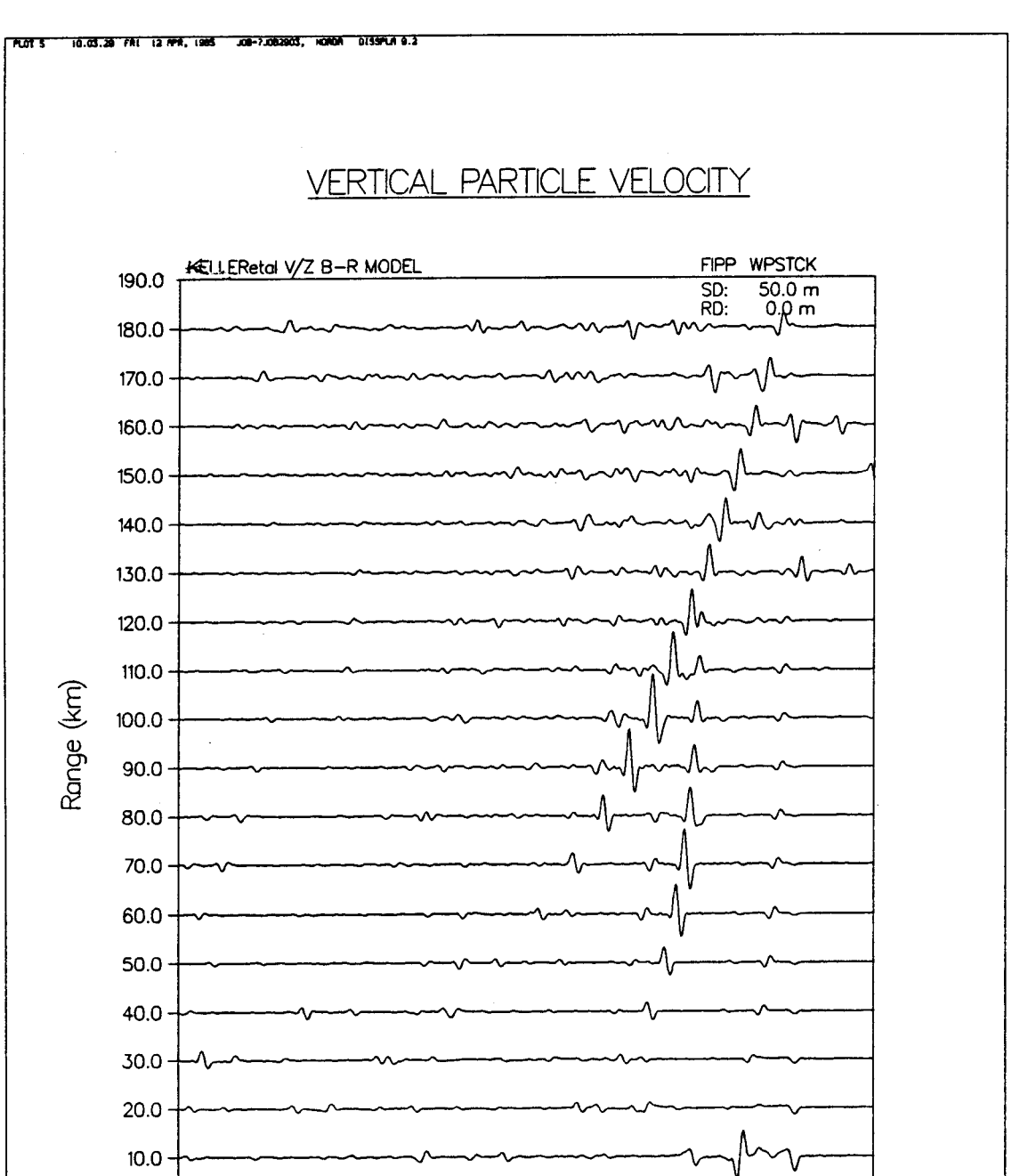
VERTICAL PARTICLE VELOCITY
KELLERetal V/Z B-R MODEL
FIPP WPSTCK
SD: 50.0 m
RD: 0.0 m
Range (km)
190.0
180.0
170.0
160.0
150.0
140.0
130.0
120.0
110.0
100.0
90.0
80.0
70.0
60.0
50.0
40.0
30.0
20.0
10.0
0.0
8.0
7.0
6.0
5.0
4.0
3.0
2.0
1.0
0.0
Reduced time t-r/6.0 (secs.)

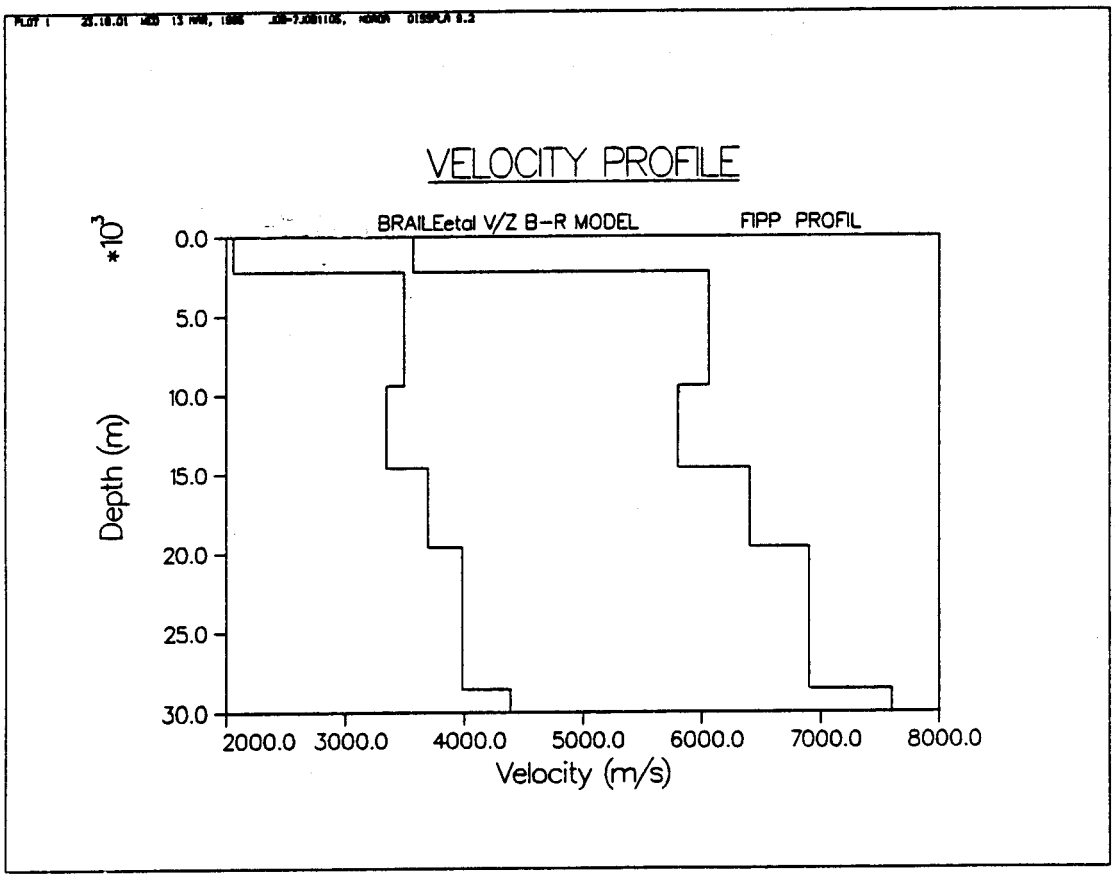
VELOCITY PROFILE
BRAILEetal V/Z B-R MODEL
FIPP PROFIL
*10^3
Depth (m)
0.0
5.0
10.0
15.0
20.0
25.0
30.0
2000.0
3000.0
4000.0
5000.0
6000.0
7000.0
8000.0
Velocity (m/s)

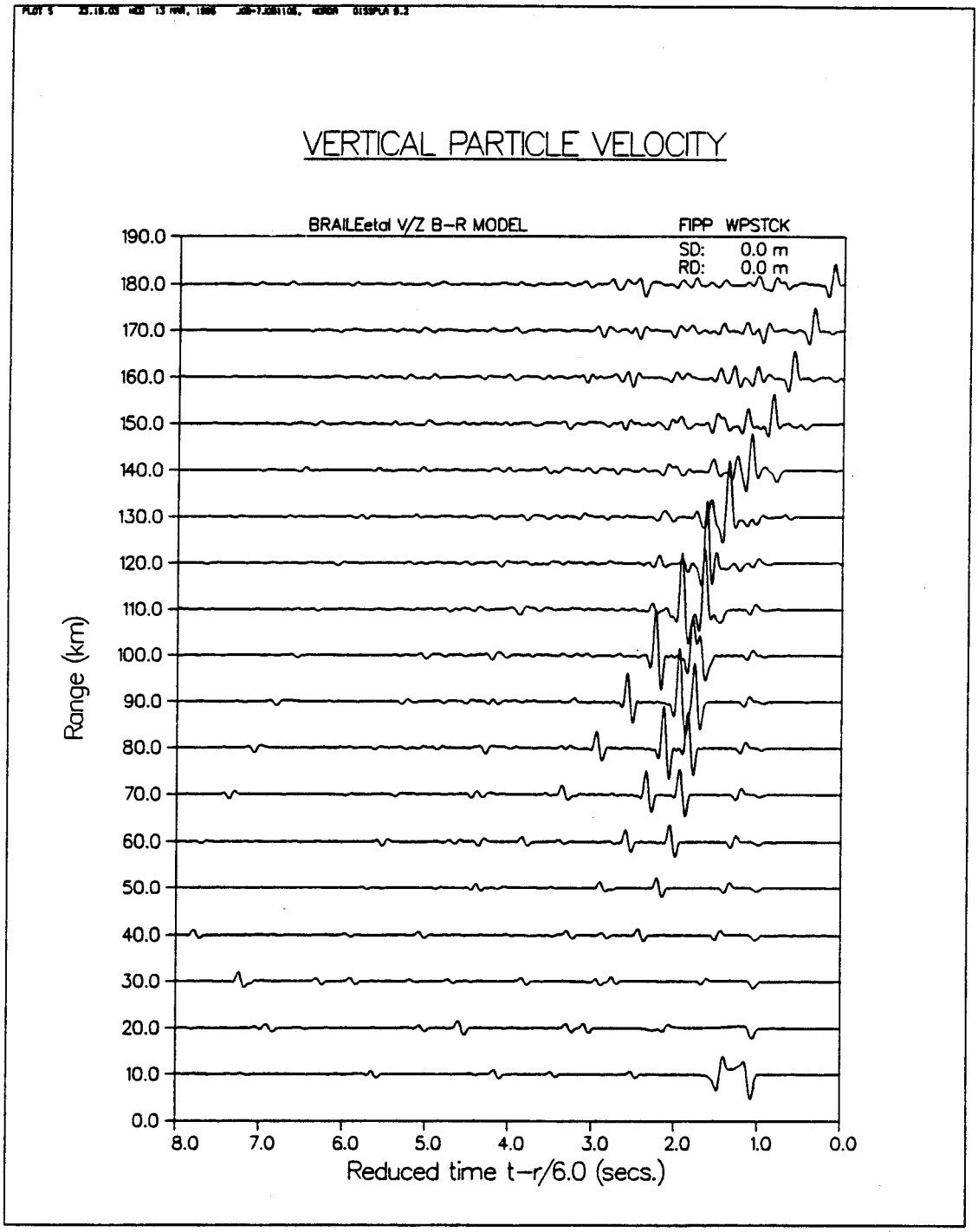
VERTICAL PARTICLE VELOCITY
BRAILEetal V/Z B-R MODEL
FIPP WPSTCK
SD: 0.0 m
RD: 0.0 m
190.0
180.0
170.0
160.0
150.0
140.0
130.0
120.0
110.0
100.0
90.0
80.0
70.0
60.0
50.0
40.0
30.0
20.0
10.0
0.0
Range (km)
8.0
7.0
6.0
5.0
4.0
3.0
2.0
1.0
0.0
Reduced time t-r/6.0 (secs.)

models. However, the PN and PnR pair at long ranges has a distinctly different separation, PnR intersecting the t=0 axis at x=240 km in the synthetic and x=180 in the data. In addition, the large clearly-defined width of the intermediary subcritical phases exceeds that of the actual data. Furthermore, and most importantly, closer inspection reveals that the "shadow zone" where only a few arrivals of specific structure can be seen on the data (65-85 km) is not reproduced in the BR2 model.

Following the suggestions of ZSCHAU and KOSCHYNK, in GIESE et al (1976), we specifically reconsidered this shadow zone in terms of the possible kinds of LVL v/z models implied by Giese's Herglotz-Wiechert method. Examining in particular the parameter space defined for a simple LVL, for an assumed constant gradient distribution within the inversion zone, the above authors show that class of equivalent LVL velocity models are all bounded above and below by a negative and positive sloping gradient. These are seen as two sides of a triangle formed by the miminum velocity depth point and the entry and departure depths to the proposed LVL. Triangular-based velocity distributions can thus be expected whenever raytrace inversion is invoked (as in PRODEHL's models; see GIESE et al, 1975).

Independent of the above (Earth-model) considerations, triangular velocity depth distributions have also been proposed, from the results of both near-vertical reflexion seismic data as well as petrologic evidence. The explicit case of a triangular-shaped

velocity distribution as a crustal model, first discussed by KOSCHYNK (1973), interestingly includes all the most recent re-interpretations of Delta West profile as an LVL candidate, specifically given by MUELLER and MULLER (1979), and more generally by MCMECHAN (1982) and BANDA & DEICHMANN (1983).

In all the above mentioned LVL models, special attention is given to attempting to account for the precise number nature and location of nearfield arrivals in the observed "shadow zone". Here it is argued that each high-velocity peak of any purported LVL structure reaching or exceeding the velocity at the top LVL point should generate a detectable reflexion and/or refraction event at the surface. For such a structured LVL model, nearfield traveltime branches of subcritical reflexions should in principle be produced, arranged in essentially interrupted concave traveltime curves parallel between both Pn and PmP arrivals (**Figure** 30). In addition, it can also be shown that multiple reflexions from one or more pre-LVL layers or from the refraction head wave phase can result in further structured arrivals within the shadow zone. Both these proposals as cited above are discussed below, using the results of both reflectivity and full wave seismogram synthesis, in attempt to further refine the Delta Shoal/West profile interpretation.

MUELLER and MULLER (1979) use the statistical 'hedgehog' method (KEILIS-BOROK and YANPOVSKAJA, 1967) to derive a set of initial models for studying the requirements necessary to better account for shadow zone wavefield events in the Delta West profile.

Considering Pc as a reflexion from either a discontinuity or from a gradient transition zone within the would-be LVL, MUELLER and MULLER initially consider the general class of 3 and 4 isovelocity layer models separated only by velocity discontinuities. Of those falling within the proposed velocity bounds, no three-layer model was found adequate to explain all major wavefield features, and all acceptable 4-layer models implied an LVL zone.

The final subset of possible models remaining was subsequently modified by addition of a suite of positive velocity gradients, in attempting to better match the observed sharpness of the Pc amplitude versus distance curve. Replacing the original discontinuity by a sufficient number of transition layers, much more peak-pronounced amplitude behaviour results, at the same time, however, as shifting the theoretical amplitude maximum about 10 km toward the farfield ranges (figures in MUELLER and MULLER, 1979).

In the simplest plane layered case, the desired agreement between synthetic and observed amplitude-distance behaviour was achieved

Figure 46 - 47

Velocity-depth profile (figure 46a) and corresponding reflectivity (46b) and fullwave (47) synthetic seismograms

The agreement between reflectivity and fullwave responses for this model (excepting nearsurface ghost features following first arrival on fullwave record) is almost total.

VELOCITY PROFILE

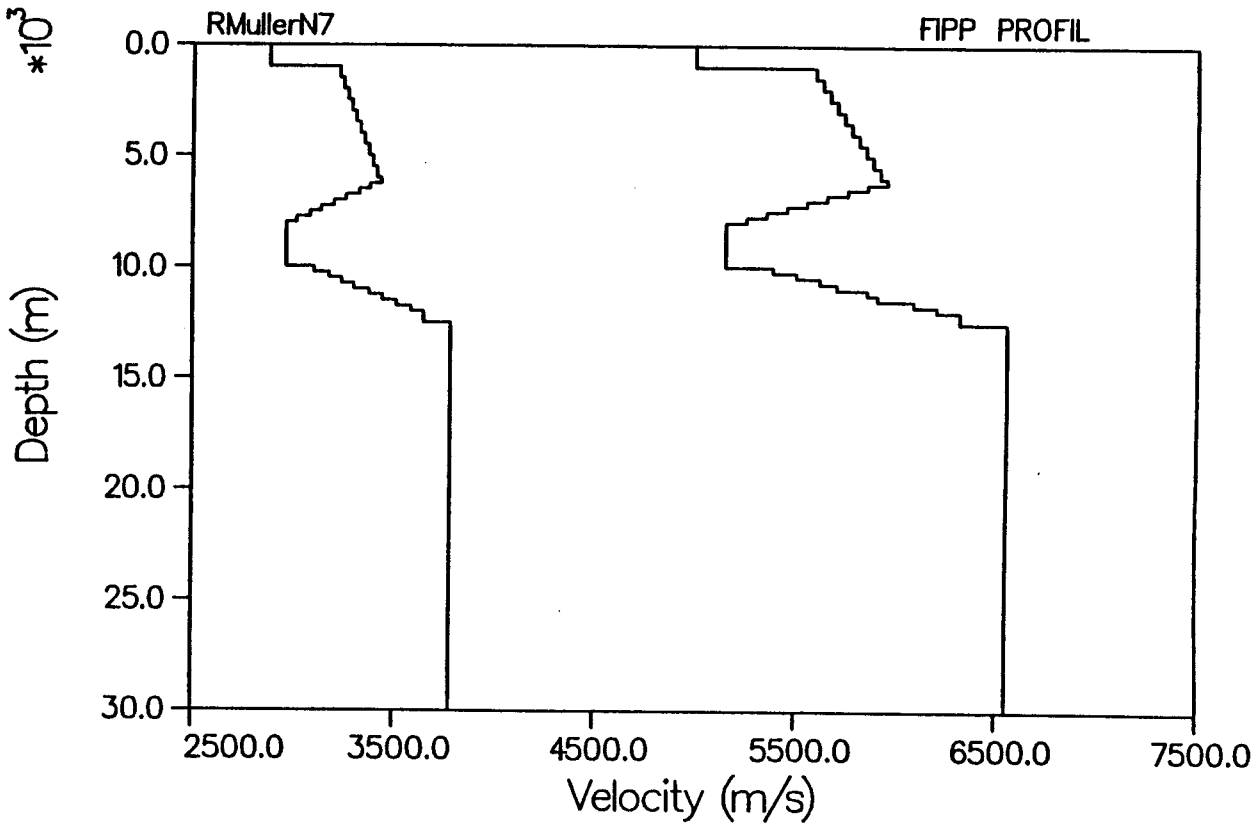

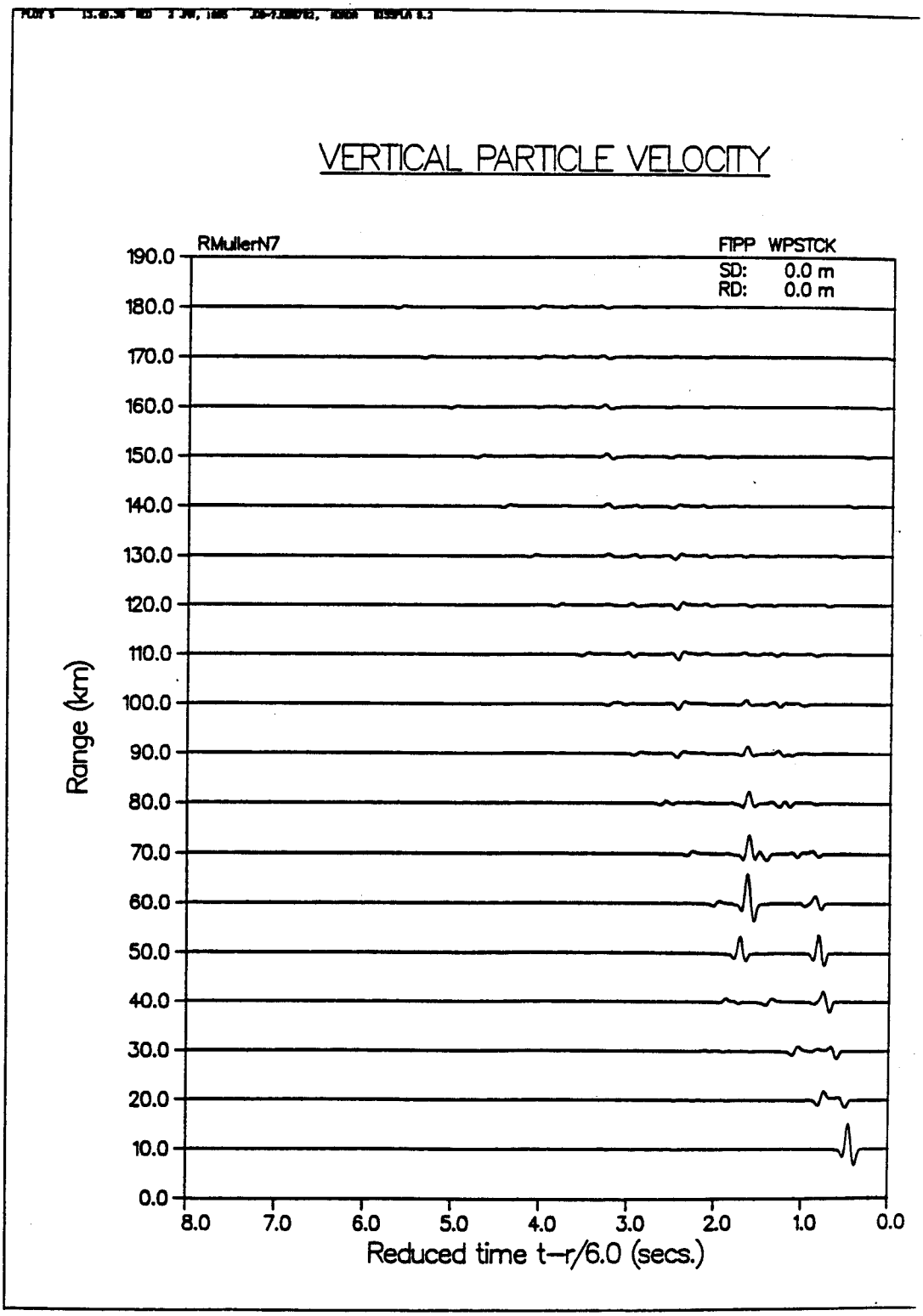
VERTICAL PARTICLE VELOCITY
RMullerN7
FIPP WPSTCK
SD: 0.0 m
RD: 0.0 m
190.0
180.0
170.0
160.0
150.0
140.0
130.0
120.0
110.0
100.0
90.0
80.0
70.0
60.0
50.0
40.0
30.0
20.0
10.0
0.0
Range (km)
8.0
7.0
6.0
5.0
4.0
3.0
2.0
1.0
0.0
Reduced time t−r/6.0 (secs.)

17.07.38 WED 10 APR, 1985 JOB=7J0B1701, NORDA DISSPLA 9.2

VERTICAL PARTICLE VELOCITY

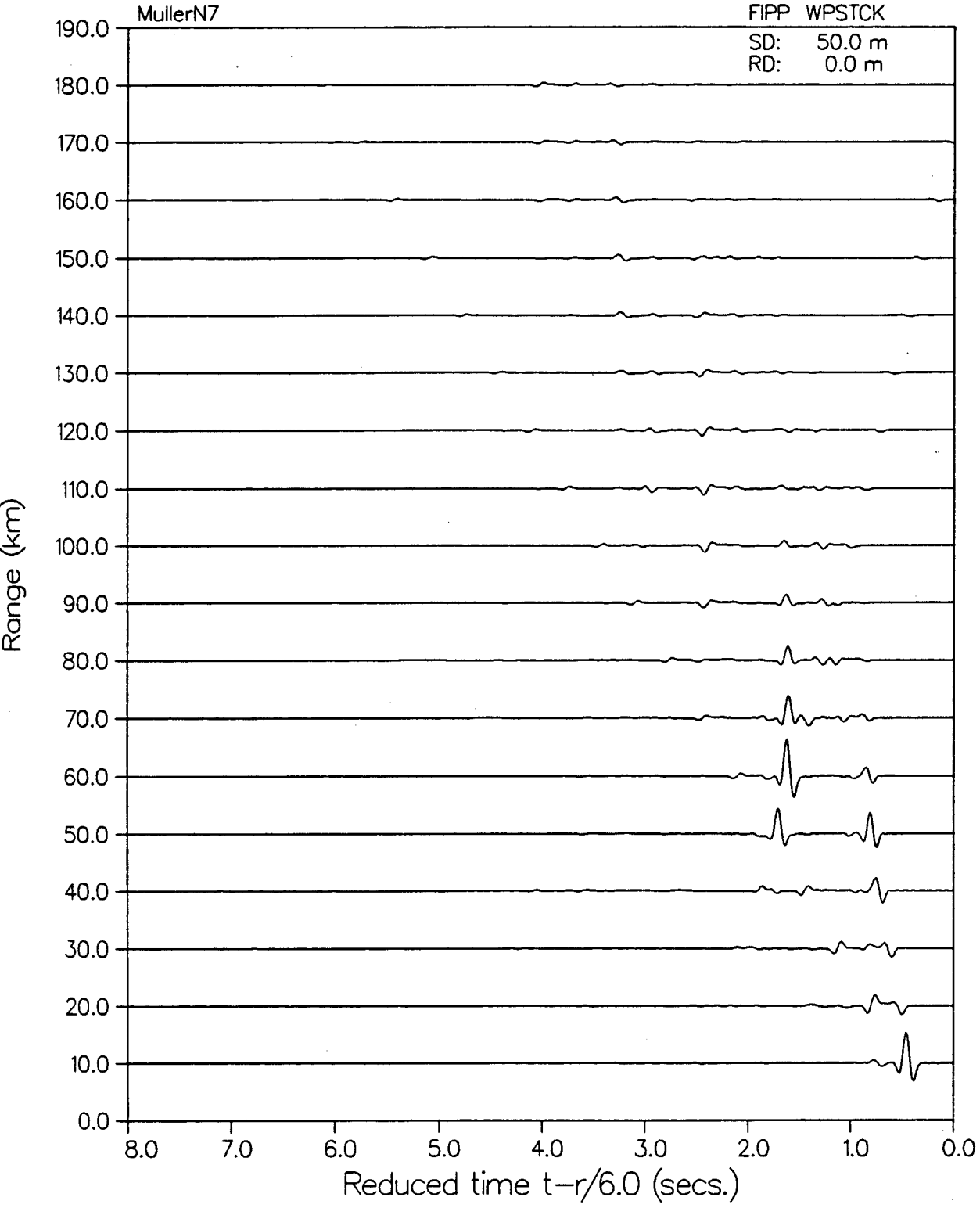

by MUELLER and MULLER via introducing an LVL on top of the deepest (Pc) reflecton. To accurately match maximum amplitude ranges, both LVL gradients were modified to a final Model (N7) shown in (MUELLER and MULLER, 1979). Good data/model agreement was achieved for most gross features using Model N7, with synthetics computed by the generalised ray method (neglecting both multiple reflexions and attenuation). A similar modelling strategy was also previously employed by PAKISER and HILL (1971) in their analysis of other refraction profiles in the western Cordillera.

It must at this point be underscored that only a complete reflectivity synthetic can offer a correct wavefield response. As MULLER (1970) has observed, any partial wavefield solution (generalised ray) will not in general give the correct or complete wavefield for an LVL transition zone at ranges near and greater-than critical. MUELLER and MULLER further note that additional reduction of the bottom LVL gradient would improve Pn head wave amplitude agreement. To test these proposals, complete reflectivity (**Figure** 46) and fullwavefield synthetic seismograms (**Figure** 47) were computed by SAFARI for MUELLER-MULLER Model N7, considering two differing bottom LVL velocity gradients.

Although some Pg amplitude change can be observed in simple reflectivity synthetics for both increased attenuation and for increased velocity gradients, the overall degree of model/data agreement for the shadowzone region remains essentially

unchanged. In particular, the aforementioned intermediate (concave) subcritical reflexions and possible multiply-reflected head wave (PgPg) across Pg to Pc traveltime curves) remain entirely unaccounted for in the simple (transmitting only nearsurface) reflectivity computation for an unstructured LVL.

Although some Pg amplitude change can be observed in the reflectivity and fullwave synthetics, the overall degree of model/data agreement for the geometrical shadow zone remains essentially unchanged from that of the published generalized ray results of MUELLER and MULLER (1979), with, however, several notable exceptions.

In particular, the aforementioned intermediate (concave-up) subcritical reflections and multiply-reflected refraction (PgPg) headwave crossing in retrograde fashion the Pg to Pc traveltime curves can only be accounted for in a complete reflectivity or exact fullwave computation (where all orders of primary, multiple and converted mode arrivals are automatically considered). In a generalized ray computation, such as used by MUELLER and MULLER in their re-evaluation of the Delta profile, the effects of free surface reflections at the source and/or receiver were not included. The effects of internal multiple reverberations within model layers were also neglected (MUELLER and MULLER, 1979). WIGGINS and HELMSBERGER (1974) have shown that multiples of one or more orders arising between major velocity discontinuities (such as an LVL) can notably contribute to a model's total

response, and cannot in general be ignored. In a generalized ray computation (SPUDICH, 1977), it is necessary to first determine and then computationally include all "important" rays. In the complete reflectivity solution (with reflection zone very near or at the surface), however, this is automatically obtained. In addition, in these later cases, there are no high or low frequency limits of validity to the synthetic obtained, so long as the isovelocity layer step size (used to approximate a gradient in velocity) is sufficiently small with respect to the dominant seismic wavelength (WHITE & STEPHEN, 1980).

As can be seen in both the reflectivity and fullwave responses for the MUELLER-MULLER N7 model, fairly strong secondary arrival appears in the geometrical shadow zone between Pg and PcP when using the complete reflectivity algorithm, even without assuming any additional discontinuities within the LVL. The present model N-7 velocity/depth profile agrees very closely to that of BANDA and DEICHMANN (1983) using a related LVL model, incorporating a 2-gradient nearsurface instead of the isospeed plus gradient Model N7 from MUELLER and MULLER. The importance at this stage of careful choice of maximum integration angle/wavenumber or minimum phase velocity is dramatically shown in **Figures 42c-d.** Here the Green's function reflectivity response integrand was cut prematurely and without sufficient smoothing.

The importance of internal multiples originating from within the LVL is underlined if varying intra-LVL discontinuities in

addition to velocity gradient zones are instead of the original discontinuities. We explicitly consider the idealised LVL of MCMECHAN (1983) and BANDA and DEICHMANN (1984), whih replaces the more complex interlayering expected above, within and/or below an LVL with a simpler 1st order gradient and few-step discontinuity series (**Figure 48**). Here the intermediary double-reflected arrival from within the LVL is plainly visible between 10 and 50km range, at reduced times of 3 to about 6 seconds. For the present reflectivity maximum angle (60°), there are in fact seen 2 closely spaced intermediary arrivals in the shadow zone, which converge as they approach intersection with the main concave-up Pn branch. The near-vertical nature (and hence numerical model sensitivity) of these features is further underscored by this example, which shows the sythetic reflectivity seismogram as computed for the same simple LVL model, this time inclusive of a relatively thin high velocity zone at central LVL depths.

Since the same maximum angle of integration as previously (60°) is used here, the interior high-angle sets of parallel multiple reflections are only very weakly in evidence, at 3.8 to 4.0 seconds, between 10 and 30km range, and again slightly below the main Pn branch at ~ 4.8 seconds between 30 and 60km. That this interpretation is correct can be further corraborated by repeating this structured LVL computation at higher maximum angles of integration (here 75°), or by considering the direct full wavefield solution (**Figures 49** and 50).

Figure 48

Velocity/depth model and corresponding reflectivity synthetic seismogram for generalized Basin & Rangle LVL model (after BANDA and DEICHMANN, 1983, and MCMECHAN, 1983)

Figure 49

Reflectivity synthetic for Banda and Deichmann LVL model, using maximum angle of wavenumber integration

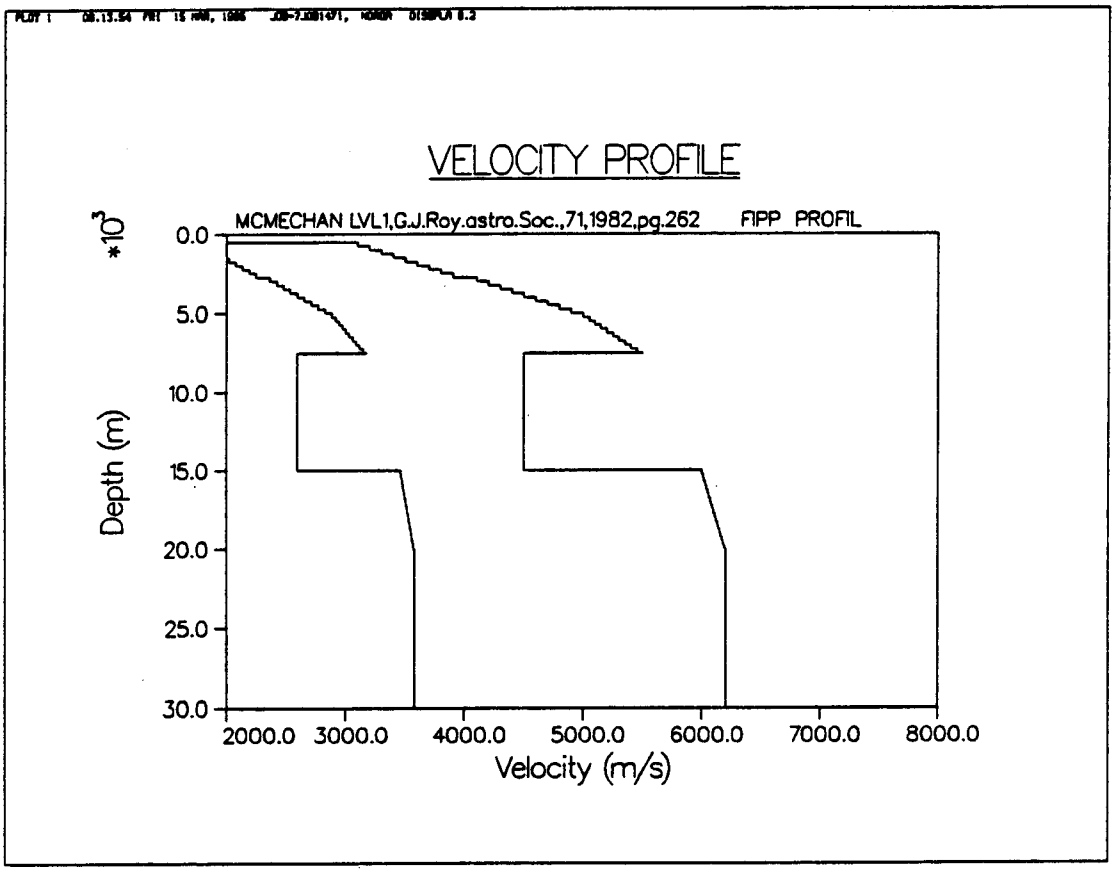
VELOCITY PROFILE
MCMECHAN LVL1,G.J.Roy.astro.Soc.,71,1982,pg.262 FIPP PROFIL
*10^3
Depth (m)
0.0
5.0
10.0
15.0
20.0
25.0
30.0
2000.0
3000.0
4000.0
5000.0
6000.0
7000.0
8000.0
Velocity (m/s)

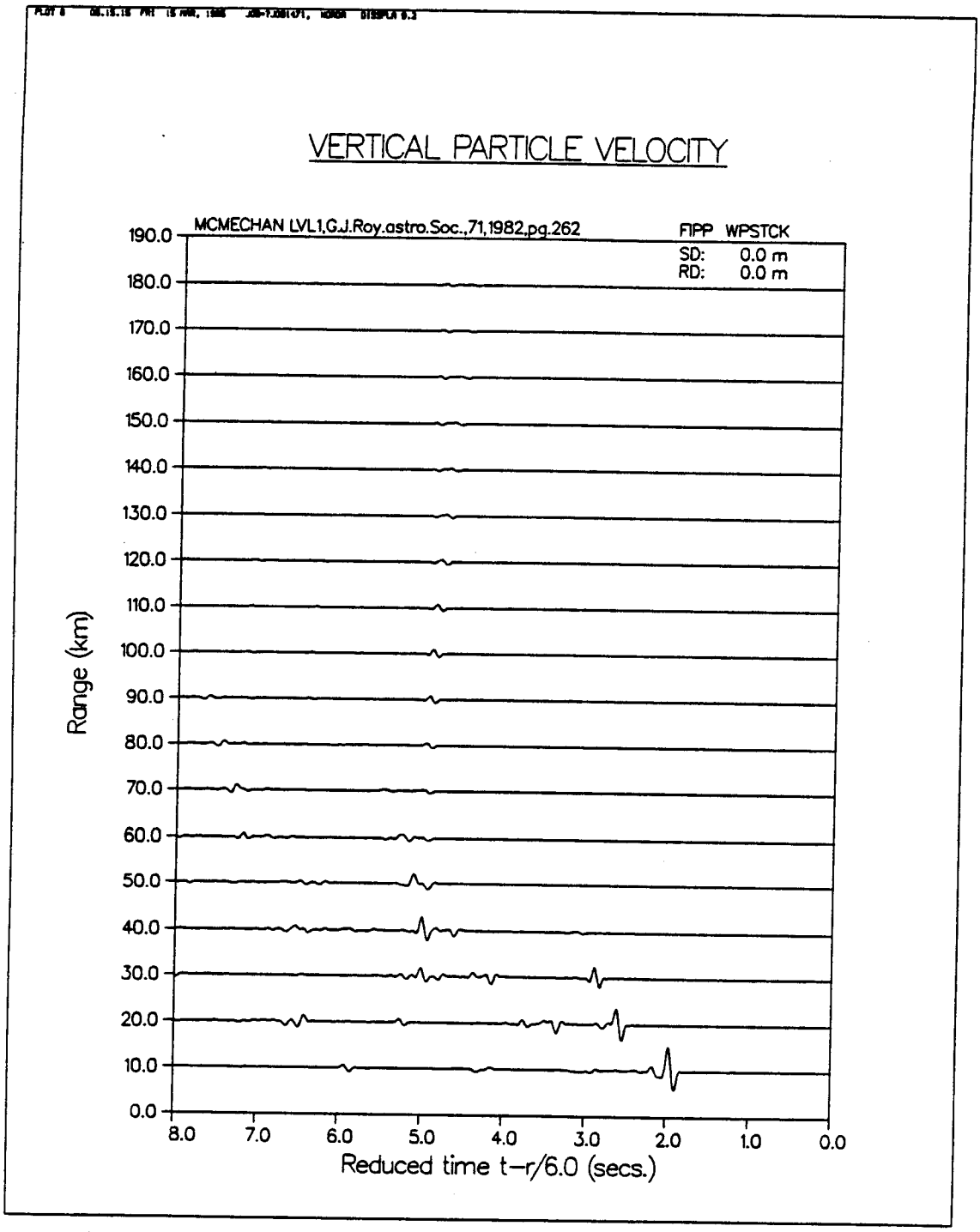
VERTICAL PARTICLE VELOCITY
MCMECHAN LVL1,G.J.Roy.astro.Soc.,71,1982,pg.262
FIPP WPSTCK
SD: 0.0 m
RD: 0.0 m
Range (km)
190.0
180.0
170.0
160.0
150.0
140.0
130.0
120.0
110.0
100.0
90.0
80.0
70.0
60.0
50.0
40.0
30.0
20.0
10.0
0.0
8.0
7.0
6.0
5.0
4.0
3.0
2.0
1.0
0.0
Reduced time t−r/6.0 (secs.)

VERTICAL PARTICLE VELOCITY

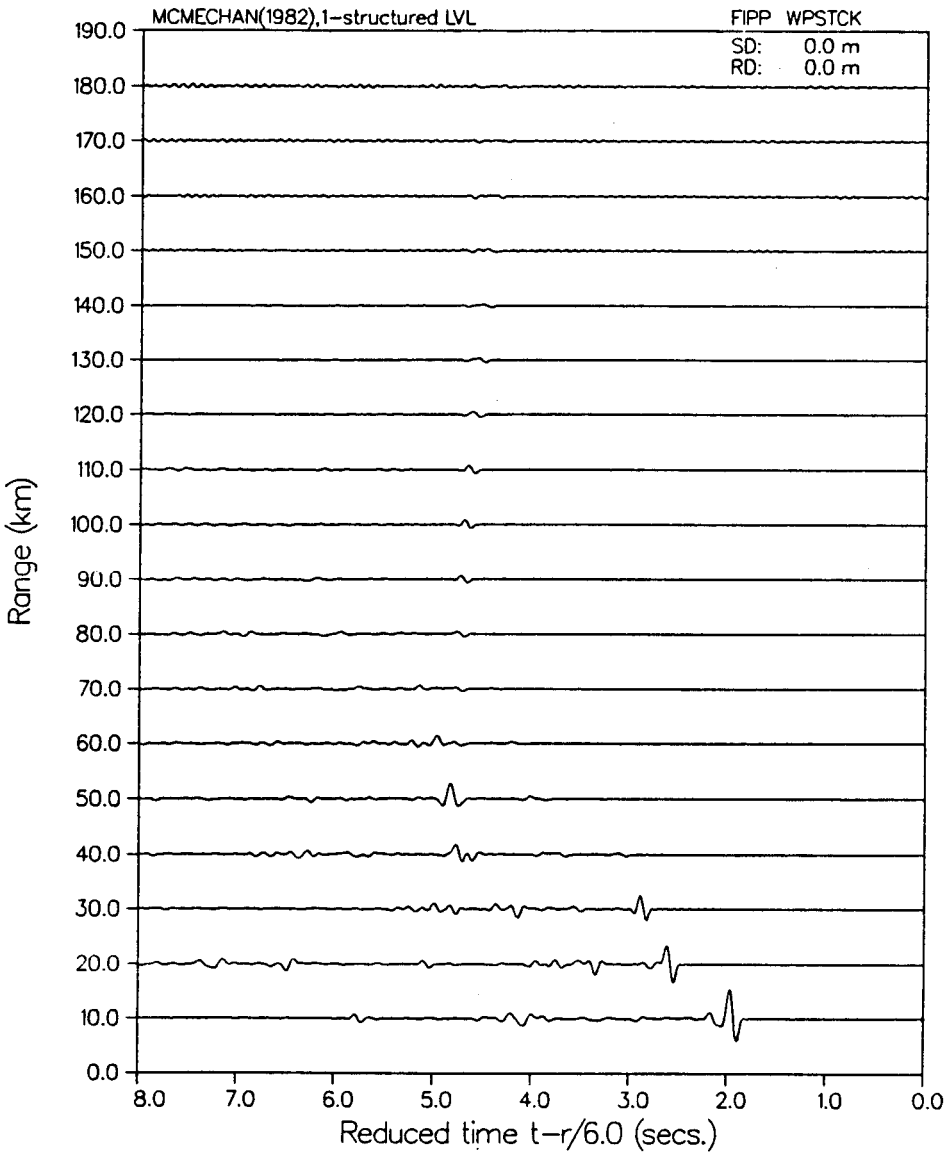

Figure 50

Velocity-depth model and corresponding reflectivity & full wavefield synthetic seismograms for 'structured LVL' (after MCMECHAN, 1984). NB the complexity of the full wavefield response, its agreement with published features of MCMECHAN (1983) and BANDA & DEICHMANN (1984), as well as its improvement over nearfield ranges

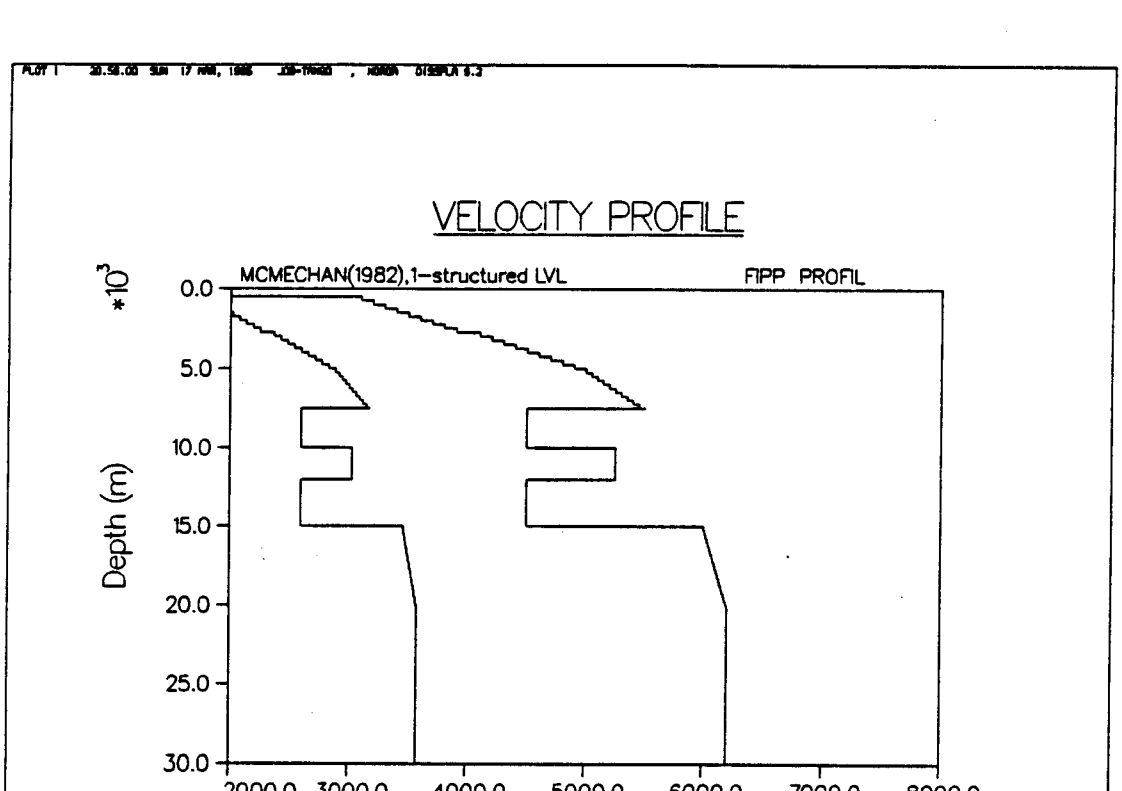
VELOCITY PROFILE
MCMECHAN(1982),1-structured LVL
FIPP PROFIL
*10^3
Depth (m)
0.0
5.0
10.0
15.0
20.0
25.0
30.0
2000.0
3000.0
4000.0
5000.0
6000.0
7000.0
8000.0
Velocity (m/s)

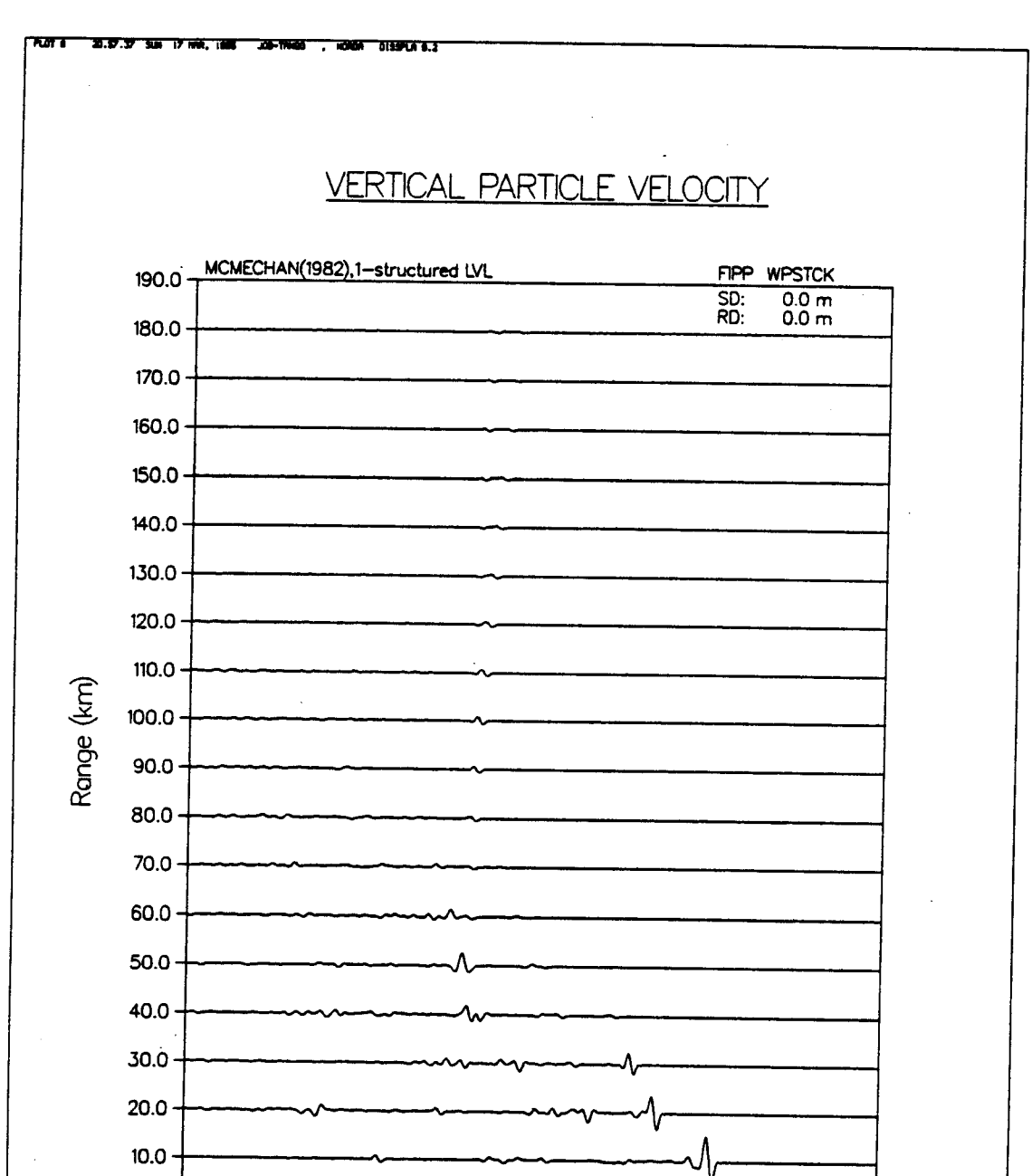
VERTICAL PARTICLE VELOCITY
MCMECHAN(1982),1-structured LVL
FIPP WPSTCK
SD: 0.0 m
RD: 0.0 m
Range (km)
190.0
180.0
170.0
160.0
150.0
140.0
130.0
120.0
110.0
100.0
90.0
80.0
70.0
60.0
50.0
40.0
30.0
20.0
10.0
0.0
8.0
7.0
6.0
5.0
4.0
3.0
2.0
1.0
0.0
Reduced time t-r/6.0 (secs.)

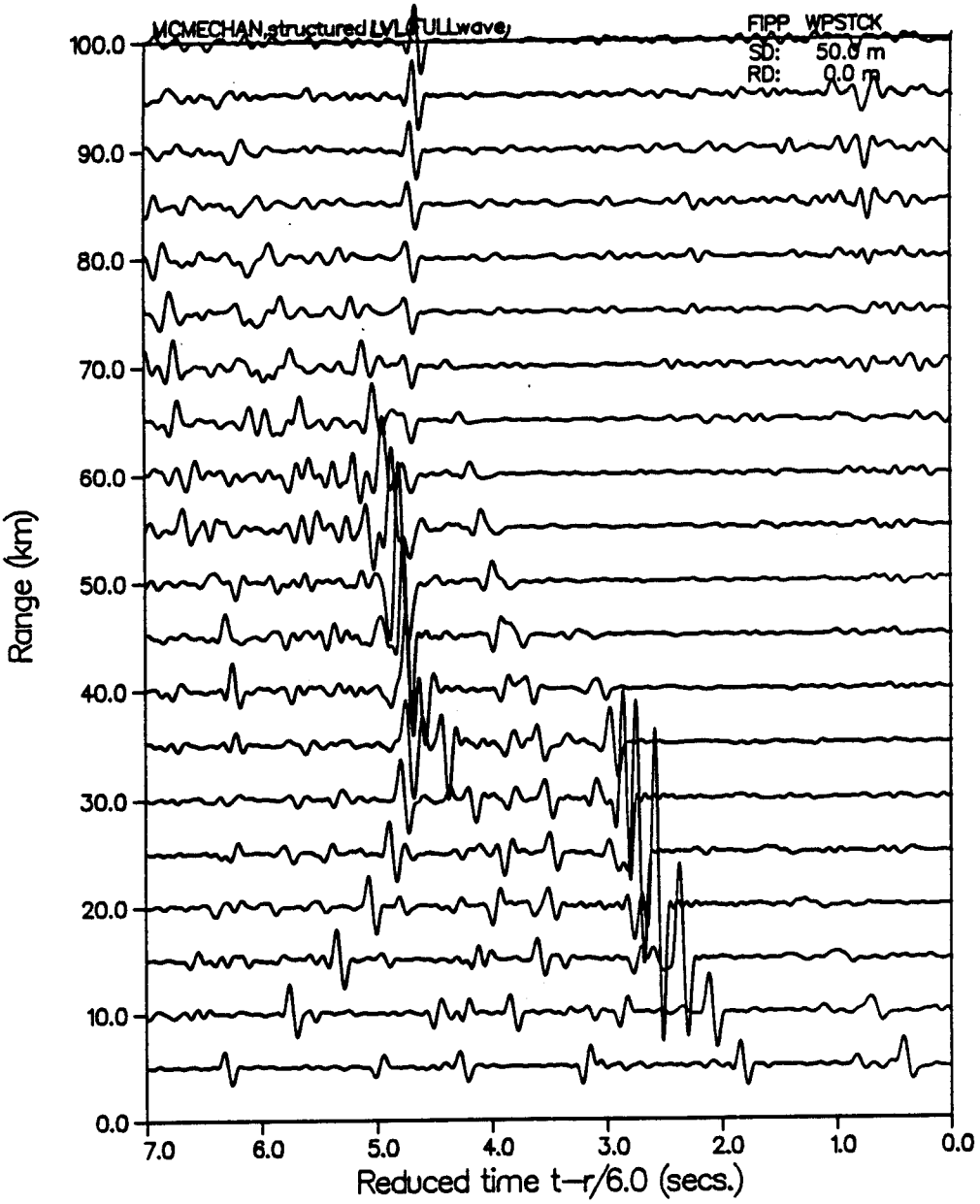
VERTICAL PARTICLE VELOCITY
MCMECHAN,structured LVL&ULLwave)
FIPP WPSTCK
SD: 50.0 m
RD: 0.0 m
100.0
90.0
80.0
70.0
60.0
50.0
40.0
30.0
20.0
10.0
0.0
Range (km)
7.0
6.0
5.0
4.0
3.0
2.0
1.0
0.0
Reduced time t−r/6.0 (secs.)

Consideration of the seismograms resulting from a 3d LVL model (with the 3d LVL at a depth immediately below the main LVL) shows results very suggestive of the strong interference nature of the localized high amplitude features in the observed Delta profile. In addition, several other intermediate-amplitude nearvertical arrival trains are also seen, visibly coherent for only relatively short profile distances (15-25km).

In attempt to further improve model/data match, thin hi-velocity layers (with varying velocity contrasts) of the type used in McMECHAN were added to the LVL interior of the Prodehl-modified Model N7 of MUELLER and MULLER, as computed with the reflectivity and fullwavefield solution of SAFARI. These results are shown in **Figure** 49 and 50.

Considering the reflectivity synthetic for MCMECHAN Model 1 in **Figure 49**, a definite body of precritically reflected multiples can now be plainly seen, as additional arrival branches between the main Pn and Pg head wave traveltime curves. Their pattern, however, is comparatively indistinct in the reflectivity synthetic (here computed over arrival angles from 0 to 70 degrees), in comparison to the highly prominent and well-separated arrival branches of MCMECHAN's asymptotic ray calculation. Various other maximum arrival angles (from 75 thru 90 degrees) were subsequently employed, without, however, any noticeable increase in intermediary arrival number or definition (these results not shown). In contrast to the above results, the

intra-LVL Pg-Pg reflected refraction, however, is relatively clear and well defined, between 3 and 5 seconds reduced time and 20 to 50 km offset range.

In attempt to obtain better agreement with both MCMECHAN's theoretical results and the DELTA data profile, a fullwave synthetic seismogram was computed for the same velocity/depth profile as above. These results are given in FIGURE 50.

The results reveal an almost total agreement in both the number and character of intra-LVL arrivals in the geometric shadow zone and nearfield, plus additional features confirming both the extended post-publication discussion of his results by MCMECHAN (1984) and the Delta field profile itself.

Of immediate importance is the vast increase in the total number of P1R type arrival branches visible within an even smaller reduced time window than that originally used in the previous reflectivity calculations. Unlike MCMECHAN's artificially isolated and simplistic multiple arrival branches, the true interference character of,and the mode conversions associated with each of the expected intra-LVL multiple branches is strongly apparent in the fullwave solution. Their correct amplitude-distance and phase behaviour (especially for the shadow zone branches between 3.5-4.5 seconds at 40-80 km range) is plainly in evidence. Furthermore, in agreement with MCMECHAN's discussion of expected and observed data from LVL zones, the retrograde Pg-Pg

reflected refraction arrival, while still evident between about 25 and 45 km at 4-5 seconds reduced time, is now much less distinct against the total background of nearfield multiples and mode conversions. The striking improvement of agreement between the fullwave synthetic and the Delta profile data in the nearfield underscores the necessity of considering all arrival orders and modes, and thereby the utility of a fast fullwave solution which correctly achieves this in one economic computational pass.

Further considering these results in regard to the DELTA data itself, an apparent interference complex in the nearfield, of locally high amplitude along the Pc branch (between 35 and 60 km range at ~ 5 seconds), in agreement with that shown by BANDA and DEICHMANN Model 1 and discussed by MUELLER and MULLER. This proposed Pg-Pg + PcP interference complex plus respective amplitude maxima is strongly suggestive of the main interference complex visible on the DELTA profile itself. This is also true for the much smaller amplitude high on the lower refraction branch. Additional high velocity stringers appropriately located as well as of smaller individual thickness could likely increased the dispersed ringy character of the present synthetic.

We next undertook several detailed reflectivity calculations, which retain the single LVL structure, albeit one intermediate to that of MUELLER and MULLER and BANDA and DEICHMANN. At the same time, we attempted to systematically introduce both near-surface

and deeper crustal features into the total v/z profile, as implied by the PRODEHL data sets, and other work on Basin and Range crustal modeling (PAKISER, 1985). These results are shown in **Figures 51 - 55.**

Figures 51 - 55

Velocity-depth model and corresponding reflectivity synthetic for:

51) MULLER-MUELLER nearsurface + LVL with PRODEHL subLVL model

52) MULLER-MUELLER nearsurface + LVL with PRODEHL subLVL model: (thicker LVL)

53) MULLER-MUELLER nearsurface + LVL with PRODEHL subLVL model: (LVL of greater velocity contrast)

54) MULLER-MUELLER nearsurface + LVL with PRODEHL subLVL model: (with additional velocity gradient structure)

55) MULLER-MUELLER nearsurface + LVL with PRODEHL subLVL model: (maximum velocity contrast of LVL)

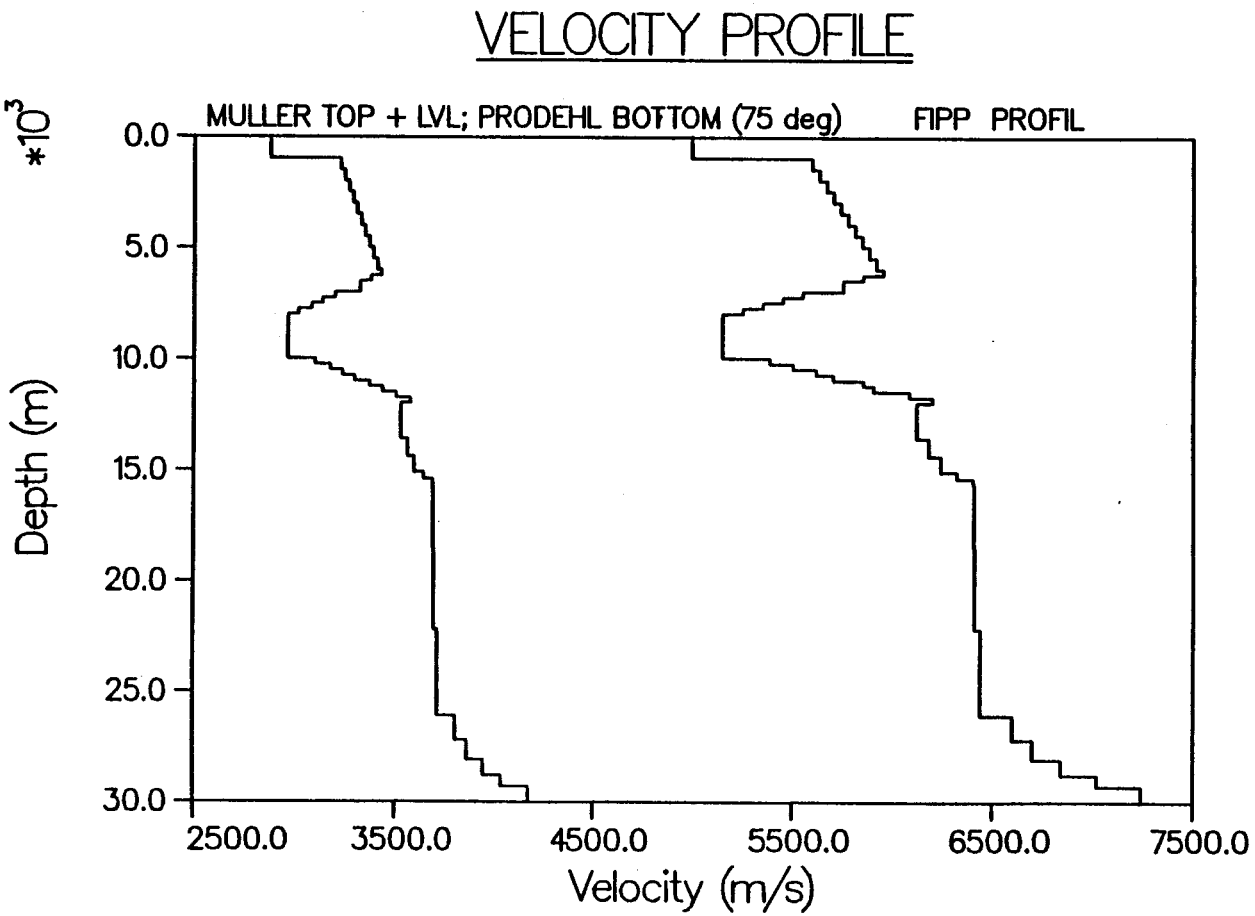
VELOCITY PROFILE
MULLER TOP + LVL; PRODEHL BOTTOM (75 deg)
FIPP PROFIL
*10^3
Depth (m)
0.0
5.0
10.0
15.0
20.0
25.0
30.0
2500.0
3500.0
4500.0
5500.0
6500.0
7500.0
Velocity (m/s)

VERTICAL PARTICLE VELOCITY

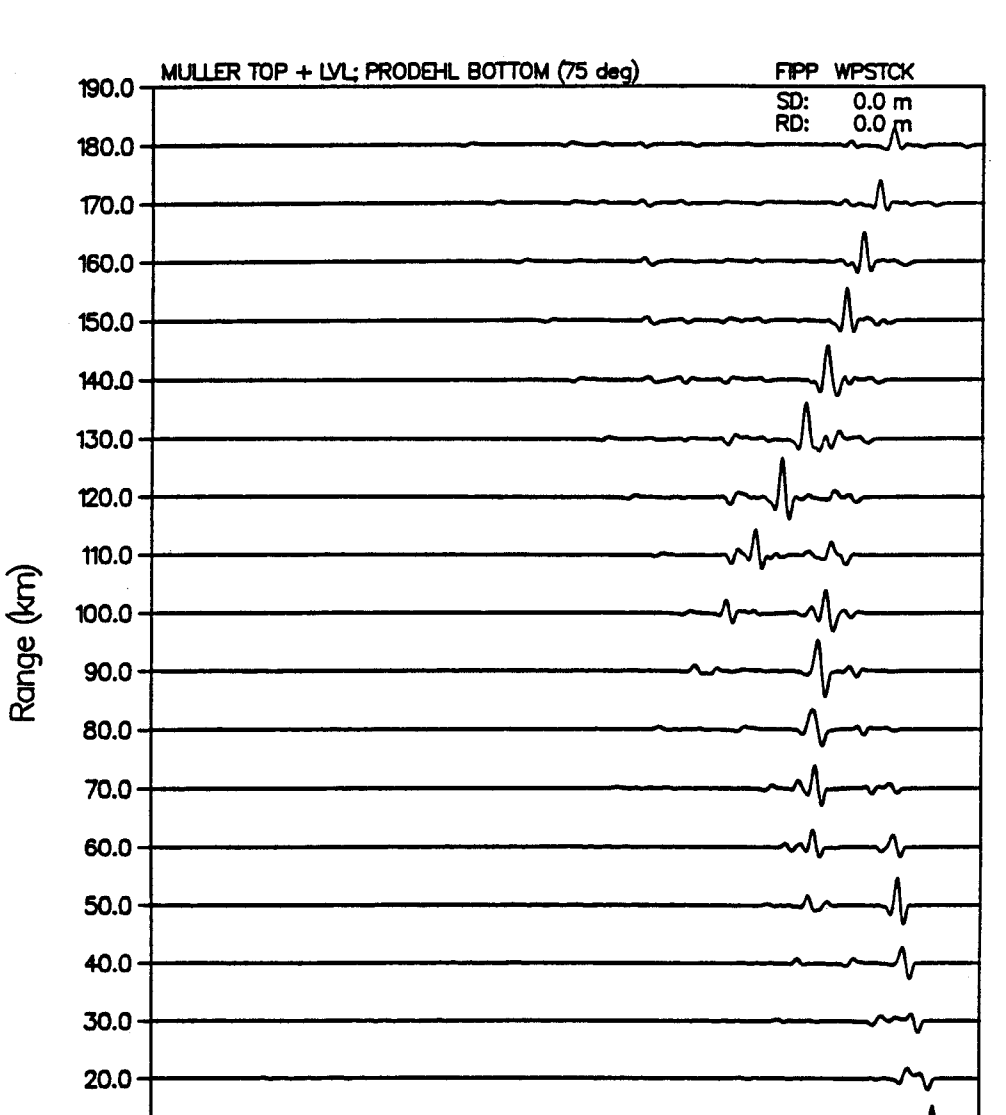

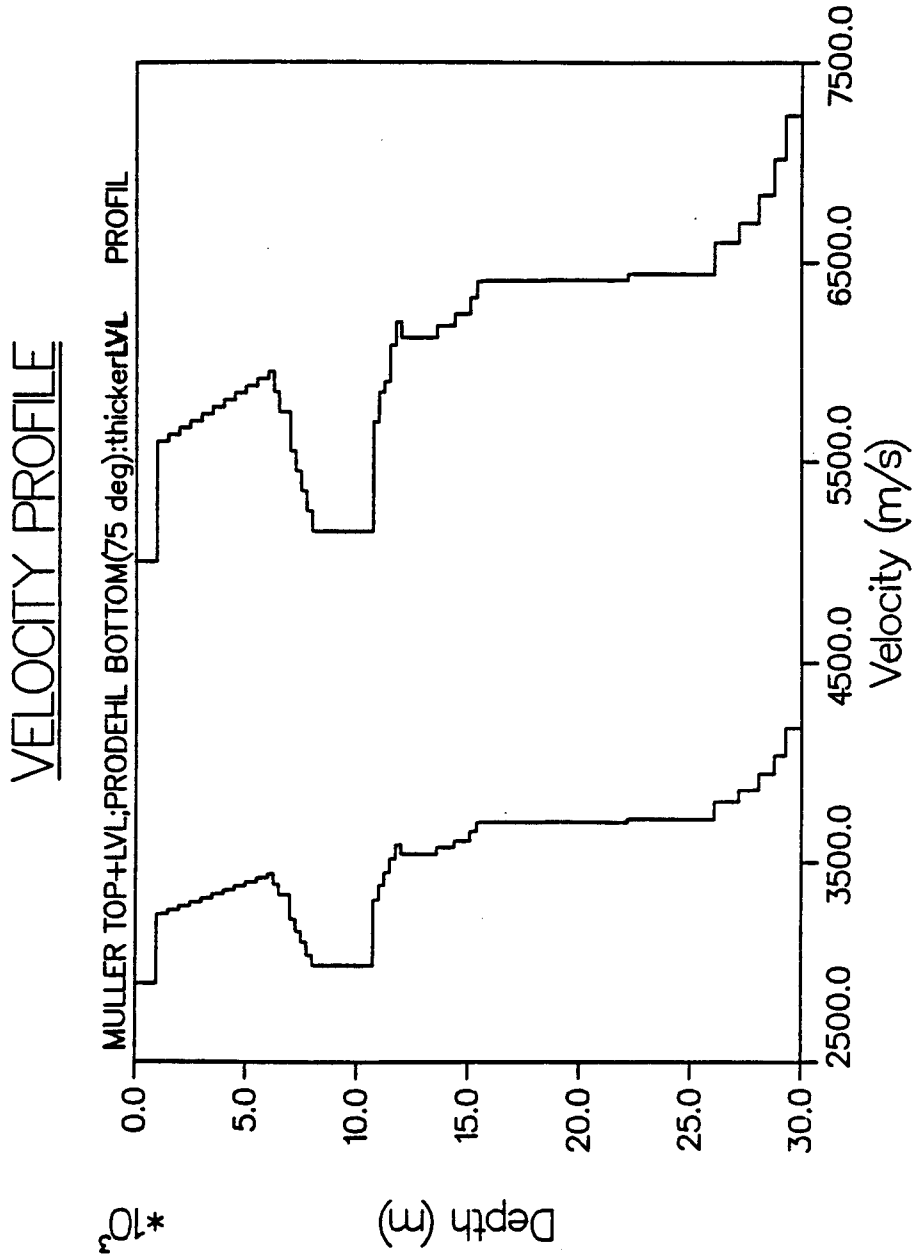
VELOCITY PROFILE
MULLER TOP+LVL;PRODEHL BOTTOM(75 deg):thickerLVL PROFIL
*10²
Depth (m)
0.0
5.0
10.0
15.0
20.0
25.0
30.0
2500.0
3500.0
4500.0
5500.0
6500.0
7500.0
Velocity (m/s)

VERTICAL PARTICLE VELOCITY

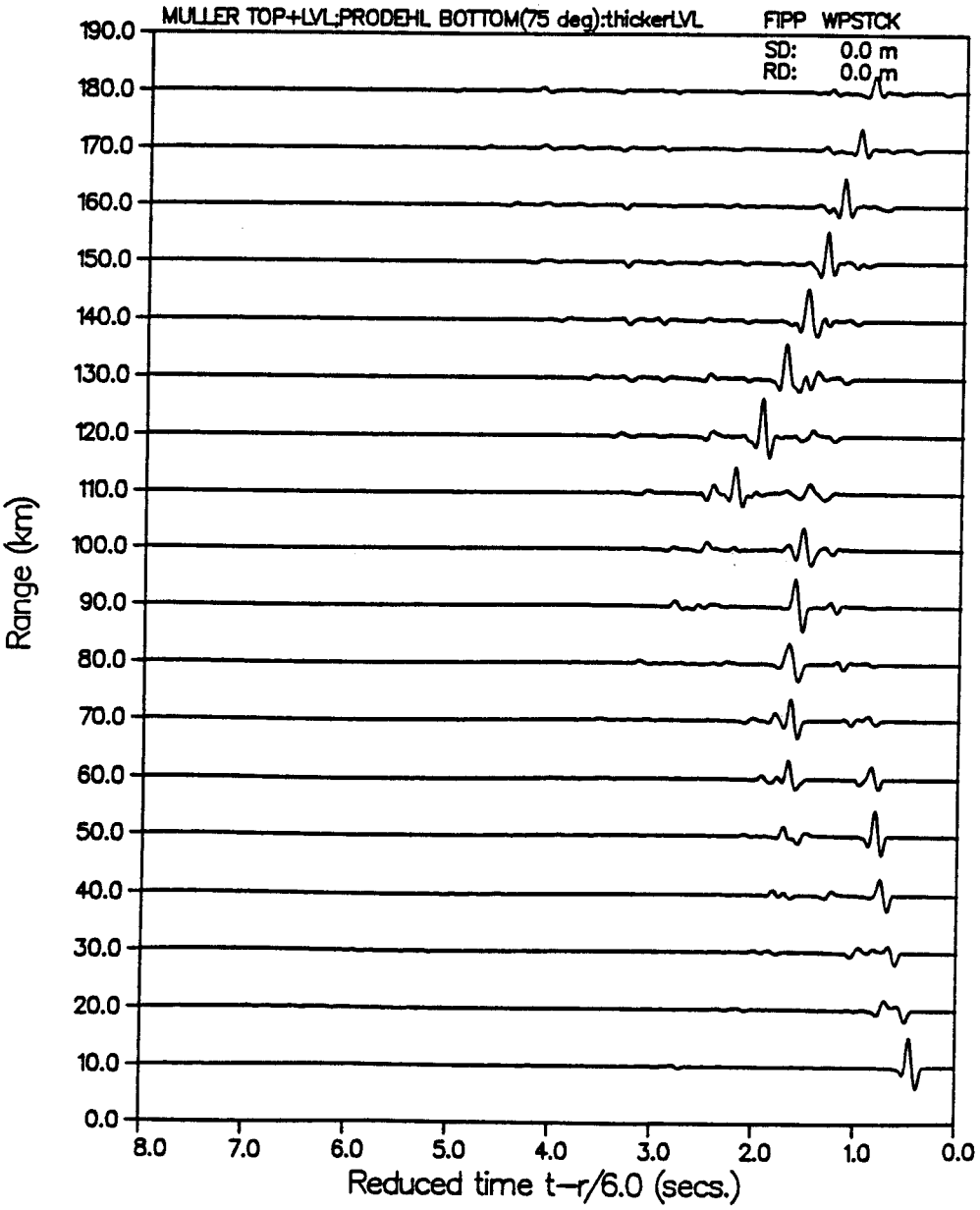

Figure 51 comprises a near-surface and LVL velocity distribution taken from that of MUELLER and MULLER, and a sub-LVL structure derived from PRODEHL. The resulting reflectivity synthetic does not differ significantly from the PRODEHL-based seismograms computed earlier. Although a single very weak P1R arrival, as well as the PgPg retrograde, are seen well into the nearfield, the localized interference complexes and amplitude maxima are totally absent.

Increasing the total LVL thickness by a nominal amount (here shown for 2km) as per **Figure 52** has a small observable effect on the single P1R arrival noted above, apparently altering its intrinsic phase (to that of a 1st derivative of the corresponding arrival waveform shown above in Figure 51). In addition, in the farfield, the characteristic en echelon PmP arrival branches are now also significantly reduced in both maximum amplitude and discernability.

VELOCITY PROFILE

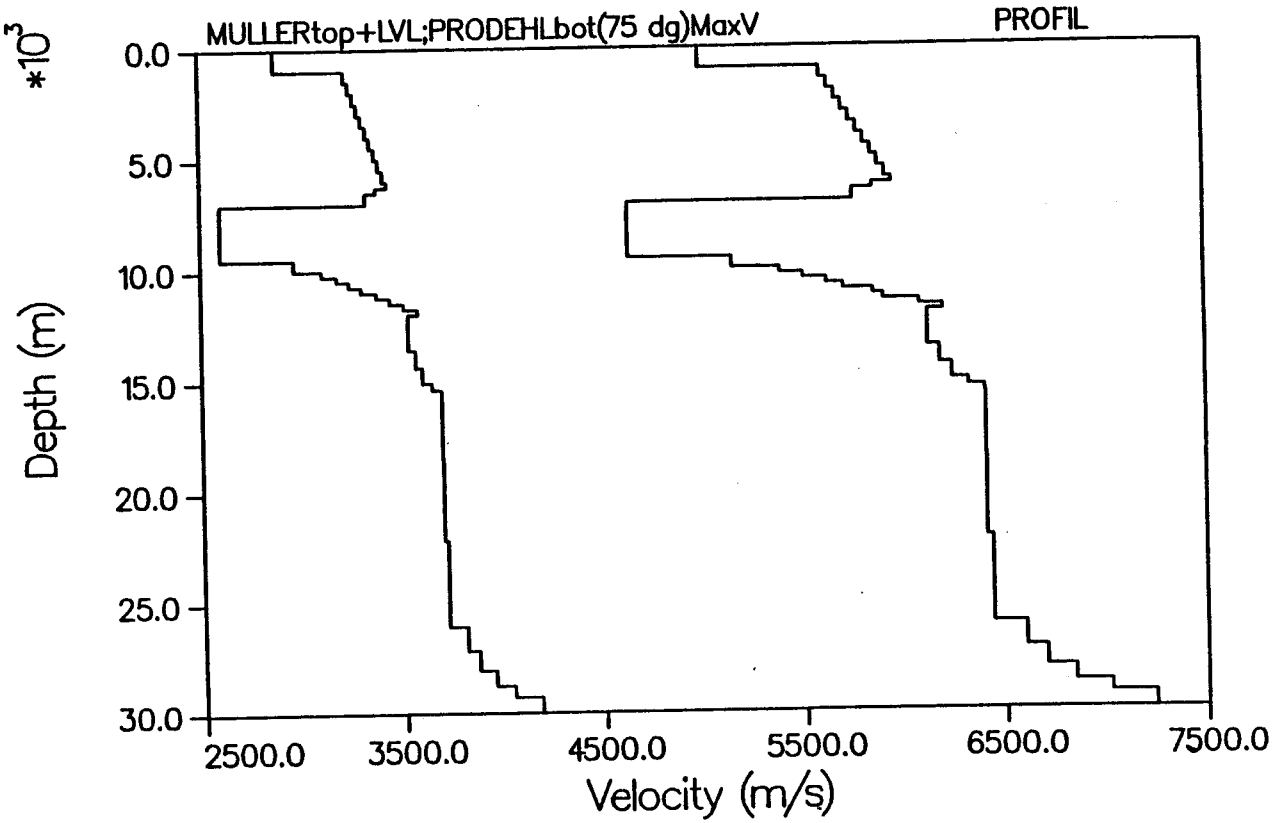

VERTICAL PARTICLE VELOCITY

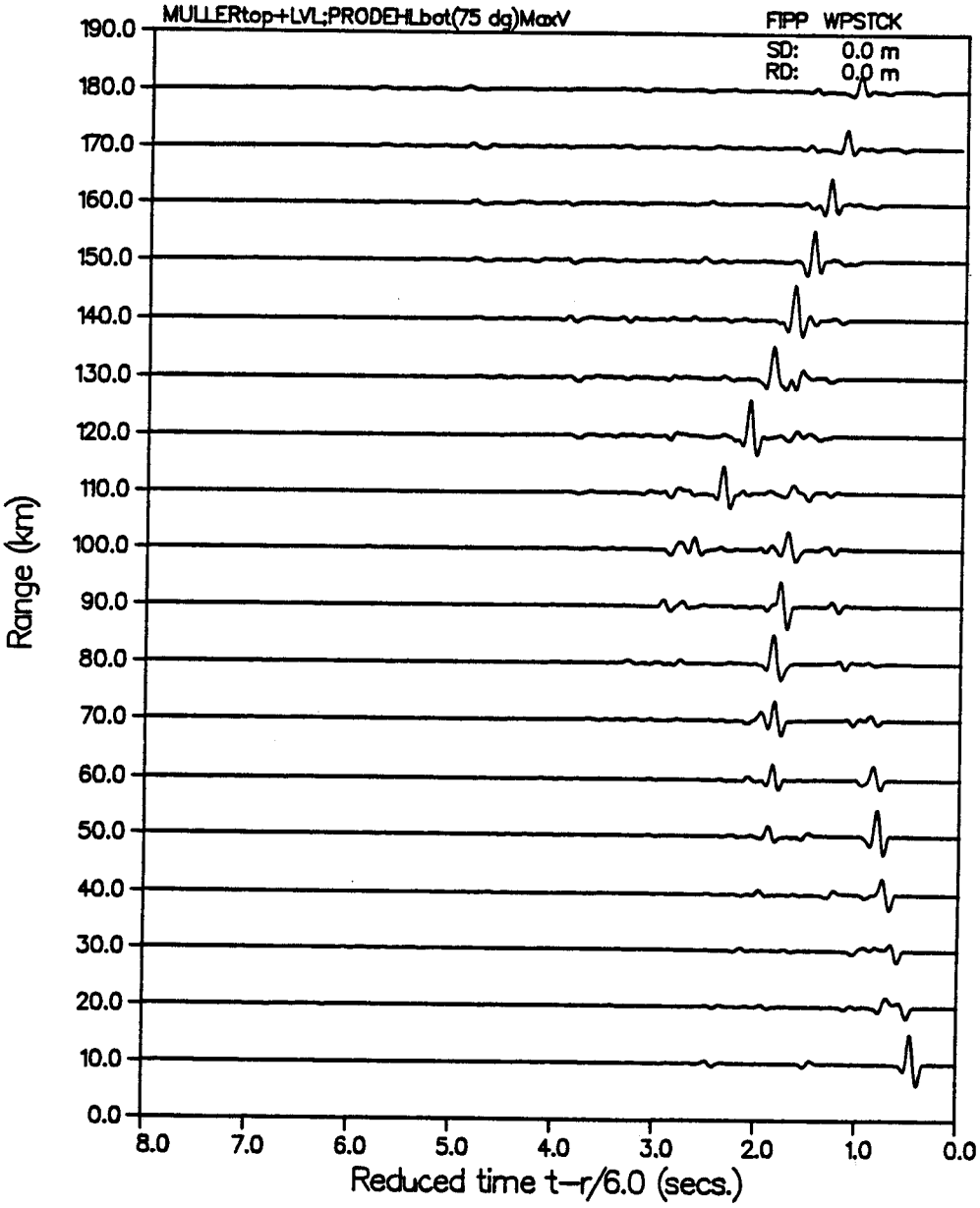

The model in **Figure 53** returns to the original LVL thickness of MUELLER and MULLER (as per Figure 51). In this case, however, we increase the total velocity-contrast of the LVL by 500 m/sec. Here, in addition to the above noted PgPg and PcP features, are 2 additional P1R type branches (analogous to those previously seen in the fullwave synthetic for MCMECHAN Model 1; Figure 51). at reduced time of about .5 - 1.5 and 1.5 - 2.5 seconds respectively for ranges of 0-30 and 0-50 km.

Some lessening in the total amplitude and rate of amplitude variation with distance is also evident for the PcP-Pc branches, along with an apparent increase in PcP waveform complexity, due to interference with one of the above cited additional P1R reflection branches.

VELOCITY PROFILE

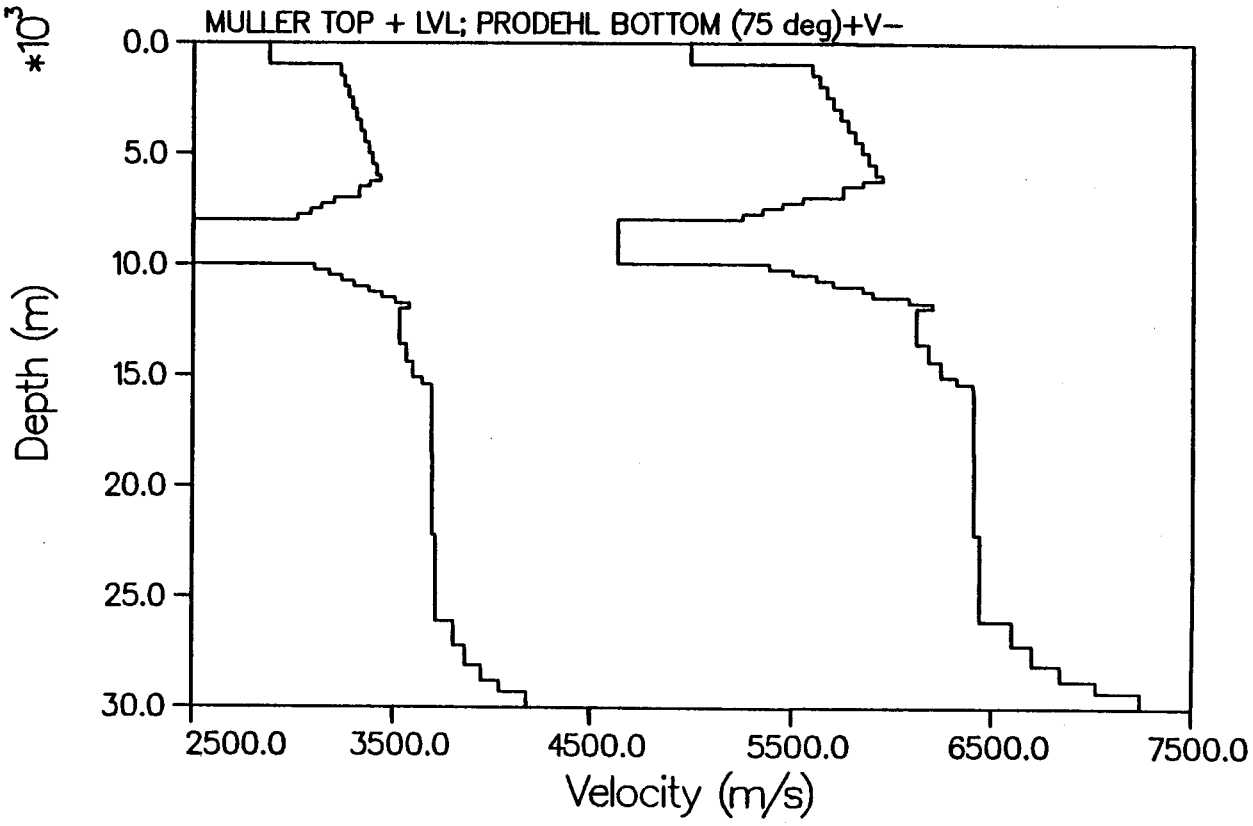

PLOT 5 21.01.51 THUR 10 JAN, 1985 JOB-7.0897605, NORSAR DISSPLA 8.2

VERTICAL PARTICLE VELOCITY

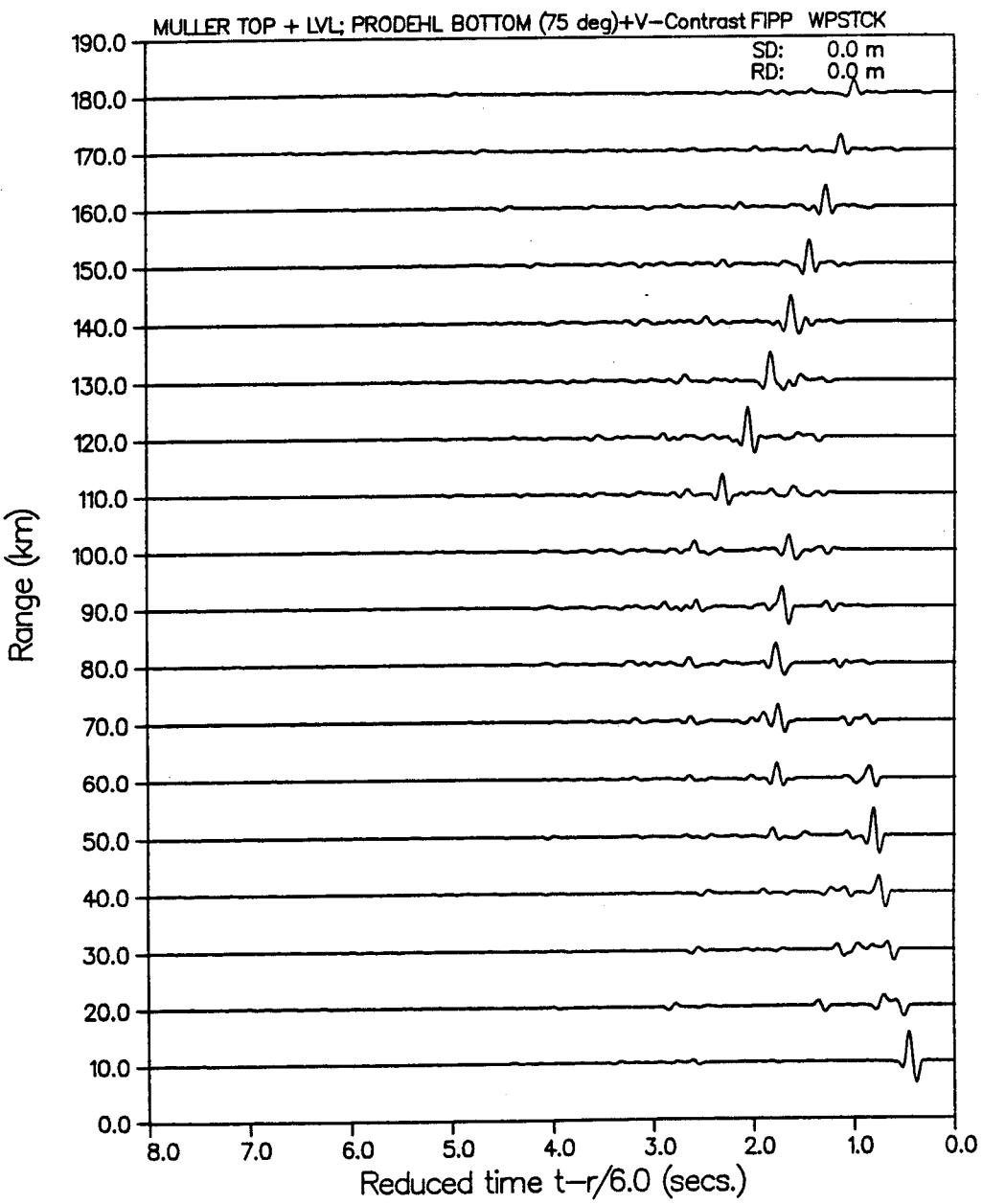

VELOCITY PROFILE

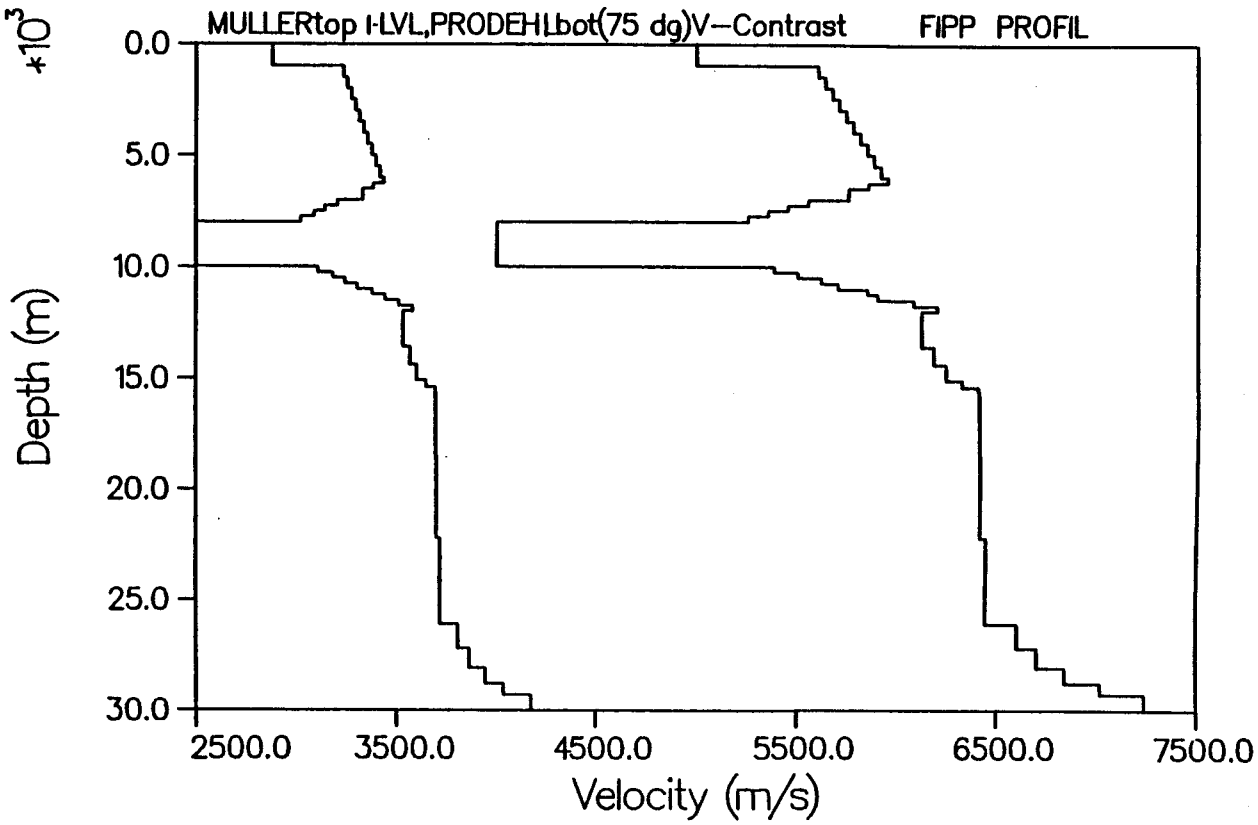

VERTICAL PARTICLE VELOCITY

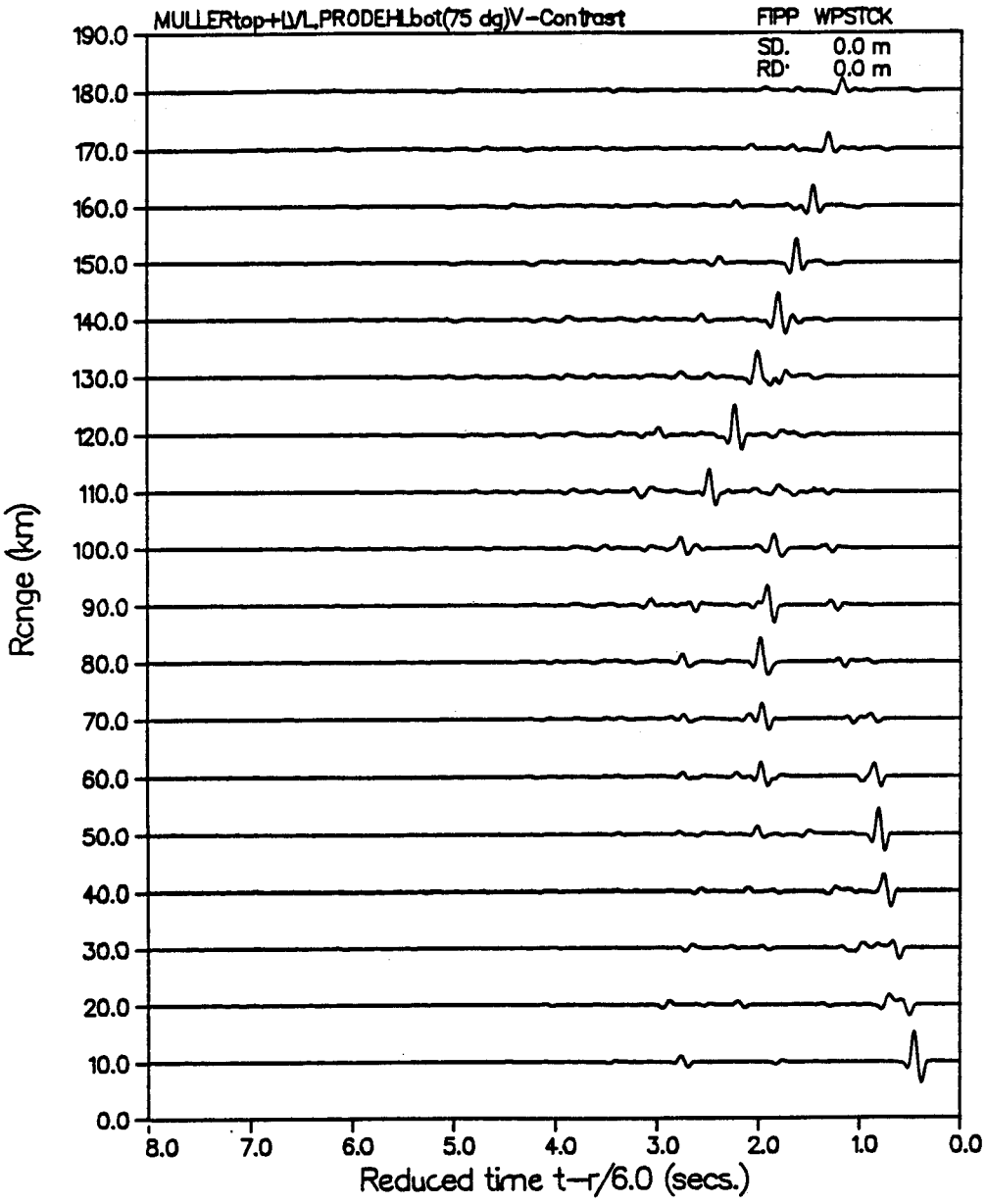

A significant number (5+) of precritical reflections and multiples can now be seen as additional arrival branches above, below and within the shadow zone over the nearfield receiver range, for the case of a single hi-velocity layer of thickness = 1km. As considered here, an increase in velocity contrast serves only to increase the amplitudes of arrivals at less than 2 seconds reduced time, between 0 and 40 km.

The combined results of both maintaining an increased LVL thickness and total LVL velocity contrasts are shown in FIGURE 54. The additional P1R multiple branches as above are retained, with however a decreased presence in the PgPg retrograde, due to destructive cancellation by the lowermost additional P1 branch. Further reverberant PmP arrivals appear at farfield offsets for t greater than 3 seconds.

These features are clarified by the results of **Figure 55**, which increases the total LVL velocity contrast by about 1000 m/sec (ie, the limit of what might be geologically feasible). While the farfield PmP arrivals have almost completely lost any distinct character whatsoever, the PgPg retrograde is now clearly evident again, accompanied by a total of 4 additional P1 type nearfield branches.

As stated by MCMECHAN (1977; 1983), FUCHS (1975) and others, the structure of a real LVL zone need not always necessarily comprise only a single isolated velocity inversion, but perhaps may be better represented as a complex zone over which P and S wave velocities vary discontinuously with depth. Such a structure could be accounted for (e.g.) in terms of fine scale velocity inversions and thin low and/or high velocity layers.

Some of the same effects (in terms of increased number and complexity of nearfield arrivals) can be achieved by retaining the original LVL model of MUELLER and MULLER, supplemented by one or more smaller LVLs at lesser and/or greater depths.

Figure 56 shows the same LVL model as considered previously, here with a much shallow LVL at about 3km depth. The only effect directly attributable to this new feature is a small and rapidly decaying phase between 20 and 50 km range, at about t = 1 second reduced time. This phase strongly interferes with one of the main expected P1 phases from the central LVL, masking the PgPg retrograde.

In **Figure 57** the effect of increasing the net velocity contrast of this 2nd shallow LVL is displayed. The additional short-path P1 type phase is now more clearly resolved, while the apparent amplitude of the underlying Pg phase is reduced.

Figure 56

Velocity/depth profile and corresponding reflectivity synthetic for MULLER-MUELLER + PRODEHL model, with second LVL in nearsurface

Figure 57

Velocity/depth profile and corresponding reflectivity synthetic for MULLER-MUELLER + PRODEHL model, with second LVL (as above) in nearsurface, of greater velocity contrast

VELOCITY PROFILE

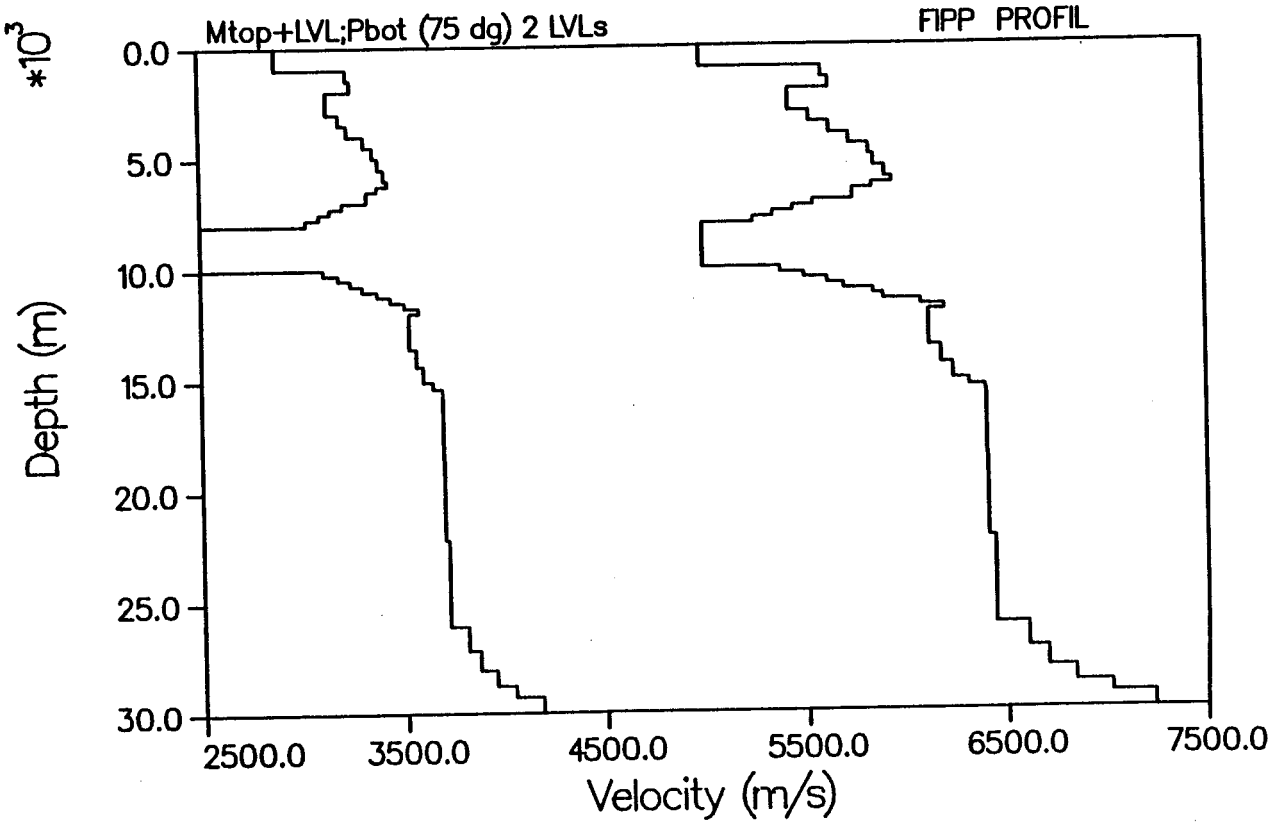

VERTICAL PARTICLE VELOCITY

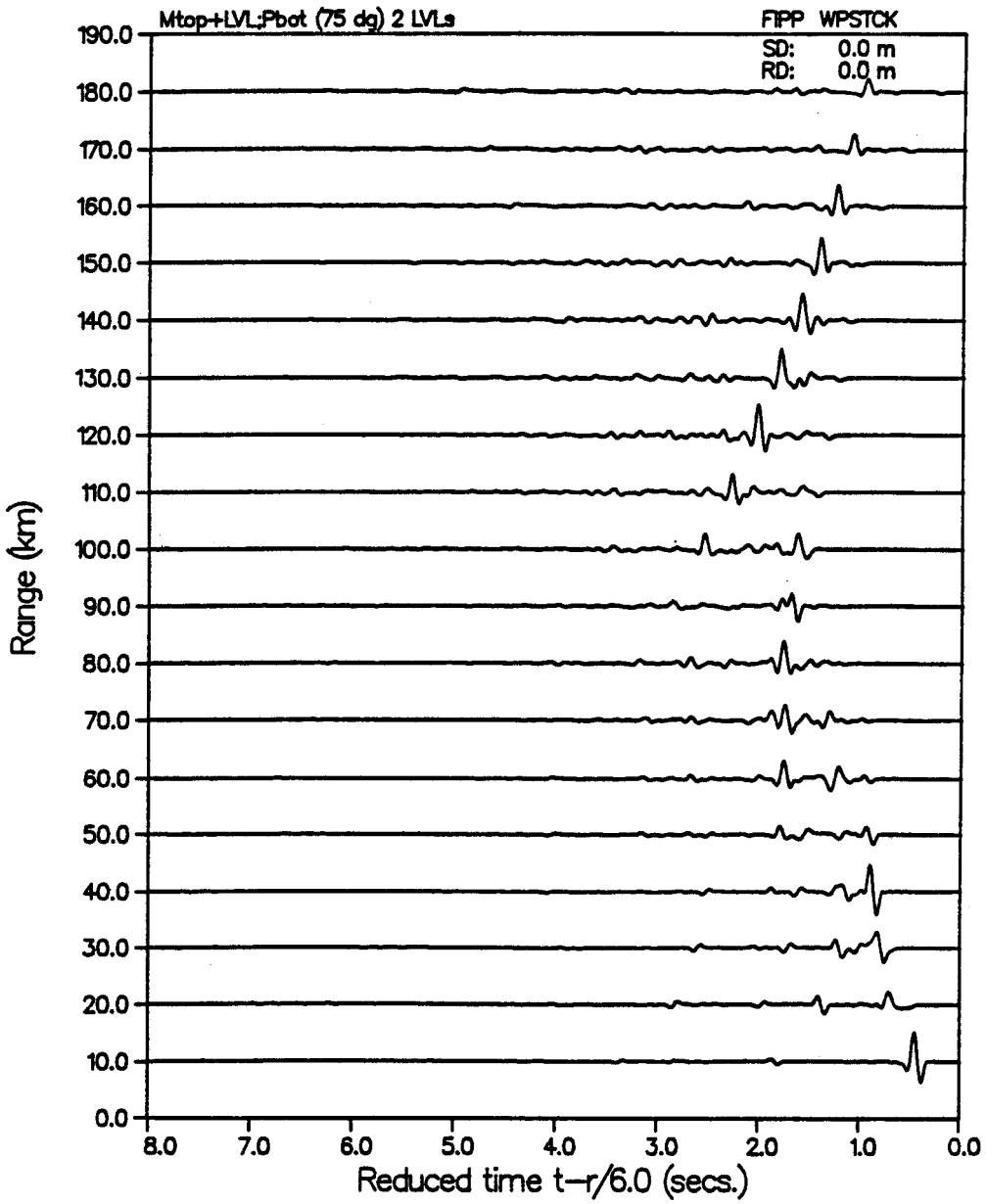

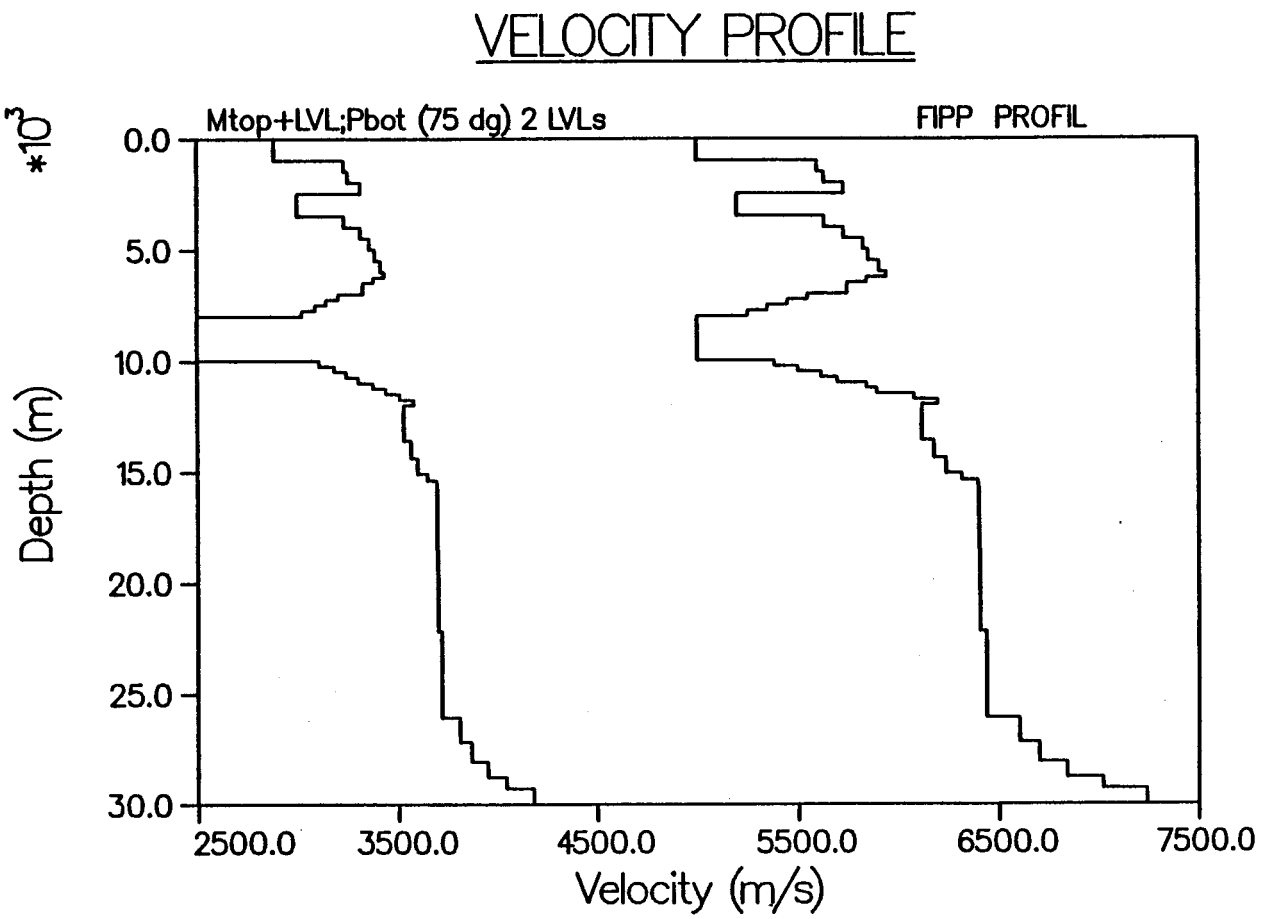
VELOCITY PROFILE
Mtop+LVL;Pbot (75 dg) 2 LVLs
FIPP PROFIL
*10^3
Depth (m)
0.0
5.0
10.0
15.0
20.0
25.0
30.0
2500.0
3500.0
4500.0
5500.0
6500.0
7500.0
Velocity (m/s)

VERTICAL PARTICLE VELOCITY

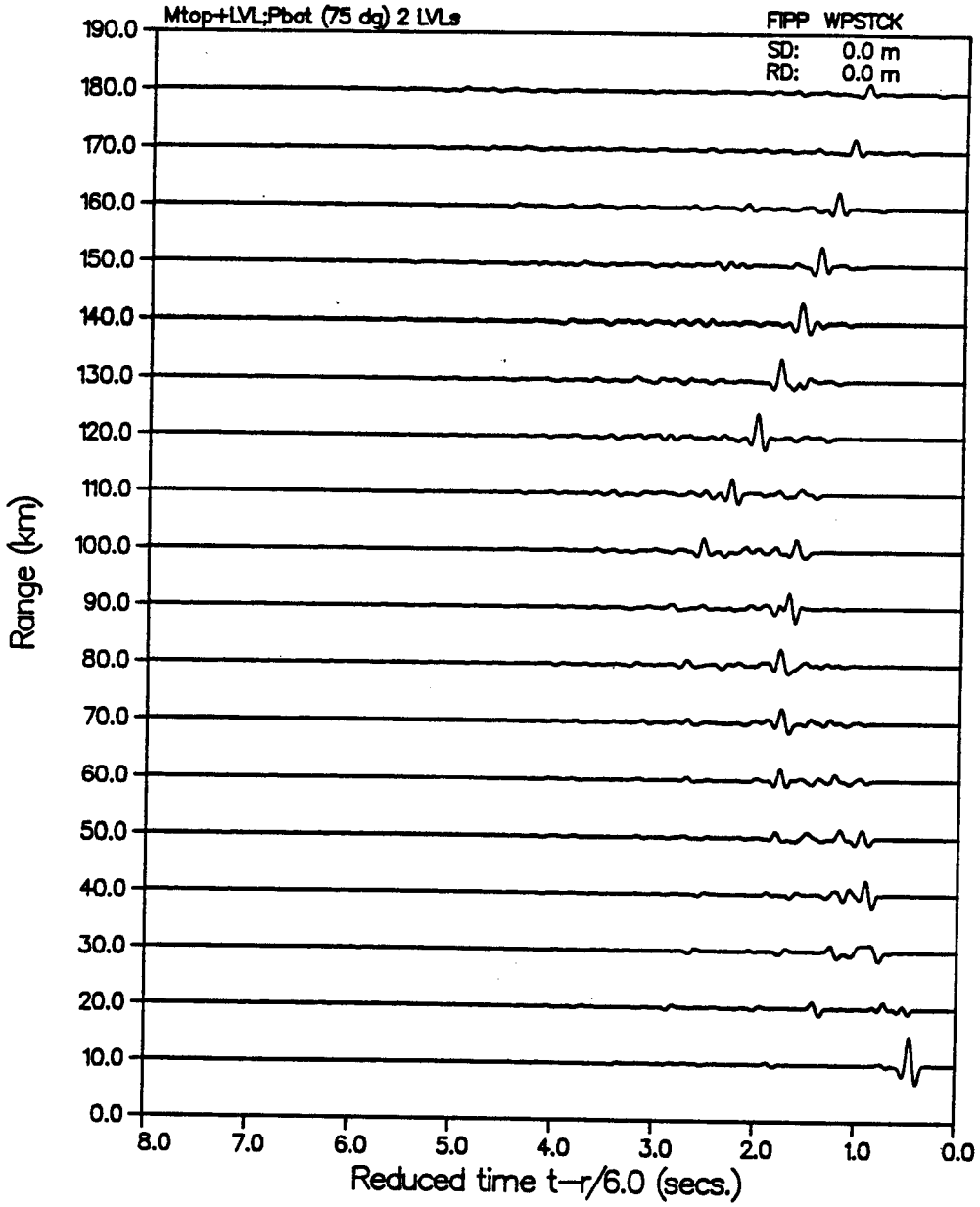

-2 LVLs, the second of which lying in the near-surface zone, having both weak and strong velocity-contrasts

-a 3rd LVL, placed immediately below the main LVL

In these cases, one or more parallel branches of subcritical concave-up reflexions can be observed from the critical distance back to zero offset range. Increase of the total LVL velocity-contrast effectively enhances these arrivals. In addition, the intermediary contra-parallel arrival (described by BANDA and DEICHMANN, 1983) is also in plain evidence, at about t = .8 -1.0 secs reduced time, from 20 thru 60 km offset.

Addition of a 2nd nearsurface LVL introduces several strong concave-up nearfield branches, at 1-2 seconds, from 10 thru 40 km, and at 3-3.5 seconds from 10 to 70 km. In addition, several new strong but diffuse amplitude arrivals are also evident in the classic shadow zone. However in this case the clear far he clear farfield en echelon sequence of PmP reflections are seriously disrupted. the maximum amplitudes of the major Pg and Pn phases are also seen to be somewhat reduced with respect to the single LVL case.

When the velocity contrast between surrounding layers and the first near surface LVL is decreased, most of the previously-observed amplitude of the major refraction arrivals is seen to return, in addition to at least some degree of better definition and coherence in the supercritical reflection phases.

When a 3d deeper LVL is added to the near-surface and main LVL model (as in Figure 57 above), a later P1 type phase at critical offsets, between 50 and 100 km at t=2 seconds, is observed to interfere destructively with the local amplitude maximum at about 70-90 km range (**Figure 58**).

Figure 58

Velocity-depth profile and corresponding reflectivity synthetic for MULLER-MUELLER nearsurface + LVL with PRODEHL subLVL, having 2nd nearsurface (smaller) LVL as in figure 56 (with additional 3d smaller LVL below central LVL)

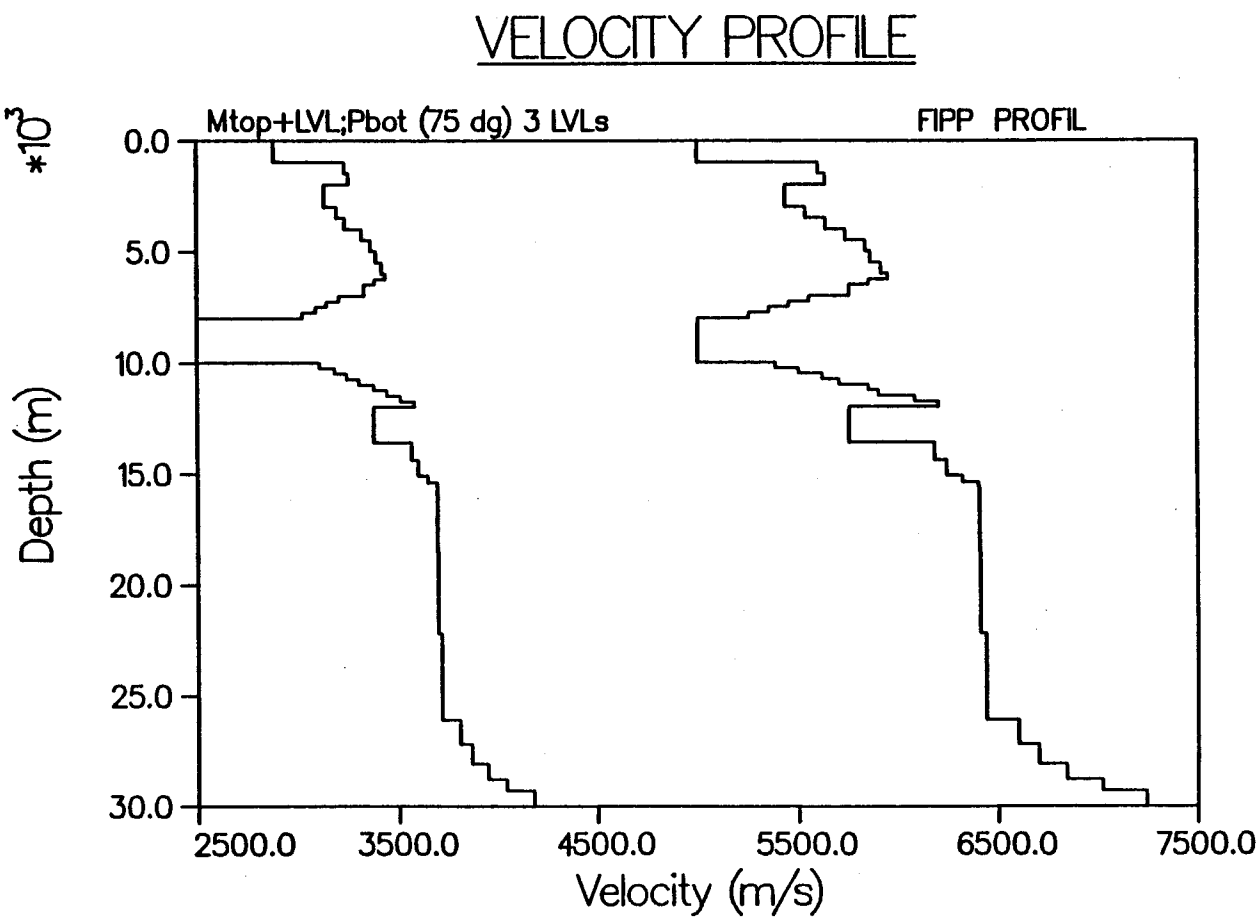
VELOCITY PROFILE
Mtop+LVL;Pbot (75 dg) 3 LVLs
FIPP PROFIL
*10^3
Depth (m)
0.0
5.0
10.0
15.0
20.0
25.0
30.0
2500.0
3500.0
4500.0
5500.0
6500.0
7500.0
Velocity (m/s)

VERTICAL PARTICLE VELOCITY

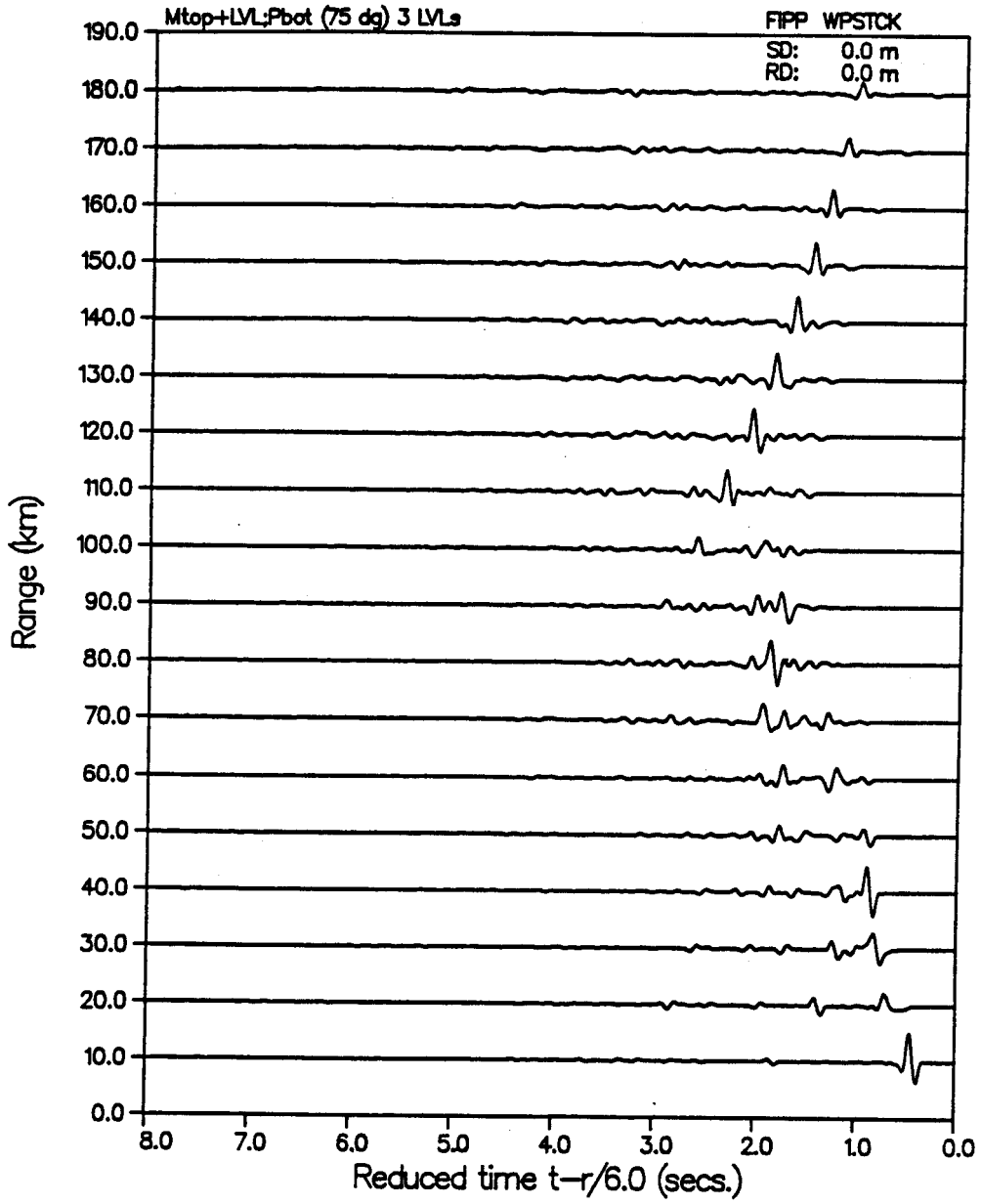

Figure 59 - 60

(59) Velocity-depth model and corresponding reflectivity synthetic seismogram for MULLER-MUELLER nearsurface + LVL with PRODEHL subLVL, (having single thin high-velocity layer centered in main LVL)

(60) same as figure 59 above, instead with high-velocity thin inner-LVL layer of greater velocity contrast

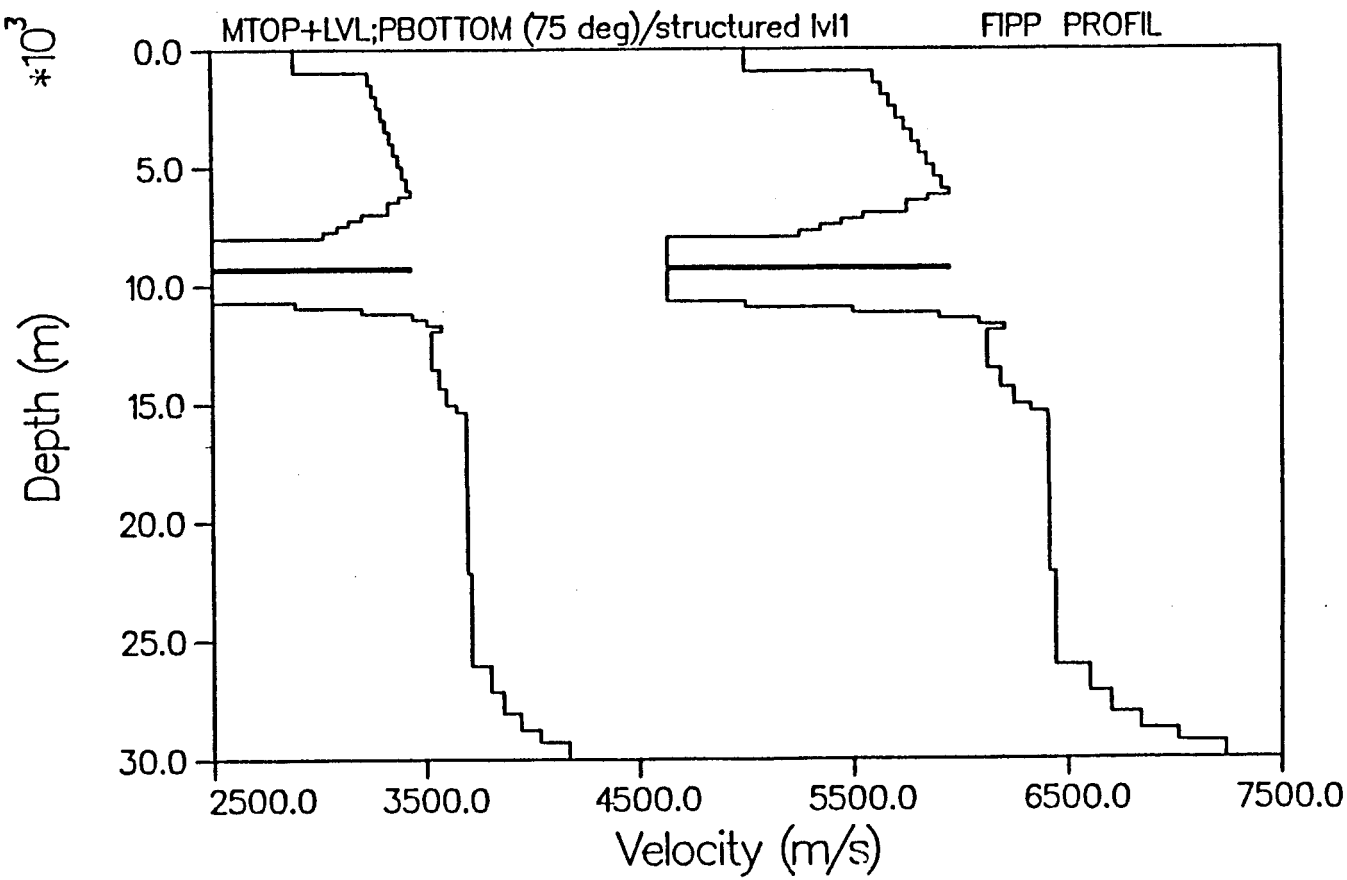
MTOP+LVL;PBOTTOM (75 deg)/structured lvl1
FIPP PROFIL
*10^3
Depth (m)
0.0
5.0
10.0
15.0
20.0
25.0
30.0
2500.0
3500.0
4500.0
5500.0
6500.0
7500.0
Velocity (m/s)

VERTICAL PARTICLE VELOCITY

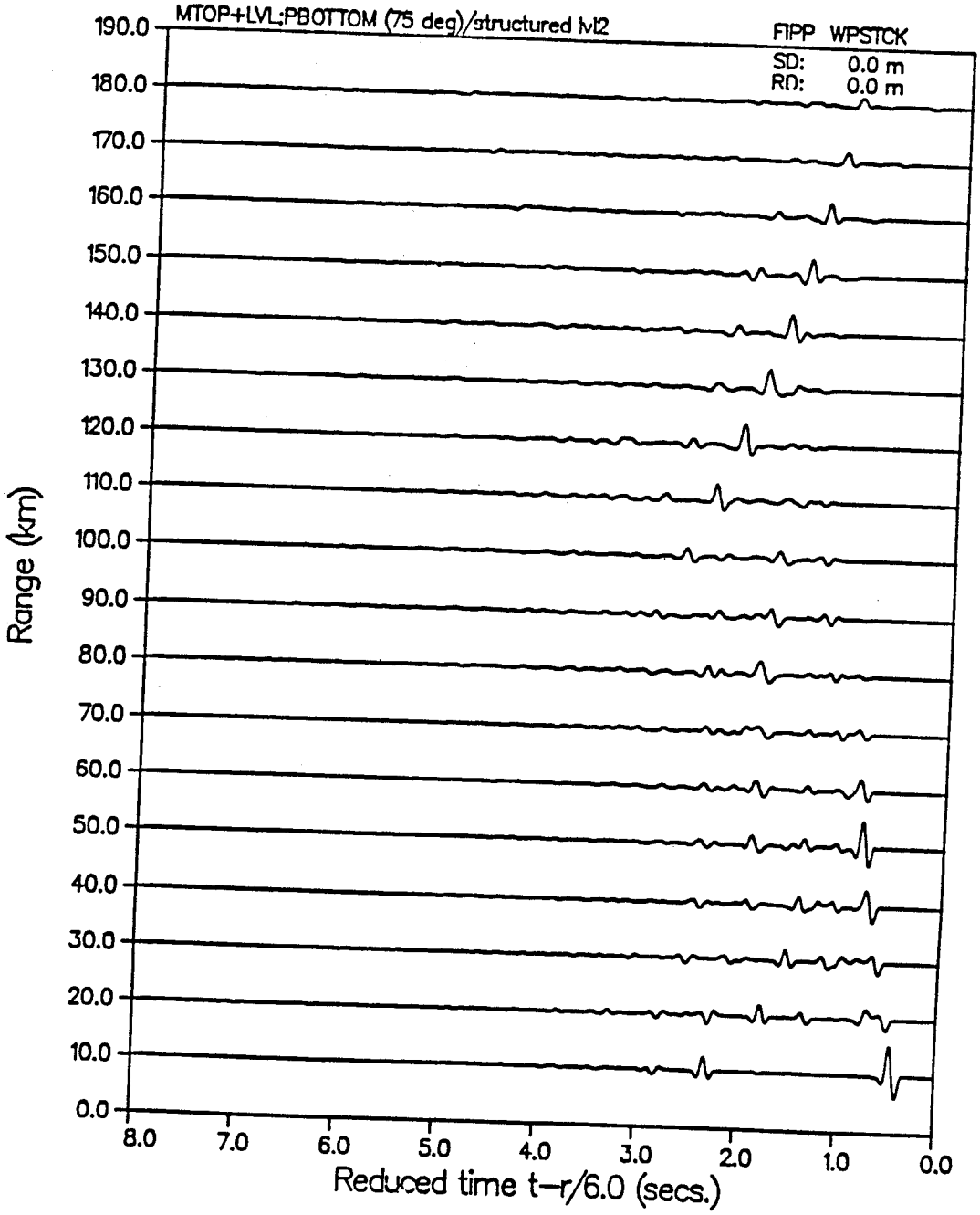

VELOCITY PROFILE

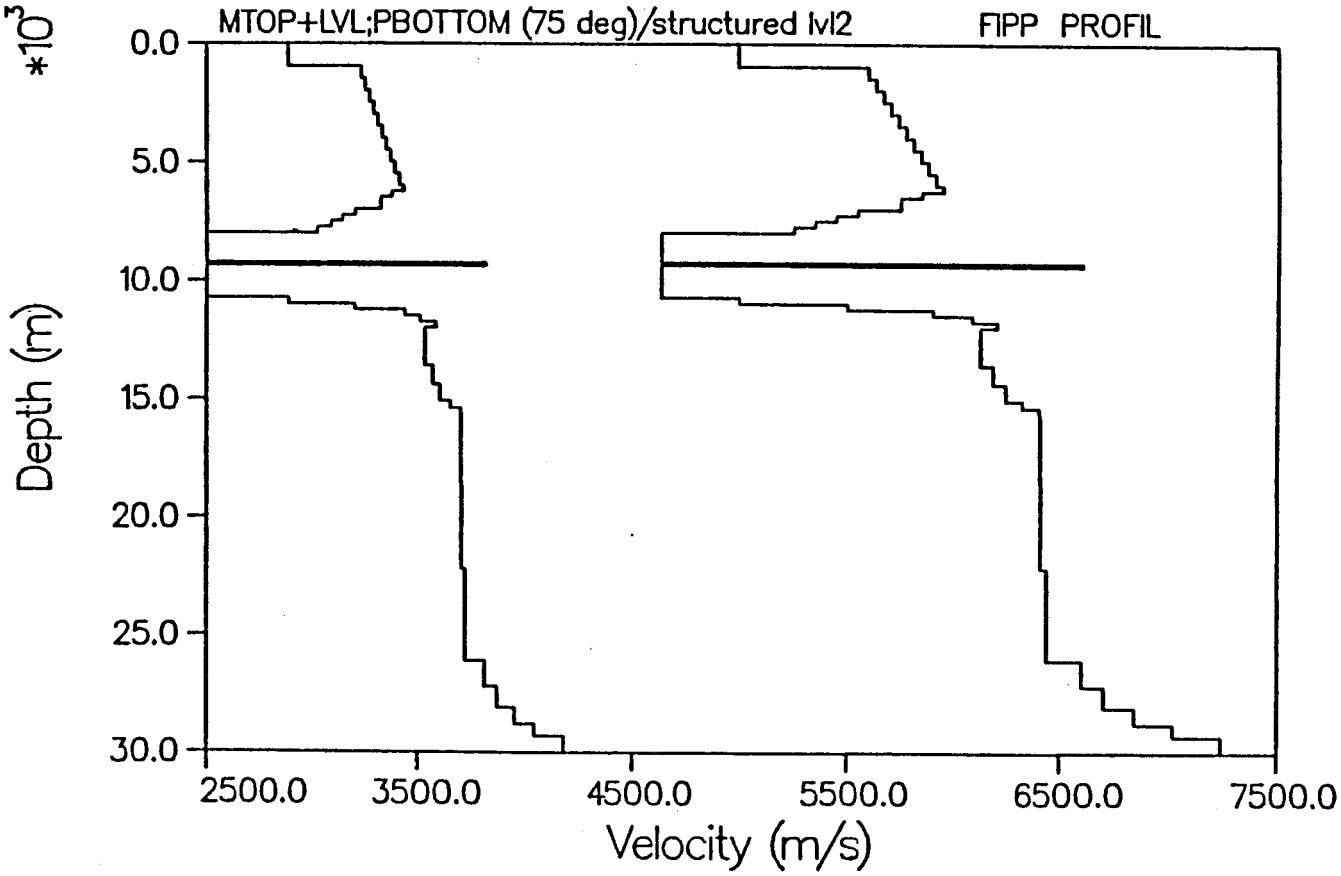

VERTICAL PARTICLE VELOCITY

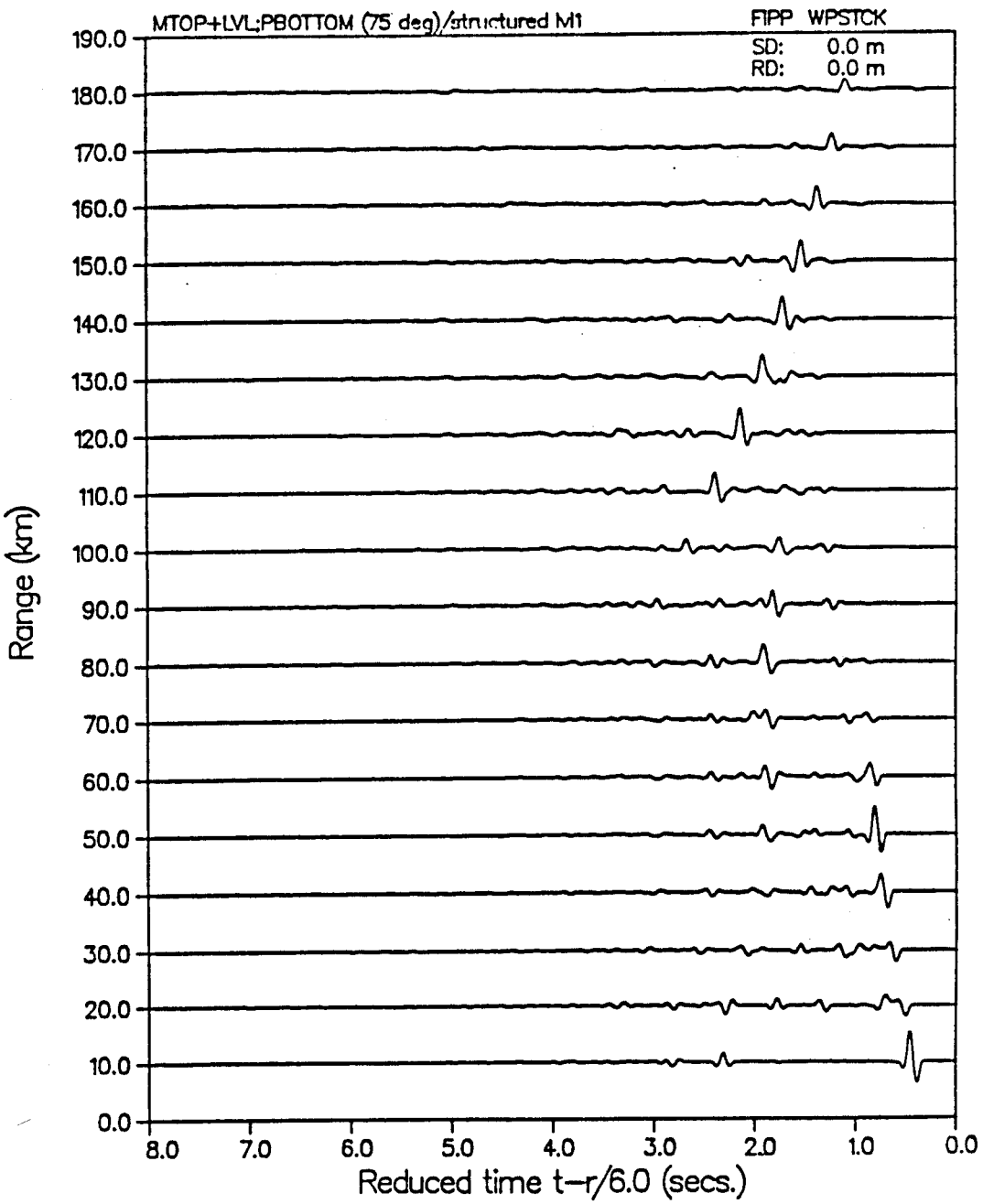

To consider the effects of wave interference more directly, when the number and location of an alternating high/low velocity lamina sequence is examined (**Figure 61**), the overall result is the introduction of a drastically dispersed character to the basic travel-time structure of the entire seismogram. Some of this highly resonant and wave-tunnelling character is suggestive of some overall features of the DELTA and other data profiles from the Basin and Range. However, no local amplitude maxima remain in this case, and in addition a plainly spurious near-vertical arrival is introduced from about 0 - 30km offset at 1-2 seconds reduced time. Variations in the thickness and location of lamina components will locally enhance this dispersed character for one or more arrival types.

The importance of these observations is that very fine velocity structure, on the scale of only 1/4 to 1/8 the shear wavelength at depths of proposed crustal LVLs can have an enormous effect on the variable angle P and S near-field arrivals. Further studies of these effects should be closely guided not only by the previous results of wave tunnelling (FUCHS and SCHULTZ, 1975) and reflection crustal profiling (OLIVER et al, 1980), but by specific geological considerations (HALE and THOMPSON, 1983).

Figure 61

Velocity-depth model and corresponding reflectivity synthetic seismogram for MULLER-MUELLER nearsurface + LVL with PRODEHL subLVL, (having many thin high-velocity layers alternating with low velocity layers, centered in main LVL: laminated LVL)

VELOCITY PROFILE

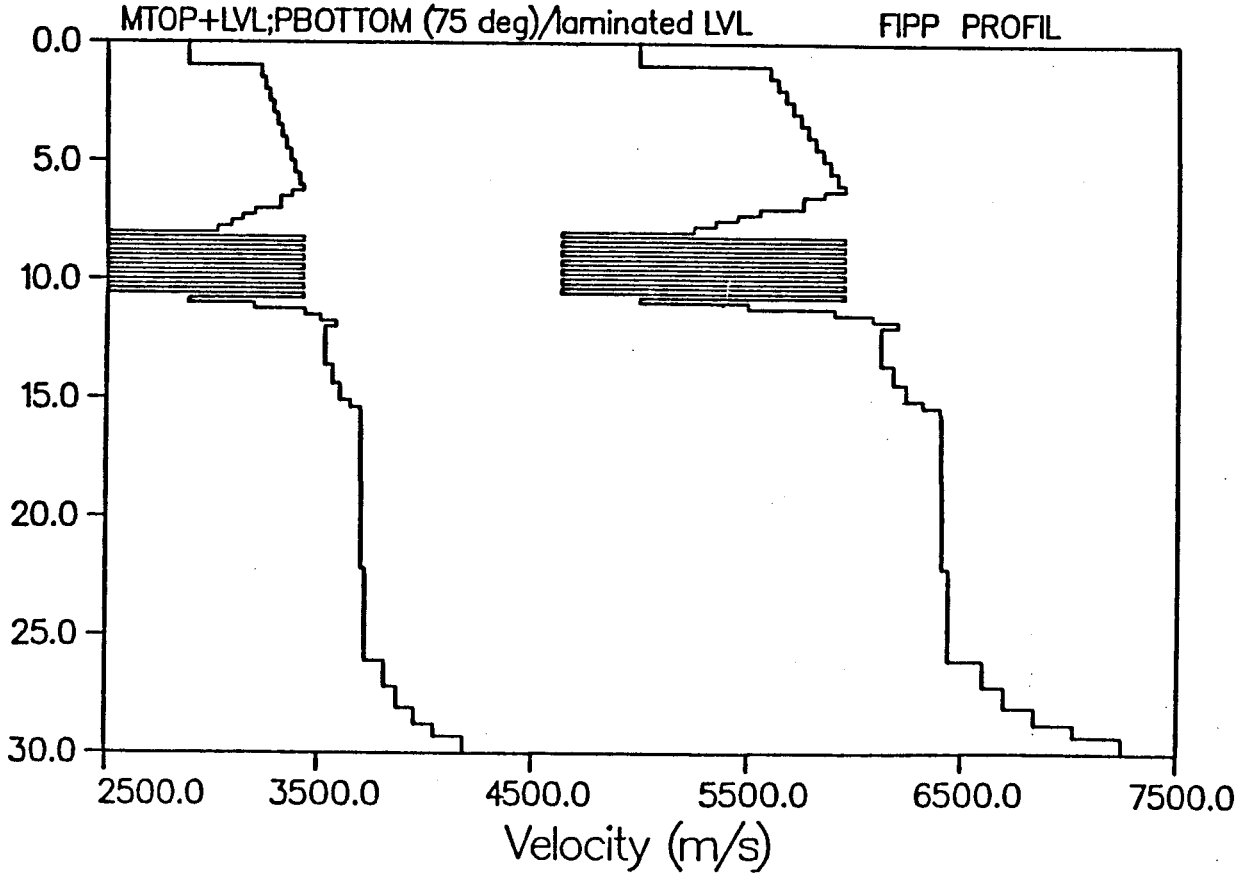

VERTICAL PARTICLE VELOCITY

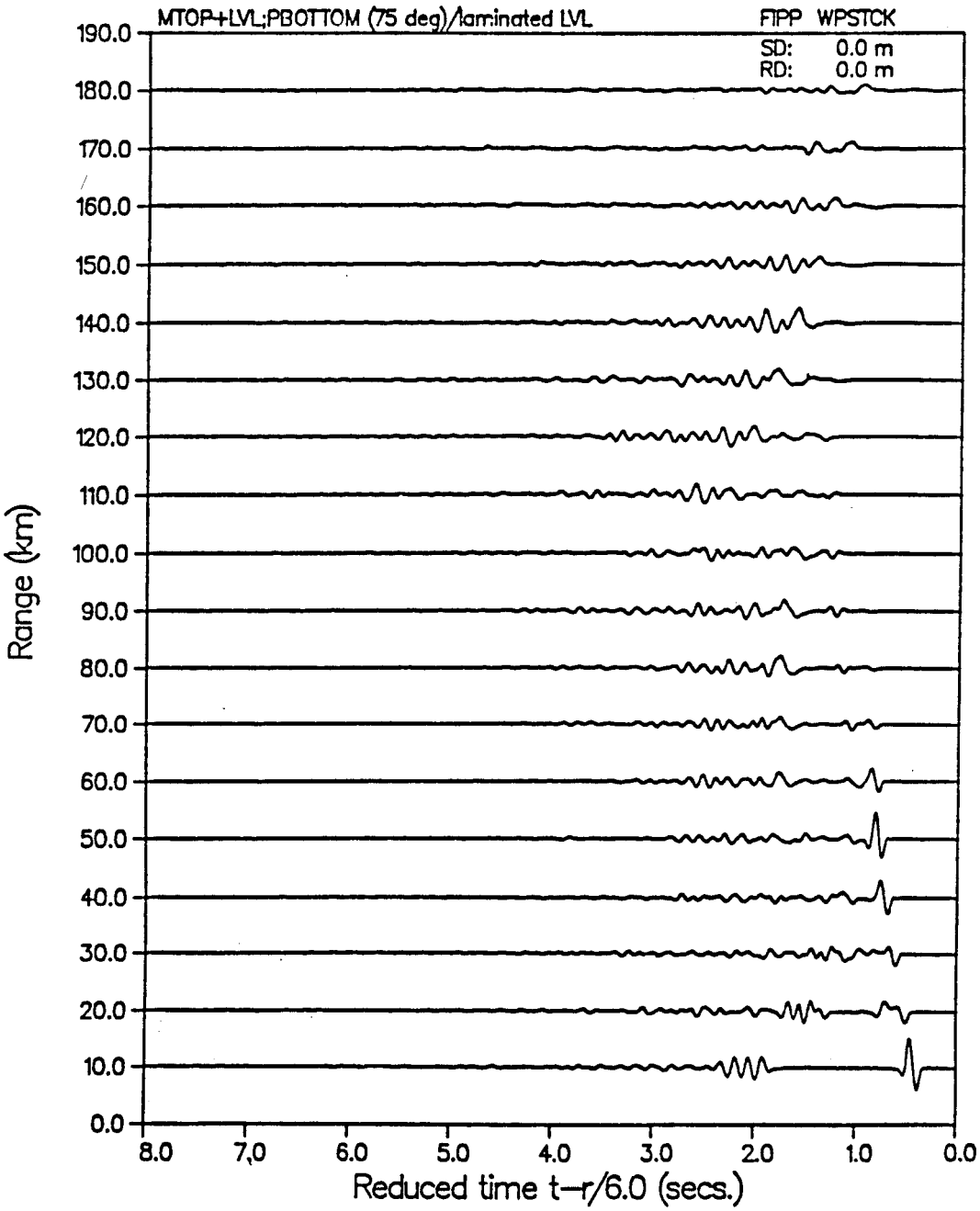

Many of the models previously depicted could themselves serve as the subject of considerable extended modeling and study. Thus we consider any conclusions made here as only tentative. If, however, an initial attempt is made to combine pertinent elements of the velocity profiles above, the basic resulting (modified Model N7) velocity depth distribution is suggestive of the so-called 'comb'-layered total crustal models given by KOSMINSKYA et al (1971), KIND (1974) and in GIESE et al (1976). These represent essentially a gradient -with- velocity discontinuities structure including both the extreme nearsurface (0-5km) and subMOHO (z>40km) (**Figure 62**). The importance of fine-scale structure in both nearsurface and subMOHO velocity-depth distributions has been emphasized by recent results of COCORP reflexion seismic profiling and teleseismic propagation studies, which stress the interference and trapped wave nature respectively of near vertical reflexions and longrange regional phases. As HELMSBERGER (1971) among others has shown, higher order multiples in the shallow nearsurface layers can significantly effect net seismic results (at higher source frequencies).

As only an initial study of the above composite, a model-only computation, for the KOSMINSKYA v/z profile, modified to include both the above N7 model and similar additional LVL gradient zones is shown above. The corresponding full wavefield synthetic seismogram (**Figure 63**) here suggests the increased degree of complexity inevitable from such very large multi-layered earth models when a full wavefield synthetic seismogram is computed.

Figure 62

Composite velocity-depth model, derived from previous results and published proposals (KOSMINSKYA et al, 1972 and ZOSCHYNK et al, 1976: multi-structured-LVL)

100 LAYER V/Z MODEL

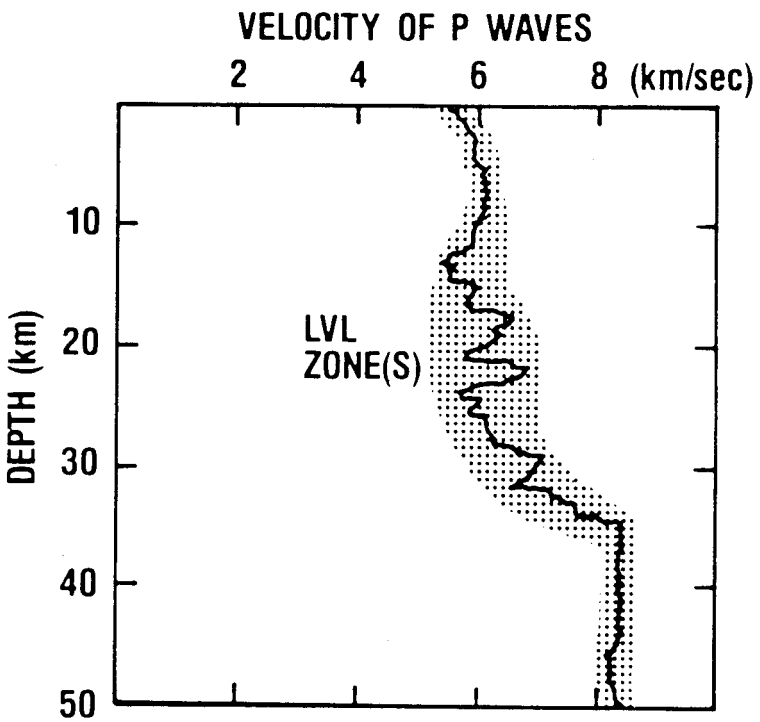

Figure 63

Partially-digitized velocity-depth model, after KOSMINSKYA et al (1972) and corresponding fullwave synthetic seismogram: initial study

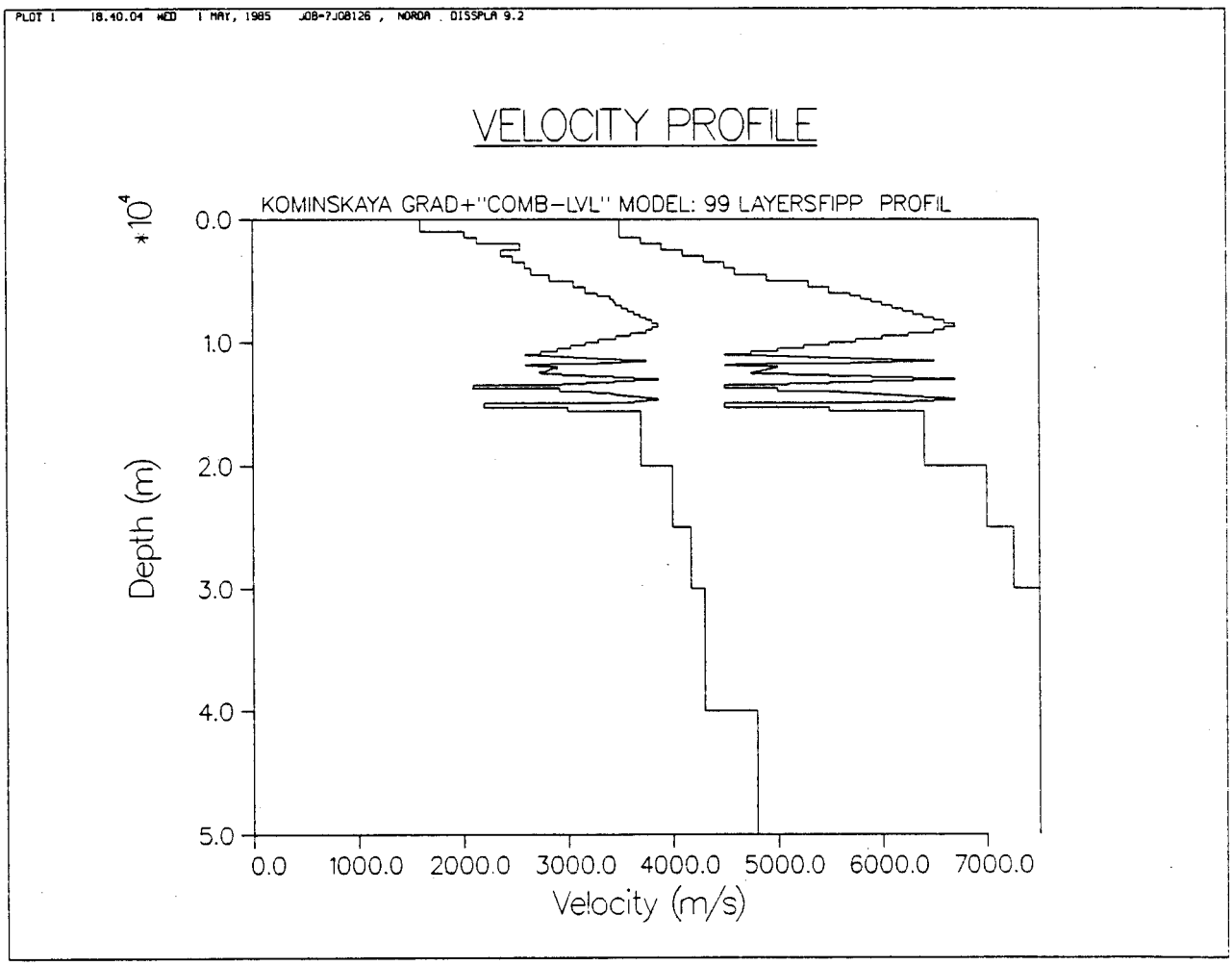
PLOT 1 18.40.04 WED 1 MAY, 1985 JOB=7J08126 , NORDA . DISSPLA 9.2
VELOCITY PROFILE
KOMINSKAYA GRAD+"COMB-LVL" MODEL: 99 LAYERSFIPP PROFIL
*10^4
0.0
1.0
2.0
3.0
4.0
5.0
Depth (m)
0.0
1000.0
2000.0
3000.0
4000.0
5000.0
6000.0
7000.0
Velocity (m/s)

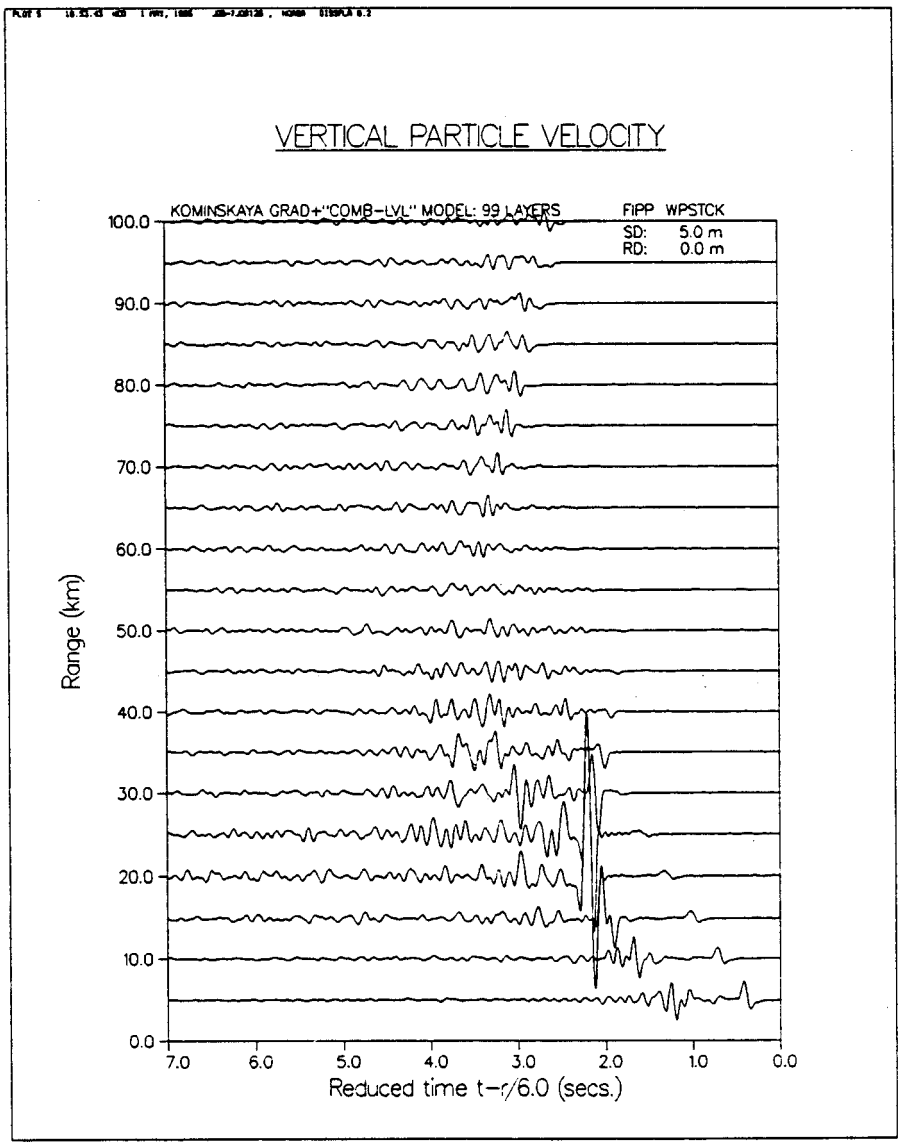
VERTICAL PARTICLE VELOCITY
KOMINSKAYA GRAD+"COMB-LVL" MODEL: 99 LAYERS
FIPP WPSTCK
SD: 5.0 m
RD: 0.0 m
Range (km)
100.0
90.0
80.0
70.0
60.0
50.0
40.0
30.0
20.0
10.0
0.0
7.0
6.0
5.0
4.0
3.0
2.0
1.0
0.0
Reduced time t−r/6.0 (secs.)

point source solution when considered at somewhat larger offsets ($x > .30$ km).

Recent results of MCMECHAN et al (1985, personal communication) suggests that even further complexities could be considered with the given velocity/depth model above. Comprising a nominal 99 layers, it is believed to be the largest synthetic full wavefield seismic model successfully run to date.

As has been noted previously by several authors, and by personal communications to the present author (PECHMANN, 1985; KENNETT, 1985), any attempt to make any more than a first tentative general analysis and provisional conclusions for further study would be premature. Comparison of seismograms for all the near DELTA Shoal-West lines of PRODEHL show significant variation in individual trace and amplitude patterns within nearfield ranges, even for lines shot in the same (dip) direction. This obfuscating behaviour may simply be the result of inadequate geophone-ground coupling or amplitude distortion in recording or plotting. Alternatively, the effects of local receiver near-surface statics (departures from planar topography and lateral velocity homogeneity) may also further complicate the picture. It would be desirable in future analyses to obtain one or more velocity logs from wellsites in the general DELTA profile region.

Although it seems clear from the present results that an all-step discontinuity (no gradient) model simply cannot account for all major DELTA profile including varying sharp P and S wave velocity gradients need to be investigated. As known from the results of recent marine crustal seismic modeling, seismic data from continuous velocity gradient structures are not necessarily lacing in diagnostic secondary and other observable fine structured arrival information. Although the nearsurface and deeper continuous gradient models considered here as variations of PRODEHL's data derived v/z distribution are plainly not able

to comprehend pre- and critical-offset arrivals, the possibility of other more adequate velocity gradient distributions (ie, those involving a number of small localised velocity inversions) cannot yet be ruled out.

Our comparisons of the DELTA profile with synthetic reflectivity and fullwave seismograms for data-derived and other recently suggested models has underscored that multiply reflected refractions and reflections as well as interference complexes impose considerable constraints on probable velocity depth structures, and argue strongly for the need of employing consistently a complete wavefield solution for forward modeling efforts. The comparatively large number of candidate models that have been examined here has been possible because of the improved CPU savings and automatically complete solution offered by the DGM method used in "SAFARI". We have also here suggested the utility of jointly employing, for example as a first pass, standard reflectivity synthetics with a variable reflectivity zone, to be subsequently followed by fullwave synthetics when all possible consequences of one or more analysed features are to be studied.

Each of the synthetic horizontal (surface-based receiver) seismograms examined here could also be interpreted additionally using what we have termed 'hypothetical VSPs' to graphically determine to what depths refracted and interference head waves have penetrated and with what precise structures intracrustal

multiples can be associated. Perhaps the most diagnostic features of hypothetical VSPs for the synthetic seismic modeler are its ability to unravel local interference complexes as well as the cumulative effects of repeated passages thru the "near-surface".

Limited time, computer resources and the absence of available ray-trace or generalised linear inverse routines have limited the present initial investigation of the Delta profiles of the eastern Basin and Range. However, although no final decision is made here on the "best" possible v/z model for the DELTA profile, the "SAFARI" synthetic seismogram program used in the above study has allowed us to rule out many previously proposed models and specific model features, as well as to independently confirm the recent results of several researchers. For example, as a corralary to the work of BRAILE and SMITH, MUELLER and MULLER, MCMECHAN and BANDA and DEICHMANN, synthetic reflectivity and fullwave seismograms have also been computed for various combinations of their proposed v/z distributions for the DELTA profile, as well as variations of the original data derived models of PRODEHL. As a result of these computations, it has been possible to tentatively identify aspects of the DELTA profile which are in need of continued study.

Further work in LVL identification must involve:

(1) inclusion of realistic multilayered "stochastic" nearsurface layering overlying deeper crustal structure, as per HALE and NUR (1985);

(2) remodeling of original 'discontinuity' and 'gradient' dependent features in terms of larger mixed multilayered 'discontinuity + gradient' models, noting 'wavefield averaging' effects, following the Kosminsaya model in GIESE et al (1976) and in KOSMINSKAYA et al (1972);

(3) more closely examine SV wave data, allowing in v/z models for more complex Sv wave velocity variations/relations to P velocities, as per FUCHS (1976);

(4) consideration of extreme farfield regional arrival phases, after HADDON (1984);

(5) incorporation of realistic compressional and shear wave attenuation coefficients with depth (THOUVENOT, 1982; PRIESTLY et al, 1980).

(6) The provisional outcome of the present investigations is an overall general agreement between the 'reflectivity' and 'full wavefield' solutions for many crustal models examined here. The conditions of agreement and departure must be examined more completely and from a theoretic viewpoint.

(7) The success of the present forward-propagation modeling approach depends critically on having a good initial v/z model as well as an efficient and consistent pattern recognition and event correlation scheme (HEALY, 1970), when establishing the degree and kinds of agreement between synthetic and field data.

However, to date analysis of crustal seismic data has largely been more qualitative than quantitative. For example, the number, type and layer origin of given arrivals as discernible from arrival times and waveform character are often not very precisely defined and hence at least somewhat dependent upon subjective judegement. In particular, the "stochastic" character of most deep crustal arrival trains resulting from passage through a large and complex number of intermediary layers has been recently emphasised as requiring extensive further study. As in recent exploration seismics, considerable effort is now being placed on a more systematic and rigorous approach to deep crustal model construction, appraisal and refinement. Within the framework of a generalised linear inverse methodology, (PECHMANN, 1985, personal communication) improved answers can be given to questions regarding the ultimate resolving power of the data, the class of models which reproduce the data to within a definable error measure, the importance of additional constraining iinformation and the effects of observational inaccuracies.

As is well known, however, all such earth models so derived by geophysically-guided trial and error forward modeling are not necessarily unique or even correct (SABATIER, 1974). Furthermore, the actual problem at hand must eventually consider the nonlinear inverse problem and for crustal applications must as such await viable inverse methods for a more systematic solution.

The above numerical computations by "SAFARI" represent

only a limited initial effort to delineate the applications accuracy and scope of the DGM method for crustal seismic modeling. Further model-model reviews are currently underway (TANGO and SCHMIDT, 1985), and both pre-experimental planning and model-data analyses are envisioned for the future.

Section 3(d)

Synthetic Vertical Seismic Profiles (VSPs) for Exploration and Marine Crustal Seismic Modelling

The geophysical literature has recently documented the rapidly increasing number of applications of VERTICAL SEISMIC PROFILING (VSP) to a variety of exploration and deep crustal reconnaissance problems (TOKSZOZ and STEWART, 1984; HARDAGE, 1983; BALCH, 1983; KENNETT et al, 1982; TANGO, 1981; GANLEY and KANASEWICH, 1980; OMNES, 1979; WUENSCHEL, 1976). VSP, a powerful investigative technique developed principally by GAL'PERIN (1973 op cit), permits observation of a seismic wavefield incident upon one or more subsurface layers as well as the resultant reflected converted and transmitted wavefields. In this way the source waveform and its evolution with travel time and depth within the medium can be directly observed, including the origin and travelpaths of all orders of multiply-reflected and mode-converted arrivals, for both body and interface waves.

In the field, vertical wave tests, generalized borehole arrays or Vertical Seismic Profile's (VSPs) are the records obtained by recording a transient source pulse taken separately into a number of different geophone positions, separated at depth over a given vertical borehole distance (**Figure 64**).

Figure 64

Data acquisition and seismic wave arrival types for shallow-depth Vertical and Horizontal seismic profiles

HSP RECORD

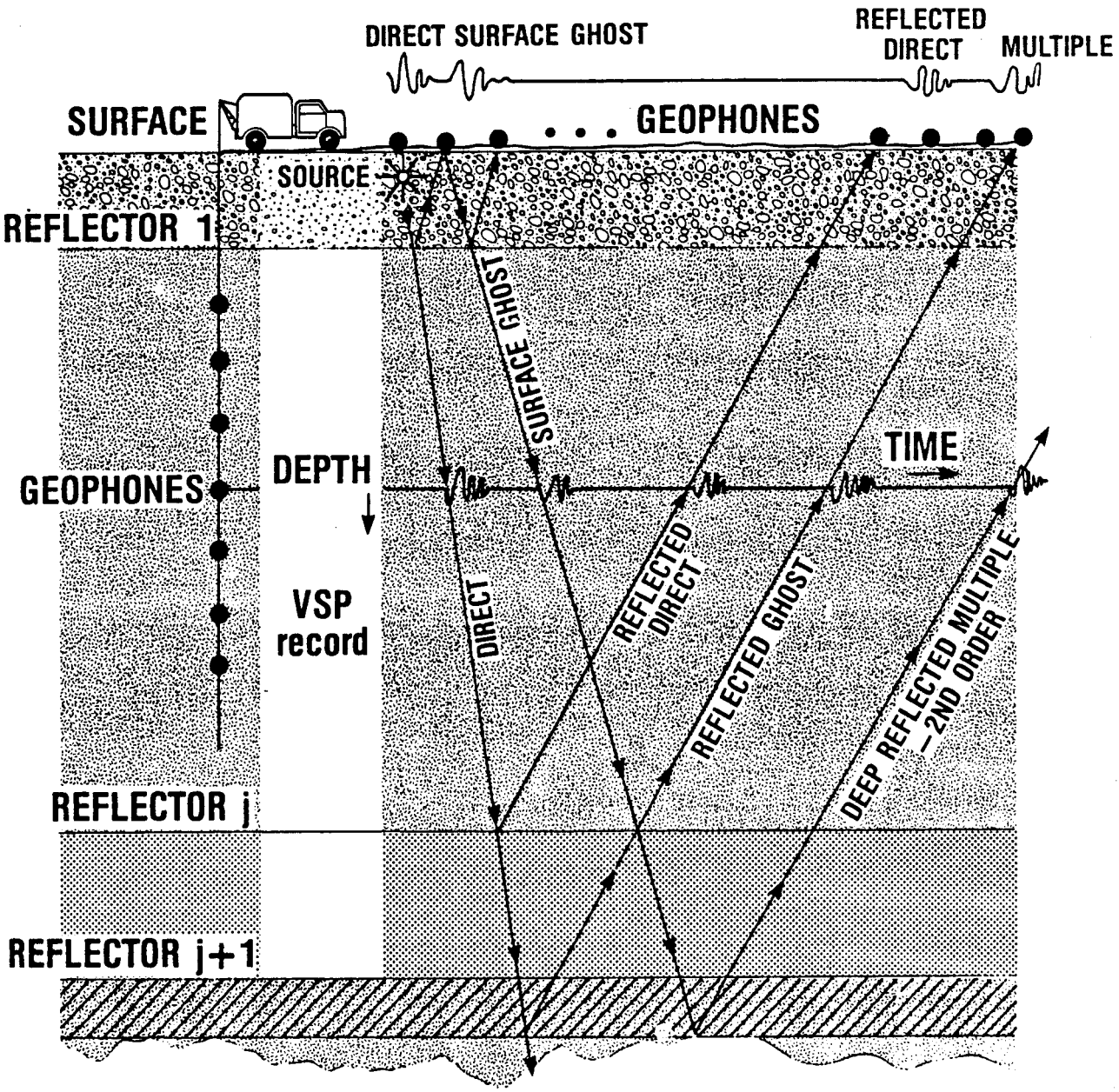
DIRECT SURFACE GHOST
REFLECTED
DIRECT
MULTIPLE
SURFACE
GEOPHONES
SOURCE
REFLECTOR 1
SURFACE GHOST
TIME
GEOPHONES
DEPTH
VSP
record
DIRECT
REFLECTED
DIRECT
REFLECTED GHOST
DEEP REFLECTED MULTIPLE
– 2ND ORDER
REFLECTOR j
REFLECTOR j+1

In a similar manner, synthetic seismograms can be produced from velocity/depth profiles, with a point or plane wave source and an array of borehole receivers simulated for different depths in the geologic column. In extant synthetic VSP algorithms, for a constant source depth, the geophone depth is successively varied in (often uniform) t- or z-increments for each successive synthetic seismic trace generated. The end result of this process repeated over all depth levels of interest constitutes a synthetic VSP.

Both prior to field acquisition as well as in conjunction with subsequent data analysis, synthetic VSPs can be used not only to optimise survey planning of receiver-source offsets, depths and spacing, but also to back-locate and identify often complicated wavefield paths as well as waveform character change with layer velocity and depth.

Given the inherent uncertainties both in knowledge of real elastic parameter distributions with depth, and the true laws governing their behaviour in the seismic frequency/small strain regime in real (microfractured, porous, three-dimensional) earth media, it is crucial to utilise the most correct and complete synthetic seismic modeling algorithm available. Major limitations in extant convolutional and ray-type approaches to synthetic VSP modeling can, however, arise from the assumptions of high frequency dominance, relatively thick equispaced layers, plane waveforms, neglegible mode conversion and reverberation, and

simple or no attenuation. Additional complications can arise in the nearfield from source-nearsurface interactions (nb with surface waves) which can arise in many cases and be significant in the presence of many complexly-layered thin beds.

In the catagory of "exact" synthetic VSP modeling, in the last few years several investigators (DIETRICH et al, 1985; TEMME and MULLER, 1982) have used a modified reflectivity approach, with promising initial results. These numerical models, however, have in general been computationally limited as to the size and/or type of environmental and experimental source-receiver configurations which can be treated, due to inherent difficulties in the propagator-matrix formulation.

In this section, we describe a new approach for exact fullwavefield synthetic VSP modeling, based upon the direct global reflectivity method of SCHMIDT (1982; 1983). In particular, as has been discussed elsewhere (TANGO and SCHMIDT, 1985), the present global algorithm " SAFARI " can be shown to automatically consider in one step the complete up and downgoing wavefield in an n layered plane homogeneous media, as excited and seen respectively by any arbitrary number of subsurface sources and receivers. With a standard VAX 11/780 + FPS164 having added external buffer, models involving more than 400 layers can readily be considered. Thus the natural application of SAFARI to VSP modeling is immediate.

In particular, since the global " SAFARI " algorithm in vectorized form reduces computational time by at least an order of magnitude with respect to extant reflectivity codes (TANGO and SCHMIDT, 1985), complete and exact wavefield solutions for realistically layered earth systems having many more layers and elastic parameter variations than previously possible can now be routinely considered. Hence a wider range of detailed practical and theoretical VSP modeling applications can be pursued.

In the present section, a synopsis describing interpretation of a 'generic' VSP record is given, and a discussion of other 'exact' synthetic VSP algorithms presented. The unique capabilities of the direct global algorithm "SAFARI" of SCHMIDT for synthetic VSP modeling is then described. Two selected examples are considered here for VSP synthesis, as have been very recently treated in the literature. These are the representative stratigraphic coal seam model previously investigated by FERTIG and MULLER (1979) and TEMME and MULLER (1982), and the generalised ocean crustal models studied by STEPHEN (1977; 1980; 1984). The first shallow exploration model was chosen to illustrate the recently-discussed difficulties in using synthetic VSP modeling to unambiguously identify multiply-reflected reverberations (that have not undergone additional mode conversion) from direct and multiply converted modes, when attempting to resolve finely stratified earth models. The second deep marine crustal model was selected to detail the need to carefully consider all arrival types (both body and interface waves) for geobottom and crustal

reconnaissance from marine borehole data. In both cases the requirement of using synthetic VSP to optimise field VSP survey parameters (source-receiver offsets, number and location of sources and source wave type) prior to actual data acquisition is underlined.

Background: VSP Method and Full Wavefield Record

Basic principles and procedures for field acquisition, data processing and record interpretation for VSPs have been discussed in detail by GAL'PERIN (1971), TANGO (1981), HARDAGE (1982), LEE and BALCH (1983) and BALCH (1984). Therefore only schematic discussions of some important aspects of VSP are considered here.

As outlined above, a vertical seismic profile is basically the record obtained by n receivers in a borehole from one or more sources on or near the surface (**Figure** 65). Ideally, one would energize the seismic source only once and record the observed wavefield record for several seconds over all depths simultaneously (by means of an array of vertical receivers). However, because of borehole configuration and coupling requirements, in almost all cases only one depth level at a time is recorded, the receiver moved to the next depth and the source refired etc for all levels of interest. In VSP data processing, input source waveforms are generally assumed to be impulsive and identical at each depth level (in practice, however, this is only rarely if ever the case). In real field scenarios, an optimal offset distance between receiver at borehole top and source must be determined, so as on the one hand to be sufficiently close to the well to obtain truely "vertical" travel paths, while on the other hand sufficiently far away so that strong noise levels of both ground and borehole surface wave ("tube wave") noise will

Figure 65

Schematic of seismic travelpaths for Vertical and Horizontal seismic profiles

VSP HSP SCHEMATIC

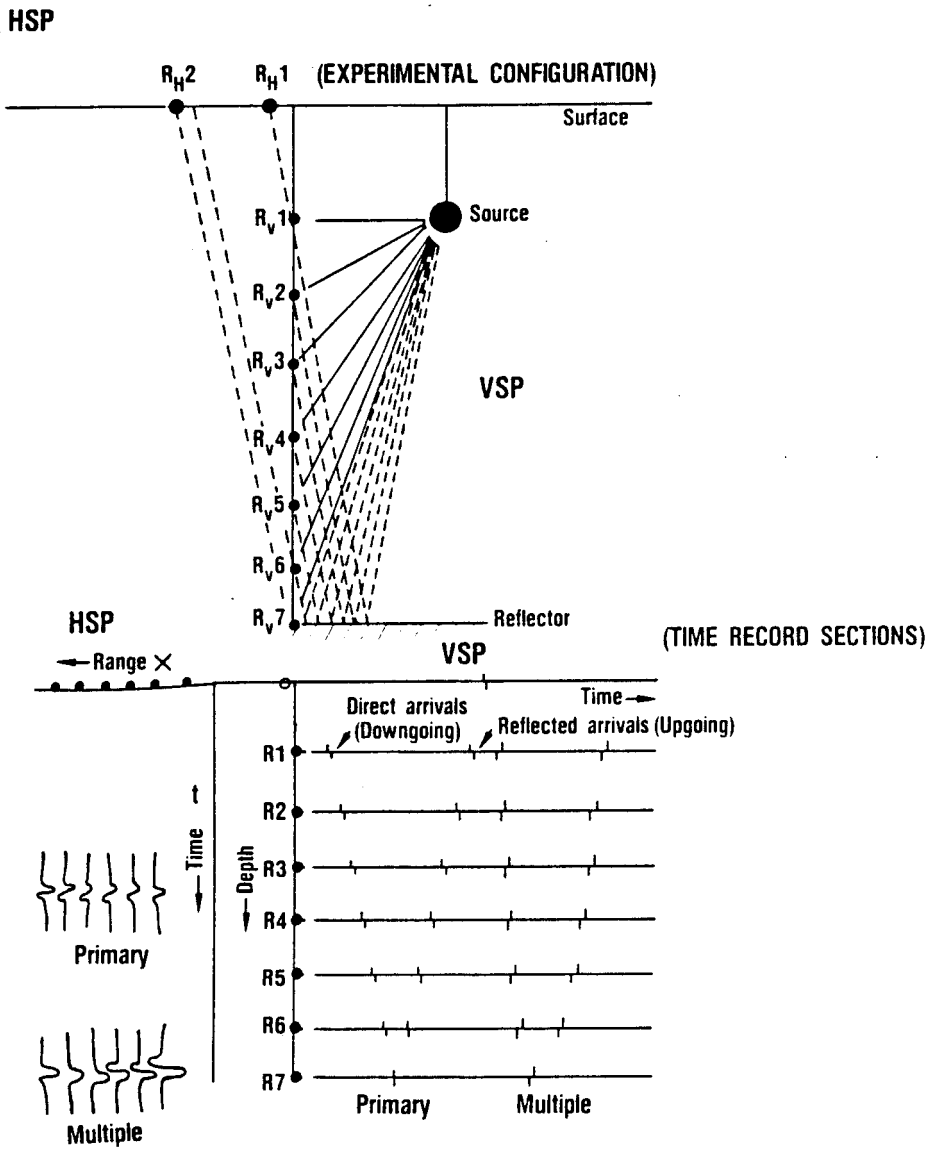

not be excited to mask desired up and downgoing head and body wave information.

In a VSP time/depth record, primary reflections can be identified via the characteristic pattern of traveltime-depth alignments defining both up and downgoing ray-type patterns thruout the section. However, as noted by LEVIN and LYNN (1958) and GAL'PERIN (1971), each such 'ray-tracable' wavefield event on a total VSP record is not a true ray in the geometric sense, but rather a net alignment complex of several overlapping adjacent reflection interactions of the outgoing signal. Each single trace will itself be seen to consist of the superposition of upcoming and downgoing waves (CLAERBOUT, 1968), due to the decomposition possible for a finite layered system (SCHELKUNOFF, 1951; SLUITJER, 1970; CLAERBOUT, 1976). An important point to remember when using VSP alignment paths to follow the evolution of down and upgoing travel paths and waveforms (for time-depth tying VSP events to surface events recorded in time) is the wave nature of the event. Thus, when inspecting the same wavefield event trace after trace on adjacent depth recordings, each trace represents in fact a different ray, but one however which is closely identifiable with its neighbours as belonging to the same wavefront.

One of the major advantages for both exploration and deep crustal seismology (as yet only partially exploited) is the fact that VSP records the entire up and downgoing wavefields, including

those from reflector depths greater than the depth of the borehole (HARDAGE, 1983). This in principle allows details of deeper structure to be revealed which cannot otherwise be observed (by surface based receivers). When the near surface zone is complex, these advantages are especially obvious.

Simple kinematic laws define the traveltime behaviour of VSPs. For any VSP, all P wave phases not directly above the receiver line must necessarily have an arrival time greater than that of a pure vertically-travelling P wave. Upcoming waves are readily identified by their upgoing (positive) slope, likewise downgoing waves by their equal and oppositely directed travel paths. An obvious feature on many VSP records is the characteristically long succession of downtraveling waves closely parallel to the direct P wave (first) arrival. Here, at short source-receiver offsets, P-to-SV mode conversions are generally observed to be zero, and close to 100% reflection of direct P waves into multiples seen to occur.

In the case of a comparatively simple (nonreverberant) layer system, where coherent and continuous direct downgoing and reflected upgoing wavepaths can be identified, any given arrival in question can literally be time/depth traced up to the surface, having an average wave shape just above the major reflecting interface closely resembling the wave shape recorded by receivers on the surface.

For most realistic multilayered earth systems, however, perhaps the most important step in correctly processing and interpreting VSP data is the complex separation of upcoming from downgoing waves, and thus multiple identification. In general the downgoing waves from the source are neither an impulse nor a simple wavelet, but in general a highly complicated wave train of long duration and oftentimes large amplitudes. These downgoing waves can be readily identified with multiple reverberation, both between major reflectors and the air/surface interface as well as internally between reflectors, often having highly complex ray-reverberation paths. This is especially true in geologic areas having complex near surface stratigraphy (which in general is not well sampled by current lithologic or seismic techniques). Here the downgoing waveform need not be a constant waveform, the departure from stationarity being large where changes in acoustic impedence is large.

For arrivals having travel paths involving only a few layers, geometric optics suffices to identify any given event as primary or multiple. For example, any reflection alignment which extended to the line of first arrivals is a primary reflection; else at least part of its travelpath must have involved reverberation. More notably, the multiple is terminated at the same depth as the primary with which it is associated. Thus for receivers dropped below the main layer of reverberation, multiple amplitude should decrease significantly, becoming zero in the case where the entire reverberant layer system lies above the receiver depth.

If the downgoing multiple reflection amplitudes are sufficiently strong so as to interfere with identification of upgoing primary reflection paths, it is necessary to "separate" up and downgoing reflections to determine the wavefield that would have been recorded if the original downtraveling wave train had been a single short impulsive source. (This complex problem for real VSP field data is straightforward in synthetic VSP modeling; see below).

At farther source-receiver offsets (as governed by the reflexion coefficient response with angle and the critical angle of the layers in question), the total wavefield can become considerably more complicated. For example, even if it is assumed that only pure P waves are set up in the immediate vicinity of the point source, experimental field evidence and numerical modeling results strongly suggest that at least some proportion of P-to-SV converted waves are generated within a comparatively small radius of the source (HEELAN, 1956; DIETRICH et al, 1985). The most probable mechanism here simply involves reaction of the directly incident P wave impinging obliquely upon one or more (near surface) interfaces having a sufficiently strong acoustic impedence contrast; for example, a shallow gradient.

The characteristic P-SV arrival pattern is distinctively more curved than corresponding direct or reflected P wave paths (AMINZADEH and MENDEL, 1985). This is due both to the lower SV velocities and to the fact that the P-SV mode is often refracted

when traveling away from the borehole at comparatively short source-receiver offsets. The P-SV conversion chain can be continued at deeper layers, and can cause serious event identification problems when unconverted P wave reverberations intermingle with multiply converted P-SV and P-SV-P mode conversions (LASH, 1980; 1982).

Although in general all subsequently-converted P-SV waves describe a travel path more nearly vertical than the direct P wave that produced them, its own apparent velocity is generally less than that of the "original' vertically-travelling nearsurface P-SV wave, often making wave identification (between P multiples, P-SV and P-SV-P arrivals) an extremely difficult task. Thus a further important consideration in resolving, identifying and tracking the time depth progress of P-SV waves is the proper use of both **horizontal** and **vertical** particle velocity records (and in synthetics between all acoustic and full elastic VSP records). In general which component to display depends critically on both the layer depth(s) of interest and source-receiver offsets. Thus for a given (pre-conversion) offset, the horizontal component of SV waves intensifies when considering deeper wavefronts that are travelling more nearly vertical. At near surface depths the P-SV wave is more clearly evident on the **vertical** component display, since at shallow depth, the refracted P-SV wave is travelling almost horizontal (with resulting vertical particle motion). At greater depths/larger offset ranges, both P and P-SV waves arrive obliquely at deeper

receivers; hence both arrivals can be equally well correlated on both horizontal and vertical displays.

At what are generally even greater source-receiver offsets, in addition to mode conversion, head wave refraction can result from one or more layers. When these overtake the usual direct P wave, refracted P (or P-SV converted refraction) can become the new first arrival. This can considerably complicate the net wavefield picture if not explicitly allowed for.

Background: Synthetic VSP Modeling Algorithms

The above outlined difficulties in extracting the fullwavefield information contained in a VSP record has underscored the need for a flexible, complete and correct synthetic VSP modeling algorithm.

Ever since the original "layer transfer matrix" studies of KUNETZ and GOUPILLIARD (1959; 1960), synthetic seismograms have proven invaluable in understanding forward propagation and in interpretative modeling of seis-acoustic wave propagation in real media.

Notwithstanding the many practical successes of synthetic seismic modeling to date, the ever increasing importance of obtaining an exact and complete wavefield solution for better understanding complex wave phenomena is often much less widely appreciated. To cite but two recent examples, the current revival of emphasis on multiply-converted and refracted modes in exploration seismology, and the current "rediscoveries" of major "new" nongeometric arrivals (for shallow buried sources) both reflect basic wave propagation phenomena in principle implicit in the full elastodynamic response of Lamb's classic problem.

As detailed in the works of GAL'PERIN and only later reinvestigated by others in Europe and America, generalised

borehole seismometry -VSP- has increasingly shown itself as a major resource for detailed investigation of seismic wave propagation in real media. Because VSP directly allows all up and downgoing waves to be recorded simultaneously within all layers, both time-depth correlation and waveform evolution are immediately possible for the most complex applications.

Given the generally high cost and complexity of actual VSP field data acquisition, and the complexity of analysing a complete wavefield response, strong emphasis has been focused in recent years on improved numeric seismogram synthesis for deterministic modeling of vertical seismic profiling. YOUNG et al (1983) and TOKSZOZ and STEWART (1984; references) have discussed the assumptions and approximations employed in developing computer algorithms from the initial Helmholtz wave equation, with regard to both theoretical capability and convenience. (The following discussion considers only those exact wave algorithms reported in the literature).

In the class of "exact" synthetic VSP models, all extant algorithms have to date been based entirely upon local propagator matrices to obtain the total multilayer solution. Using the related "transfer matrix" approach to convolutional modeling first put forward in seismology by KUNETZ and GOUPILLARD (1959; 1960) WUENSCHEL, 1960; ROBINSON and TREITEL, 1966, 1980), WYATT et al (1981) implemented the first published time domain propagator matrix scheme to find the plane wave zero offset

source VSP response for an acoustic-only medium. This has been described in more detail by CLAERBOUT (1968) and FITCH (1981). In similar fashion, AMINZADEH and MENDEL (1982; 1985) developed a "state space" approach to computing the synthetic seismic response of an elastic layered media to plane wave or line sources, based again on time domain recursive relations which effectively delimit initial downgoing "ray" departure angles and wavelet shape. This method however is valid only for source angles less than critical (head waves are not considered).

From the main body of reflectivity models, it was originally problematic for a receiver to reside within the same layer as the source. STEPHEN (1977) developed an extended version of KENNETT's (1974) recursive reflexion matrix algorithm allowing repeated wavefield calculations for a single receiver within the source layers. From the related point of view of the Fuchs-Muller model, GANLEY (1981) developed a more sophisticated frequency-domain wave equation solution technique, involving propagator matrices allowing oblique incident from a single point source, attenuation and dispersion. Likewise, TEMME and MULLER (1982) presented an acoustic-only model similar to that of GANLEY, using propagator matrices to calculate the synthetic VSP at any single receiver point in the media, in response to line or point sources.

More recently, DIETRICH et al (1985) have described a dedicated synthetic VSP algorithm, employing the multi-source discrete wavenumber formulation of BOUCHON (1982). This interesting

approach solves the elastic wave equation by repesenting the horizontal wavenumber integral as a discrete Bessel function sum (BOUCHON and AKI, 1977). This is effected by assuming N fictitious periodic surface sources in the presence of attenuation, where both these effects are removed in the final synthetic wavefield calculation. The multilayer Green's function is in this case also computed by modified Thomson-Haskell propagator matrices.

Many of the above exact complete wavefield solution techniques are comparatively new with only limited opportunity for detailed application and testing. To date each has proven highly useful in the published model problems around which they were originally designed. In general, however, the formal and computational limits of propagator matrices common to all the above algorithms have distinctly limited their range and validity of application.

From the above survey, a number of assumptions become apparent that impose limitations on accuracy and application of the underlying numerical models for VSP synthesis (**Figure** 66):

1). shear waves neglected (WYATT; TEMME and MUELLER)

2). attenuation neglected (WYATT)

3). # of layers computationally fesible limited by stability and speed of recursive propagator matrix (ALL of the above)

Figure 66

Table summary of extant synthetic VSP modelling algorithms (complete as of 12/31/84) {sans AMINZADEH & MENDEL, 1985}

REVIEW OF EXISTING EXACT-WAVE SYNTHETIC VSP ALGORITHMS

	STEPHEN REFLECTIVITY	TEMME-MULLER REFLECTIVITY	BOUCHON-PRANGE DISCRETE WAVENUMBER	GANLEY REFLECTIVITY	KUTSCHALE-JOHNS HOPKINS FFP	SCHMIDT SAFARI HP/REFLECTIVITY
WAVE EFFECTS	✓	✓	✓	✓	✓	✓
ACOUSTIC MEDIA	✓	✓	✓	✓	✓	✓
ELASTIC MEDIA	✓		✓		✓	✓
ATTENUATION	✓	✓	✓	✓		✓
MULTIPLES	✓	✓	✓	✓		✓
ARBITRARY NUMBER MULTIPLE SOURCES						✓
ARBITRARY NUMBER MULTIPLE RECEIVERS						✓
ARBITRARY SOURCE/RECEIVER TYPE			✓			✓
ARBITRARY SOURCE/RECEIVER LOCATION						✓
MAX NUMBER LAYERS (24 HR MAX RUN TIME)	10	50	50	50	10	200
CPU TIME (50 LAYER SOLID)	20hr	5hr	?	?	?	1hr
OTHER (NON VSP) APPLICATIONS					✓	✓
PUBLICATION DATE	1977	1982	1985	1980	1985	1982
NUMBER OF PUBLICATIONS (1985)	6	1	2	2	0	6

4). upper frequency " " " (ALL of the above, sans WYATT)

5). type, number and placement of sources " " " (ALL)

6). number and position of Multiple receivers (ALL)

Items 3). to 6). represent fundamental limitations, where accuracy of environment and experimental conditions is limited or dependent upon a maximum computational capacity inherent in the local propagator matrix formulation and algorithm.

As has been described elsewhere, another Global approach to computing the complete multilayer/multisource Green's function response has been developed by SCHMIDT (1982), which allows any arbitrary number of colinear subsurface sources and/or arbitrarily located receivers to be completely considered for a generalised plane layered homogeneous fluid or solid media. As was first noticed by TANGO (1983), because wavefield solutions in the "SAFARI" algorithm of SCHMIDT are written in terms of general up and downgoing scalar potentials, and because homogeneous (scattered) and inhomogeneous (source) terms are completely separated in the Direct Global matrix formulation so that the **complete** wavefield in all layers is computed simultaneously, the "SAFARI" algorithm innately and automatically treats the VSP wavefield case (**Figure** 67).

In "SAFARI", the standard inline VSP record seen by any number of arbitrarily located vertical receivers for a given source-receiver offset can be rapidly computed. However, several additional types of synthetic VSP records can also be obtained from the same direct global algorithm. In particular, the suite of synthetic seismograms obtained via lowering a horizontal surface-based string of hydrophones or geophones thru increasing depths corresponds exactly to the increasingly important case of offset VSP. The resulting offset VSP, obtained via a series of increasing source offsets from the borehole, are calculated by "SAFARI" at very small additional cost of about 7% of the total

Figure 67

Representation of SAFARI single & multiple offset VSP modelling capabilities

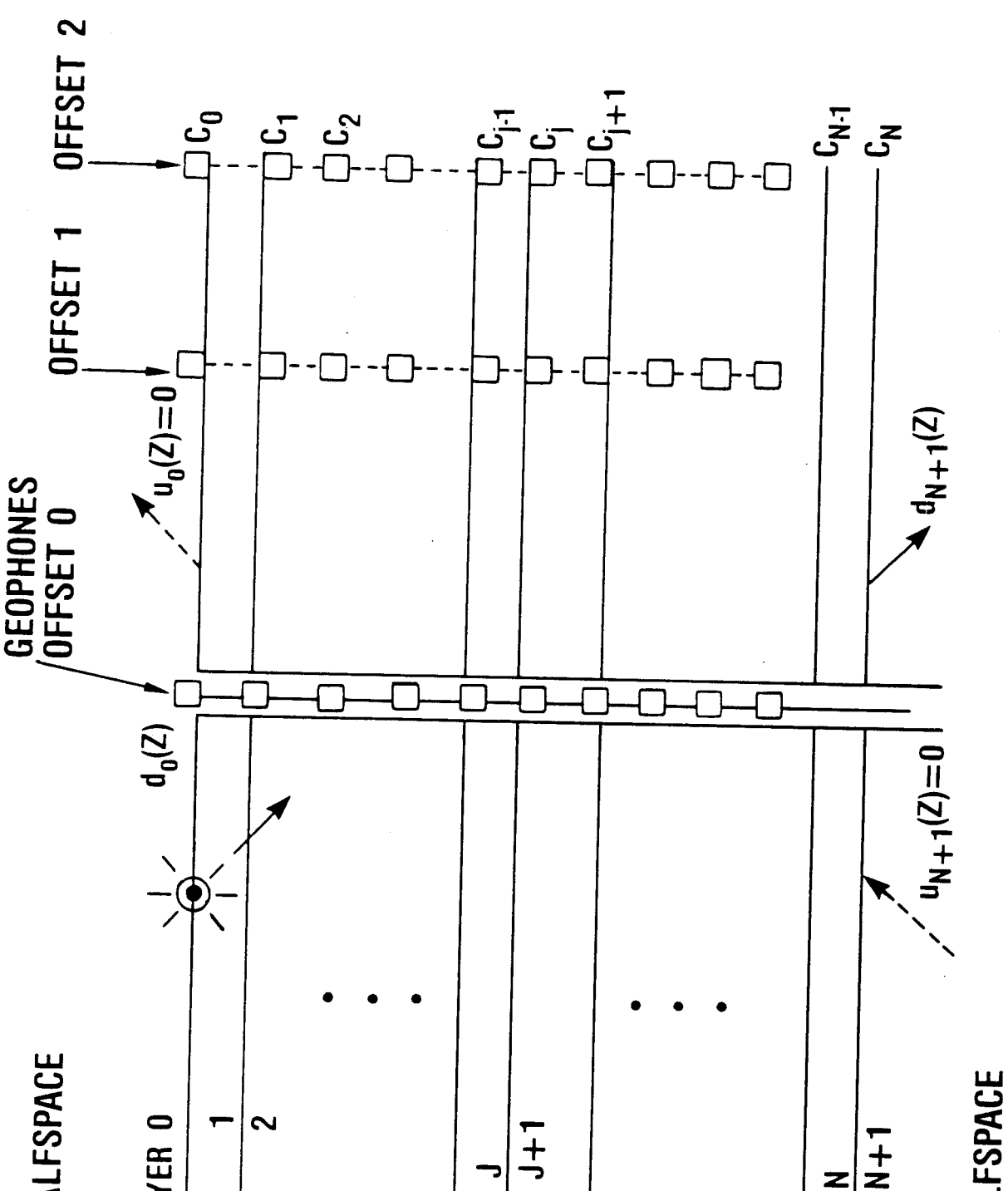
HALFSPACE
LAYER 0
1
2
J
J+1
N
N+1
HALFSPACE
GEOPHONES
OFFSET 0
OFFSET 1
OFFSET 2
$d_0(Z)$
$u_0(Z)=0$
C_0
C_1
C_2
C_{j-1}
C_j
C_{j+1}
C_{N-1}
C_N
$d_{N+1}(Z)$
$u_{N+1}(Z)=0$

VSP computation for a single offset. The reason for this economy is that the desired information is in fact already contained in the complete multilayer Green's function, and is merely accessed in efficient fashion. It is important to emphasise here that the "SAFARI" algorithm used to generate in and offline VSPs is exactly the **same** general applications program as that used to compute the standard surface-recorded synthetic seismograms previously discussed for deep crustal and exploration applications, without any special modifications necessary to comprehend the VSP case.

Application of "SAFARI" to Exploration and Deep Crustal VSP Modeling

In the present discussion, the "SAFARI" algorithm is demonstrated for 2 VSP cases, for which actual geologic models and synthetic VSP results from other algorithms already exists. These are the exploration stratigraphy model of TEMME and MULLER (1982), and the deep crustal models examined by STEPHEN (1977; 1984).

In the first example, we compute the fullwavefield VSP for a model of canonic stratigraphic layering, previously investigated by FERTIG and MULLER (1979) and TEMME and MULLER (1982).

The stratigraphic model selected is characterised by cyclic repitition of relatively thin hi velocity anhydrite beds interlayered with lower velocity shale and coal units, shown in **Figure** 68. Above the central 6-seam coal sequence of interest, a complex multilayer nearsurface overburden of semiconsolidated regolith and weaker sedimentary strata are present. The sequence here, comprising 48 total layers, approximates a typical velocity/depth profile from a multilayered coal seam in the Ruhr district of W. Germany.

The specific coal seam sequence of interest covers the depth range 600 to 1100 m, showing strong velocity inversions/ reflecting horizons at approximately 700 and 900 m. However, as discussed by FERTIG and MULLER (1979), when mapped by conventional horizontal (surface receiver) seismic profiles, the detailed stratigraphic information from the deeper layers can be effectively shielded by multiply-reflected, mode-converted and visco-elastic attenuated arrivals resulting from passage thru the uppermost portion of the stratigraphic sequence. This is shown in **Figure** 69, which is essentially that of FERTIG and MULLER (1979). For the VSPs considered in this example below, 25 3-component receivers (having interval spacing of 25m) are emplaced in a

vertical array extending from the surface to the lowest preseam level (z=600m). A single seismic source, exciting plane or spherical waves, is located at a nominal depth of 10m. The source-receiver offset can be varied arbitrarily (below).

Figure 68

Velocity-depth profile for a (full shear elastic) multilayered model of 50 layers, representing a Ruhr valley cyclic coal seam example (after TEMME and MULLER, 1982). This is the basic v/z model used for all subsequent full shear elastic VSP computations

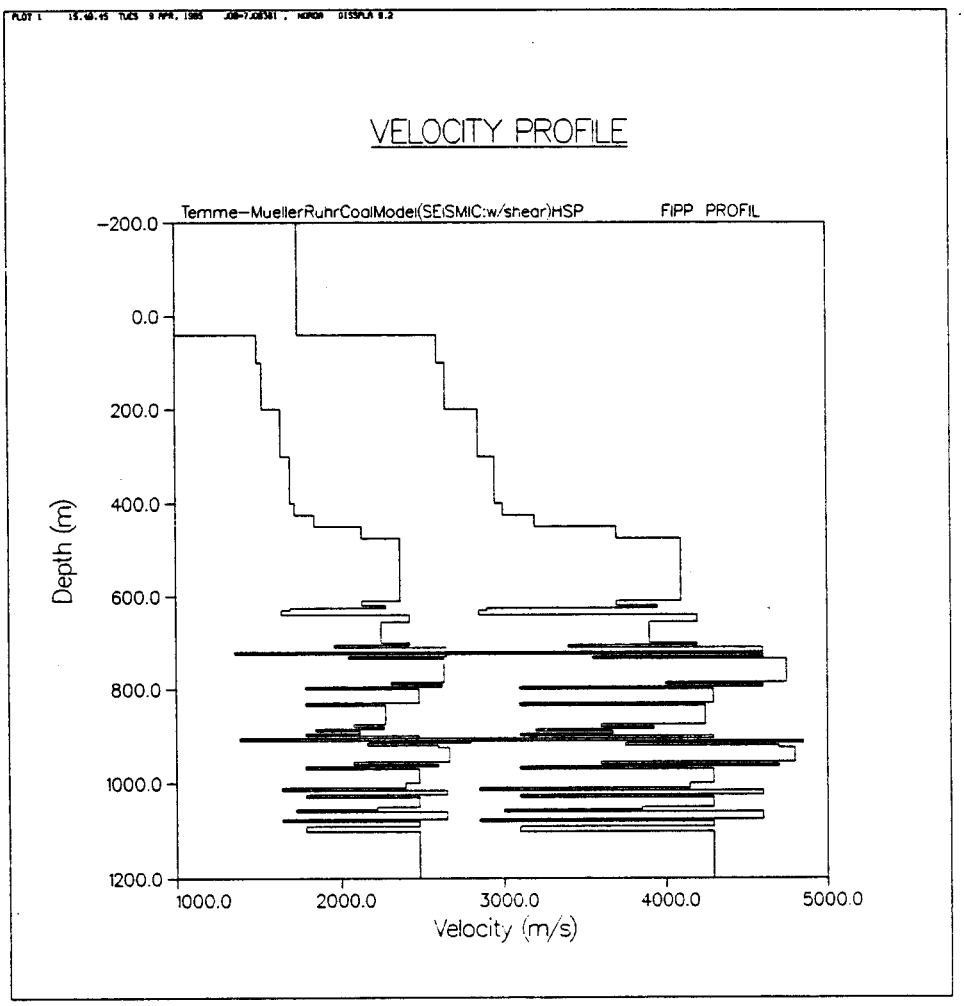
VELOCITY PROFILE
Temme–MuellerRuhrCoalModel(SEISMIC:w/shear)HSP
FIPP PROFIL
-200.0
0.0
200.0
400.0
600.0
800.0
1000.0
1200.0
Depth (m)
1000.0
2000.0
3000.0
4000.0
5000.0
Velocity (m/s)

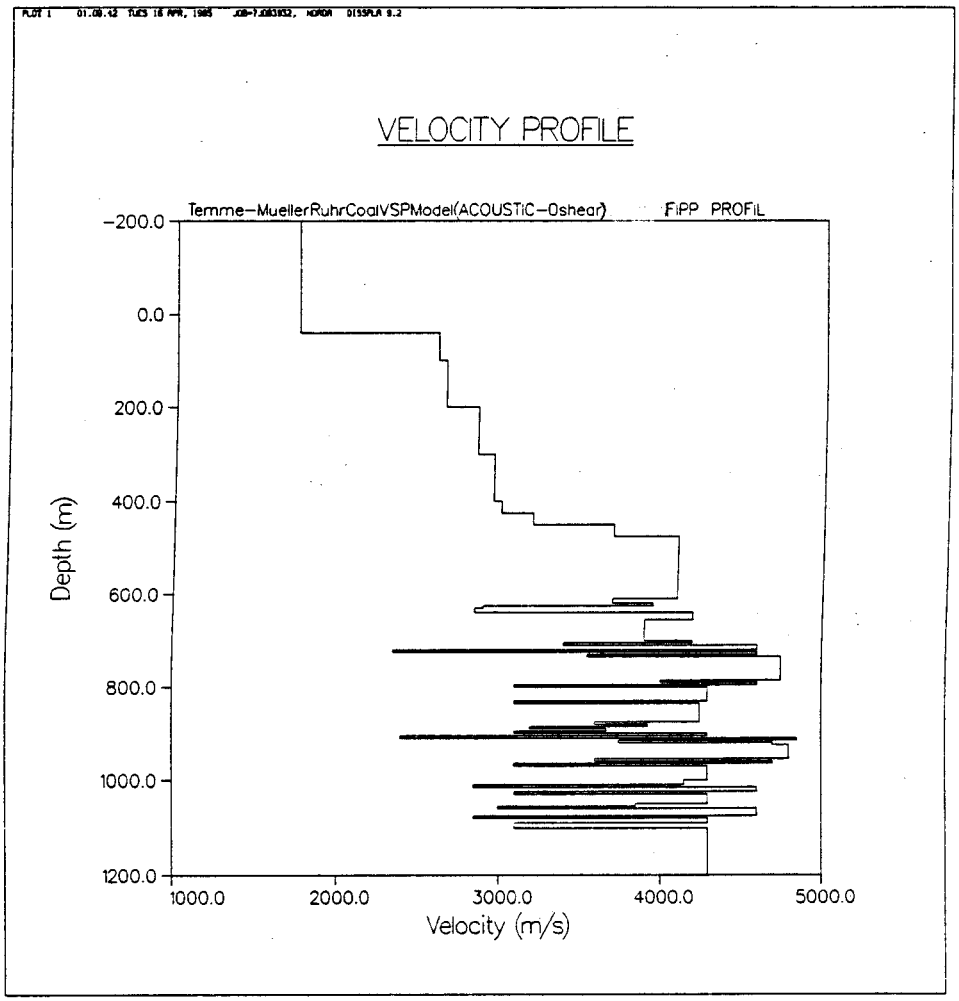
VELOCITY PROFILE
Temme-MuellerRuhrCoalVSPModel(ACOUSTIC-Oshear)
FiPP PROFiL
-200.0
0.0
200.0
400.0
600.0
800.0
1000.0
1200.0
Depth (m)
1000.0
2000.0
3000.0
4000.0
5000.0
Velocity (m/s)

Figure 69

Synthetic reflectivity horizontal seismic profile for full shear elastic Temme-Muller v/z model (compare with FERTIG and MULLER, 1978)

VERTICAL PARTICLE VELOCITY

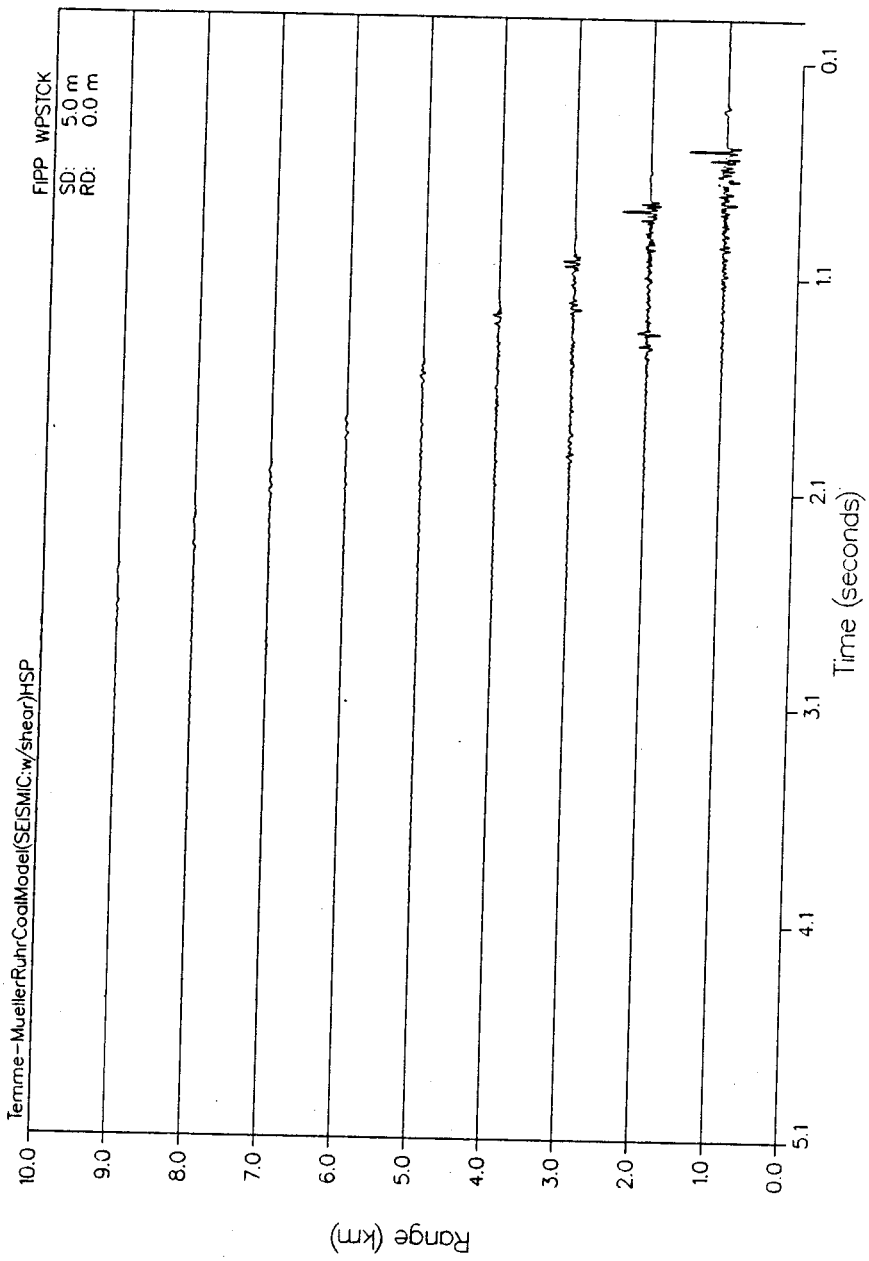

To examine the question of whether the plane or spherical wave type for VSP is appropriate for improving resolution when modeling the full range of near, mid and farfield offsets, **Figure 70** shows the synthetic Green's function integrand and VSP for a spherical wave point source, in an acoustic-only medium, having peak power frequency of 100Hz with power f=0 to f=200Hz, for a weak uniform absorption (α=.1 db/λ) in all layers. A series of 3 extreme nearfield offsets (50m to 150m) are considered. A standard double sine (N=2) input pulse shape is employed. The full wavefield Green's function integrand is here cut and tapered at kmax (minimum phase velocity) to exclude surface waves. As in the deep crustal fullwave, considerable trial and error in exactly determining an optimal $c_{phase_{Min}}$ was also required here; only final results are shown below.

For the initial source-receiver offset of 50m, the first direct P wave arrival shows abnormally high amplitudes for receivers approaching source depth. This graphically displays the singular amplitude error in extreme nearfield calculations using spherical waves in a radial Hankel function expansion neglecting (1) higher order and (2) ingoing wave terms. This computation was then repeated for the same offset, now however using plane wave source in an exact representation, which is well-behaved at any source-receiver offset range; **Figure 71**. Repeating the point source calculations for additional offsets shows that accurate wave-offset amplitude behaviour is also found for the original

Figure 70

Full wavefield synthetic VSP (spherical wave point source) for full shear elastic v/z profile, at 3 extreme nearfield source/receiver offsets (50m, 100m, 150m), to exhibit the singular amplitude behaviour due to outgoing-only and asymptotic Hankel function approximation.

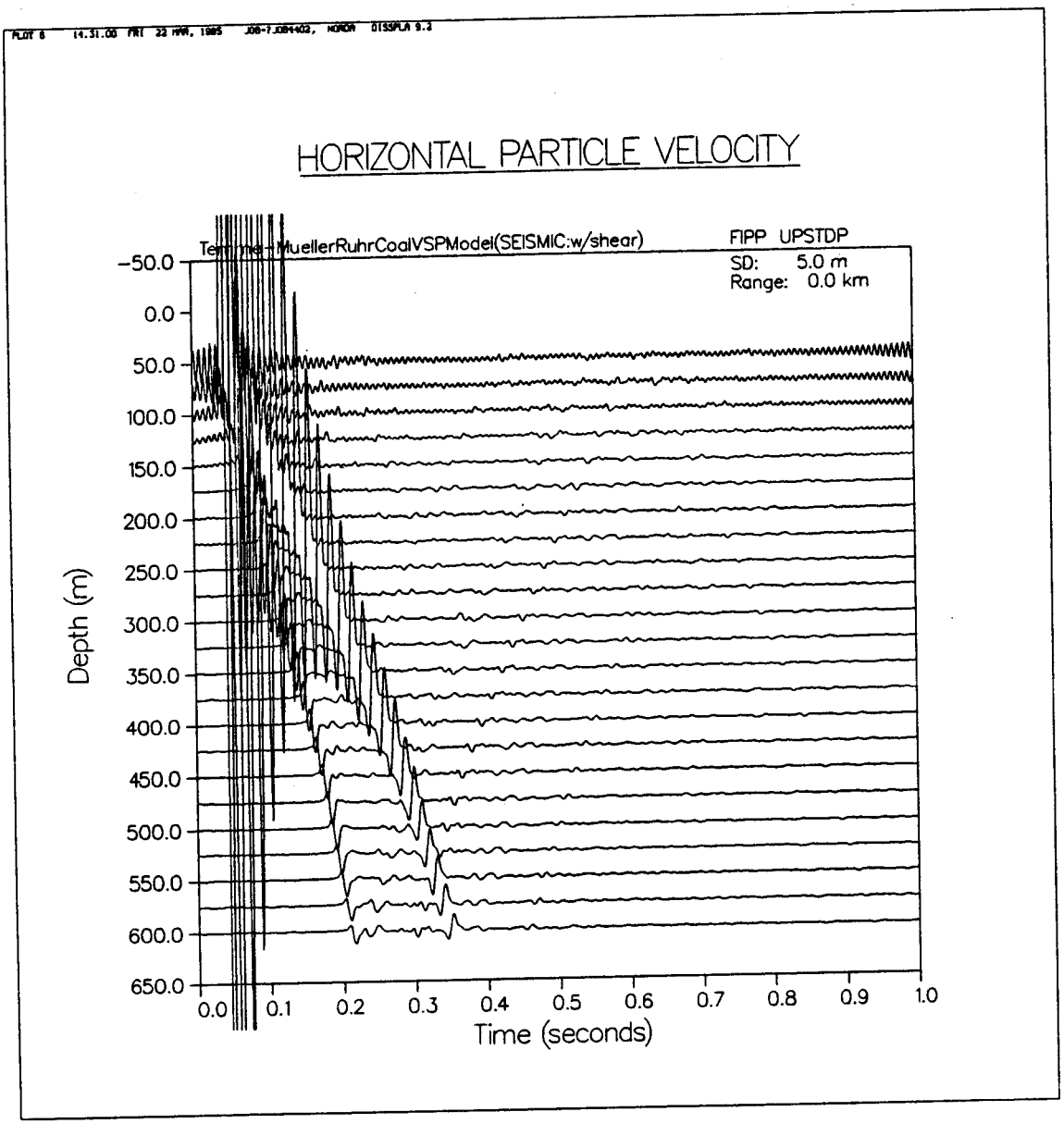
HORIZONTAL PARTICLE VELOCITY
Test name - MuellerRuhrCoalVSPModel(SEISMIC:w/shear)
FIPP UPSTDP
SD: 5.0 m
Range: 0.0 km
Depth (m)
-50.0
0.0
50.0
100.0
150.0
200.0
250.0
300.0
350.0
400.0
450.0
500.0
550.0
600.0
650.0
0.0
0.1
0.2
0.3
0.4
0.5
0.6
0.7
0.8
0.9
1.0
Time (seconds)

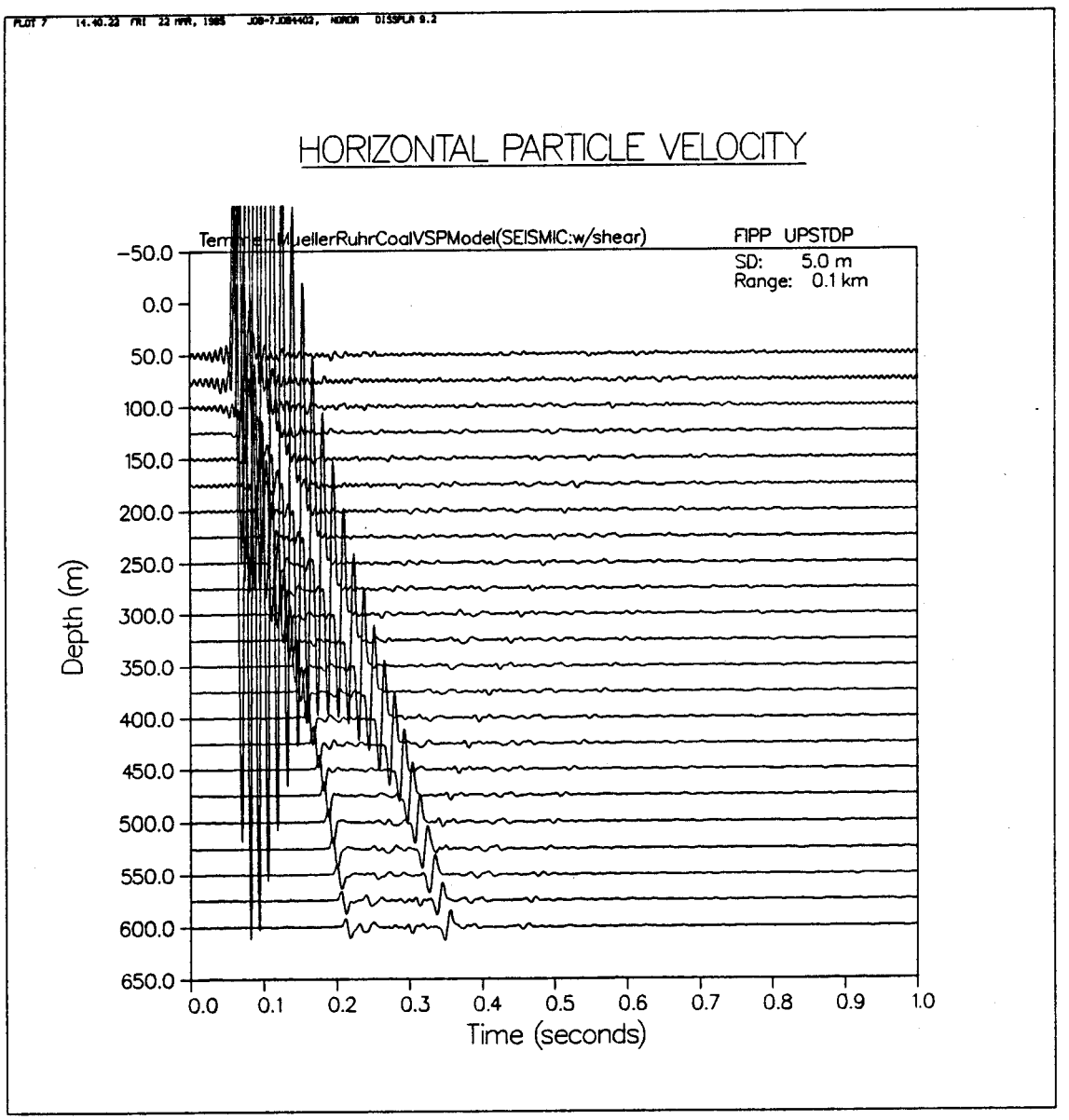
HORIZONTAL PARTICLE VELOCITY
FIPP UPSTDP
SD: 5.0 m
Range: 0.1 km
Depth (m)
-50.0
0.0
50.0
100.0
150.0
200.0
250.0
300.0
350.0
400.0
450.0
500.0
550.0
600.0
650.0
0.0
0.1
0.2
0.3
0.4
0.5
0.6
0.7
0.8
0.9
1.0
Time (seconds)

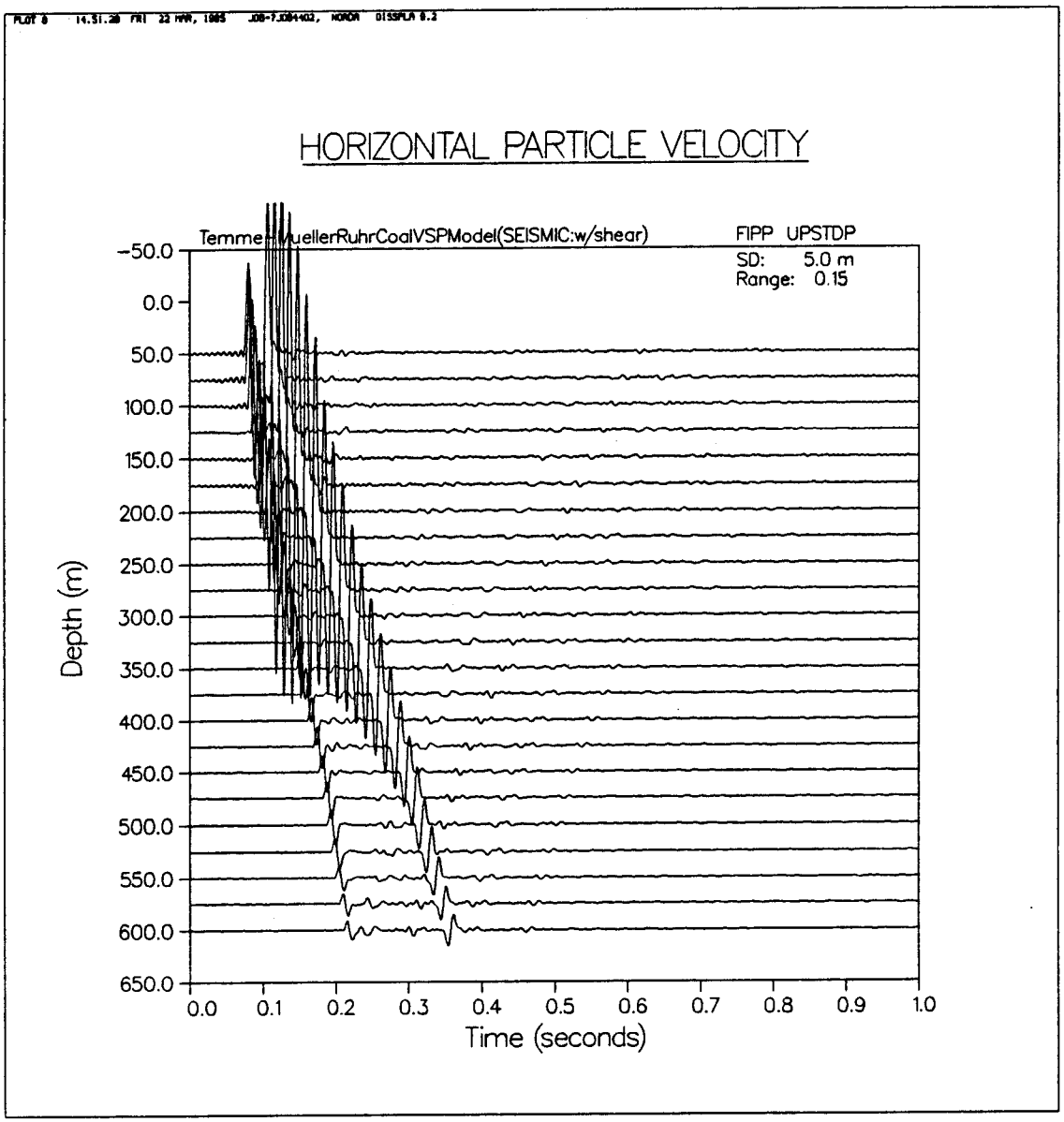
HORIZONTAL PARTICLE VELOCITY
Temme-MuellerRuhrCoalVSPModel(SEISMIC:w/shear)
FIPP UPSTDP
SD: 5.0 m
Range: 0.15
Depth (m)
-50.0
0.0
50.0
100.0
150.0
200.0
250.0
300.0
350.0
400.0
450.0
500.0
550.0
600.0
650.0
0.0
0.1
0.2
0.3
0.4
0.5
0.6
0.7
0.8
0.9
1.0
Time (seconds)

Figure 71

Full wavefield synthetic VSP (plane wave line source) for full shear elastic v/z profile, at 2 extreme nearfield source-receiver offsets (x=.1km and x=.3km)

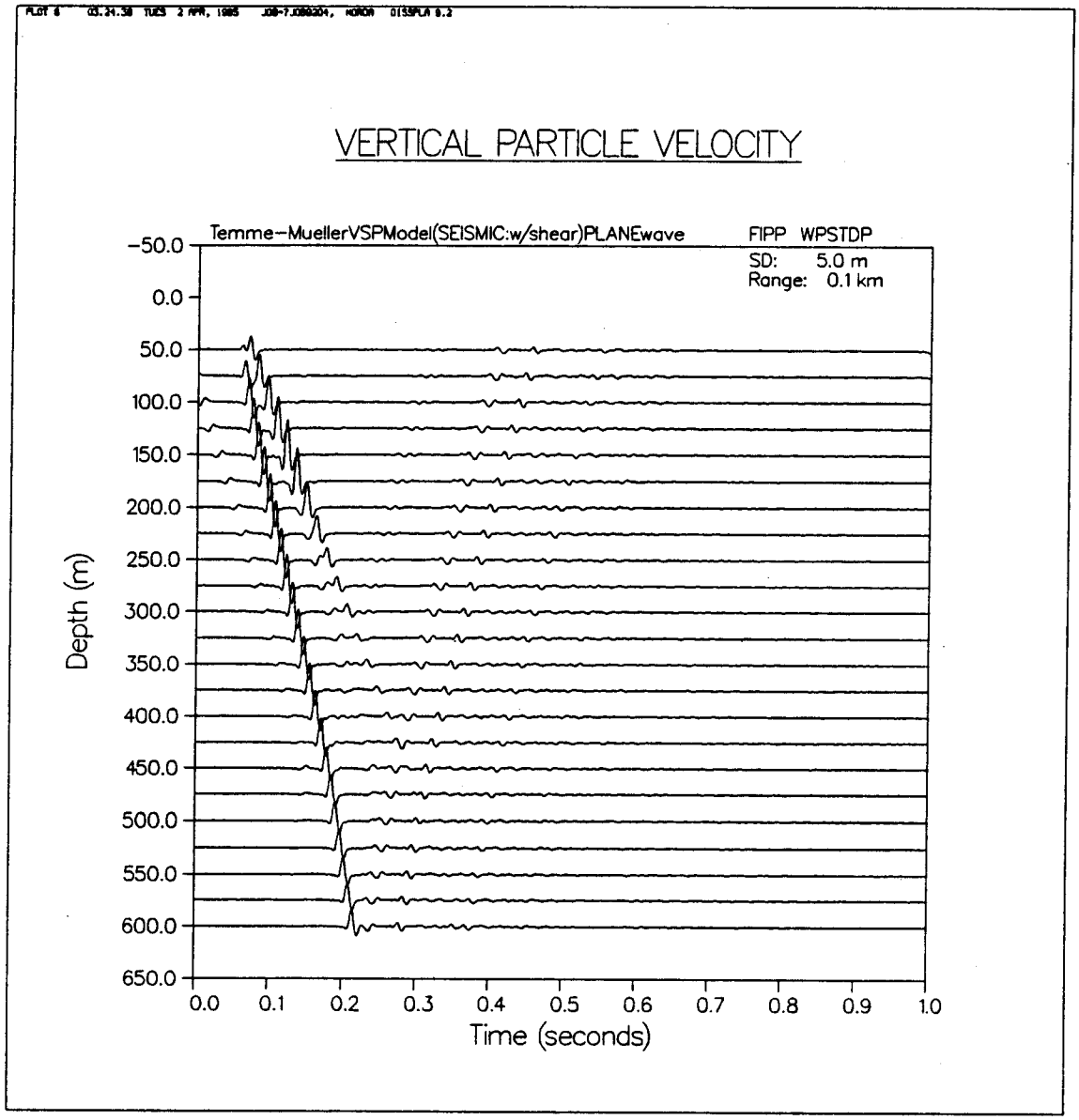
VERTICAL PARTICLE VELOCITY
Temme-MuellerVSPModel(SEISMIC:w/shear)PLANEwave
FIPP WPSTDP
SD: 5.0 m
Range: 0.1 km
Depth (m)
-50.0
0.0
50.0
100.0
150.0
200.0
250.0
300.0
350.0
400.0
450.0
500.0
550.0
600.0
650.0
0.0
0.1
0.2
0.3
0.4
0.5
0.6
0.7
0.8
0.9
1.0
Time (seconds)

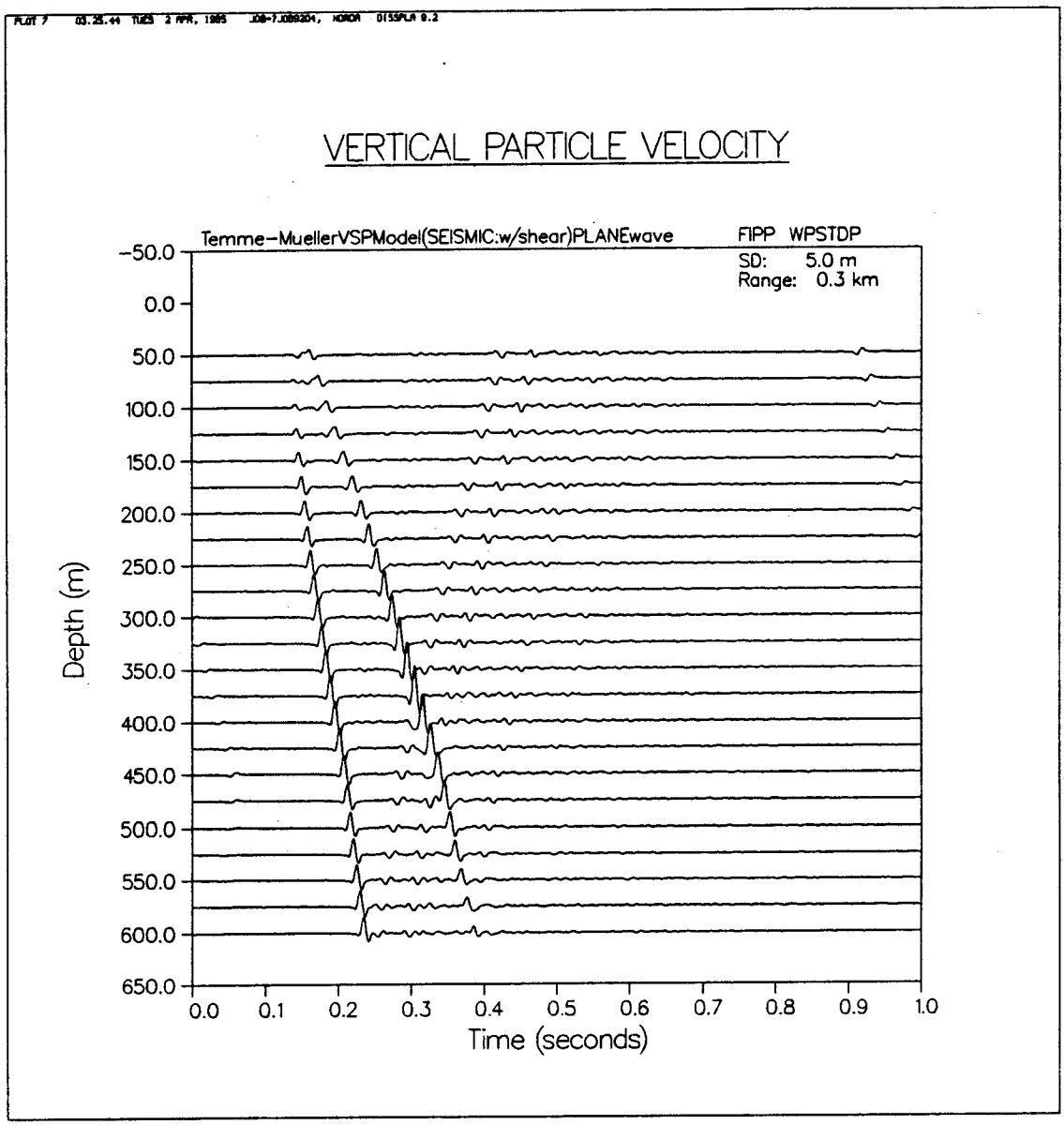
VERTICAL PARTICLE VELOCITY
Temme-MuellerVSPModel(SEISMIC:w/shear)PLANEwave
FIPP WPSTDP
SD: 5.0 m
Range: 0.3 km
Depth (m)
-50.0
0.0
50.0
100.0
150.0
200.0
250.0
300.0
350.0
400.0
450.0
500.0
550.0
600.0
650.0
0.0
0.1
0.2
0.3
0.4
0.5
0.6
0.7
0.8
0.9
1.0
Time (seconds)

In addition, as TEMME and MULLER point out, although resolution per se is not improved for the above changes of input center frequency and bandwidth, the relative amplitude ratios between the first 3 seam reflexions is now seen to be altered (from 2,1 and 3 to 3,1 and 2, in order of decreasing amplitude). This weakening of the upgoing reflexion from coal seam 2 can here be interpreted as a possible frequency-dependent "tuning effect" where at the new (higher) source frequency the thickness of the layer of origin for this reflection is no longer $\sim \lambda/4$. The end result is that the reflections from nearby layers have become the dominant controlling amplitudes near the zones of interest; given realistic real earth attenuations, attempts at even higher frequency source input would not significantly improve these results.

Since little difference in waveforms was observed between point and line sources for offsets of .3 km or greater, we next examine this later (representative) offset of x=.3km in more detail, for direct comparison with some of the results of TEMME and MULLER (1982) (**Figure 72**).

In addition to the gradually decreasing amplitude of the first direct arrival, the reflecting interfaces of the complex multi-layered overburden results in a strong "ghost" reflection (due to noncoincidence of source and surface depths), as well as several strong downgoing multiple reflections (from the first and third interfaces at z=35m and z=150m). Although in principle it would be possible to place the source at a deeper location, in this way avoiding the attenuative and multiple noise effects of the near surface layers, this would inevitably cause long period ghosts to interfere considerably with the identification of deeper primary events. Conversely, any shallower source depths used here would reduce the ghost effect.

The multiples immediately following the primary are themselves subsequently reflected from the surface and other near surface reverberant zones on one or more occassions, producing a "ringing" chain of multiple events across all later recording times in the shallow receivers. Because the receiver spacing interval is here larger than the nearsurface layer thicknesses in the overburden, this strongly-reverberant nature of the uppermost

layers is not clearly decomposable into individual layer/ ray contributions, due to interference between adjacent primaries and stronger surface multiples. However, if the VSP response is computed for a much finer spatial sampling of receivers, here emplaced so as to cover the nearsurface zone, the up and downgoing multiple paths causing the strong ringing after the secondary arrivals can more clearly be seen (**Figure** 73), the complexity of which, however, increases with offset.

Returning to the previous VSP, despite the fact that the (plane wave) amplitudes of reflections at the surface are doubled (WHITE, 1978) and are therefore optimistic with respect to true spherical wave amplitudes, as noted the late-arriving upgoing primary reflections from the last 4 deep seam coal groups become more difficult to identify in near-surface based receivers, due to the strongly interfering background from surface multiples and deeper upgoing primaries. In particular, the upgoing events from deeper seams cannot be traced to the surface closer than about half the borehole depth (z=300m).

The above difficulties are not improved significantly at either higher or lower source frequencies; **Figures** 74 and 75. Here the reflection character for a surface-receiver string of the deeper response appears highly dependent upon the adjacent units above and below the level(s) of interest. Even for the present short-period/nonoscillatory input wavelet, confusing patterns of

constructive and destructive intereference due to wavelet "ringing" can arise.

As the number and local interference of deeper primaries with varying mulitples are here important, the conditions of origin and cumulative effects of near-surface multiples are here considered further. For multiple-event analysis, as is well known, synthetic VSPs have several advantages over synthetic surface seismograms. Perhaps most notably, it is always possible as noted above to selectively "edit" or decompose total synthetic VSPs by selectively deleting one or more layer interfaces from the total v/z profile, and regenerating the corresponding new VSP, minus the deleted layer. It is also conversely possible to compute the specific synthetic VSP response from the given (deleted) layer(s) in question directly.

To consider an example of this feature in the present case, **Figures 76a & b** shows the synthetic VSP for a nearfield offset of 300 meters, using a central spherical (point) source center frequency of 50Hz and a bandwidth of 0 to 125Hz, for an assumed acoustic-only medium (zero shear), computed separately over the deep-seam only and upper near-surface only reverberant zones, compared to the total (coalseam+shallow) response (**Figure 72**).

Figure 72

Full wavefield synthetic VSP (plane wave line source) for acoustic-only Temme-Muller v/z profile, x_{offset}=.3km with f_{center}= 50Hz, power from 0-125Hz.

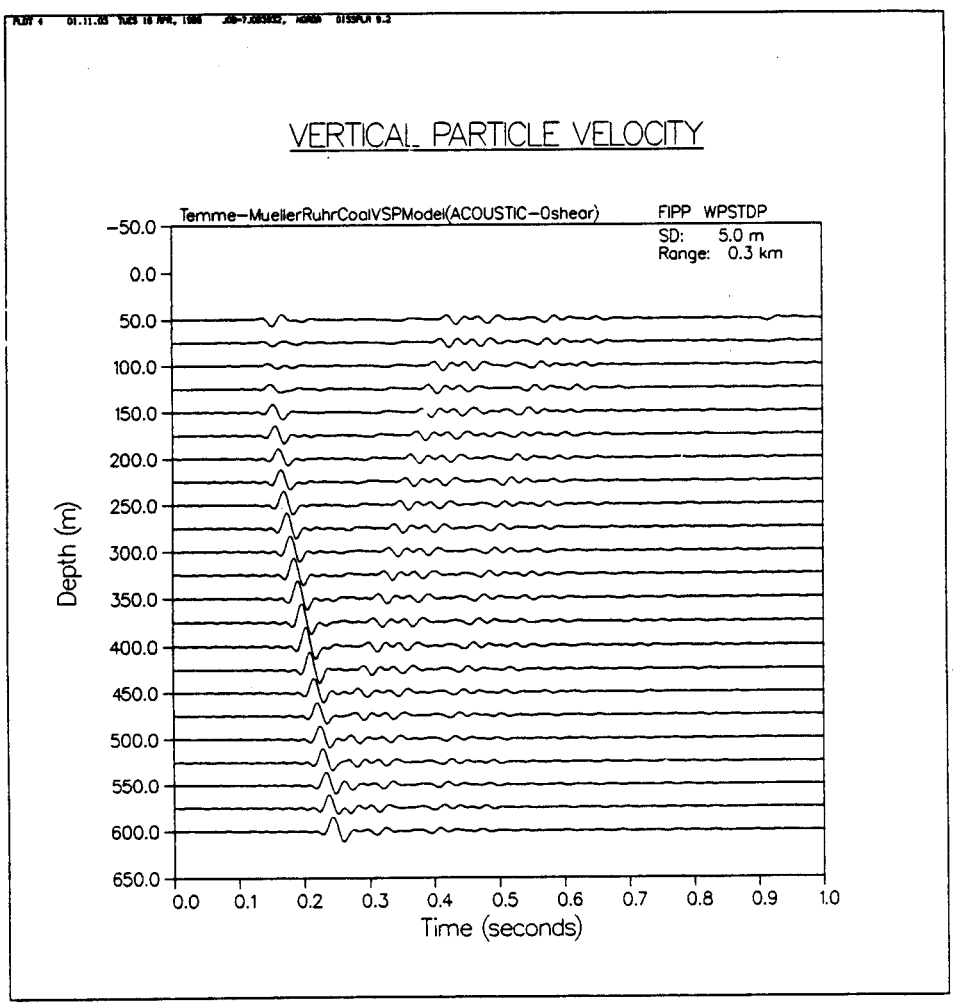
VERTICAL PARTICLE VELOCITY
Temme-MuellerRuhrCoalVSPModel(ACOUSTIC-0shear)
FIPP WPSTDP
SD: 5.0 m
Range: 0.3 km
Depth (m)
-50.0
0.0
50.0
100.0
150.0
200.0
250.0
300.0
350.0
400.0
450.0
500.0
550.0
600.0
650.0
0.0
0.1
0.2
0.3
0.4
0.5
0.6
0.7
0.8
0.9
1.0
Time (seconds)

Figure 73

Full wavefield synthetic VSP (plane wave line source) for acoustic-only Temme-Muller v/z profile, x_{offset}=.3km with f_{center}= 50Hz, power from 0-125Hz. Number of receivers=46, showing (marginally) improved resolution of first-break and subsequent traveltime branches

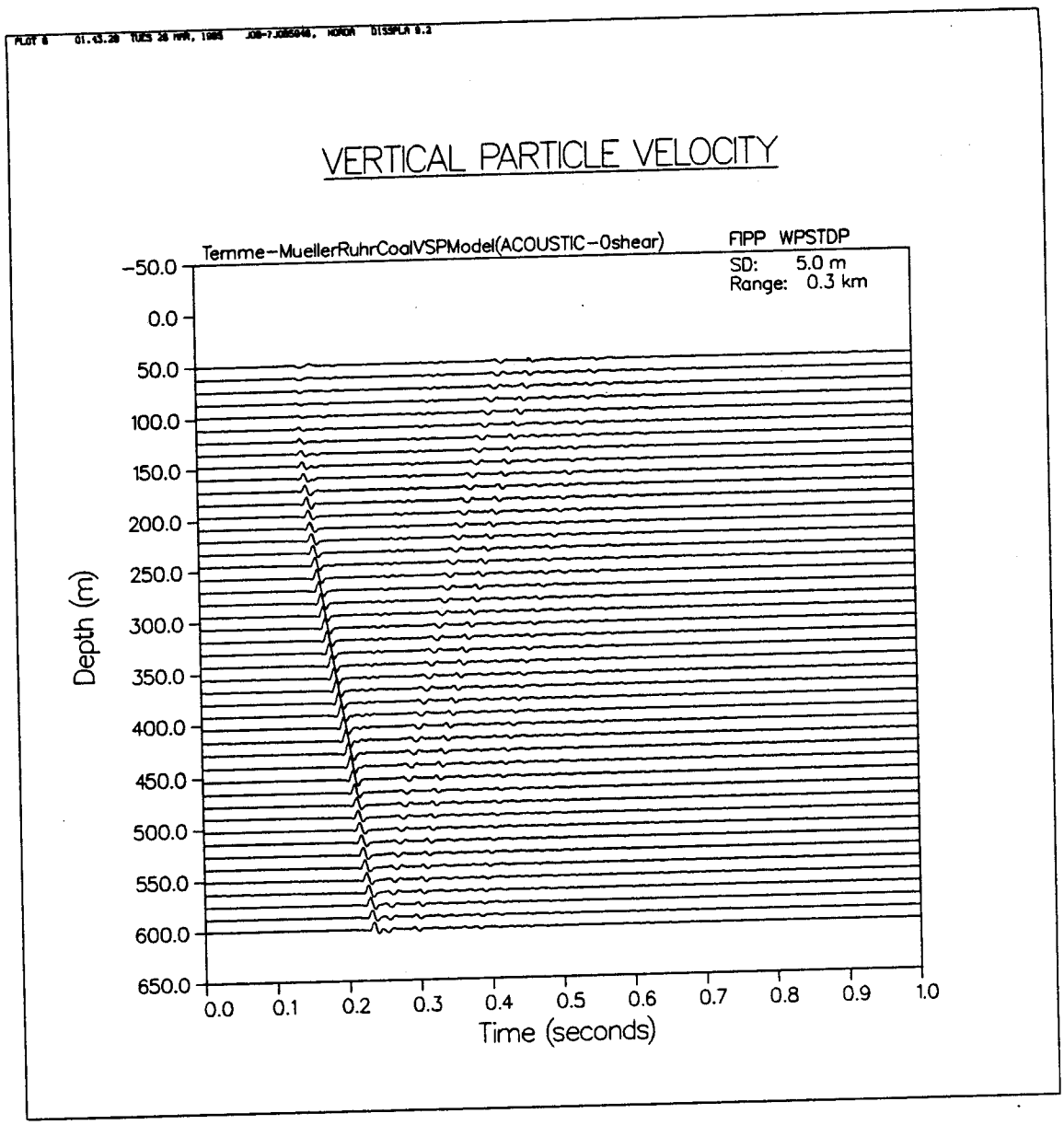
VERTICAL PARTICLE VELOCITY
Temme-MuellerRuhrCoalVSPModel(ACOUSTIC-0shear)
FIPP WPSTDP
SD: 5.0 m
Range: 0.3 km
Depth (m)
-50.0
0.0
50.0
100.0
150.0
200.0
250.0
300.0
350.0
400.0
450.0
500.0
550.0
600.0
650.0
0.0
0.1
0.2
0.3
0.4
0.5
0.6
0.7
0.8
0.9
1.0
Time (seconds)

Figure 74 and 75

74) Full wavefield synthetic VSP, (plane wave line source), for acoustic-only Temme-Muller v/z model, x_{offset}= .3km, f_{center}= 100Hz, power from 0 to 225Hz

75) Full wavefield synthetic VSP, (plane wave line source), for acoustic-only Temme-Muller v/z model, x_{offset}= .3km, f_{center}= 25Hz, power from 0 to 50Hz

Comparatively, these show the relative lack of any notable resolution gain by resorting to standard alternate frequencies (except in clarity of first arrival branch)

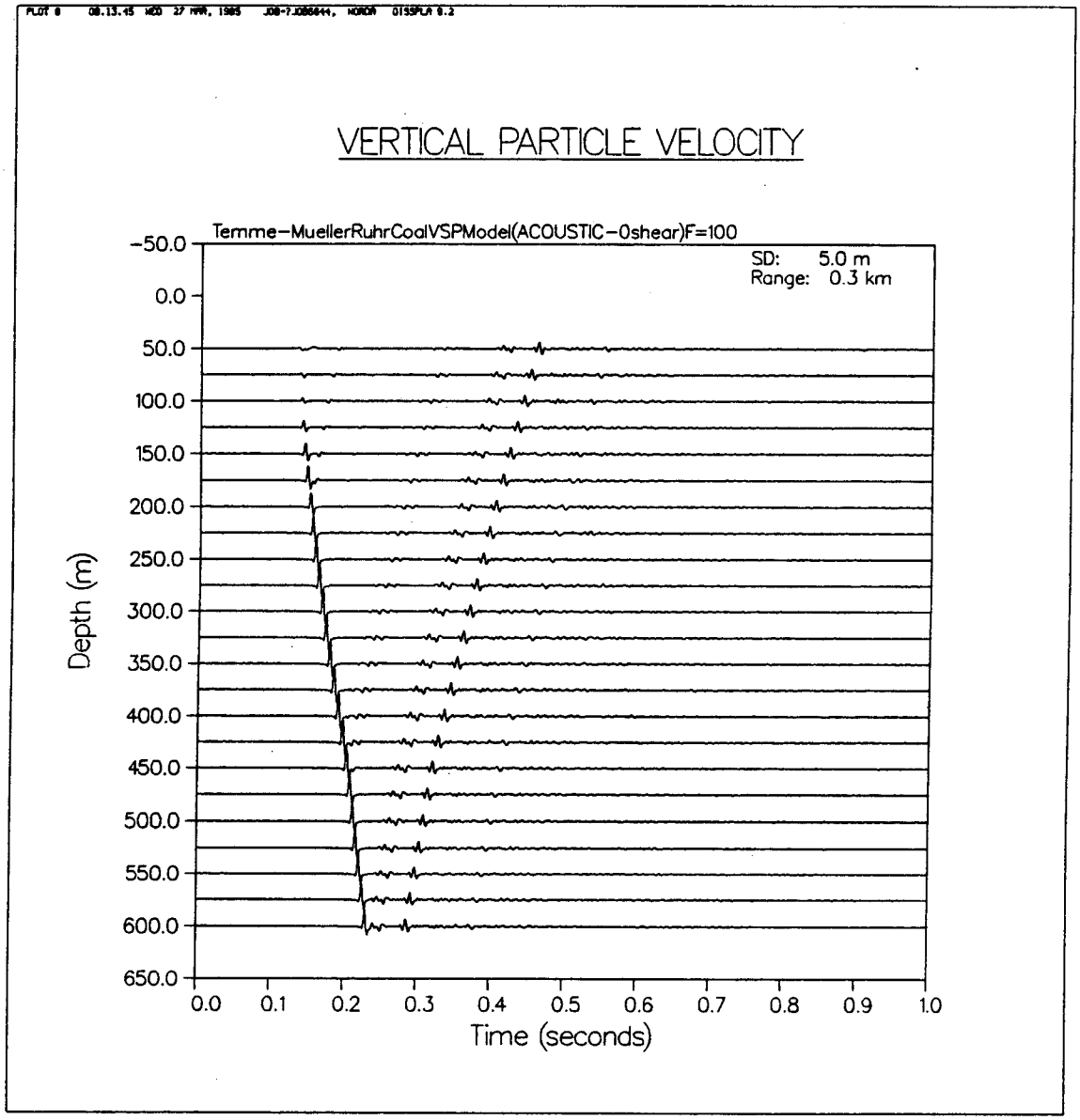
VERTICAL PARTICLE VELOCITY
Temme-MuellerRuhrCoalVSPModel(ACOUSTIC-0shear)F=100
SD: 5.0 m
Range: 0.3 km
Depth (m)
-50.0
0.0
50.0
100.0
150.0
200.0
250.0
300.0
350.0
400.0
450.0
500.0
550.0
600.0
650.0
0.0
0.1
0.2
0.3
0.4
0.5
0.6
0.7
0.8
0.9
1.0
Time (seconds)

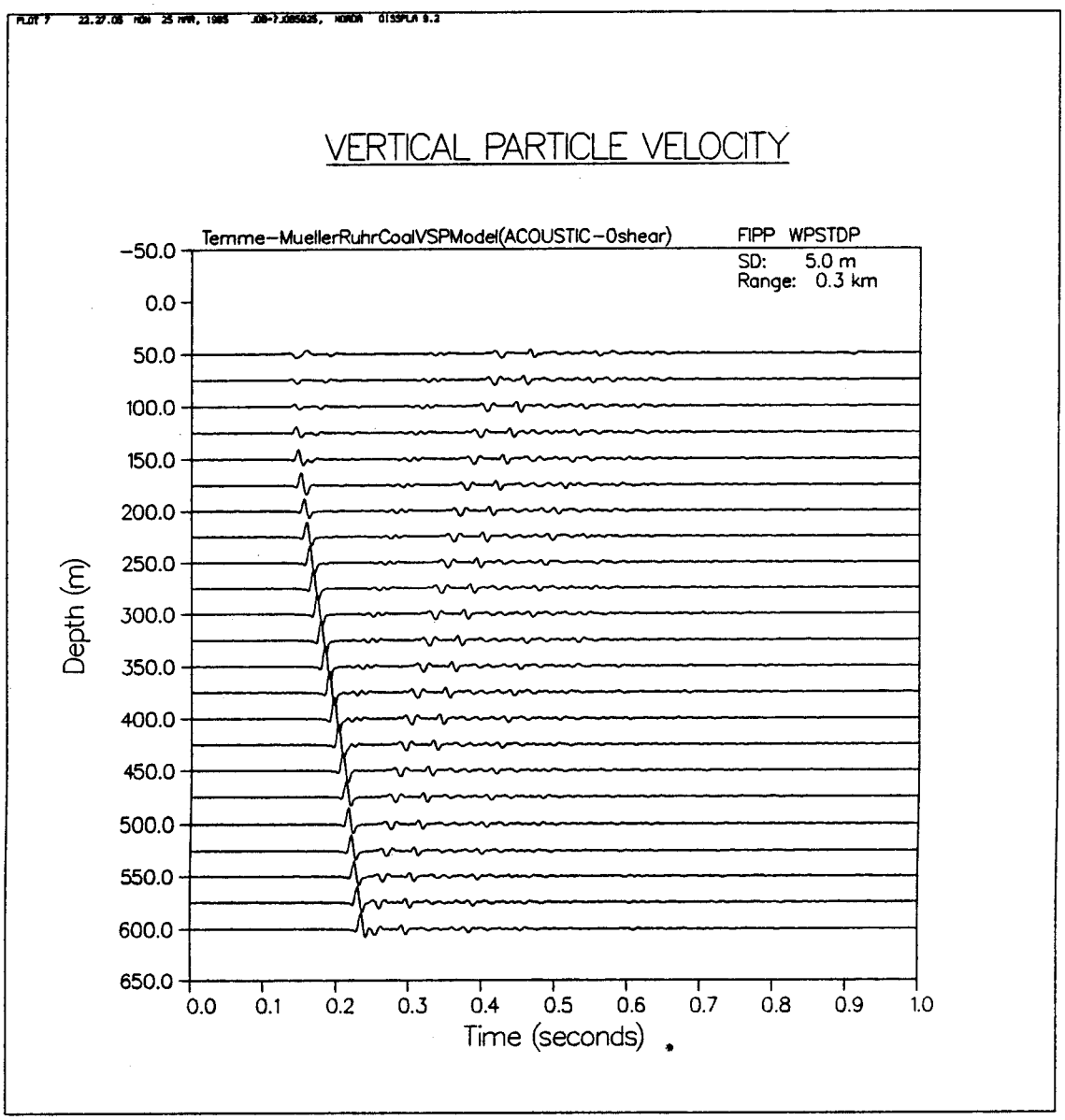
VERTICAL PARTICLE VELOCITY
Temme-MuellerRuhrCoalVSPModel(ACOUSTIC-0shear)
FIPP WPSTDP
SD: 5.0 m
Range: 0.3 km
Depth (m)
-50.0
0.0
50.0
100.0
150.0
200.0
250.0
300.0
350.0
400.0
450.0
500.0
550.0
600.0
650.0
0.0
0.1
0.2
0.3
0.4
0.5
0.6
0.7
0.8
0.9
1.0
Time (seconds)

Figure 76

Velocity-depth models and corresponding full wavefield synthetic VSP (plane wave line source) for acoustic-only Temme-Muller v/z model, with

(a) no near-surface [deep seams only]

(b) no deep seams [near-surface only]

(c) total layer (near-surface + deep seams) response

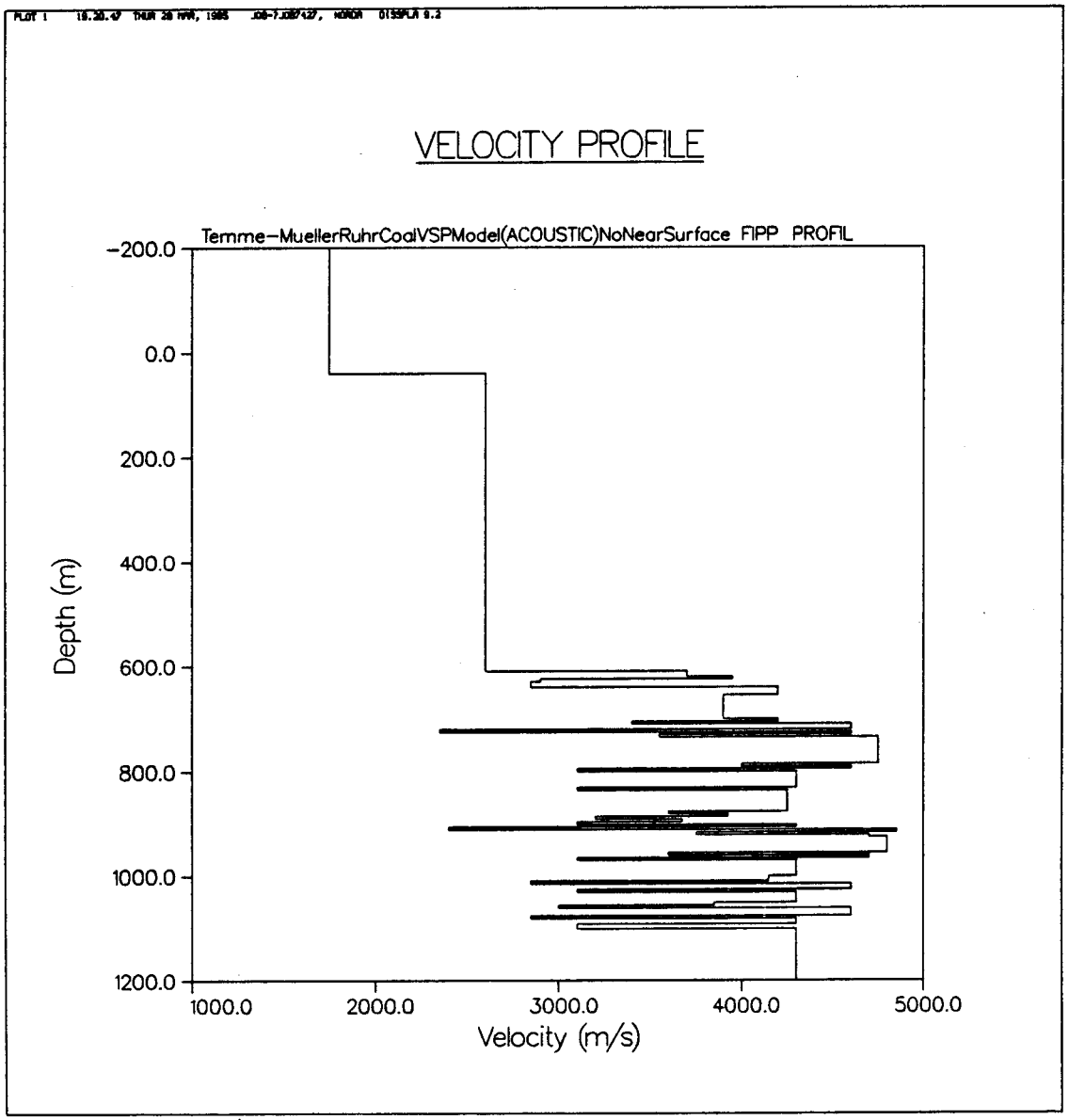
VELOCITY PROFILE
Temme-MuellerRuhrCoalVSPModel(ACOUSTIC)NoNearSurface FIPP PROFIL
-200.0
0.0
200.0
400.0
600.0
800.0
1000.0
1200.0
Depth (m)
1000.0
2000.0
3000.0
4000.0
5000.0
Velocity (m/s)

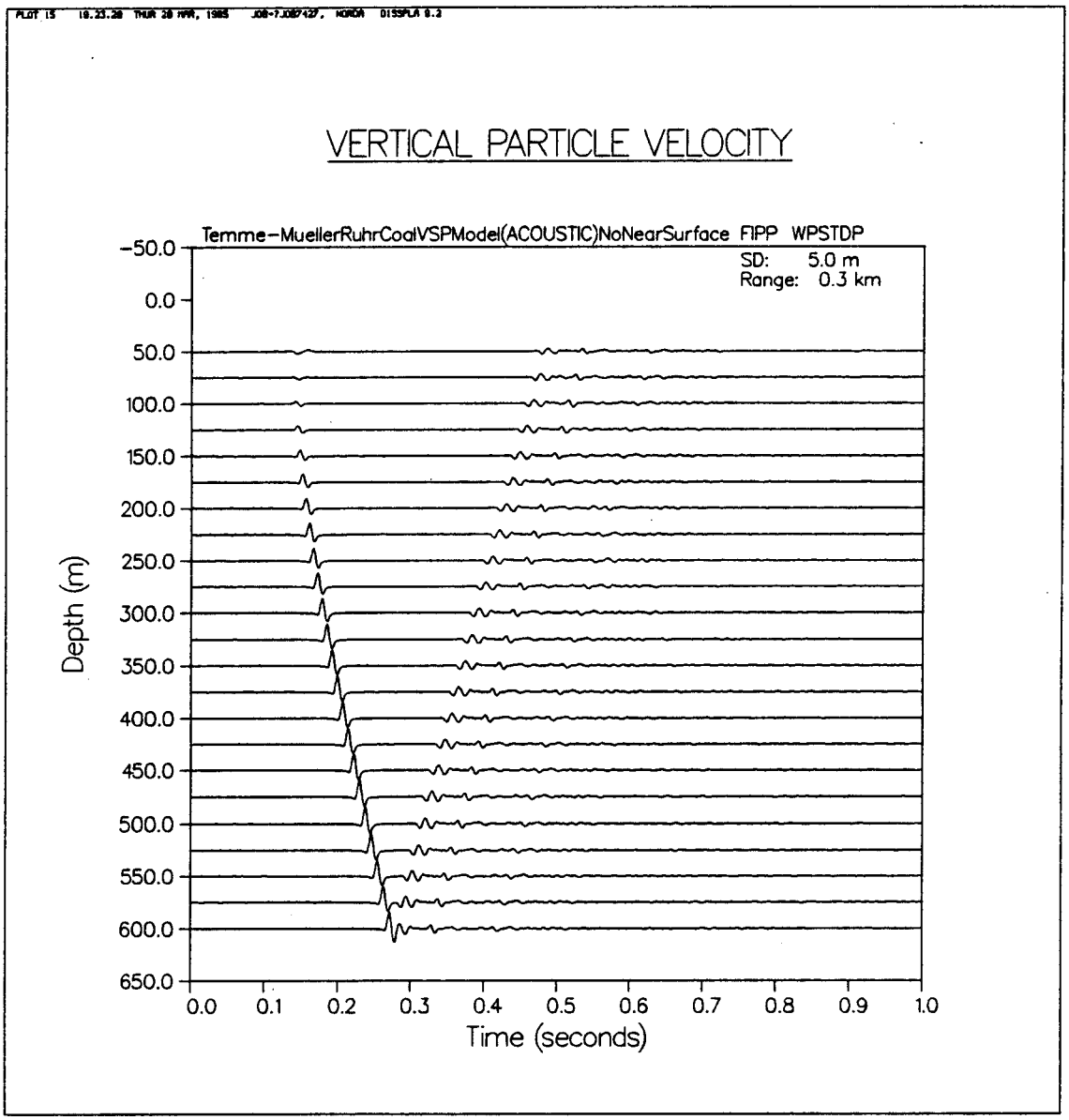
VERTICAL PARTICLE VELOCITY
Temme-MuellerRuhrCoalVSPModel(ACOUSTIC)NoNearSurface FIPP WPSTDP
SD: 5.0 m
Range: 0.3 km
Depth (m)
-50.0
0.0
50.0
100.0
150.0
200.0
250.0
300.0
350.0
400.0
450.0
500.0
550.0
600.0
650.0
0.0
0.1
0.2
0.3
0.4
0.5
0.6
0.7
0.8
0.9
1.0
Time (seconds)

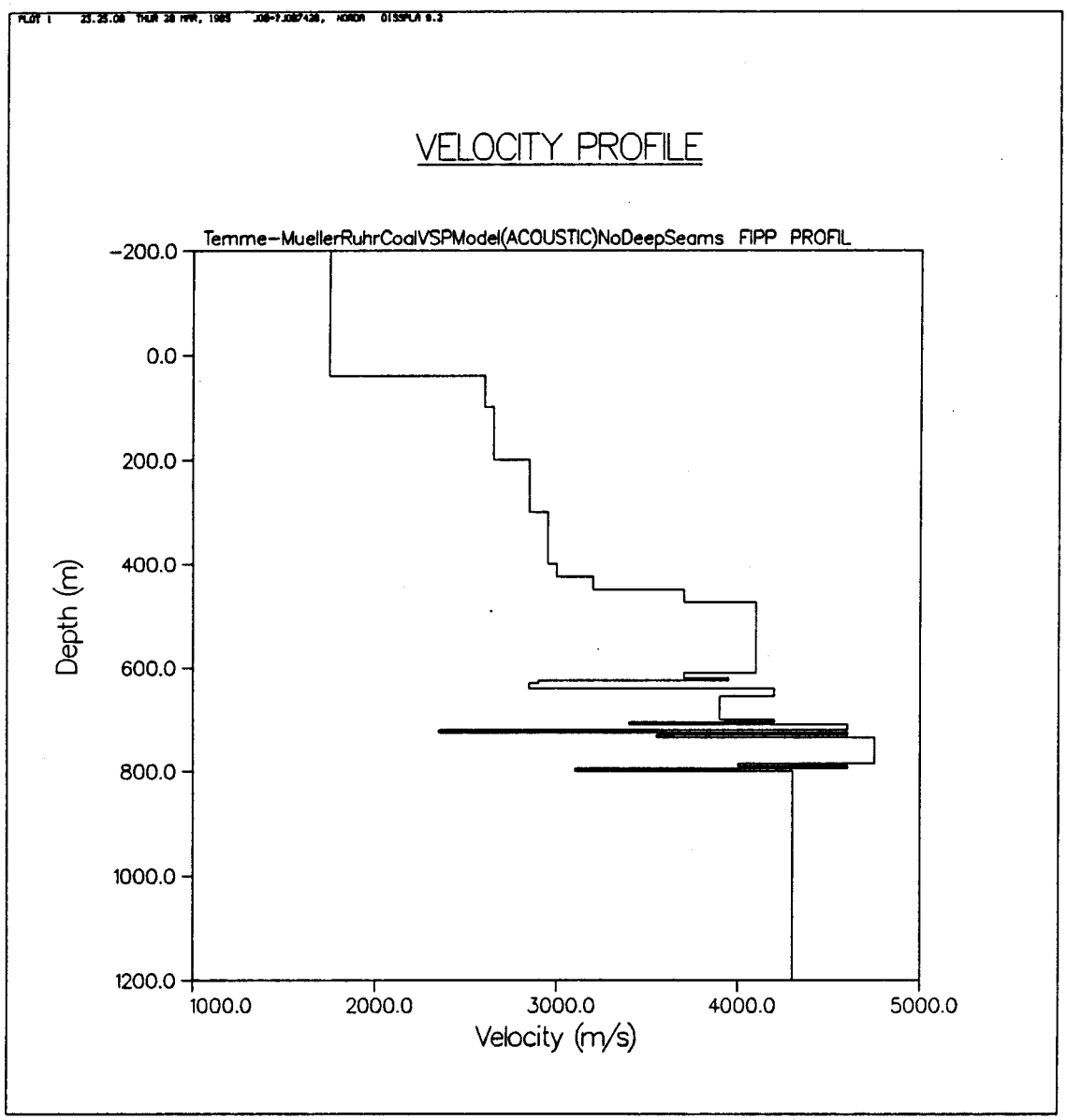
VELOCITY PROFILE
Temme-MuellerRuhrCoalVSPModel(ACOUSTIC)NoDeepSeams FIPP PROFIL
-200.0
0.0
200.0
400.0
600.0
800.0
1000.0
1200.0
Depth (m)
1000.0
2000.0
3000.0
4000.0
5000.0
Velocity (m/s)

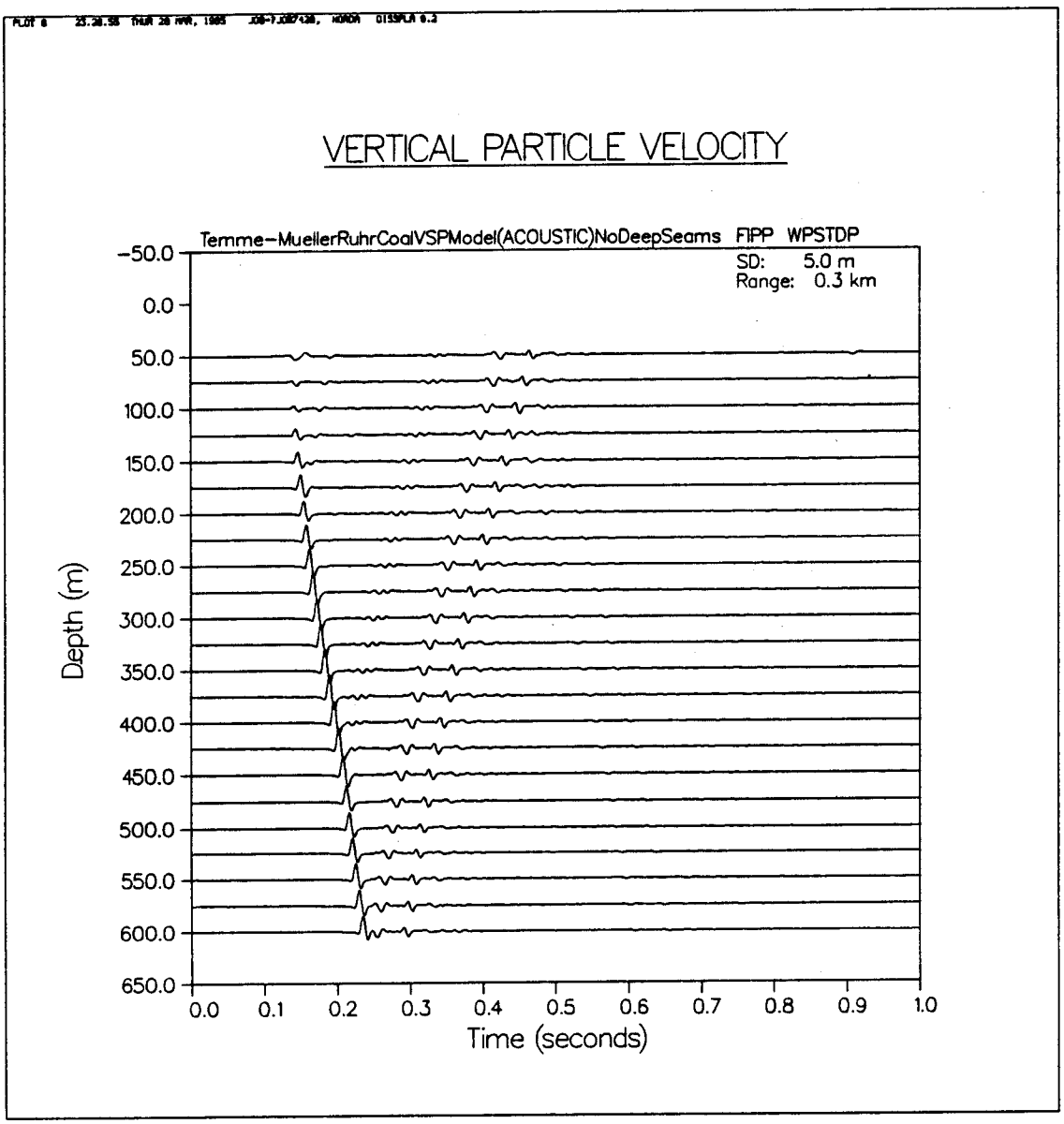
VERTICAL PARTICLE VELOCITY
Temme-MuellerRuhrCoalVSPModel(ACOUSTIC)NoDeepSeams FIPP WPSTDP
SD: 5.0 m
Range: 0.3 km
Depth (m)
-50.0
0.0
50.0
100.0
150.0
200.0
250.0
300.0
350.0
400.0
450.0
500.0
550.0
600.0
650.0
0.0
0.1
0.2
0.3
0.4
0.5
0.6
0.7
0.8
0.9
1.0
Time (seconds)

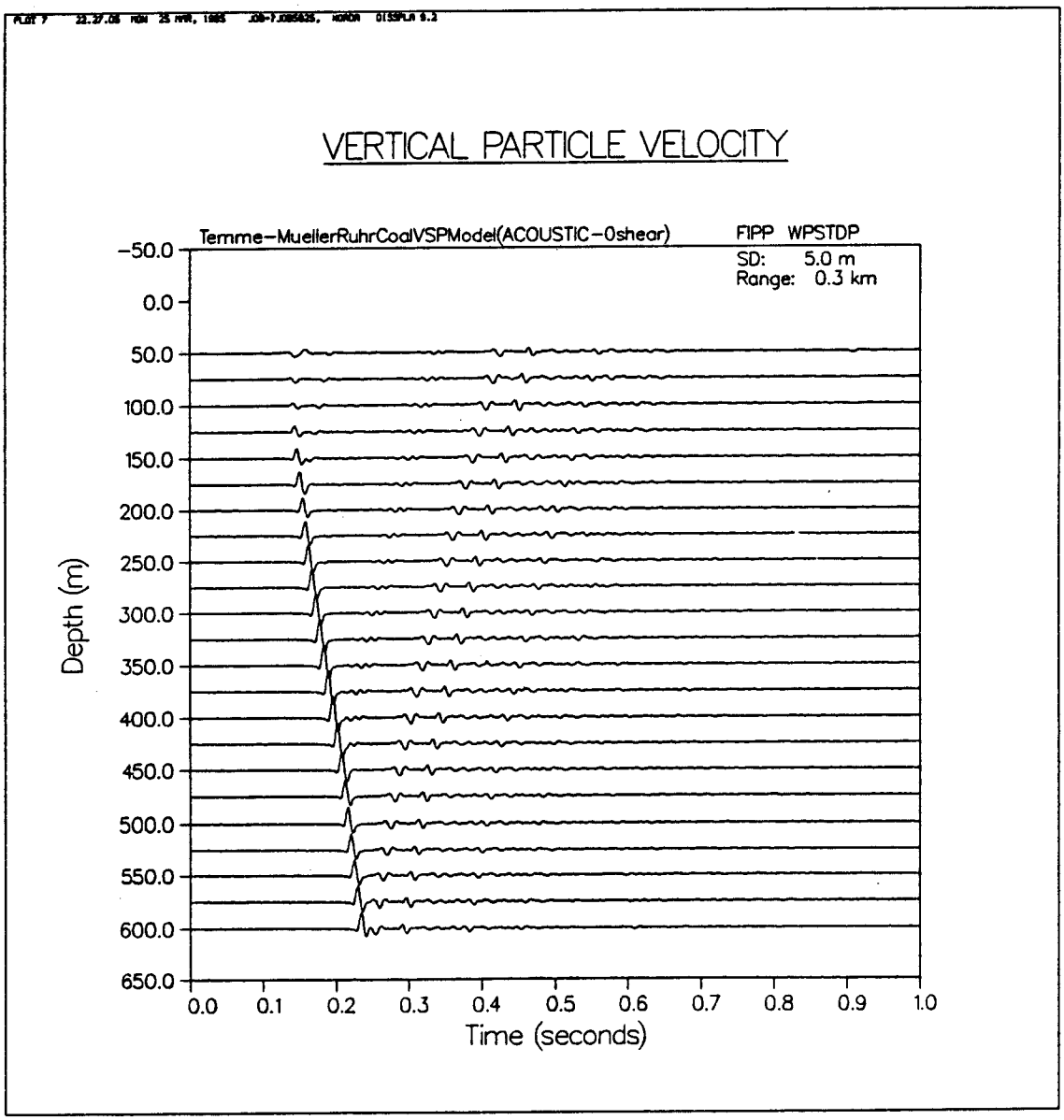
VERTICAL PARTICLE VELOCITY
Temme-MuellerRuhrCoalVSPModel(ACOUSTIC-0shear)
FIPP WPSTDP
SD: 5.0 m
Range: 0.3 km
Depth (m)
-50.0
0.0
50.0
100.0
150.0
200.0
250.0
300.0
350.0
400.0
450.0
500.0
550.0
600.0
650.0
0.0
0.1
0.2
0.3
0.4
0.5
0.6
0.7
0.8
0.9
1.0
Time (seconds)

As expected, for the major primary reflections, the waveforms show a gradual increase in reflexion amplitudes as the geophone approaches each reflexion level of origin. This can be seen, for example, for the intermediate depth events in **Figure 76a.** The very strong surface multiples, by constrast, show an abrupt amplitude change (generally decrease) as the geophone drops below the major reflection interface making up its reverberent system. This is clearly shown in **Figure 76b.** This confirms the expectation that the more reverberent legs of a multiple event are reflected from the upper interface of a two layer system, the greater will be the amplitude decrease when dropping the geophone thru the upper interface. In this regard, the lack of an effect from of the thin hi-velocity beds above the main seam body on generally-strong interbed multiples, as should be seen by the abrupt change in the synthetic VSP response as the geophones are lowered below this event horizon, is suprizing, and clearly shows the overwhelming dominance on the record section of surface-reflected over interbed and pegleg multiples in this particular geomodel.

Because the effects of shortpath intrabed multiples due to finely layered stratigraphy are widely believed to significantly alter the net transmitted waveform in addition to material-specific intrinsic attenuation (MORLET et al, 1982), and because the multiples themselves are often nontrivially difficult to identify and examine, it is problematic to differentiate between the

nature and magnitude of these two loss mechanisms by simple visual inspection alone. Waveform amplitude changes due to attenuation intrinsic to rocks qua frictional absorption are inevitably superposed upon changes in the contributions from shortperiod intrabed multiples (SPENCER et al, 1982), as a function of rock layers qua layered strata. In particular, GAMBURSTSVEJ (1970), O'DOHERTY and ANSTEY (1971), SCHOENBERGER and LEVIN (1974) and SPENCER (1977) have demonstrated that cyclic nondissipative layers ($\alpha \sim 0$) act like low pass filters, increasing rapidly with increased layer thickness the shift of energy from high to lower wavelet frequencies.

From their results, it is thus clear that many downgoing events at later arrival times thruout the VSP section show complexly varying depth dependent amplitudes, from one or more depth-dependent mechanisms, with (as noted above) often abrupt changes in relative amplitude corresponding to transmission across one or more layer interfaces. These cumulative effects become particularly difficult to analyse for the cyclic stratigraphic sequences at greater depths, involving fine scale repitition of low and high velocity (thin) beds ('fine' with respect to the dominant seismic wavelength).

To specifically consider the effects of realistic viscoelastic intrinsic attenuation as may apply to the present geomodel, we assign a nominally high (.1dB/λ) and low (.01dB/λ) constant P wave attenuation to all layers, to obtain the synthetic VSP,

Figure 77

Full wavefield synthetic VSP (plane wave line source) for acoustic-only Temme Muller v/z model, with values of low and high intrinsic attenuation (α_{high}= .1 dB/λ and α_{low}= .01 dB/λ)

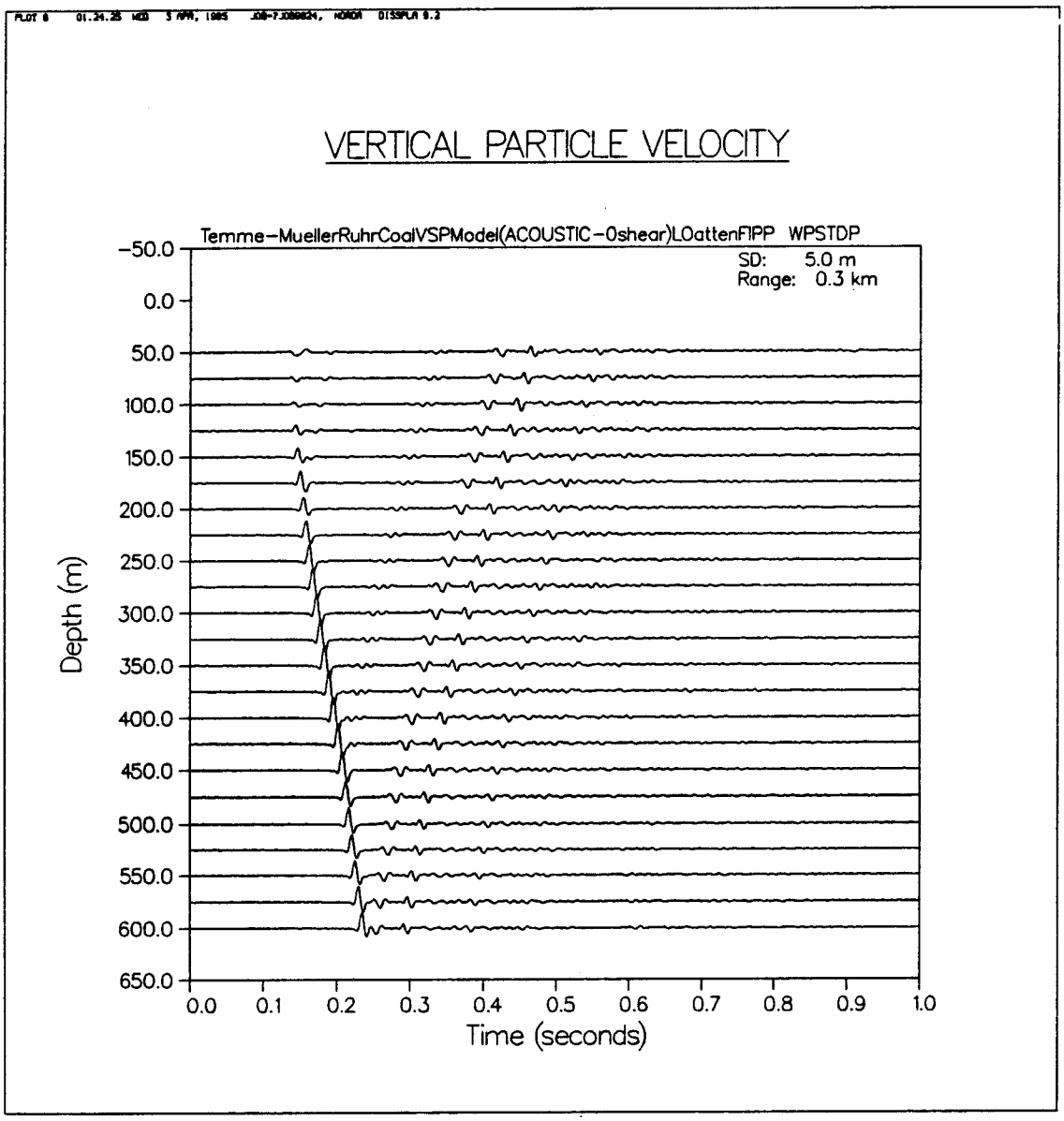
VERTICAL PARTICLE VELOCITY
Temme-MuellerRuhrCoalVSPModel(ACOUSTIC-0shear)L0attenF1PP WPSTDP
SD: 5.0 m
Range: 0.3 km
Depth (m)
-50.0
0.0
50.0
100.0
150.0
200.0
250.0
300.0
350.0
400.0
450.0
500.0
550.0
600.0
650.0
0.0
0.1
0.2
0.3
0.4
0.5
0.6
0.7
0.8
0.9
1.0
Time (seconds)

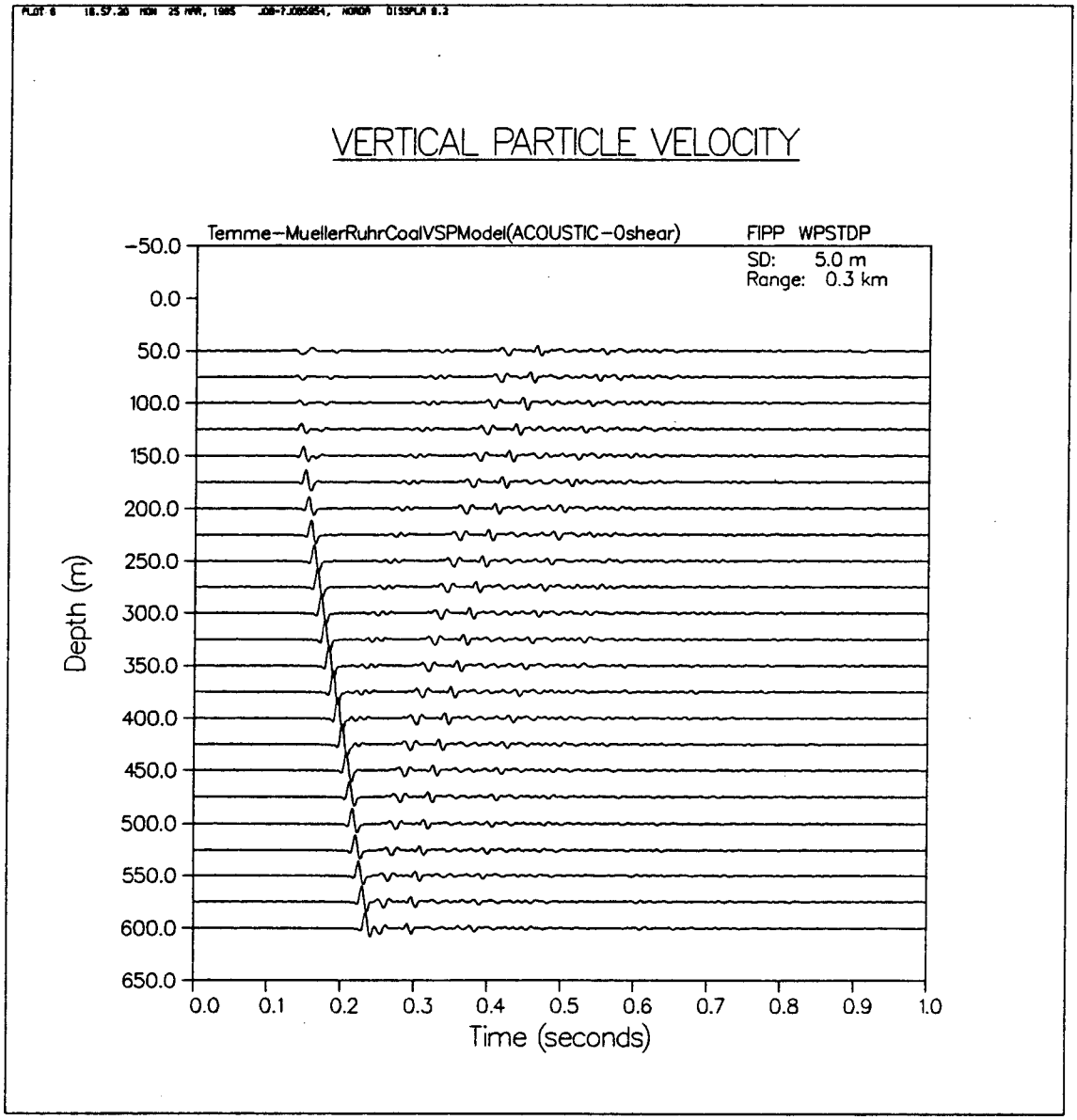
VERTICAL PARTICLE VELOCITY
Temme-MuellerRuhrCoalVSPModel(ACOUSTIC-0shear)
FIPP WPSTDP
SD: 5.0 m
Range: 0.3 km
Depth (m)
-50.0
0.0
50.0
100.0
150.0
200.0
250.0
300.0
350.0
400.0
450.0
500.0
550.0
600.0
650.0
0.0
0.1
0.2
0.3
0.4
0.5
0.6
0.7
0.8
0.9
1.0
Time (seconds)

shown in **Figure 77a** and **b**. Here it is obvious that all wave amplitudes are not strongly attenuated compared to those in the previous low-α model. Some small degree of accompanying frequency-dependent dispersion can be seen qua a changed wavelet width for deeper and/or multiply-reflected events. However, although the previously disturbing "ringing" noise from multiple reflections in the nearsurface is almost entirely unaffected as still strongly in evidence, it is also true that all deeper primary events from seams greater than 600 m are not more plainly visible than previously. As a final investigation of shortperiod multiple effects on net wavelet shape (preservation of primary amplitudes despite instrinsic attenuation) using the present modeling algorithm, since it is not currently possible to decouple primary and multiple orders in the fullwavefield solution, it is necessary to effectively vary the magnitude of multiple contributions by varying the number and thickness of cyclic strata. The results of replacing the first major high-velocity seam with a seismically-equivalent cyclic stack of alternating high and low velocity layers is given in **Figure 78.** We note that the present example constitutes only the briefest examination of the difficult subject of attenuation measurement via VSP (SPENCER, 1982; References in TOKZSOZ and STEWART, 1984).

Figure 78

Velocity-depth model (variation of Temme-Muller acoustic only) and corresponding synthetic VSP (plane wave line source), x_{offset} = .3km, with 1st major deep coal seam replaced by a 'seismically-equivalent' cyclic sequence of thin alternating high and low velocity layers

VERTICAL PARTICLE VELOCITY

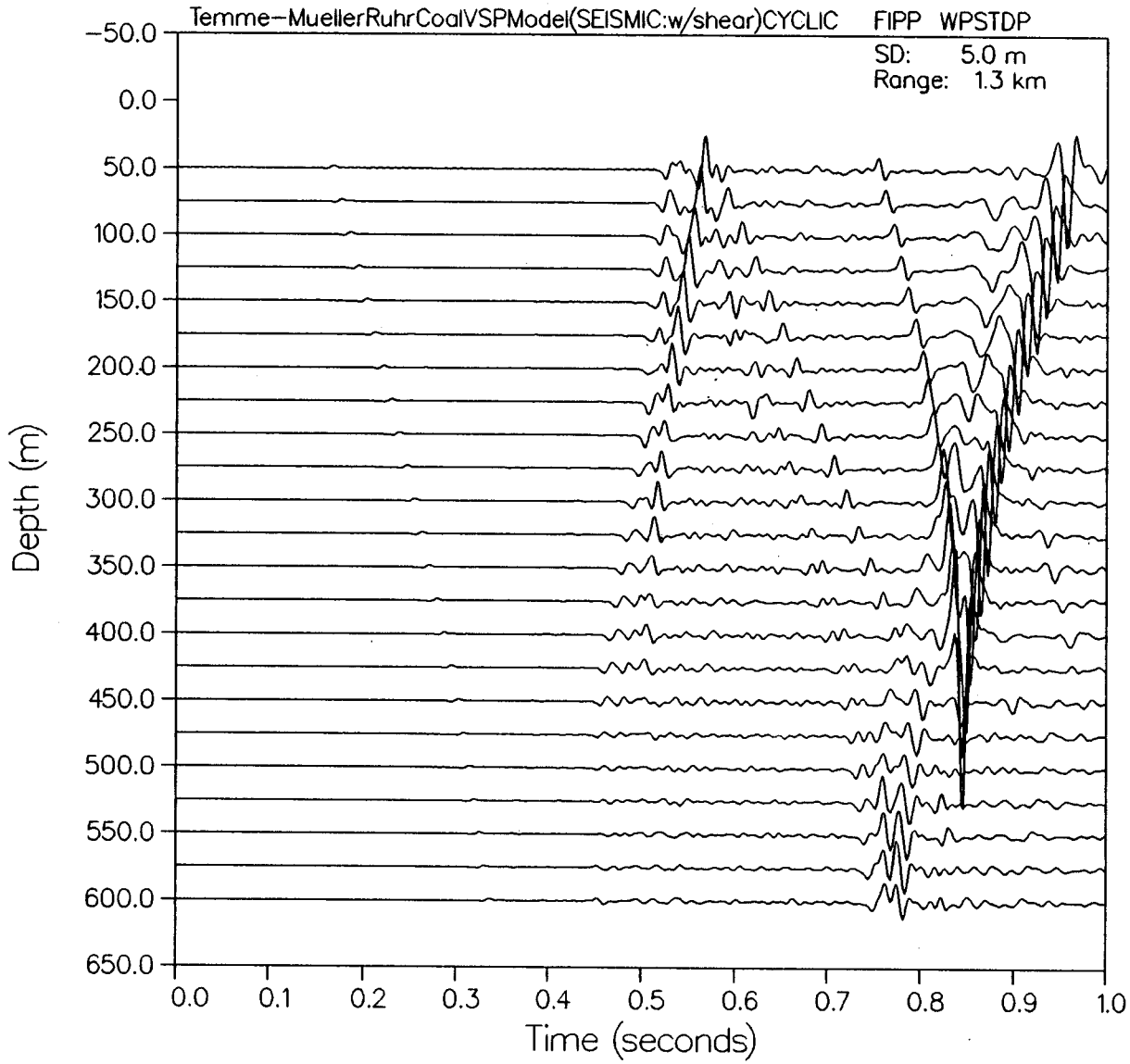

VERTICAL PARTICLE VELOCITY

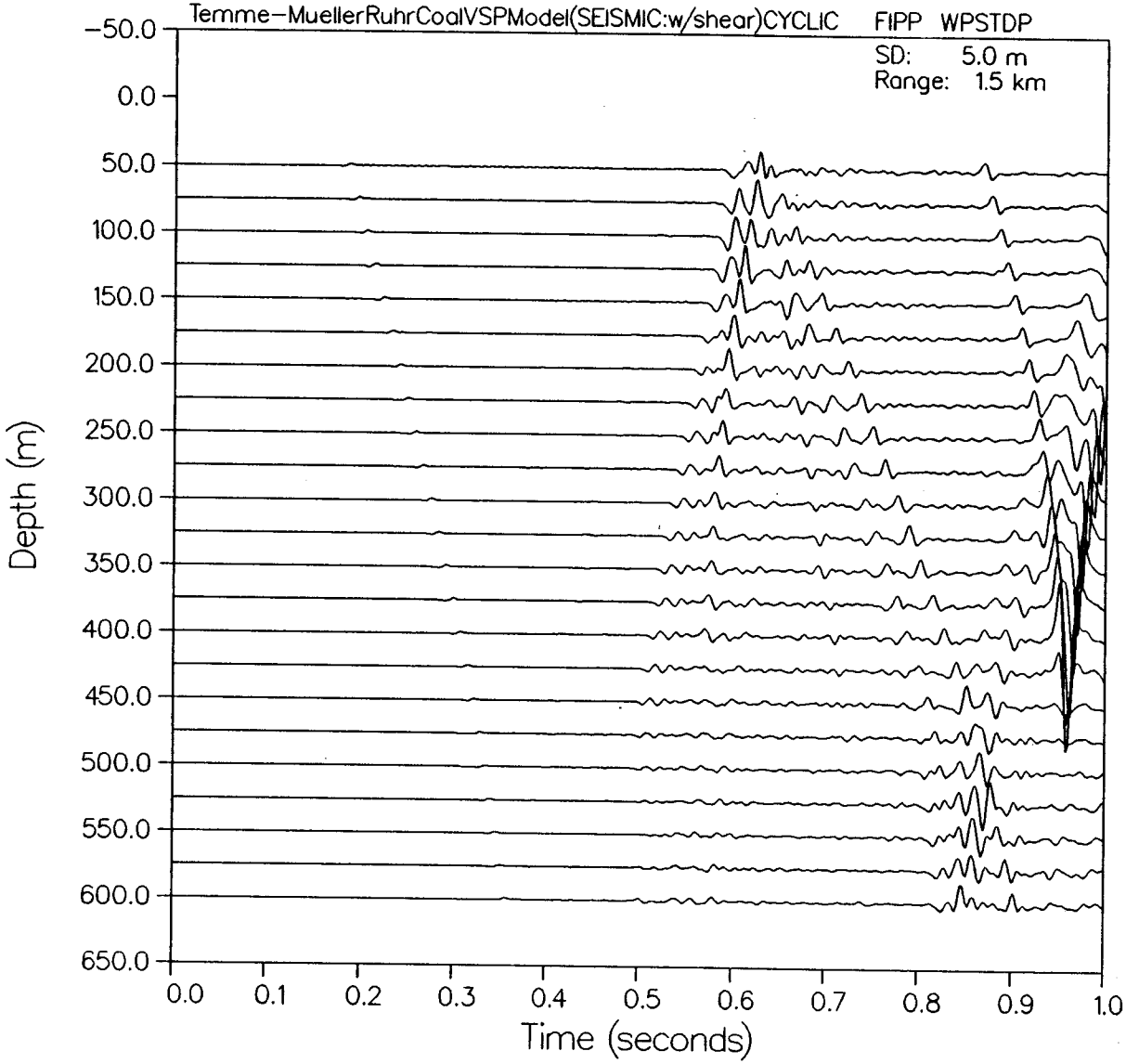

VERTICAL PARTICLE VELOCITY

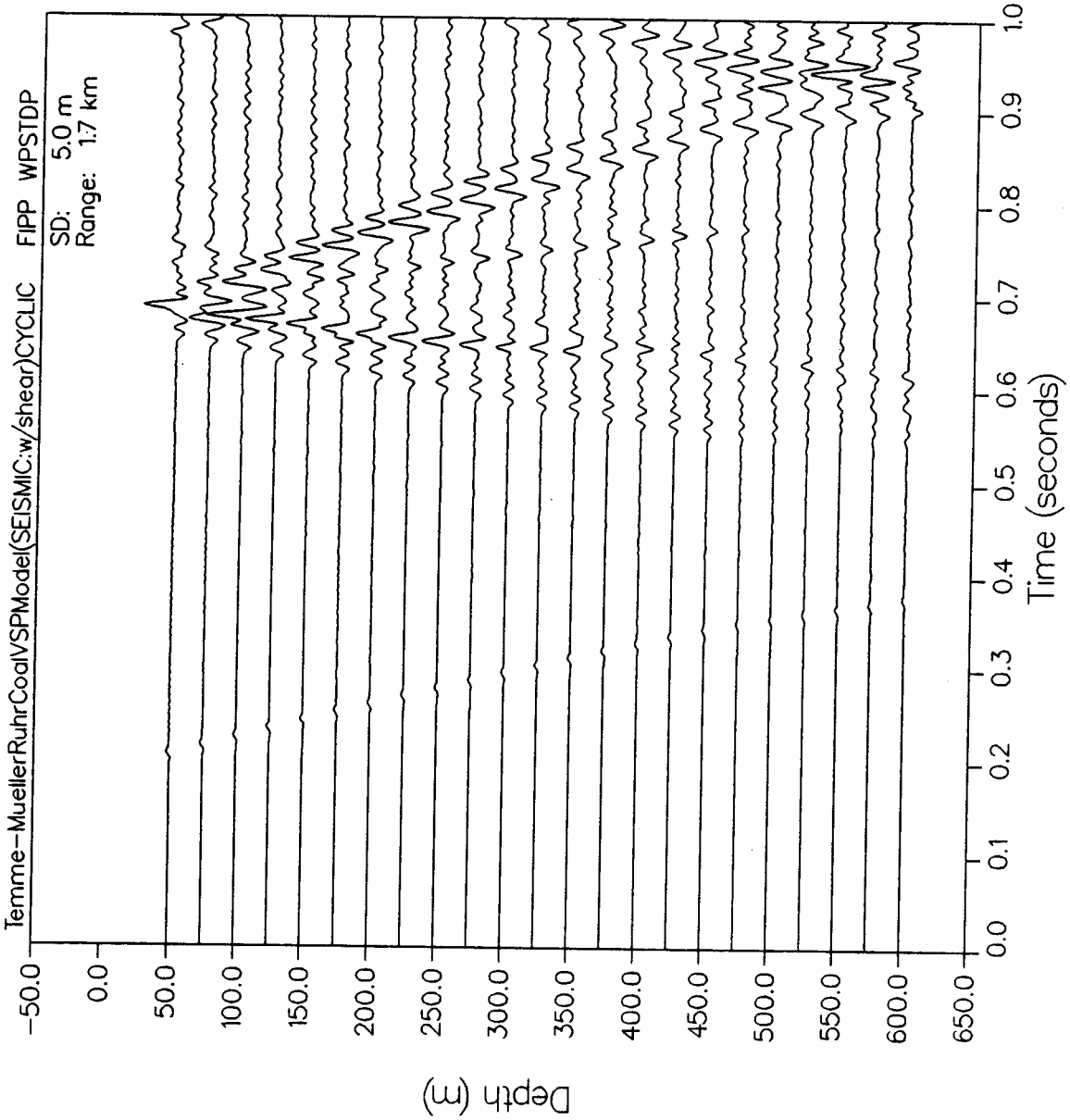

VERTICAL PARTICLE VELOCITY

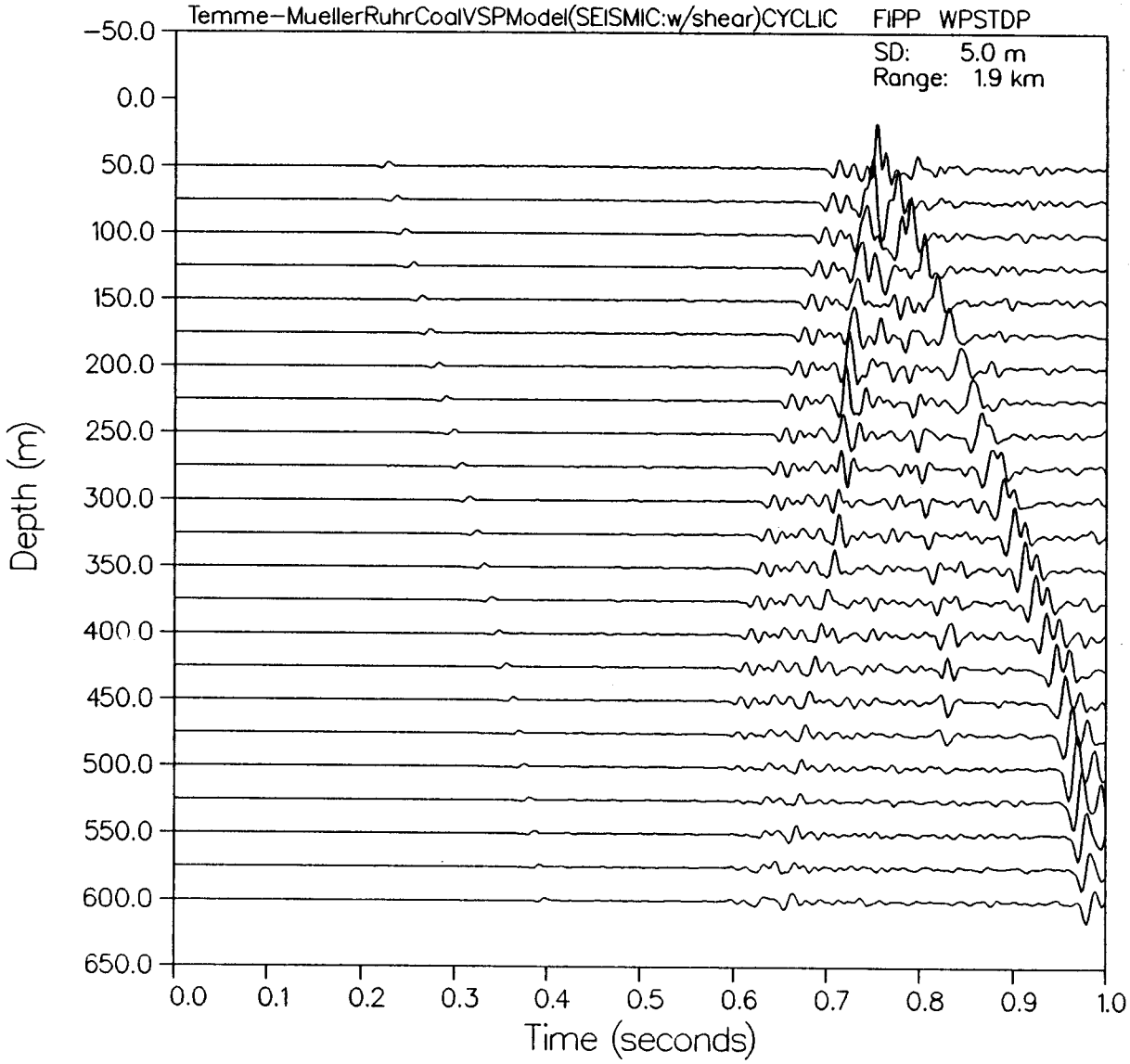

Figure 79

Synthetic full wavefield VSP (plane wave line source) for acoustic-only Temme-Muller v/z model, over a range of increasing source-receiver offsets:

x = .1km
.3km
.5km
.7km
.9km
1.1km
1.3km
1.5km
1.7km

demonstrating maximum compressional wave amplitude enhancement from successively deeper horizons with progressively larger offsets (includes P head wave effects)

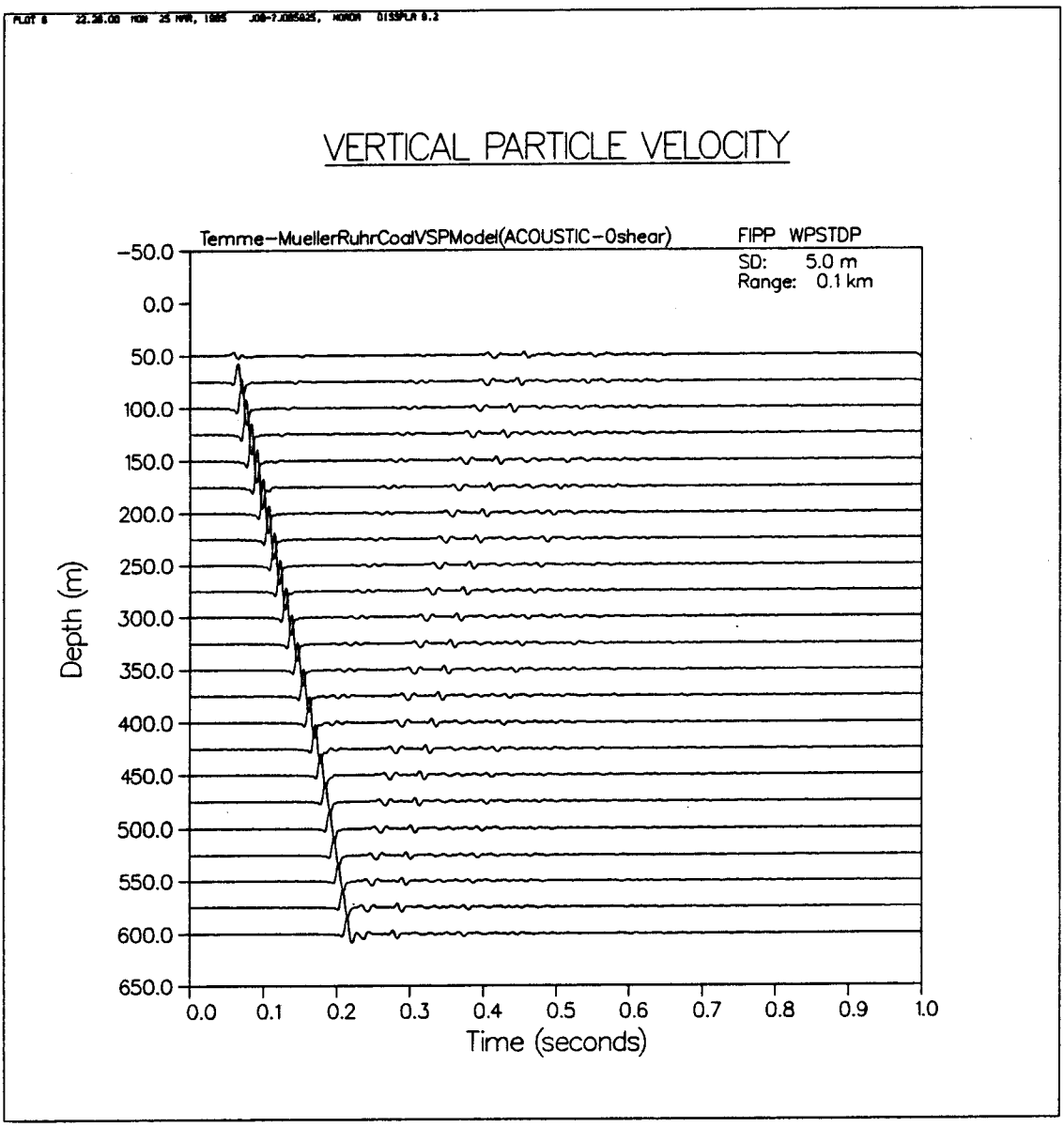
VERTICAL PARTICLE VELOCITY
Temme-MuellerRuhrCoalVSPModel(ACOUSTIC-0shear)
FIPP WPSTDP
SD: 5.0 m
Range: 0.1 km
Depth (m)
-50.0
0.0
50.0
100.0
150.0
200.0
250.0
300.0
350.0
400.0
450.0
500.0
550.0
600.0
650.0
0.0
0.1
0.2
0.3
0.4
0.5
0.6
0.7
0.8
0.9
1.0
Time (seconds)

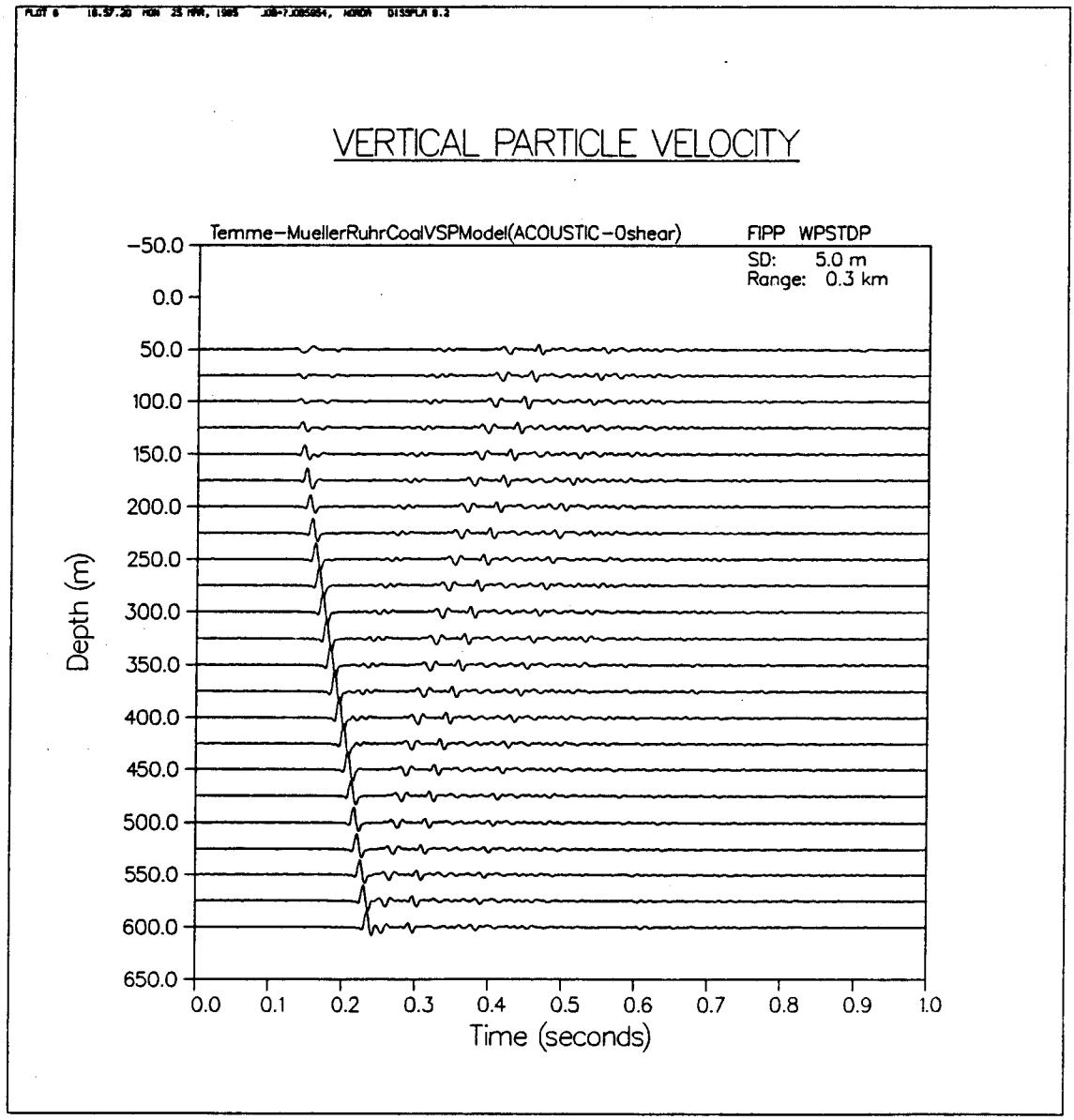
VERTICAL PARTICLE VELOCITY
Temme-MuellerRuhrCoalVSPModel(ACOUSTIC-0shear)
FIPP WPSTDP
SD: 5.0 m
Range: 0.3 km
Depth (m)
-50.0
0.0
50.0
100.0
150.0
200.0
250.0
300.0
350.0
400.0
450.0
500.0
550.0
600.0
650.0
0.0
0.1
0.2
0.3
0.4
0.5
0.6
0.7
0.8
0.9
1.0
Time (seconds)

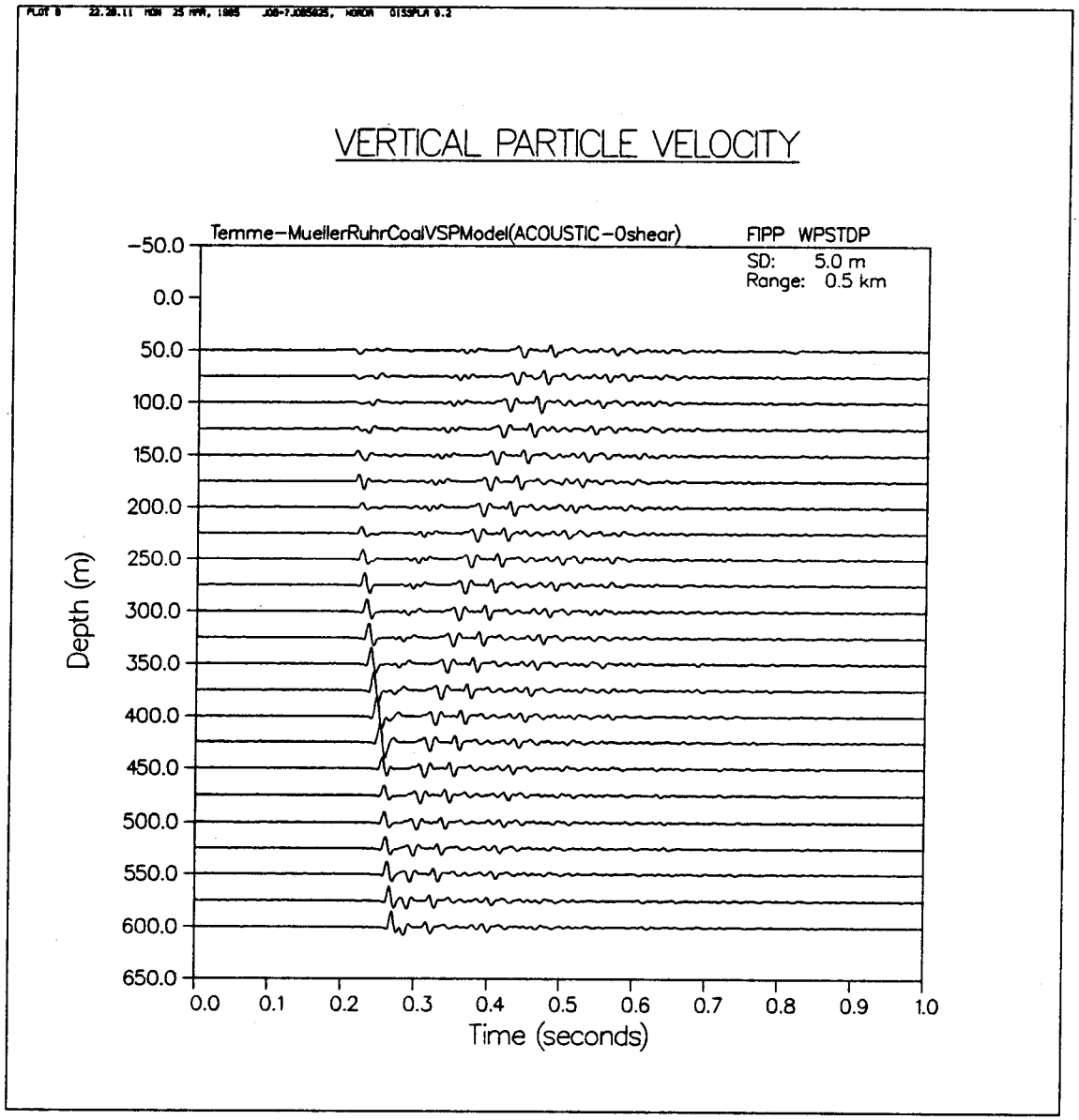
VERTICAL PARTICLE VELOCITY
Temme-MuellerRuhrCoalVSPModel(ACOUSTIC-0shear)
FIPP WPSTDP
SD: 5.0 m
Range: 0.5 km
Depth (m)
-50.0
0.0
50.0
100.0
150.0
200.0
250.0
300.0
350.0
400.0
450.0
500.0
550.0
600.0
650.0
0.0
0.1
0.2
0.3
0.4
0.5
0.6
0.7
0.8
0.9
1.0
Time (seconds)

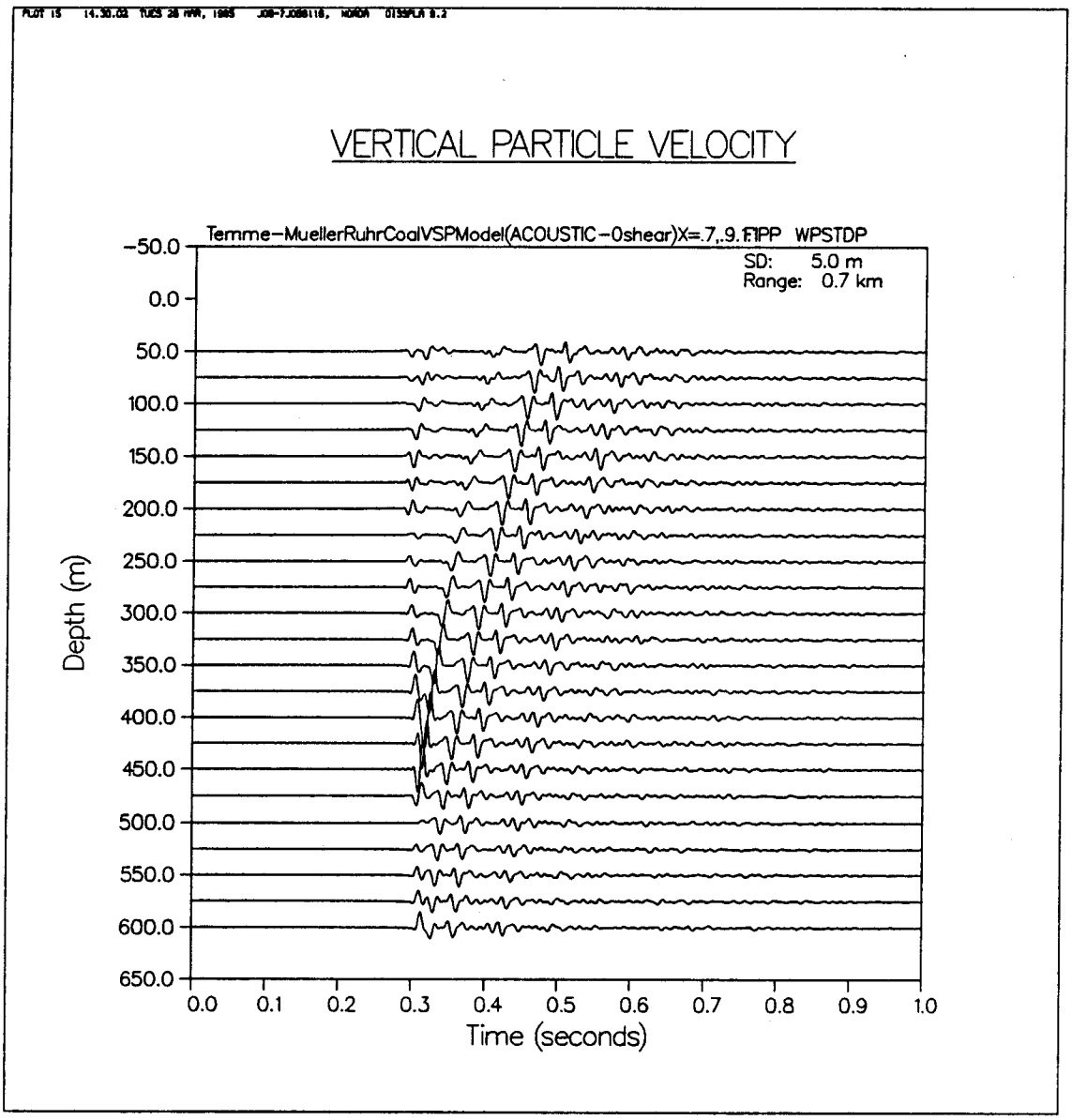
VERTICAL PARTICLE VELOCITY
Temme-MuellerRuhrCoalVSPModel(ACOUSTIC-0shear)X=.7,.9.1.1PP WPSTDP
SD: 5.0 m
Range: 0.7 km
Depth (m)
-50.0
0.0
50.0
100.0
150.0
200.0
250.0
300.0
350.0
400.0
450.0
500.0
550.0
600.0
650.0
0.0
0.1
0.2
0.3
0.4
0.5
0.6
0.7
0.8
0.9
1.0
Time (seconds)

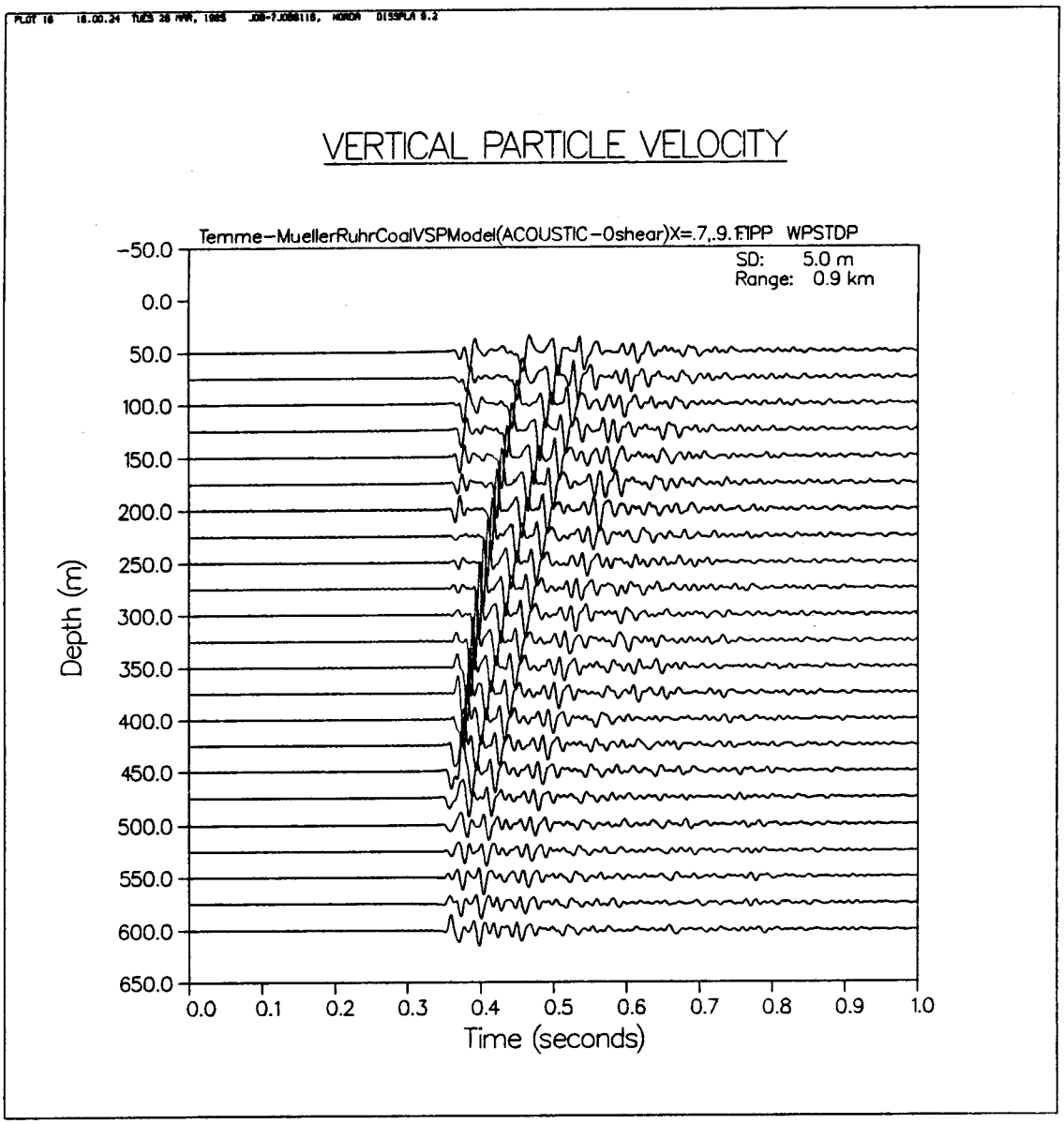
VERTICAL PARTICLE VELOCITY
Temme-MuellerRuhrCoalVSPModel(ACOUSTIC-0shear)X=.7,.9.EIPP WPSTDP
SD: 5.0 m
Range: 0.9 km
Depth (m)
-50.0
0.0
50.0
100.0
150.0
200.0
250.0
300.0
350.0
400.0
450.0
500.0
550.0
600.0
650.0
0.0
0.1
0.2
0.3
0.4
0.5
0.6
0.7
0.8
0.9
1.0
Time (seconds)

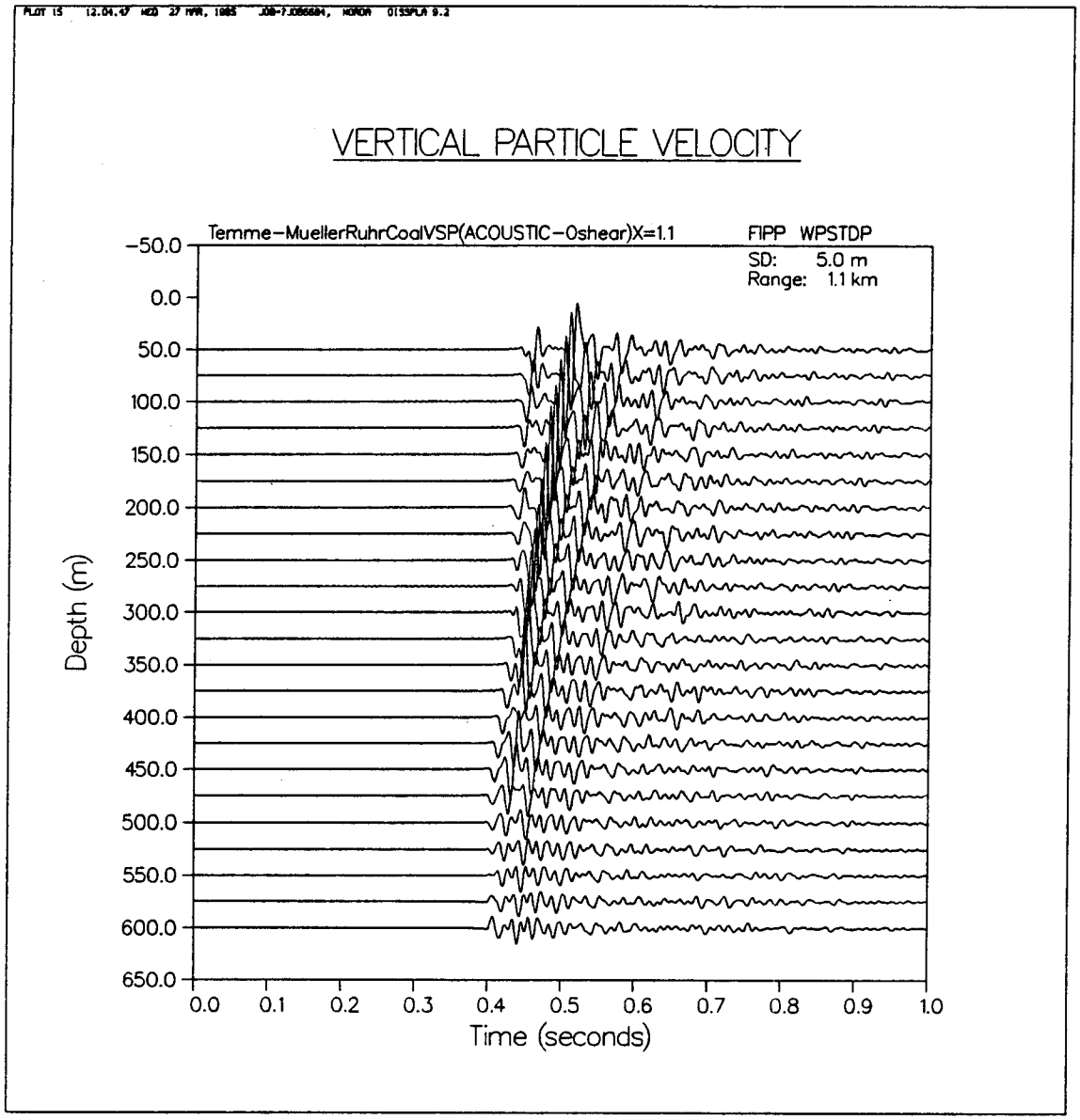
VERTICAL PARTICLE VELOCITY
Temme-MuellerRuhrCoalVSP(ACOUSTIC-0shear)X=1.1
FIPP WPSTDP
SD: 5.0 m
Range: 1.1 km
Depth (m)
-50.0
0.0
50.0
100.0
150.0
200.0
250.0
300.0
350.0
400.0
450.0
500.0
550.0
600.0
650.0
0.0
0.1
0.2
0.3
0.4
0.5
0.6
0.7
0.8
0.9
1.0
Time (seconds)

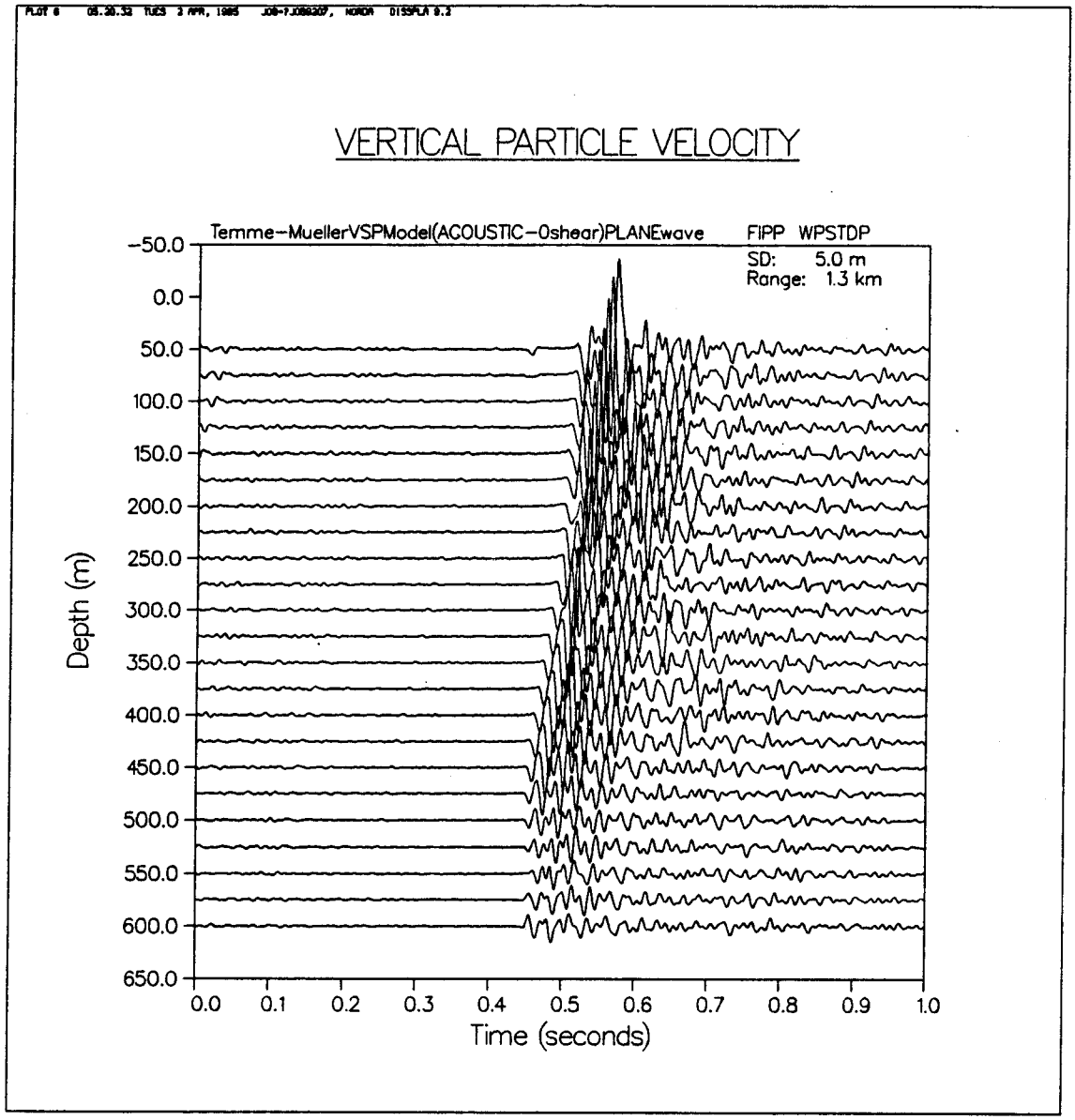
VERTICAL PARTICLE VELOCITY
Temme-MuellerVSPModel(ACOUSTIC-0shear)PLANEwave
FIPP WPSTDP
SD: 5.0 m
Range: 1.3 km
Depth (m)
-50.0
0.0
50.0
100.0
150.0
200.0
250.0
300.0
350.0
400.0
450.0
500.0
550.0
600.0
650.0
0.0
0.1
0.2
0.3
0.4
0.5
0.6
0.7
0.8
0.9
1.0
Time (seconds)

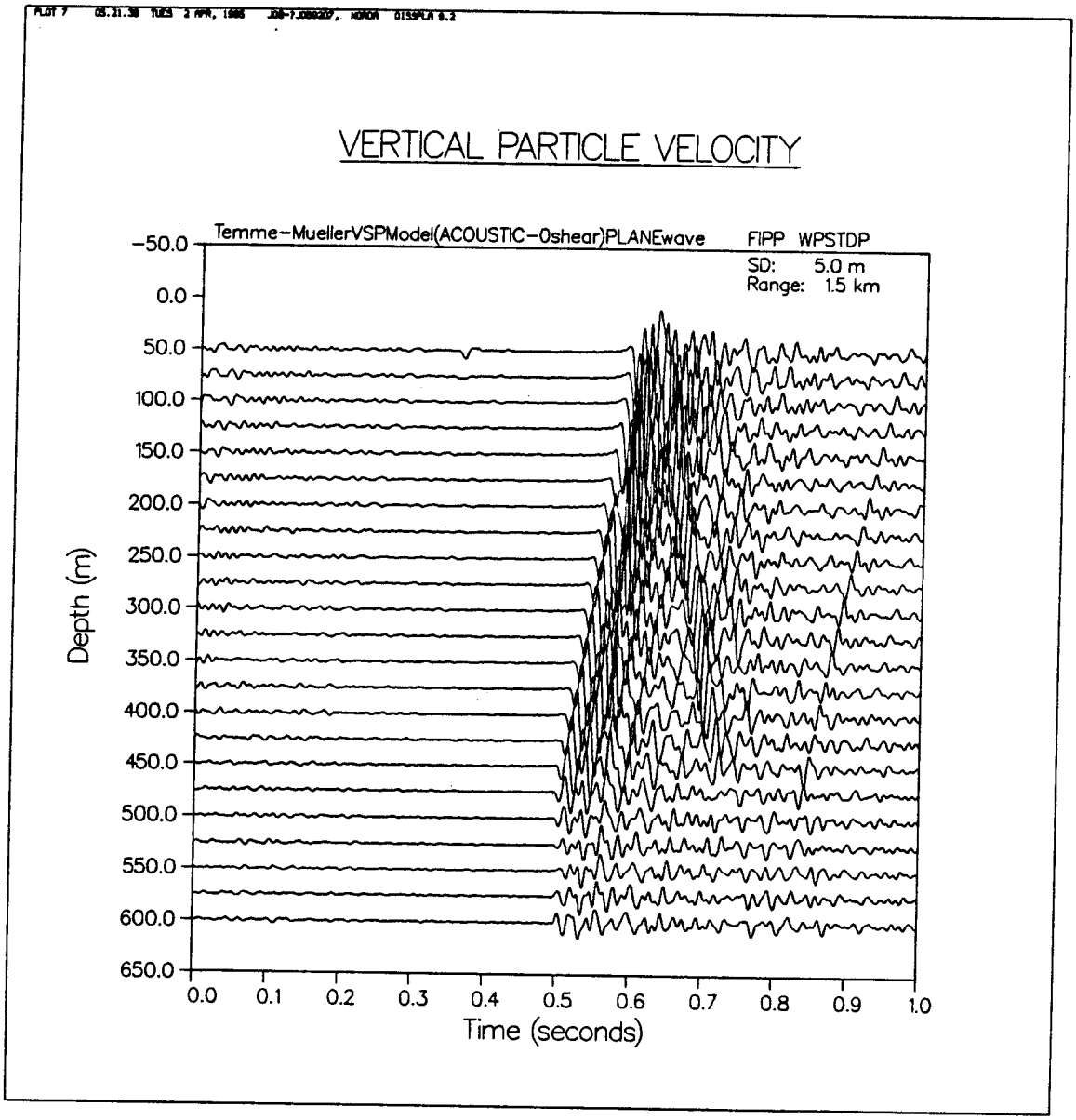
VERTICAL PARTICLE VELOCITY
Temme-MuellerVSPModel(ACOUSTIC-0shear)PLANEwave
FIPP WPSTDP
SD: 5.0 m
Range: 1.5 km
Depth (m)
-50.0
0.0
50.0
100.0
150.0
200.0
250.0
300.0
350.0
400.0
450.0
500.0
550.0
600.0
650.0
0.0
0.1
0.2
0.3
0.4
0.5
0.6
0.7
0.8
0.9
1.0
Time (seconds)

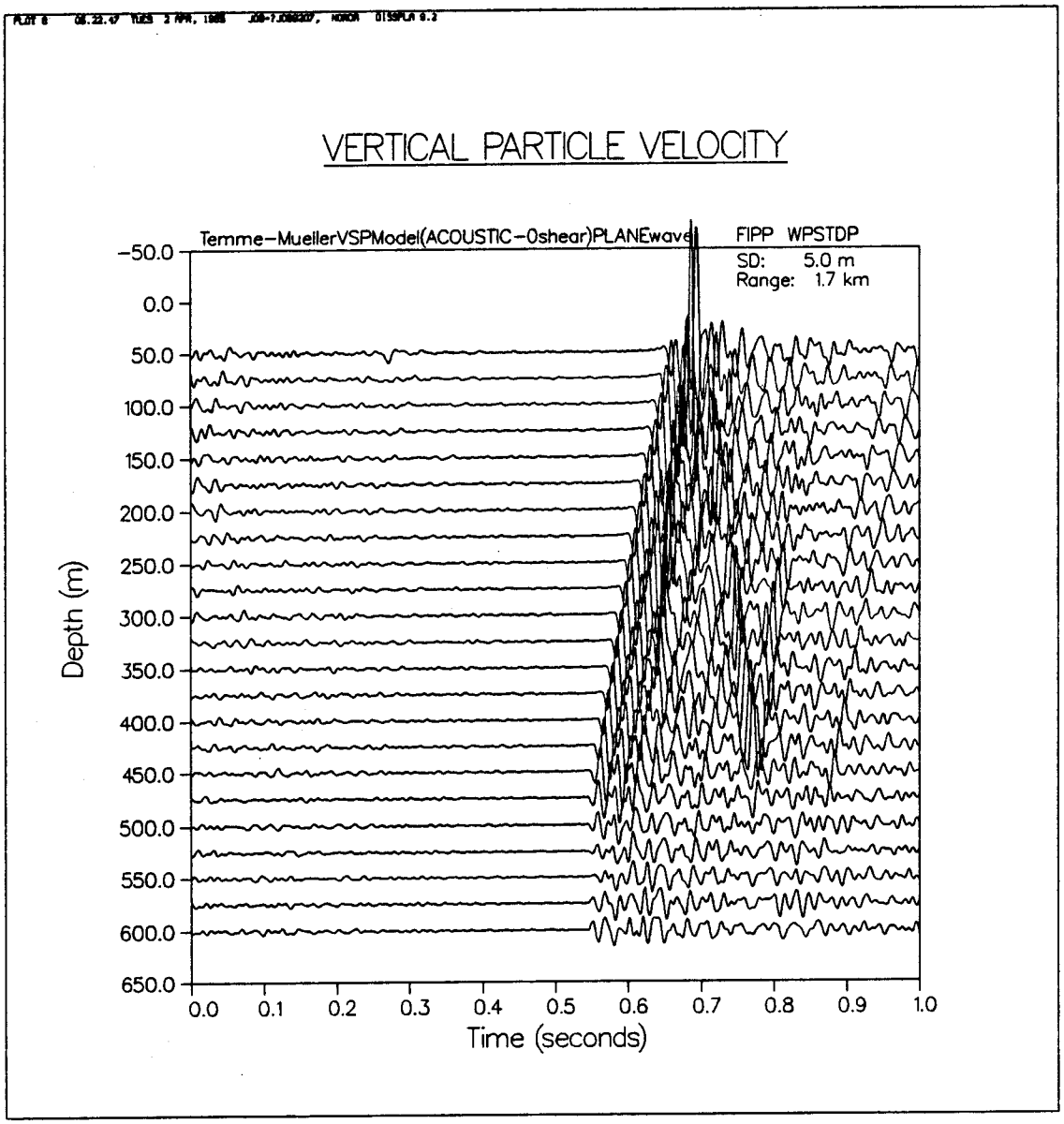
VERTICAL PARTICLE VELOCITY
Temme-MuellerVSPModel(ACOUSTIC-0shear)PLANEwave
FIPP WPSTDP
SD: 5.0 m
Range: 1.7 km
Depth (m)
-50.0
0.0
50.0
100.0
150.0
200.0
250.0
300.0
350.0
400.0
450.0
500.0
550.0
600.0
650.0
0.0
0.1
0.2
0.3
0.4
0.5
0.6
0.7
0.8
0.9
1.0
Time (seconds)

Having briefly considered some of the effects of receiver location with respect to multiple reverberation effects, **Figure 79a-d** shows the synthetic VSP for the same (acoustic-only) model as above, for a suite of successively increasing source-receiver offsets (from x=.1km to x=1.7km), to examine the effects of angle-dependent reflection coefficient strengths as well as refraction head wave generation. In the case of increasing incident angles with respect to the major deep seam reflecting layers, reflection amplitudes increase as expected. Events from greater depths become especially prominent at the later arrival times, but the first arrival curve becomes progressively more complicated as (e.g.) refractions from the uppermost layers overtake the direct wave at larger offsets.

In the present acoustic-only earth model (no shear), for geophones traversing a relatively low velocity zone just above a high velocity formation, refracted head waves can arrive at the geophone before direct P waves. This manifests itself as an apparent "cusp" of generally small amplitude in the first arrival curve for far-offset VSPs. As KANESTROEM (1982) has recently discussed, at offset distances large compared to the depth of boundaries of interest, head and critically refracted waves will be in evidence even from relatively thin layers with respect to the dominant seismic wavelength. Likewise, for geophones positioned within the higher velocity sections, refraction effects can also lead to additional timing inversions of direct

arrivals, wherein direct arrivals may reach deeper geophones before arriving at shallow receivers. Other examples of such complex VSPs are given by GAL'PERIN (1973), and correspond to the traveltime cusp noted above. (The noise type arrivals ahead of the true first arrival curve for the VSPs shown below, at very far offsets of 1.3, 1.5 and 1.7km, are due to wraparound aliasing, which would require an extremely wide time window/larger number of time sample points (NT>8192) to be entirely avoided).

For general multilayered media, it is necessary to determine the maximum lateral distance the source may be placed from a given downhole geophone before refracted head wave arrivals precede the direct arrival. Although experience with VSP has shown that velocity in general increases with depth, this is obviously not always the case. In this event, since the critical distance is a function of both depth and velocity of the layer(s) in question, the critical source offset distance can be smaller for deeper layers of lesser velocity, and thus not necessarily increase for layers at increasing depth.

These refraction effects are shown graphically in the last 3 panels of the previous Figure 79. This shows the synthetic VSP computed for source-receiver offsets greater than critical distance for the deepest seam reflector of interest. Because the seam model here is not comprised of a small number of uniform layers but instead a relatively large number of thin components,

only very low intensity head waves are observed. However, as the thickness of the bottommost high-velocity (refracting) layer of interest is increased, the intensity of the resultant head wave increases. This is shown in **Figure 80**, where the thickness of the 1st seam layer is increased, and the corresponding strong head wave arrival identified by its characteristically curved travelpath with respect to reflected and direct arrivals. In this model, at very large (supercritical) offsets, it is also possible that transcritically reflected waves closely approach the first arrival curve and/or interfere with the first curved-path refractions and direct first arrivals. Other than the limited survey given by GAL'PERIN (1973) almost nothing in the seismologic or exploration literature has been presented on the recording and analysis of transcritical arrivals on VSPs. The implications of far-offset refractions and reflections on the VSP record requires additional investigation, and is the object of current research in both exploration (HARDAGE, 1984, personal communication) and underwater sensing (MOSELEY, 1985, personal communication) endeavours.

Figure 80

Full wavefield synthetic VSP (plane wave line source) for acoustic-only Temme-Muller v/z model, with increased thickness and velocity contrast of 1st major deep seam (z_{seam}=720m)

VERTICAL PARTICLE VELOCITY

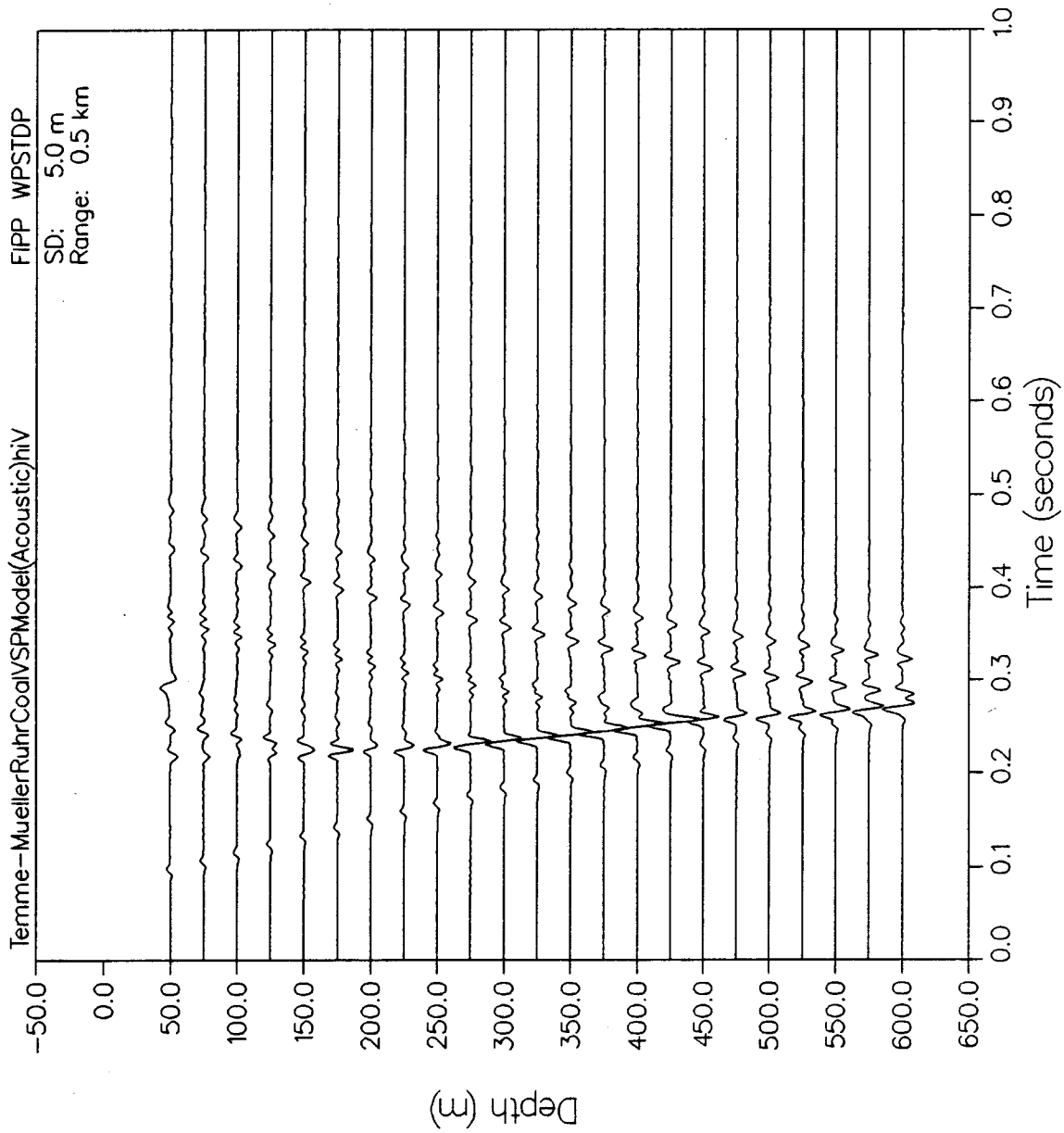

VERTICAL PARTICLE VELOCITY

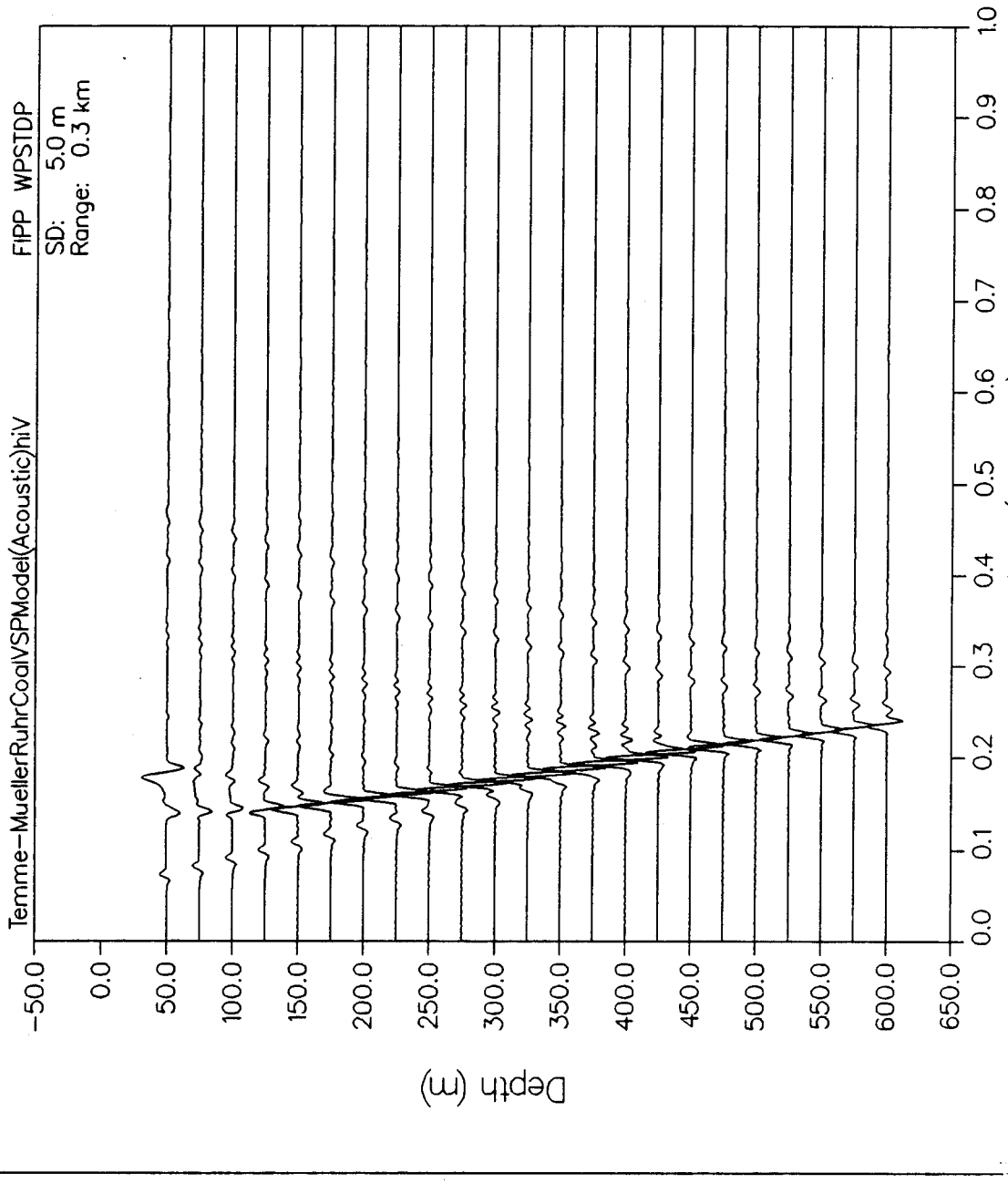

In the final model considered here, formulated to most closely approach realistic seismic propagation, **Figure** 81, show the synthetic VSPs resulting from a solid earth model now including both shear velocity and attenuation, computed over a range of nearfield and post critical offsets.

As can be seen when comparing the previous figures (for acoustic medium) with **Figure** 81 (for solid) medium, at small offsets, shear contributions even from shallow layers are comparatively small. In the present v/z model and small number of closely spaced receivers distributed over a small depth, the angle of incidence of the direct wave on the boundaries of conversion varies only within very narrow limits. For registration of converted reflections or refractions along lower depth intervals, the angle of incidence of the P wave varies by only a few degrees. Likewise, for the SV wave-which has a smaller velocity and hence a smaller critical refraction distance-for such a small angular variation, coefficients of refraction and reflection vary smoothly and here only insignificantly. This can also be seen by examining the plane wave reflection loss curves computed by "SAFARI" for the TEMME-MULLER v/z model (**Figure** 82).

However, the comparative results above dramatically show that the downgoing P-SV converted mode arrival in fact dominates the VSP record section relative to the original P wave arrival, even at nominally greater field acquisition S-R offset ranges beyond

Figure 81

Full wavefield synthetic VSP (plane wave line source) for full shear elastic Temme-Muller v/z model, over a range of source-receiver offsets:

x =.1km
=.3km
=.5km
=.7km
=.9km
=1.1km

demonstrating increased P to Sv mode conversion from localized layers with increased offset

Figure 81

Full wavefield synthetic VSP (plane wave line source) for full shear elastic Temme-Muller v/z model, over a range of source-receiver offsets:

x =.1km
=.3km
=.5km
=.7km
=.9km
=1.1km

demonstrating increased P to Sv mode conversion from localized layers with increased offset

Figure 81

Full wavefield synthetic VSP (plane wave line source) for full shear elastic Temme-Muller v/z model, over a range of source-receiver offsets:

x =.1km
=.3km
=.5km
=.7km
=.9km
=1.1km

demonstrating increased P to Sv mode conversion from localized layers with increased offset

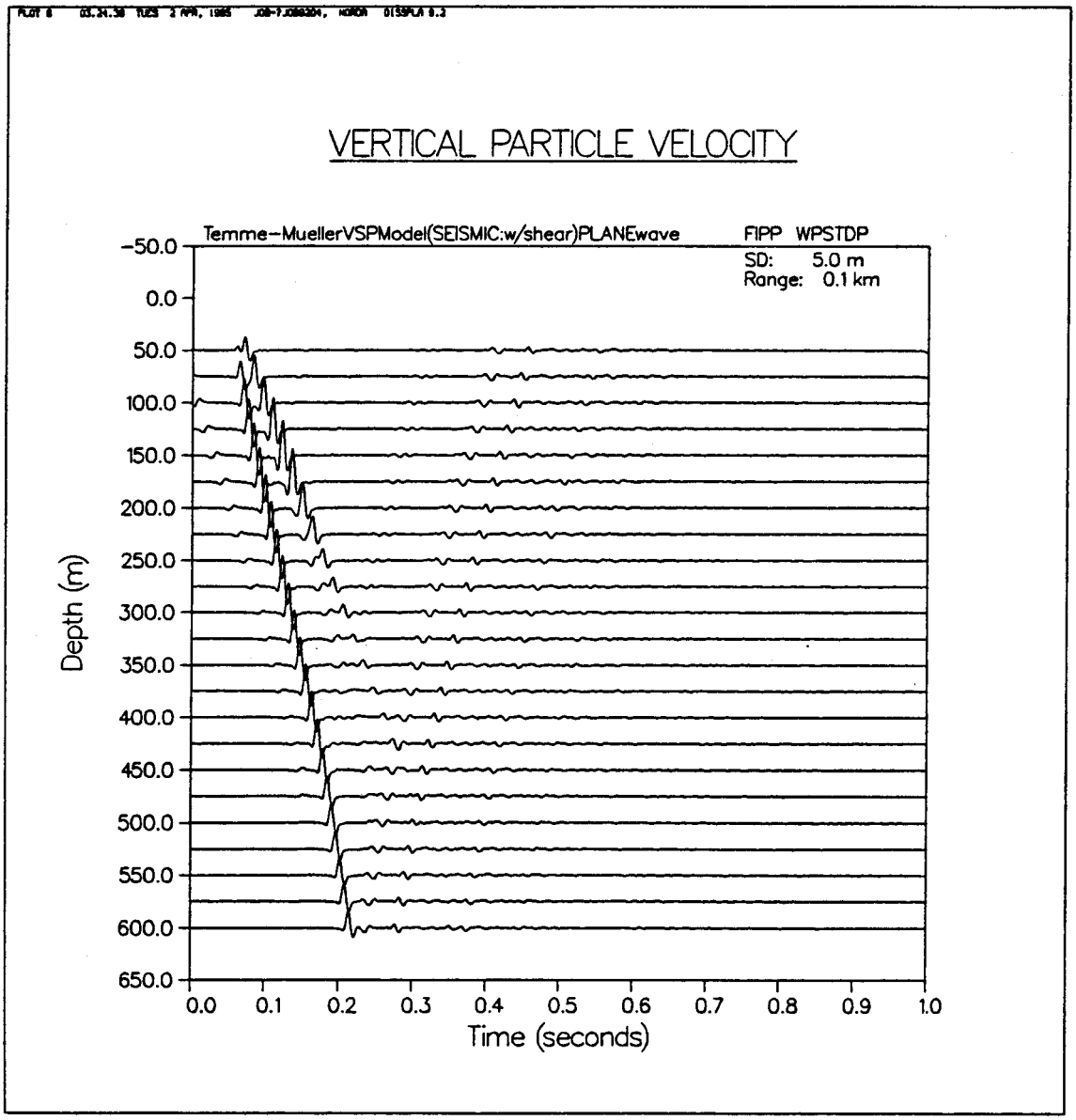
VERTICAL PARTICLE VELOCITY
Temme-MuellerVSPModel(SEISMIC:w/shear)PLANEwave
FIPP WPSTDP
SD: 5.0 m
Range: 0.1 km
Depth (m)
-50.0
0.0
50.0
100.0
150.0
200.0
250.0
300.0
350.0
400.0
450.0
500.0
550.0
600.0
650.0
0.0
0.1
0.2
0.3
0.4
0.5
0.6
0.7
0.8
0.9
1.0
Time (seconds)

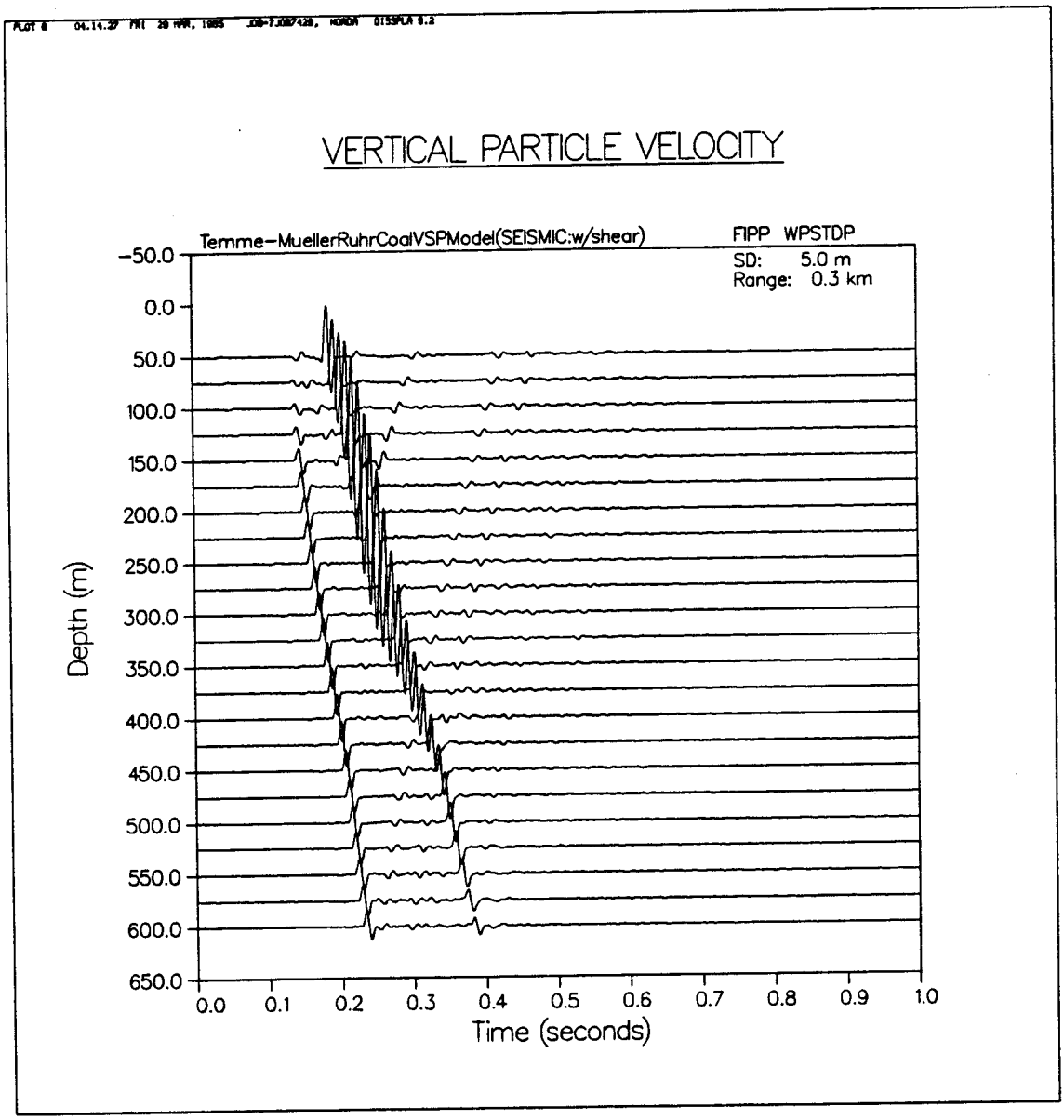
VERTICAL PARTICLE VELOCITY
Temme-MuellerRuhrCoalVSPModel(SEISMIC:w/shear)
FIPP WPSTDP
SD: 5.0 m
Range: 0.3 km
Depth (m)
-50.0
0.0
50.0
100.0
150.0
200.0
250.0
300.0
350.0
400.0
450.0
500.0
550.0
600.0
650.0
0.0
0.1
0.2
0.3
0.4
0.5
0.6
0.7
0.8
0.9
1.0
Time (seconds)

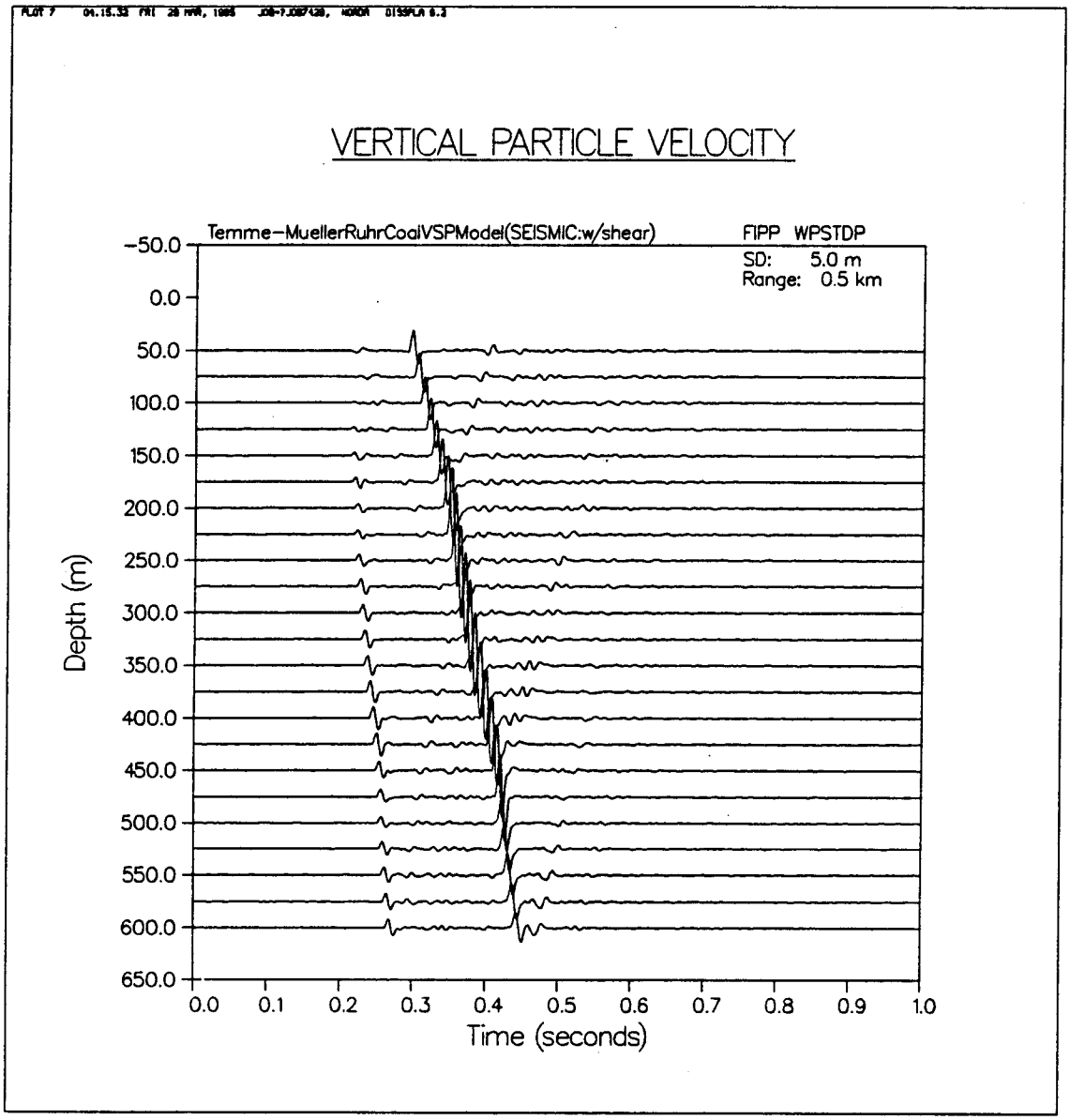
VERTICAL PARTICLE VELOCITY
Temme-MuellerRuhrCoalVSPModel(SEISMIC:w/shear)
FIPP WPSTDP
SD: 5.0 m
Range: 0.5 km
Depth (m)
-50.0
0.0
50.0
100.0
150.0
200.0
250.0
300.0
350.0
400.0
450.0
500.0
550.0
600.0
650.0
0.0
0.1
0.2
0.3
0.4
0.5
0.6
0.7
0.8
0.9
1.0
Time (seconds)

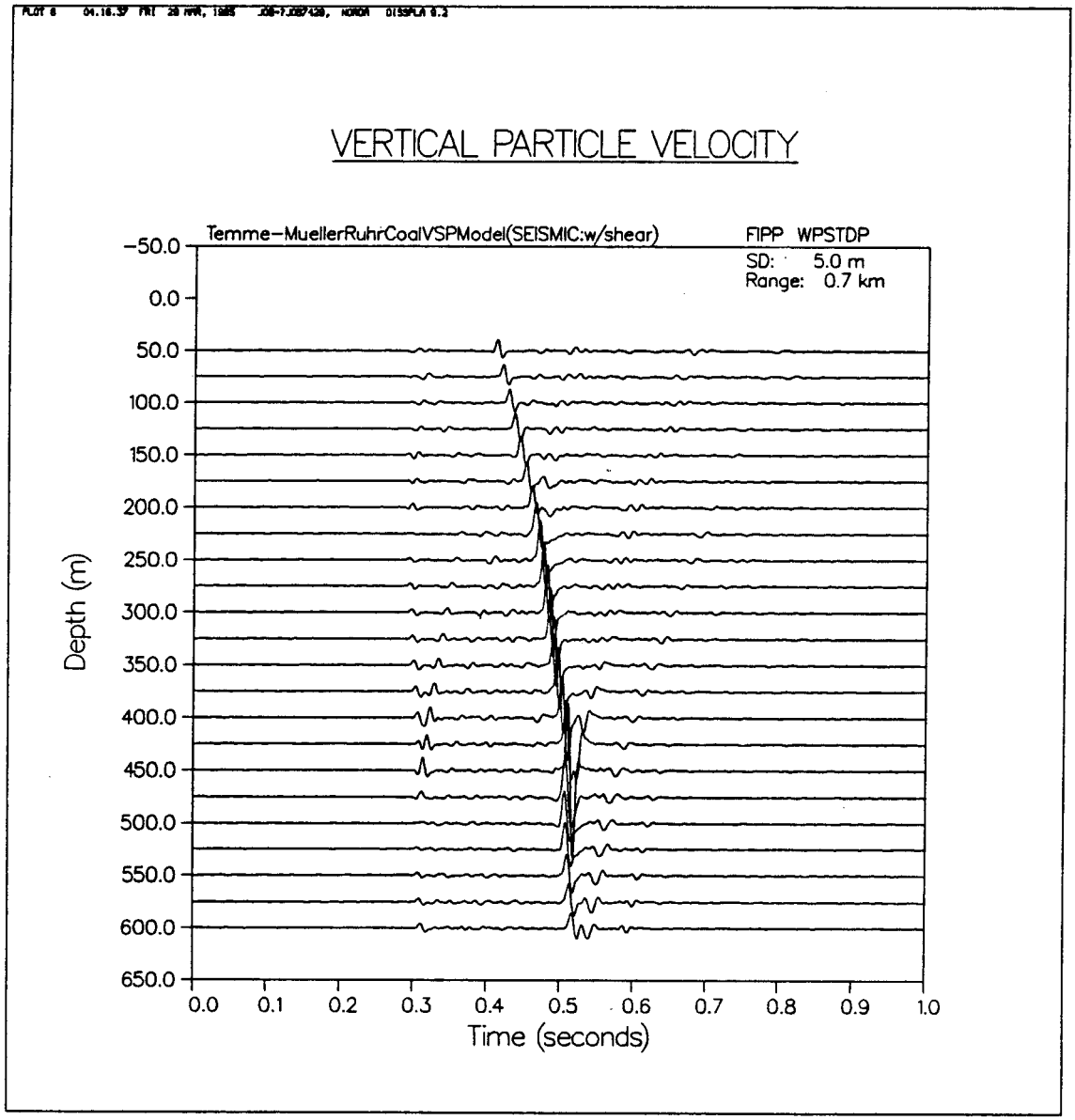
VERTICAL PARTICLE VELOCITY
Temme-MuellerRuhrCoalVSPModel(SEISMIC:w/shear)
FIPP WPSTDP
SD: 5.0 m
Range: 0.7 km
Depth (m)
-50.0
0.0
50.0
100.0
150.0
200.0
250.0
300.0
350.0
400.0
450.0
500.0
550.0
600.0
650.0
0.0
0.1
0.2
0.3
0.4
0.5
0.6
0.7
0.8
0.9
1.0
Time (seconds)

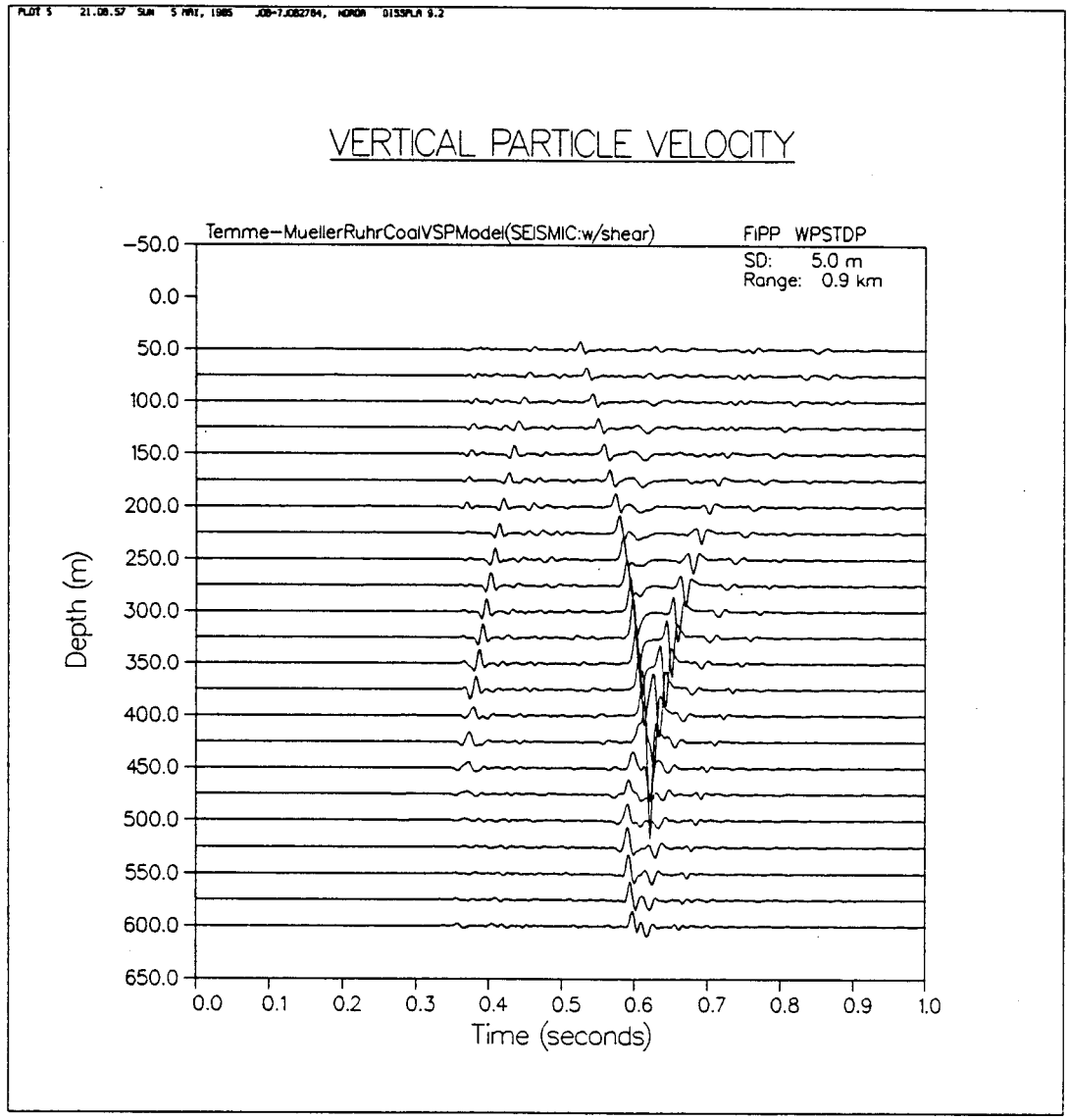
PLOT 5 21.08.57 SUN 5 MAY, 1985 JOB-7.082784, NORDA DISSPLA 9.2
VERTICAL PARTICLE VELOCITY
Temme-MuellerRuhrCoalVSPModel(SEISMIC:w/shear)
FIPP WPSTDP
SD: 5.0 m
Range: 0.9 km
Depth (m)
-50.0
0.0
50.0
100.0
150.0
200.0
250.0
300.0
350.0
400.0
450.0
500.0
550.0
600.0
650.0
0.0
0.1
0.2
0.3
0.4
0.5
0.6
0.7
0.8
0.9
1.0
Time (seconds)

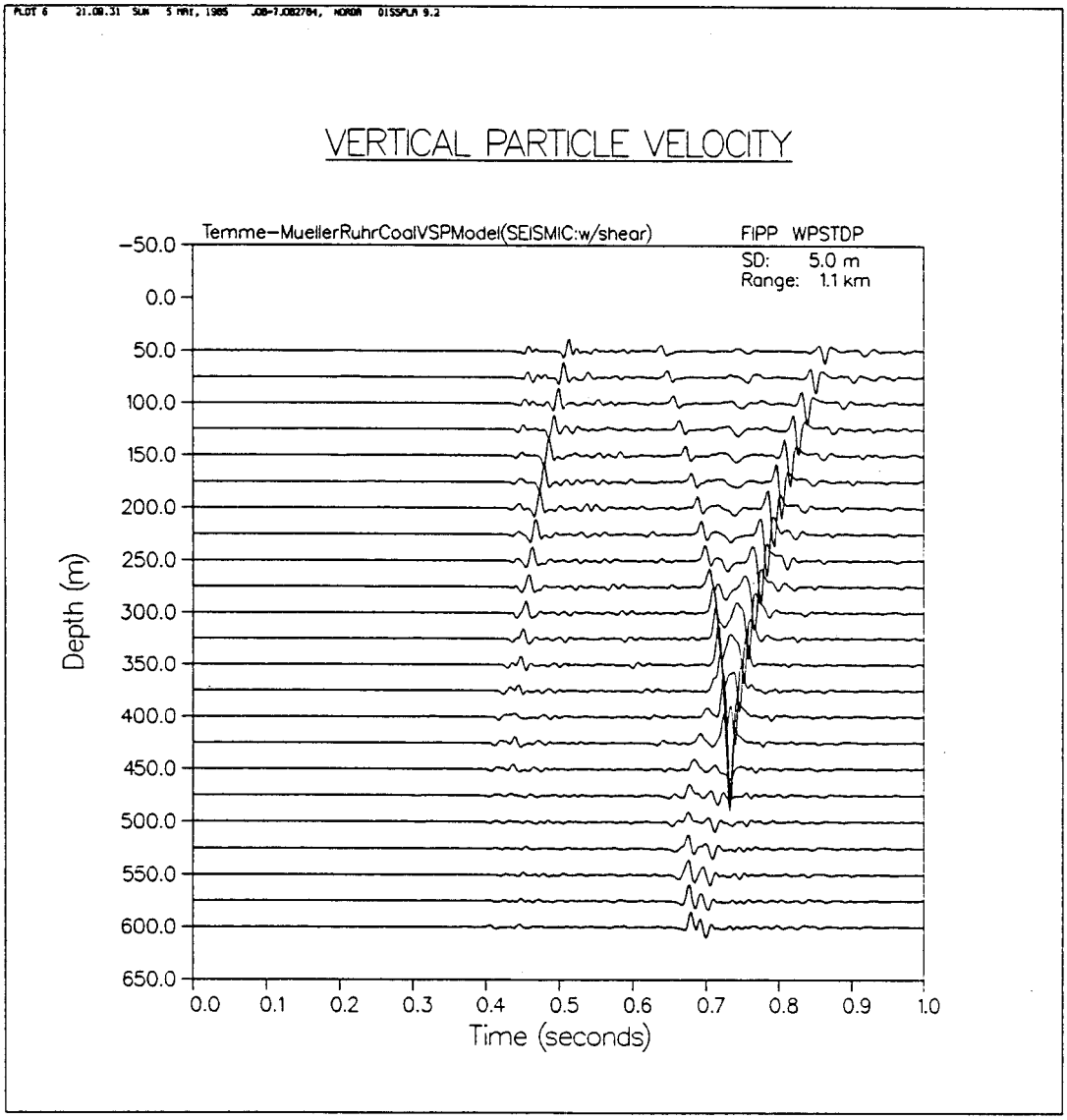
PLOT 6 21.08.31 SUN 5 MAY, 1985 JOB=7.082784, NORDA OISSPLA 9.2
VERTICAL PARTICLE VELOCITY
Temme-MuellerRuhrCoalVSPModel(SEISMIC:w/shear)
FIPP WPSTDP
SD: 5.0 m
Range: 1.1 km
Depth (m)
-50.0
0.0
50.0
100.0
150.0
200.0
250.0
300.0
350.0
400.0
450.0
500.0
550.0
600.0
650.0
0.0
0.1
0.2
0.3
0.4
0.5
0.6
0.7
0.8
0.9
1.0
Time (seconds)

Figure 82

Plane wave reflexion coefficients (scaled as per bottom loss) for full shear elastic Temme-Muller v/z model, over selected frequencies between 0 and 125Hz

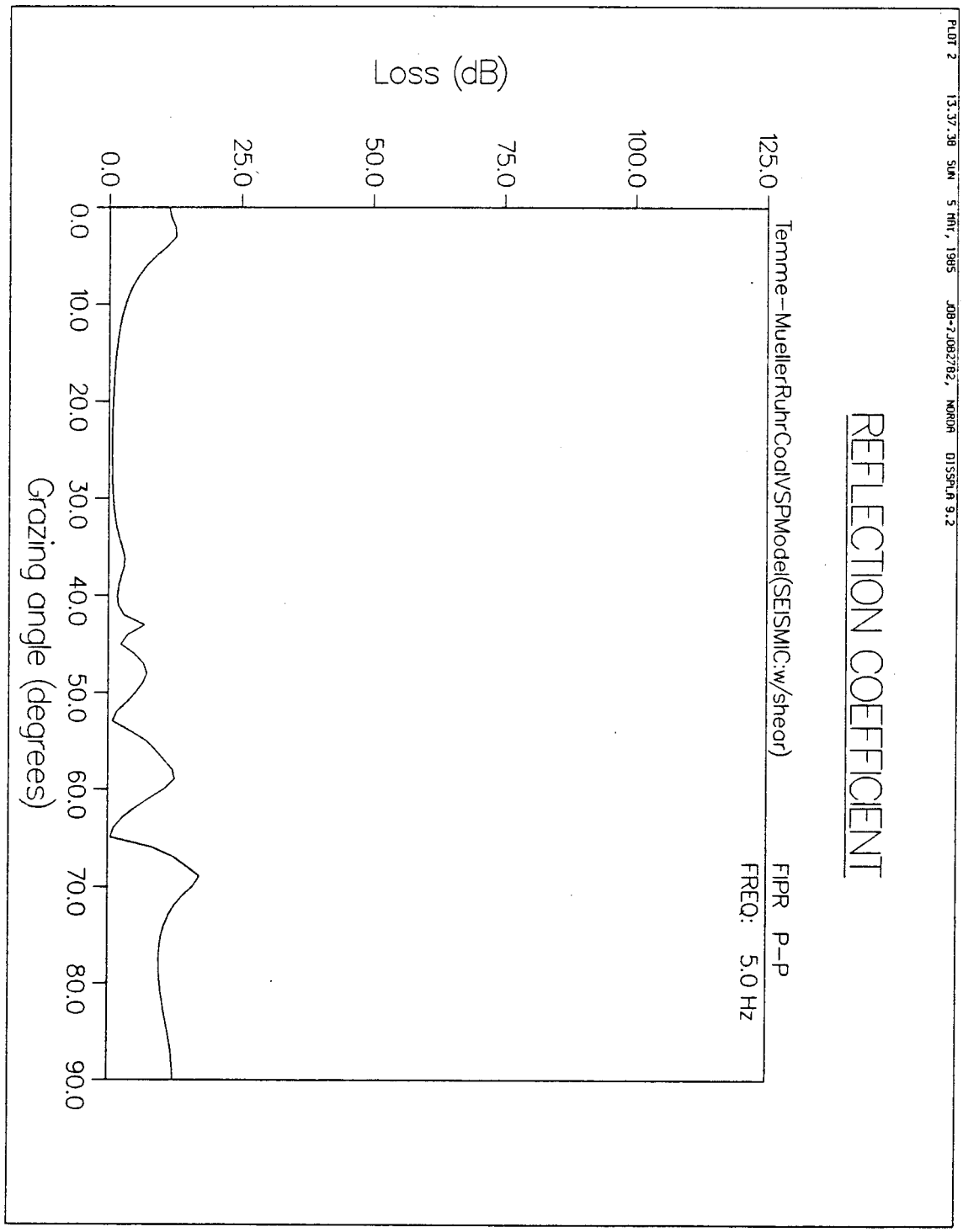
PLOT 2 13.37.38 SUN 5 MAY, 1985 JOB=7J0827B2, NORDA DISSPLA 9.2
REFLECTION COEFFICIENT
Temme-MuellerRuhrCoalVSPModel(SEISMIC:w/shear)
FIPR P-P
FREQ: 5.0 Hz
Loss (dB)
125.0
100.0
75.0
50.0
25.0
0.0
0.0 10.0 20.0 30.0 40.0 50.0 60.0 70.0 80.0 90.0
Grazing angle (degrees)

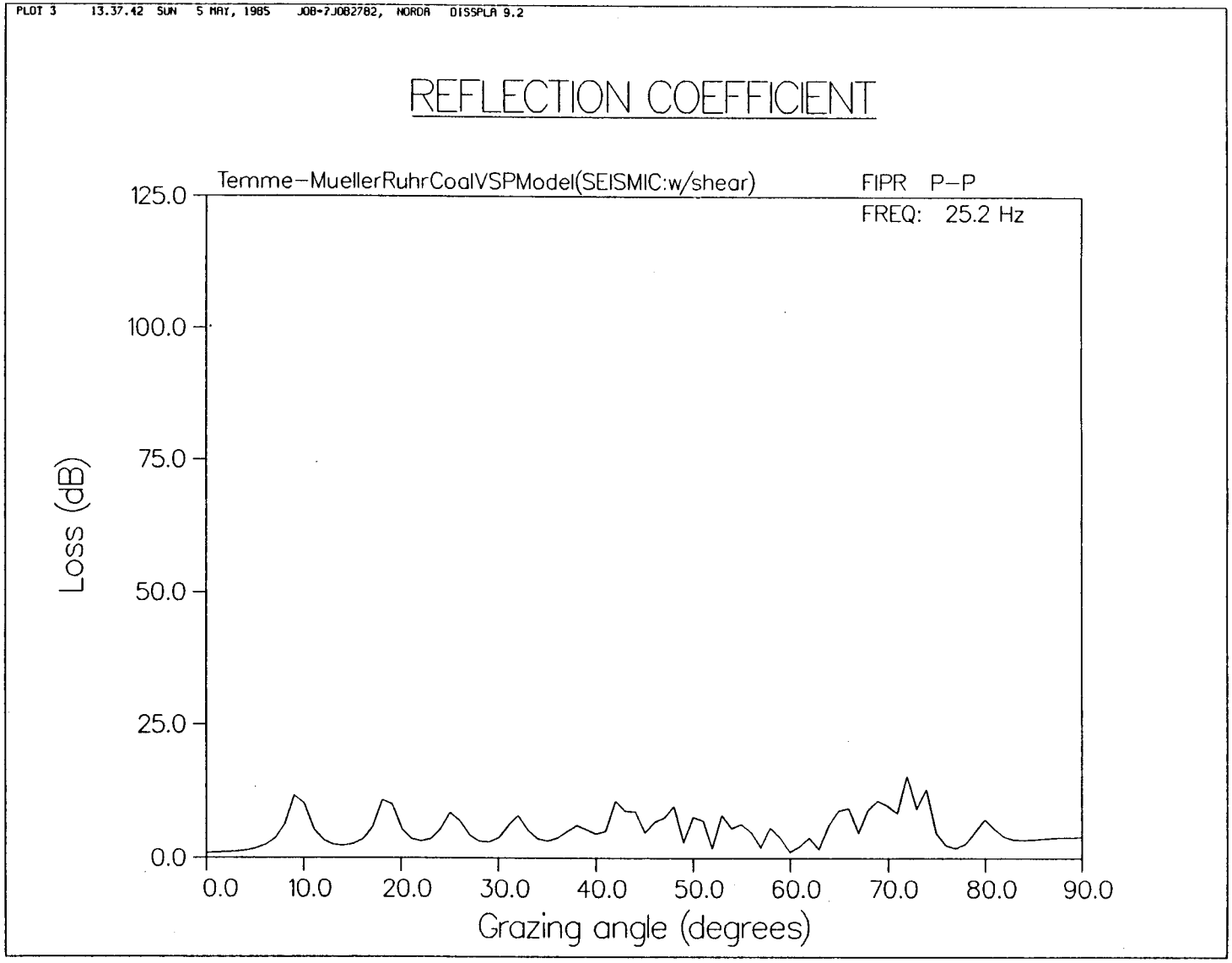
PLOT 3 13.37.42 SUN 5 MAY, 1985 JOB=7J082782, NORDA DISSPLA 9.2
REFLECTION COEFFICIENT
Temme-MuellerRuhrCoalVSPModel(SEISMIC:w/shear)
FIPR P-P
FREQ: 25.2 Hz
125.0
100.0
75.0
50.0
25.0
0.0
Loss (dB)
0.0
10.0
20.0
30.0
40.0
50.0
60.0
70.0
80.0
90.0
Grazing angle (degrees)

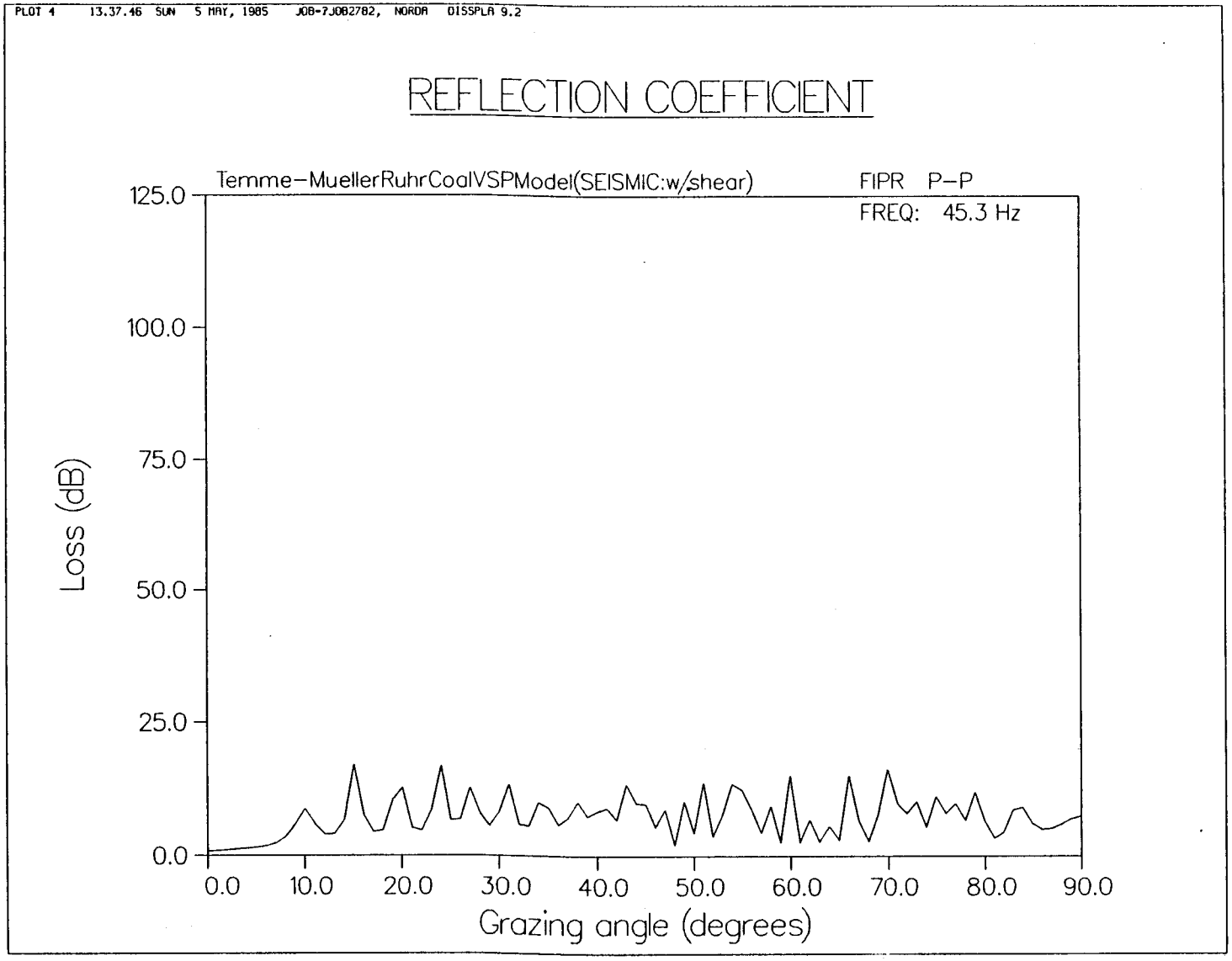
PLOT 4 13.37.46 SUN 5 MAY, 1985 JOB-7J082782, NORDA DISSPLA 9.2
REFLECTION COEFFICIENT
Temme-MuellerRuhrCoalVSPModel(SEISMIC:w/shear)
FIPR P-P
FREQ: 45.3 Hz
125.0
100.0
75.0
50.0
25.0
0.0
Loss (dB)
0.0
10.0
20.0
30.0
40.0
50.0
60.0
70.0
80.0
90.0
Grazing angle (degrees)

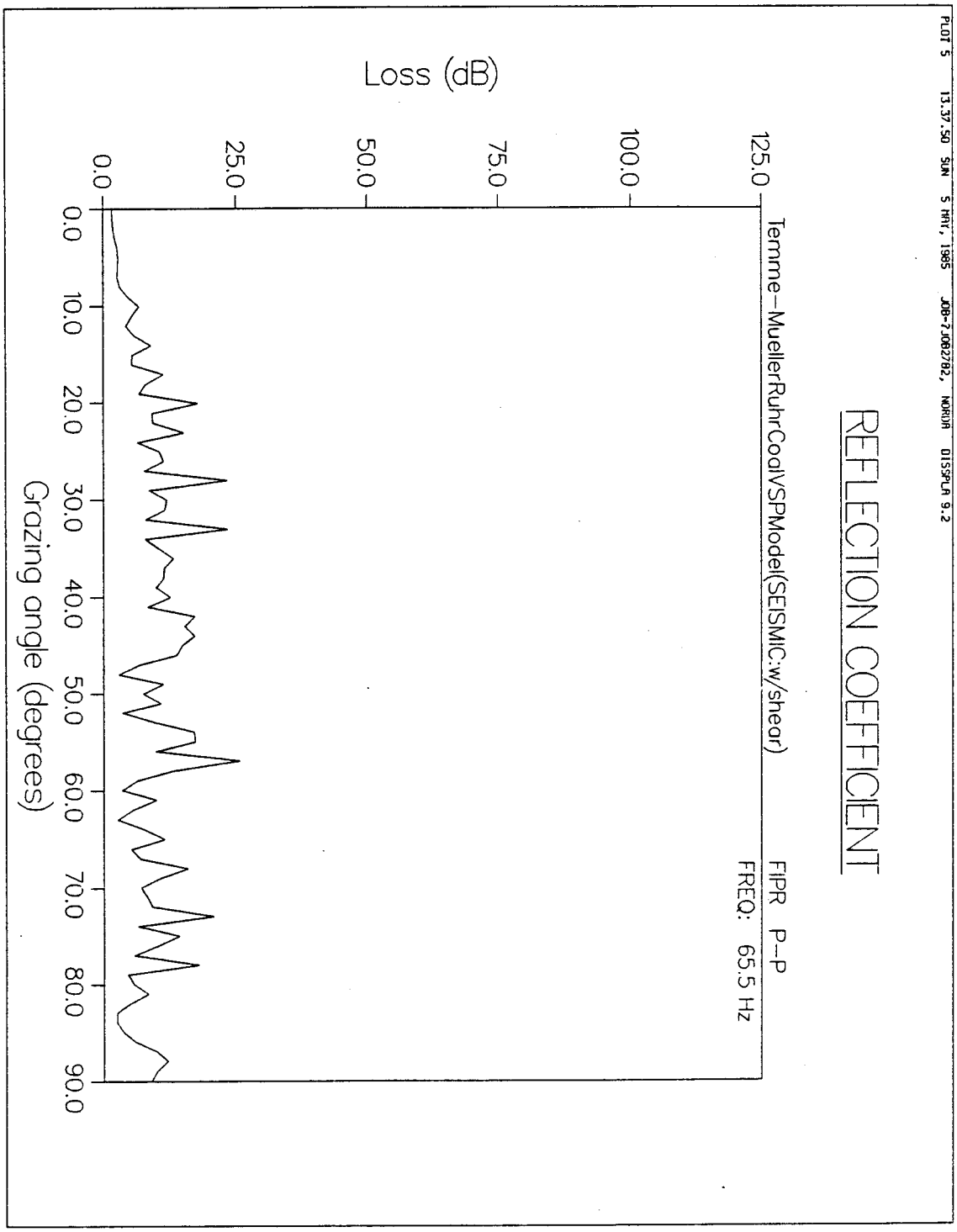
PLOT 5 13.37.50 SUN 5 MAY, 1985 JOB-7.J082782, NORUA DISSPLA 9.2
REFLECTION COEFFICIENT
Temme-MuellerRuhrCoalVSPModel(SEISMIC:w/shear)
FIPR P--P
FREQ: 65.5 Hz
Loss (dB)
125.0
100.0
75.0
50.0
25.0
0.0
0.0 10.0 20.0 30.0 40.0 50.0 60.0 70.0 80.0 90.0
Grazing angle (degrees)

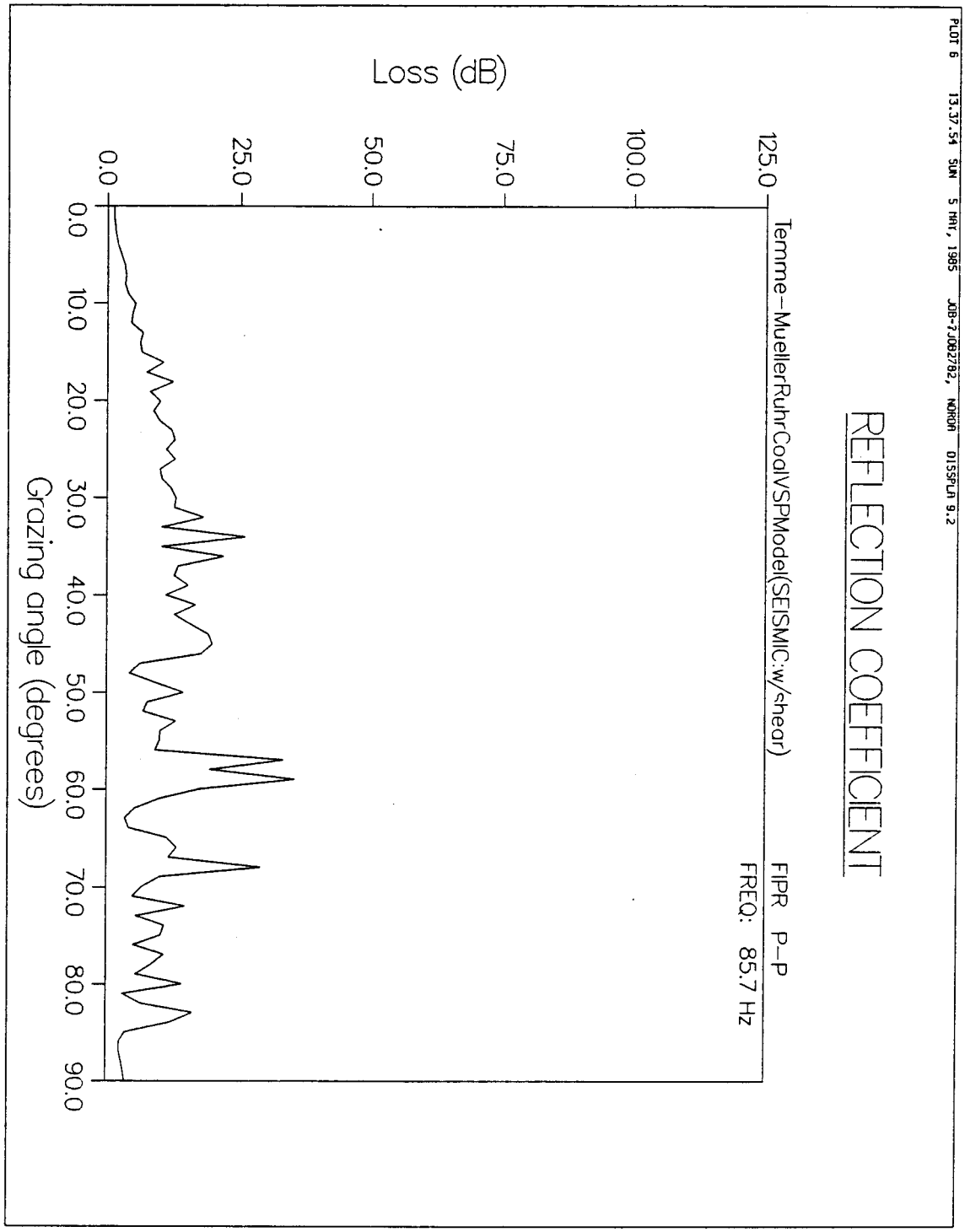
PLOT 6 13:37:54 SUN 5 MAY, 1985 JOB-?-J062782, NORDA DISSPLA 9.2
REFLECTION COEFFICIENT
Temme-MuellerRuhrCoalVSPModel(SEISMIC:w/shear)
FIPR P-P
FREQ: 85.7 Hz
Loss (dB)
125.0
100.0
75.0
50.0
25.0
0.0
0.0 10.0 20.0 30.0 40.0 50.0 60.0 70.0 80.0 90.0
Grazing angle (degrees)

x=300 m. This conversion arrival can be tentatively identified as originating from the nearsurface layer, due to the interval of interference between the converted transverse wave and the original incident longitudinal wave in the immediate vicinity of the conversion boundary. For all post-critical offset records, the intensity of downgoing converted waves (on vertical component records) clearly exceeds that of the first longitudinal wave. This confirms the recent results (e.g.) of AMINZADEH and MENDEL (1985) and of DIETRICH and BOUCHON (1985). In addition, some upward travelling transmitted converted waves are also seen associated with high velocity layers at depth. Due to much larger S attenuation in the nearsurface, all the above converted arrivals are seen to have a generally lower-frequency appearance.

Because of P/Sv interference, correlation of transverse waves along a (nb, large offset) VSP, without the aid of a polarizational scheme (GAL'PERIN, 1974) is in general a much more difficult task, requiring use of both horizontal and vertical particle velocity, as well as comparative seismic/acoustic VSP records. As noted, even for relatively shallow receiver arrays the direction of wave approach from the source can vary substantially as a function of offset for a given receiver array depth. Thus the approach direction of the converted Sv wave is close to horizontal in the near surface, and hence is here satisfactorily registered by geophones measuring vertical particle velocity. However, as the source-receiver offset distance increases, ie, as the direction of approach of the converted Sv wave more closely approximates the vertical, the intensity of the Sv wave on vertical seismometers diminishes, at the same time as the amplitude of the first P wave arrival increases. Conversely, on the horizontal particle velocity record, P wave events decrease and Sv events are optimised for far offset records. This is shown in **Figures 83a-b** over a 0-50/25Hz bandwidth and center frequency.

However, although P wave amplitudes can be approximately separated from converted Sv waves when using orthogonal particle velocity records, it will also be seen that the converted Sv waves can themselves give rise to their own complicated pattern of multiple reverberations. As LASH (1980;1982) has pointed out,

Figure 83

VSPs for same v/z model, at selected receiver offsets as per Figure 81, in Horizontal particle velocity records, with f_c= 50 and f_c= 25 Hz

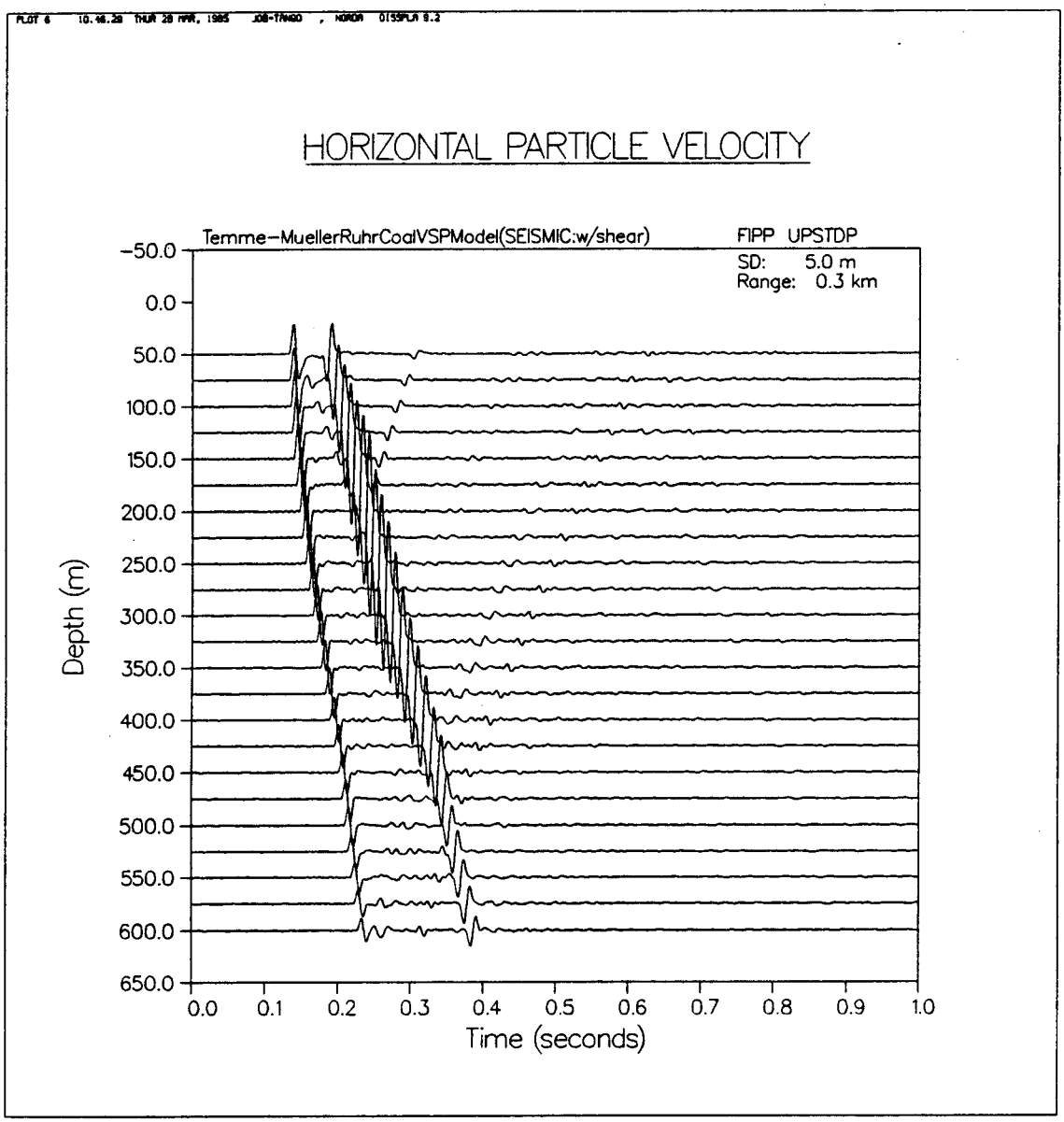
HORIZONTAL PARTICLE VELOCITY
Temme-MuellerRuhrCoalVSPModel(SEISMIC:w/shear)
FIPP UPSTDP
SD: 5.0 m
Range: 0.3 km
Depth (m)
-50.0
0.0
50.0
100.0
150.0
200.0
250.0
300.0
350.0
400.0
450.0
500.0
550.0
600.0
650.0
0.0
0.1
0.2
0.3
0.4
0.5
0.6
0.7
0.8
0.9
1.0
Time (seconds)

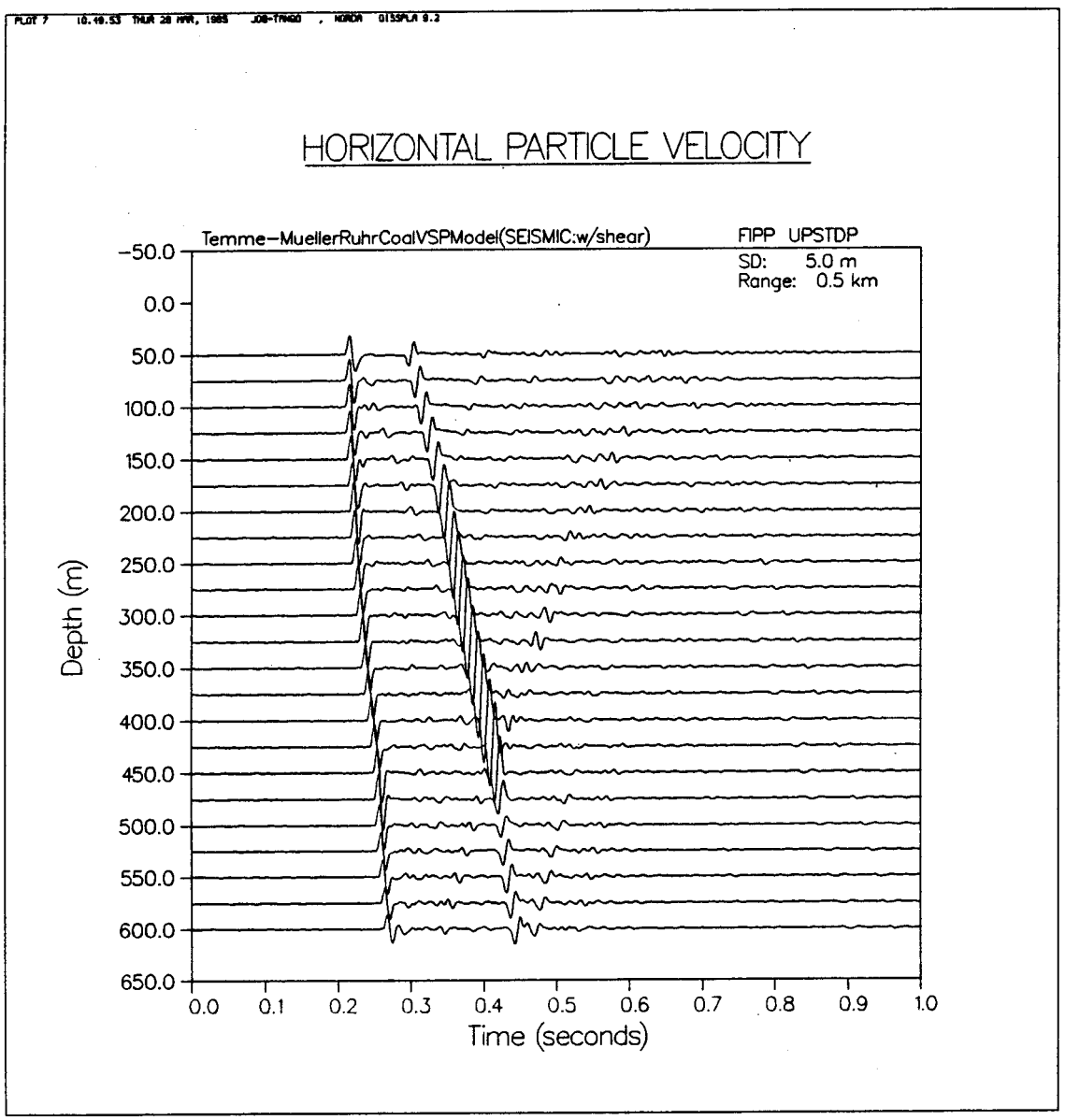
HORIZONTAL PARTICLE VELOCITY
Temme–MuellerRuhrCoalVSPModel(SEISMIC:w/shear)
FIPP UPSTDP
SD: 5.0 m
Range: 0.5 km
Depth (m)
-50.0
0.0
50.0
100.0
150.0
200.0
250.0
300.0
350.0
400.0
450.0
500.0
550.0
600.0
650.0
0.0
0.1
0.2
0.3
0.4
0.5
0.6
0.7
0.8
0.9
1.0
Time (seconds)

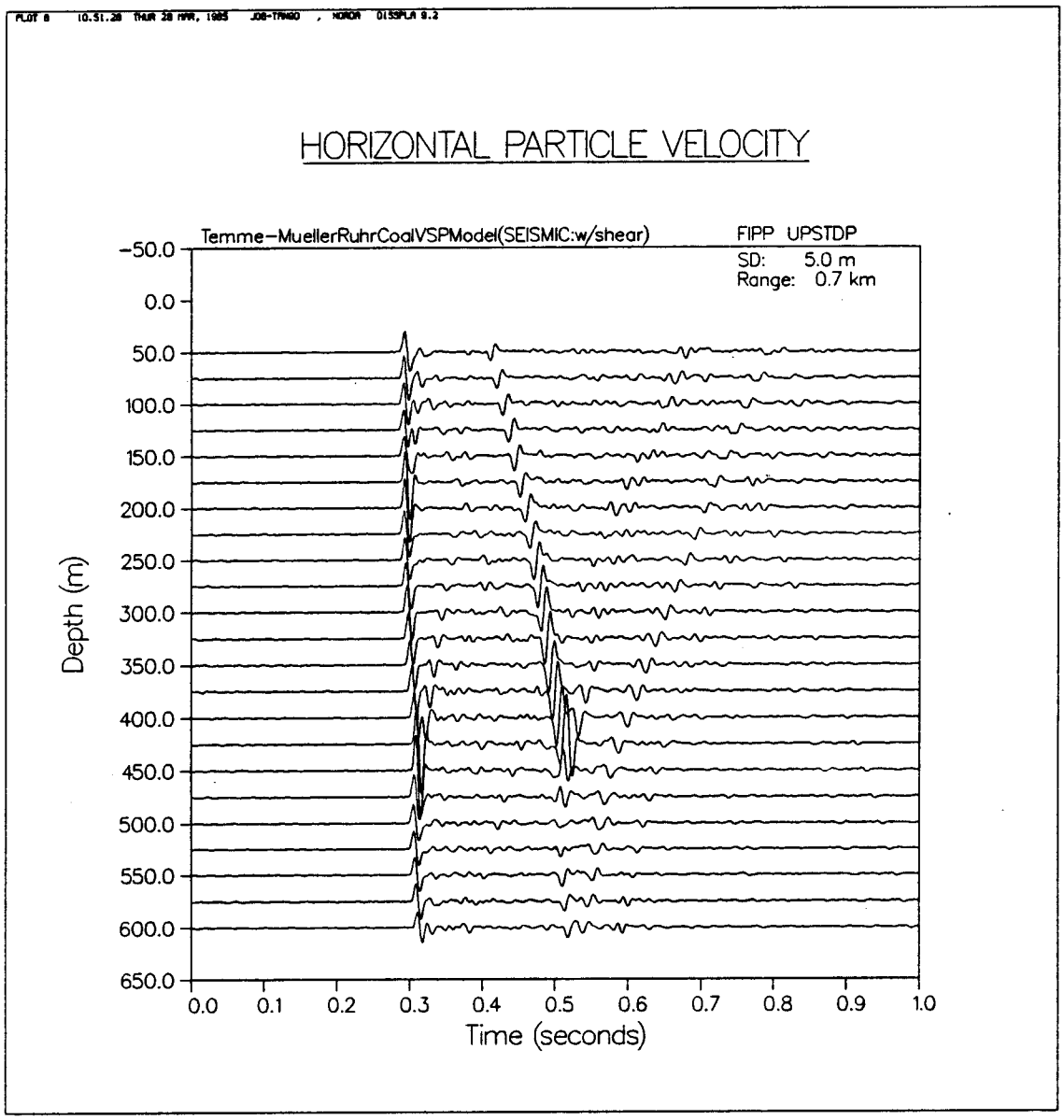
HORIZONTAL PARTICLE VELOCITY
Temme-MuellerRuhrCoalVSPModel(SEISMIC:w/shear)
FIPP UPSTDP
SD: 5.0 m
Range: 0.7 km
Depth (m)
-50.0
0.0
50.0
100.0
150.0
200.0
250.0
300.0
350.0
400.0
450.0
500.0
550.0
600.0
650.0
0.0
0.1
0.2
0.3
0.4
0.5
0.6
0.7
0.8
0.9
1.0
Time (seconds)

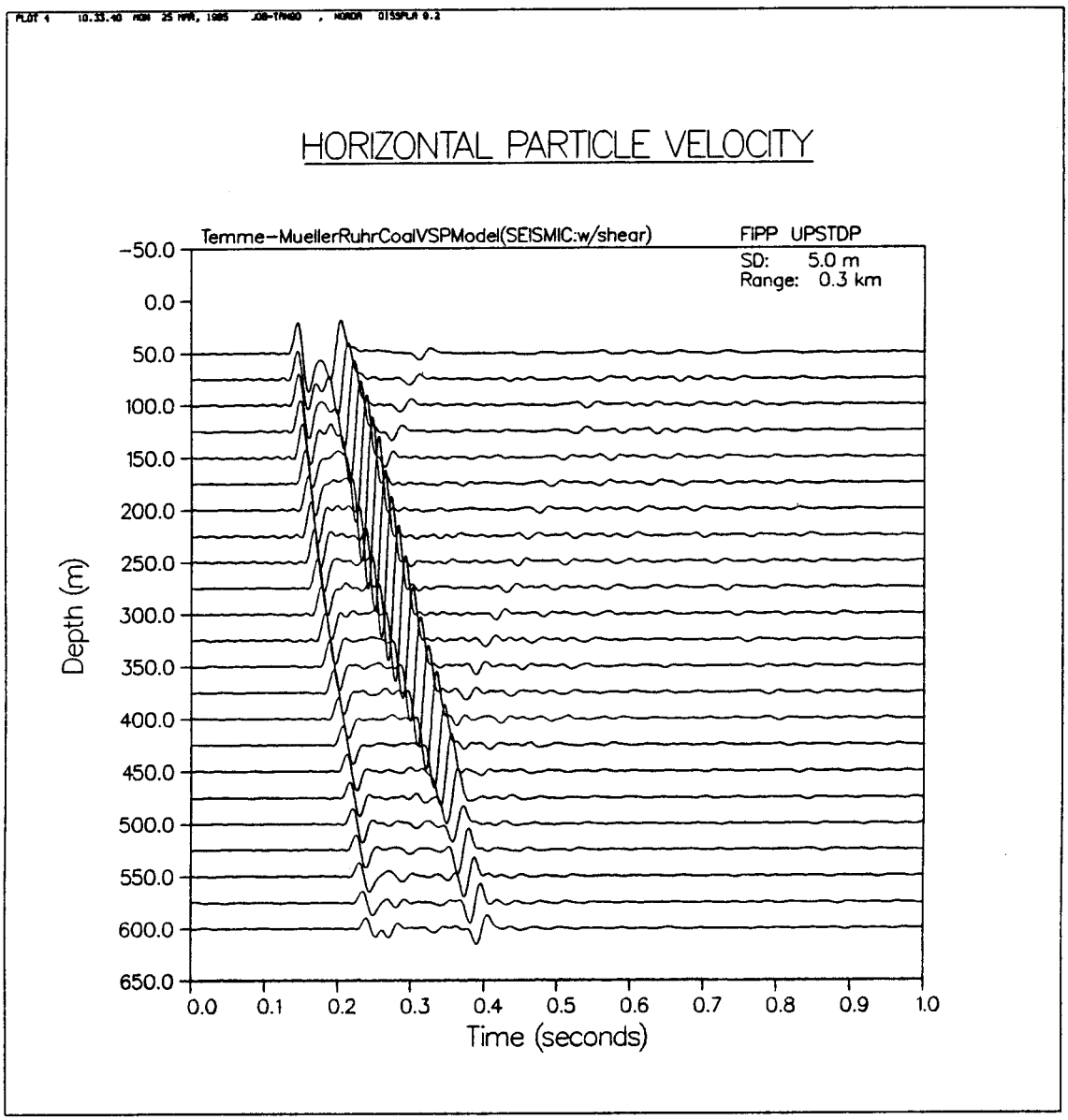
HORIZONTAL PARTICLE VELOCITY
Temme-MuellerRuhrCoalVSPModel(SEISMIC:w/shear)
FIPP UPSTDP
SD: 5.0 m
Range: 0.3 km
Depth (m)
-50.0
0.0
50.0
100.0
150.0
200.0
250.0
300.0
350.0
400.0
450.0
500.0
550.0
600.0
650.0
0.0
0.1
0.2
0.3
0.4
0.5
0.6
0.7
0.8
0.9
1.0
Time (seconds)

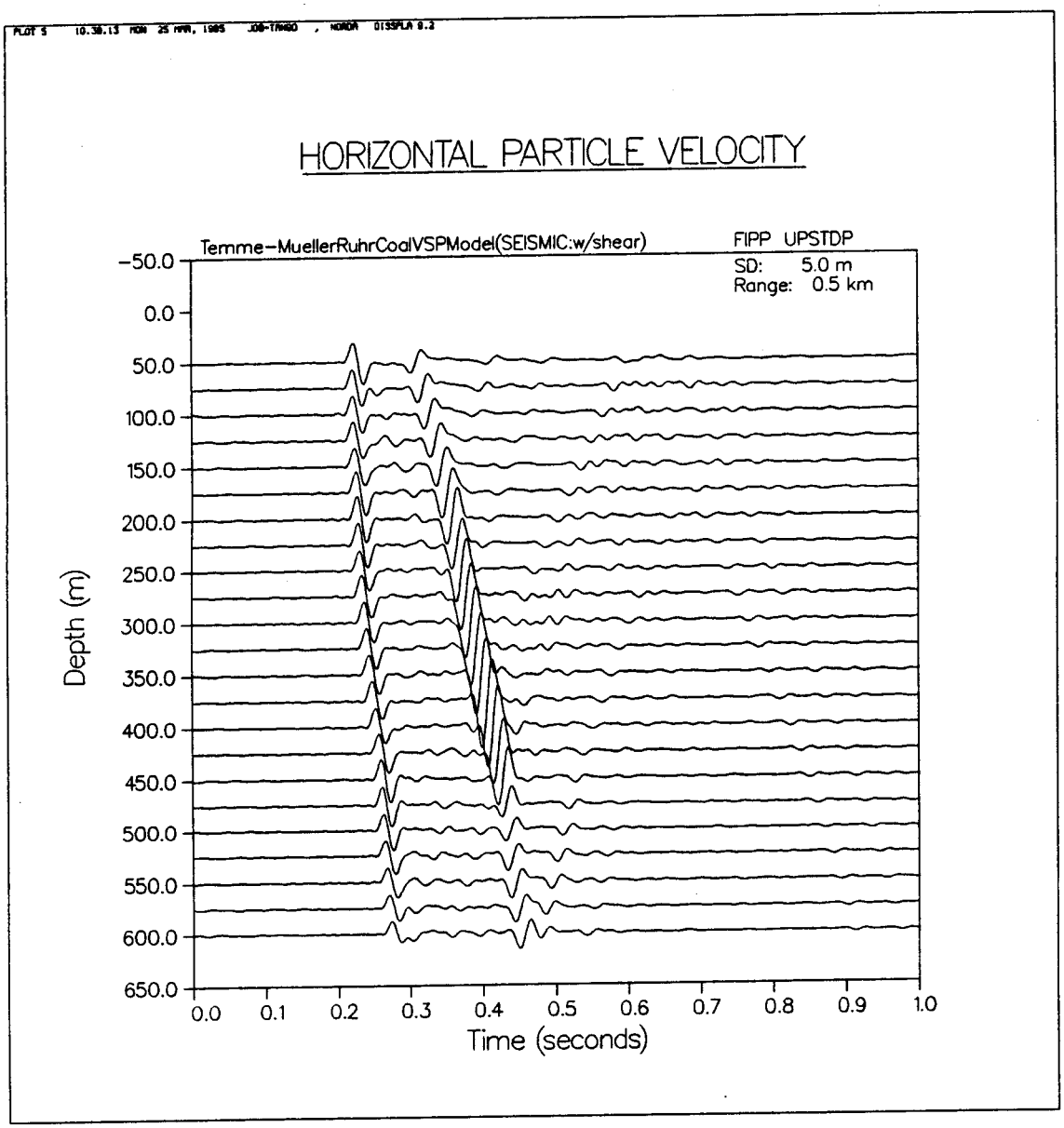
HORIZONTAL PARTICLE VELOCITY
Temme-MuellerRuhrCoalVSPModel(SEISMIC:w/shear)
FIPP UPSTDP
SD: 5.0 m
Range: 0.5 km
Depth (m)
-50.0
0.0
50.0
100.0
150.0
200.0
250.0
300.0
350.0
400.0
450.0
500.0
550.0
600.0
650.0
0.0
0.1
0.2
0.3
0.4
0.5
0.6
0.7
0.8
0.9
1.0
Time (seconds)

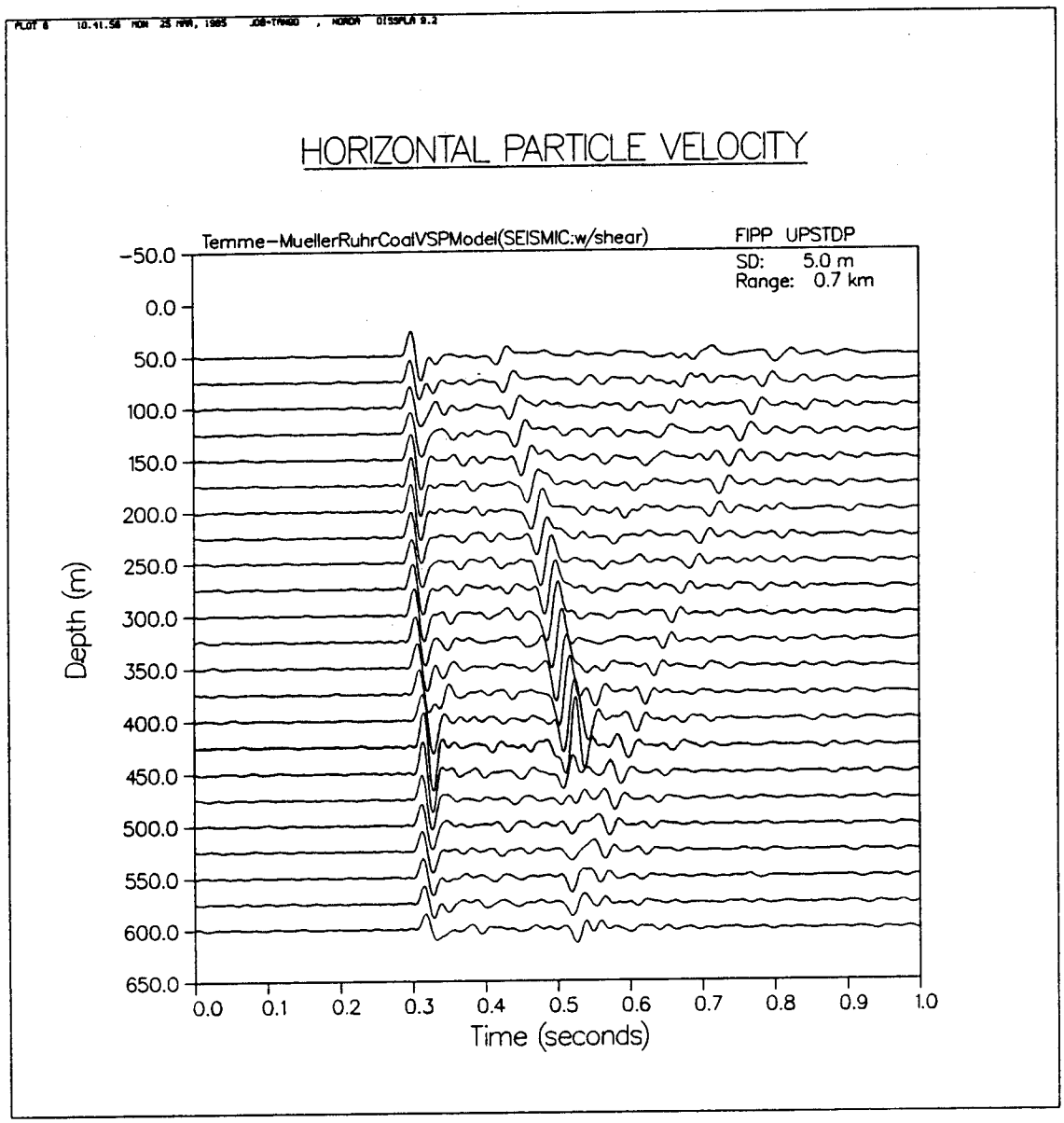
HORIZONTAL PARTICLE VELOCITY
Temme-MuellerRuhrCoalVSPModel(SEISMIC:w/shear)
FIPP UPSTDP
SD: 5.0 m
Range: 0.7 km
Depth (m)
-50.0
0.0
50.0
100.0
150.0
200.0
250.0
300.0
350.0
400.0
450.0
500.0
550.0
600.0
650.0
0.0
0.1
0.2
0.3
0.4
0.5
0.6
0.7
0.8
0.9
1.0
Time (seconds)

practical interpretation in such events is complicated on account of the difficulties in correctly identifying all the major possibilities of higher order multiple P-SV-P conversions. Fast fullwave synthetic modeling algorithms allowing separable P and Sv only calculations would be ideally suited to further facilitate this analysis (SCHMIDT, 1985, personal communication).

From the above, it is thus clear, that for most actually-encountered multilayered velocity-depth distributions, no one source-receiver offset is optimal for all VSP applications, and that layer resolution can be enhanced only by particular consideration of refracted and SV converted modes in addition to direct and reflected P wave arrivals. By optimally selecting the offset distance it is possible to selectively enhance the correlation and identification of a specific P and/or SV arrival, at the expense of deriving clear information about arrivals from other depth levels. GAL'PERIN (1971) has proposed offsets in the range of about two times the boundary depth of interest as the most favourable distances for observing converted reflected waves. This is shown in **Figure 84a-e**, where mode conversions from the deepest seam layers are clearly evident. A split panel comparison of P and P+S VSP models for the same geomodel, at 2 different offsets, is given in **Figure 84f**.

Figure 84

VSPs for same v/z model as in Figure 81, over extreme far field offsets (x=1.3,1.5,1.7,1.9 and 2.1km), and split-panel of acoustic and full shear elastic VSPs at 2 offsets (showing increases P-Sv conversion at even nominal S-R separations)

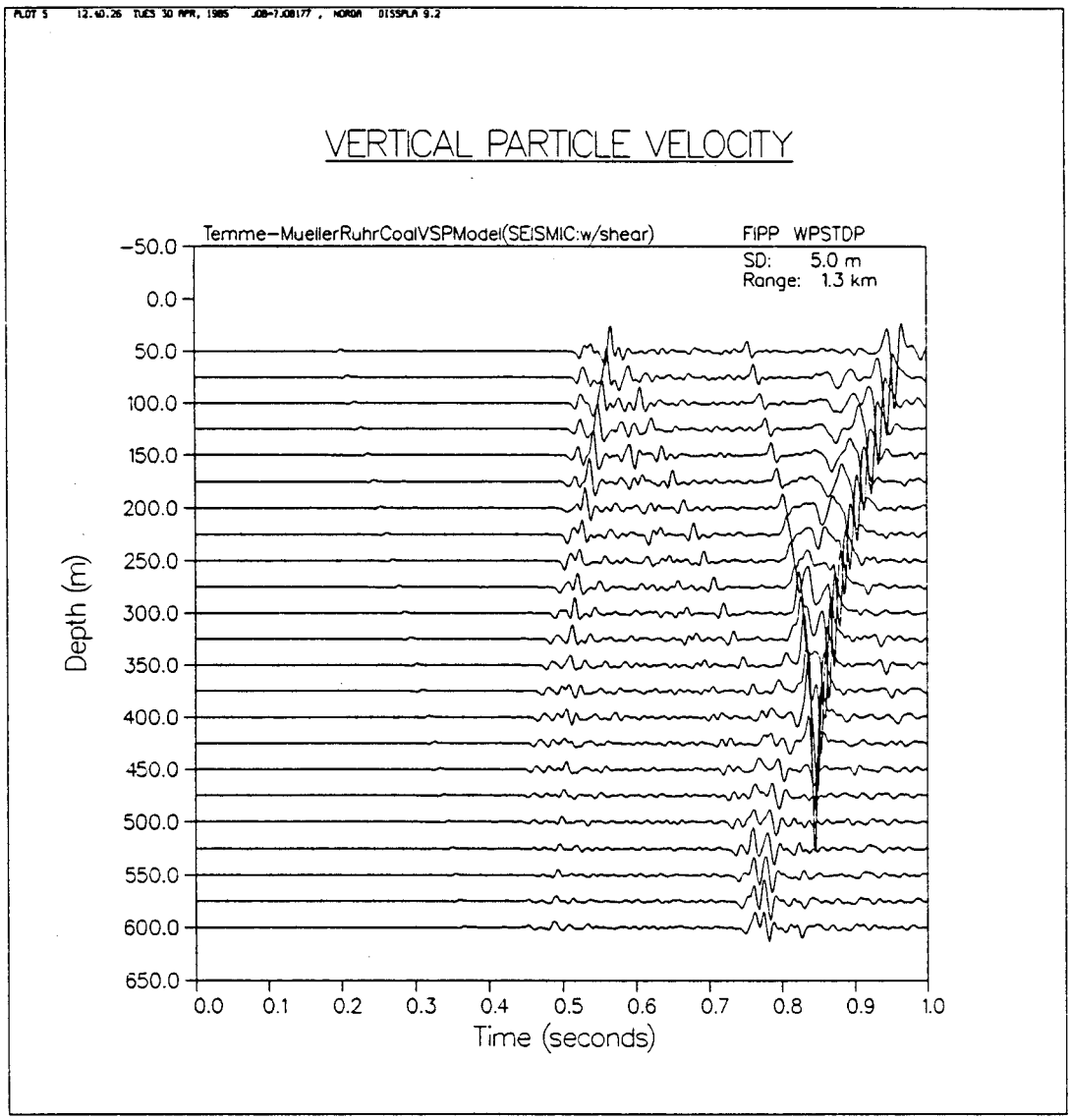
PLOT 5 12.40.26 TUES 30 APR, 1985 JOB=7.08177 , NORDA DISSPLA 9.2
VERTICAL PARTICLE VELOCITY
Temme-MuellerRuhrCoalVSPModel(SEISMIC:w/shear)
FiPP WPSTDP
SD: 5.0 m
Range: 1.3 km
Depth (m)
-50.0
0.0
50.0
100.0
150.0
200.0
250.0
300.0
350.0
400.0
450.0
500.0
550.0
600.0
650.0
0.0
0.1
0.2
0.3
0.4
0.5
0.6
0.7
0.8
0.9
1.0
Time (seconds)

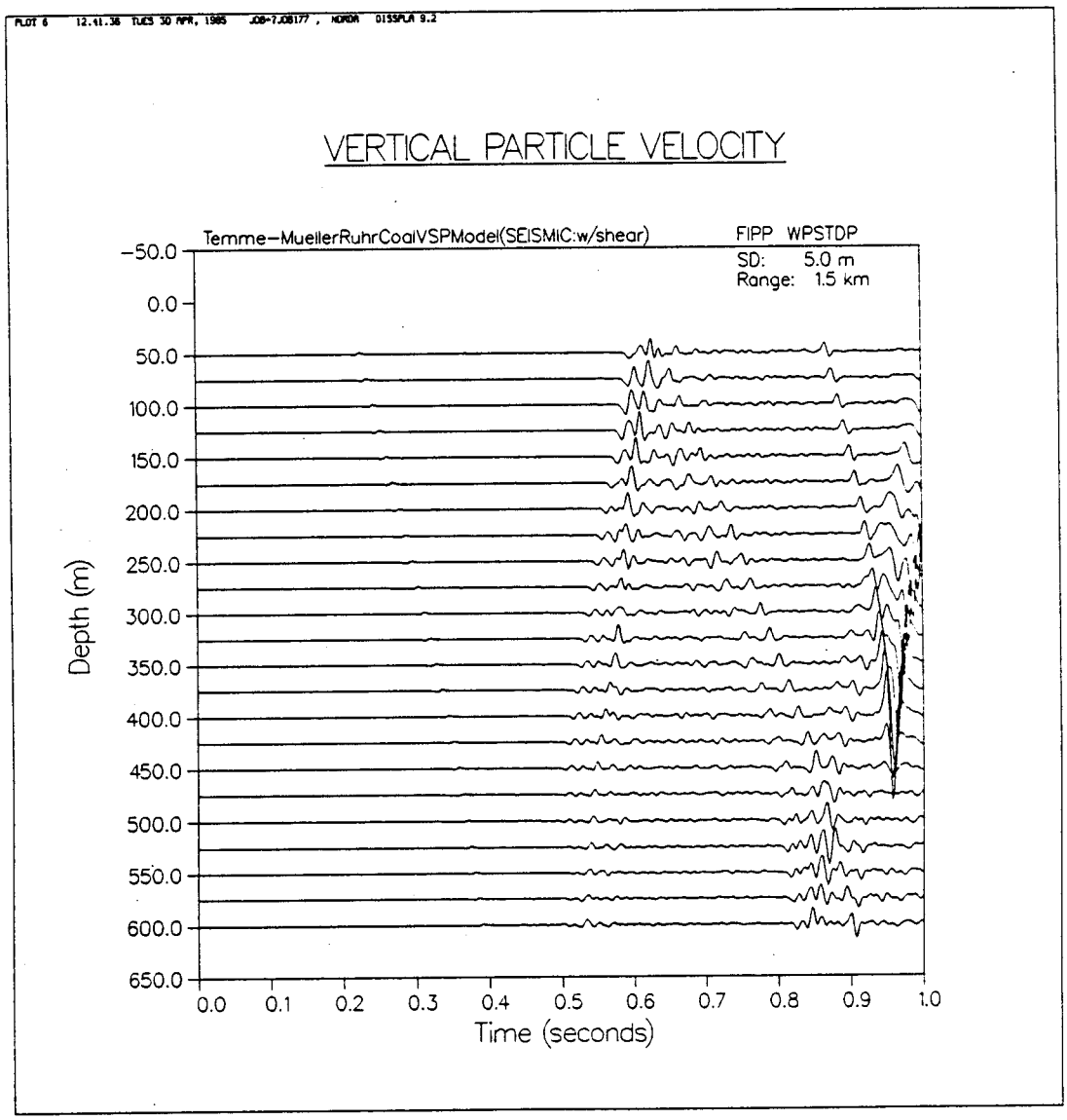
PLOT 6 12.41.36 TUES 30 APR, 1985 JOB=7.08177 , NORDA DISSPLA 9.2
VERTICAL PARTICLE VELOCITY
Temme-MuellerRuhrCoalVSPModel(SEISMIC:w/shear)
FIPP WPSTDP
SD: 5.0 m
Range: 1.5 km
Depth (m)
-50.0
0.0
50.0
100.0
150.0
200.0
250.0
300.0
350.0
400.0
450.0
500.0
550.0
600.0
650.0
0.0
0.1
0.2
0.3
0.4
0.5
0.6
0.7
0.8
0.9
1.0
Time (seconds)

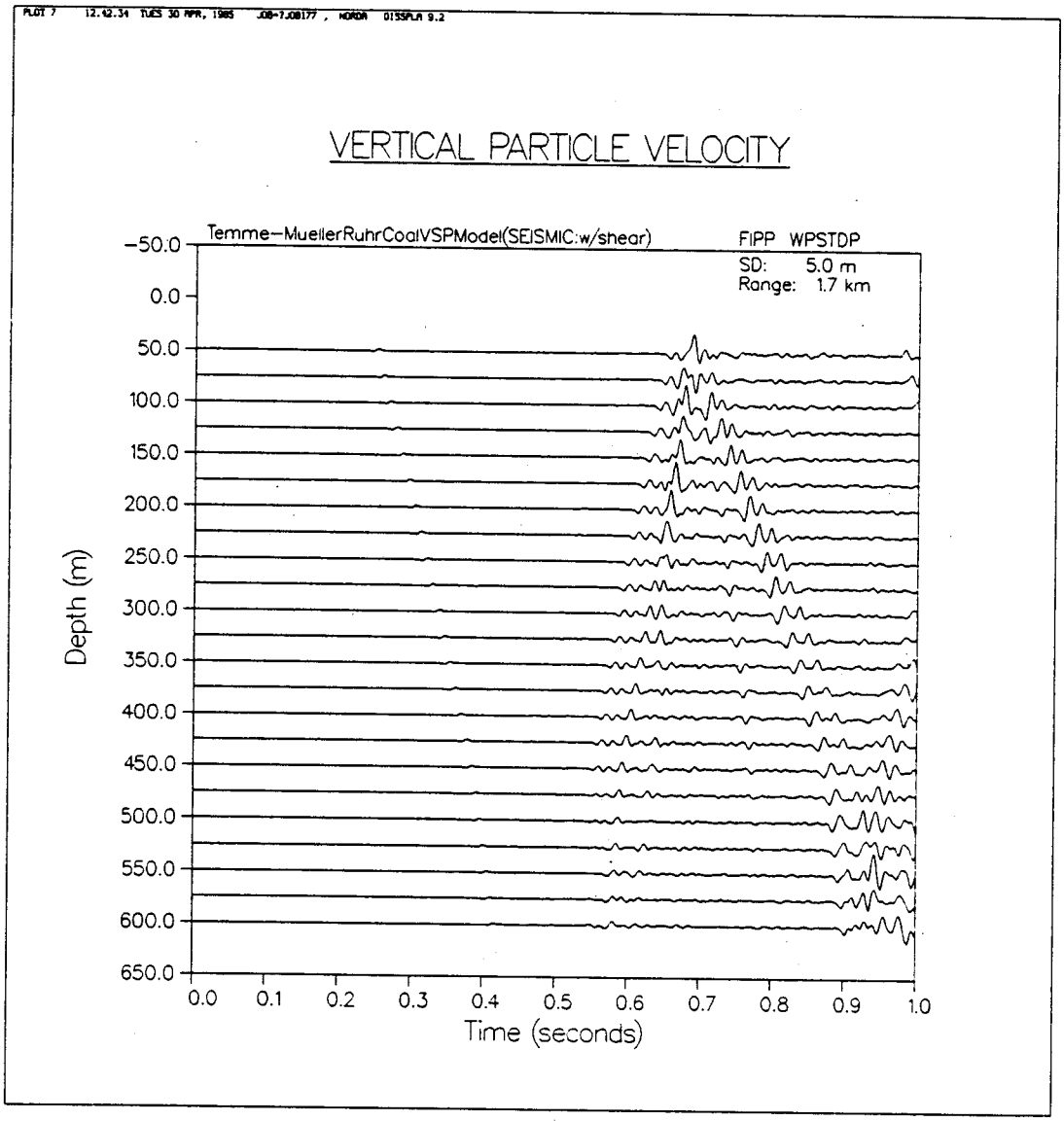
PLOT 7 12.42.34 TUES 30 APR, 1985 JOB=7.JOB177 , NORDA DISSPLA 9.2
VERTICAL PARTICLE VELOCITY
Temme–MuellerRuhrCoalVSPModel(SEISMIC:w/shear)
FIPP WPSTDP
SD: 5.0 m
Range: 1.7 km
Depth (m)
-50.0
0.0
50.0
100.0
150.0
200.0
250.0
300.0
350.0
400.0
450.0
500.0
550.0
600.0
650.0
0.0 0.1 0.2 0.3 0.4 0.5 0.6 0.7 0.8 0.9 1.0
Time (seconds)

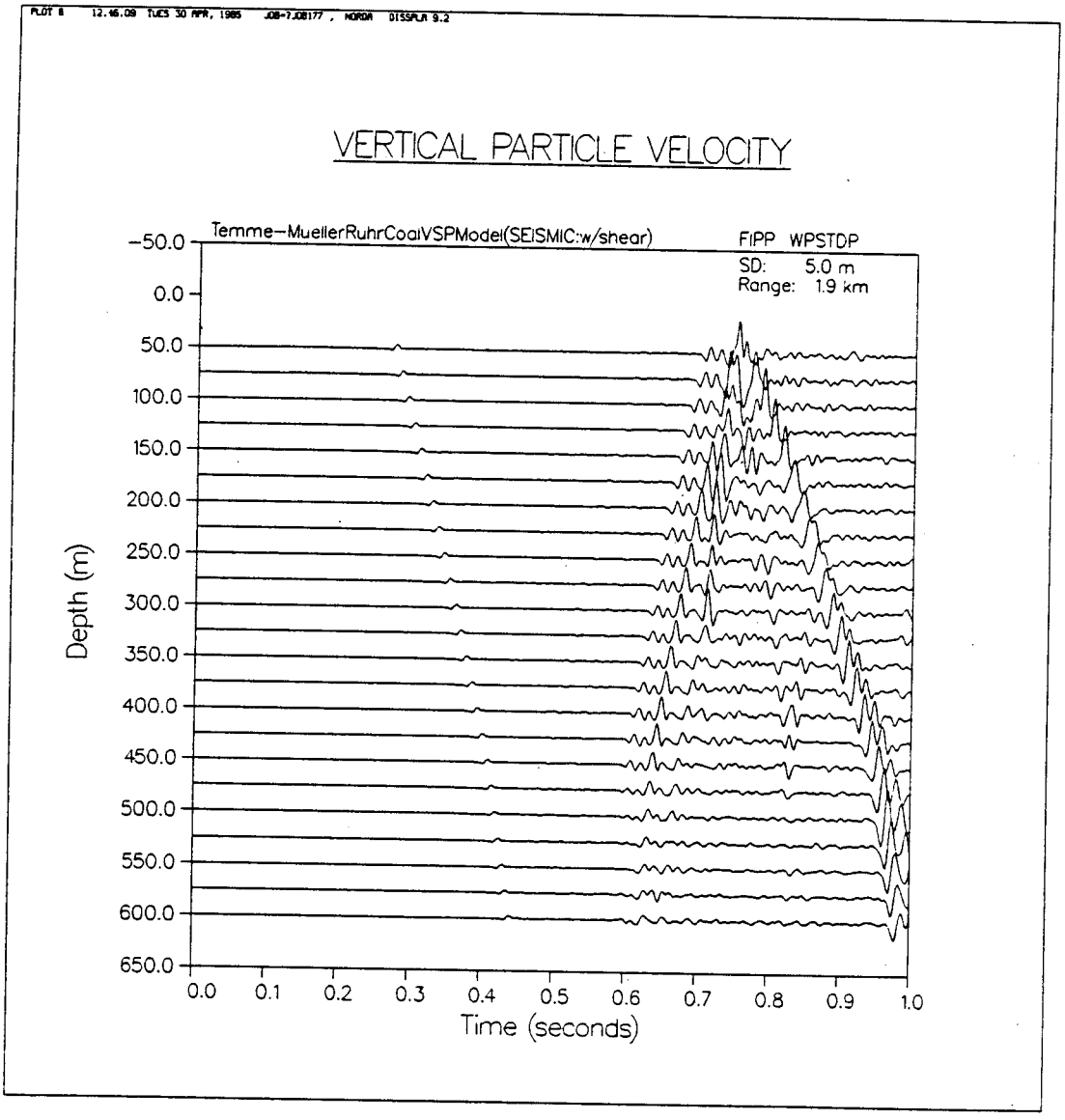
PLOT 8 12.46.09 TUES 30 APR, 1985 JOB=7.JOB177 , NORDA DISSPLA 9.2
VERTICAL PARTICLE VELOCITY
Temme-MuellerRuhrCoalVSPModel(SEISMIC:w/shear)
FIPP WPSTDP
SD: 5.0 m
Range: 1.9 km
Depth (m)
-50.0
0.0
50.0
100.0
150.0
200.0
250.0
300.0
350.0
400.0
450.0
500.0
550.0
600.0
650.0
0.0
0.1
0.2
0.3
0.4
0.5
0.6
0.7
0.8
0.9
1.0
Time (seconds)

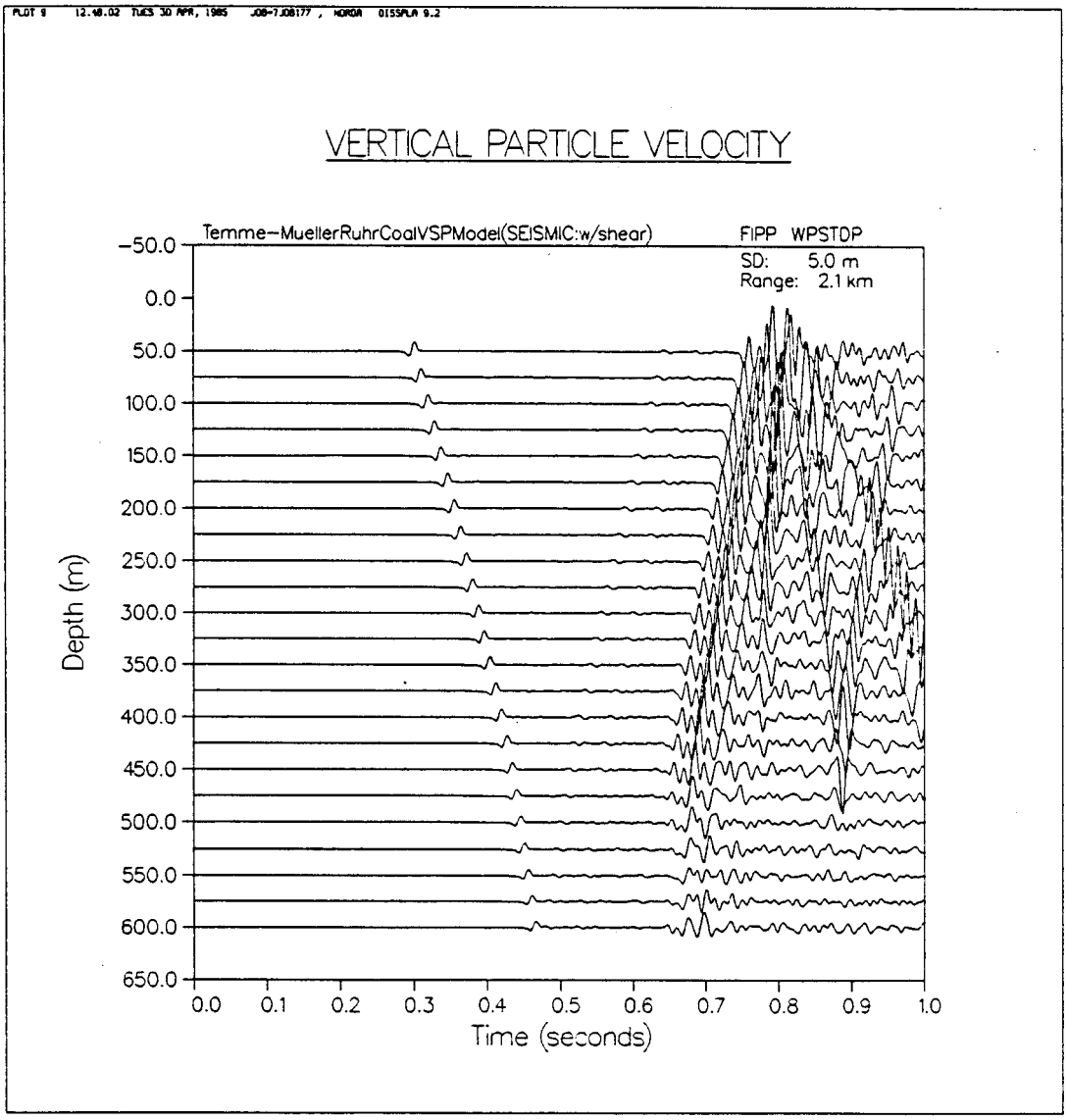
PLOT 9 12.48.02 TUES 30 APR, 1985 JOB-7.JOB177 , NORDA DISSPLA 9.2
VERTICAL PARTICLE VELOCITY
Temme–MuellerRuhrCoalVSPModel(SEISMIC:w/shear)
FIPP WPSTDP
SD: 5.0 m
Range: 2.1 km
Depth (m)
-50.0
0.0
50.0
100.0
150.0
200.0
250.0
300.0
350.0
400.0
450.0
500.0
550.0
600.0
650.0
0.0
0.1
0.2
0.3
0.4
0.5
0.6
0.7
0.8
0.9
1.0
Time (seconds)

VERTICAL PARTICLE VELOCITY

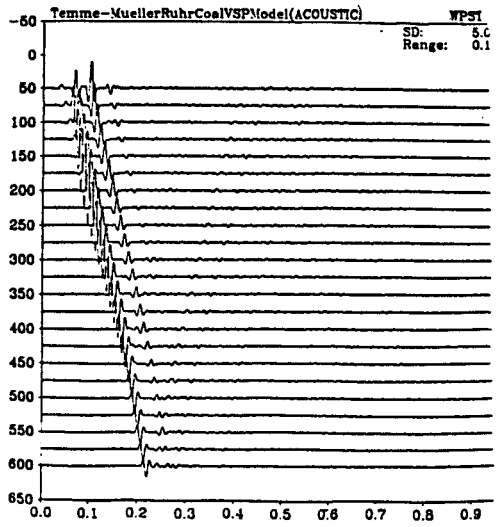

VERTICAL PARTICLE VELOCITY

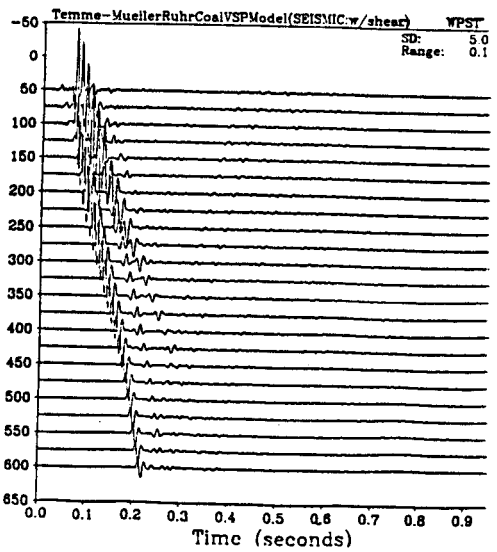

VERTICAL PARTICLE VELOCITY

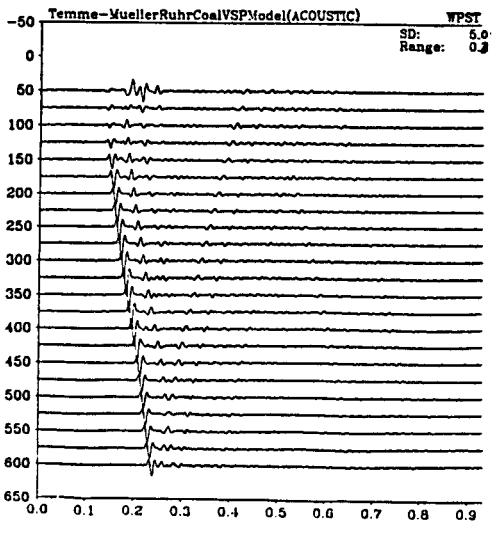

VERTICAL PARTICLE VELOCITY

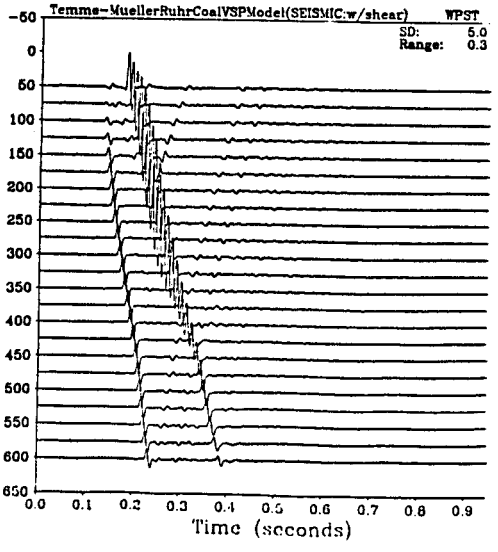

Deep Crustal Marine Seismic VSP

Recent results of marine crustal studies of the midocean ridge from standard surface-towed or ocean bottom seismic data are often inadequate to determine the fine structure of seismic transition boundaries within crustal Layers 2 and 3 (RAITT, 1963; KENNETT, 1976; KARSON, 1984). In particular, there can be a complex velocity change at mid Layer 2 depths which have not been consistently observed for horizontal towed array and OBS refraction seismic records.

In the last 5 years, it has become possible to carry out deep crustal marine seismic experiments with borehole geophones in the same fashion as "conventional" exploration VSP. STEPHEN (1977) has extensively discussed the advantages of insitu borehole seismic data for further resolving upper marine crustal velocity structures.

As in conventional shallow borehole seismic reconnaissance, the present marine crustal application of VSP offers many potential advantages not otherwise attainable, including:

detection of direct waves for accurate (shallow) sediment velocity determination;

improved resolution of interference complexes and traveltime triplications;

Since (at the time of this writing) there does not yet exist a specific marine crustal VSP data set in the public domain (STEPHEN, 1984; PUJHOL etal, 1984), the above applications of deep crustal VSP are investigated in the following for the simplest 3-layer ocean crustal model due to RAITT (1963). In particular, the following aspects are considered:

1. up vs. downgoing wave information, via traveltime and raypath analysis, as a function of source-receiver offsets
2. Refraction information " "
3. Deep shear wave data, via horizontal and vertical components
4. Shallow shear wave effects from minor nearsurface model variations (Sv velocity gradients on top of Layer 1)
5. Seismic interface waves/channeled evanescent waves

In the context of experimental VSP geometries, STEPHEN (1977; 1980; 1983) has discussed the necessity of carefully considering the optimal location of a buried source in respect of improved resolution of specific bodywave arrivals from deeper transition layers of interest.

Because of the relative newness and general unfamiliarity with the techniques of field and analytical VSP procedures, it is necessary to carefully assess experimental requirements (S-R offset, S depth, # and location of receivers, etc) with regard to environmental complexities (trapped modes; multiples and mode conversions) via synthetic VSP modeling, before actual field surveys are undertaken.

The present section reports the results of computing synthetic VSPs using the fullwavefield solution of "SAFARI", for the simplest possible ocean crustal model due to RAITT (1963), to assess the significance of possible realistic experimental parameters (**Figure 85**). Figure 85 shows the corresponding fullwave horizontal seismic profile for the RAITT v/z model. Here considerable trial and error testing was necessary in order to find an optimal value of $c_{phase_{MIN}}$, which would cut out the overpoweringly strong direct water wave arrival, while at the same time preserving all body wave data. Only the final results of this testing are shown below.

Figure 85

Idealized ocean crustal v/z model (after RAITT, 1963) with corresponding suite of Greens function integrands and synthetic reflectivity horizontal (OBS) seismic profile

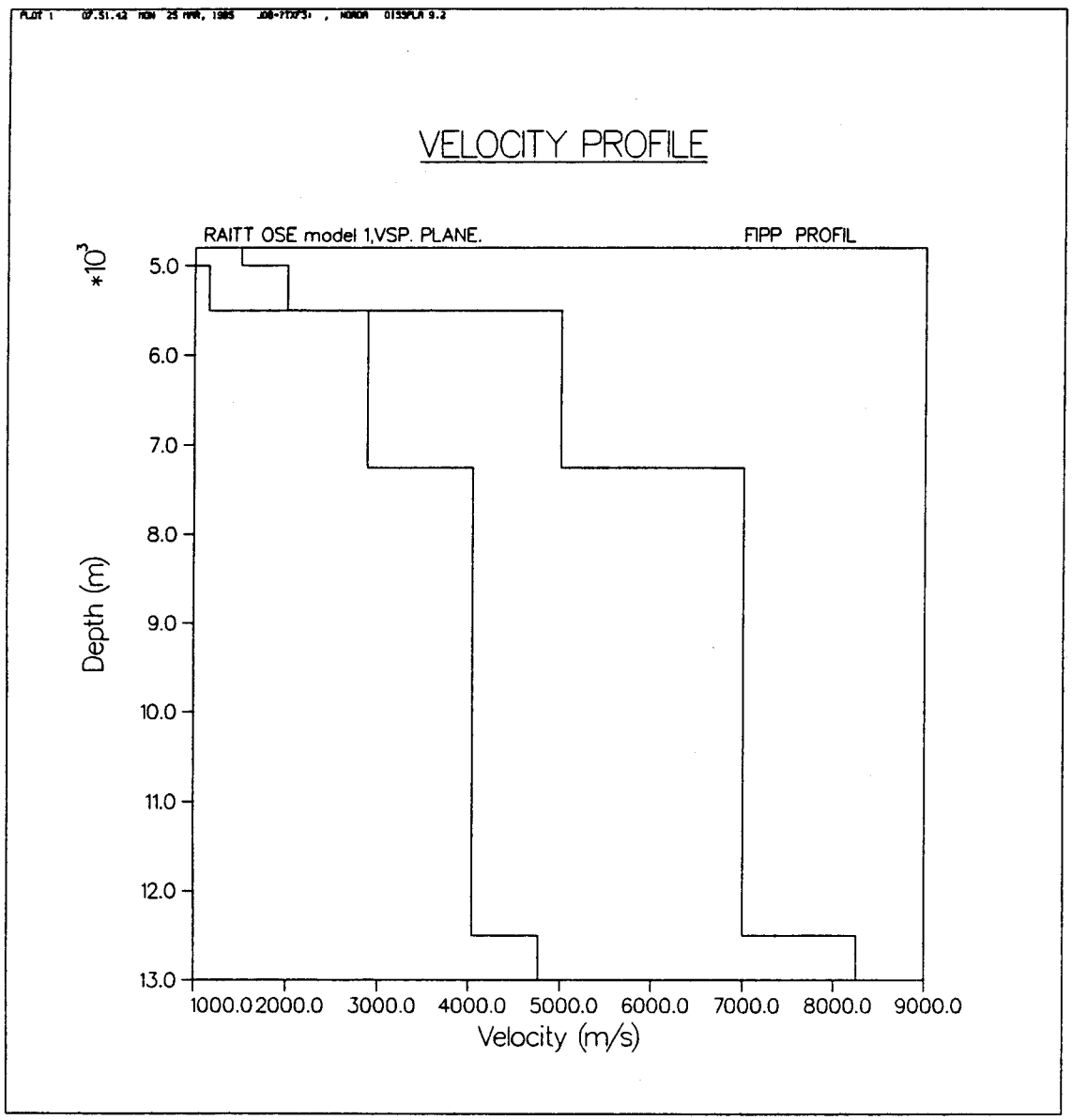
VELOCITY PROFILE
RAITT OSE model 1,VSP. PLANE.
FIPP PROFIL
*10^3
5.0
6.0
7.0
8.0
9.0
10.0
11.0
12.0
13.0
Depth (m)
1000.0 2000.0 3000.0 4000.0 5000.0 6000.0 7000.0 8000.0 9000.0
Velocity (m/s)

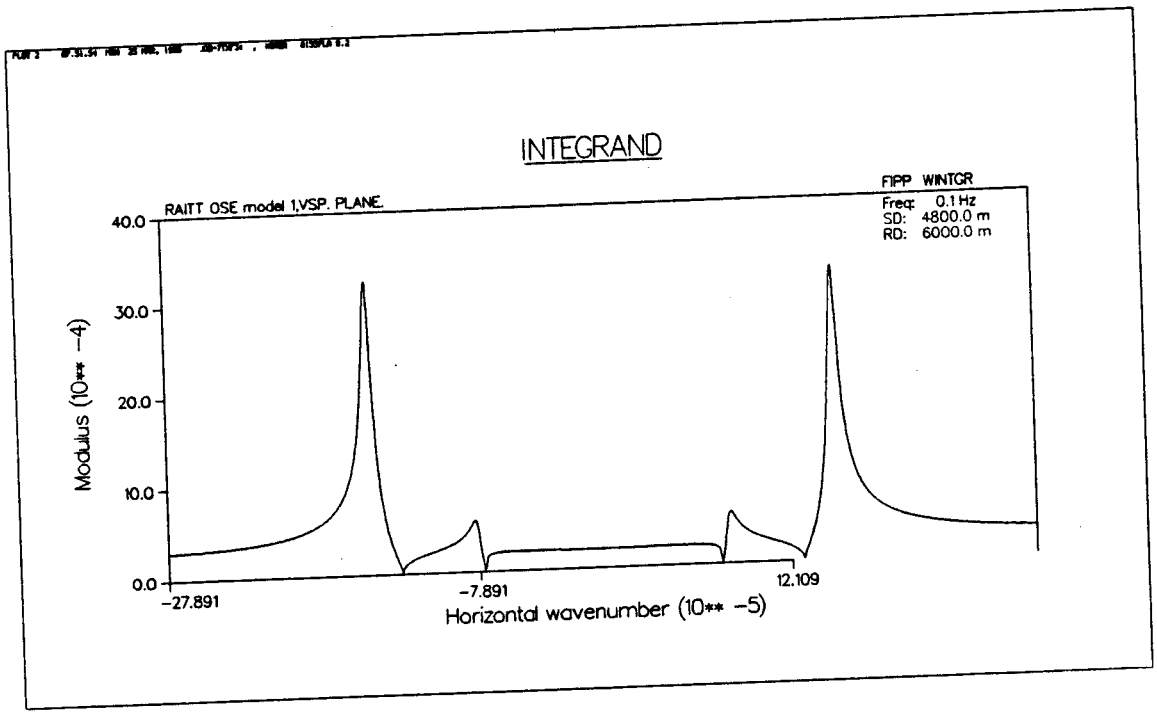
INTEGRAND
RAITT OSE model 1,VSP. PLANE.
FIPP WINTGR
Freq: 0.1 Hz
SD: 4800.0 m
RD: 6000.0 m
40.0
30.0
20.0
10.0
0.0
Modulus (10** -4)
-27.891
-7.891
12.109
Horizontal wavenumber (10** -5)

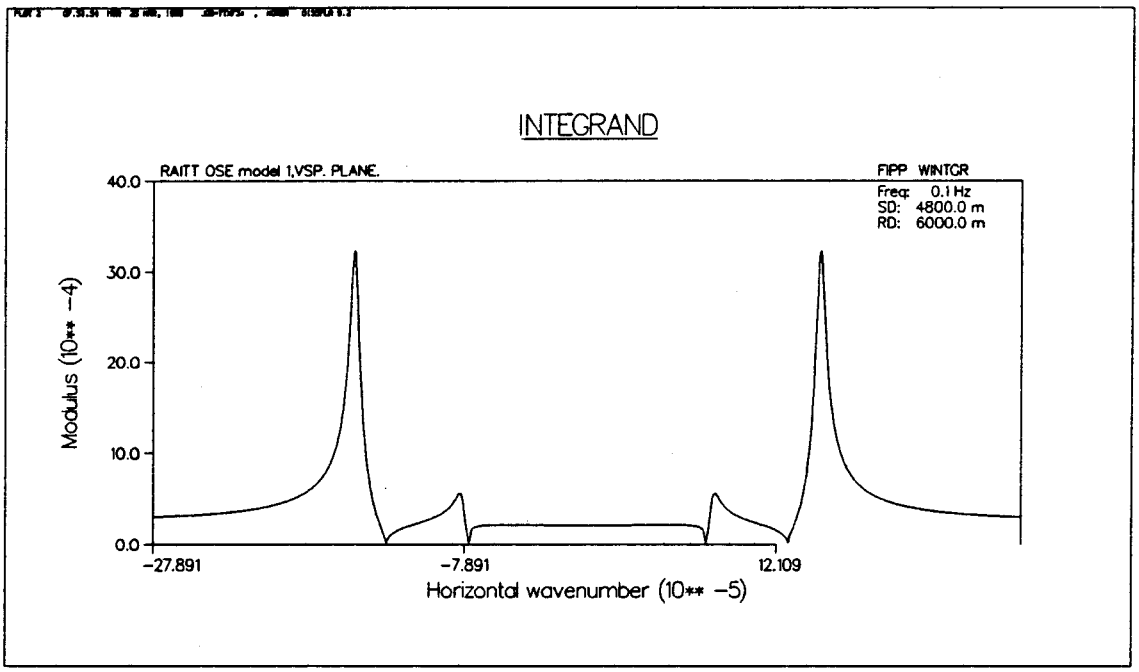
INTEGRAND
RAITT OSE model 1,VSP. PLANE.
FIPP WINTGR
Freq: 0.1 Hz
SD: 4800.0 m
RD: 6000.0 m
40.0
30.0
20.0
10.0
0.0
Modulus (10** -4)
-27.891
-7.891
12.109
Horizontal wavenumber (10** -5)

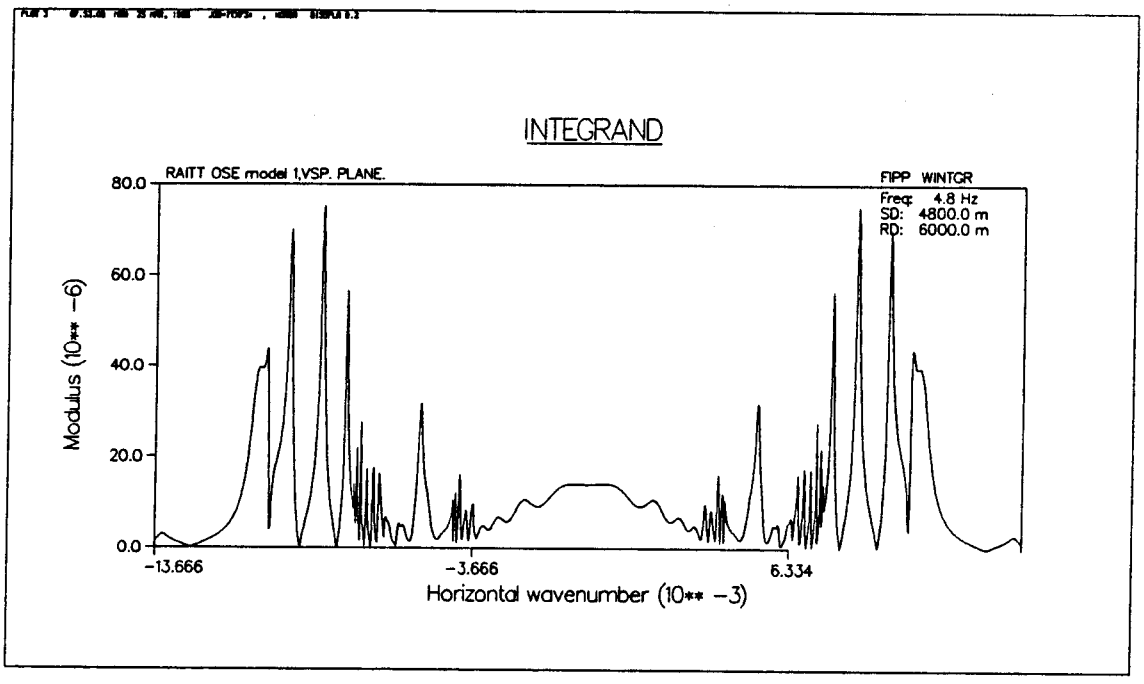
INTEGRAND
RAITT OSE model 1,VSP. PLANE.
FIPP WINTGR
Freq: 4.8 Hz
SD: 4800.0 m
RD: 6000.0 m
80.0
60.0
40.0
20.0
0.0
Modulus (10** -6)
-13.666
-3.666
6.334
Horizontal wavenumber (10** -3)

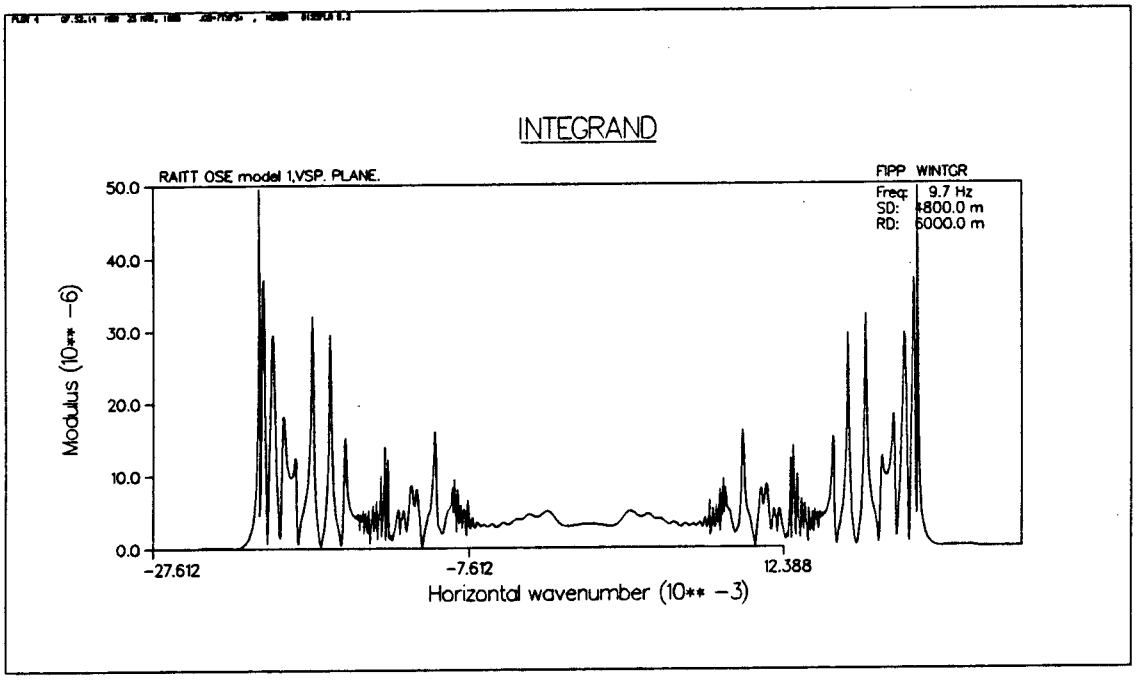
INTEGRAND
RAITT OSE model 1,VSP. PLANE.
FIPP WINTGR
Freq: 9.7 Hz
SD: 4800.0 m
RD: 6000.0 m
Modulus (10** -6)
50.0
40.0
30.0
20.0
10.0
0.0
-27.612
-7.612
12.388
Horizontal wavenumber (10** -3)

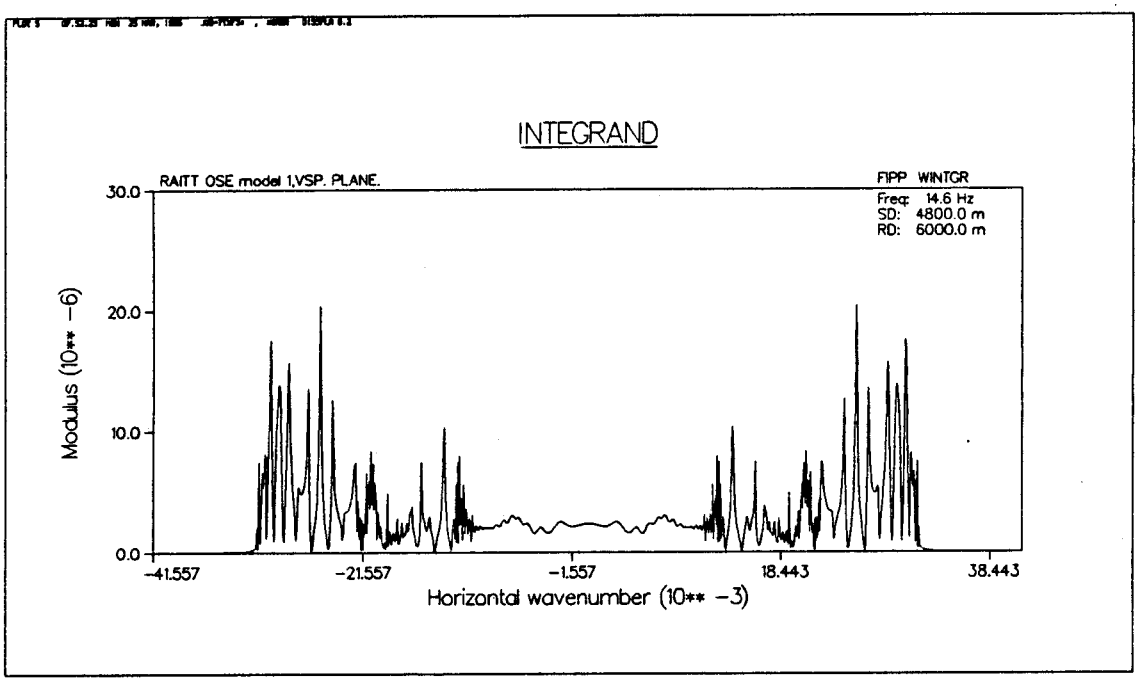
INTEGRAND
RAITT OSE model 1,VSP. PLANE.
FIPP WINTGR
Freq: 14.6 Hz
SD: 4800.0 m
RD: 6000.0 m
30.0
20.0
10.0
0.0
Modulus (10** −6)
−41.557
−21.557
−1.557
18.443
38.443
Horizontal wavenumber (10** −3)

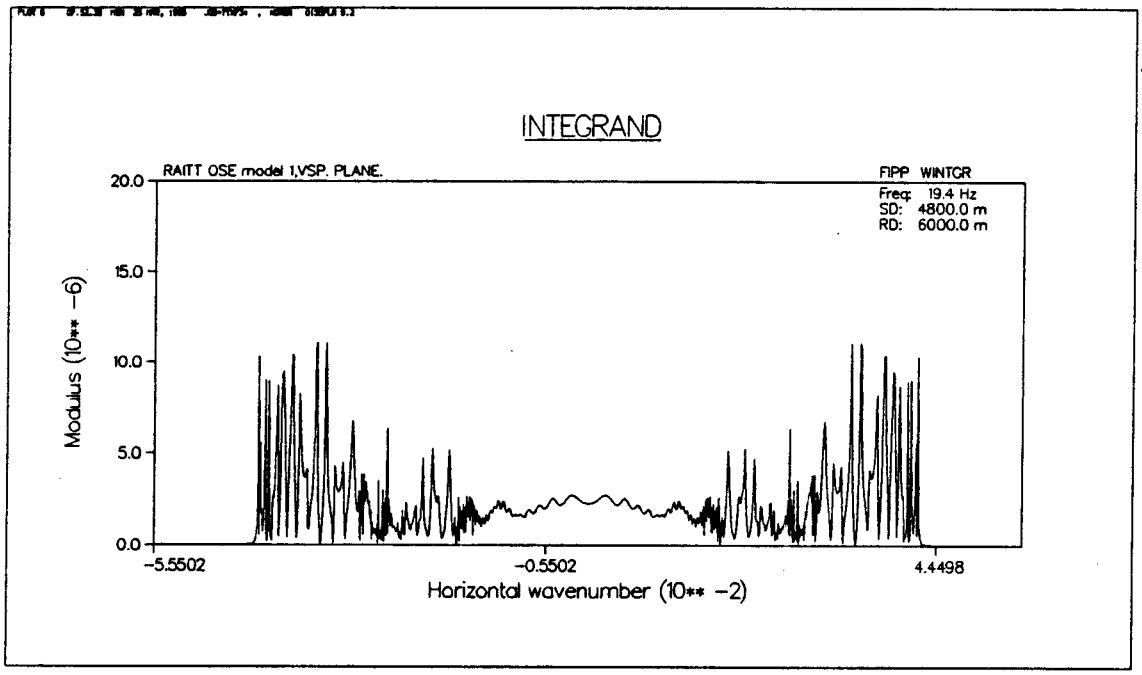
INTEGRAND
RAITT OSE model 1,VSP. PLANE.
FIPP WINTGR
Freq: 19.4 Hz
SD: 4800.0 m
RD: 6000.0 m
20.0
15.0
10.0
5.0
0.0
Modulus (10** −6)
−5.5502
−0.5502
4.4498
Horizontal wavenumber (10** −2)

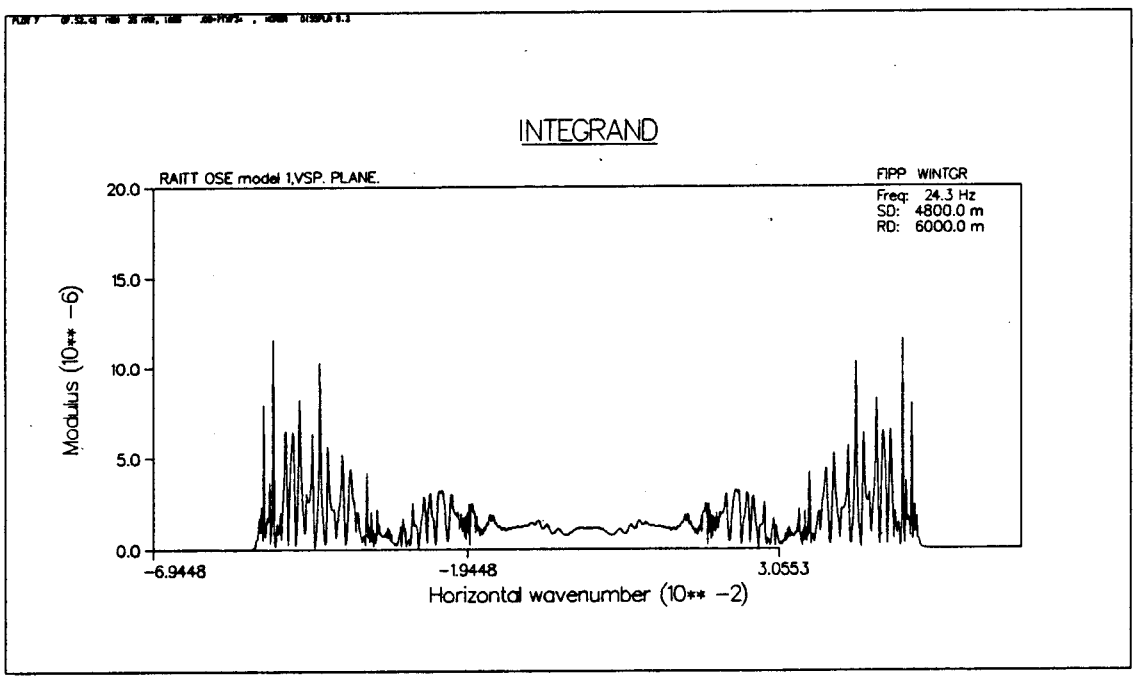
INTEGRAND
RAITT OSE model 1,VSP. PLANE.
FIPP WINTGR
Freq: 24.3 Hz
SD: 4800.0 m
RD: 6000.0 m
20.0
15.0
10.0
5.0
0.0
Modulus (10** -6)
-6.9448
-1.9448
3.0553
Horizontal wavenumber (10** -2)

VERTICAL PARTICLE VELOCITY

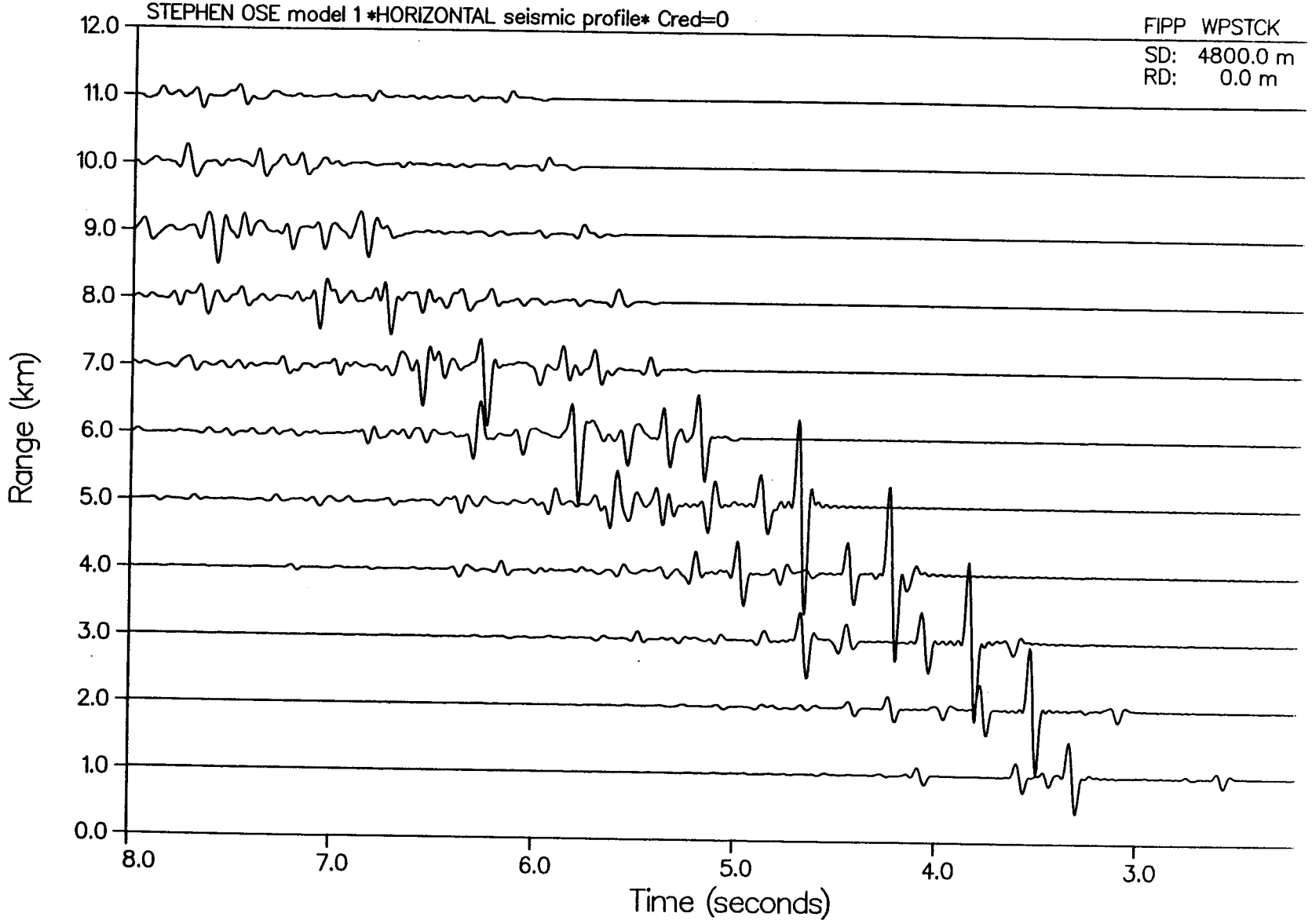

Figures 86, 87 and **88** shows the synthetic VSPs computed over a number of source-receiver offset ranges, here spanning distances from 1.0km to 5.0km, in geophone/vertical and horizontal particle velocity, and hydrophone/normal stress=pressure records. Because $\Delta z < V_{min}/2f_{max} = 75$, here the response is adequately sampled by 10 equispaced subsurface receivers positioned between 6000 and 7000 m depth into Layer 2. An elastic solid v/z model incorporating velocity = vp/1.5 and $\beta = 2\alpha$.

Comparing any V, H or P component synthetic VSP record for 1, 3 and 5km offsets plainly shows the dramatic change in the relative strengths of first and multiple arrivals as S-R offsets/angle of incidence and hence reflexion coefficients are increased. As can be seen, until a certain range is reached for the simple structural layer features here in question, downgoing waves dominate the VSP section. By contrast, for a 5km offset, visible downgoing waves have almost completely vanished, and the record response is dominated by upgoing reflected refracted and converted modes, except for two near vertical upgoing (refracted) arrivals. In this model, between 2 and 3km offsets produced an optimal balance of clearly resolved up and downgoing wavefield information for all layer interfaces. Comparing records for the same source-receiver offset over pressure, horizontal and vertical particle velocities, the corresponding VSPs are shown to differ radically even for clearly main features on the basic RAITT v/z model. Most notable perhaps are the phase inversions of

Figure 86, 87 and 88

Full wavefield synthetic VSPs (plane wave line source) for full shear elastic Raitt v/z model, over selected range of OSE offsets $x_{min/max}$= 1km/5km, in:

Geophone	Vertical particle velocity
Geophone	Horizontal particle velocity
Hydrophone	Pressure

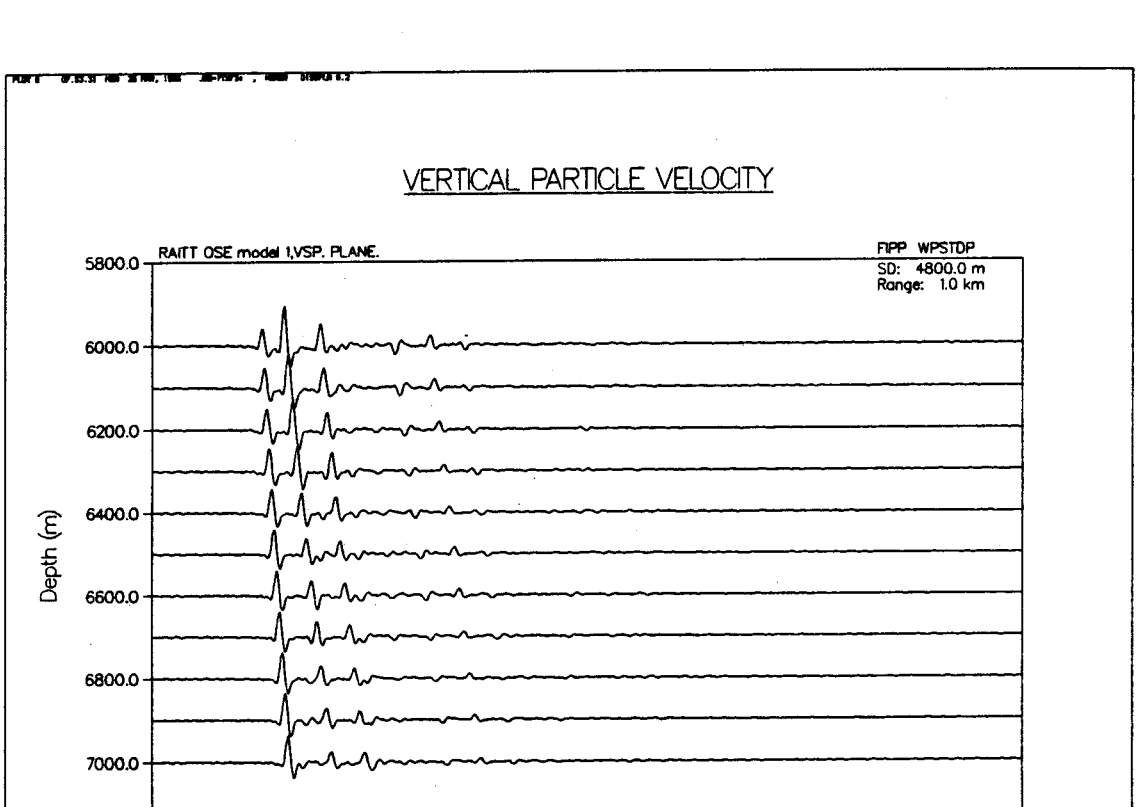
VERTICAL PARTICLE VELOCITY
RAITT OSE model 1,VSP. PLANE.
FIPP WPSTDP
SD: 4800.0 m
Range: 1.0 km
Depth (m)
5800.0
6000.0
6200.0
6400.0
6600.0
6800.0
7000.0
7200.0
0.0
1.0
2.0
3.0
4.0
5.0
Time (seconds)

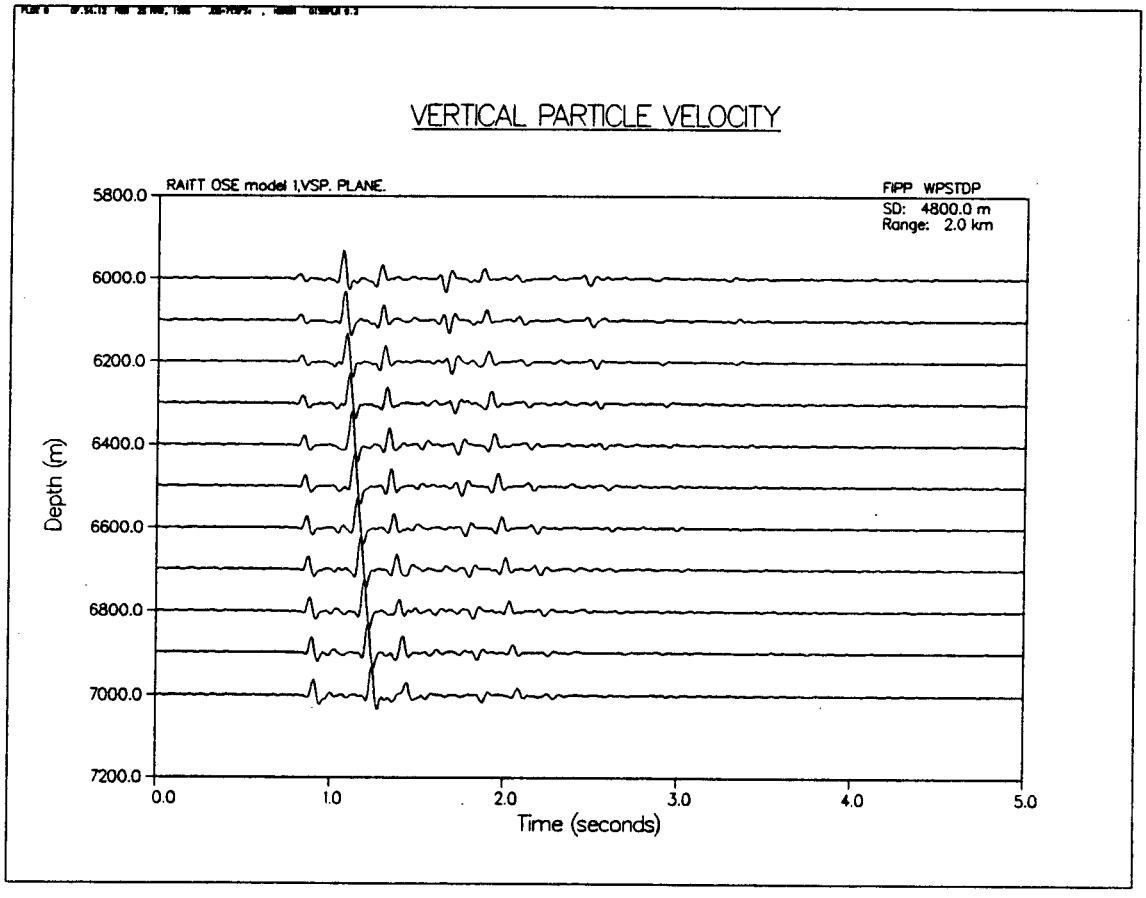
VERTICAL PARTICLE VELOCITY
RAITT OSE model 1,VSP. PLANE.
FIPP WPSTDP
SD: 4800.0 m
Range: 2.0 km
Depth (m)
5800.0
6000.0
6200.0
6400.0
6600.0
6800.0
7000.0
7200.0
0.0
1.0
2.0
3.0
4.0
5.0
Time (seconds)

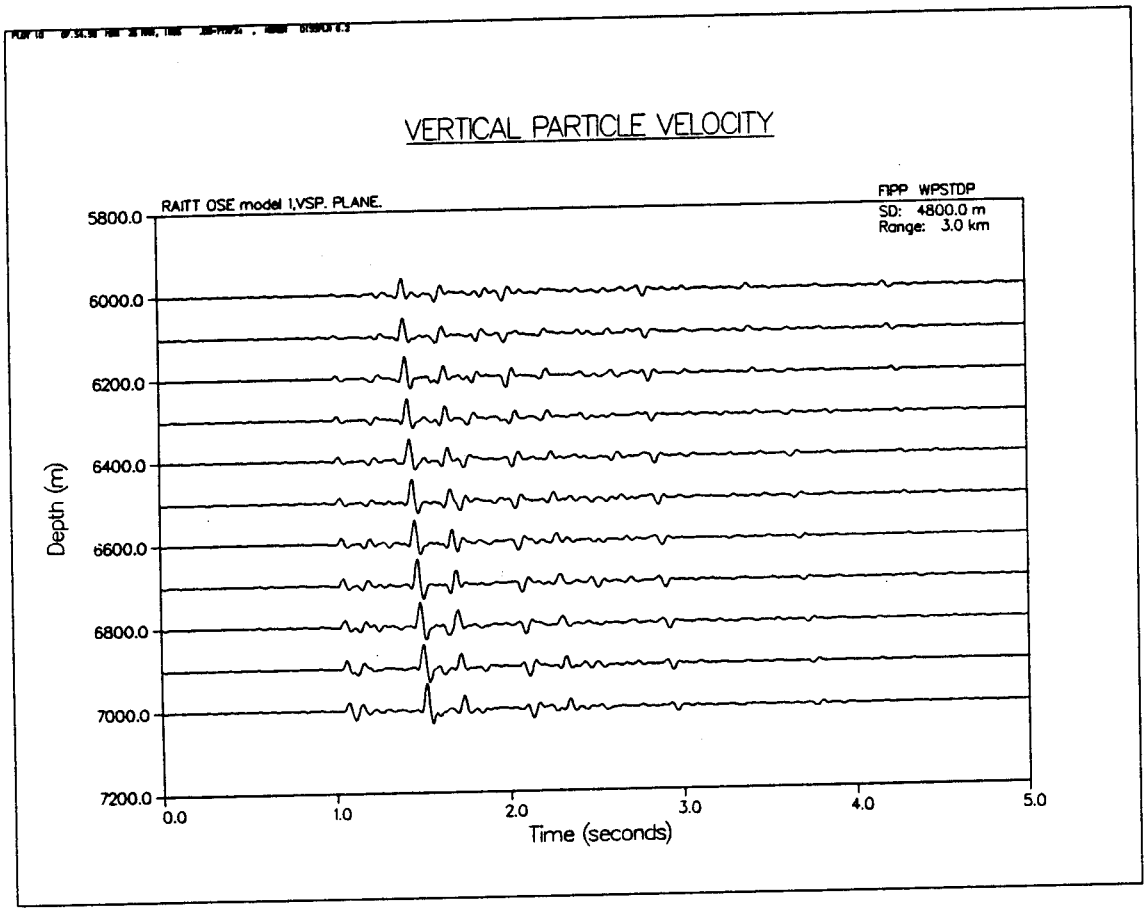
VERTICAL PARTICLE VELOCITY
RAITT OSE model 1,VSP. PLANE.
FIPP WPSTDP
SD: 4800.0 m
Range: 3.0 km
Depth (m)
5800.0
6000.0
6200.0
6400.0
6600.0
6800.0
7000.0
7200.0
0.0
1.0
2.0
3.0
4.0
5.0
Time (seconds)

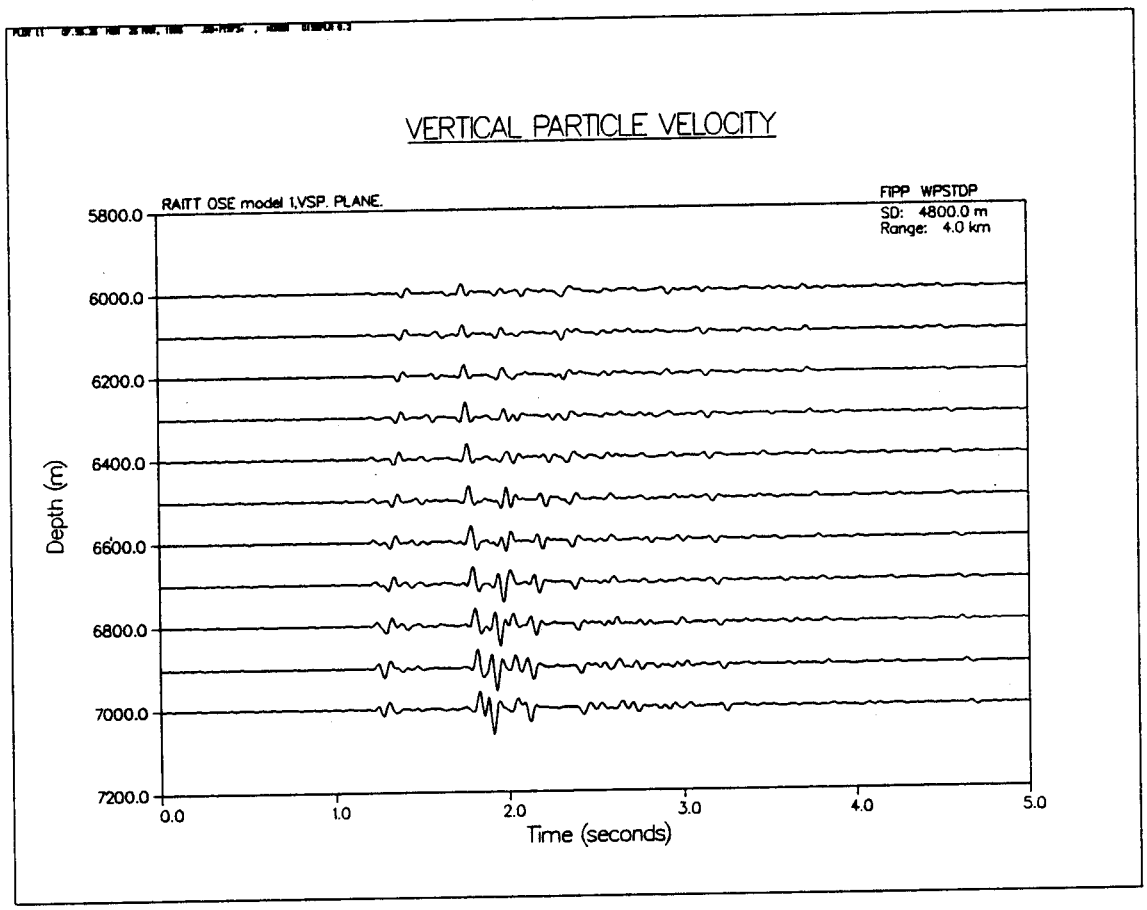
VERTICAL PARTICLE VELOCITY
RAITT OSE model 1.VSP. PLANE.
FIPP WPSTDP
SD: 4800.0 m
Range: 4.0 km
Depth (m)
5800.0
6000.0
6200.0
6400.0
6600.0
6800.0
7000.0
7200.0
0.0
1.0
2.0
3.0
4.0
5.0
Time (seconds)

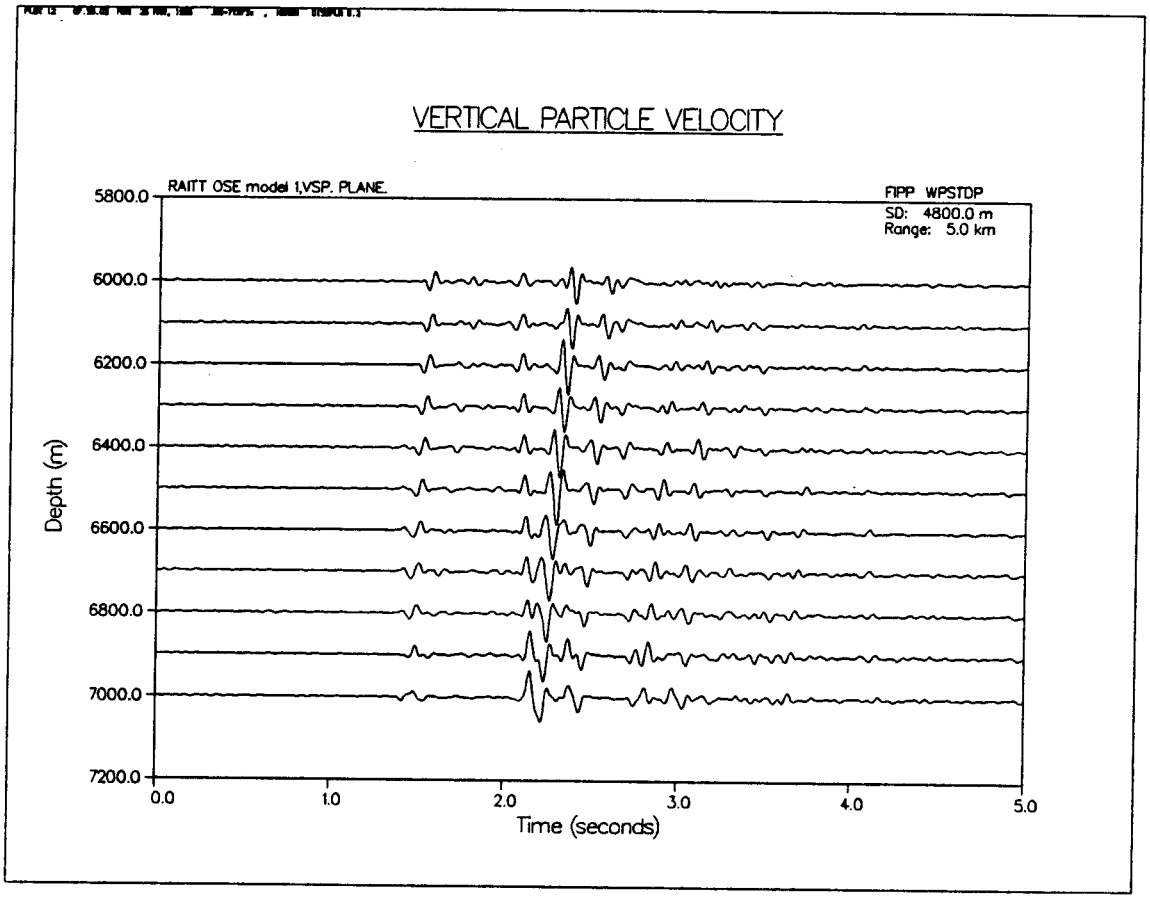
VERTICAL PARTICLE VELOCITY
RAITT OSE model 1,VSP. PLANE.
FIPP WPSTDP
SD: 4800.0 m
Range: 5.0 km
Depth (m)
5800.0
6000.0
6200.0
6400.0
6600.0
6800.0
7000.0
7200.0
0.0
1.0
2.0
3.0
4.0
5.0
Time (seconds)

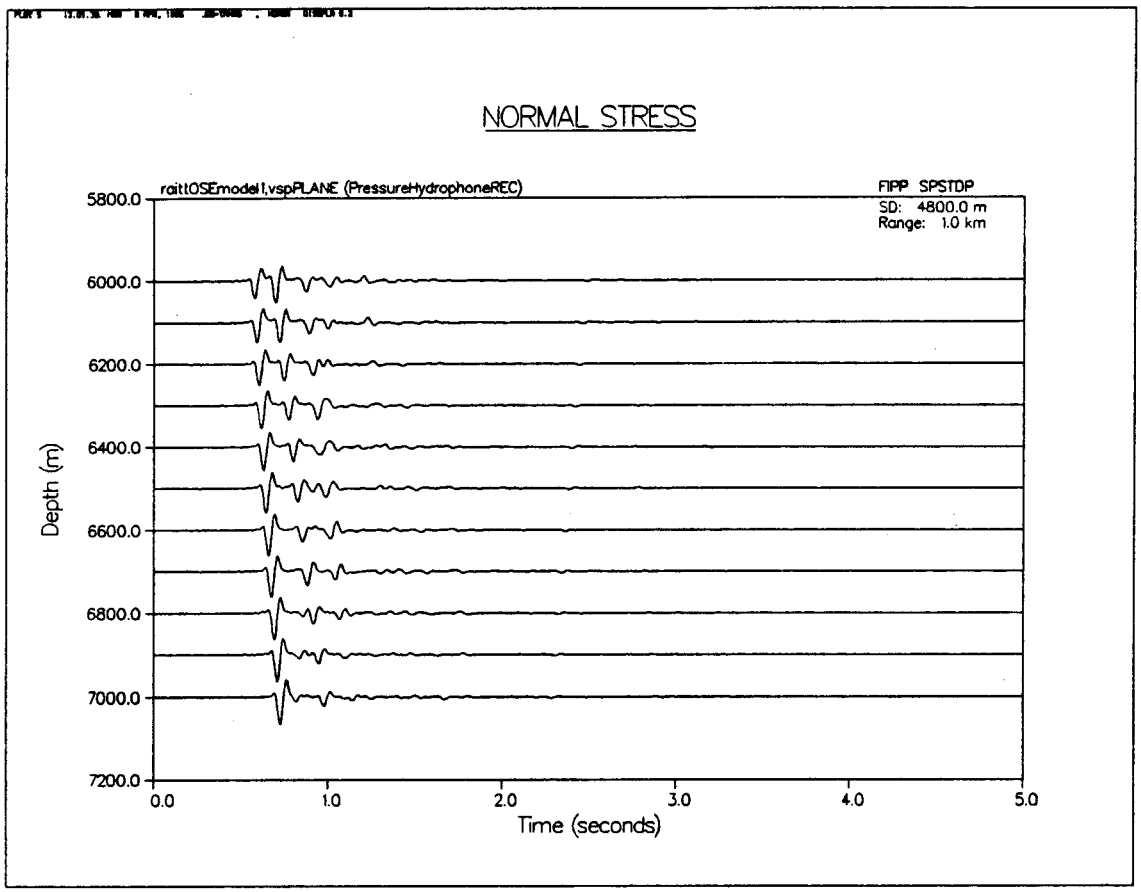
NORMAL STRESS
raitt0SEmodel1.vspPLANE (PressureHydrophoneREC)
FIPP SPSTDP
SD: 4800.0 m
Range: 1.0 km
5800.0
6000.0
6200.0
6400.0
6600.0
6800.0
7000.0
7200.0
Depth (m)
0.0
1.0
2.0
3.0
4.0
5.0
Time (seconds)

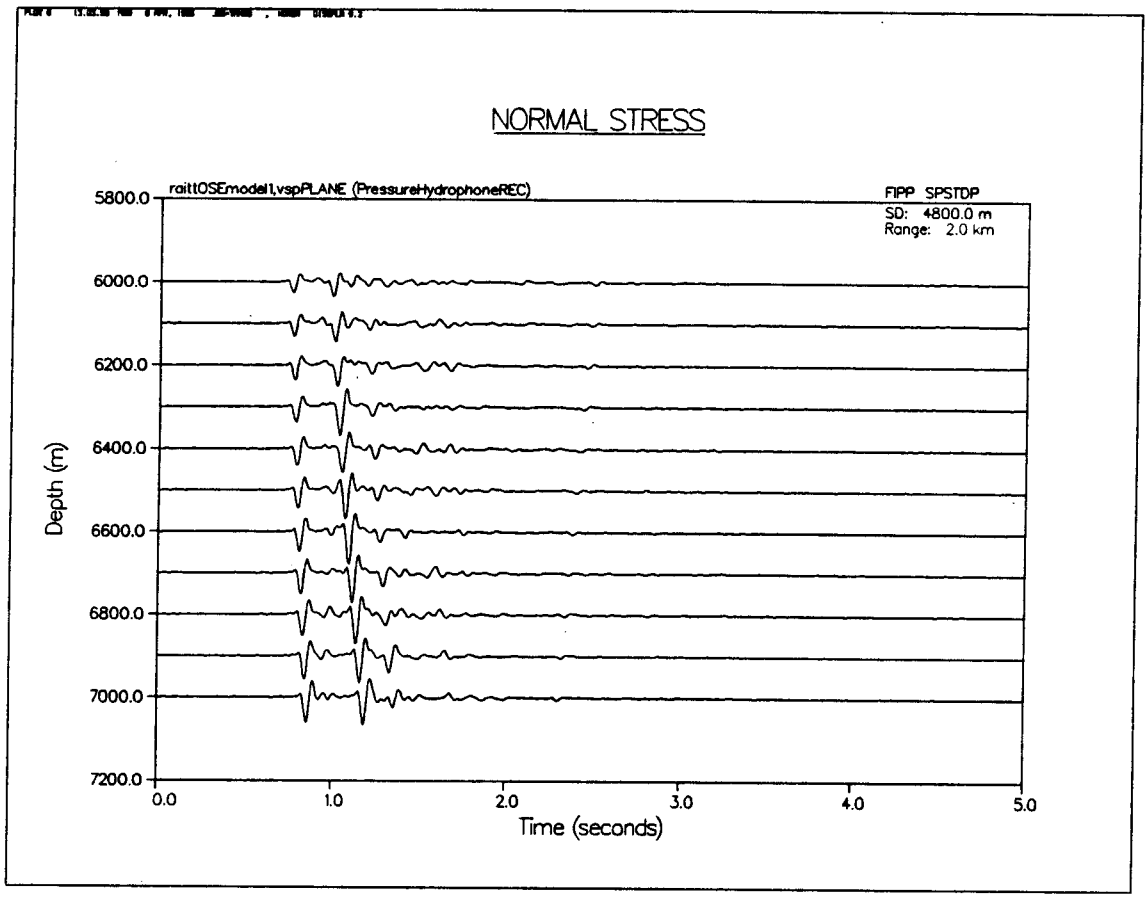
NORMAL STRESS
raittOSEmodel1.vspPLANE (PressureHydrophoneREC)
FIPP SPSTDP
SD: 4800.0 m
Range: 2.0 km
Depth (m)
5800.0
6000.0
6200.0
6400.0
6600.0
6800.0
7000.0
7200.0
0.0
1.0
2.0
3.0
4.0
5.0
Time (seconds)

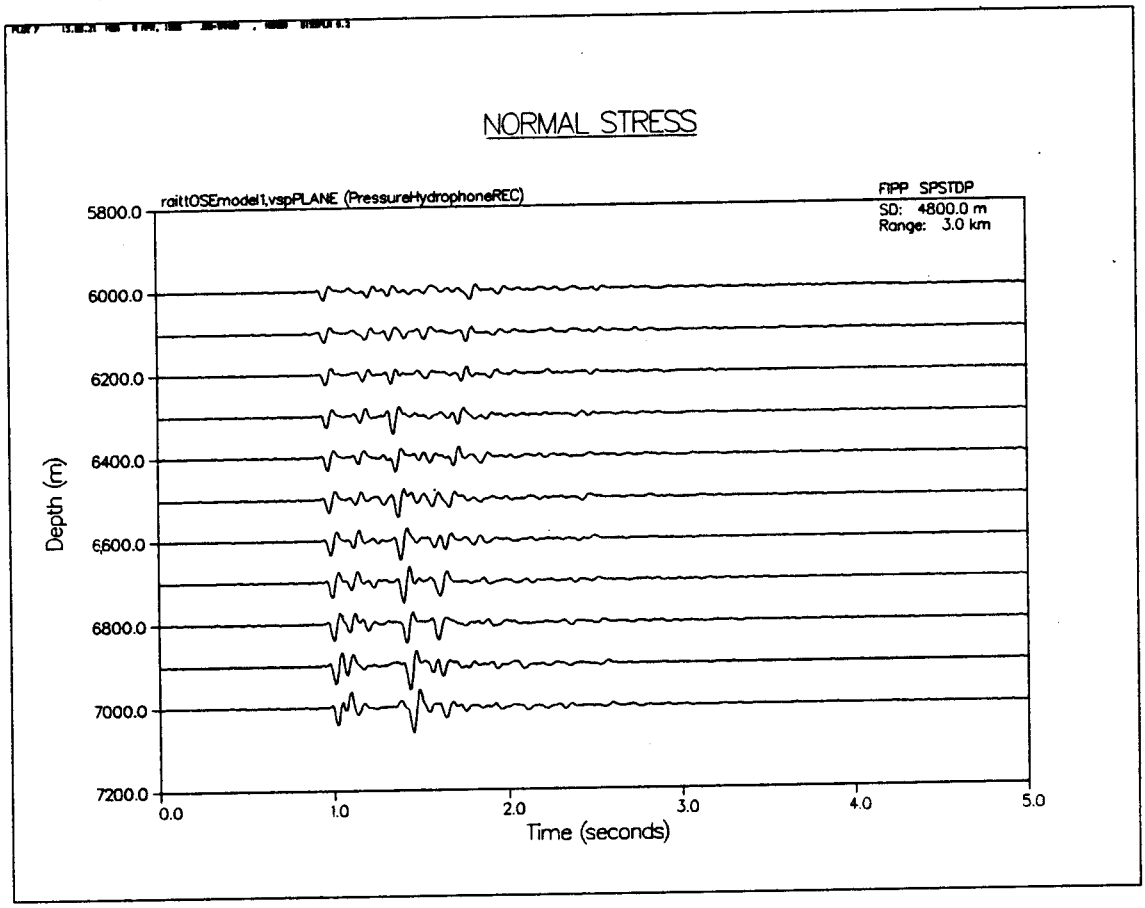
NORMAL STRESS
raitt0SEmodel1.vspPLANE (PressureHydrophoneREC)
FIPP SPSTDP
SD: 4800.0 m
Range: 3.0 km
5800.0
6000.0
6200.0
6400.0
6600.0
6800.0
7000.0
7200.0
Depth (m)
0.0
1.0
2.0
3.0
4.0
5.0
Time (seconds)

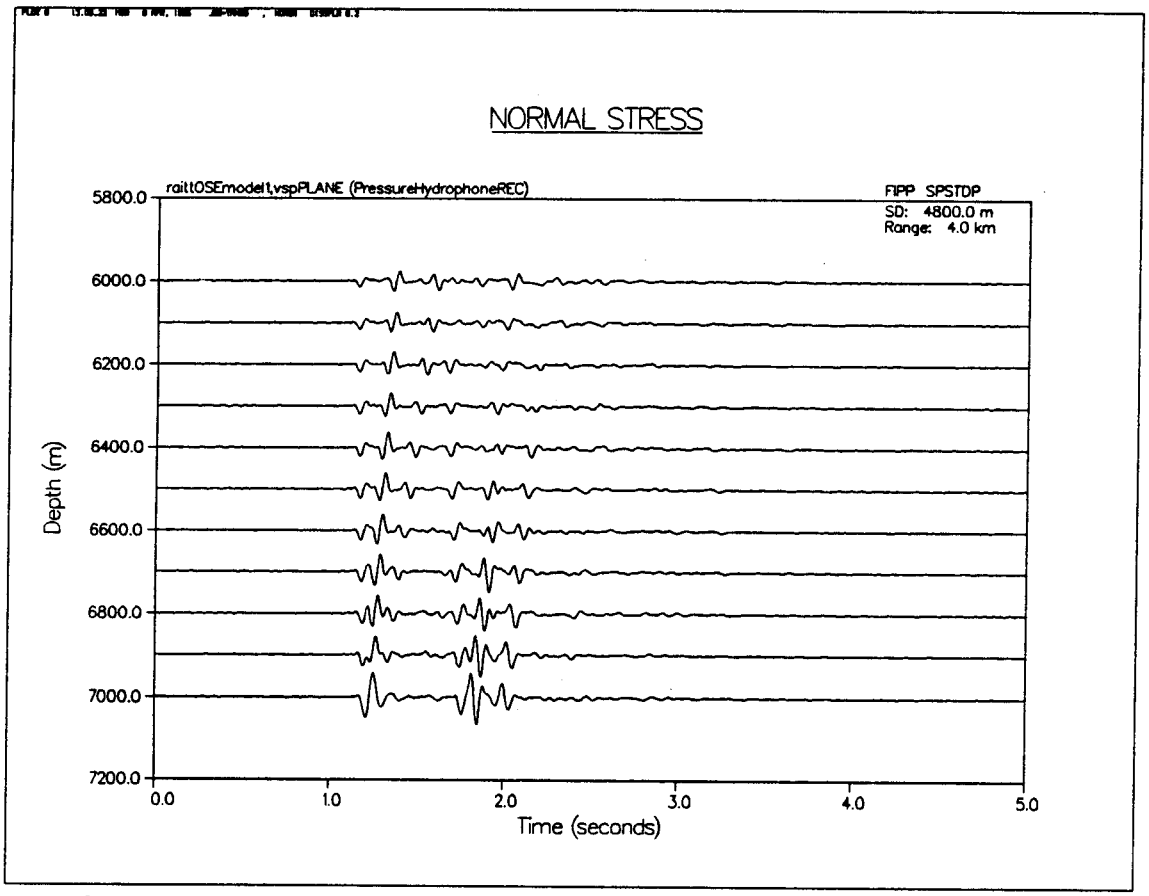
NORMAL STRESS
raitt0SEmodel1,vspPLANE (PressureHydrophoneREC)
FIPP SPSTDP
SD: 4800.0 m
Range: 4.0 km
5800.0
6000.0
6200.0
6400.0
6600.0
6800.0
7000.0
7200.0
Depth (m)
0.0
1.0
2.0
3.0
4.0
5.0
Time (seconds)

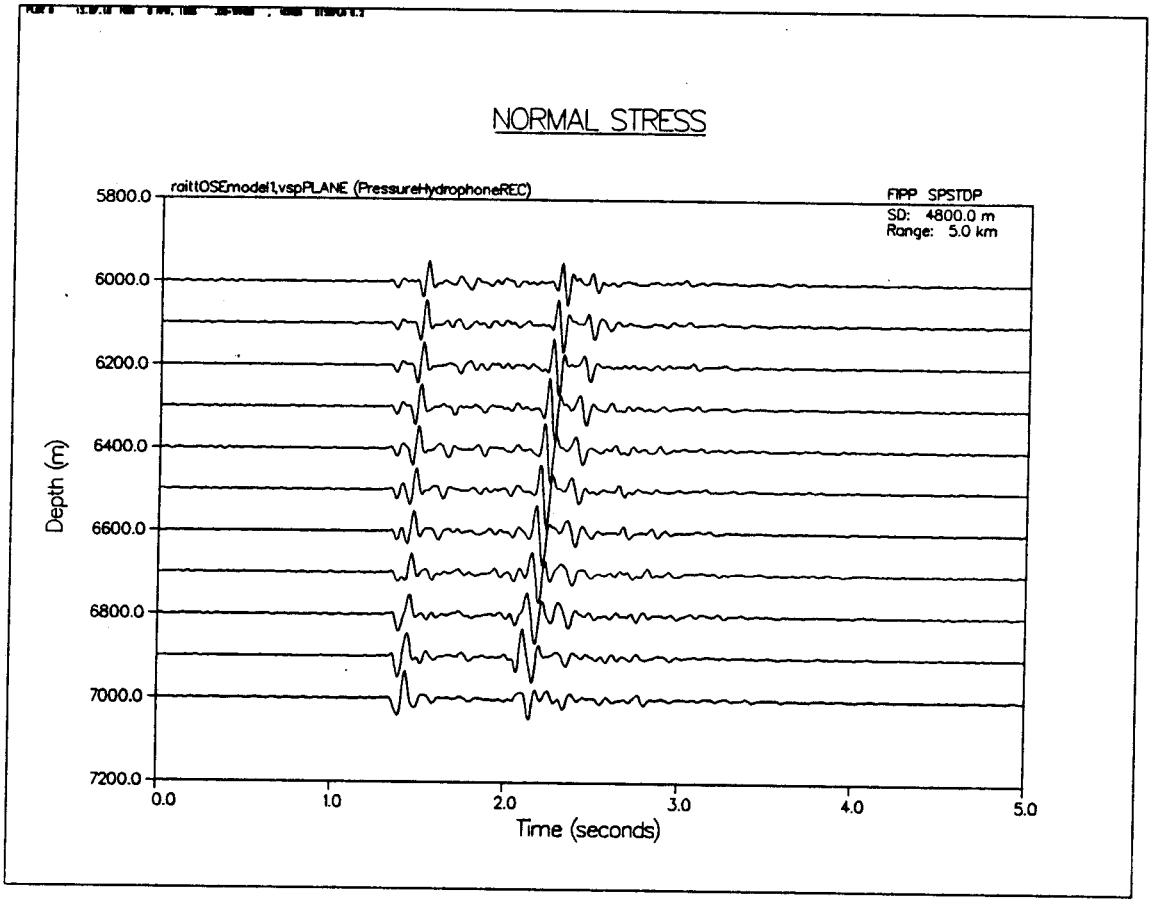
NORMAL STRESS
raittOSEmodel1.vspPLANE (PressureHydrophoneREC)
FIPP SPSTDP
SD: 4800.0 m
Range: 5.0 km
Depth (m)
5800.0
6000.0
6200.0
6400.0
6600.0
6800.0
7000.0
7200.0
0.0
1.0
2.0
3.0
4.0
5.0
Time (seconds)

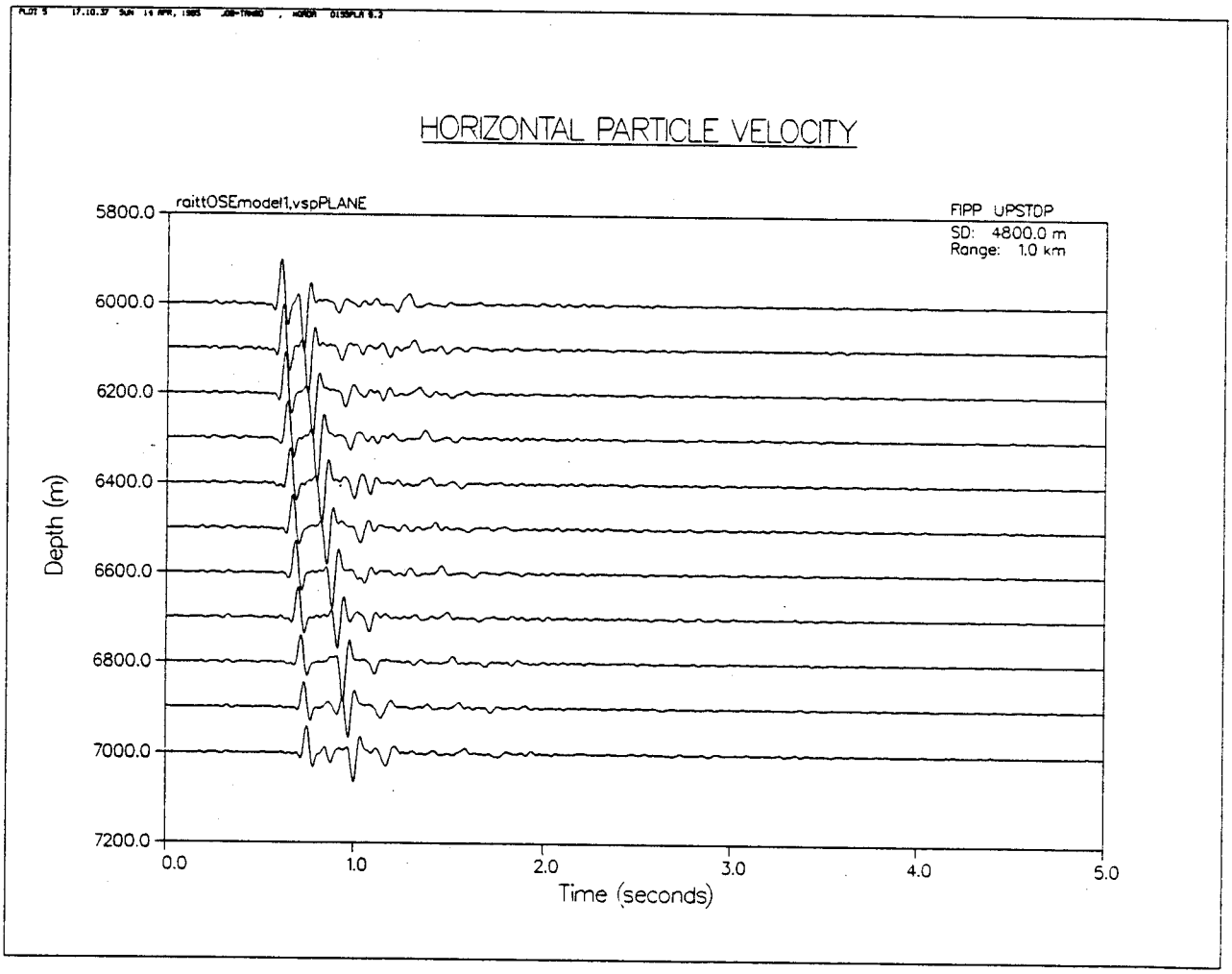
HORIZONTAL PARTICLE VELOCITY
raittOSEmodel1.vspPLANE
FIPP UPSTDP
SD: 4800.0 m
Range: 1.0 km
Depth (m)
5800.0
6000.0
6200.0
6400.0
6600.0
6800.0
7000.0
7200.0
0.0
1.0
2.0
3.0
4.0
5.0
Time (seconds)

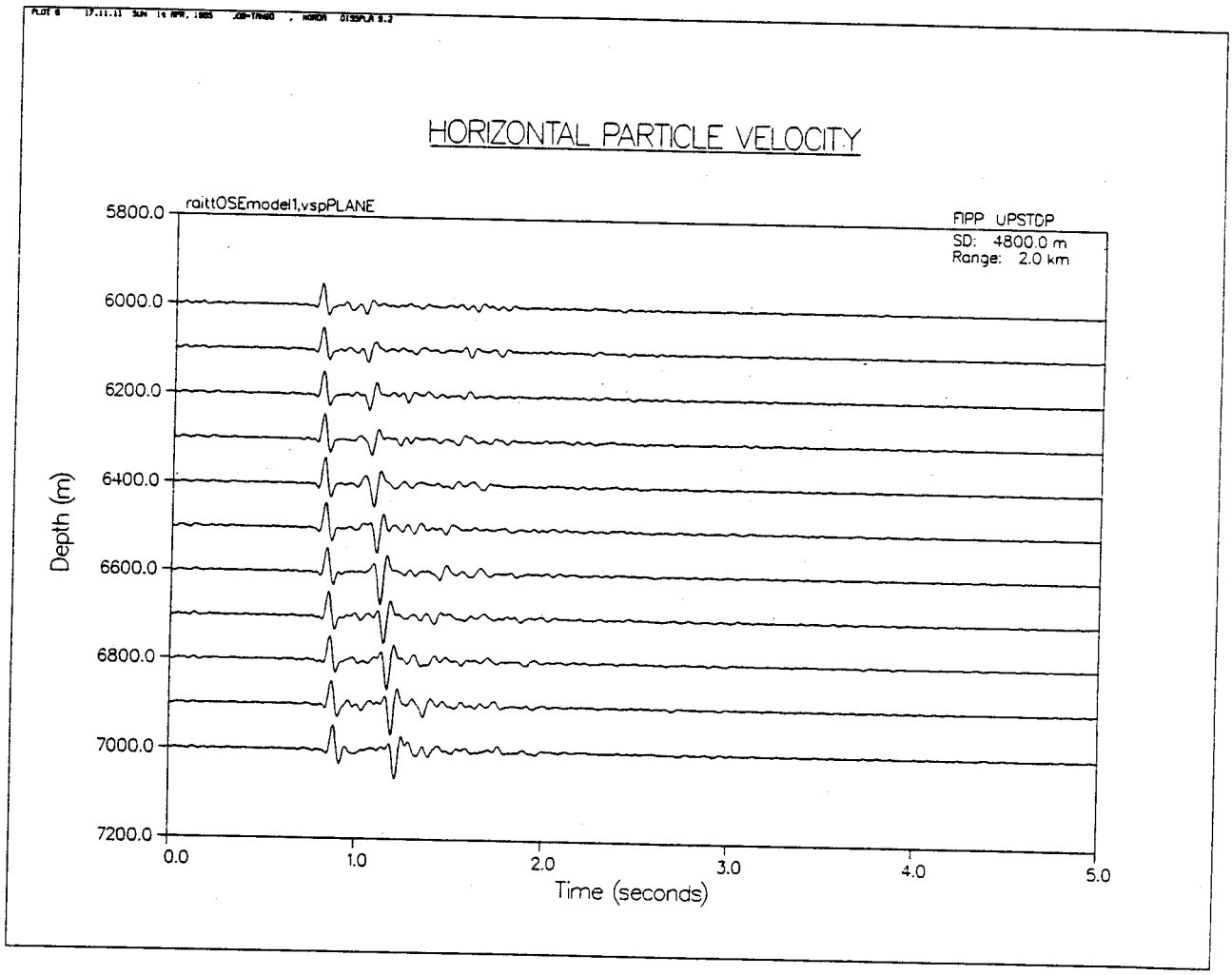
HORIZONTAL PARTICLE VELOCITY
raittOSEmodel1.vspPLANE
FIPP UPSTOP
SD: 4800.0 m
Range: 2.0 km
Depth (m)
5800.0
6000.0
6200.0
6400.0
6600.0
6800.0
7000.0
7200.0
0.0
1.0
2.0
3.0
4.0
5.0
Time (seconds)

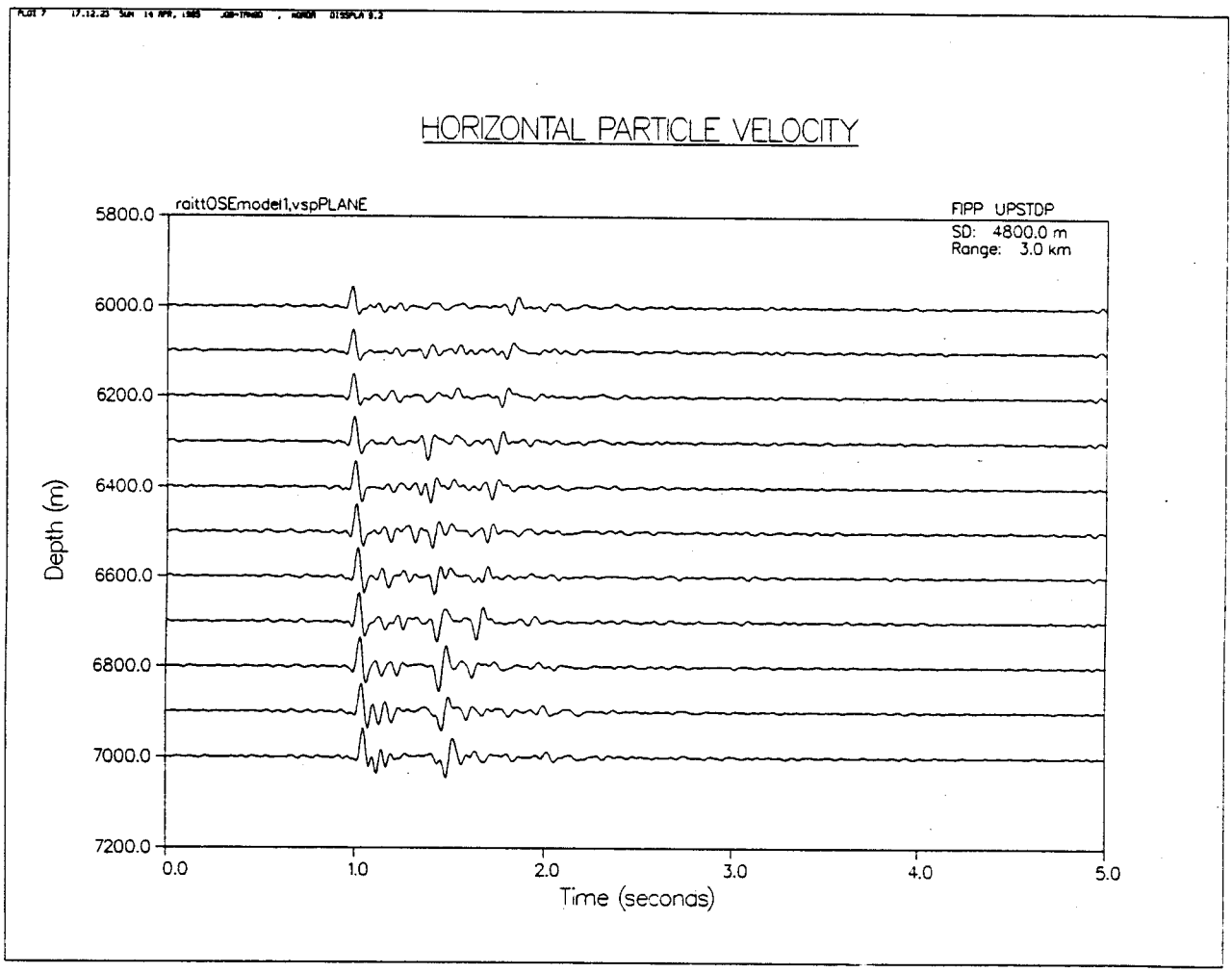
HORIZONTAL PARTICLE VELOCITY
raitt0SEmodel1.vspPLANE
FIPP UPSTDP
SD: 4800.0 m
Range: 3.0 km
Depth (m)
5800.0
6000.0
6200.0
6400.0
6600.0
6800.0
7000.0
7200.0
0.0
1.0
2.0
3.0
4.0
5.0
Time (seconds)

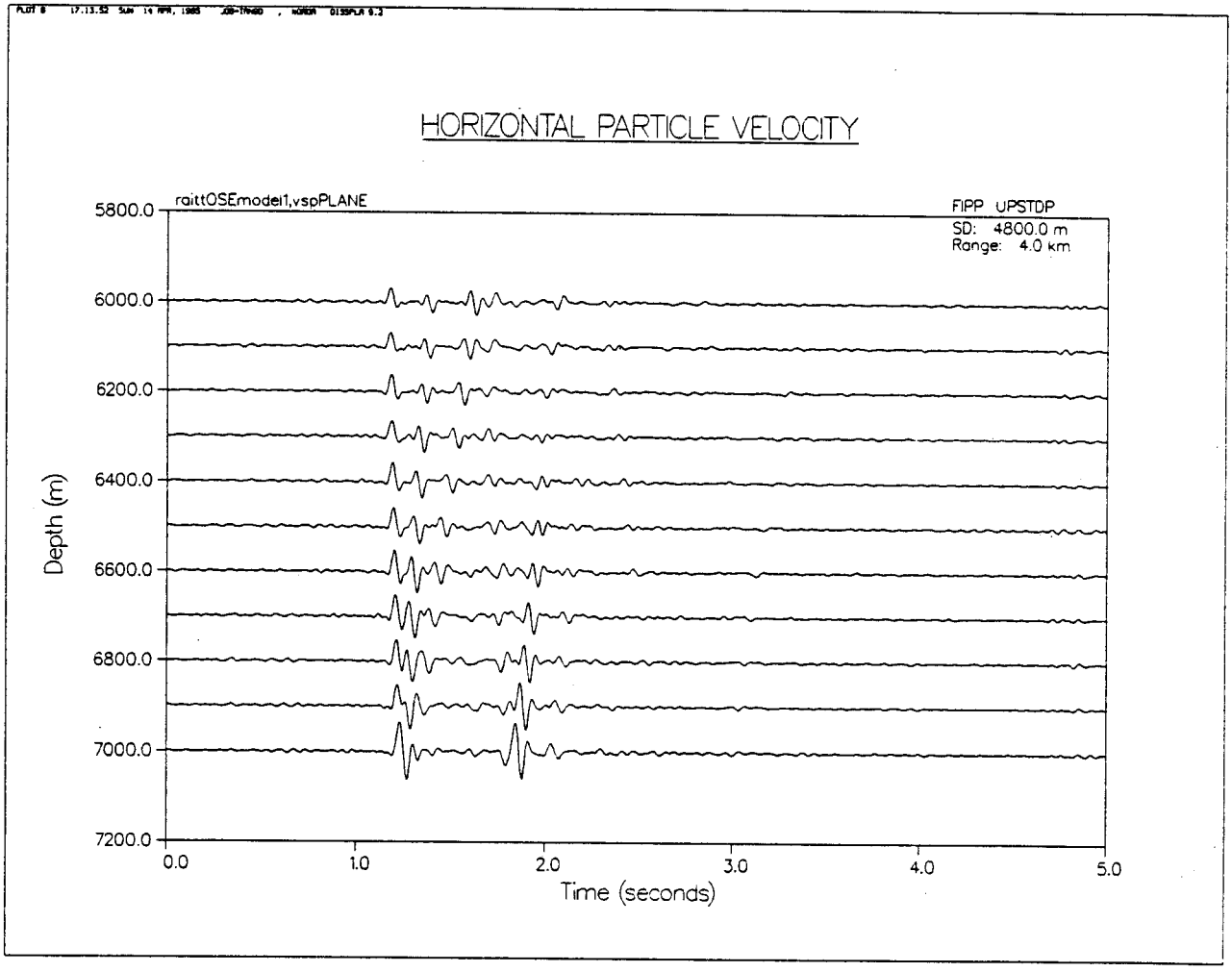
HORIZONTAL PARTICLE VELOCITY
raittOSEmodel1,vspPLANE
FIPP UPSTDP
SD: 4800.0 m
Range: 4.0 km
Depth (m)
5800.0
6000.0
6200.0
6400.0
6600.0
6800.0
7000.0
7200.0
0.0
1.0
2.0
3.0
4.0
5.0
Time (seconds)

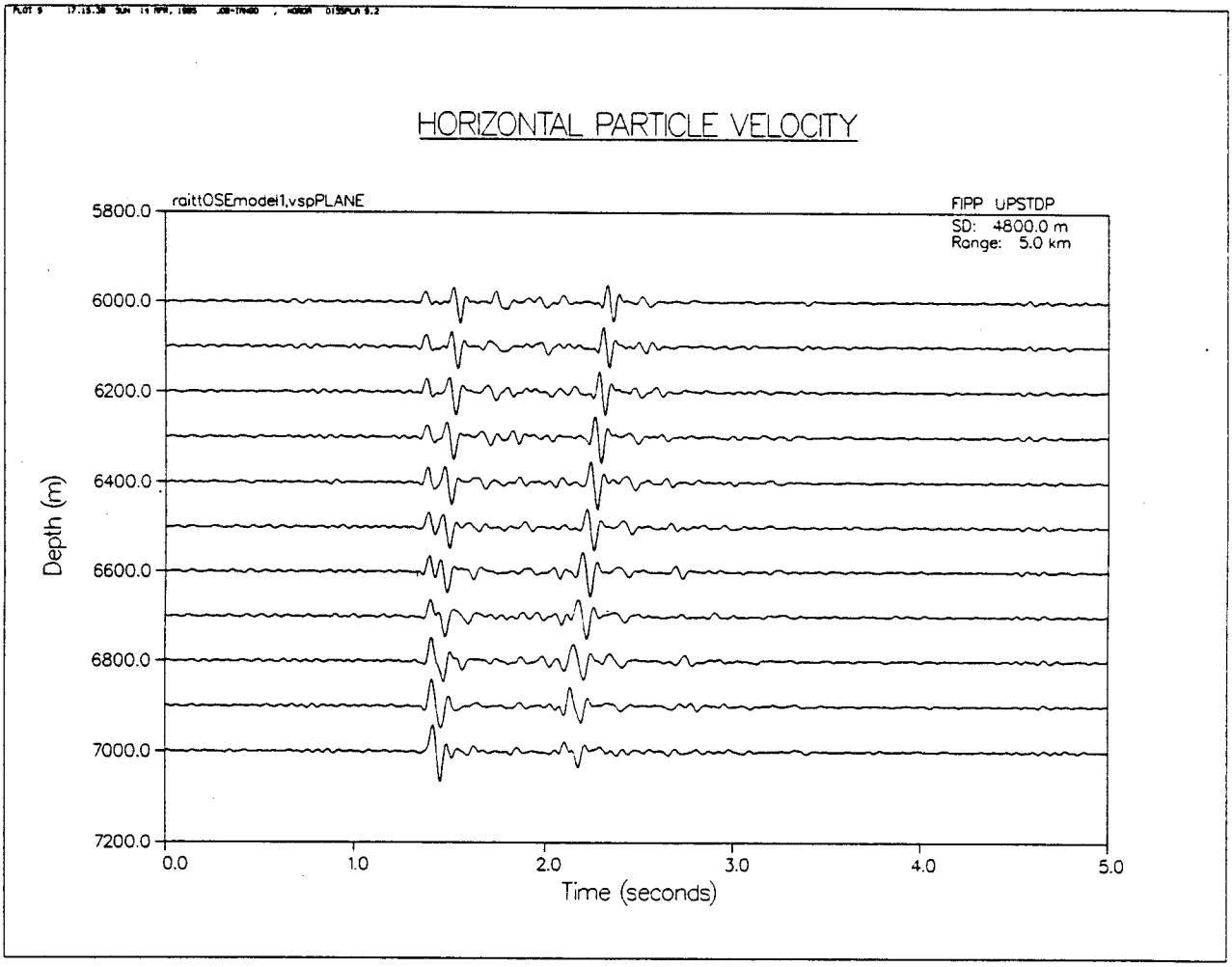
HORIZONTAL PARTICLE VELOCITY
raittOSEmodel1.vspPLANE
FIPP UPSTDP
SD: 4800.0 m
Range: 5.0 km
Depth (m)
5800.0
6000.0
6200.0
6400.0
6600.0
6800.0
7000.0
7200.0
0.0
1.0
2.0
3.0
4.0
5.0
Time (seconds)

the first arrivals between the acoustic pressure and vertical particle velocity records. Also evident is the much lesser total number of arrivals on the hydrophone record than on either geophone record. The exception here is the direct and reflected water water found at all offsets only on the hydrophone pressure records (and not on any geophone traces).

As can readily be seen (particularly for the far offset VSP records), even in the simplest possible generic ocean crustal model, the resultant VSP wavefield exhibits considerable complexity, comprising a mixture of direct, reflected and multiple P wave arrivals of all orders, P-to-SV mode conversions of both reflected and refracted type including multiples, and pure intermode conversions (P-SV-P). To further determine the precise origin of each arrival, the simple decompositional facility of a layered fullwavefield solution can be employed, to compute the P-wave only, no-surface and no-bottom synthetic VSP responses. When compared to the full elastic response previously computed above, these should respectively show the relative degee of P-SV conversion, surface multiple percentage and deep upgoing primary contributions (**Figure 89**). Here, as in the TEMME-MULLER case above, the free surface multiples are without doubt the most significant in both number and amplitude.

For very large source-receiver offsets with respect to maximum layer depths of interest, as noted in the previous example, the importance of refracted head wave contributions should be considered. If the velocity increases across the interface in question, the critical distance for the layers here in question will occur between the source and receiver array. In this case, the critically refracted wave arrives just ahead of the reflected wave (increasing its lead over the direct P wave as S-R offset is

Figure 89

Full wavefield synthetic VSPs (plane wave line source) in Vertical particle velocity records for full shear elastic Raitt v/z model, x_{offset}=3km:

(a) with

(b) without

free surface reflection events

VERTICAL PARTICLE VELOCITY

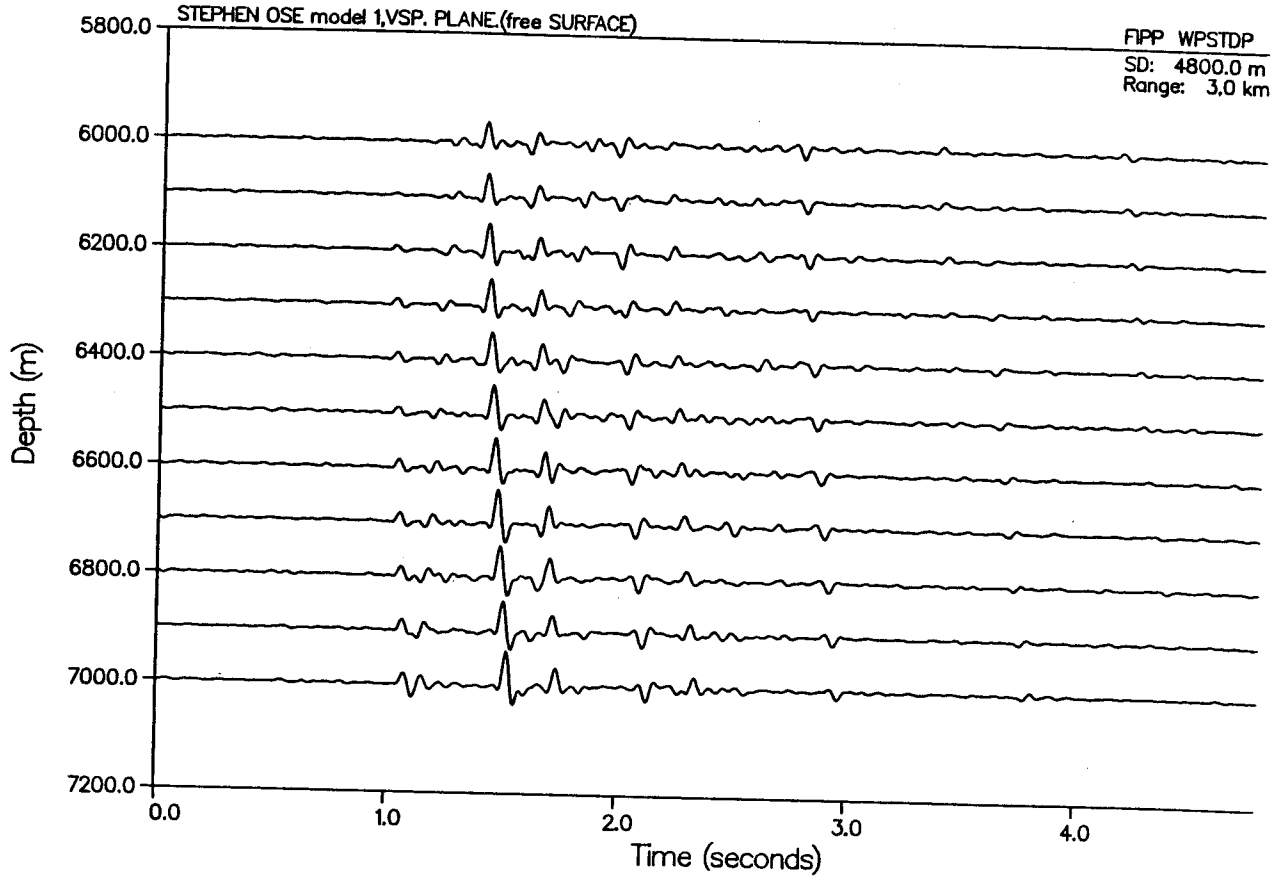

VERTICAL PARTICLE VELOCITY

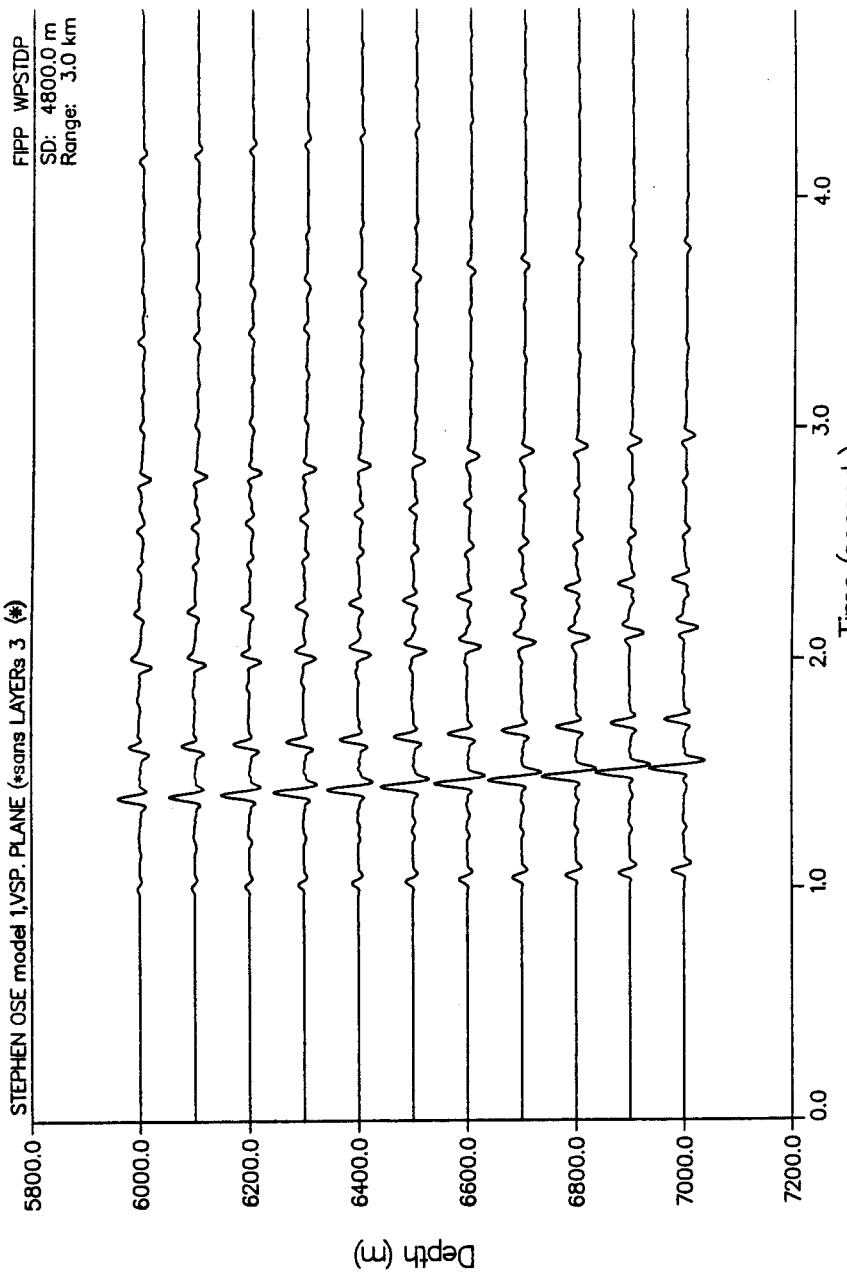

increased). For sufficiently large velocity contrasts, critically refracted P-SV converted waves can also result, at correspondingly smaller offset ranges, for an increased acoustic impedance contrast.

With this in mind, it is clear from comparative inspection of horizontal and vertical particle velocity records from mid to far offset ranges that both P and SV refracted and reflected waves are present in large number. This is especially well shown in source-receiver offsets of 3 km. Thus the major impedence change occuring at depth z=5500 (top of Layer 2) shows an obvious P-SV conversion at several seconds from this depth. The second SV headwave mode can be traced upward on the H component record from the bottom of Layer 2/top of Layer 3 interface, lagging the P head wave arrival at longer lags for increasing shallow receiver positions. Some obliquely traveling P wave events are also present at later arrival times.

STEPHEN (1984) has recently shown that the often high-velocity contrasts between water/sediment and (nb) sediment/basalt-type basement interfaces can cause refracted P waves to arrive almost horizontally for borehole receivers in the first upper crustal layer. Thus, in this case, the maximum P wave amplitude should occur for the horizontal rather than the vertical velocity component (as expected on an OBS).

In the underwater acoustic case (for a CW point source in water and one or more receivers at depth), hydrophones are generally unaffected by any "deep crustal" layering structure below what is effectively a 'hidden depth' determined by the geometric turning depth of a maximally incident ray x twice the dominant wavelength (GILBERT, 1985, personal communication). However, as WHITE and STEPHEN (1980) have further pointed out that, in many cases, even a very small velocity-transition zone comprised of sediments at the top of the 1st basement Layer 1 can have a considerable effect on the amount and kind of P-SV mode conversion. **Figure 90a-f, 90g-l** and **90m-r** shows a plot of plane wave bottom loss (scaled reflection coefficients) versus grazing angle (compliment of angle of incidence) for 3 different sediment layer thicknesses (500m, 50m, 5m). As will be seen, in particular, at typical marine crustal seismic source frequencies, an additional change of only a few meters to a few tens of meters ($\sim \lambda_{shear}$), resulting from adding a small shearwave velocity transition zone thickness on top of Layer 1, although much less than $\lambda_{compressional}$, can nevertheless considerably alter the resulting

Figure 90

Raitt v/z ocean crustal model, modified to include a range of 'thin' sediment layer thicknesses (after WHITE and STEPHEN, 1980), with corresponding plane wave reflection loss plots over all grazing angles for 5 selected frequencies betwee 0 and 25Hz, over 3 sediment layer thicknesses (5m, 50m, 500m)

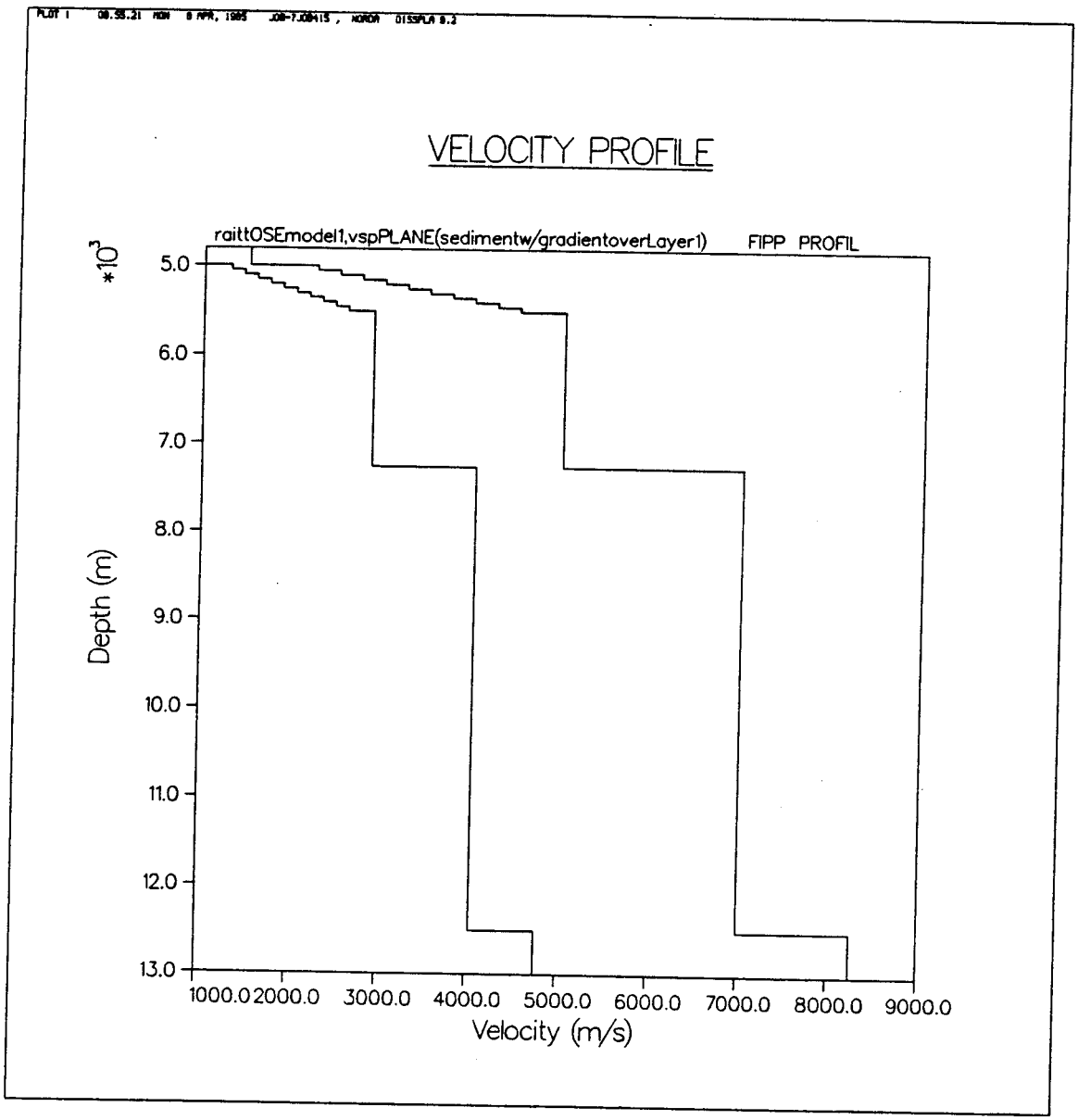
VELOCITY PROFILE
raittOSEmodel1,vspPLANE(sedimentw/gradientoverLayer1) FIPP PROFIL
*10^3
Depth (m)
5.0
6.0
7.0
8.0
9.0
10.0
11.0
12.0
13.0
1000.0 2000.0 3000.0 4000.0 5000.0 6000.0 7000.0 8000.0 9000.0
Velocity (m/s)

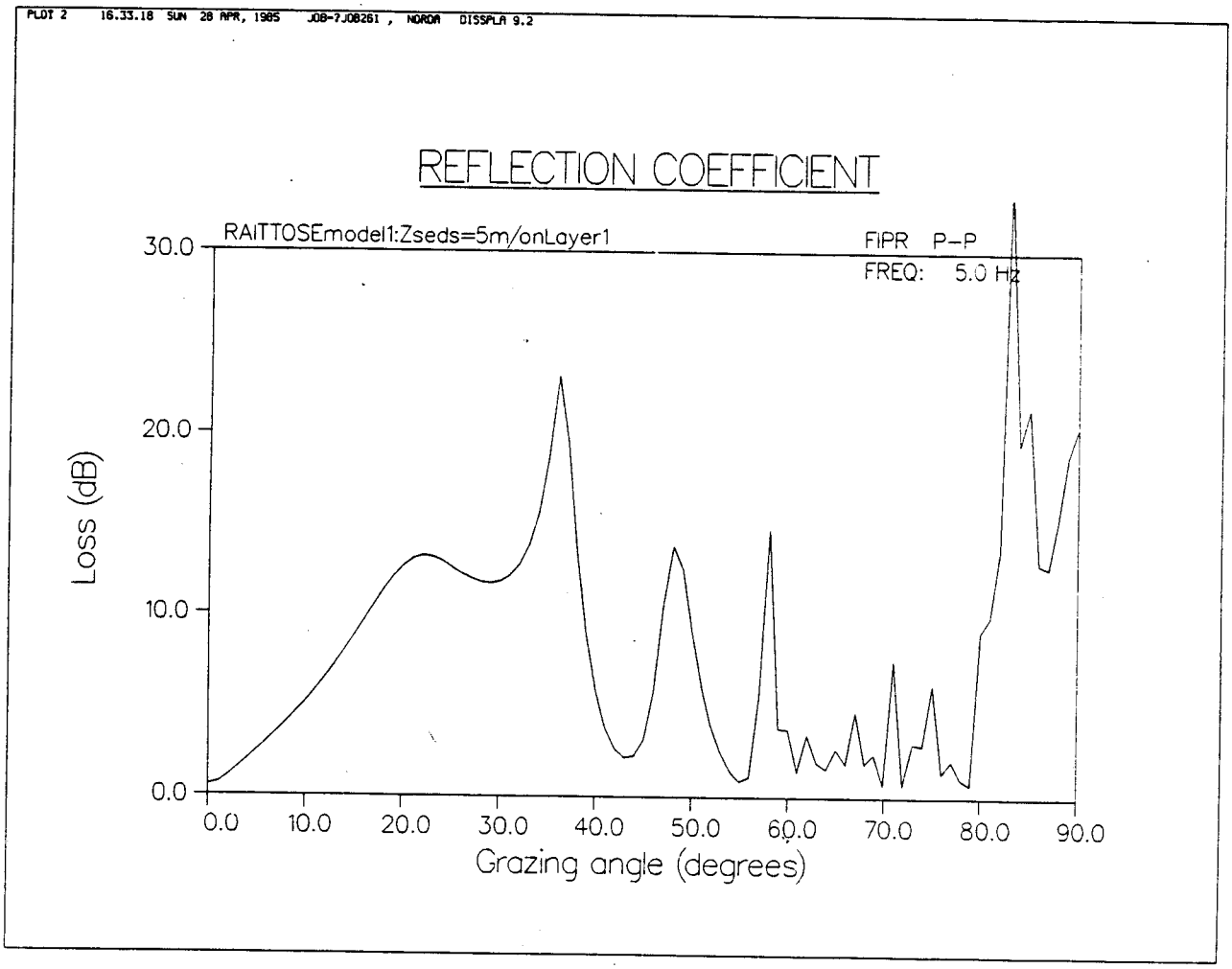
PLOT 2 16.33.18 SUN 28 APR, 1985 JOB-7JOB261 , NORDA DISSPLA 9.2
REFLECTION COEFFICIENT
RAITTOSEmodel1:Zseds=5m/onLayer1
FIPR P-P
FREQ: 5.0 Hz
30.0
20.0
10.0
0.0
Loss (dB)
0.0
10.0
20.0
30.0
40.0
50.0
60.0
70.0
80.0
90.0
Grazing angle (degrees)

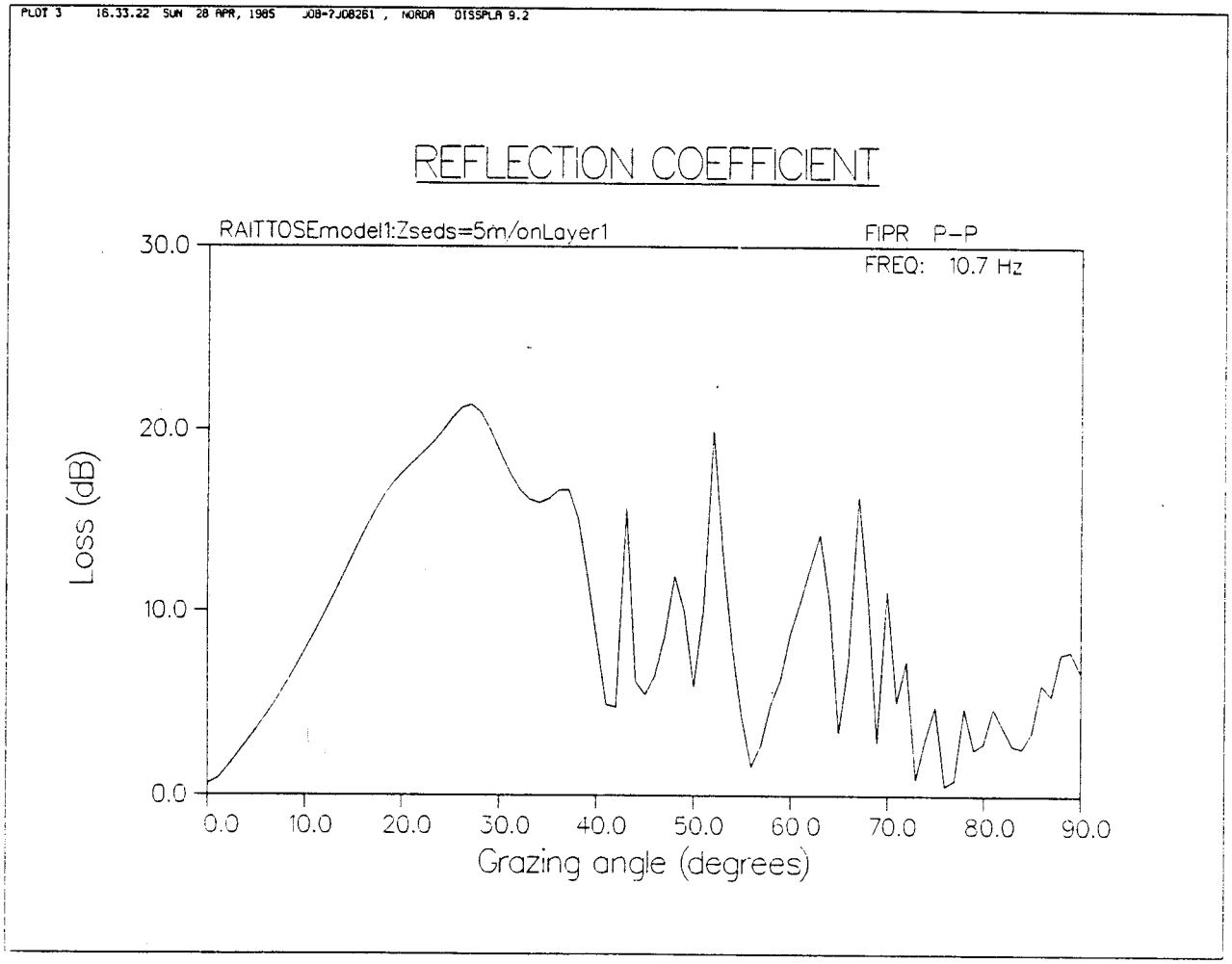
PLOT 3 16.33.22 SUN 28 APR, 1985 JOB=?J08261 , NORDA DISSPLA 9.2
REFLECTION COEFFICIENT
RAITTOSEmodel1:Zseds=5m/onLayer1
FIPR P-P
FREQ: 10.7 Hz
30.0
20.0
10.0
0.0
Loss (dB)
0.0
10.0
20.0
30.0
40.0
50.0
60.0
70.0
80.0
90.0
Grazing angle (degrees)

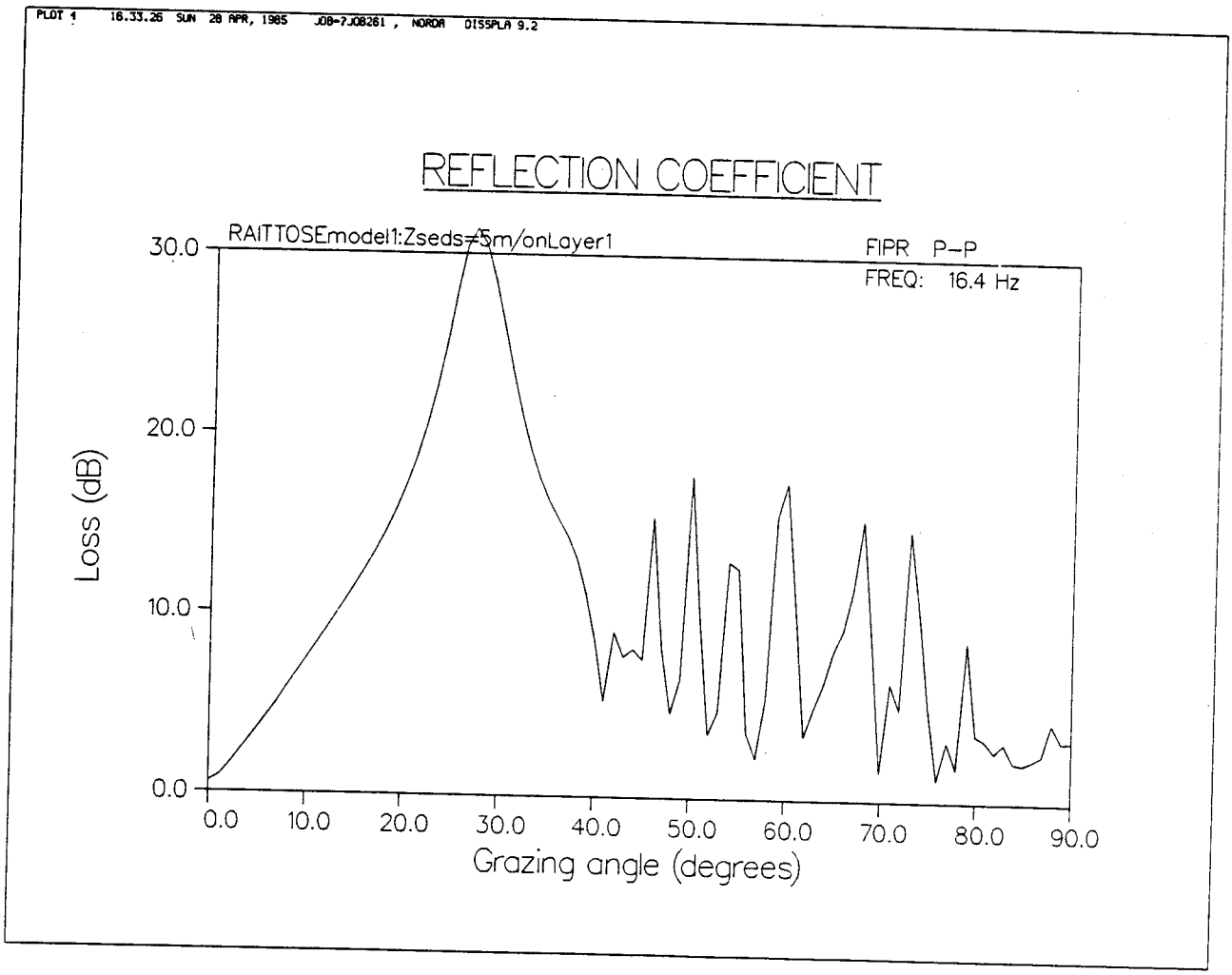
PLOT 1 18.33.26 SUN 20 APR, 1985 JOB-7J08261 , NORDA DISSPLA 9.2
REFLECTION COEFFICIENT
RAITTOSEmodel1:Zseds=5m/onLayer1
FIPR P-P
FREQ: 16.4 Hz
Loss (dB)
30.0
20.0
10.0
0.0
0.0
10.0
20.0
30.0
40.0
50.0
60.0
70.0
80.0
90.0
Grazing angle (degrees)

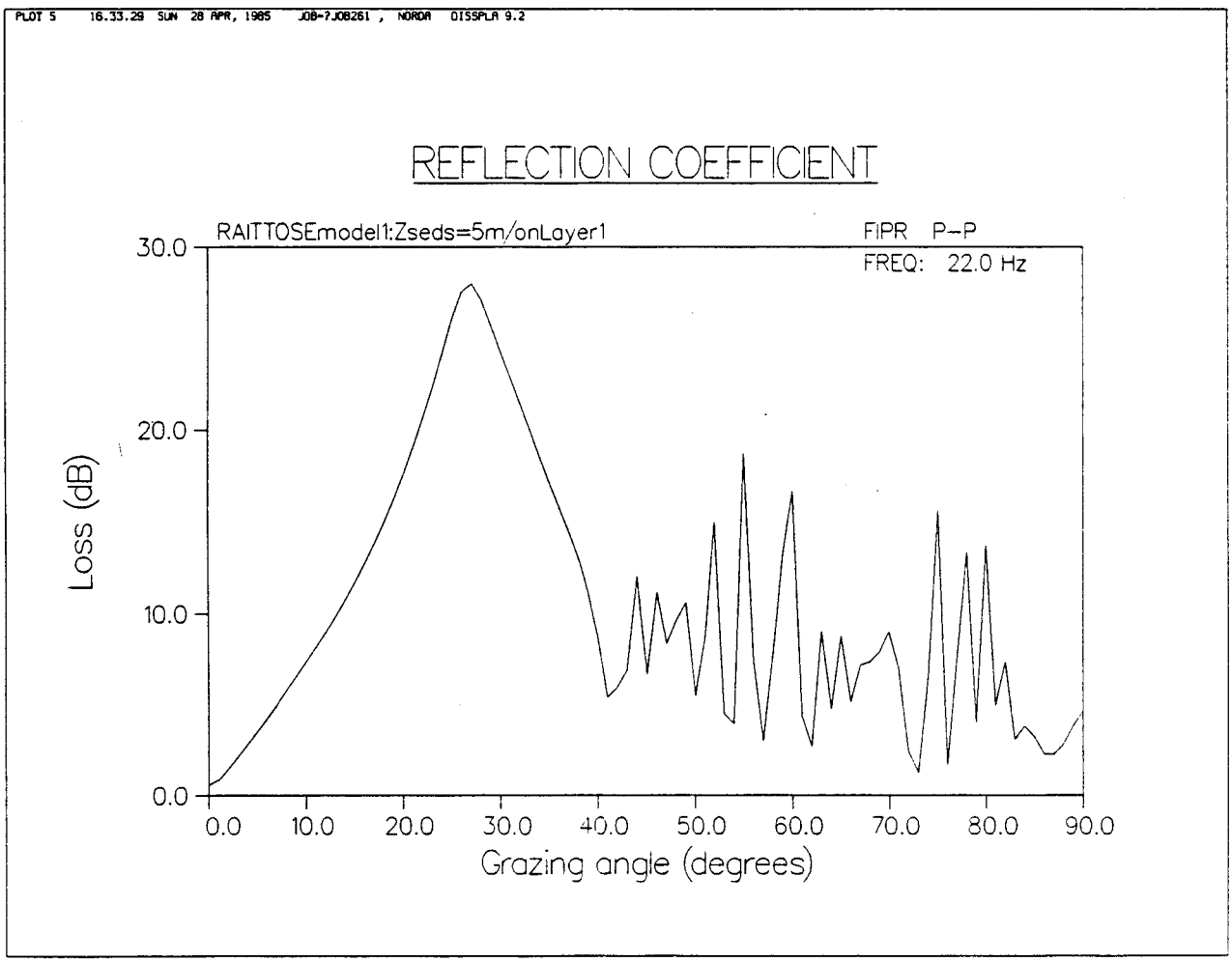
PLOT 5 16.33.29 SUN 28 APR, 1985 JOB=?J08261 , NORDA DISSPLA 9.2
REFLECTION COEFFICIENT
RAITTOSEmodel1:Zseds=5m/onLayer1
FIPR P-P
FREQ: 22.0 Hz
Loss (dB)
30.0
20.0
10.0
0.0
0.0
10.0
20.0
30.0
40.0
50.0
60.0
70.0
80.0
90.0
Grazing angle (degrees)

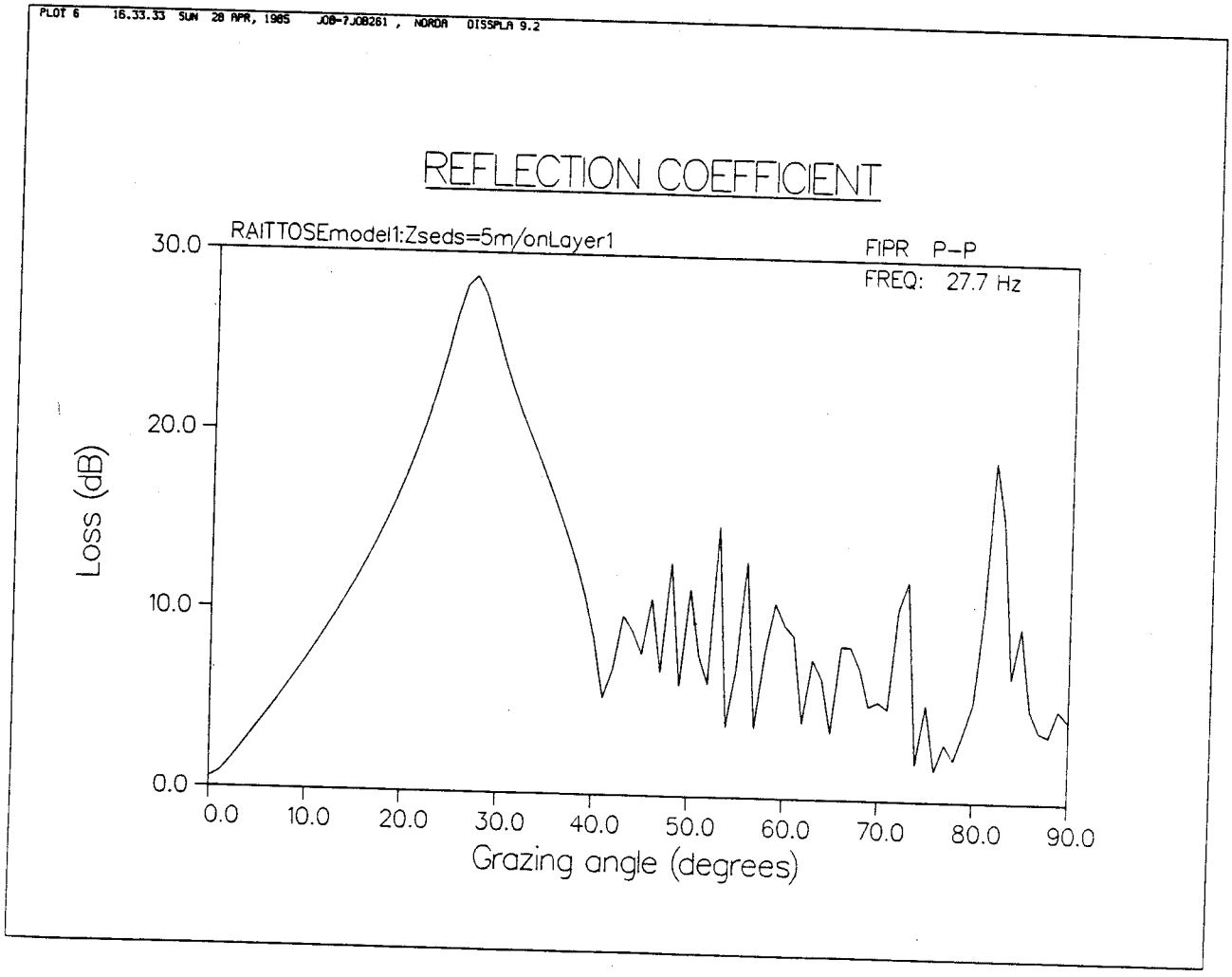
PLOT 6 16.33.33 SUN 28 APR, 1985 JOB-7J0B261 , NORDA DISSPLA 9.2
REFLECTION COEFFICIENT
RAITTOSEmodel1:Zseds=5m/onLayer1
FIPR P-P
FREQ: 27.7 Hz
30.0
20.0
10.0
0.0
Loss (dB)
0.0
10.0
20.0
30.0
40.0
50.0
60.0
70.0
80.0
90.0
Grazing angle (degrees)

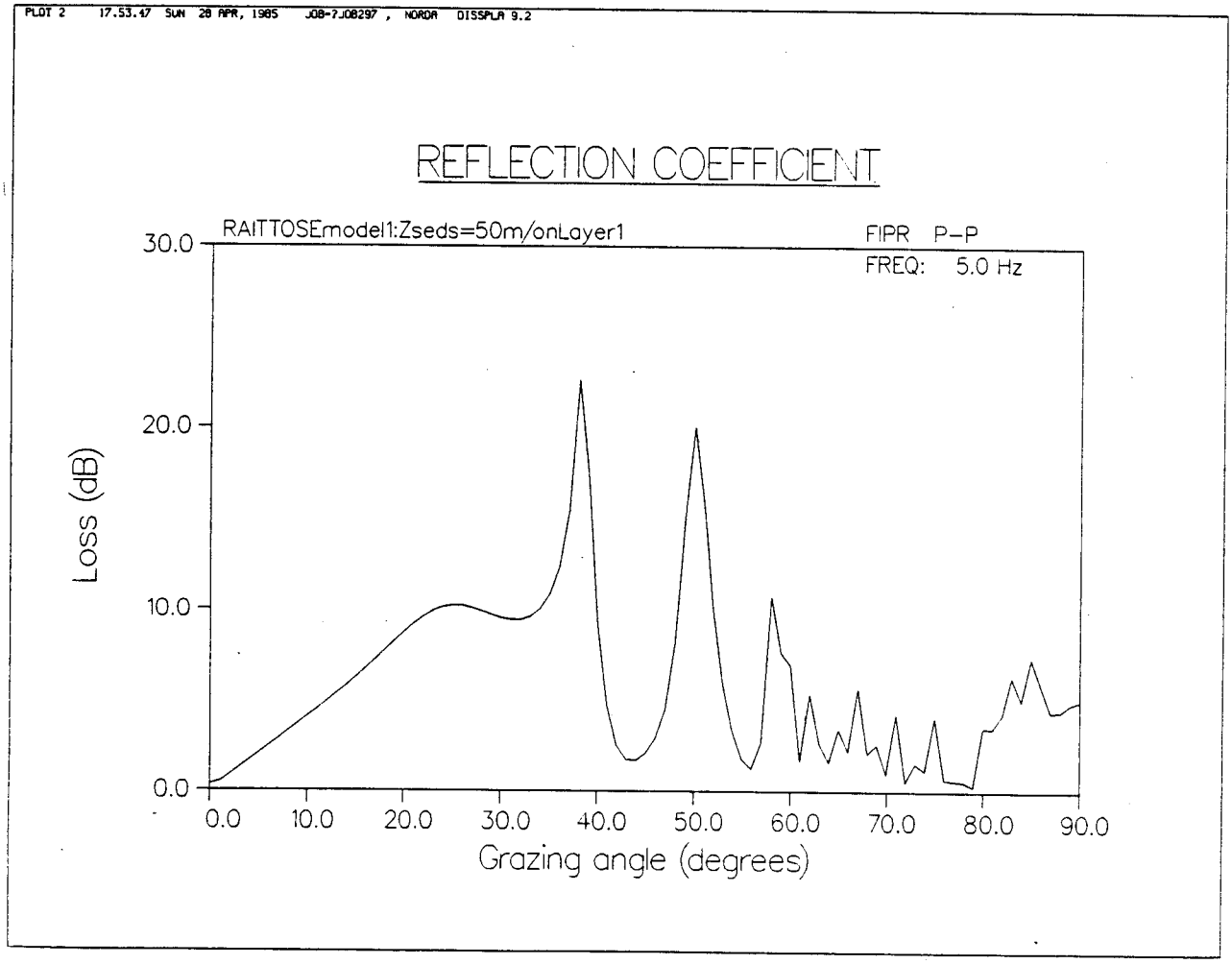
PLOT 2 17.53.47 SUN 28 APR, 1985 JOB-?J08297 , NORDA DISSPLA 9.2
REFLECTION COEFFICIENT
RAITTOSEmodel1:Zseds=50m/onLayer1
FIPR P-P
FREQ: 5.0 Hz
30.0
20.0
10.0
0.0
Loss (dB)
0.0
10.0
20.0
30.0
40.0
50.0
60.0
70.0
80.0
90.0
Grazing angle (degrees)

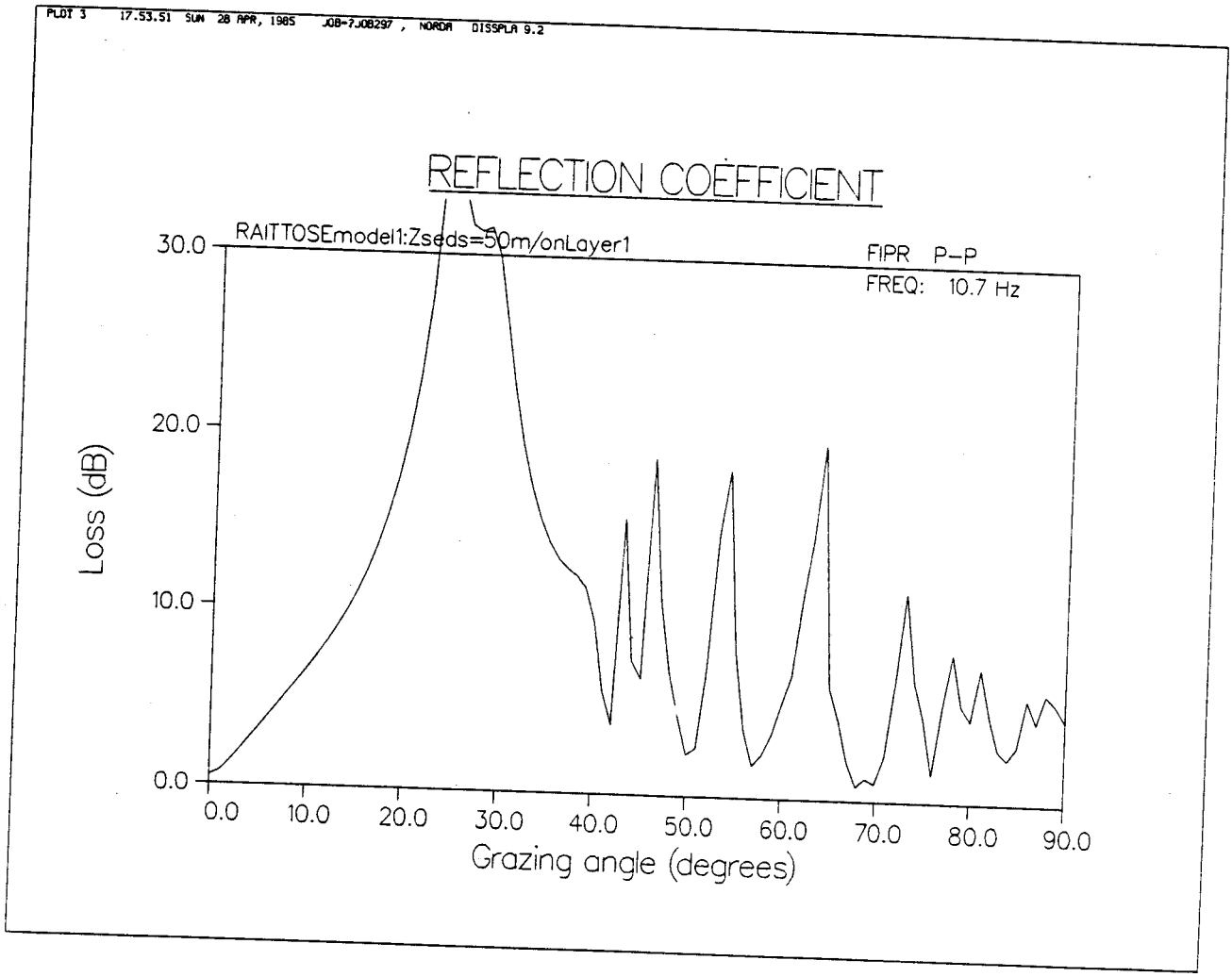
PLOT 3 17.53.51 SUN 28 APR, 1985 JOB=?JOB297 , NORDA DISSPLA 9.2
REFLECTION COEFFICIENT
RAITTOSEmodel1:Zseds=50m/onLayer1
FIPR P-P
FREQ: 10.7 Hz
Loss (dB)
30.0
20.0
10.0
0.0
0.0
10.0
20.0
30.0
40.0
50.0
60.0
70.0
80.0
90.0
Grazing angle (degrees)

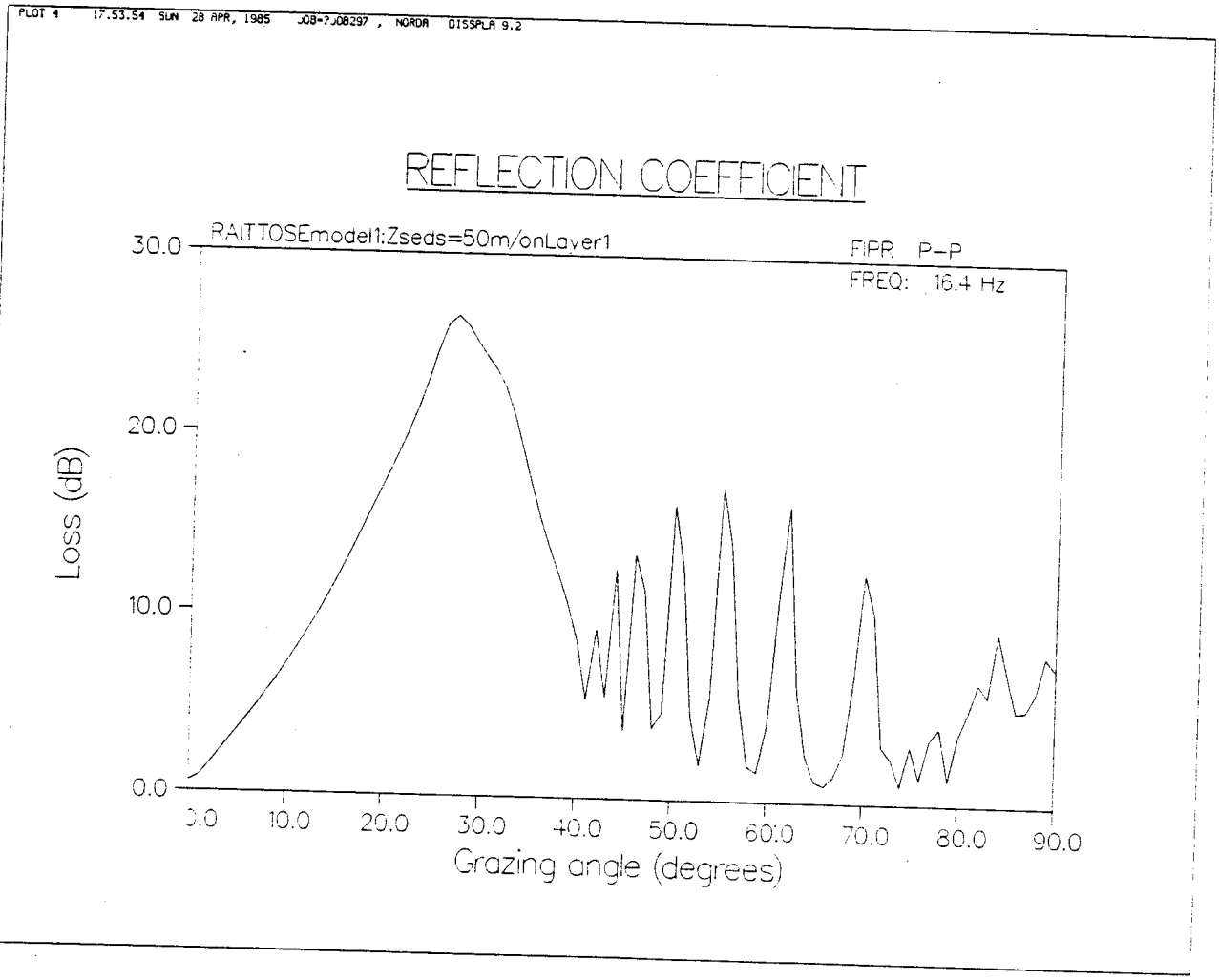
PLOT 1 17.53.54 SUN 28 APR, 1985 JOB=?J08297 , NORDA DISSPLA 9.2
REFLECTION COEFFICIENT
RAITTOSEmodel1:Zseds=50m/onLayer1
FIPR P-P
FREQ: 16.4 Hz
30.0
20.0
10.0
0.0
Loss (dB)
0.0
10.0
20.0
30.0
40.0
50.0
60.0
70.0
80.0
90.0
Grazing angle (degrees)

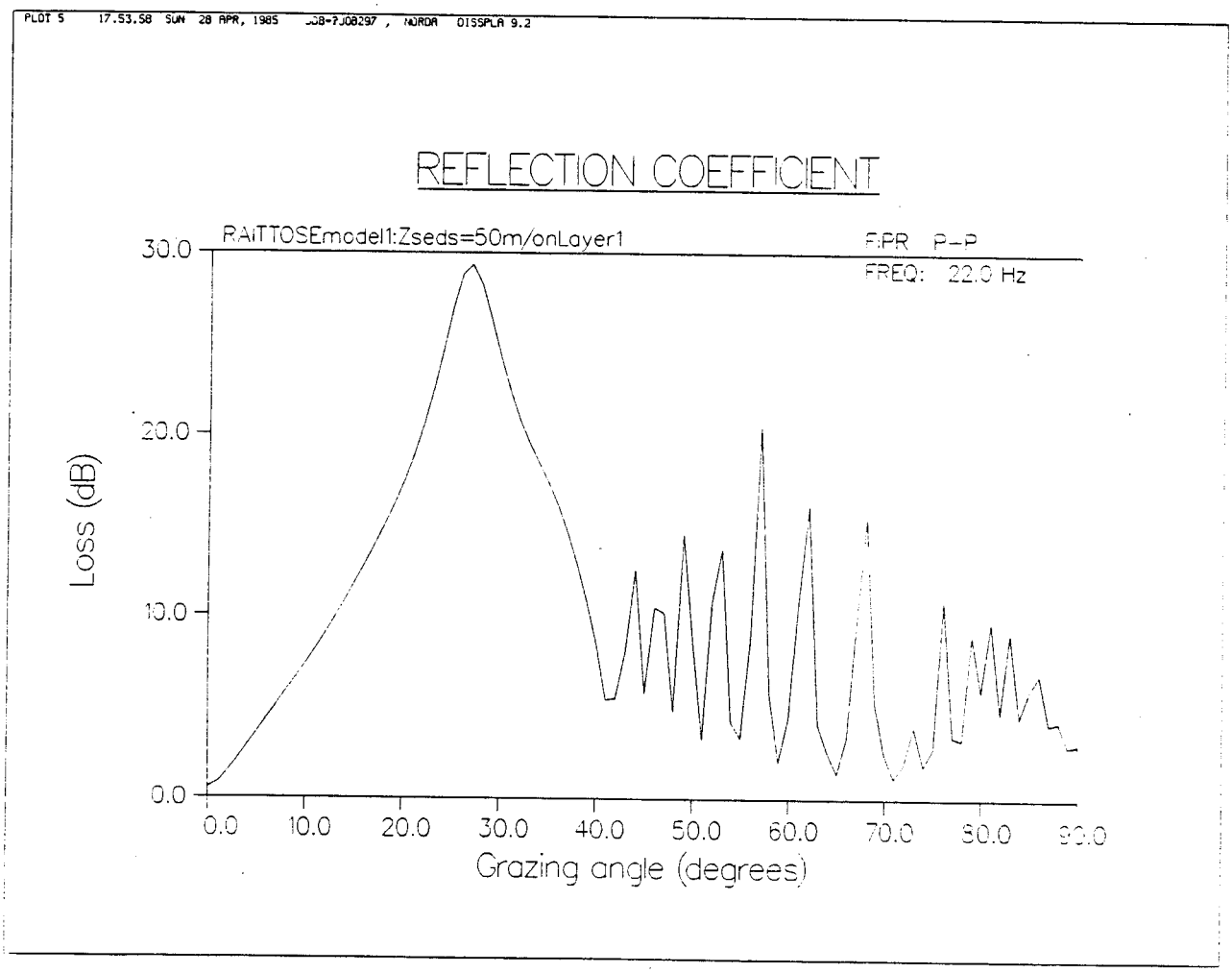
PLOT 5 17.53.58 SUN 28 APR, 1985 JOB=?J08297 , NORDA DISSPLA 9.2
REFLECTION COEFFICIENT
RAITTOSEmodel1:Zseds=50m/onLayer1
F:PR P-P
FREQ: 22.0 Hz
Loss (dB)
30.0
20.0
10.0
0.0
0.0
10.0
20.0
30.0
40.0
50.0
60.0
70.0
80.0
90.0
Grazing angle (degrees)

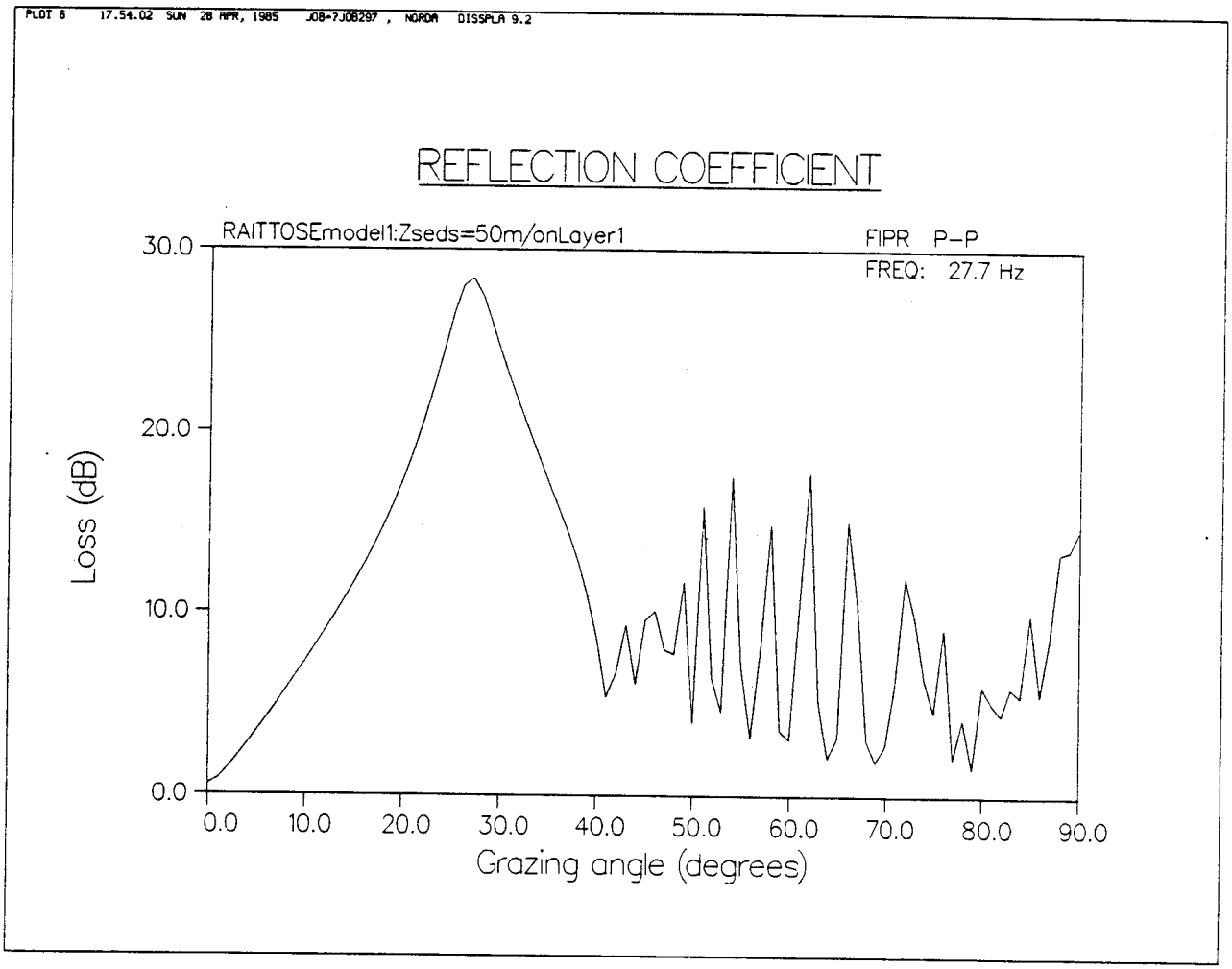
PLOT 6 17.54.02 SUN 28 APR, 1985 JOB=7J08297 , NORDA DISSPLA 9.2
REFLECTION COEFFICIENT
RAITTOSEmodel1:Zseds=50m/onLayer1
FIPR P-P
FREQ: 27.7 Hz
Loss (dB)
30.0
20.0
10.0
0.0
0.0
10.0
20.0
30.0
40.0
50.0
60.0
70.0
80.0
90.0
Grazing angle (degrees)

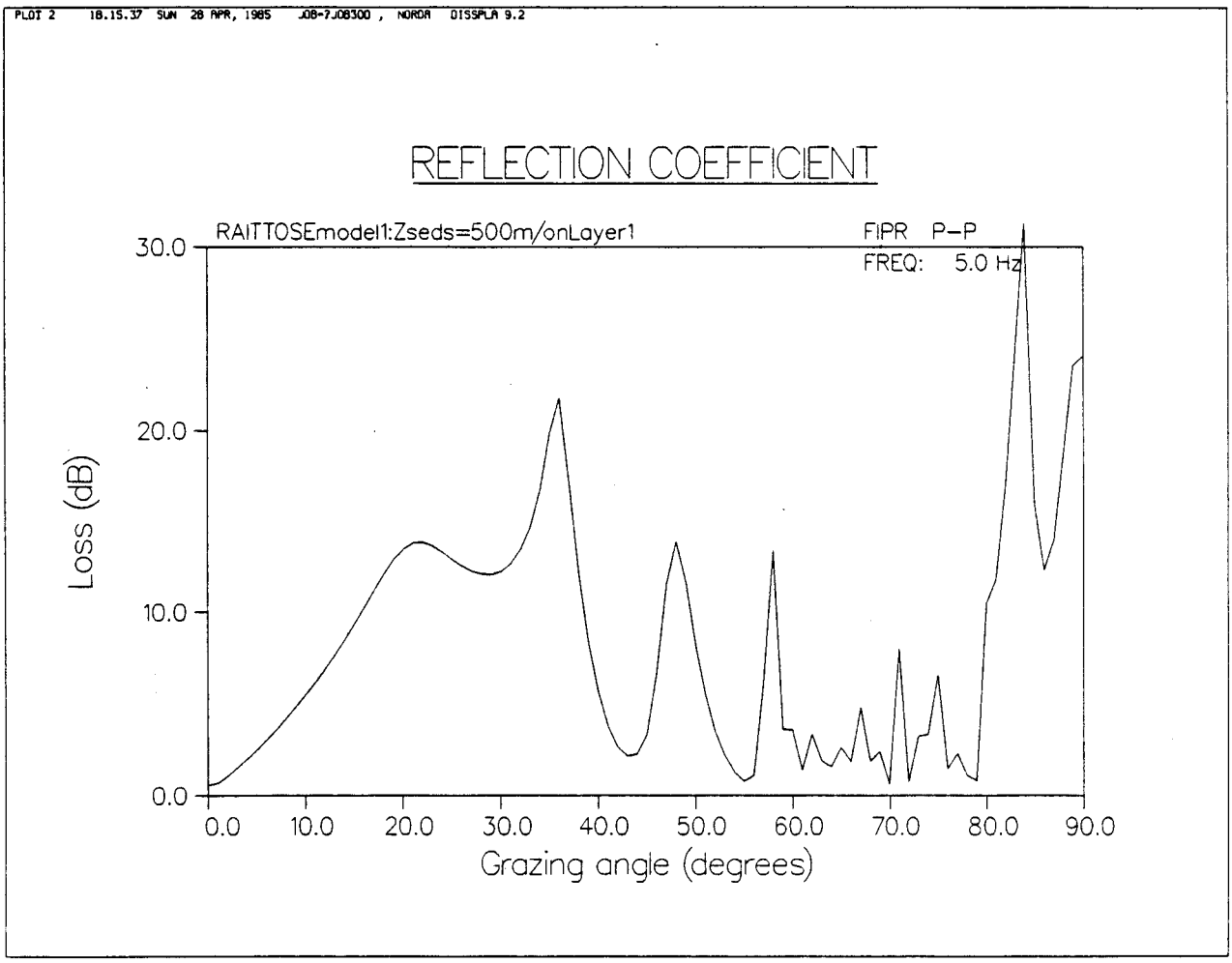
PLOT 2 18.15.37 SUN 28 APR, 1985 JOB=7J08300 , NORDA DISSPLA 9.2
REFLECTION COEFFICIENT
RAITTOSEmodel1:Zseds=500m/onLayer1
FIPR P-P
FREQ: 5.0 Hz
Loss (dB)
30.0
20.0
10.0
0.0
0.0
10.0
20.0
30.0
40.0
50.0
60.0
70.0
80.0
90.0
Grazing angle (degrees)

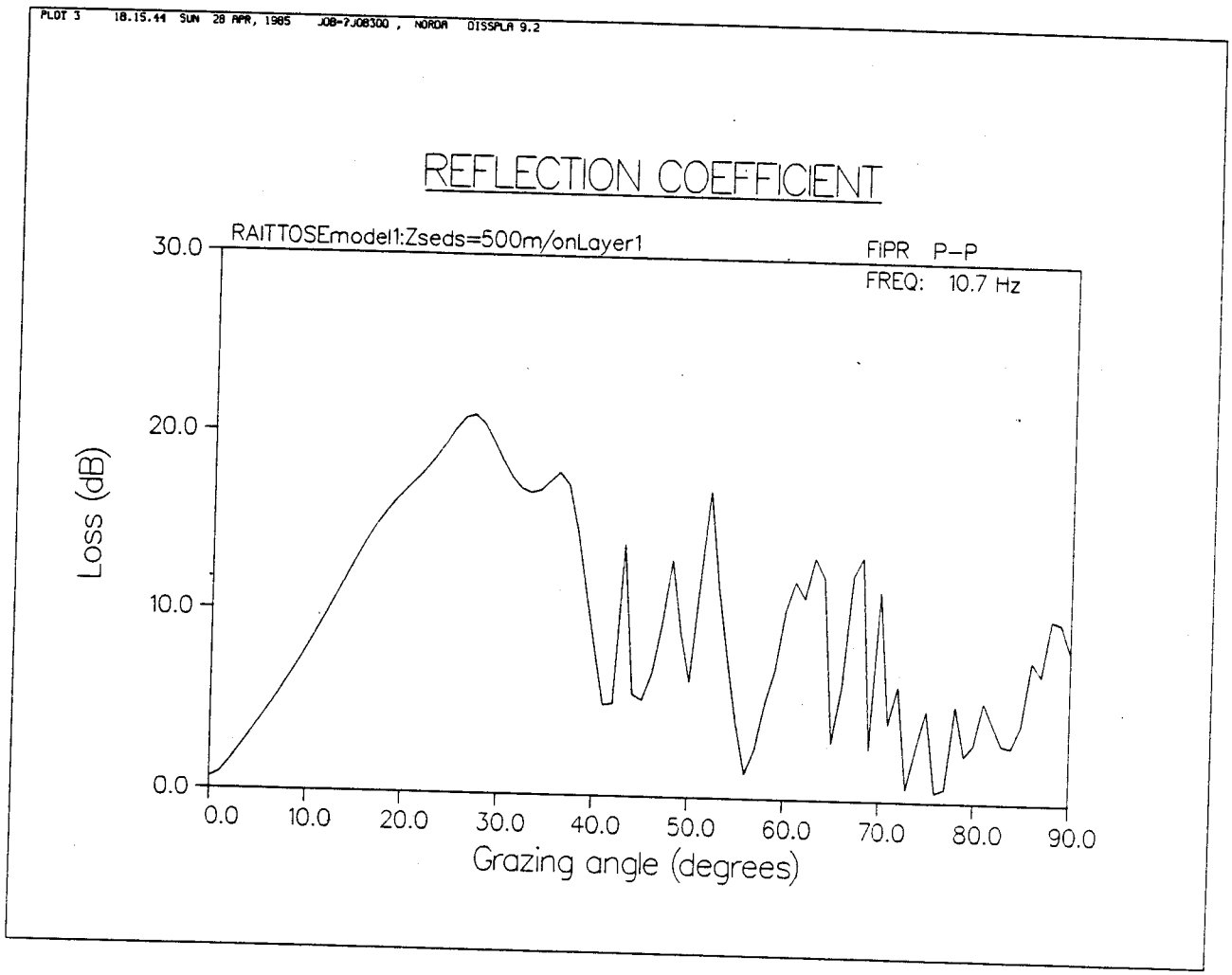
PLOT 3 18.15.44 SUN 28 APR, 1985 JOB=?J08300 , NORDA DISSPLA 9.2
REFLECTION COEFFICIENT
RAITTOSEmodel1:Zseds=500m/onLayer1
FIPR P-P
FREQ: 10.7 Hz
Loss (dB)
30.0
20.0
10.0
0.0
0.0
10.0
20.0
30.0
40.0
50.0
60.0
70.0
80.0
90.0
Grazing angle (degrees)

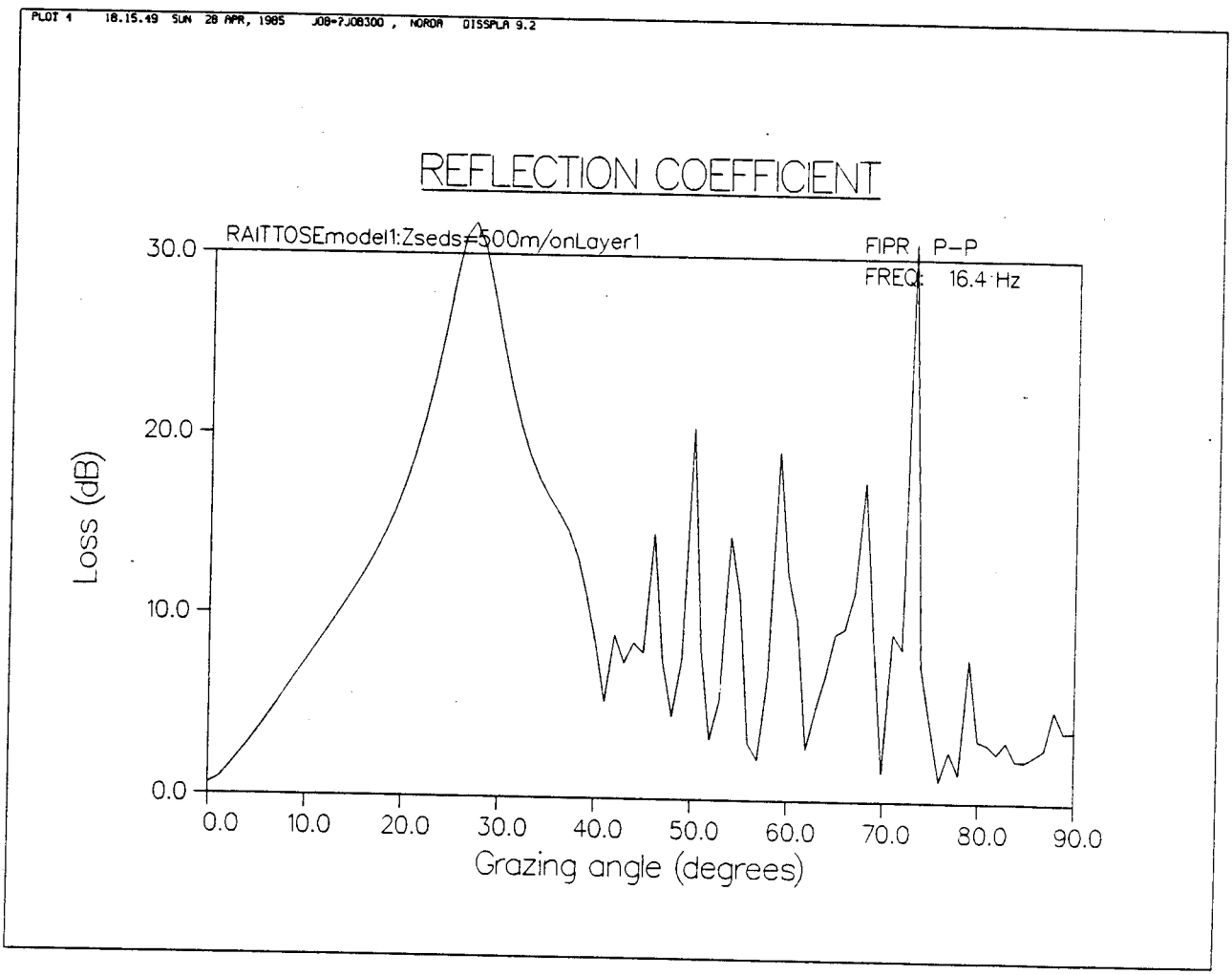
PLOT 1 18.15.49 SUN 28 APR, 1985 JOB=?JOB300 , NORDA DISSPLA 9.2
REFLECTION COEFFICIENT
RAITTOSEmodel1:Zseds=500m/onLayer1
FIPR P-P
FREQ: 16.4 Hz
30.0
20.0
10.0
0.0
Loss (dB)
0.0
10.0
20.0
30.0
40.0
50.0
60.0
70.0
80.0
90.0
Grazing angle (degrees)

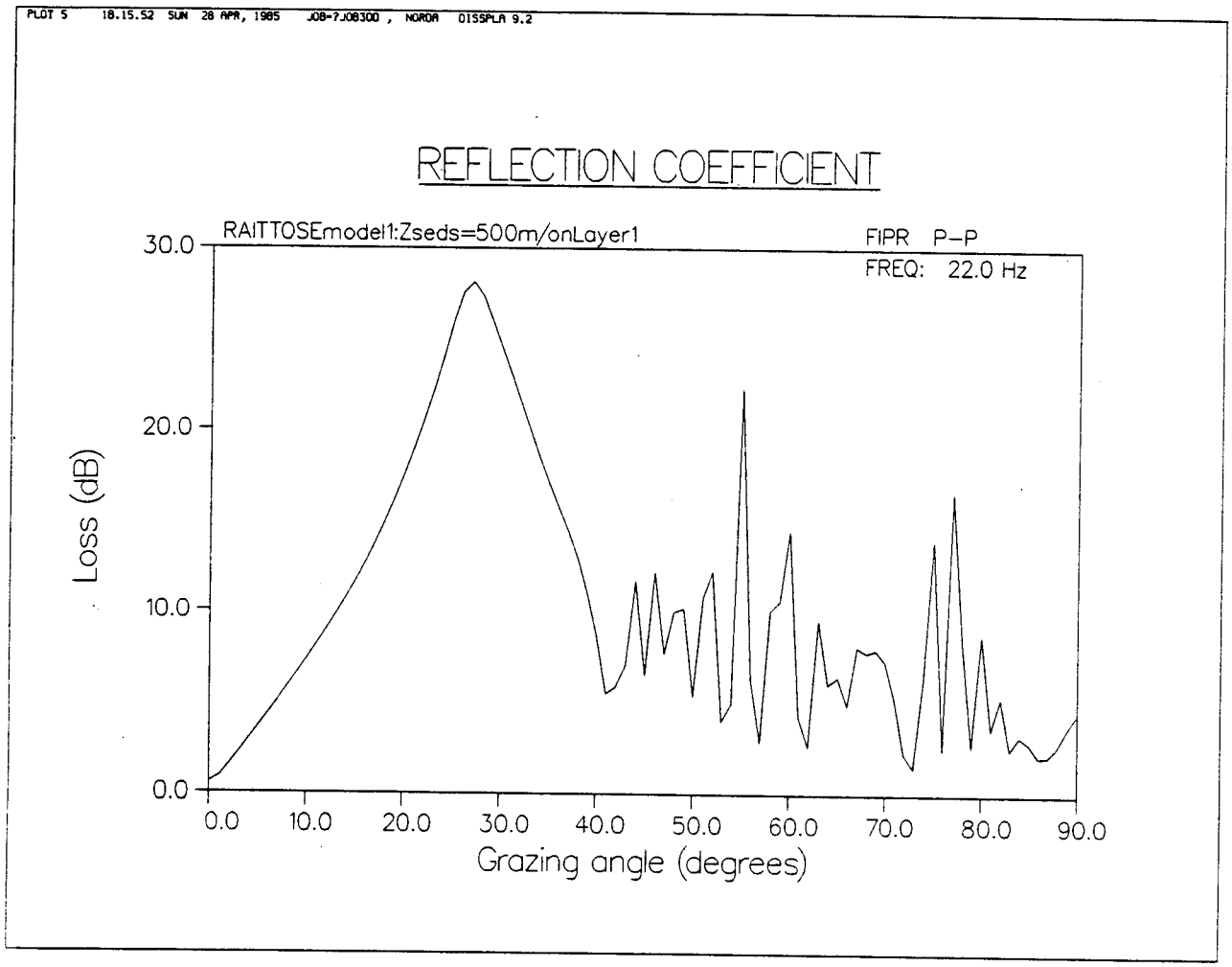
PLOT 5 18.15.52 SUN 28 APR, 1985 JOB=?J08300 , NORDA DISSPLA 9.2
REFLECTION COEFFICIENT
RAITTOSEmodel1:Zseds=500m/onLayer1
FlPR P-P
FREQ: 22.0 Hz
30.0
20.0
10.0
0.0
Loss (dB)
0.0
10.0
20.0
30.0
40.0
50.0
60.0
70.0
80.0
90.0
Grazing angle (degrees)

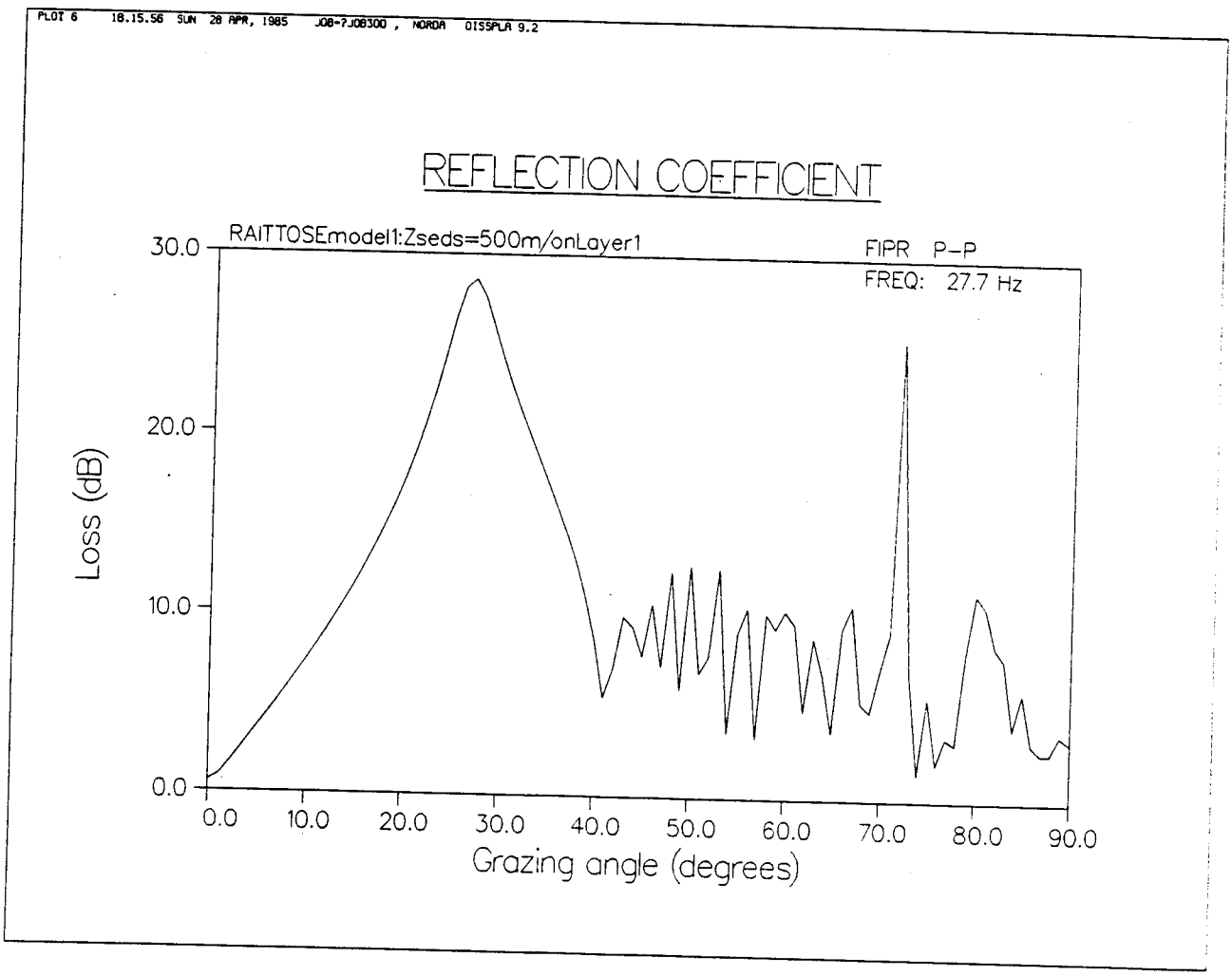
PLOT 6 18.15.56 SUN 28 APR, 1985 JOB=7J08300 , NORDA OISSPLR 9.2
REFLECTION COEFFICIENT
RAITTOSEmodel1:Zseds=500m/onLayer1
FIPR P-P
FREQ: 27.7 Hz
30.0
20.0
10.0
0.0
Loss (dB)
0.0
10.0
20.0
30.0
40.0
50.0
60.0
70.0
80.0
90.0
Grazing angle (degrees)

P wave seismogram. The resulting head wave intensity, for example, can be readily seen for the corresponding OBS synthetic seismic profile shown in **Figure 93.**

This can also be seen in the horizontal and vertical particle velocity VSPs in **Figure 91a-e** and **92a-e,** where additional P-SV multiples and multiple conversion can be observed. Here it will be seen that the additional P wave energy loss mechanism through conversion within the sediments strongly manifests itself even at small grazing angles for the present geomodel.

Comparing the present sediment+Raitt versus the original Raitt crustal model previously shown, it will be apparent immediately that whereas the 2 synthetic VSPs still give the approximate location and amplitude of the first shallow crustal arrival, the sediment+Raitt VSP shows a strong waveform preceding the crustal wave as a first arrival. In addition, the water/crust interface surface multiple, so plainly evident as a triplet of 3 wavelets of alternating phase on the Raitt model, is now totally absent on the sediment+Raitt model.

When comparatively considering the Raitt and sediment+Raitt models in terms of VSPs at progressively larger offsets, it becomes clear that the sediment layer acts to greatly reduce the net acoustic impedence contrast, thereby vastly lessening the number and amplitude of surface reflected multiples observed. Further, the upgoing waveform form the major discontinuity at

Figure 91 and 92

Full wavefield synthetic VSPs (plane wave line source) for full shear elastic thin sediment + Raitt crustal v/z model, at 5 offset ranges (x=1,5km) in:

Geophone: Vertical particle velocity

Geophone: Horizontal particle velocity

showing differential shear effects

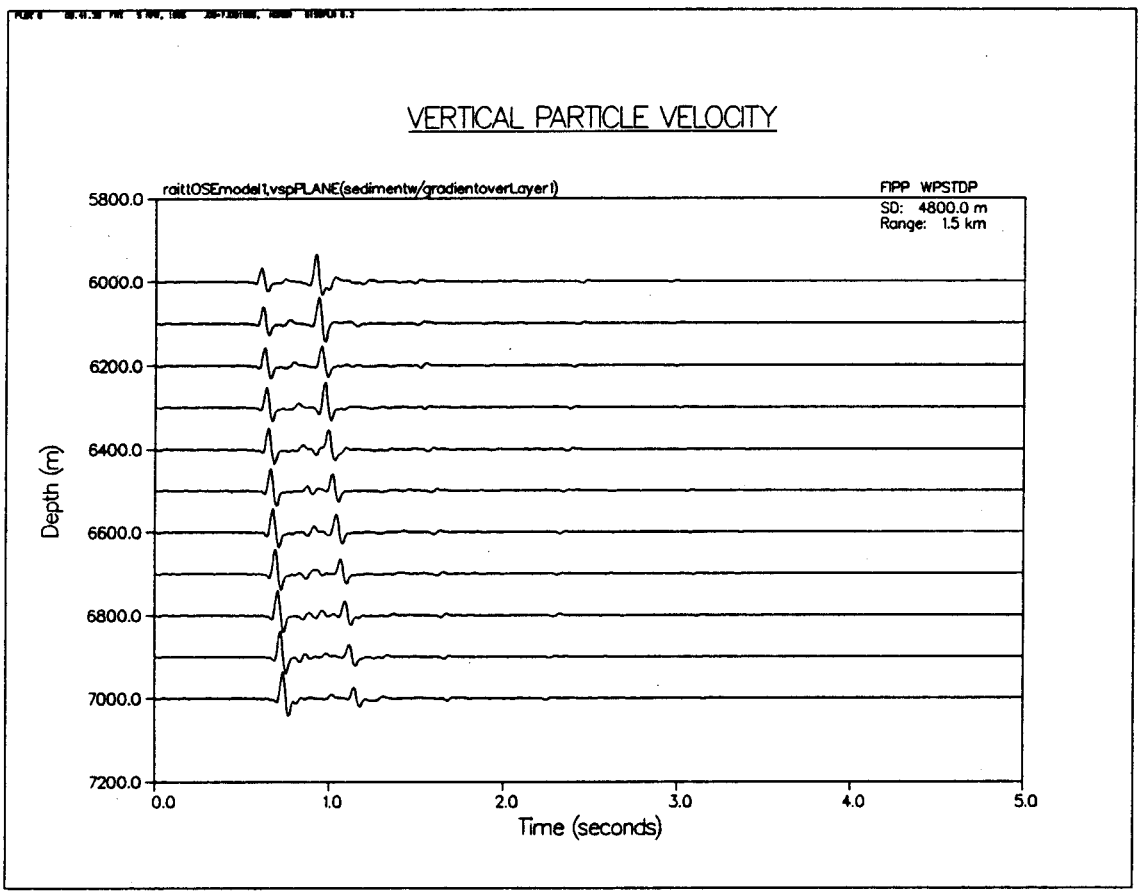
VERTICAL PARTICLE VELOCITY
raitlOSEmodel1,vspPLANE(sedimentw/gradientoverLayer1)
FIPP WPSTDP
SD: 4800.0 m
Range: 1.5 km
Depth (m)
5800.0
6000.0
6200.0
6400.0
6600.0
6800.0
7000.0
7200.0
0.0
1.0
2.0
3.0
4.0
5.0
Time (seconds)

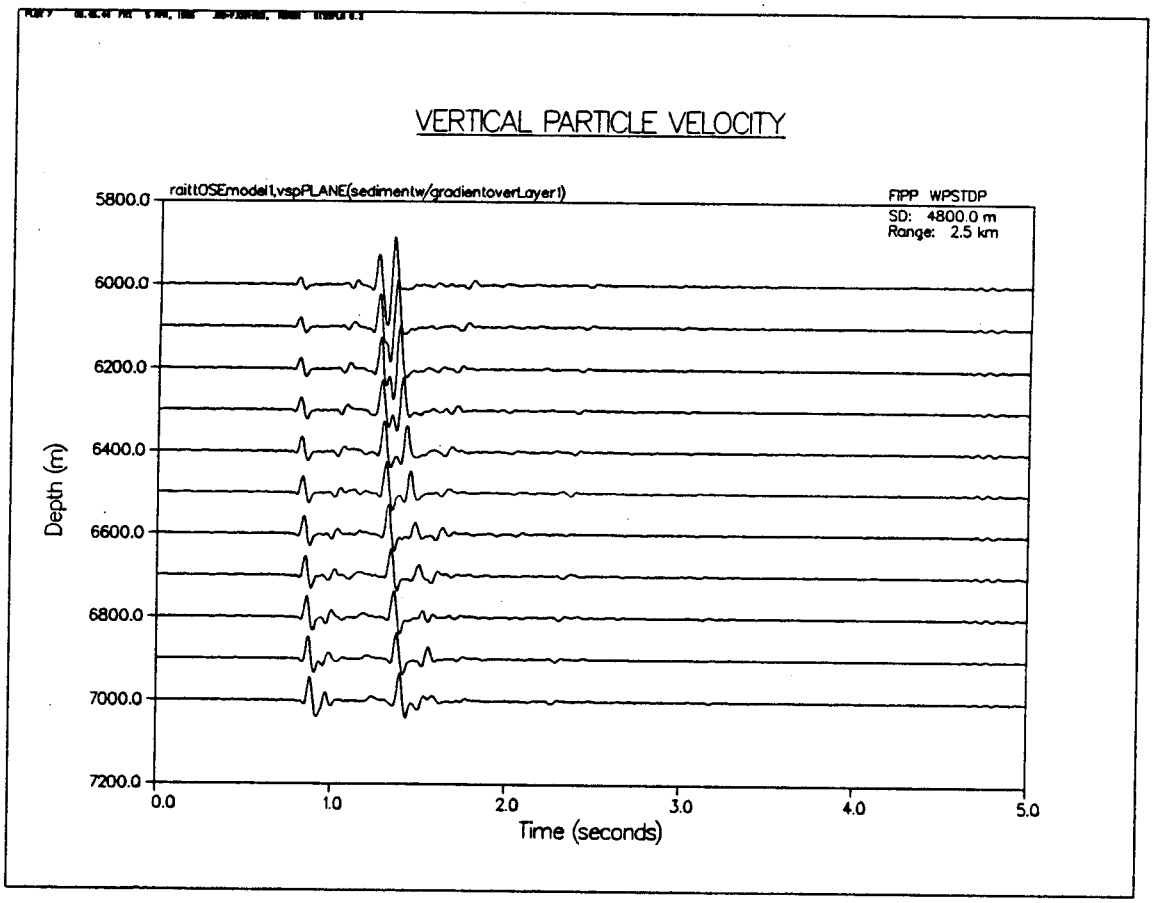
VERTICAL PARTICLE VELOCITY
raittOSEmodel1.vspPLANE(sedimentw/gradientoverLayer1)
FIPP WPSTDP
SD: 4800.0 m
Range: 2.5 km
Depth (m)
5800.0
6000.0
6200.0
6400.0
6600.0
6800.0
7000.0
7200.0
0.0
1.0
2.0
3.0
4.0
5.0
Time (seconds)

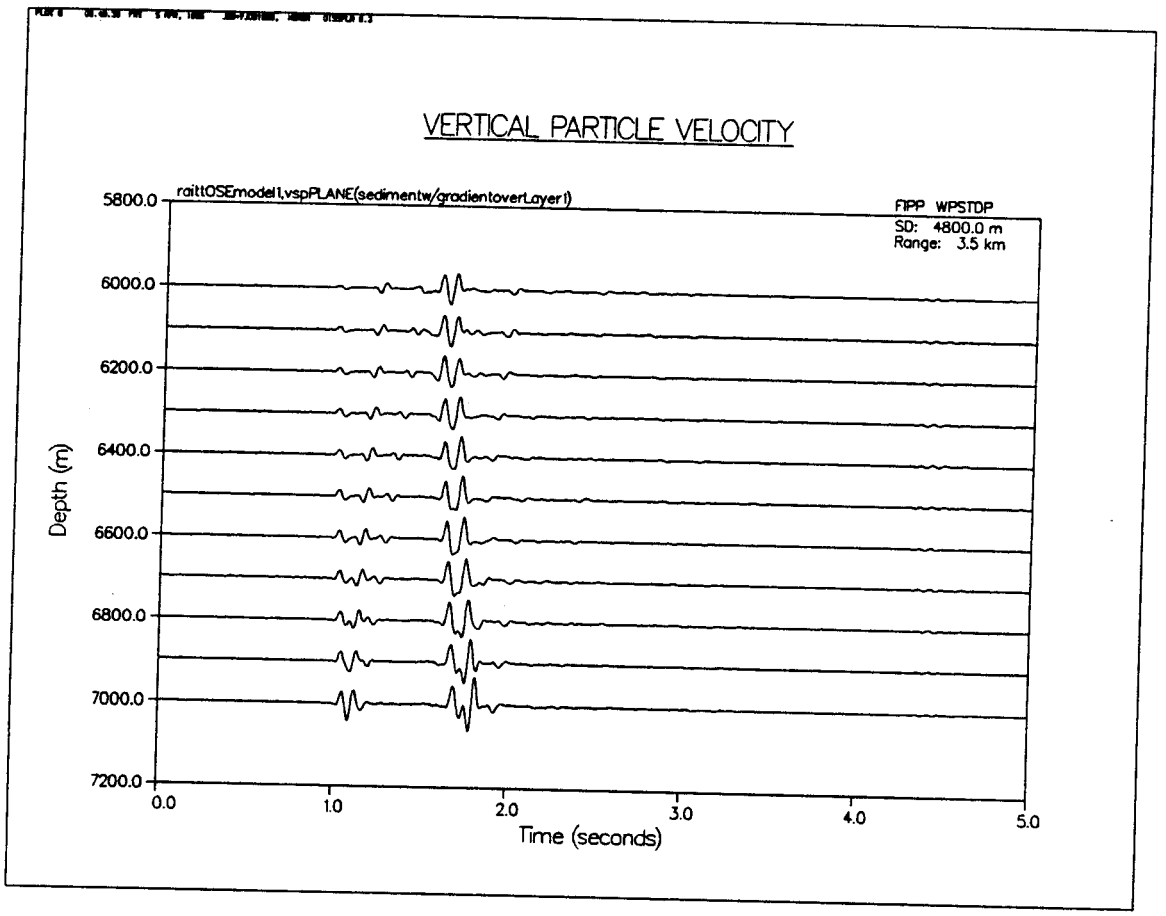
VERTICAL PARTICLE VELOCITY
raittOSEmodel1.vspPLANE(sedimentw/gradientoverLayer1)
FIPP WPSTDP
SD: 4800.0 m
Range: 3.5 km
Depth (m)
5800.0
6000.0
6200.0
6400.0
6600.0
6800.0
7000.0
7200.0
0.0
1.0
2.0
3.0
4.0
5.0
Time (seconds)

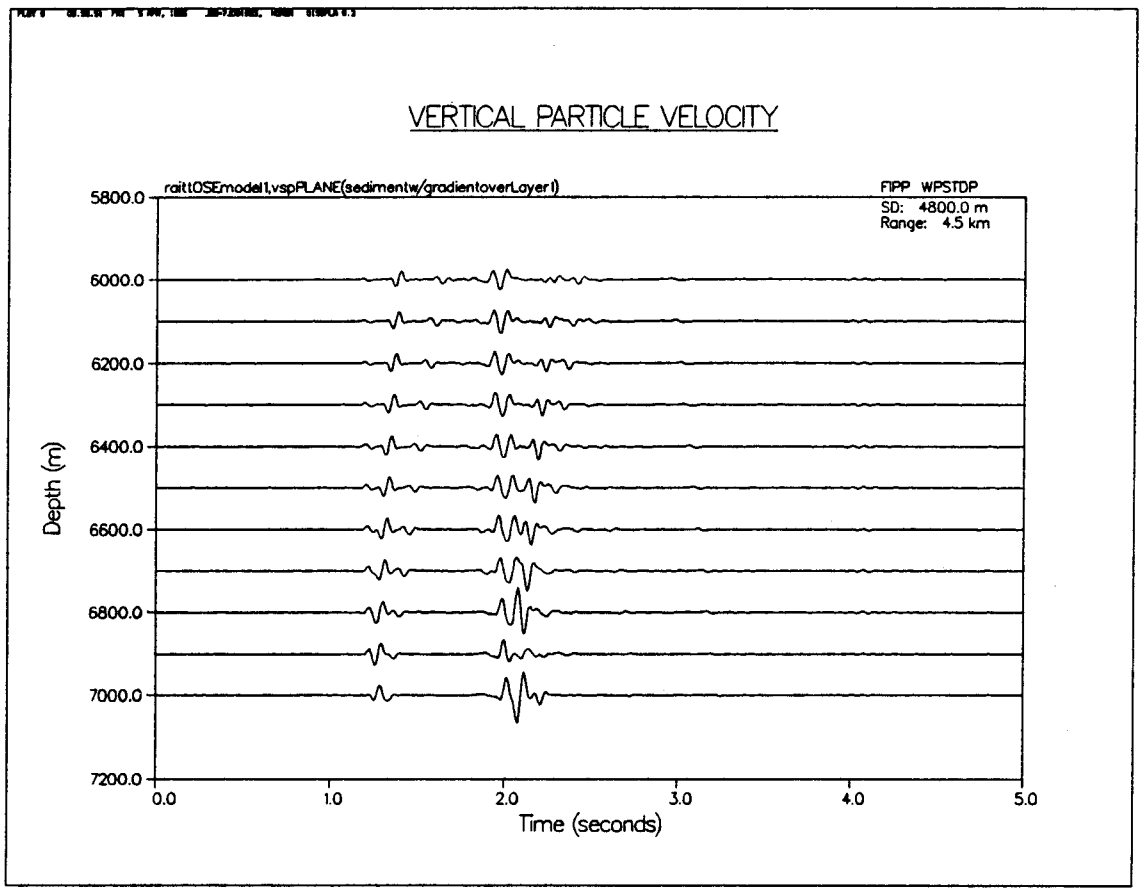
VERTICAL PARTICLE VELOCITY
raitt0SEmodel1,vspPLANE(sedimentw/gradientoverLayer1)
FIPP WPSTDP
SD: 4800.0 m
Range: 4.5 km
Depth (m)
5800.0
6000.0
6200.0
6400.0
6600.0
6800.0
7000.0
7200.0
0.0
1.0
2.0
3.0
4.0
5.0
Time (seconds)

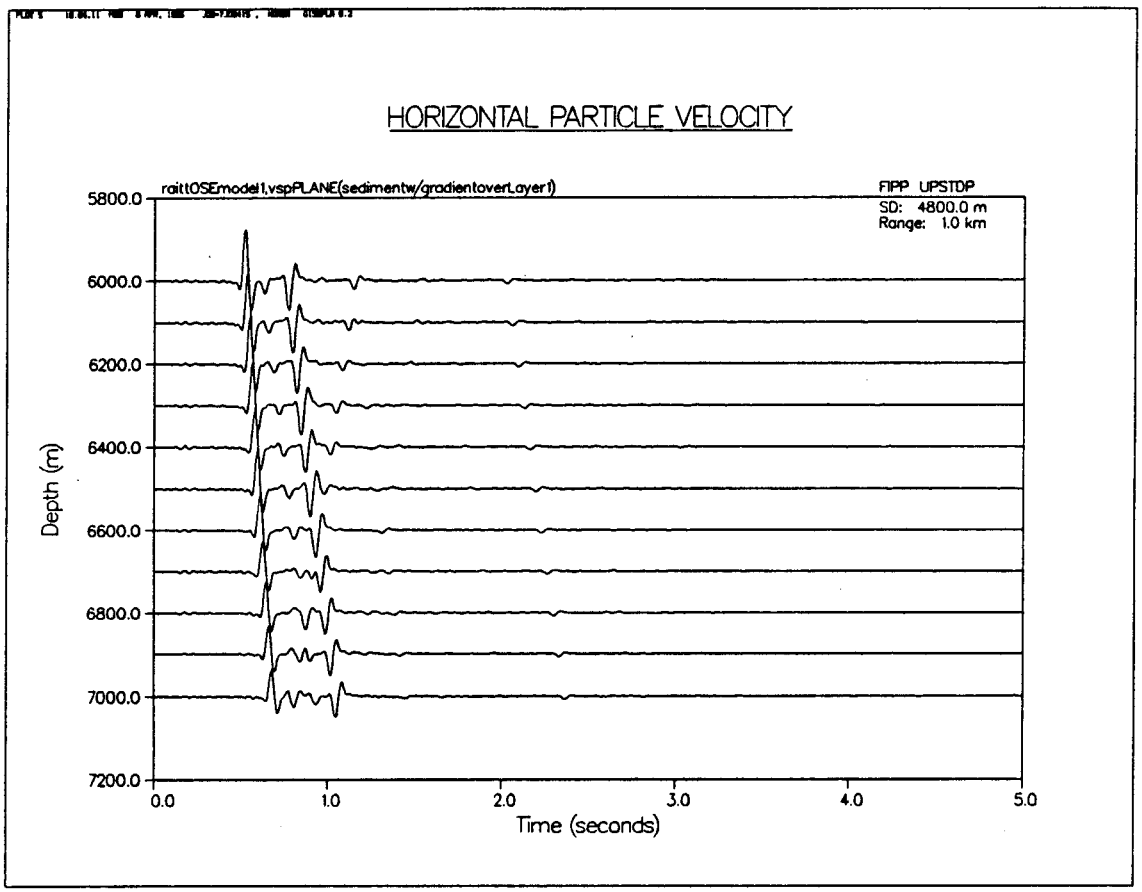
HORIZONTAL PARTICLE VELOCITY
raitt0SE.model1.vspPLANE(sedimentw/gradientoverLayer1)
FIPP UPSTDP
SD: 4800.0 m
Range: 1.0 km
Depth (m)
5800.0
6000.0
6200.0
6400.0
6600.0
6800.0
7000.0
7200.0
0.0
1.0
2.0
3.0
4.0
5.0
Time (seconds)

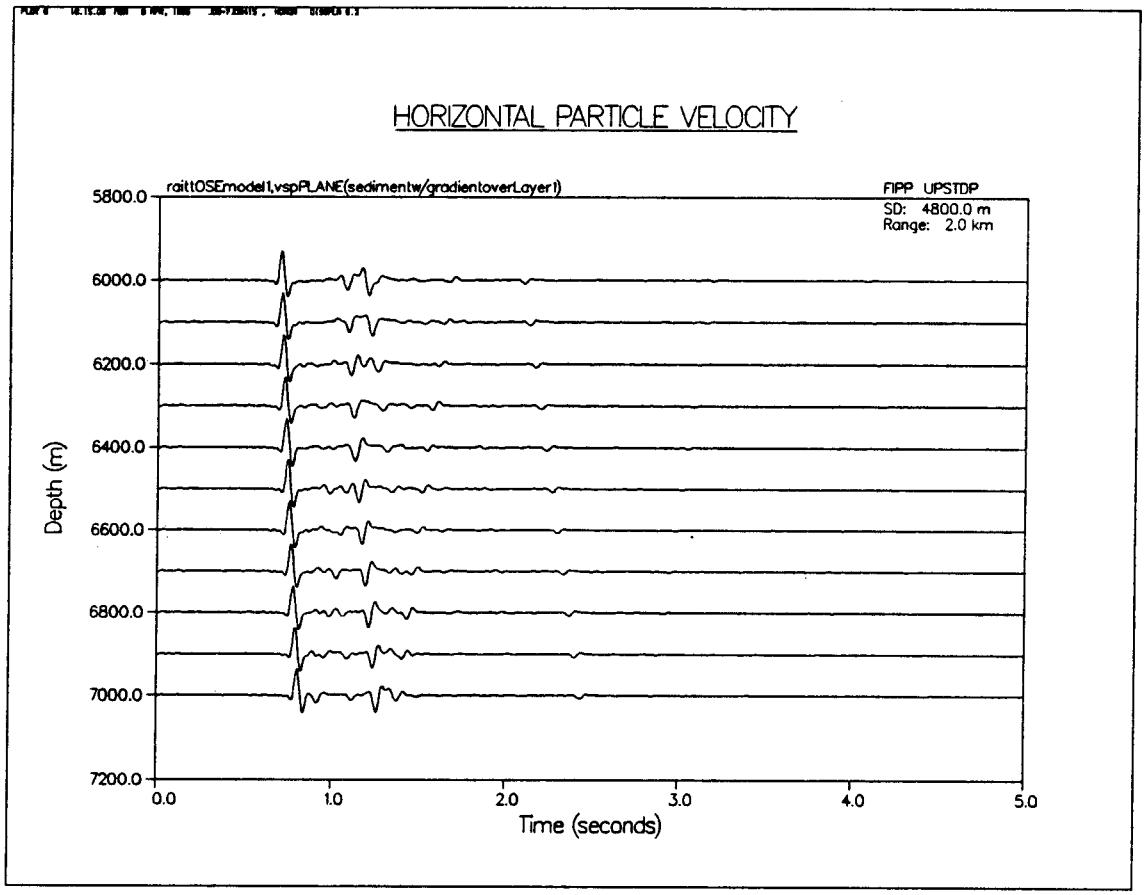
HORIZONTAL PARTICLE VELOCITY
raittOSEmodel1,vspPLANE(sedimentw/gradientoverLayer1)
FIPP UPSTDP
SD: 4800.0 m
Range: 2.0 km
Depth (m)
5800.0
6000.0
6200.0
6400.0
6600.0
6800.0
7000.0
7200.0
0.0
1.0
2.0
3.0
4.0
5.0
Time (seconds)

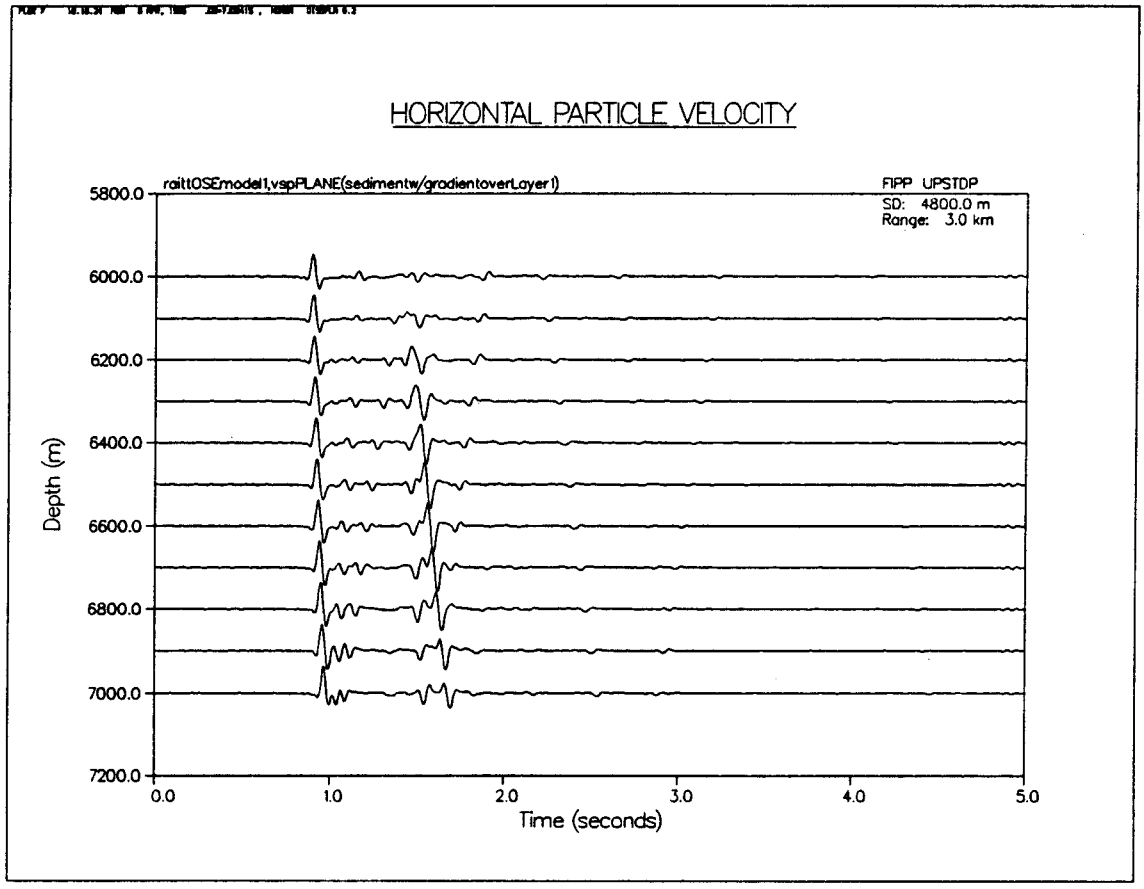
HORIZONTAL PARTICLE VELOCITY
raittOSEmodel1,vspPLANE(sedimentw/gradientoverLayer1)
FIPP UPSTDP
SD: 4800.0 m
Range: 3.0 km
Depth (m)
5800.0
6000.0
6200.0
6400.0
6600.0
6800.0
7000.0
7200.0
0.0
1.0
2.0
3.0
4.0
5.0
Time (seconds)

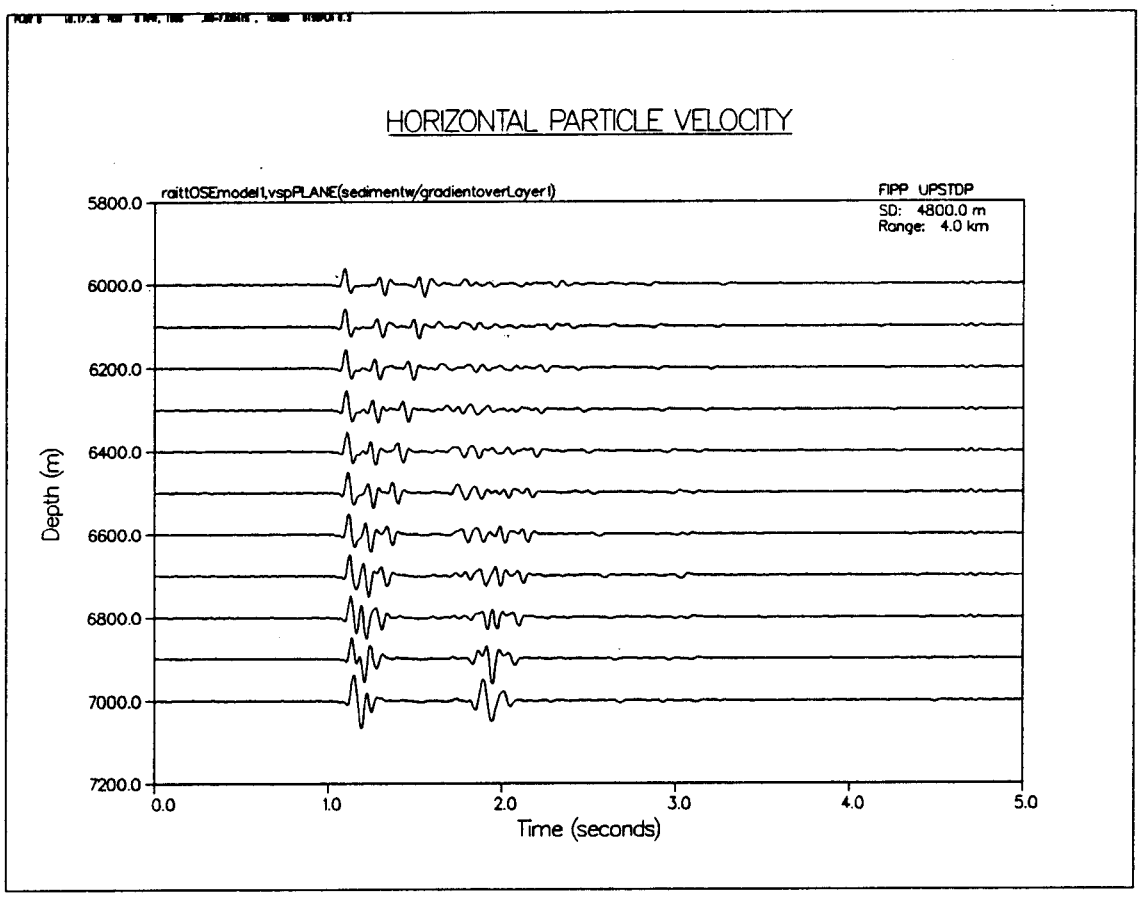
HORIZONTAL PARTICLE VELOCITY
raittOSEmodel1,vspPLANE(sedimentw/gradientoverLayer1)
FIPP UPSTDP
SD: 4800.0 m
Range: 4.0 km
Depth (m)
5800.0
6000.0
6200.0
6400.0
6600.0
6800.0
7000.0
7200.0
0.0
1.0
2.0
3.0
4.0
5.0
Time (seconds)

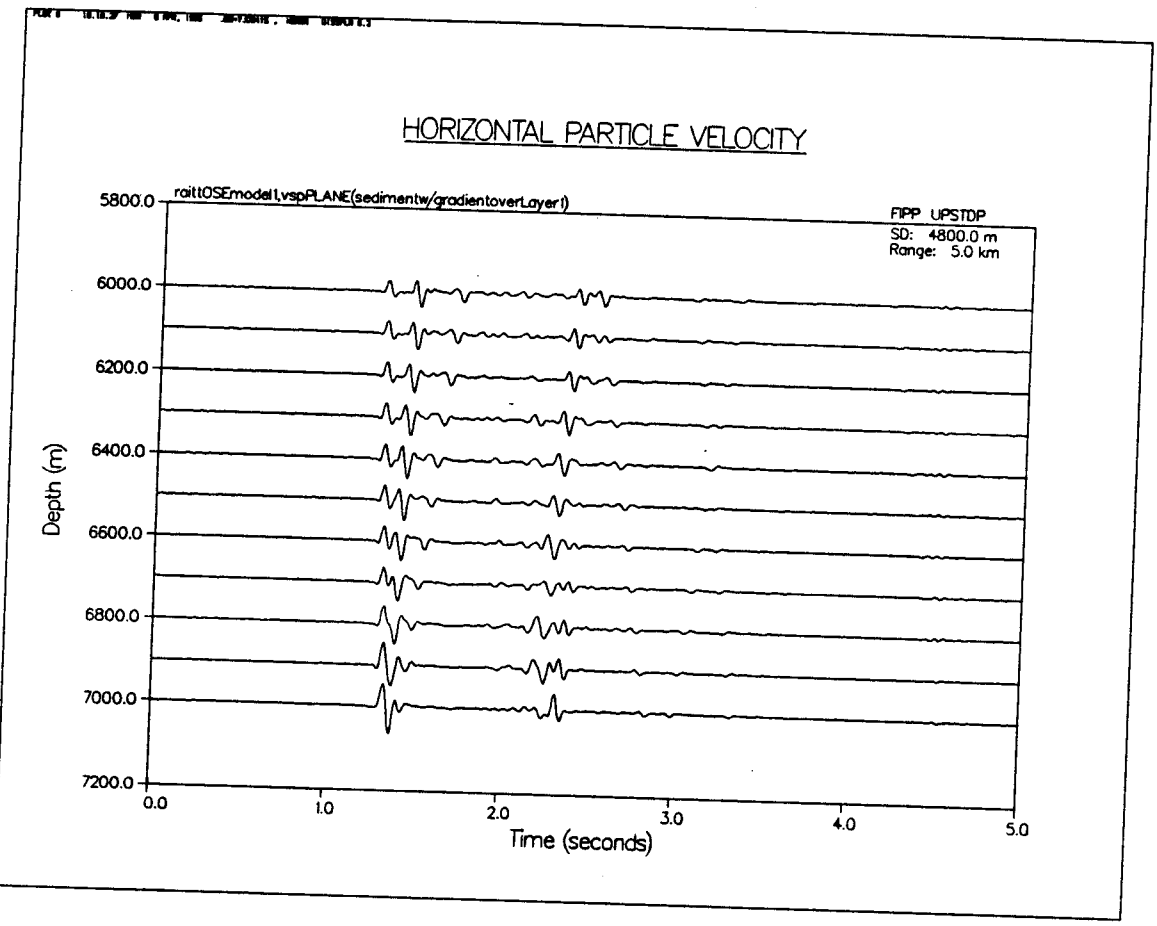
HORIZONTAL PARTICLE VELOCITY
raittOSEmodel1.vspPLANE(sedimentw/gradientoverLayer1)
FIPP UPSTDP
SD: 4800.0 m
Range: 5.0 km
Depth (m)
5800.0
6000.0
6200.0
6400.0
6600.0
6800.0
7000.0
7200.0
0.0
1.0
2.0
3.0
4.0
5.0
Time (seconds)

Layer 3 (at ~ 7200 m depth), while barely notable on the Raitt model, is now clearly evident on the sediment+Raitt VSP.

If there is a sharp jump in the P wave velocity at the ocean/sediment bottom or (nb) at the base of the sediment/crust interface, such that the S wave velocity below an interface is equal to or greater than the P wave velocity above, then the P-SV transformed shear waves can be prominent arrivals (SPUDICH, 1977). This is shown in **Figure 93d**, which shows the horizontal seismic profile from a velocity/depth model incorporating a shear wave velocity structure as above.

Figure 93

Full wavefield HSP (spherical wave point source) for fullshear elastic thin sediment + Raitt crustal v/z model, over a suite of OBS ranges in:

Geophone: Horizontal particle velocity

Geophone: Vertical particle velocity

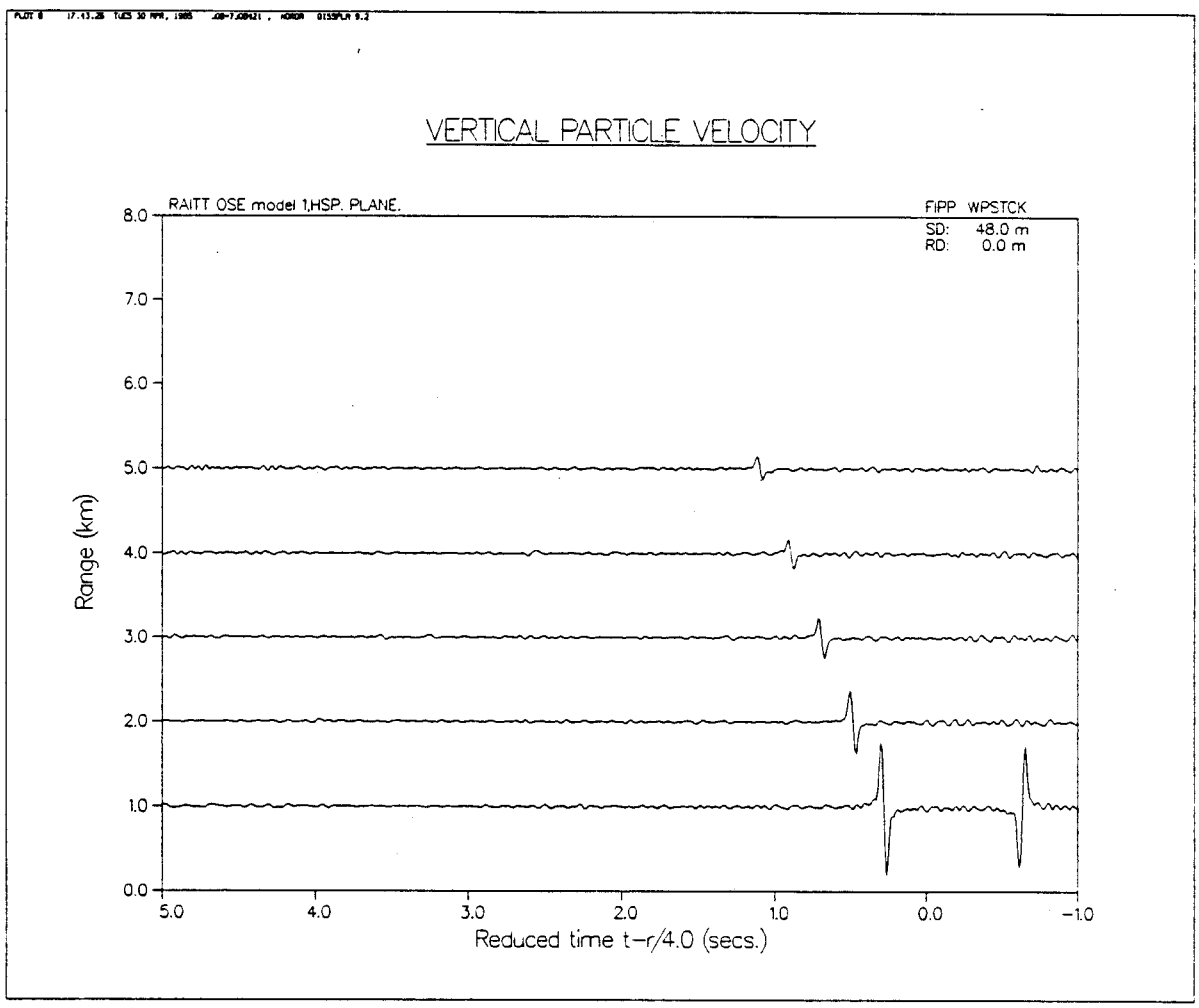
VERTICAL PARTICLE VELOCITY
RAITT OSE model 1,HSP. PLANE.
FIPP WPSTCK
SD: 48.0 m
RD: 0.0 m
Range (km)
8.0
7.0
6.0
5.0
4.0
3.0
2.0
1.0
0.0
5.0
4.0
3.0
2.0
1.0
0.0
−1.0
Reduced time t−r/4.0 (secs.)

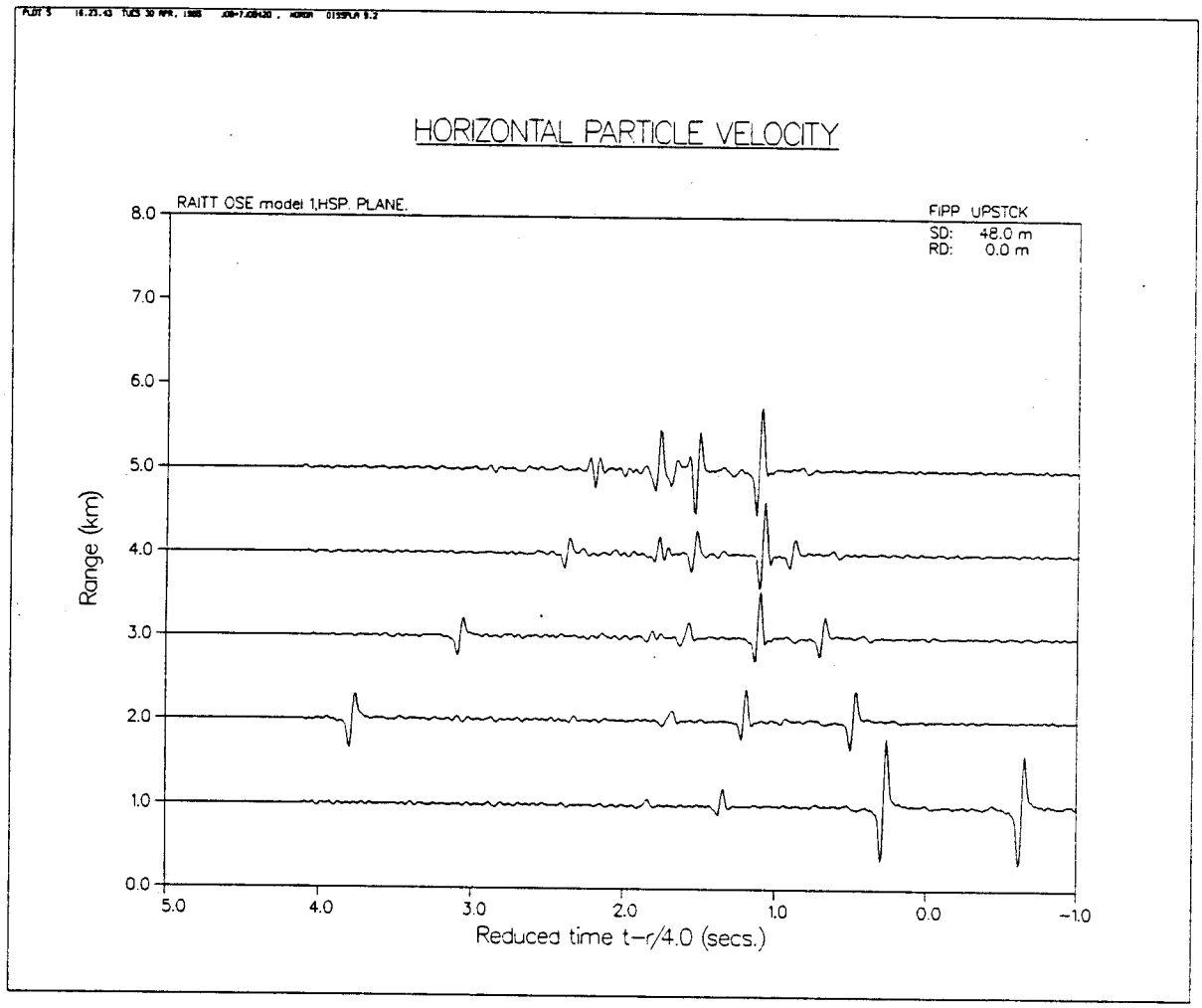
HORIZONTAL PARTICLE VELOCITY
RAITT OSE model 1,HSP. PLANE.
FIPP UPSTCK
SD: 48.0 m
RD: 0.0 m
Range (km)
8.0
7.0
6.0
5.0
4.0
3.0
2.0
1.0
0.0
5.0
4.0
3.0
2.0
1.0
0.0
-1.0
Reduced time t-r/4.0 (secs.)

Finally, STEPHEN (1984) has recently discussed what he calls the "direct wave root" as a previously-neglected nearfield effect for shallow VSP receivers. This arrival corresponds to the case of one or more receivers stationed very close to a major acoustic impedence boundary, where a large amplitude evanescent interface wave is generated by the direct water arrival. For sources in the water column sufficiently near the first major reflecting interface, the "direct wave root" is the largest amplitude (inhomogeneous/pseudo-spherical/non-geometric) arrival on shallow borehole receivers at supercritical S-R offset ranges.

Even after many repeated trials, it was not possible to unambiguously identify the direct wave root on several attempted fullwave VSPs. This arrival, however, is apparently in evidence in **Figures 94a-b**, where in both cases a single point source is placed in the water column at the near air/water interface depth of 40 m, with respect to 25 receivers located at several depths from 0 to 200 m into the subsediment basement layer. The basic total record of STEPHEN (1984, figure 2, pg. 4) is matched in both arrival number and character (with, however, the direct root wave remaining somehow less evident).

The figures cited above are horizontal seismic profiles (with bottom-based receivers), computed for two (a and b) frequency bandwidths (0-25 and 2-18 Hz) in attempt to optimally enhance the

Figure 94

Full shear elastic v/z model from Costa Rica DSDP experiment (after STEPHEN et al, 1984), with corresponding full wavefield HSP (spherical wave point source), for OBS receiver string at two depths into bottom, to highlight the direct water root (inhomogeneous) wave, at 2 center frequencies and bandwidths (f_c= 10 and f_c= 5, 0-20 and 2.5-18 Hz), and 2 gradient samplings (# layers =45; # layers = 90)

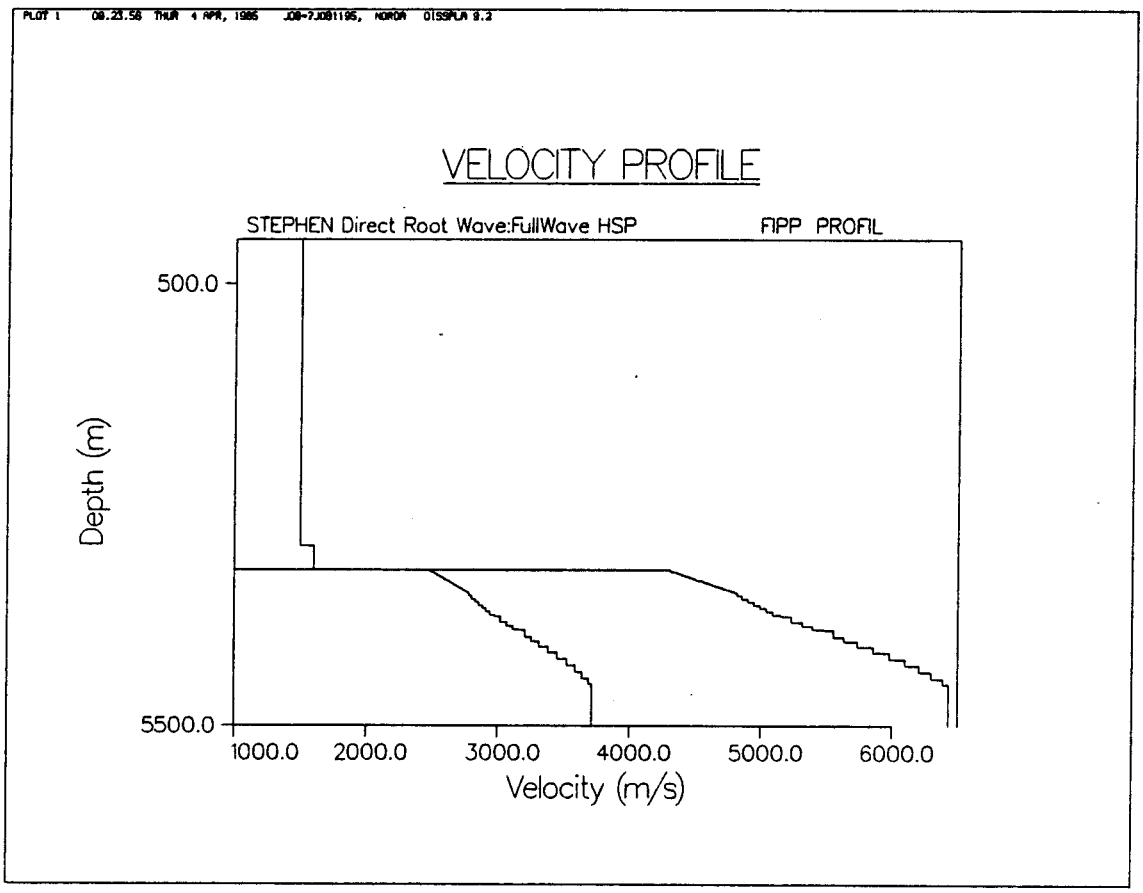
PLOT 1 08.23.56 THUR 4 APR, 1985 JOB=7J0891195, NORDA DISSPLA 9.2
VELOCITY PROFILE
STEPHEN Direct Root Wave:FullWave HSP
FIPP PROFIL
500.0
5500.0
Depth (m)
1000.0
2000.0
3000.0
4000.0
5000.0
6000.0
Velocity (m/s)

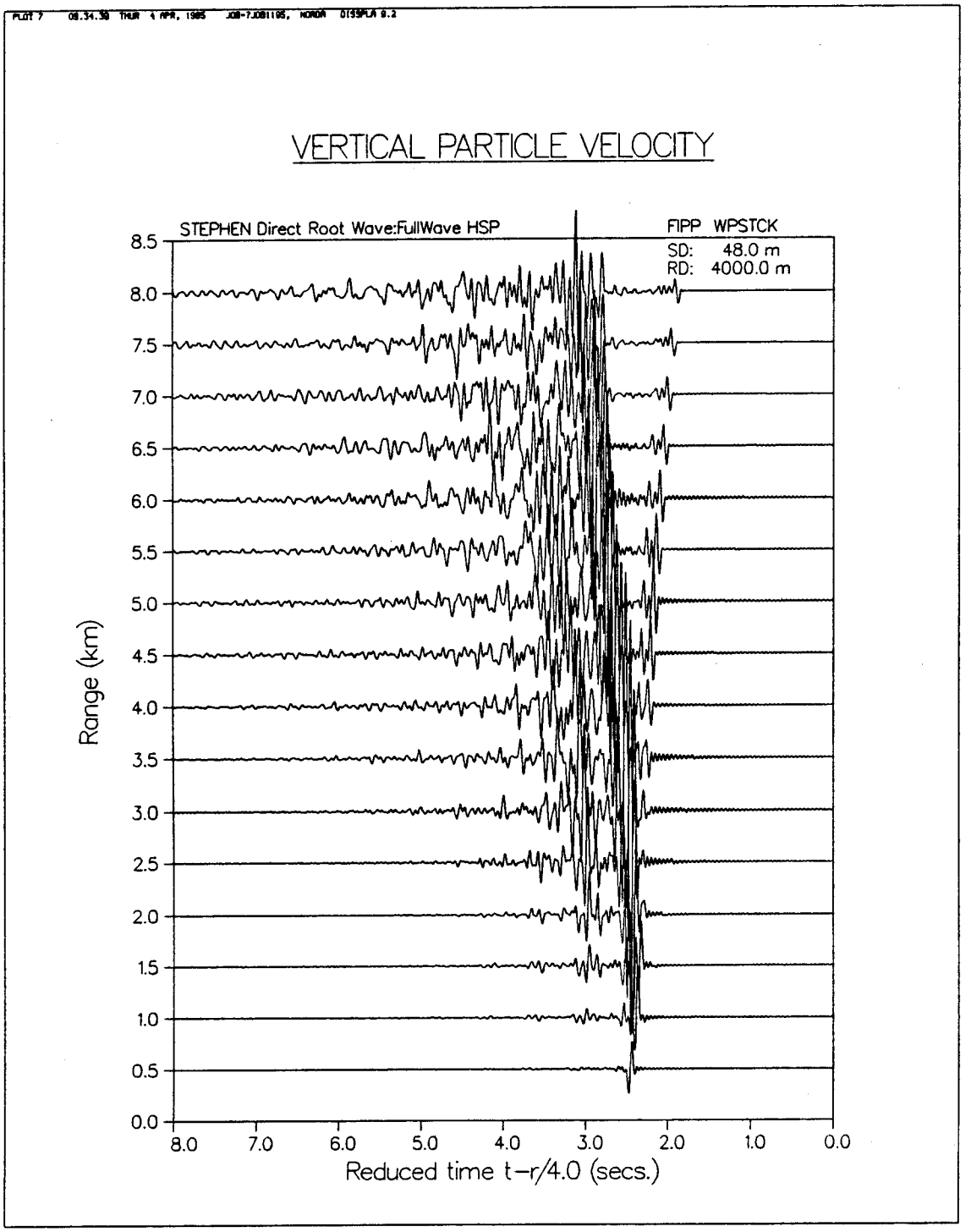
VERTICAL PARTICLE VELOCITY
STEPHEN Direct Root Wave:FullWave HSP
FIPP WPSTCK
SD: 48.0 m
RD: 4000.0 m
Range (km)
8.5
8.0
7.5
7.0
6.5
6.0
5.5
5.0
4.5
4.0
3.5
3.0
2.5
2.0
1.5
1.0
0.5
0.0
8.0 7.0 6.0 5.0 4.0 3.0 2.0 1.0 0.0
Reduced time t−r/4.0 (secs.)

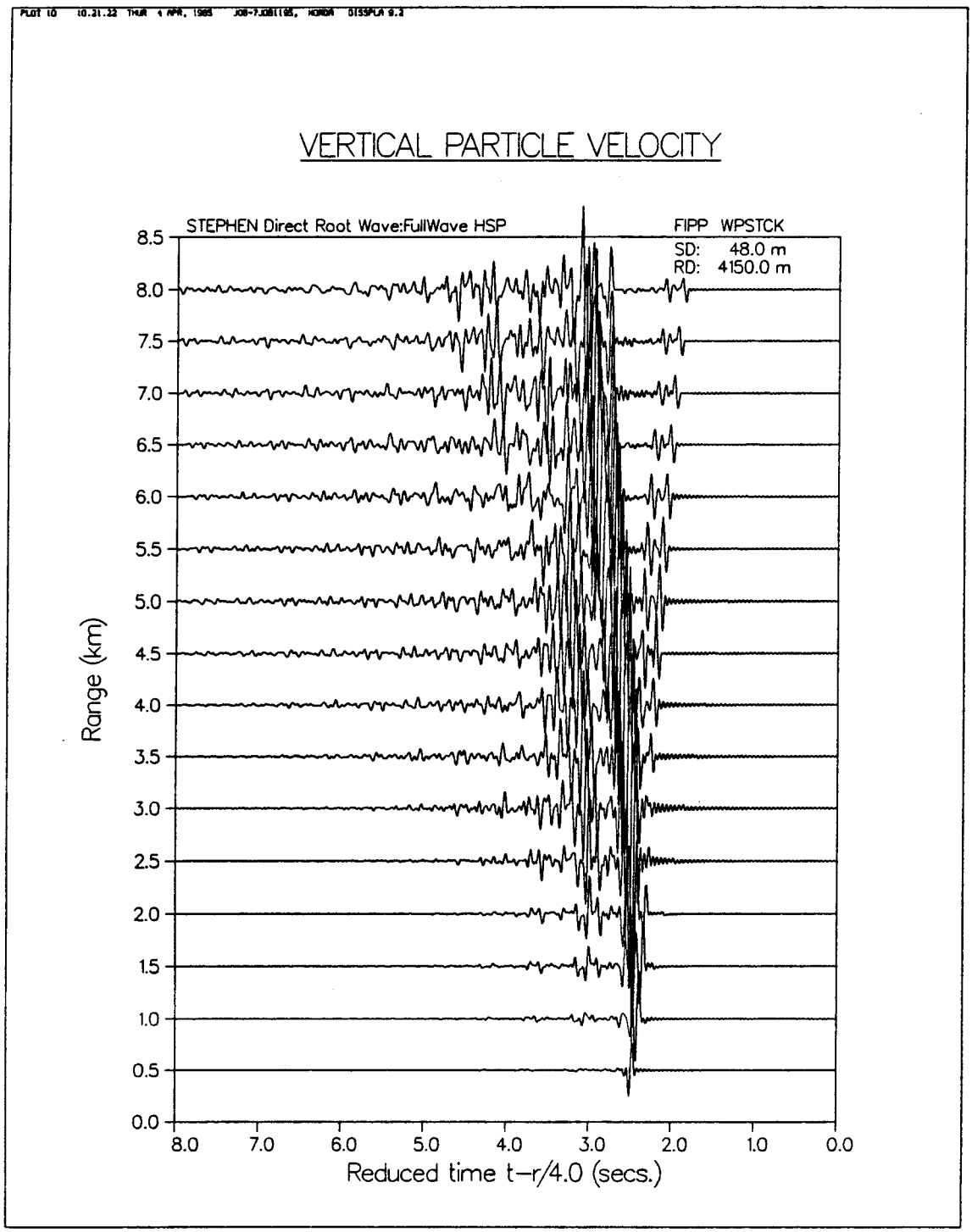
VERTICAL PARTICLE VELOCITY
STEPHEN Direct Root Wave:FullWave HSP
FIPP WPSTCK
SD: 48.0 m
RD: 4150.0 m
Range (km)
8.5
8.0
7.5
7.0
6.5
6.0
5.5
5.0
4.5
4.0
3.5
3.0
2.5
2.0
1.5
1.0
0.5
0.0
8.0 7.0 6.0 5.0 4.0 3.0 2.0 1.0 0.0
Reduced time t−r/4.0 (secs.)

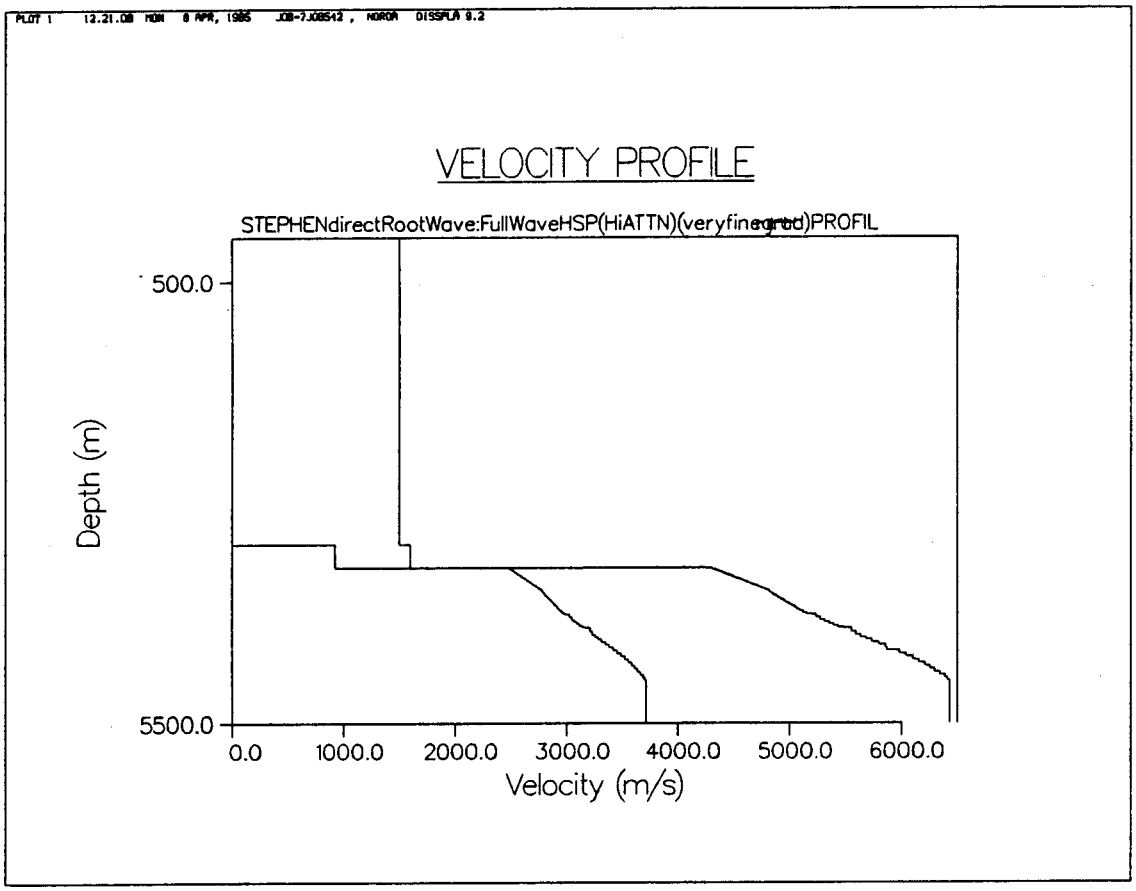
PLOT 1 12.21.08 MON 8 APR, 1985 JOB=7.00542 , NORDA DISSPLA 9.2
VELOCITY PROFILE
STEPHENdirectRootWave:FullWaveHSP(HiATTN)(veryfinegrid)PROFIL
500.0
5500.0
Depth (m)
0.0
1000.0
2000.0
3000.0
4000.0
5000.0
6000.0
Velocity (m/s)

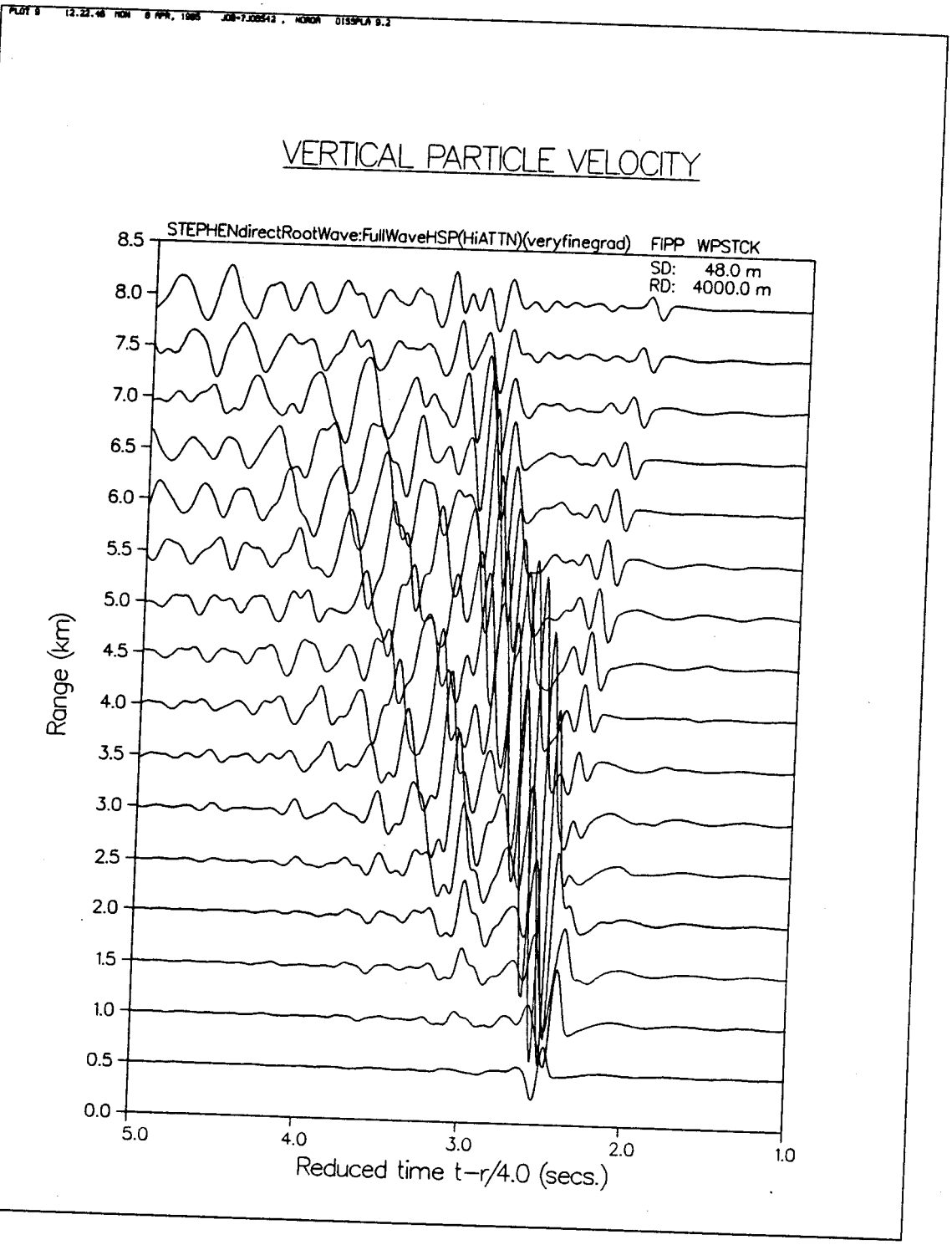
PLOT 9 12.22.48 MON 8 APR, 1985 JOB=7.008542 , NORDA OISSPLA 9.2
VERTICAL PARTICLE VELOCITY
STEPHENdirectRootWave:FullWaveHSP(HiATTN)(veryfinegrad) FIPP WPSTCK
SD: 48.0 m
RD: 4000.0 m
Range (km)
8.5
8.0
7.5
7.0
6.5
6.0
5.5
5.0
4.5
4.0
3.5
3.0
2.5
2.0
1.5
1.0
0.5
0.0
5.0
4.0
3.0
2.0
1.0
Reduced time t−r/4.0 (secs.)

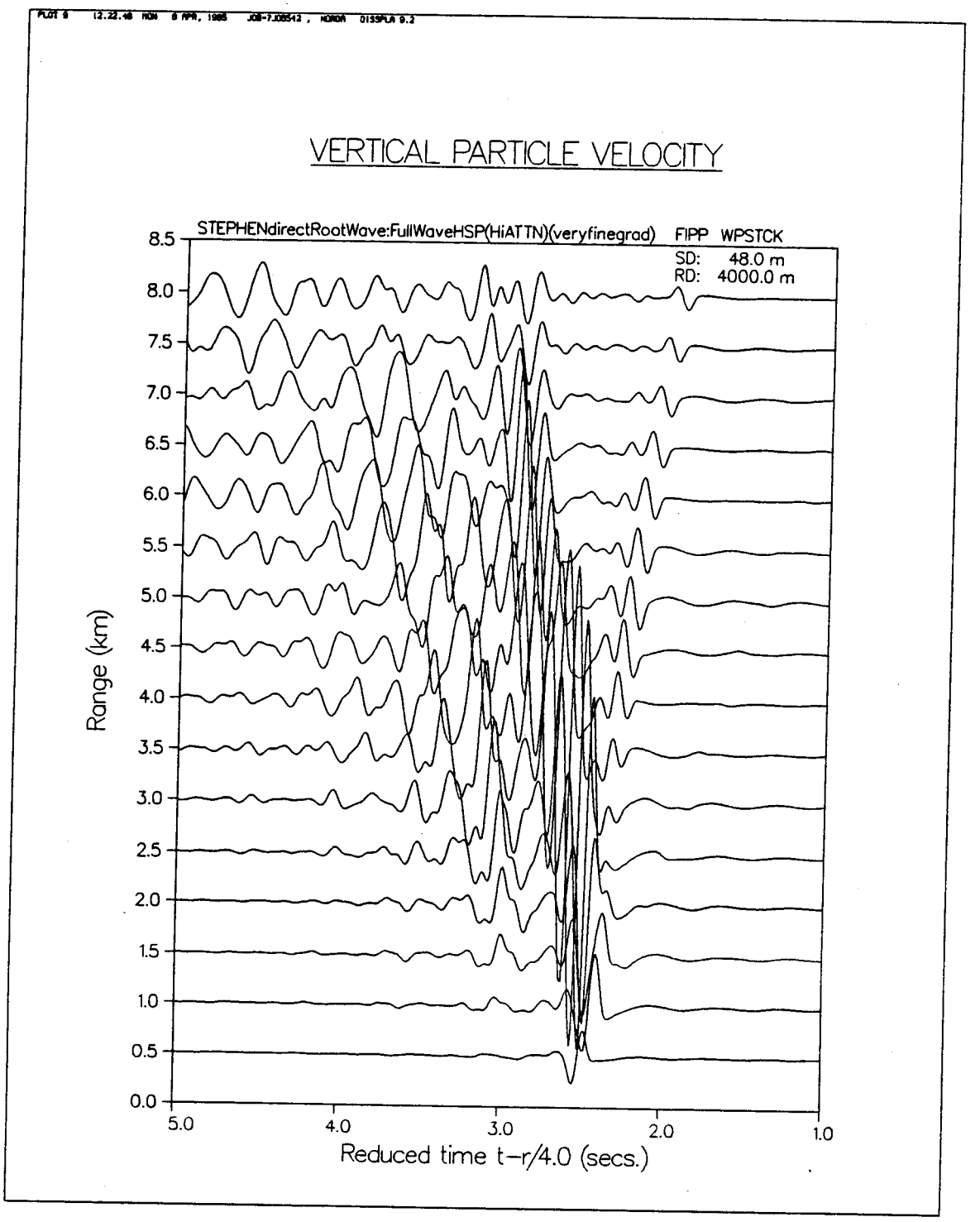
VERTICAL PARTICLE VELOCITY
STEPHENdirectRootWave:FullWaveHSP(HiATTN)(veryfinegrad) FIPP WPSTCK
SD: 48.0 m
RD: 4000.0 m
Range (km)
8.5
8.0
7.5
7.0
6.5
6.0
5.5
5.0
4.5
4.0
3.5
3.0
2.5
2.0
1.5
1.0
0.5
0.0
5.0
4.0
3.0
2.0
1.0
Reduced time t−r/4.0 (secs.)

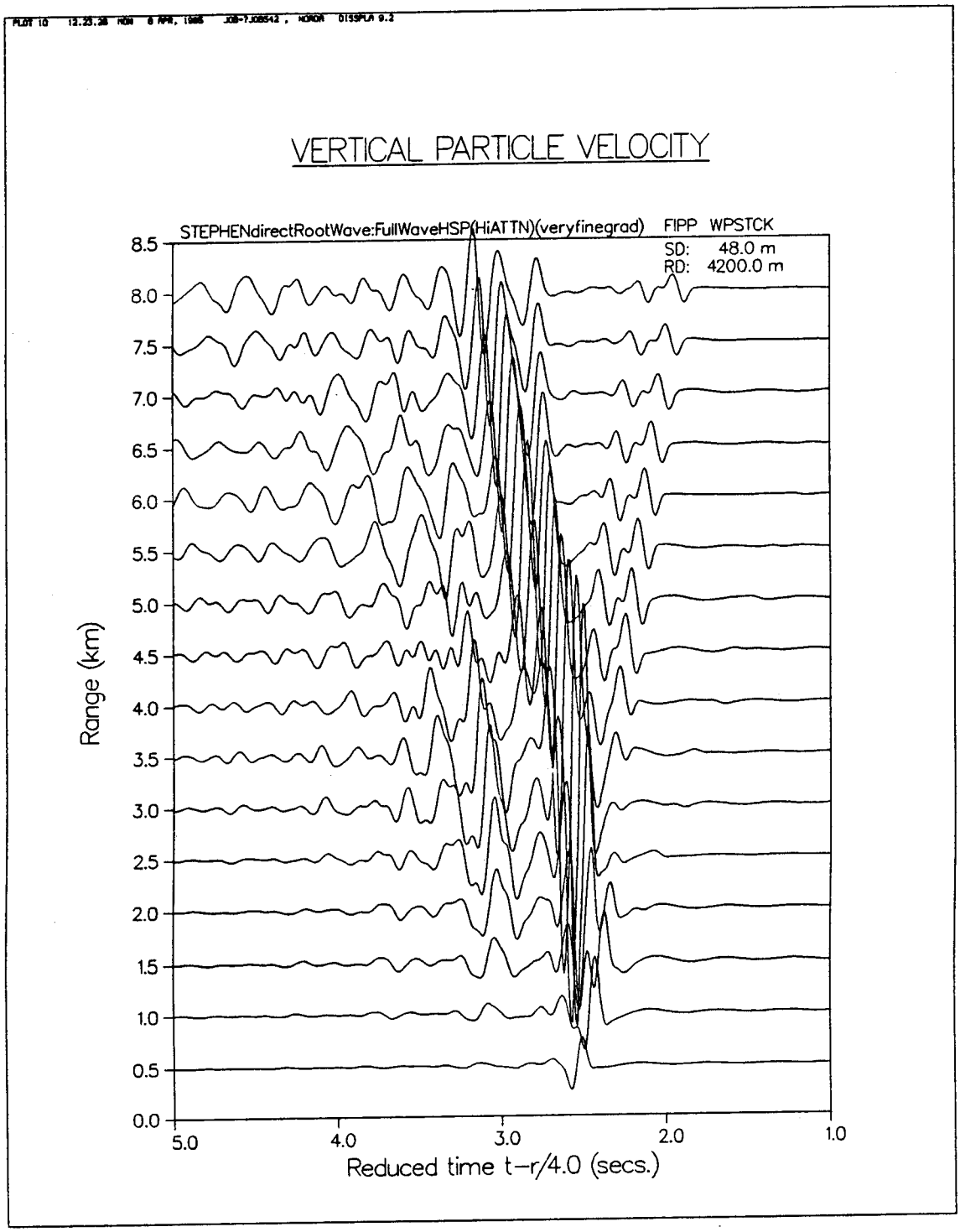
VERTICAL PARTICLE VELOCITY
STEPHENdirectRootWave:FullWaveHSP(HiATTN)(veryfinegrad) FIPP WPSTCK
SD: 48.0 m
RD: 4200.0 m
Range (km)
8.5
8.0
7.5
7.0
6.5
6.0
5.5
5.0
4.5
4.0
3.5
3.0
2.5
2.0
1.5
1.0
0.5
0.0
5.0
4.0
3.0
2.0
1.0
Reduced time t−r/4.0 (secs.)

inhomogeneous root arrival against the background of locally large-amplitude surface multiples and P and Sv headwaves.

In the examples of **Figure 94a-b**, we have also considered also two approximations, involving a lesser and a greater number of component isovelocity layers to approximate the continuous gradient of STEPHEN. It will be noted that the more continuous gradient approximation decreases the head wave amplitude features at higher grazing angles (longer offsets, at about 2.5 seconds reduced time), otherwise entirely preserving the same number and basic character of arrival phases.

It must be repeated that the "direct wave root" or source-related inhomogeneous wave is unobservable for the case of vertical receivers located in the uppermost sediment layers (not shown), and is in any case not as clearly evident on any attempted seismograms computed by us as on the reflectivity seismograms originally published by STEPHEN (1984).

The full nature of this discrepancy is at present unknown (STEPHEN, 1985, personal communication), and is the subject of further investigation. It is believed that at least some part of this discrepancy can be accounted for as a function of:

(a) the number of isovelocity layer steps used to approximate the subsediment velocity gradient

(b) the precise choice of minimum, center-power and maximum spectral frequencies

(c) the minimum phase velocity (maximum horizontal wavenumber and its truncation/smoothing)

(d) operational treatment of reverberant effects at the free/pressure release surface.

As noted, many fullwave calculations using "SAFARI" require the computational replacement of the free surface with (e.g.) an equivalent halfspace having the same (or slightly different) properties as the first media layer. This is done as a functional measure, in order to reduce the amplitudes of the otherwise very strong and disruptive trains of surface-reflected multiples. However, the treatment of the uppermost solid layer/air interface is in need of additional consideration, as the "true" seismic response plainly lies somewhere between the free surface and absorbing upper halfspace cases.

The direct root wave effect is in need of much additional study, and is currently being investigated by us and others with respect to its conditions of generation and detection over diverse geobottom environments and experimental configurations, in attempt to further quantify possible improvements in S/N for water-column, OBS and subbottom receivers. It is possible, for example, that at least some of the generally high amplitude "noise" routinely observed in marine exploration VSPs in and thru shallow sediment layers can be attributed to an inhomogeneous wave effect like that of the direct root.

Section 4

Current Areas of Development of the "SAFARI" Algorithm

Improving runtime reduction, startup capacity, and range of possible applications via postprocessors are all among the important areas of current program development for "SAFARI".

On the level of code development and implementation, it is desirable to maintain insofar as possible the sparse banded block diagonally-dominant global matrix form in whatever change of field equations and/or boundary conditions are considered. It is possible that the direct global matrix resulting from one or more of these departures from the plane homogeneous isotropic layer case could be more readily solved by another sequence of assembly and linear equation solution techniques than those currently employed.

It is also anticipated that the development of new generation array processors and associated parallel software algorithms will help make feasible considerable further savings in storage and runtime for even the present direct global matrix implementation in "SAFARI".

However, outside the area of formal program development, there are many other more fundamental areas of great interest and

possible new application, which can be considered with relative ease within the direct global matrix/finite wave element framework. For example, the non-ideal earth model cases including weak anisotropy, variable porosity via a Biot model, and alternate layer connectivity conditions (such as 'slipping' interfaces) are but 3 examples of more or less direct extensions possible. In the case of transverse anisotrophy, the local layer submatrices are now 6x6 in dimension; it is not anticipated that this should adversely affect solubility using the present global scheme. The cases of interlayer slippage and/or Biot media conditions do not change the matrix dimensions but only their entries.

It should also be noted immediately that numerous other applications-specific options (such as intermediate slowness-plane wave seismograms, SV and complex nonpoint source types) could also be readily developed within the present "SAFARI" framework. In a similar fashion, approximate rough-scattering phenomenologies can also be introduced, via an appropriate change in the field equations to reflect an additional net attenuation mechanism.

Section 4(a)

Spherically stratified media

As the scalar wave equation is separable not only in cylindrical and cartesian coordinates as discussed here, but also in spherical polar coordinates, this leads to solutions in terms of spherical harmonics and hence the possibility of exactly treating spherically stratified earth models (BEN MENAHEM and SINGH, 1981). In this case, as in the above, the global matrix form is directly applicable for determining the radially dependent Green' function in spherically stratified environments. The main modifications necessary here are the replacement of the current exponential depth functions by spherical Bessel functions. It is envisioned that such a spherically-stratified SAFARI would have immediate applications to earthquake and teleseismic propagation studies.

Section 4(b)

3-dimensional source

Considering problems with a three-dimensional distributed source, rather than pursue a 'hybridization' approach, which combines analytical integral transform methods with finite difference or finite element numerical techniques, it has only been necessary to use the possibility of total wavefield superposition inherent in the finite wave element approach to provide an exact analytical solution for arbitrary 3D source arrays in the transform domain, to successfully simulate ultrasonic beamforming, seismic and towed acoustic array effects.

SCHMIDT and GLATTETRE (1985) have recently developed both theory and working numerical model, based upon expansion of the 3 dimensional source potentials in a Fourier series of the azimuthal Fourier order. This is a major computational advantage, making the numerical code extremely efficient even when hundreds of Fourier orders are needed, since these are simply introduced as additional right hand source terms in the direct global matrix equations (**Figure 95**).

Figure 95

Outline of governing field equations and local-global mapping for 3D source version of SAFARI (after SCHMIDT and GLATTETRE, 1985)

LOCAL – GLOBAL MAPPING

Local unknowns: $\{a\}_l^m = \{A_1^m, B_1^m, C_1^m, A_2^m, B_2^m, C_2^m\}^T$

Global unknowns: $\{a\}_l^m = [S]_l \{A\}^m$

Local field parameters $\{v\}_i^m = \{w_i^m, u_i^m \pm v_i^m, \sigma_{zz}^m, \sigma_{rz}^m \pm \sigma_{\theta z}^m\}$

Global field parameters $\{V\}^m = \sum_{i=1}^{N-1} [T]_i \{v\}_i^m$

FOURIER EXPANSIONS

$$\Phi(r,\theta,z) = \sum_{m=0}^{\infty} \Phi^m(r,z) \begin{cases} \cos\ m\theta \\ \sin\ m\theta \end{cases}$$

$$\Lambda(r,\theta,z) = \sum_{m=0}^{\infty} \Lambda^m(r,z) \begin{cases} \cos\ m\theta \\ \sin\ m\theta \end{cases}$$

$$\Psi(r,\theta,z) = \sum_{m=0}^{\infty} \Psi^m(r,z) \begin{cases} \sin\ m\theta \\ -\cos\ m\theta \end{cases}$$

DISPLACEMENT EXPANSION COEFFICIENTS

$$w^m(r,z) = \int_0^\infty [-A_1^m \alpha e^{-z\alpha} + A_2^m \alpha e^{z\alpha} + B_1^m s e^{-z\beta} + B_2^m s e^{z\beta}] s J_m(rs) ds$$

$$u^m(r,z) \pm v^m(r,z) = \int_0^\infty [\mp A_1^m s e^{-z\alpha} \mp A_2^m s e^{z\alpha} \pm B_1^m \beta e^{-z\beta} \mp B_2^m \beta e^{z\beta} + C_1^m s e^{-z\beta} + C_2^m s e^{z\beta}] s J_{m\pm1}(rs) ds$$

EXPANSION COEFFICIENTS

Use of the Hankel transform yields the following integral representations:

$$\Phi^m(r,z) = \int_0^\infty [A_1^m(s)e^{-z\alpha} + A_2^m(s)e^{z\alpha}]\, sJ_m(rs)ds$$

$$\Lambda^m(r,z) = \int_0^\infty [B_1^m(s)e^{-z\beta} + B_2^m(s)e^{z\beta}]\, J_m(rs)ds$$

$$\Psi^m(r,z) = \int_0^\infty [C_1^m(s)e^{-z\beta} + C_2^m(s)e^{z\beta}]\, sJ_m(rs)ds$$

$$\alpha = \sqrt{s^2-h^2} \qquad \beta = \sqrt{s^2-k^2}$$

SOURCE FIELD REPRESENTATION

Compressional point source at $\{r_i,\theta_i,z_i\}$:

$$\Phi_i^m(r,z) = \frac{\varepsilon_m}{4\pi\omega}\int_0^\infty \left[\begin{Bmatrix}\cos\ m\theta_i\\ \sin\ m\theta_i\end{Bmatrix}\frac{\exp(-\alpha|z-z_i|)}{\alpha}J_m(r_i s)\right]$$

$$\times s J_m(rs)\,ds$$

$$\Lambda_i^m(r,z)\ ,\ \Psi_i^m(r,z) = 0$$

Although this model in its present implementation is set up to treat problems with simple axial source distributions (horizontal arrays), it is readily extended to the case of more complex nonaxial source types.

Section 4(c)

Range Dependent/Laterally-inhomogeneous media

The previous investigations of wave propagation in layered media have been almost exclusively restricted to (2D) range Independent media, wherein elastic material properties effecting propagation are allowed to change in only one (eg, depth) direction, with assumed constancy in the other (lateral/horizontal range) direction. The exact solution of problems in the more general media case of vertical and horizontally variant media is of considerable importance in predicting propagation effects and behaviour in bottom-interacting underwater acoustics, deep crustal and exploration seismology, where cross-sectional models are required to adequately describe the environment.

However, for the case of simultaneous depth and range dependent elastic media, the Helmholtz wave equation can no longer be solved by simple separation. In the case of range dependent media, the question of P and SV wave coupling leads almost immediately to major difficulties in even defining what is meant by P and S components of displacement and stress. Thusfar only approximate or brute force solutions to the complete problem, or else exact solutions to some approximate problem form, have been attempted, with varying success and applicability. A subset of "exact" approaches is reviewed briefly below.

Figure 96

Schematic of basic finite wave element concept (in a range Independent environment) for generalized source-receiver configuration

MULTILAYER ELASTIC WAVEGUIDE MODEL

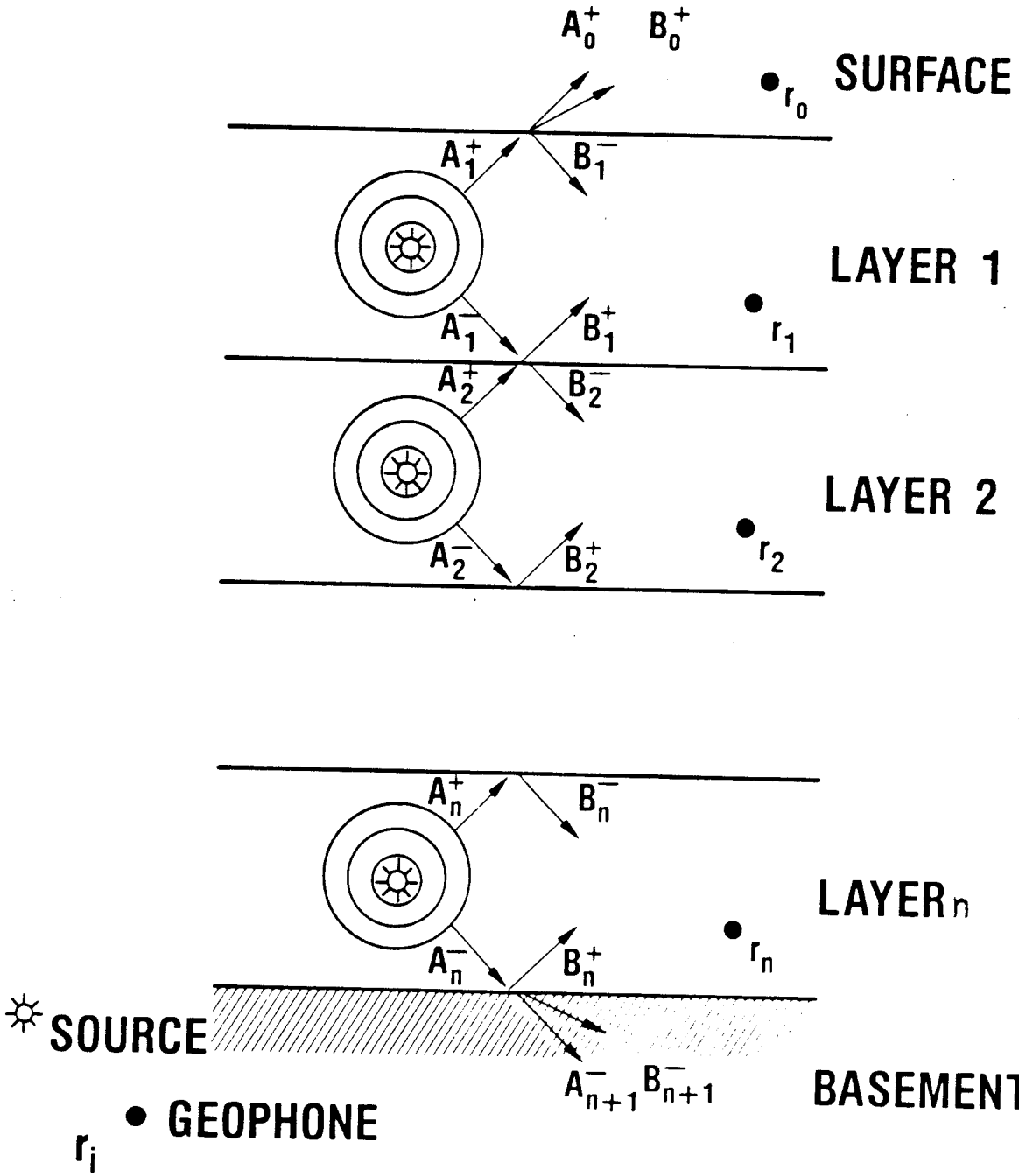

Various 'exact' attempts have sought to consider only an incomplete set of the total number of 'interaction terms' in the full vector wave equation. However, to date no such attempt has notably succeeded. A major difficulty here is in precisely identifying the specific kinds and importance of contributions to the total observable wavefield arising from retained/neglected terms. It has generally proven impossible to find other Helmholtz representations in which the coupling terms are either simply expressed or else demonstrably negligible over realistic frequencies of interest. This is essentially equivalent to making the medium only "weakly" inhomogeneous in a given sense.

Additional efforts have been directed at considering an approximate solution to exact inhomogeneous media, by employing asymptotic approximations in which P and SV components of displacement decouple as frequency increases. These have been very limited in their hi-frquency/large scale applications, and their accuracy to fine-structured media over most real exploration and deep crustal frequencies is open to question.In particular, as KENNETT has discussed, in both surface wave phenomena, and for seismic wave propagation to moderate distances from the source, coupling of P and SV waves in laterally inhomogeneous media cannot apriori be neglected.

Recently KENNETT (1984) has presented a formal solution to seismic propagation in range dependent media via modified

coefficient matrices. The essence of this approach separation of the spatial distribution of material properties into a primary part (depending only on z) and an additional perturbation (depend ing on both z and x). In this way, the net displacement and stress can be obtained by operation of the standard propagator matrix for the laterally homogeneous component, plus the effective contribution of distributed sources having intensity per unit distance given by a measure of the perturbation. In particular, if the inhomogeneous contribution is in some sense smaller than the homogeneous result, the integral equation representation can be iteratively solved for until a sufficient accuracy is achieved.

Here the reflection/transmission operator for such a composite zone can be seen as a "reverberation" operator coupling the adjacent regions, where each term in the total operator expansion represents the behaviour of all possible incident fields. If the horizontal extent of the inhomogeneity in question is large with respect to the incident seismic wavelength, the above mentioned possibility of partial operator expansion provides the formal link to modeling propagation in more general media. An advantage of this representation is that it exposes the physical character of that portion of the total response modeled.

An objection to this approach is that simple spatial convolution characteristics are preserved only in the case of Horizontally stratified media. Thus, in a rapidly varying heterogeneous

medium, intermode coupling here neglected becomes important, and other approximations to the reflection/transmission operators must be invoked.

To date considerable difficulty has ensued when practically attempting to algorithmically implement such a formal solution. In addition, the physical interpretation of the new local matrix is not as transparent as in the case of the original vertically inhomogeneous media. As in the above approaches, interpretation of the various terms in this (or any) approximation scheme will depend heavily on the specific choice of potential and/or matrix representation, as well as on any subsequent approximations adopted.

As in the simpler case of range-independent propagation, identification of an appropriate model formulation for treating both field equations and boundary conditions in the case of a general layered medium is essential for profitable consideration of the range dependent problem. In this section, it will be briefly argued that for the general case of an n plane layered vertically and laterally inhomogeneous medium, it can be equally advantageous to resort to a global finite wave element methodology. Because the algebraic expressions encountered in the problem of defining, assembling and solving for the wavefield here are rather formidable, in the following, only a conceptual analysis is used to motivate and gain insight into a globally formulated range dependent propagation problem.

Here, to model seismic-acoustic wave propagation in and between horizontal and verticaly contiguous layered regions, one seeks simply to model a global inhomogeneous depth and range dependence in elastic parameters via an appropriate number of local homogeneous layer mega-blocks or super-elements. The total wavefield solution in each superelement cell is determined simply by solving the direct global matrix via the present (vertically-inhomogeneous/range independent) "SAFARI" program. The complete and exact wavefield solutions from one or more buried sources can then be computed for each individual "local" layer block in terms of up and downtravelling wave potentials, which are then matched simulteneously via classical boundary conditions across all vertical and horizontal boundaries across each superelement.

For a sufficient number of superlements, the total wavefield for the entire media is completely described to specifiable accuracy by assembling all "local" superelements and solving the resultant "superglobal" matrix. In this way, the grid-reduced global matrix for an individual (vertically inhomgeneous; laterally homogeneous) media sector can be treated as if it were itself a "local" element submatrix. Once these are defined for all superelements, the resulting matrices may then be assembled to form a super global matrix. In exact analogy to the range independent case, a new "mega global" matrix containing complete wavefield solutions for each of the component super-elements (hence a "finite wave-element) can be likewise assembled and solved by standard (if somewhat more involved) finite element matrix techniques.

A high degree of generality is retained by allowing arbitrary representations of a vertically and horizontally inhomogeneous medium in finite wave element form. All depth and range dependent elastic parameters are completely variable, as well as the use of any source number or depth(s). In this entirely general formulation, as a natural extension of the previous range-independent direct global matrix approach, no restriction whatsoever is made upon the size and/or kind of variation in elastic properties between adjacent finite layer elements. As in the range-independent methodology, instead of considering a fixed discretised approximation of the the continuous boundary value problem in terms of local propagator matrices, this finite wave

element approach centers on construction of an adequate sequence of local discretized problems that when assembled properly approximate the continuous problem.

In this way, the numerical approach advocated here overcomes the difficulties and limitations of the attempted analytical methods previously described (concerning degree, nature and/or location of P-SV coupling), by avoiding an explicit formulation, solution and interpretation of complicated interaction expressions, and utilising an exact Numerical solution for a specifiably approximate problem (instead of an unspecifiable-approximation Analytic solution to an exact problem).

One possible difficulty is that, in practice, it is necessary to compute solutions on a very large ("infinite") number of subregions. Such a computational grid that adequately covers the full region for the most general case is presently prohibitive in terms of CPU and storage on most present computers. Thus consideration must be given to optimise the number and location of computational elements introduced.

The main concern here is for an efficient superglobal matrix assembly and solution strategy, built around the present direct global matrix technique for determining the multilayer Green's function in vertically inhomogeneous media. This involves some type of FEM algorithm that uses an indexing system to identify and optimally regroup individual superelement matrices into an

optimally sparse and/or diagonally dominant matrix form admitting of rapid stable solution. In exact parallel to the previous formulation in range independent media, such a rearrangement in the interest of computational stability and economy is readily undertaken, as is routinely the case in Finite Element methods, precisely because it is the total superGlobal solution over all superelements that is sought for. The main difference between the original (range independent) strategy of assembling all vertical local element matrices followed by solving the linear equations on the one hand and the new proposed strategy of assembling all horizontal local superelement matrices followed again by solution is that in the latter case, assembly and solution of the overall super-global set of equations must in some sense be interleaved in parallel.

The correctness and completeness of the above outline superglobal solution of course assumes that the source(s) and/or receiver(s) are "sufficiently far" away from the 4 outer edge boundaries, so that backscattering would be negligible. The construction of 'nonreflecting' boundary conditions offers at least a numerical approximation to attenuating and/or removing backscattered reflections at intersecting edge boundaries.

A further extension of the above global approach to range dependent propagation can at this point be considered, which at the same time considers the backscattering problem as well as computational feasibility. As is well known, the representation of elastic wave fields in terms of one or more configurations of point sources provides a source of sufficiently general character such that nearly any seismic source model can be written in this form. However, the present direct global matrix represenation - allowing separable homogeneous (source-free) and inhomogeneous (source) solutions - yields the possibility of treating any desired vertical source configuration, either in the form of a large number of discrete point sources or else continuous source distributions.

It has been shown that consideration of the effects of lateral inhomogeneity on wave propagation can be equivalently reconsidered in terms of a source distribution, appropriately modified by the conditions of inhomogeneity. The displacement and stress fields generated by a single source in a range dependent media will be shown to be equivalent to that produced by taking the radiation from the source into the homogeneous medium and subsequently regarding this itself as the new incident field at the next superelement interface. This process can be continued to cover the entire gridded media. The depth dependent Green's function solution for the vertically inhomogeneous/laterally homogeneous media presented previously could therefore be readily

A further extension of the above global approach to range dependent propagation can at this point be considered, which at the same time considers the backscattering problem as well as computational feasibility. As is well known, the representation of elastic wave fields in terms of one or more configurations of point sources provides a source of sufficiently general character such that nearly any seismic source model can be written in this form. However, the present direct global matrix represenation - allowing separable homogeneous (source-free) and inhomogeneous (source) solutions - yields the possibility of treating any desired vertical source configuration, either in the form of a large number of discrete point sources or else continuous source distributions.

It has been shown that consideration of the effects of lateral inhomogeneity on wave propagation can be equivalently reconsidered in terms of a source distribution, appropriately modified by the conditions of inhomogeneity. The displacement and stress fields generated by a single source in a range dependent media will be shown to be equivalent to that produced by taking the radiation from the source into the homogeneous medium and subsequently regarding this itself as the new incident field at the next superelement interface. This process can be continued to cover the entire gridded media. The depth dependent Green's function solution for the vertically inhomogeneous/laterally homogeneous media presented previously could therefore be readily

used for propagating the total wavefield from one lateral superelement to another, by simply employing Huygen's principle in an analogous use to its application in parabolic equation techniques. This viewpoint accords well with the previous discussion of finite wave elements, where we consider the total superglobal Wavefield solution to be simply that derived from (simultaneously) computing the exact solution in each superlocal wave element and assembling these by matching boudary and radiation conditions.

A complete analysis and solution of this new source problem, and the associated numeric techniques for assembly discussed above, appears to be very complicated within the present solution representation. In addition, the computational problems of selecting the proper element size, determining ultimate accuracy and identifying model features governing correct parameterisation for relevant types of real laterally-inhomogeneous media must be subsequently examined. Further work is currently underway to determine the conditions for optimal source representation and superglobal matrix assembly and solution.

Section 5.

Conclusion.

The main results of this thesis have shown how seismic-acoustic wave propagation problems in plane layered range-independent media can be readily and completely solved in terms of numerical integration of a fast direct global matrix solution for the exact multilayered/multisource Green's function.

The general direct global matrix/finite wave element implementation of the integral transform solution to the Helmholtz wave equation, first given by EWING JARDETZKY and PRESS, provides a simple and physically appealing solution of the **general** problem of wave propagation in layered media. It generates a correct and complete solution for the global wavefield (from n arbitrary sources) at n arbitrary surface or depth positioned receivers simultaneously, based on an efficient formulation, assembly and solution of the local layer equations as governed by classical interface boundary conditions.

In a 2 dimensional isotropic homogeneous plane-welded elastic model, the Green's function kernel involves a Hankel function transform of a superposition, in each layer interface, of source -produced fields and homogeneous scattered fields, expressed in

terms of general up and downgoing wave potentials on the layer interface as the basic unit of consideration.

The DGM/FWE approach of SCHMIDT has a simple and effective representation in terms of "finite wave elements". The principle problem here is simple solution of a system of linear equations, which, however, turns out to be sparse banded block bidiagonal on account of the simple boundary conditions connecting all interfaces. The resultant kernel of the integral transform defines the correct and complete multilayer and multisource Green's impulse response function. All desired field parameters can be derived directly from this Green's function by numeric integration.

Even for very large numbers of layers and/or source-receiver combinations, the solutions of the globally assembled local continuity equations are both unconditionally stable and efficient, typically providing at least an order of magnitude savings in total computational time, as implemented on a typical minicomputer configuration (VAX 11/780). Because of the high degree of inate parallelism in the resulting algorithm of SCHMIDT ("SAFARI"), significant additional time savings are available for attached array processor configurations. Depending upon the specific application and hardware, any desired numerical accuracy and quality of output can be specified simply by dividing the total integration and Green's function computation intervals into

a sufficient number of finite wavenumber, frequency and layer intervals.

It should be stressed that the DGM/FWE method, here developed for the 2D, plane welded homogeneous and isotropic layer model, provides a complete and correct solution within this discretely approximated model.

The multilayered Green's function obtained by solution of the direct global matrix requires specification of integration path with respect to singularities of the integrand. To preserve the completeness of the exact fullwavefield response, problems with poles and branch cuts are avoided by introducing vanishingly small attenuative loss into the system, thereby removing all singularities from the real wavenumber axis so that direct numerical integration can be implemented. (Because of the completeness of the Green's function solution, all "ray trajectories" and "mode orders" are automatically included.)

Computationally convenient forms of kernels are furnished by taking the outgoing wave approximation, in the farfield asymptotic limit, using Fast Fourier transform. Since almost all conceivable seismic-acoustic applications consider only the outgoing wave (which is the only contribution experimentally ever seen), this truncated formulation is generally valid. The subsequent asymptotic approximation only weakly limits the range of numeric integration validity at very low frequencies, for

steep incident angles and extremely small source-receiver offset ranges. It must be emphasised, however, that the above choices for numeric integration are arbitrarily made only in the interest of computational economy when evaluating the integrands, and that exact Bessel function relations could equally well be employed (giving a totally correct complete solution for all angles, offsets and frequencies). In view of actual experience with quadrature integration employed, it is proposed that alternative correct and complete numeric integration schemes (adaptive quadrature/generalised Filon method) be investigated.

The stability, accuracy and completeness, and versatility of the direct global matrix/finite wave element solution was examined by comparing numerical results from "SAFARI" to a number of related canonic propagation problems admitting of solution both by analytic and established numerical methods.

Comparison of standard underwater acoustic, synthetic crustal and vertical seismic outputs to those computed by extant "exact" methods has shown that, in both stability and accuracy, completeness and economy, and versatility of solution, the SAFARI algorithm compares very favourably, or even improves upon, results of extant FFP and Reflectivity techniques. In particular, the order of magnitude CPU time savings allows routine consideration of a vastly increased number of layers in stratified models. The general multi-source formulation of the solution allows ready modeling of line and other more complex

source types, in one or more layers. Especially worthy of note is the fact that the simultaneous solution for the complete up and downgoing wavefield at all depths, for n arbitrary receivers at one or more source-receiver offsets, is such as to immediately comprehend the simulation of Vertical Seismic Profiling (VSP).

As noted, the DGM/FWE solution provides a ready complete exact benchmark solution for many applications. Because the total response of an exact Green's function is preserved, many additional wave phenomena (trapped/leaky/inhomogeneous phases), not always available in other "exact" modeling algorithms, are here readily evident. For both deep crustal and exploration seismic applications, it is felt that many fundamental properties of the exact complete fullwavefield response may reveal themselves more directly thru the "SAFARI" algorithm than in more complex solution representations. As a consequence, perhaps the only basic "shortcoming" of the "SAFARI" solution is precisely that it provides the complete total wavefield without intrinsic identification of individual arrivals (as possible with matrix-expansion based reflectivity models such as those of KENNETT). The full implications of the above are a subject of continuing study.

The ready development of the DGM/FWE method of SCHMIDT for other more complex layered media models has been here suggested in outline. The range of validity and application of the method embodied in "SAFARI" is not limited to the integro-differential

equation of visco-elastic wave propagation, but can be also applied to electromagnetic wave propagation.

Further theoretic and applications modeling studies are continuing, to further explore the wide class of propagation applications and extensions of "SAFARI" to more complex media approachable in a global finite wave element framework.

Figure 97

Overview of SAFARI algorithm capabilities (as of 12/31/84)

Figure 97

Overview of SAFARI algorithm capabilities (as of 12/31/84)

OVERVIEW OF SAFARI CAPABILITIES

	CW FIP	FULL WAVEFIELD PULSE FIPP	REFLECTION COEFFICIENT FIPR	REFLECTIVITY REFP	3D SOURCE SAFARI
MONOFREQUENCY GREEN'S FUNCTIONS	✓	✓		✓	✓
MONOFREQUENCY TL VS RANGE PLOTS	✓				✓
Z-CONTOURED TL VS RANGE PLOTS	✓				✓
ULTRASONIC SCATTERING	✓				
FULL WAVEFIELD PULSE WAVEFORMS		✓			
FULL WAVEFIELD SYNTHETIC SEISMOGRAMS		✓			
FULL WAVEFIELD SYNTHETIC VSPs		✓			
PLANE WAVE REFLECTION COEFFICIENT VS FREQUENCY			✓		
PLANE WAVE REFLECTION COEFFICIENT VS ANGLE			✓		
FREQUENCY-ANGLE CONTOURED REFLECT COEFFICIENT			✓		
FUCHS-MULLER REFLECTIVITY SYN SEISMOGRAMS				✓	
FUCHS-MULLER REFLECTIVITY SYNTHETIC VSPs				✓	
KENNETT DECOMPOSABLE REFLECT SYN SEISMOGRAMS				(✓)	
KENNETT DECOMPOSABLE REFLECTIVITY SYN VSPs				(✓)	
CROSSHOLE S/R TOMOGRAPHY					(✓)

Thesis Contributions:

Re-detailed derivation and documented chief computational and programming features of the DGM method and the "SAFARI" algorithm

Gave first extended discussion of the DGM with respect to local recursive propagation matrix methods in seismology

Co-Developed the general crustal seismic modeling capabilities in "SAFARI"

Recognized the potential for, and co-implemented, the VSP modeling capabilities in "SAFARI"

Carried out first extended verification tests and applications research of Crustal Seismic and VSP outputs of "SAFARI"

Re-examined an important crustal refraction profile from the E. Basin & Range province, in attempt to better account for nearfield arrivals

Confirmed and extended synthetic VSP modeling results of TEMME and MULLER for exploration and of STEPHEN for marine crustal VSP

Included examination and discussion of inhomogeneous/pseudo-

spherical/nongeometric arrivals, and the recent direct wave root arrival

We have newly presented the DGM wave propagation modeling method introduced to underwater acoustics by SCHMIDT, and both tested and applied this method in 3 diverse seismic-acoustic problems. We have discussed in detail the background history, field equation derivation, and DGM solution technique (including its analogy to FEM), centering on the relations of "SAFARI" to other FFP, discrete wavenumber and reflectivity models.

Accurate and realistic modelling requirements as a practical matter have also been discussed. In particular we have compared the fullwave and reflectivity responses, as available from SAFARI, in terms of surface, inhomogeneous and multiply-reflected contributions. A tentative result of these comparisons is that traditional reflectivity modeling will generally be a suitable prelude to fullwave analysis (which later requires considerable foreknowledge and care in Green's function integrand truncation). The DGM method implemented in SAFARI is very effective CPU-wise for even few-layered cases, and allows practical consideration of very large (NLayers>100) multilayered models heretofore generally unfeasible or impossible computationally.

We emphasize that the DGM method, as perceived by the author and by SCHMIDT, is characterized by a simultaneous **global** solution for the total wavefield amplitudes in all layers, in a simple physically intuitive formalism that separates source from resultant wavefield terms (thereby increasing its potential applicability to multi and complex source cases). The underlying

'finite wave element' philosophy here stems by analogy from the direct finite element method, when applied to the solutions first proposed by EWING JARDETZKY and PRESS. The key to the realization of the DGM-FWE technique in SAFARI is the exact mapping between local and global wave solutions, in precise isomorphism to that of FEM, which can be very efficiently implemented via a general index pointer scheme.

What is need in practice in many seismic-acoustic modeling scenarios is a fast general—applications numerical method that gives, using a discrete finite layer approximation, physically exact solutions, whose sum approximates reasonably well the exact analytic continuous solution. This has been the main motivation for the diverse development and testing of the present SAFARI algorithm. We believe that the present work exhibits the important consequences and applications of SAFARI to seismic acoustic modeling of diverse types, and suggests its fruitful further development and application for other fields in the future.

Bibliography.

Abramowitz,M. and I.A. Stegun, 1965. Handbook of Mathematical Functions. New York: Dover Publishers.

Achenbach, J.D., 1973. Wave Propagation in Elastic Media. Amsterdam-New York: North-Holland.

Aki, K. and P.G. Richards, 1980. Quantitative Seismology, vols. 1 and 2. San Francisco: W.H. Freeman.

Alekseyev, A.S. and B.G. Mikhailenko, 1976. "Solution of Lamb's problem for a vertically-inhomogeneous elastic halfspace", Izvestiya, Physics of the Solid Earth, December, p.11-25.

Aminzadeh, F. and J.M. Mendel, 1982. "Non-normal incidence state space model and line source reflexion synthetic seismogram", Geophysical Prospecting, 30, p.541-568.

, 1985. "Synthetic Vertical seismic Profiles for Non-normal incidence plane waves", Geophysics, 50(1), p.127-135.

Apsel, R.J., 1979. 'Dynamic Green's functions for Layered media and applications to Boundary-value problems', Ph.D. thesis, University of California at San Diego, La Jolla.

Apsel, R.J. and J.E. Luco, 1983. "On the Green's function for a Layered half-space, parts I and II", Bull. Seismo. Soc. Amer., 73(4), pp.909-930 and 931-949.

Aziz, A.K. (ed)., 1972. The Mathematical Foundations of the Finite Element Method, with applications to Partial Differential Equations. New York: Academic Press.

Bache, T.C. and D.G. Harkrider, 1976. "The Body Waves due to a General seismic Source in a layered Earth model: I", Bull. Seismo. Soc. Am., 66, p.1805-1819.

Bakun, W.H. and A. Eisenberg, 1970. "Fourier Integrals and Quadrature-introduced Aliasing", Bull. Seismo. Soc. Am., 60(4), p.1291-1296.

Balch, A.H. and M.W. Lee (eds), 1984. Vertical Seismic Profiling. Boston: IHRDC.

Banda, E. and N. Deichmann, 1983. "Comments on 'Low Velocity zone reflections observed in geometrical shadows of refraction profiles' by G.A. McMechan,", Geophys.J.R.astro.Soc., 74(2), p.633-636.

Baranzangi, M. and J. Ni, 1982. "Velocities and Propagation characteristics of Pn and Sn phases beneath the Himalayan arc and Tibetan plateau", Geology, 10, p.179-185.

Bath, M., 1984. Mathematical Aspects of Seismology. London-Amsterdam: Geophysical Press.

Bathe, K.E. and E.L. Wilson, 1976. Numerical Methods in Finite Element Analysis. Englewood Cliffs, NJ: Prentice Hall.

Bathe, K.E., J.T. Oden and W. Wunderlich (eds)., 1977. Formulation and Computational Algorithms in Finite Element Analysis. Cambridge: Cambridge University Press.

Ben Menahem, A. and S.J. Singh, 1981. Seismic Waves and Sources. New York-Berlin: Springer Verlag.

Bleistein, N., 1984. Mathematical methods for Wave propagation . New York: Academic Press.

Boore, D.M., 1972. "Finite Difference Methods for Seismic Wave Propagation in heterogeneous materials", in: B.A. Bolt (ed)., Methods in Computational Physics, Vol.11:Seismology. New York: Academic Press.

Bortfeld, R., 1967. "Elastic Waves in Layered Media", Geophys. Prosp. 15, p.644-650.

Bouchon, M. and K. Aki, 1977. "Discrete Wavenumber representation of Seismic source Wave fields", Bull. Seismo. Soc. Am., 67, p.259-277.

Bouchon, M., 1981. "A Simple Method to calculate Green's functions for Elastic layered media", Bull. Seismo. Soc. Am., 71, p.959-971.

Boyles, C.A., 1984. Acoustic Waveguides. New York: Wiley.

Bracewell, R., 1978. The Fourier Transform and its Applications. New York: McGraw Hill.

Braile, L.W., 1973. "Inversion of Crustal Seismic Reflexion Data", J. Geophys. Res., 78, p.7738-7744.

Braile, L.W. and R.B. Smith, 1975. "Guide to the Interpretation of Crustal refraction profiles", Geophys.J.R. astro. Soc., 40, p.145-176.

Brekhovskikh, L.M., 1960. Waves in Layered Media. New York: Academic Press.

Brigham, E.O., 1974. The Fast Fourier Transform. Englewood Cliffs, NJ: Prentice Hall.

Budden, K.G., 1962. The Wave Guide-Mode Theory of Wave Propagation. Englewood Cliffs, NJ: Prentice Hall.

Burridge, R., 1980. "The Gelfand-Levitan, the Marchenko and the Gopinath-Sondhi Integral Equations of Inverse Scattering Theory", Wave Motion, 2, pp.305-323.

Cagniard, L., 1962. Reflection and Refraction of Progressive Seismic Waves. New York: McGraw Hill.

Carson, J.R., 1924. "The Guided and Radiated Energy in Wire Transmission", AIEE Journ., 1(10).

Cerveny, V., 1962. "On the Position of the Maximum of the Amplitude curves of Reflected waves", Studia Geophys. Geod., 6, p.215-234.

, 1965. "The Dynamic Properties of Reflected and Head waves around the Critical point", Inst.Geophys.Acad.Tchech.Sci., 221, p.135-245.

,1967. "The Amplitude-Distance curves for waves Reflected at a plane interface for different frequency ranges", Geophys.J.R.astro.Soc., 13, p.187-196.

Cerveny, V. and R. Ravindra, 1971. Theory of Seismic Head Waves. Toronto: University of Toronto Press.

Cerveny, V. and B. Pscenik, 1972. "Refraction of Elastic Waves into a Medium of Lower velocity - pseudoSpherical waves", Pure and Appl. Geophys., 92, p.115-132.

Cerveny, V. and A.B. Frangie, 1980. "Seismic Wave Fields in Media with Causal Absorption", in: Proceedings of the 17th Assembly of the ESC, Budapest., p.250ff.

Chapman, C.H., 1978. "Body Waves in Seismology", in: J.Miklowitz and J.D. Achenbach (eds)., Modern Problems in Elastic Wave Propagation. New York: Wiley Interscience.

Chapman, C.H. and S. Orcutt, 1984. "The Computation of body-Wave synthetic seismograms", manuscript (prepared for Review of Geophysics and Space Physics, March, 1984).

Chin, R.C.Y., G.Hedstrom and L.Thigpen, 1984. "Numerical Methods in Seismology", Comput.Phys., 54. (manuscript).

, 1984. "Matrix Methods in Seismogram Synthesis", Geophys.J.R.astro.Soc., 77., p.483-502.

Chin, R.C.Y., 1980. "Wave Propagation in viscoelastic Media", in: A.M. Dziewonski and E.Boschi (eds). Physics of the Earth's Interior, Proc. of Corso LXXVIII, International School of Physics 'Enrico Fermi', 23 July-4 August 1979. New York: North Holland.

Christiansen, R.E., J.A. Frank and W.H. Geddes, 1976. "Low-Frequency Propagation via shallow Refracted paths through Deep

ocean unconsolidated Sediments", J.Acoust.Soc.Am., 57(6/7), p.1421-1426.

Choy, G.L., 1977. "Theoretical Seismograms of Core phases calculated by frequency-dependent FullWave theory and their Interpretation", Geophys.J.R.astro.Soc., 51, p.275-312.

Choy, G.L., V.F. Cormier, R.Kind, G.Muller and P.G.Richards, 1980. "A Comparison of Synthetic Seismograms of Core phases generated by Full wave theory and the Reflectivity method", Geophys.J.R.astro.Soc., 61, p.21-40.

Cisternas, A., O.Betancourt and A.Leiva, 1973. "Body in a 'real' Earth, Part I", Bull. seismo. Soc. Am., 63, p.145-156.

Claerbout, J., 1968. "Synthesis of a Layered medium from its Acoustic transmission response", Geophysics, 33, p.264-269.

, 1969. "Coarse grid Calculations of waves in Inhomogeneous media with Application to delineation of complicated seismic structure", Geophysics, 35, p.407-418.

, 1976. Fundamentals of Geophysical Data Processing. New York: McGraw Hill.

Clowes, A.M. and E.R. Kanasewich, 1970. "Seismic attenuation and the nature of Reflecting horizons within the Crust", J. Geophys. Res., 75, p.6693-6708.

Cooley, J.W., P.A.W. Lewis and P.D. Welch, 1969. "The fast Fourier transform and its applications", IEEE Trans.Audio and Electroacoustics, 17, p.77-85.

Davidoya,N.I., (ed), 1975. Seismic Properties of the Mohorovicic discontinuity. Springfield, Virginia: US Dept. of Commerce, National Technical Information Service.

Davis, J.J. and P.Rabinowitz, 1984. Methods of Numerical Integration, 2nd edition. New York: Academic Press.

Davis, J.A., D.White and R.C.Cavanagh, 1982. NORDA Parabolic Equation Workshop, Norda Tech Note Rpt. # TN-143. NSTL Station, MS: NORDA.

Deavenport, R.L. and F.R. DiNapoli, 1977. "An Evaluation of Computer Models in Underwater Acoustics", in: J.B. Keller and J.S. Papadakis (eds)., Wave Propagation and Underwater Acoustics. Berlin-New York: Springer Verlag.

DeBoor, C. and R. Weiss, 1980. "Almost Block-Diagonal Linear Systems", ACM Trans.Math.Softw., 6(1), p.80-87.

DeBremaecker, J.-Cl., 1967. "Body waves as Normal and Leaking modes, Introduction", Bull. Seismo. Soc. Am., 16, p.191-198.

Desai, C.S. and J.F. Abel, 1972. An Introduction to the Finite Element Method. New York: Van Nostrand Reinhold.

Dietrich, M. and M. Bouchon, 1985. "Synthetic vertical Seismic profiles in elastic media", Geophysics, 50(2), p.224-234.

DiNapoli, F.R., 1971. 'The Fast field program for multilayered media', NUSC Tech. rept. 4103. New London, CT.

DiNapoli,F.R. and R.L. Deavenport, 1980. "Theoretical and Numerical Green's function field Solution in a plane multilayered Medium", J.Acoust.Soc.Am., 67, p.92-105.

Dix, C.H., 1961. "The seismic head pulse, reflexion and pseudo-reflexion pulses", J. Geophys. Res., 66, p.2945-2951.

Dolph, C.L. and R.A. Scott, 1978. "Recent Developments in the Use of Complex Singularities in Electromagnetic Theory and Elastic Wave Propagation", manuscript.

Eaton, J.P., J.Healy, W.H. Jackson and L.C. Pakiser, 1964. "Upper Mantle Velocity and Crustal Structure in the Eastern Basin and Range province, determined from Shoal and chemical explosions near Delta, Utah", Bull. Seismo. Soc. Am., 1964 Annual Mtg. Program., pg.30-31.

Ellis, D.D. and D.M.F. Chapman, 1984. 'Modeling of Shear-wave Related Acoustic propagation on the UK continental shelf'. Dartmouth, Canada: DREA. Tech Report 84/P.

Essen, H.H., 1980. "Model Computations for Low-velocity Surface Waves on Marine Sediments", in: W.A. Kuperman and F.B. Jensen (eds)., Bottom-interacting Ocean Acoustics. New York: Plenum Press., p.299-306.

Ewing, W.M., W.C. Jardetzky and F. Press, 1957. Elastic Waves in Layered Media. New York: McGraw Hill.

Faber, S. and G. Muller, 1980. "Sp Phases from the Transition zone between the Upper and Lower Mantle", Bull. Seis. Soc. Am., 70, p.487-508.

Ferla, M.C., F.B. Jensen and W.A. Kuperman, 1982. "High Frequency normal Mode calculations in deep Water", J.Acoust.Soc.Am., 72, p.505-509.

Fertig, J. and G. Muller, 1979. "Computations of Synthetic Seismograms with the Reflectivity method", Geophysical Prospecting, 26, p.868-883.

Fitch, A.A., 1981. "Vertical Seismic Profiling", in: G.Tango and W.Murphy (eds)., Proceedings of the SGS Conference on VSP. New Orleans: SGS.

Forsythe, G.A., M.A. Malcomb and C.B. Moler, 1977. Computer Methods for Mathematical Computations. Englewood Cliffs, NJ: Prentice Hall.

Franssens, G.R., 1983. "Calculation of the Elasto-dynamic Green's function in layered Media by means of a modified Propagator matrix method", Geophys.J.R.astro.Soc., 75, p.669-691.

Frazer, L.N., and A.J. Rudman, 1981. 'Generation of Synthetic Seismograms for an Acoustic layer over an Acoustic halfspace", Indiana Dept. Nat. Res. Geological Survey Occ. Pap. 35.

Frazer, L.N. and J.F. Gettrust, 1984. "On a generalization of Filon's method and the computation of the oscillatory integrals of seismology", Geophys.J.R.astro.Soc., 76, p.461-481.

Fryer, G.J. 1978. "Reflectivity of the Ocean bottom at Low Frequencies", J.Acoust.Soc.Am., 63(1), p.35-42.

Fuchs, K., 1968. "The Reflection of Spherical Waves from Transition Zones with arbitrary Depth-dependent Elastic moduli and Density", J.Phys.Earth, 16, special issue.

, 1969. "On the Properties of Deep Crustal Reflectors", Z. Geophys., 35, p.133-149.

, 1969. "The Method of Stationary Phase as a diagnostic aid in estimating the Field pattern of Body waves from Transition zones", Z. Geophys., 35, p.431-435.

Fuchs, K. and G. Muller, 1971. "Computation of Synthetic Seismograms with the Reflectivity method and comparison with Observations", Geophys.J.R.astro.Soc., 23, p.417-433.

Fuchs, K., 1975. "Snythetic Seismograms of PS-reflections from Transition Zones computed with the Reflectivity method", J. Geophys., 41, p.445-462.

Fuchs, K. and K. Schultz, 1976. "Tunneling of Low-frequency Waves through the subCrustal lithosphere", J. Geophys., 42, p.175-190.

Galligani, I. and E. Magenes (eds), 1977. Mathematical Aspects of Finite Element Method. New York-Berlin: Springer Verlag.

Gal'perin, E.I., 1974. Vertical Seismic Profiling. Moscow, NEDRA, 1971., English translation, Society of Exploration Geophysicists, Special Publication #12, Tulsa, Oklahoma.

Gamburtsvej, A.G., 1969. "Determing velocity characteristics of a medium using well-shooting with observation points inside the Medium", in: G.V. Keller (ed)., Exploration Geophysics, Vo.99. New York: Consultants Bureau.

Ganley, D.C. and E.R. Kanasewich, 1980. "Measurement of Attenuation and Dispersion from Check-Shot Surveys", J.Geophys.Res.,85, p.5219-5226.

Ganley, D.C., 1981. "A Method of Calculating Synthetic Seismograms which includes the Effects of Attenuation and Dispersion", Geophysics, 46(8), p.1100-1107.

George, A. and J.Liu, 1980. Computer Solution of Large Sparse Positive - Definite Systems. New York: Prentice Hall.

Giese, P. and A. Stein, 1971. "Versuch einer einheitlichen Auswertung tiefenseismicher Messungen aus dem Bereich zwischen der Nordsee und den Alpen", Zeit.Geophys., 37, p.237-272.

Giese, P., C. Prodehl and A. Stein (eds)., 1976. Explosion Seismology in Central Europe. New York-Berlin: Springer-Verlag.

Gilbert, F., 1964. "Propagation of Transient Leaking Modes in a Stratified Elastic Wavefield", Rev. Geophys., 2, p.123-153.

Gilbert, F. and G.E. Backus, 1966. "Propagator matrices in Elastic and Vibration problems", Geophysics, 31, p.326-332.

Gilbert, K.E., 1980. "Reflection of sound from a Randomly-layered ocean", J.Acoust.Soc.Am., 68(5), p.1454-1458.

, 1983. "A propagator matrix method for periodically-stratified media", J.Acoust.Soc.Am., 73(1), p.137-142.

Goupillaud, P.L., 1961. "An approach to Inverse Filtering of near-surface layer effects from Seismic Records", Geophysics, 26, p.754-760.

Green, R., 1962. "The Hidden-layer Problem", Geophys. Prosp. 10, p.166-170.

Gutenberg, B., 1913. "Ueber die Konstitution des Erdinnern erschlossen aus Erdbeben beobachtungen", Zeits. Geophys., 14, p.1217-1218.

Gutowski, P.R., F.Hron, D.E.Wagner and S.Treitel, 1984. " S* ", Bull. Seismo. Soc. Am., 74(1), p.1-78.

Ha, J., 1984. "Propagation of SH waves in a Layered Medium", Geophys.J.R.astro.Soc., p.291-306.

Haddon, R.A., 1984. "Computation of Synthetic Seismograms in Layered earth models of Leaking Modes", Bull. Seismo. Soc. Am., 74(4), p.1225-1248.

Hale, L.D. and G.A. Thompson, 1982. "The Seismic reflexion character of the Mohorovicic discontinuity", J. Geophys. Res., 81, p.4625-4635.

Hamilton, E.L., 1975. "Acoustic Properties of the Seafloor: a Review", Oceanic Acoustic Modeling Conference, Part 4, The Seafloor. SACLANTCEN Conference Proceedings., #17, October 15, 1975.

Hamming, R.W. and M.P. Epstein, 1972. "Non-interpolation quadrature formulas", SIAM J. Numer. Analy., 9, p.464-475.

Hardage, B.A., 1983. Vertical Seismic Profiling, Part A: Basic Principles. London and Amsterdam: Geophysical Press.

Harkrider, D.G., 1964. "Surface Waves in Multilayer Elastic Media, I: Rayleigh and Love Waves from Buried Sources in a Multilayered halfspace", Bull. Seismo. Soc. Am., 54, p.627-679.

Harrison, C.H., 1982. "Modeling low-frequency Sound propagation in Solid/fluid layers", in: N.G. Pace (ed)., Acoustics of the SeaBed. Bath: Bath University Press.

Haskell, N.A., 1953. "The Dispersion of Surface Waves on Multilayered Media", Bull. Seismo. Soc. Am., 43, p.17-34.

Healy, J.H. and D.H. Warren, 1969. "Explosion seismic studies in North America", in: P.J. Hart (ed)., The Earth's Crust and Upper Mantle. Washington: American Geophysical Union. Monograph 13, p.242-246.

Hecht, R.J., 1978. "Background of the Problems Associated with Seismic Detection of Signal Sources in the Ocean", in: Proceedings of a Workshop on Seismic Propagation in Shallow Water. Washington, DC: Office of Naval Research.

Heelan, P.A., sj., 1953. "Radiation from a Cylindrical Source of Finite Length", Geophysics, 18, p.685-696.

Heller, D., 1978. "A Survey of Parallel algorithms in Numerical linear Algebra", SIAM Review, 20(4), p.740-777.

Helmsberger, D.V. and R.A. Wiggins, 1971. "Upper mantle structure in the midWestern US", J. Geophys. Res., 76, p.3239-3245.

Helmsberger, D.V., 1973. "On the structure of the low-velocity zone", Geophys.J.R.astro.Soc., 48, p.81-80.

Herglotz, G., 1907. "Ueber das Benndorfische Problem der Fortplanzungsgeschwindigkeit der Erdbebenstrahlen", Phys. Zeit., 8, p.145-147.

Hill, D.P. and L.C. Pakiser, 1966. "Crustal structure beneath the Nevada Test Site and Boise Idaha from seismic Refraction measurements", in: J.S. Steinhart and T.J. Smith (eds)., The Earth Beneath the Continents. Washington: American Geophysical Union. Monograph #10, p.391-419.

Hill, D.P., 1971. "Velocity gradients in the earth from Head wave amplitudes", in: J.G.Heacock (ed)., American Geophysical Union Monograph #14. Washington: AGU., p.71-75.

Hinton, E. and D.R.J. Owens, 1977. Finite Element Programming. New York: Academic Press.

, 1980. An Introduction to Finite Element Computations. London: Pineridge Press.

Hron, F. and B.G. Mikhailenko, 1980. "Discovery of a 'new' S* arrival generated at a free interface", in: Proceedings of the 17th Assembly of the ESC, Budapest, p.293-298.

Hudson, J.A., 1980. The Excitation and Propagation of Elastic Waves. Cambridge: Cambrigde University Press.

Ida, N. and W. Lord, 1984. "Solution of Linear Systems for Small Computer Scenarios", Int.Journl.Num.Meth.Engin., 20, p.625-641.

Ingenito, F., R. Ferris, W.A. Kuperman and S.N. Wolf, 1978. "Shallow Water Acoustics- Summary Report". Rpt.#8179. Washington, DC: Naval Research Labs.

Jardetzky, W.S., 1953. "Period Equation for a n-Layered halfspace and some related Questions", Columbia University Lamont-Doherty Geological Observatory Technical Report #29. New York: Columbia University.

, 1954. "On Evaluation of Solutions to Equations of Wave Propagation in a Layered Halfspace", Columbia University Lamont-Doherty Geological Observatory Technical Report #35. New York: Columbia University.

Jeffreys, H., 1957. "Elastic Waves in a continuously-stratified Medium", Mon. Not. R. astro. Soc., Geophysics, suppl. 2, p.101-111.

, 1968. The Earth. Cambridge: Cambridge University Press.

Jensen, F.B. and W.A. Kuperman, 1982. "Consistency tests of Acoustic Propagation Models", SACLANTCEN Rept. #SM-157. La Spezia, Italy: SACLANT ASW Research Center.

, 1983. "Optimum Frequency of Propagation in Shallow Water Environments", J.Acoust.Soc.Am., 73, p.813-819.

Jensen, F.B. 1983. "Numerical Models in Underwater Acoustics", presented at the NATO Advanced Research Workshop on Hybrid Formulation of Wave Propagation and Scattering, Roma Italy, July 1983. In": G.Felsen (ed)., Hybrid Formulation of Wave Propagation and Scattering. The Hague: Martinus Nijhoff.

Johnson, L.R., 1974. "Green's function for Lamb's problem", Geophys.J.R.astro.Soc., 37, p.99-131.

Jones, T. and A. Nur, 1984. "The Nature of Seismic Reflexions from Deep Crustal Fault Zones", J. Geophys. Res., 89(B5), p.3153-3171.

Kanestrom, R., 1983. "Refracted arrivals and P-to-S converted waves in offset VSPs", paper presented at the 45th Meeting of the European Association of Exploration Geophysicists, Oslo, June, 1983.

Keilis-Borok, V.I., 1951. "On the Surface Waves in a Layer Overlying a Solid Halfspace", Izvest.Akad.Nauk.S.S.S.R.,Ser.Geograf.i Geofiz.,2.

, 1954. "On the Propagation of Vibrations in a Multilayered HalfSpace", Doklady Akad.Nauk.S.S.S.R., 45, p.733-735.

Kennett, B.L.N., 1974. "Reflections, Rays and Reverberations", Bull. Seismo. Soc. Am., 64, p.1685-1696.

, 1975. "The effects of Attenuation on Seismograms", Bull Seismo. Soc. Am., 65, p.1643-1651.

, 1977. "Towards a more detailed Seismic picture of the Oceanic Crust and Mantle", Marine Geophys. Res., 3, p.7-42.

, 1979. "Theoretical reflectivity seismograms for an elastic medium", Geophys. Prosp., 27, p.301-321.

, 1981. "Elastic Waves in Stratified Media", in: C.S.-Yih (ed)., Advances in Applied Mechanics, vo.21. New York: Plenum Press.

, 1983. Seismic Wave Propagation in Stratified Media. Cambridge: Cambridge University Press.

, 1984. "Reflection operator methods for Elastic Waves, I: irregular interfaces and regions", Wave Motion, 6, p.407-418.

Kind, R. and G. Muller, 1975. "Computation of Sv Waves in realistic earth models", J. Geophys., 41, p.149-172.

Kind, R., 1976. "Computation of Reflection Coefficients for Layered media", J. Geophys., 42, p.191-200.

, 1978. "The Reflectivity Method for a buried Source", J. Geophys., 45, p.450-462.

, 1979. "Extensions of the Reflectivity method", J. Geophys., 45, p.373-380.

Korn, M. and G. Muller, 1983. "Comparison of the Alekseev-Mikhailenko method and the Reflectivity method", Geophys.J.R.astro.Soc., 72, p.541-556.

Kosminskaya, I.P., 1971. Deep Seismic Sounding of the Earth's Crust and Upper Mantle. New York: Consultants Bureau.

Kosminskaya, I.P, N.N. Puzyrev and A.S. Alexeev, 1972. "Explosion Seismology: its past, present and future", Tectonophysics, 13, p.309-323.

Krenk, S. and H. Schmidt, 1982. "Elastic Wave Scattering by a circular Crack", Phil.Trans. R. Soc. Lond., A308, p.167-198.

Kunetz, G. and I. D'Erceville, 1962. "Sur certaines proprietes d'une onde acoustique plane de compression dans un milieu stratife", Annales de Geophysique, 18, p.351-359.

Kupper, F.J., 1958. "Theoretische Untersuchung ueber die Mehrfachaufstetung von Geophonen", Geophys. Prosp., 6, p.194-256.

Kurita, T., 1976. "Crustal and upper-Mantle structure in the central U.S. from body-wave Spectra, surface-wave Dispersion, travel-time Residuals and synthetic Seismograms", Phys. Earth and Planet. Inter., 12, p.65-86.

Kutschale, H., 1970. 'The Integral solution of the Sound field in a Multilayered Liquid-Solid Halfspace with Numerical Calculations for low-frequency in the Arctic Ocean', Columbia University Tech. Report CU1-1-70.

, 1973. 'Rapid Computation by Wave Theory of Propagation Loss in the Arctic Ocean', Report CU-8-73. Palisades, NY: Lamont-Doherty Geological Observatory, Columbia University.

Lamb, H., 1904. "On the Propagation of Tremors over the surface of an Elastic Solid", Phil.Trans.Roy.Soc.Lon., A203, p.1-42.

Lamé, G., 1852. Lecons sur la Theorie Mathematique de l'Elasticite des Corps Solides. Paris: Bachelier.

Landismann, M., S. Mueller and B.J. Mitchell, 1971. "Review of Evidence for velocity Inversions in the continental Crust", in: J.G. Heacock (ed)., The Structure and Physical Properties of the Earth's Crust. Washington: American Geophysical Union. Monograph #14, p.11-34.

Lawrie, D.H., 1975. "Access and alignment of data in an Array Processor", IEEE Trans.Comp., C-24(12), p.1145-1155.

Lawrie, D.H. and A.H. Sameh, 1984. "The Computation and Communication Complexity of a Parallel-Banded System Solver", ACM Trans.Math.Softw., 10(2), p.185-195.

Lee, M.W. and A.H. Balch, 1983. "Computer Processing of Vertical Seismic Profile data", Geophysics, 48, p.272-283.

Levin, F.K. and R.D. Lynn, 1958. "Deep-hole Geophone Studies", Geophysics, 23, p.639-664.

Lash, C.C., 1980. "Shear waves, Multiple reflections and Converted waves formed by a deep vertical wave test (VSP)", Geophysics, 45, p.1373-1411.

, 1982. "Investigation of Multiple reflections and Wave conversions by means of Vertical Wave Tests (VSP) in S. Mississippi", Geophysics, 47, p.977-1000.

Luke, Y.L., 1954. "On the Computation of oscillatory Integrals", Proc.Cambridge Philosop.Soc., 50, p.269-277.

Mainardi, F. (ed)., 1982. Wave Propagation in Viscoelastic Media. London: Pitman Advanced Publishing.

Marsh, H.W. and S.R. Elam, 1967. "Report on numerical integral for electromagnetic field calculations", Internal Document, Raytheon Co., Marine Research Lab, New London, CT.

Martin, H., 1935. "Einschwingvorgaenge and ihre Bedeutung bei der Aufzeichnung von Stossaehnlichen Erschuetterungen", Vrf.R.Anstalt f.Erdbebenforschung, Jena, Heft 26, p.1-40.

Martin, R.S. and J.H. Wilkinson, 1965. "Symmetric decomposition of positive-definite band matrices", Numer.Math., 7, p.355-361.

McMechan, G.A., 1977. "Low velocity zone Parameters as functions of Focal depth", Geophys.J.R.astro.Soc., 51, p.217-228.

, 1982. "Low velocity zone Reflections observed in Geometrical shadows of Refraction profiles", "Geophys.J.R.astro.Soc.,71, p.261-268.

Meissner, R.O. and E.R. Flueh, 1979. "Probable relations between seismic Anisotropy and a Fine structure of the Lithosphere", J. Geophys., 45, p.349-352.

Meissner, R.O., 1967. "Exploring deep Interfaces by seismic Wide-angle measurements", Geophys. Prosp., 15, p.598-617.

, 1973. "The 'MOHO' as a Transition zone", Geophys. Surveys, 1, p.195-215.

Menke, W., 1984. "A formula for the Apparent attenuation of acoustic waves in a randomly-layered media", Geophys.J.R.astro.Socl, 75(2), p.541-544.

Miklowitz, J., 1978. The Theory of Elastic Waves and Waveguides. New York: North-Holland.

Moler, C. and C. Van Loan, 1978. " Nineteen Dubious ways to Compute the Exponential of a Matrix ", SIAM Review, 20(4), p.801-836.

Mooney, H.M., 1974. "Some numerical Solutions to Lamb's problem", Bull. Seismo. Soc. Am., 64, p.473-491.

1983. "Synthetic Seismograms for body waves: a review", First Break Newsletter, 1(12), p.9-20.

Morlet, J., G. Arens, E. Fourgeau and D. Giard, 1982. "Wave Propagation and Sampling Theory, I & II", Geophysics, 47(2), pp. 203-221 and 222-236.

Muller, G., 1968. "Theoretical Seismograms for some Types of Point-sources in Layered media, I", Zeits. Geophys., 34(1), p.15-35.

, 1968. "Theoretical Seismograms for some Types of Point-sources in Layered media, II", Zeits. Geophys., 34(1), p.147-162.

Muller, G. and W. Schott. 1981. "Some Recent Extensions of the Reflectivity Method", in: E.S. Husebye and S. Mykkelveit (eds)., Identification of Seismic Sources-Earthquake or Underground Explosion. New York: Plenum Press, p.347-371.

Muller, G. and S. Mueller, 1979. "Traveltime and Amplitude Interpretation of Crustal phases on the Refraction profile DELTA-W.Utah", Bull. Seismo. Soc. Am., 69, p.1121-1132.

Mueller, S. and M. Landismann, 1966. "Seismic studies of the Earth's Crust in Continents, I: Evidence for a Low-velocity zone in the upper part of the Lithosphere", Geophys.J.R.astro.Soc., 10, p.525-538.

Newton, R.G., 1981. "Inversion of Reflection Data for Layered Media: a Review of Exact Methods", Geophys.J.R.astro.Soc., 65, pp.191-215.

O'Doherty, R.F. and N. Anstey, 1971. "Reflections on Amplitudes", Geophys. Prosp., 19, p.430-458.

Officer, C.B., 1958. Introduction to the Theory of Sound Transmission. New York: McGraw Hill.

Oliver, J., 1964. "Propagation of PL waves across the US", Bull. Seismo. Soc. Am., 50, p.151-160.

Oliver, J. and S. Kaufman, 1977. "Complexities of the deep Basement from seismic reflexion profiling", in: J.G. Heacock (ed)., American Geophysical Union monograph 20, p.243-253. Washington, DC: AGU.

Oliver, J., 1982. "Tracing surface features to great depths: a powerful means of exploring the crust", Tectonophysics, 81, p.257-272.

Omnes, G., 1978. "Vertical Seismic Profiling: a Bridge between Velocity logs and surface Seismograms", SPE paper #7436, 53rd Annual SPE Fall Conference.

O'Neill, M.E. and D.P. Hill, 1979. "Causal Absorption: its effect on Synthetic Seismograms computed by the Reflectivity method", Bull. Seismo. Soc. Am., 69, p.17-26.

Ostrander, J.J., 1984. "Plane wave reflexion coefficients for gas sands at non-normal angles of incidence", Geophysics, 49(10), p.1637-1648.

Pakiser, L.C., 1963. "Structure of the Crust and Upper mantle in the western United States", J. Geophys. Res., 68, p. 5747-5756.

Pakiser, L.C. and Isidore Zeitz, 1965. "Transcontinental Crustal and Upper mantle structure", Rev. Geophysics, 3, p.505-520.

Pakiser, L.C., 1985. "Historical review of Seismic exploration of the Crust and upper Mantle of the Basin and Range province", (manuscript).

Patton, H.J. and S.R. Taylor, 1984. "Q Structure of the Basin and Range from Surface Waves", J. Geophys. Res., 89, p.6929-6940.

Pei, I.M., 1960. "Stiffness Method of Rigid Frame Analysis", Proc. 2nd ASCE Conference Elec.Comput, p.225-248.

Pekeris, C.L., 1935. "The Propagation of Rayleigh Waves in heterogeneous media", Physics, 6, p.133-138.

, 1948. "Theory of Propagation of Explosive Sound in Shallow Water". In: Geological Society of America Memor #27. New York: GSA.

, 1955. "The surface Seismic pulse", Proced. Nat. Acad. Sci., 41, p.629-639.

Pekeris, C.L., Z.Alterman, F.Abramovici and H.Jarosch, 1965. "Propagation of a compressional Pulse in a Layered solid", Rev. Geophys., 3, p.25-47.

Phinney, R.A., 1961. "Leaking modes in the Crustal wave-guide,I: the oceanic PL wave", J. Geophys. Res., 66, p.1445-1469.

Pilant, W., 1979. Elastic Waves in the Earth. New York-Amsterdam: Elsevier.

Priestly, K., J.A. Orcutt and J.N. Brune, 1980. "Higher-mode surface waves and the structure of the Great Basin of Nevada and western Utah", J. Geophys. Res., 85, p.7166-7174.

Prodehl, C., 1970. "Seismic refraction study of Crustal structure in the western United States", Geol.Soc.Am.Bull., 81, p.2629-2646.

, 1979. 'Crustal Structure of the western United States', U.S. Geol. Surv. Prof. Pap. #1034. Reston, VA: USGS.

Pujol, J.M., S.B. Smithson and R. Burridge, 1984. "Vertical Seismic Profiling, Crustal Reflections and Deep Scientific Drilling", EOS, 65(16), April 17, 1984, paper presented at the 1984 Spring AGU Meeting.

Raitt, R.W., 1963. "The Crustal Rocks", in: M.N. Hill (ed)., The Sea, Vol.3. New York: Interscience

Rauch, D., 1982. "Experimental and Theoretical Studies of Seismic Interface waves in crustal waters", in: W.A. Kuperman and F.B. Jensen (eds)., Bottom-interacting Ocean Acoustics. New York: Plenum Press, p.307-328.

Redwood, M., 1960. Mechanical Waveguides. New York: Pergammon Press.

Rice, J.R., 1974. "Adaptive Quadrature", Bull.Amer.Math.Soc., 80, p.1250-1254.

, 1981. Matrix Computations and Mathematical Software. New York: McGraw Hill.

, 1983. Numerical Methods, Software and Analysis. IMSL Reference Edition. New York: McGraw Hill.

Robinson, E. and S. Treitel, 1966. "Multichannel z-transforms and minimum delay", Geophysics, 31, p.482-500.

Robinson, E. and S. Treitel, 1980. Geophysical Signal Analysis. Englewood Cliffs, NJ: Prentice Hall.

Rosenbaum, J.H., 1960. "The long-time response of a layered elastic medium to explosive sound", J.Geophys.Res., 65, p.1577-1613.

, 1961. "Refraction arrivals along a thin elastic plate submerged in a fluid medium", J. Geophys. Res., 66, p.3899-3906.

, 1974. "Synthetic microseismograms: logging in porous formations", Geophysics, 39(1), p.14-32.

Rubano, L.A., 1980. "Acoustic propagation in shallow water over a low-velocity bottom", J.Acoust.Soc.Am., 67(5), p.1608-1613.

Rubenstein, M.F., 1980. Matrix Computer Analysis of Structures. Englewood Cliffs, NJ: Prentice Hall.

Sabatier, P.C., 1974. "Remarks on approximate methods in geophysical inverse problems", Proc. Roy. Soc. Lon., A337, p.49-71.

Sameh, A.H., 1977. "Numerical Parallel algorithms- a Survey", in: D.J. Kucks, D.H. Lawrie and A.H. Sameh (eds). High-Speed Computer and Algorithm organization. New York: Academic Press.

Schelkunoff, S.A.,1934. "The Electromagnetic theory of coaxial transmission lines and cylindrical shields", Bell Sys Tech Journ., 17, October, p.17ff.

,1951. "Remarks concerning Wave propagation in stratified Media", Commun. Pure Appl. Math., 4, pp.117-128.

Schendel, U., 1984. Introduction to Numerical Methods for Parallel Computers. London: E.Harwood Ltd.

Schmidt, H., 1975. 'Revnelokaliseringsudtyr basaret pae deteston af akustisk emission', Inter. Report., Nr. I-43. Lyngby: Danmarks Tekniske Hojskole.

, 1977. 'Udbredelse Afakustisk emission i beton', Report # NR-93. Lyngby: Danmarks Tekniske Hojskole.

Schmidt, H. and S. Krenk, 1982. "Asymmetric Vibrations of a circular Elastic plate on an Elastic halfspace", Int. J. Solids Struct., 18, p.91-105.

, 1982. "Excitation and Propagation of Interace waves in a Stratified SeaBed", in: N.G. Pace (ed)., Acoustics and the SeaBed. Bath: Bath University Press.

, 1983. "A new Fast field solution to Propagation in Multilayered Solid-Fluid Environments", paper presented at the 1983 Fall Meeting of the Acoustical Society of America.

Schmidt, H. and F.B. Jensen, 1984. "Efficient numerical Solution technique for wave Propagation in Horizontally-stratified environments", presented at the Workshop on Computational Ocean Acoustics, Yale University, August 1-3, 1984.

1985. "A Full wave solution for Propagation in Multilayered viscoelastic media with application to Gaussian beam reflection at fluid-solid interfaces", J.Acoust.Soc.Am., 77(3), p.813-825.

H. Schmidt and G.J. Tango, 1984. "Efficient Global Matrix solution for Theoretical Seismograms", submitted to Geophys. J. R. astro. Soc., January, 1985.

, 1985. 'SAFARI: User's Guide and Introduction. NORDA-SACLANT joint Technical Memo (in review).

H. Schmidt and J.Glatetre, 1985. "A 3-dimensional Fast field solution to wave Propagation in Stratified environments, based on the Global matrix method", submitted to J. Acoust. Soc. Am., March, 1985.

Schoenberger, M. and F.K. Levin, 1974. "Apparent attenuation due to intrabed multiples", Geophysics, 39, p.278-291.

, 1978. "Apparent attenuation due to intrabed multiples, II", Geophysics, 43, p.730-737.

Sluijter, F.W., 1970. "Arbitrariness of dividing the Total field in an Optically-inhomogeneous medium into Direct and Reversed waves", J. Opt. Soc. Am., 60, pp. 8-10.

Smith, W.D., 1975. "The application of Finite element analysis to body wave Propagation problems", Geophys. J. Roy. astro. Soc., 72, p.747-768.

Sneddon, I.N., 1972. The Use of Integral Transforms. New York: McGraw Hill.

Spencer, T.W., 1960. "The Method of generalised Reflection and Transmission Coefficients", Geophysics, 25, p.624-641.

Spencer, T.W., J.R. Sonnad and T.M. Butler, 1982. "Seismic Q - stratigraphy or dissipation", Geophysics, 47, p.16-24.

Spudich, P., 1977. 'A Study of Underwater Seismic Propagation using generalized Ra theory', PhD Thesis, University of California at San Diego, Dept of Marine Geophysics.

Spudich, P. and J. Orcutt, 1980. "A new look at the Seismic velocity structure of the Oceanic crust", Revs. Geophys. Space Physics, 18, p.627-645.

Steinberg, D.I., 1974. Computer Matrix Algebra. New York: McGraw Hill.

Stephen, R.A., 1977. "Synthetic seismograms for the receiver within the Reflectivity zone", Geophys.J.R.astro.Soc., 51, p.169-181.

, 1979. "The Oblique Seismic Experiment in Oceanic Crust - Equipment and Technique", Marine Geophys. Res., 4, p.213-226.

Stephen, R.A., K.E. Louden and D.H. Mathews, 1980. "The Oblique Seismic Experiment on DSDP Leg 52", Geophys.J.R.astro.Soc., 60, p.289-300.

Stephen, R.A., 1981. "Seismic anistrophy observed in upper ocean crust", Geophys.Res.Let., 8, p.865-870.

, 1983. " A Comparison of Finite difference and Reflectivity seismograms for marine models", Geophys.J.R.astro.Soc., 72, p.39-58.

Stephen, R.A. and A.J. Harding, 1983. "Travel-time inversion of borehole seismic data", J. Geophys. Res., 88, p.8289-8298.

Stephen, R.A., and S.T. Boumer, 1984. " The Direct Wave Root in Marine Seismology", Woods Hole Report (submitted to Bull. Seismo. Soc. Am.)

Stewart, R.R., 1983. 'Vertical Seismic Profiling: the 1-dimensional Forward and Inverse problems'. Ph.D. Thesis, Dept. of Earth and Planetary Sciences, MIT, Cambridge, MA.

Tango, G.J., 1981. "Vertical Seismic Profiling-an Overview", in: G.J.Tango and W.Murphy (eds), Proceedings of the SGS Symposium on VSP. New Orleans, LA: SEG. March 25, 1981.

, 1983. "Note on Potential Horizontal and Vertical Seismic applications of a new Fast field program, 'SAFARI'", NORDA Memo.

Tango, G.J. and H.Schmidt, 1985a. "Exact Full wave synthetic VSPs using a new Fast Direct global matrix solution", paper submitted for presentation at the 55th annual meeting of the Society of Exploration Geophysicists. Washington, D.C., October 1-5, 1985.

Tango, G.J., K.E. Gilbert and H.Schmidt, 1985b. "An extended FFP method for generalized numerical modeling of soundwave propagation in a stratified atmosphere/earth", invited paper presented at the 2nd Symposium on Long Range Sound Propagation and Ground Coupling, New Orleans, LA., February 13-15, 1985 (to appear in Proceedings).

Tango, G.J. and T. Lawrence, 1985c. "Numerical modeling of ice-interacting acoustic signals in the Arctic using a new Fast field program", paper presented at the Spring 1985 meeting of the Acoustical Society of America, Austin, Texas, April 17, 1985; Abstract in Spring Suppl. J.Acoust.Soc.Am., March, 1985.

Tango, G.J. and H.Schmidt, 1985d. "Background and Applications of a rapid Seismic-Acoustic Wave propagation modeling program configured for the FPS-164", invited paper presented at the 8th Annual meeting of the FSP-ARRAY Users Society, New Orleans, LA., April 15, 1985 (to appear in Proceedings).

Tappert, F., 1977. "Selected applications of the Parabolic equation method in Underwater acoustics", in: Proceedings of an International Workshop on Low-frequency propagation and noise. Washington,DC: Maury Center for Ocean Sciences.

Tatel, H.E. and M.A. Tuve, 1955. "Seismic Exploration of a continental Crust", in: A. Poldevaart (ed)., The Crust of the

Earth. Washington, DC: Geological Society of America. Special Paper #62, p.35-50.

Temme, P. and G. Muller, 1982. "Numerical simulation of Vertical seismic Profiling", J. Geophys., 50, p.177-188.

Tezcon, S.S., 1963. "Discussion of 'A Simplified Formulation of Stiffness Matrices' by P.M. Wright", J.Struct.Div.ASCE, 89, p.179-204.

Thigpen, L., 1980. 'Seismic Waves in a Horizontally-stratified Halfspace", Lawrence Livermore Nat. Lab. Rept. UCRC-53072.

Thomson, W.T., 1951. "Transmission of elastic waves through a stratified solid", Journ.Appl.Phys., 21, p.89-93.

Thouvenot, F., 1980. "Quality factor in the Crust - a deep seismic sounding approach", in: Proceedings of the 17th Assembly of the ESC. Budapest, 1980, p.557-560.

, 1983. "Frequency-depedence of the Quality factor of the Crust: a Deep Seismic Sounding approach", Geophys.J.R.astro.Soc., 73(2), p.427-448.

Tolstoy, I., 1973. Wave Propagation. New York: McGraw-Hill.

Tokszoz, N. and R.R. Stewart (eds)., 1984. Vertical Seismic Profiling, PartB: Advanced Concepts. Amsterdam and London: Geophysical Press.

Tsang, L. R. Brown, J.A. Kong and G. Simmons, 1974. "Numerical evaluation of Electromagnetic fields due to dipole antennaes in the presence of stratified media", J. Geophys. Res., 79, p.2077-2080.

Ursin, B., 1983. "Review of elastic and electromagnetic wave propagation in horizontally-layered media", Geophysics, 48(8), p.1063-1081.

Van Cittert, P.H., 1939. "Propagation of Light in Inhomogeneous Media", Physics, 6, p.840-848.

Vidmar, P.J., 1980. "The effect of Sediment rigidity on bottom Reflection loss in a typical Deep sea sediment", J.Acoust.Soc.Am., 68(2), p.634-638.

Wait, J.R., 1982. Geo-Electromagnetism. New York: Academic Press.

Warren, D.H. and J.H. Healy, 1973. "Structure of the Crust in the coterminous United States", Tectonophysics, 20, p.203-213.

Watson, W.H., 1947. The Physical Principles of Wave Guide Transmission and Antenna Systems. Oxford: Clarendon Press.

Watson, T.H., 1972. "A Real-frequency, Complex-wavenumber analysis of Leaking modes", Bull. Seismo. Soc. Am., 62, p.369-384.

White, J.E., 1965. Seismic Waves: Radiation, Transmission and Attenuation. New York: McGraw Hill.

White, R.S. and R.A. Stephen, 1980. "Compressional to Shear wave conversion in Oceanic crust", Geophys.J.R.astro.Soc.,63,p.547-565.

Wiggins, R.A., G.A. McMechan and M.N. Tokszoz, 1973. "Range of earth structure Nonuniqueness implied by Body wave observations", Rev. Geophys. Space Phys., 11, p.87-113.

Wilkinson, J.H., 1963. Rounding Errors in Algebraic Processes. New York: Prentice Hall.

Woodhouse, J.H., 1978. "Asymptotic results for Elastodynamic Propagator matrices in plane-stratified and spherically-stratified earth models", Geophys.J.R.astro.Soc., 54, p.263-280.

, 1981. "Efficient and stable Methods for performing Seismic calculations in stratified media" in: A. Dziewonski and E. Boschi, (eds). Physics of the Earth's Interior. New York: Plenum.

Wuenschel, P., 1976. "The Vertical Array in Reflexion Seismology - some Experimental studies", Geophysics, 41, p.219-232.

Wyatt, K.D., 1981. "Synthetic vertical Seismic profiles", Geophysics, 46(6), p.880-891.

Young, T.K., C.B. Monash and R.B. Turpening, 1984. "Computer modeling of VSP", Geophysical Prospecting, 32(5), p.851-870.

Zienkiewicz, D.C., 1973. The Finite Element Method in Engineering Science. New York: McGraw Hill.

Zschau, J. and K. Koschyk, 1976. "Results of a combined Evaluation of Longitudinal and Transverse waves on a Seismic profile along the northern Margin of the Alps", in: P.Giese, C.Prodehl and A.Stein (eds)., Explosion Seismology in Central Europe. New York-Berlin-Heidelberg: Springer Verlag.

VITA

Gerard Joseph TANGO was born on July 17, 1955 in New Orleans, Louisiana, the son of Mr. and Mrs. Louis J. Tango. He graduated from Strake Jesuit Preparatory in Houston, Texas in 1973, and enrolled at Cornell University, graduating in 1977 with a B.S. degree in Physics and History of Science. After work with Geophysical Service Incorporated in the US and Saudi Arabia, and subsequently with Services Techniques Schlumberger, in the spring of 1983 he enrolled in the UNO Graduate Physics program, at the same time beginning work with the Numerical Modeling Group, Code 221 of the Navy Ocean Research and Development Activity (NORDA), NSTL Station, Mississippi, thru ODSI Defense Systems Incorporated. After a summer internship at the NATO SACLANT ASW Research Centre in La Spezia, Italy, he completed course and thesis work for the MS degree of Applied Physics in April of 1985.

Major Field of Study: Applied Physics - Geophysics

Studies in Seismology: Drs.L.Pakiser, H.Schmidt, K.Gilbert

Studies in Numerical Modeling: Dr.H.Schmidt, Prof. G.Ioup

Studies in Underwater Acoustics: Prof.J.Murphy, Dr.K.Gilbert

Affiliations:

Society of Exploration Geophysicsts (Active Member)

Acoustical Society of America (Member)

Seismological Society of America (Member)

Institute of Electrical & Electronics Engineers (Member)

Association of Professional Engineers, Geologists and Geophysicists of Alberta (APEGGA) (License Exam Candidate)